REFERENCE ONLY

UNIVERSITY OF LONDON THESIS

Degree PhD Year 2006 Name of Author GILSIANN, E.G

STRATEGIES TO PREVENT MOTONEURON DEGENERATION IN MODELS OF AMYOTROPHIC LATERAL SCLEROSIS

A thesis submitted to the University of London

for the degree of Doctor of Philosophy

in the Faculty of Science

By

Lynsey Gail Bilsland BSc (Hons)

Sobell Department of Motor Neuroscience and Movement Disorders

Institute of Neurology,

University College London

November 2005

ProQuest LLC
789 East Eisenhower Parkway
P.O. Box 1346
Ann Arbor, MI 48106-1346

ACKNOWLEDGEMENTS

I have been part of the Watts Laboratories in the Sobell Department at the Institute of Neurology and the Department of Physiology at UCL for 4 years and there are a large number of people that I must thank for their help during this time. In particular, I would like to thank my supervisors Dr Linda Greensmith and Professor Michael Duchen. I would like to thank Linda for her continual encouragement and the enormous amount of advice and support that I have received throughout my PhD. I would also like to thank Michael for all his advice in the imaging aspects of this PhD. Furthermore, there are numerous colleagues whose assistance has been invaluable, in particular Jim Dick for all his technical assistance and expertise. Also thanks to Dairin Kieran, Bernadett Kalmar, Andrey Abramov, Paul Sharp, Jake Jacobson, Joanna Riddoch-Contreras, Niran Nirmalananthan and Virginie Bros for their practical experience and for making the lab an enjoyable place to work.

Thank you also to my collaborators, who have made significant contributions to the studies in this Thesis: David Baker and Gareth Pryce at the ION, Mimoun Azzouz and Scott Ralph at Oxford Biomedica and Vincenzo Di Marzo and Stefania Petrosino from the Endocannabinoid Research Group in Naples.

Finally, I must also thank all my family and friends for all their support, particularly over this last year.

ABSTRACT

Amyotrophic Lateral Sclerosis (ALS) is a fatal neurodegenerative disorder, characterised by progressive motoneuron degeneration in the spinal cord, motor cortex and brainstem. The pathogenic mechanisms underlying selective motoneuron degeneration are unclear and currently there is no effective treatment.

In this Thesis, strategies designed to prevent motoneuron degeneration are investigated in both *in vivo* and *in vitro* models of ALS. Furthermore, interaction between motoneurons and astrocytes is studied to examine the influence of astrocytes on disease progression.

In the $SOD1^{G93A}$ mouse model of ALS, the glial cell genotype influences the susceptibility of motoneurons to degeneration (Gong et al., 2000; Clement et al., 2003). In this Thesis, the effect of mutant SOD1 expression in astrocytes on motoneuron properties is examined in an *in vitro* co-culture system using confocal microscopy.

Cannabinoids exert anti-excitotoxic, anti-inflammatory and anti-oxidant actions, all of which may contribute to ALS pathogenesis. In these experiments, the potential neuroprotective effect of manipulating the endocannabinoid system is investigated *in vivo* in $SOD1^{G93A}$ mice. Augmentation of the endocannabinoid system, by pharmacological and genetic manipulation, ameliorates disease symptoms in $SOD1^{G93A}$ mice. Furthermore, genetic ablation of the CB_1 receptor significantly extends lifespan in $SOD1^{G93A}$ mice.

Finally, the effect of ablating the expression of mutant SOD1 protein *in vitro* in primary motoneurons using viral delivery of targeted small interfering RNA (siRNA) is

assessed. The successful transfection and ablation of the mutant protein *in vitro,* as shown in this Thesis, has since been tested successfully *in vivo*.

The results of this Thesis show that manipulation of the endocannabinoid system and siRNA technology may be successful therapeutic approaches in ALS. The results also indicate that mutant SOD1 expression in astrocytes has a deleterious influence on mitochondrial function in motoneurons even under resting conditions. Therefore, specific targeting of astrocytes may also be an appropriate strategy to prevent motoneuron degeneration in ALS.

DECLARATION

I, Lynsey Bilsland, confirm that the work presented in this Thesis is my own. Where information has been derived from other sources, I confirm that this has been indicated in the Thesis.

Lynsey Bilsland

CONTENTS

List of Figures

Chapter 1.

Chapter 2.

Chapter 3.

Chapter 4.

Chapter 5.

Chapter 6.

List of Tables

Chapter 1.

Chapter 2.

Chapter 3.

Chapter 5.

Chapter 6.

Abbreviations

$\Delta\Psi_m$	mitochondrial membrane potential
Δ^9THC	Δ^9 tetrahydrocannabinol
$[Ca^{2+}]_c$	cytosolic calcium concentration
$[Ca^{2+}]_m$	mitochondrial calcium concentration
12 – HAEA	12-Hydroxy-N-arachidonoylethanolamine
15 – HAEA	15-Hydroxy-N-arachidonoylethanolamine
2-AG	2-arachidonoyl glycerol
a.f.u.	arbitrary fluorescent units
a.u.	arbitrary units
AAV	adeno-associated virus
ABC	avidin biotin complex
ACh	acetylcholine
AChE	acetylcholine esterase
AChR	acetylcholine receptor
Ad	adenovirus
AD	Alzheimer's Disease
AEA	anandamide
AIF	apoptosis inducing factor
ALS	Amyotrophic Lateral Sclerosis
AM ester	acetoxy-methyl ester
AMPA	α-amino-3-hydroxy-5-methyl-4-isoxazole propionic acid
ANOVA	analysis of variance
Apaf – 1	apoptosis activating factor - 1
ATP	adenosine triphosphate
BDNF	brain derived neurotrophic factor

BSA	bovine serum albumin
CB_1R	cannabinoid receptor 1
CB_2R	cannabinoid receptor 2
CB_3R	cannabinoid receptor 3
CBD	cannabidiol
CCD	charge coupled device
CCS	copper chaperone protein
CGRP	calcitonin gene related peptide
ChAT	choline acetyltransferase
CLSM	confocal laser scanning microscope
CNQX	6-cyano-7-nitroquinoxaline-2,3-dione
Cnr1 -/-	CB_1 receptor knockout mouse
Cnr2 -/-	CB_2 receptor knockout mouse
CNTF	ciliary neurotrophic factor
CREAE	chronic relapsing experimental allergic encephalomyelitis
DAG	*sn*-1-acyl-2-arachidonoyl glycerol; diacylglycerol
DAGL	diacylglycerol lipase
DAPI	4'-6-Diamidino-2-phenylindole
DIV	days *in vitro*
DMEM	Dulbecco's Modified Essential Medium
DSE	depolarisation-induced suppression of excitation
DSI	depolarisation-induced suppression of inhibition
dsRNA	double stranded RNA
EAAC1	excitatory amino acid carrier 1
EAAT–2/GLT – 1	excitatory amino acid transporter 2 (humans)/glutamate transporter 1 (animals)

EDL	extensor digitorum longus muscle
EIAV	equine infectious anaemia virus
EMT	endocannabinoid membrane transporter
EPP	endplate potential
ER	endoplasmic reticulum
ERK	extracellular signal regulated kinase
F.I.	fatigue index
Faah -/-	Faah knockout mouse
FAD	Flavin adenine dinucleotide
FADD	Fas Associated protein with Death Domain
fALS	familial Amyotrophic Lateral Sclerosis
FAN	factor associated with neutral sphingomyelinase activation
FCCP	carbonyl cyanide p-trifluoromethoxyphenyl hydrazone
FGF –2	fibroblast growth factor - 2
GABA	gamma amino butyric acid
GDNF	glial derived neurotrophic factor
GEF	guanine nucleotide exchange factor
GFAP	glial fibrillary acidic protein
GFP	green fluorescent protein
GLAST	glutamate transporter (EAAT1)
H_2O_2	hydrogen peroxide
HBSS	Hanks balanced salt solution
HEt	dihydroethidium
HPLC	high pressure liquid chromatography
HSP	heat shock protein
hsp 70	heat shock protein 70

i.p.	intraperitoneal
ICAM – 1	intracellular adhesion molecule – 1
IEGs	immediate early genes
IF	intermediate filament
IGF – 1	insulin like growth factor – 1
IL-6	interleukin 6
iNOS	inducible nitric oxide synthase
IP_3	inositol 1,4,5-trisphosphate
KA	kainate
LMC	lateral motor column
Loa	legs at odd angles
LTP	long term potentiation
MAGL	monoacylglycerol lipase
MAPK	mitogen activated protein kinase
MCPG	alpha-methyl-4-carboxyphenylglycine
MK – 801	(5R,10S)-(+)-5-Methyl-10,11-dihydro-5H-dibenzo [a,d] cyclohepten-5,10-imine hydrogen maleate
MOI	multiplicity of infection
MOM	mouse on mouse
mPTP	mitochondrial permeability transition pore
MS	multiple sclerosis
mtDNA	mitochondrial DNA
MTT	maximal tetanic tension
NADH	nicotinamide adenine dinucleotide
NAE	N-acyl ethanolamines
NAPE	N-acyl phosphatidylethanolamines

NE	norepinephrine
NF – H/M/L	neurofilament heavy/medium/light chain
NMDA	N-methyl-D-aspartate
NO	nitric oxide
NOS	nitric oxide synthase
OEA	oleoylethanolamide
PAG	periaqueductal grey matter
PARP	poly (ADP-ribose) polymerase
PBS	phosphate buffered saline
PCD	programmed cell death
PCR	polymerase chain reaction
PEA	palmitoylethanolamide
PFA	paraformaldehyde
PKA	protein kinase A
PLC	phospholipase C
PLD	phospholipase D
PMT	photomultiplier tube
PPARα	peroxisome proliferator-activated receptor-alpha
RISC	RNA-induced silencing complex
RM	recording medium
ROS	reactive oxygen species
sALS	sporadic Amyotrophic Lateral Sclerosis
SDH	succinate dehydrogenase
SEM	standard error of the mean
Shh	sonic hedgehog protein
shRNA	short hairpin RNA

siRNA	small interfering RNA
Smac	second mitochondrial-derived activator of caspase
SOD1	Cu/ZN superoxide dismutase enzyme
SOD1.*Cnr1* -/-	$SOD1^{G93A}$ CB_1 receptor knockout mouse
SOD1.*Faah* -/-	$SOD1^{G93A}$ Faah knockout mouse
SODnSODa	$SOD1^{G93A}$ neurons co-cultured with $SOD1^{G93A}$ astrocytes
SODnWTa	$SOD1^{G93A}$ neurons co-cultured with WT astrocytes
STN	staurosporin
TA	tibialis anterior muscle
TCA cycle	tricarboxylic acid cycle
TMRM	tetramethyl rhodamine methyl ester
TNF – α	tumour necrosis factor α
VAPB	vesicular associated membrane protein B
VEGF	vascular endothelial growth factor
VR1	vanilloid receptor 1
VSV-G	vesicular stomatitis virus-G
WIN	WIN55,212-2
WT	wild type
WTnSODa	WT neurons co-cultured with $SOD1^{G93A}$ astrocytes
WTnWTa	WT neurons co-cultured with WT astrocytes

CHAPTER 1

GENERAL INTRODUCTION

In this Thesis, a series of experiments have been undertaken to investigate potential strategies to prevent the degeneration of motoneurons that occurs in diseases such as Amyotrophic Lateral Sclerosis (ALS). Therefore in the Introduction, the normal development of motoneurons, muscle fibres and the neuromuscular junction will be discussed to provide an understanding of the system that subsequently degenerates in ALS. Furthermore, the pathways by which motoneurons die and the pathological processes that are proposed to play a role in initiating the degeneration of motoneurons in ALS will also be discussed.

1.1. Development of the neuromuscular system

1.1.1. Motoneuron development

The vertebrate nervous system originates from the neural plate, which consists of a sheet of elongated neuroectodermal cells that form a group of multipotent proliferating progenitors. A thickening of the neural plate initiates folding and the subsequent fusion of the folds generates the neural tube (Briscoe & Ericson, 1999). The development of regional cell types in the neural tube occurs along both an anterior-posterior and dorsal-ventral axis. In the latter, the dorsal neurons are involved in the processing and relaying of sensory information and the ventrally located neurons are responsible for the co-ordination and regulation of motor systems (Briscoe & Ericson, 1999).

In the ventral horn, neural progenitor cells are subdivided into five separate domains with defined locations, each of which differentiates into a separate neuronal subtype. The patterning of neuronal subtypes in the ventral horn occurs due to the secretion of Sonic Hedgehog (Shh) protein by the notochord and floor plate adjacent to the neural tube. This signal diffuses in a graded manner over a distance of several cell diameters and via specific concentration-dependent expression of different homeodomain

transcription factors can establish segregated domains of neural progenitor cells in the ventral horn (Briscoe et al., 2000). The segregation of domains initiated in response to graded Shh signalling is further maintained by repressive interactions between the different classes of homeodomain proteins (Briscoe & Ericson, 2001). The distinct expression patterns of homeodomain proteins in progenitor cells will then activate neuronal subtype specific genes initiating the differentiation and development of each domain of progenitor cells into their appropriate post-mitotic neuronal subtypes. For example, the expression of motoneuron restricted 2 (MNR2) and homeobox 9 (HB9) homeodomain proteins, which induce post-mitotic motoneuron differentiation, is selective to the domain of progenitor cells destined to become somatic motoneurons and does not occur in neighbouring domains (Tanabe et al., 1998).

1.1.2. Motoneuron subtype specification

The graded signalling along the dorsal-ventral axis determines a single domain in which motoneurons are derived from progenitor cells. Differential signalling along the rostral-caudal axis however, classifies motoneurons according to their position in the spinal cord. Motoneurons are organised into distinct, longitudinally orientated columns depending on the target of their projected axons. Therefore, motoneurons innervating the limb musculature are arranged in the lateral motor column (LMC), whereas those innervating the axial musculature are arranged in the medial motor column (MMC; Price & Briscoe, 2004). Graded diffusion of fibroblast growth factor (FGF), produced by the paraxial mesoderm, regulates a rostrocaudal expression pattern of Hox-c homeodomain transcription factors in progenitor cells and post-mitotic motoneurons along the spinal cord (Dasen et al., 2003). This differential expression in motoneurons initiates subtype specific protein expression and determines their columnar and axon projectory fate (Dasen et al., 2003). Further subtype specification of LMC neurons into

lateral and medial subtypes, innervating dorsally and ventrally derived limb muscles respectively, is dependent on a graded retinoid signalling cascade, regulating the expression of specific LIM homeodomain transcription factors in post-mitotic motoneurons (Sockanathan et al., 2003). A final level of columnar organisation is the grouping of motoneurons, innervating a single muscle, into motor pools. Although not yet fully defined, this organisation may be regulated by the differential expression of further homeodomain transcription factors, the ETS family (Lin et al., 1998; Price & Briscoe, 2004).

Motoneurons can be classified as either upper or lower motoneurons depending on their location in the CNS. Upper motoneurons are located in the motor cortex and synapse either directly or indirectly with lower motoneurons, which are located in the spinal cord. Lower motoneurons can be subdivided into somatic, innervating skeletal muscles, or autonomic, innervating cardiac and smooth muscles. Somatic motoneurons can be further classified as either α or γ motoneurons depending on the type of muscle fibre they innervate; α motoneurons innervate the extrafusal muscle fibres, exerting muscle contraction and γ motoneurons innervate the intrafusal fibres of the muscle spindle, controlling the stretch of the muscle. The α motoneuron together with its axon and the muscle fibres it innervates constitutes a functional motor unit.

1.1.3. Skeletal muscle development

In vertebrates, skeletal muscles develop from muscle progenitor cells located in somites, which are formed from the segmentation of the paraxial mesoderm on either side of the neural tube. Somites are divided on a dorsal-ventral axis and it is the dorsal portion of the somite, the dermomyotome, in which the skeletal muscle progenitor cells are located. The dermomyotome is further divided along a medial-lateral axis, whereby

muscle progenitors in the medial portion give rise to the deep back muscles and the remaining body musculature including the limbs, derives from progenitors located laterally. The dorsal-lateral and medial-lateral patterning of the somite, and therefore myogenesis, is regulated by signals from the neural tube and notochord, including Shh and Wnt proteins (reviewed in Christ & Brand-Saberi, 2002; Buckingham et al., 2003). Progenitor cells of the limb musculature detach from the epithelia of the lateral dermomyotome and migrate to the limb "buds", a process regulated by transcription factor Pax3, where proliferation is ongoing (Epstein et al., 1996; Christ & Brand-Saberi, 2002). The expression of muscle specific transcription factors such as MyoD and Myf5, induced by Shh and Wnt proteins in the dermomyotome, ensures muscle cell identity by inducing the cessation of proliferation and stimulating differentiation of muscle progenitors into committed myoblasts. Signals from the limb mesenchyme further contribute to the muscle patterning (Christ & Brand-Saberi, 2002).

In preparation for contractile activity, the metabolic activity of myoblasts increases (Schudt et al., 1975) and mononucleated myoblasts fuse to form multinucleated myotubes, in a calcium-dependent process (Holtzer et al., 1957). Subsequently, newly formed myotubes show an increase in expression of ion channels and incorporation of acetylcholine receptors (AChR) into the muscle membrane (Fambrough & Rash, 1971; Dryden et al., 1974; Gonoi et al., 1985; Gonoi & Hasegawa, 1988) that, with further development, form clusters independently of innervation (Peng et al., 1981). Contractile protein expression also increases (Allen & Pepe, 1965; Przybilski & Blumberg, 1966) and myotubes gain the ability to conduct electrogenic responses along the entire length of the fibre (Purves & Vrbova, 1974), with a corresponding increase in spontaneous contractions (Yaffe, 1969). At this stage in muscle development, there is evidence to suggest that primary myotubes can be characterised as either phasic (fast) or tonic

(slow), indicating that early embryonic muscle patterning may occur independently of motoneuron innervation (Condon et al., 1990; Fredette & Landmesser, 1991). Further muscle development, including the formation of secondary myotubes, is however, dependent on functional motoneuron interaction (Ross et al., 1987; Wilson & Harris, 1993).

1.1.4. Development of the neuromuscular junction

Motoneuron subtypes display distinct patterns of gene expression according to their position in the spinal cord, which ultimately determines their axonal projectories. However, cellular and extracellular matrix adhesion molecules and graded signalling of chemoattractants and chemorepellants can also influence axonal guidance (Colamarino & Tessa-Lavigne et al., 1995). Prior to contact with myotubes, spontaneous as well as evoked release of acetylcholine (ACh) from nerve terminals has been observed *in vitro* (Hume et al., 1983; Young & Poo, 1983). Consistent with these findings, expression of choline acetyltransferase (ChAT) and acetylcholinesterase (AChE) increases in the axonal growth cone (Phelps et al., 1984). Myotube fusion occurs just at the time when motor axons are starting to make contact (embryonic day 12 in the mouse; Misgeld et al., 2002), accompanied by an up-regulation in AChR expression as previously described. Expression of AChE in myotubes is also elevated prior to the formation of the neuromuscular junction (Brzin et al., 1981).

1.1.4.1. Functional neurotransmission

Almost immediately upon contact between motor axons and myotubes synaptic transmission is initiated. Functional contact with myotubes induces an increase in the amplitude and frequency of spontaneous and evoked ACh release by the motor axon (Chow & Poo, 1985; Xie & Poo, 1986). This consequently induces the conductance of a

larger current, the so-called endplate potential (EPP), by postsynaptic endplate channels, stimulating action potentials and subsequent muscle depolarisation. Accumulation of AChE at the synapse accompanies this elevation in ACh release, thereby providing a mechanism for the termination of transmitter action (Brzin et al., 1981). Initially the efficiency of transmission is low due to the lack of pre- and post-synaptic specialisations. Thus, the EPP has a slower rate of rise and smaller amplitude, compared to that generated at mature neuromuscular junctions, due to the low density of synaptic AChR and the limited release of ACh (Dennis et al., 1981; Takahashi et al., 1987).

1.1.4.2. Postsynaptic differentiation

The myonuclei at the postsynaptic endplate undergo transcriptional specialisation following innervation, including a secondary elevation in the expression of AChR, which subsequently cluster directly beneath the nerve terminal. Nerve-derived neuregulin initiates the localised up-regulation of AChR mRNA transcription, therefore ensuring a synapse specific effect (Martinou et al., 1991; Loeb & Fischbach, 1995). The synaptic clustering of AChR is subsequently induced by agrin, which is similarly synthesised and released by motoneurons and becomes incorporated into the basal lamina of the synaptic cleft (Nitkin et al., 1987). Activation of MuSK, the muscle-specific tyrosine kinase agrin receptor, recruits rapsyn, a MuSK effector protein, to the synapse, and this complex mediates the clustering and stabilisation of synaptic AChR (Anderson & Cohen, 1977; Gautam et al., 1995). Simultaneously, the degradation of 'extrajunctional' AChRs is enhanced (Fambrough, 1979).

With further development, the postsynaptic membrane forms junctional folds, which lie directly across from the active zones in the nerve terminal, acting to optimise the action of neurotransmitters. Development of the postsynaptic membrane is accompanied by the

replacement of the AChR γ subunit by the ε subunit, which confers a reduction in channel opening time (Merlie & Sanes, 1985), and further stabilisation of the AChR (Sanes & Lichtman, 1999). Maturation of the endplate is reflected by an increase in amplitude, frequency and size of EPPs, (Diamond & Miledi, 1962), accompanied by an elevation in ACh synthesis presynaptically (O'Brien & Vrbova, 1978). Therefore, with the specialisation of pre- (see below) and postsynaptic components and their increased integration, transmission efficiency at the synapse gradually improves.

1.1.4.3. Presynaptic differentiation

Differentiation of the presynaptic nerve terminal and the appearance of the active zone, is thought to be triggered by an elevation in intracellular calcium (Dai & Peng, 1993), mediated by an agrin-stimulated retrograde signal released from the muscle, possibly β2-laminin (Hoch, 2003). On myotube contact, the expression of synaptic vesicle proteins increases (Campagna et al., 1997) whereas expression of growth-associated proteins is down-regulated (Caroni & Becker, 1992). With the formation of active zones, synaptic vesicles and mitochondria accumulate at the terminal, at opposite poles (Sanes & Lichtman, 1999; Misgeld et al., 2002). Furthermore, the expression of voltage-gated calcium and potassium channels in the nerve terminal increases with development, to maximise calcium-dependent transmitter release (Funte & Haydon, 1993; Robitaille et al., 1993). Target muscle contact is also required for the maturation of NMDA receptors located on motoneurons, elicited by a subunit change from NR2 to NR3B, to enable them to cope with more mature glutamatergic afferent inputs (Fukaya, 2005).

1.1.4.4. Synapse elimination

Once innervation is established, successive axons follow the routes laid down by the initial pathfinder axons and each muscle fibre consequently becomes innervated by axons from several motoneurons. This 'polyneuronal innervation' is in contrast to the situation at the adult neuromuscular junction where each muscle fibre is innervated by a single motor axon, although each axon can branch to innervate many muscle fibres (reviewed in Gillingwater & Ribchester, 2003). Maturation of the neuromuscular junction involves the gradual elimination of synapses by retraction of axon branches and consequent reduction in the peripheral field of the motoneuron, rather than the death of motoneurons (Brown et al., 1976; Balice-Gordon & Thompson, 1988; Greensmith & Vrbova, 1996). The mechanisms mediating the preferential vulnerability of certain axons and therefore synapse elimination at the neuromuscular junction have not been fully elucidated. However, the correlation between the onset of synapse elimination and a general increase in locomotor activity, suggests that synaptic activity may play a role (Redfern, 1970). Indeed, experiments carried out to investigate the importance of neuromuscular activity to synapse elimination, demonstrate that paralysis of the target muscle delays synapse elimination (Duxson, 1982). In contrast, increasing neuromuscular activity via chronic stimulation of the nerve accelerates synapse elimination (O'Brien & Vrbova, 1978). More recently, it has been suggested that the synaptic efficacy of individual innervating axon branches is the determining factor underlying synapse elimination (Buffelli et al., 2003; Kasthuri et al., 2003). The efficacy of each axon branch is related to the amount of neurotransmitter released and therefore the ability of axons to excite postsynaptic muscle fibres. Therefore, amongst competing branches, the axon with the greatest efficacy will 'outcompete' weaker branches, which will subsequently detach from the neuromuscular junction and undergo protease-mediated degradation (Buffelli et al., 2003). A variety of possible proteases

have been implicated in this process including cysteine proteases, for example calcium-activated neutral proteases (Connold et al., 1986; Tyc & Vrbova, 1995) and serine proteases such as thrombin (Zoubine et al., 1996).

1.1.4.5. Determination of motoneuron and muscle fibre phenotype

The elimination of polyneuronal innervation establishes the adult pattern of innervation, whereby each muscle fibre is innervated by a single axon terminal. The prevailing view is that the phenotype of each muscle fibre is subsequently determined by the activity of innervating motoneurons (Navarrete & Vrbova, 1984). Initially developing motoneurons are all tonically active with a low frequency of firing (Navarrete & Vrbova, 1983). However, during the first few weeks of postnatal development motoneurons differentiate, becoming either phasic, high frequency firing motor units (fast motoneurons) or remaining tonically active motor units but with an increased duration of low frequency firing (slow motoneurons). The firing pattern of motoneurons is determined by a combination of intrinsic electrophysiological properties and the descending and interneuronal inputs onto motoneurons. Meanwhile the muscle fibres they innervate differentiate into fast (type II); either fast oxidative (type IIa) or fast glycolytic (type IIb) depending on their oxidative capacity; and slow (type I) muscle fibres respectively (Navarrete & Vrbova, 1983). However, evidence also exists to suggest that muscle fibre phenotype may be predetermined to some extent, prior to innervation, and therefore mechanisms of target recognition may be involved in the guidance of motor axons to specific muscle fibre targets (reviewed in Sanes & Lichtman, 1999).

1.1.4.6. Target dependence of motdoneurons

Once contact has been initiated, developing motoneurons and muscle fibres are highly dependent on functional interaction for their survival and maintenance. Interruption of this interaction at birth, for example by peripheral nerve injury, results in a loss of muscle function and the death of motoneurons (Romanes, 1946; Lowrie et al., 1987). However, this dependency declines rapidly during early postnatal development and following a similar injury in adults, no motoneurons die although some muscle force is still lost even after adult crush (Gutmann & Young, 1944). The functional dependence of motoneurons on their target during development may be related to neurotrophic support from muscles (Oppenheim, 1991). Alternatively, the critical period of motoneuron susceptibility to target withdrawal may represent their maturation from growing cells into target-independent fully transmitting neurons (as described in **Chapter 1.1.4.3.**; Greensmith & Vrbova, 1996). Therefore, in the absence of the target muscle this functional change may fail to occur, which will render motoneurons susceptible, for example to glutamate-induced cell death (Greensmith et al., 1994).

1.2. Motoneuron degeneration

Motoneuron degeneration occurs i) naturally during normal embryonic development as a consequence of programmed cell death, ii) pathologically, for example postnatally following injury, or as a consequence of normal aging and iii) during disease, for example in motoneuron diseases such as Amyotrophic Lateral Sclerosis. Motoneuron degeneration can occur via a number of mechanisms discussed in the following sections.

1.2.1. Types of cell death

i) Apoptosis

Apoptosis, also known as programmed cell death, is a genetically controlled, ATP-dependent form of cell death characterised by an initial shrinkage of the cytoplasm and nucleus (pyknosis), chromatin condensation and blebbing of the plasma membrane. The cell then fragments into 'apoptotic bodies' that are phagocytosed by adjacent cells (Kerr et al., 1972; Wyllie et al., 1980). Depending on the initial 'death' signal, and cell type, apoptosis can proceed via two different, although interconnecting, pathways, as shown in **Figure 1.1**, either by ligation of 'death' receptors or activation of a mitochondria-dependent signalling pathway (Friedlander, 2003). Cell surface 'death' receptors include the $p75^{NTR}$ receptor, a member of the TNF family, or the Fas receptor, which initiates the activation of caspase 8 via the intermediary adaptor protein FADD. Caspase 8 subsequently activates caspase 3 as the final executioner in the cell death pathway.

The mitochondria-dependent pathway involves the translocation of pro-apoptotic molecules, Bax and Bid, to the mitochondria, which can stimulate the release and translocation of cytochrome c to the cytosol. Subsequently, cytochrome c can form an apoptosome by complexing with apoptosis activating factor-1 (Apaf-1) and procaspase 9 in an ATP-dependent manner, thus activating caspase 9 and initiating a cascade of protease activity resulting in apoptosis. The simultaneous release of Smac (second mitochondrial-derived activator of caspase)/Diablo from mitochondria potentiates this pathway by acting to inhibit endogenous caspase inhibitors (Friedlander et al., 2003). Permeabilisation of the outer mitochondrial membrane can be achieved by the Bax-induced formation of pores in the membrane (Eskes et al., 2000; Kuwana et al., 2002). Alternatively, opening of the mitochondrial permeability transition pore (mPTP),

Figure 1.1 - Extrinsic receptor-mediated and intrinsic mitochondrial-dependent mechanisms of apoptotic cell death

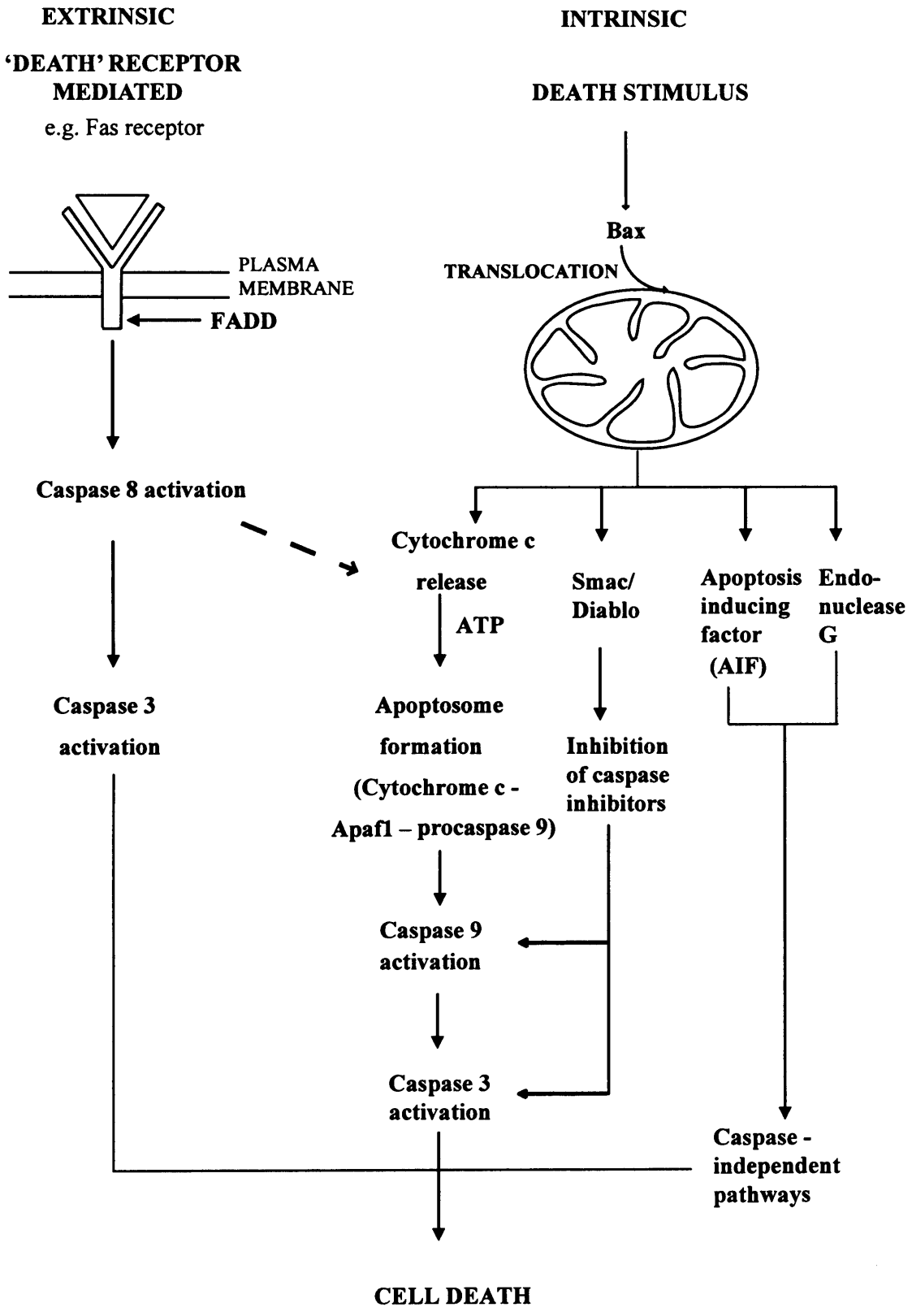

activated for example by high mitochondrial calcium and oxidative stress, will increase mitochondrial permeability and release cytochrome c to the cytosol, initiating apoptosis (reviewed in Duchen, 2004). There is evidence that these two mechanisms may be interrelated, as Bax can bind to the voltage dependent anion channel (VDAC) and adenine nucleotide transporter (ANT), which form part of the mPTP, and modulate their activity (Halestrap et al., 2002).

The main executors of cell death in both the extrinsic and intrinsic apoptotic pathways are the caspases, a family of cysteine-dependent, aspartate-specific proteases, present initially in the cell as inactive zymogens, procaspases, which once activated can cleave many cellular substrates and exert significant cellular damage (Guegan et al., 2003). 14 caspases have been identified in mammals, which can be divided into two main groups: the initiator caspases and the effector caspases. The initiator caspases can be further subdivided according to their mechanism of activation, as shown in **Figure 1.1**, and their target: caspases 2, 8, 9 and 10 initiate apoptosis by activation of effector caspases, whereas caspases 1, 4, 5, 11, 12 and 13 are involved in cytokine maturation (Friedlander, 2003). Initiator caspases are activated by the binding of a regulatory molecule to a specific activation domain. In contrast, effector caspases (3, 6 and 7) require initiator caspase-mediated cleavage for their activation. Activation of effector caspases represents the final step in the apoptotic cascade, inducing degradation of cellular components and the fragmentation of DNA (Friedlander, 2003).

Caspase-independent apoptosis may be regulated by the release of apoptosis inducing factor (AIF) and endonuclease G from damaged mitochondria. Translocation of AIF to the nucleus may be involved in chromatin condensation, whereas endonuclease G is implicated in the nucleosomal fragmentation of DNA (Orrenius et al., 2003).

ii) Necrosis

Necrosis, in contrast to apoptosis, is a passive form of cell death that occurs when cells are placed under extreme physiological stress. Necrosis is characterised by cellular oedema and swelling of organelles. Subsequently, chromatin condenses and the nucleus disintegrates. Ultimately, rupturing of the plasma membrane allows leakage of the cellular contents and the random degradation of nuclear DNA. Unlike apoptosis, necrotic cell death has a minimal ATP requirement and does not require protein synthesis. Instead, necrosis appears to be mediated by normal cellular mechanisms that, in response to altered homeostasis, mediate the degradation of cellular components and instigate cell death (Syntichaki & Tavernarakis, 2002, 2003).

It is now believed that the initial distinction between apoptosis and necrosis may have been an over-simplification. Indeed, another form of cell death, paraptosis has been described in which dying cells display characteristic features of both apoptosis and necrosis (Sperandio et al., 2000; Syntichaki & Tavernarakis, 2002). Furthermore, in response to different stimuli the same cells can undergo either apoptosis or necrosis. Therefore, the cellular decision to undergo apoptosis or necrosis appears to be dependent on the intensity of the insult and the energy state of the cell.

Various detrimental environmental factors or cellular mutations can trigger necrosis, by mediating alterations in ionic homeostasis, cellular acidification, oxidative stress and energy depletion (Syntichaki & Tavernarakis, 2003). Necrotic mediators include lysosomal and cytoplasmic proteases. The lysosomal membrane can be disrupted by either oxidative stress or by a family of calcium-activated cysteine proteases, the calpains. Cells have adapted to cope with an increase in intracellular concentrations of calcium, by sequestration in endoplasmic reticulum (ER) and mitochondria and

extrudation via plasma membrane ATPases. However, calcium overloading, for example under excitotoxic conditions, can overwhelm the cellular buffering systems and activate calpains, which can rupture lysosomal membranes releasing numerous hydrolytic enzymes including cathespins. This combination of cellular proteases will consequently degrade cellular components, deplete energy and ultimately induce rapid necrotic cell death (Nicotera et al., 1999; Yamashima, 2000; Ferri & Kroemer, 2001).

1.2.2. Developmental motoneuron death

Programmed cell death (PCD) of motoneurons occurs at several distinct developmental stages, the timing and extent of which are tightly regulated (Oppenheim et al., 1991, 1999). The reasoning behind the mass overproduction of motoneurons followed by their programmed death during development is unclear. The prevailing view is that PCD represents an important regulatory mechanism for the formation of optimally functional circuits by removing superfluous motor axons and matching the neuronal input to the target muscle size (Pettmann & Henderson, 1998). Motoneuron development is characterised by three distinct stages of PCD; i) during proliferation of precursor cells, ii) at the onset of axon projection and iii) coincident with myotube innervation. Dying motoneurons display characteristic features of apoptotic morphology including organelle shrinkage and chromatin condensation. An increase in survival of motoneurons after caspase inhibition further implicates a role for caspases in PCD (Pettmann & Henderson, 1998).

The mechanisms that determine the selective degeneration of motoneurons in PCD, is however, not fully defined. The first two stages of PCD in the spinal cord are target-independent (Banks & Noakes, 2002). However, the PCD occurring coincidently with the onset of neuromuscular contact is under the influence of the target muscle, Schwann

cells and potentially the motoneuron afferent inputs (reviewed in Oppenheim, 1991). Removal of the limb bud significantly enhances the developmental death of motoneurons (Hamburger, 1939), attributed to a dependence of motoneurons on a supply of survival-promoting neurotrophic factors from the target muscle. A limited supply of neurotrophins would initiate the PCD of unsupported motoneurons. However, it has subsequently been shown that motoneuron death is actually delayed by paralysis of the target muscle, which also increases target innervation (Oppenheim, 1987). Target muscle paralysis inhibits synaptic transmission and therefore the neuromuscular differentiation that occurs with development. Consequently, the inability of muscles to restrict the clustering of AChR, for example, enables the support of a greater number of motor axons. This suggests that competition between motoneurons for a limited number of target muscle contact sites may be the basis for PCD (Oppenheim, 1987). Upon innervation, motoneurons become dependent on their target muscles for differentiation and maturation into a fully transmitting neuron (as described in **Chapter 1.1.4.6**). Therefore, a lack of target contact may preserve motoneurons in a growth state and render them more vulnerable to apoptotic stimuli occurring in the maturing environment of the neuromuscular junction.

Potentially intrinsic properties of motoneurons may also increase the likelihood of their survival. Raoul et al, (2002) identified a cell death pathway specific to motoneurons that may be activated in PCD. Fas receptor-mediated activation of caspase 8 in combination with elevated nitric oxide (NO) production induces cell death specifically in motoneurons in culture. However, 50% of cultured motoneurons show resistance to Fas-mediated death following neurotrophin deprivation *in vitro*. Susceptible motoneurons up-regulate the Fas receptor ligand, FasL, whereas resistant motoneurons up-regulate an

endogenous inhibitor of caspase 8 activation, implying intrinsic survival-promoting properties of subpopulations of motoneurons (Raoul et al., 1999).

1.2.3. Pathological motoneuron death - Amyotrophic Lateral Sclerosis

A number of neurodegenerative diseases are characterised by specific motoneuron degeneration, as listed in **Table 1.1**. Motoneuron degeneration is evident both in developmental and adult onset disorders. For example, spinal muscular atrophy (SMA), caused by mutations in the Survival of Motor Neuron 1 (SMN1) gene, is the most common genetic cause of infantile mortality. On the other hand, Kennedy's disease, caused by a CAG repeat in the androgen receptor, manifests as late onset, progressive motoneuron degeneration, which affects predominantly males. However, the work in this Thesis focuses on Amyotrophic Lateral Sclerosis (ALS), which is characterised by a progressive loss of upper and lower motoneurons during the disease course (reviewed by Cleveland & Rothstein, 2001 and discussed in **Chapter 1.3.**). In transgenic mouse models of ALS, over 50% of motoneurons have died by disease end-stage (Kieran et al., 2004; Sharp et al., 2005). Morphological identification of motoneurons as 'apoptotic' is complicated by the presumed low daily loss of motoneurons and the very transient detection period for apoptotic cells (Wyllie et al., 1980; Chiu et al., 1995). Furthermore, although some morphological characteristics of degenerating motoneurons in post-mortem spinal cords of ALS patients are reminiscent of apoptosis, they cannot be definitely defined as apoptosis due to a lack of nuclear and chromatin condensation (Martin, 1999; Guegan et al., 2003). Therefore, alternative mechanisms of cell death, other than apoptosis, may also contribute to the death of motoneurons in ALS.

Table 1.1 - Motoneuron diseases

Motoneuron disease	Motoneurons affected
Amyotrophic Lateral Sclerosis	Upper and lower motoneurons
Progressive Muscular Atrophy	Lower motoneurons
Primary Lateral Sclerosis	Upper motoneurons
Spinal Muscular Atrophy	Lower motoneurons
Distal Hereditary Motor Neuropathy (Distal SMA)	Lower motoneurons
Hereditary Spastic Paraparesis	Upper motoneurons
Spinal and Bulbar Muscular Atrophy (Kennedy's Disease)	Lower motoneurons

i) Evidence for apoptotic cell death in ALS

In approximately 20% of familial ALS cases, motoneuron degeneration occurs due to mutations in the Cu/Zn superoxide dismutase gene (SOD1; Rosen et al., 1993). *In vitro*, the expression of human mutant SOD1 in cell lines has been shown to induce apoptotic cell death (Rabizadeh et al., 1995; Durham et al., 1997; Cozzolino et al., 2005). Similarly, although rare, apoptotic motoneurons and glia have been identified in the spinal cord tissue from transgenic mutant SOD1 mouse models of ALS (a model of familial ALS in which the mutant human SOD1 gene is expressed, as described in more detail in **Chapter 1.3.2.i**; Pasinelli et al., 2000; Vukosavic et al., 2000). However, morphological studies of the motoneuron death that occurs in ALS are largely inconclusive. However, studies investigating the expression of molecular markers of apoptosis in post-mortem spinal cord tissue from ALS patients and from mutant SOD1 mice have provided definitive evidence of an apoptotic involvement in ALS.

Coincident with the occurrence of mitochondrial defects in motoneurons in post-mortem spinal cord tissue from ALS patients and mutant SOD1 mice (described in detail in **Chapter 1.3.4.3.**), substantial evidence exists for the activation of the mitochondrial-dependent apoptotic cascade. Recently, an impaired association of cytochrome c with the inner mitochondrial membrane has been identified in the CNS of symptomatic $SOD1^{G93A}$ mice, potentially increasing the susceptibility of mitochondria to apoptotic stimuli (Kirkinezos et al., 2005). Indeed, in early symptomatic $SOD1^{G93A}$ mice, cytosolic cytochrome c levels are elevated concurrently with reduced mitochondrial levels. Similarly, in post-mortem spinal cord tissue from sALS patients, the cytochrome c immunoreactivity in surviving motoneurons is diffusely distributed, indicating a cytosolic localisation (Guegan et al., 2001). Furthermore, the mitochondrial translocation of the pro-apoptotic molecule, Bax, and the expression of truncated Bid,

which potentiates the action of Bax, increase progressively during the disease course of $SOD1^{G93A}$ mice. In fact, redistribution of Bax occurs just prior to the translocation of cytochrome c, perhaps serving as the initiating signal for permeabilisation of the outer mitochondrial membrane and release of cytochrome c (Guegan et al., 2001). Consistent with these findings, the expression of Bax mRNA is up-regulated and Bcl2 mRNA, an anti-apoptotic protein, is reduced in post-mortem spinal cord tissue from ALS patients (Martin, 1999). Interestingly, the anti-apoptotic function of Bcl-2 may be further down-regulated by its inclusion in mutant SOD1-induced protein aggregates in spinal cord mitochondria that are found in post-mortem spinal cord tissue from ALS patients and in $SOD1^{G93A}$ mice (Pasinelli et al., 2004). Overexpression of Bcl-2 in $SOD1^{G93A}$ mice, however, significantly delays the degeneration of motoneurons, extending lifespan by approximately 15% (Kostic et al., 1997). Similarly, minocycline treatment, one action of which is to inhibit the release of cytochrome c, produces a 9% extension in lifespan (Zhu et al., 2002).

The functional significance of cytochrome c translocation to the cytosol is evident by an up-regulation in levels of the active initiator caspase 9 and a delayed increase in effector caspases 7 and 3 in symptomatic $SOD1^{G93A}$ mice, particularly in motoneurons (Guegan et al., 2001). Ablation of Apaf-1 in mutant SOD1-expressing cell lines prevents the activation of caspase 3 and hence apoptosis, induced by mutant SOD1 (Cozzolino et al., 2005). Activation of caspases 9 and 3 is also evident in motoneurons in post-mortem human ALS spinal cords (Martin, 1999; Inoue et al., 2003). *In vitro*, the expression of mutant SOD1 in N2a cells induces the activation of caspase 1, but only under conditions of oxidative stress (Pasinelli et al., 1998). *In vivo*, activation of caspase 1 occurs early in $SOD1^{G93A}$ mice, significantly preceding symptom onset, with sequential activation of caspase 3 occurring at the onset of symptoms in both motoneurons and glia (Pasinelli et

al., 2000; Vukosavic et al., 2000). This suggests that caspase 1 may gradually induce cellular damage and on reaching a threshold activates caspase 3 as the final effector in the cell death pathway. The activation of caspase 1 is reflected by elevated levels of interleukin-1β in $SOD1^{G85R}$-expressing N2a cells (Pasinelli et al., 1998), which may subsequently initiate an inflammatory response. Indeed, a downstream consequence of caspase 1 activation may be microglial activation, which precedes symptom onset in mutant SOD1 mice (Hall et al., 1998; Weydt et al., 2004). Ablation of caspase 1 significantly extends the lifespan of $SOD1^{G93A}$ mice, by 8% (Friedlander et al., 1997), whereas treatment of $SOD1^{G93A}$ mice with zVAD-fmk, a broad-spectrum caspase inhibitor, produces a 22% extension in survival (Li et al., 2000).

Raoul et al, (2002) proposed the existence of a selective mechanism of apoptotic cell death for the induction of motoneuron degeneration. In primary motoneurons in culture, ligation of the death receptor, Fas, activates caspase 8 via binding of FADD adaptor protein. However, to induce cell death in cultured motoneurons, the simultaneous up-regulation of neuronal NOS transcription via a Daxx/ASK-1/p38 kinase-mediated pathway is also required. Caspase 8 activation in combination with peroxynitrite (derived from NO)-mediated cellular damage can induce the translocation of cytochrome c to the cytosol, the activation of caspase 3 and cell death (Raoul et al., 2002). Mutant SOD1-expressing motoneurons from mutant SOD1 mice show significantly greater susceptibility to NO-induced apoptotic death than that induced by excitotoxins or trophic factor deprivation (Raoul et al., 2002). The inflammatory processes known to occur in ALS, including microglial activation and reactive astrogliosis may therefore initiate apoptotic cell death via activation of this pathway. Interestingly, the activation of caspase 8 occurs near disease end-stage in $SOD1^{G93A}$ mice, suggesting this pathway may only be activated in the later stages of disease

(Guegan et al., 2001). Further evidence for involvement of death receptors in motoneuron death in ALS comes from an elevation in expression of the $p75^{NTR}$ death receptor in $SOD1^{G93A}$ mice and an increase in secretion of nerve growth factor, its endogenous ligand, by reactive astrocytes (Copray et al., 2003; Pehar et al., 2004).

ii) Evidence for necrotic cell death in ALS

The majority of degenerating motoneurons in transgenic mouse models of ALS have a non-apoptotic morphology, exhibiting swollen mitochondria, ER and golgi apparatus and condensed nuclei and cytoplasm (Dal Canto et al., 1995; Guegan et al., 2003). Indeed, a mechanism of necrotic death would be consistent with the excitotoxicity hypothesis of ALS. However, it is likely that a combination of both necrosis and apoptosis (and perhaps paraptosis) underlie motoneuron death in ALS.

1.3. Amyotrophic lateral sclerosis

1.3.1. Description of disease

Initially described in 1869 by French physician Jean-Martin Charcot, Amyotrophic Lateral Sclerosis (ALS) is the most common adult motoneuron disease in humans. ALS is characterized by a progressive degeneration of lower motoneurons in the spinal cord and brainstem, and large pyramidal neurons in the motor cortex and associated corticospinal tracts. The motoneurons of Onuf's nucleus, controlling pelvic floor musculature, and ocular motoneurons, controlling eye movement, are however, generally resistant in ALS. At an ultrastructural level, the neuropathology of degenerating motoneurons in ALS includes accumulations of intermediate filaments and ubiquitinylated intracellular aggregates in perikarya and proximal axons, abnormalities in mitochondrial structure and fragmentation of Golgi apparatus. Profound astrogliosis also accompanies motoneuron degeneration. **Table 1.2** summarises the pathological

Table 1.2 - Summary of the pathological features in human ALS

Disease stage	Pathological changes	Clinical manifestation	References
Presenting symptoms	Upper motoneuron degeneration	Muscle spasticity Hyperreflexia Extensor plantar reflexes	Rowland & Shneider, 2001
	Lower motoneuron degeneration	Slurred speech Progressive decline in motor function and muscle wasting	Rowland & Shneider, 2001
Disease progression	Upper motoneuron degeneration	Muscle spasticity Hyperreflexia Extensor plantar reflexes	Rowland & Shneider, 2001
	Lower motoneuron degeneration	Muscle atrophy Fasciculation Muscle paralysis	Rowland & Shneider, 2001
	Preservation of oculomotor neurons and neurons of the bladder		Rowland & Shneider, 2001
	Degeneration of neurons in substantia nigra and dentate gyrus cells	Dementia	Shaw, 2005
Death	Degeneration of respiratory motoneurons	Respiratory difficulties	Shaw, 2005
	Degeneration of tongue and oesophageal muscles	Swallowing difficulties	Rowland & Shneider, 2001
Post-mortem	Significant degeneration of lower and upper motoneurons		Rowland & Shneider, 2001
	Reactive gliosis		Leigh & Swash, 1991
	Mitochondrial abnormalities		Borthwick et al., 1999
	Fragmentation of golgi apparatus		Rowland & Shneider, 2001
	Ubiquitinylated proteinaceous inclusions (Bunina bodies) in motoneuron soma		Leigh, 1991
	Intermediate filament accumulations in motoneuron axons		Carpenter, 1968; Hirano, 1984
	Loss of interneurons in motor cortex and spinal cord		Cleveland & Rothstein, 2001

features of human ALS, which manifest either as clinical symptoms during disease progression or are observed in post-mortem tissue from ALS patients.

The worldwide incidence of ALS is on average 1-2 per 100,000, excluding high incidence foci, for example, Guam. Onset is normally within the fifth to sixth decade of life and clinical progression is variable, although generally limb weakness or slurred speech is the initial manifestation of disease. Degeneration of the large lower α motoneurons is reflected by a progressive decline in muscle function with accompanying muscle atrophy. Spasticity, hyperreflexia and extensor plantar reflexes are the clinical manifestations of upper motoneuron degeneration. Death ultimately occurs with the failure of respiratory muscles, often exacerbated by swallowing problems, on average 1-5 years after diagnosis.

ALS is a predominantly sporadic disorder (sporadic ALS; sALS), although approximately 10% of cases have a family history consistent with mendelian inheritance (familial ALS; fALS). Despite extensive research, the underlying pathogenic mechanisms of both sALS and fALS are still far from clearly understood, although it has been suggested that common pathogenic mechanisms are involved, as both forms are clinically indistinguishable. Therefore information gained from the study of fALS may be relevant to sALS pathogenesis (reviewed by Cleveland & Rothstein, 2001; Bruijn et al., 2004; Shaw, 2005).

1.3.2. fALS – genetic linkage

i) ALS1/Cu/Zn superoxide dismutase (SOD1)

In 1993, mutations in the Cu/Zn superoxide dismutase (SOD1) enzyme, on chromosome 21q22.1, were identified in approximately 20% of fALS patients, (Deng et al., 1993;

Rosen et al., 1993). The SOD1 enzyme is a ubiquitously expressed, predominantly cytoplasmic enzyme that acts as a cellular antioxidant by catalysing the conversion of superoxide radicals into hydrogen peroxide and water (**Figure 1.2**). The functional enzyme exists as a homodimer that requires copper and zinc binding for catalytic activity and stabilisation respectively (Shaw, 2005).

To date over 100 mutations have been identified in the SOD1 enzyme, which are scattered throughout the structure of the protein (www.alsod.org). Inheritance of ALS, induced by missense mutations in the SOD1 enzyme, is predominantly autosomal dominant with the exception of ALS induced by D90A, which can show recessive inheritance (Shaw, 2005). Initially, mutations in the SOD1 enzyme were suggested to reduce the dismutase activity and enhance oxidative stress, however, genetic ablation of endogenous SOD1 does not induce motoneuron disease in knock-out mice (Reaume et al., 1996). In contrast, transgenic mice expressing mutations in the human SOD1 enzyme develop a motoneuron disease that resembles the human condition (Gurney et al., 1994; Ripps et al., 1995; Wong et al., 1995; Bruijn et al., 1997). Furthermore, neither expression of WT human SOD1 nor ablation of endogenous SOD1 affects disease progression in $SOD1^{G85R}$ mice (Bruijn et al., 1998). Therefore, it is now widely recognised that the mutant SOD1 enzyme acquires a toxic gain of function, which is independent of activity levels (Borchelt et al., 1994; Dal Canto & Gurney, 1994; Ripps et al., 1995; Wong et al., 1995; Bruijn et al., 1997).

The generation of transgenic mice expressing mutations in the human SOD1 enzyme has provided an excellent research tool to investigate the pathogenesis of ALS. Indeed, mutant SOD1 mice demonstrate many of the pathological features seen in humans, including neurofilament inclusions, ubiquitinylated aggregates and selective

Figure 1.2 – The normal dismutase activity of the SOD1 enzyme

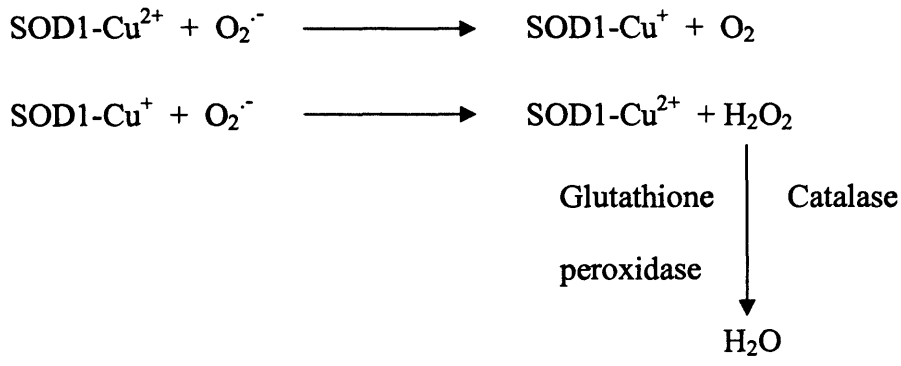

motoneuron loss (Gurney et al., 1994; Ripps et al., 1995; Wong et al., 1995; Bruijn et al., 1997). However, there are also limitations to the mutant SOD1 mouse model. For example, mutant SOD1 mice express mutant SOD1 at a level several fold higher than in ALS patients and as a consequence some mutant SOD1 mice express features that are not seen in spinal cord tissue from ALS patients, for example vacuolations (Bruijn et al., 1997). Furthermore, the disease progression and severity is significantly influenced by the copy number of the transgene (Cleveland & Rothstein, 2001). Nevertheless, research using mutant SOD1 mice provides insight into the potential neurotoxic mechanisms that may contribute to ALS pathogenesis, as described in **Chapter 1.3.4**.

ii) ALS2/Alsin

The *Als2* gene lies on chromosome 2q33 and was identified in 2001 as the causative gene for a slowly progressive, recessive form of juvenile ALS (Hadano et al., 2001; Yang et al., 2001). Two identified variants of the alsin protein are translated from alternative splicing of the *Als2* gene, a long and short form (Hadano et al., 2001; Yang et al., 2001). Sequence analysis has revealed 3 putative guanine nucleotide exchange factor (GEF) domains of the alsin protein; RCC1 like domain, DH/PH domain and VPS9 domain, which can regulate the activity of small GTPases (Hadano et al., 2001; Yang et al., 2001). GTPases cycle between an inactive GDP bound state and an active GTP bound state and GEFs activate GTPases by stimulating GTP binding (Etienne-Manneville & Hall, 2002). *In vitro*, the VPS9 domain localises alsin on the cytoplasmic side of endosomal membranes (Otomo et al., 2003). Consistent with this finding, alsin acts as a functional GEF for Rab5 GTPase, which is involved in early endocytosis, and interacts directly with this GTPase through the VPS9 domain (Otomo et al., 2003; Topp et al., 2004). Alsin may also influence the organisation of the actin cytoskeleton due to GEF-mediated stimulation of Rac1 GTPase activity (Hall & Nobes, 2000).

Nine different mutations from independent families have now been identified in the *Als2* gene, which result in variable phenotypes that generally do not resemble typical ALS including juvenile ALS, juvenile primary lateral sclerosis and infantile-ascending hereditary spastic paralysis (Yang et al., 2001; Otomo et al., 2003). The position of each mutation is predicted to induce premature truncation of the ALS2 protein. *In vitro* expression of the predicted mutant proteins in cell lines results in an altered subcellular distribution and functional inactivation, potentially due to increased degradation (Otomo et al., 2003; Yamanaka et al., 2003). A loss of function may exert toxicity on motoneurons due to impaired membrane trafficking or alternatively it may interfere with motoneuronal development (Otomo et al., 2003; Tudor et al., 2005). However, the recent generation of an *Als2* knock-out mouse revealed no obvious motor phenotype, although motoneurons had an increased susceptibility to oxidative stress (Cai et al., 2005). Interestingly, alsin can prevent mutant SOD1-mediated toxicity in cell lines *in vitro*, although the physiological relevance of this direct interaction is still unclear (Kanekura et al., 2004).

iii) ALS4/sentaxin

Analysis of a large family with a rare early childhood/juvenile onset recessive form of slowly progressing ALS, mapped a genetic locus for ALS4 at chromosome 9q34 (Chen et al., 2004). The candidate gene was identified as sentaxin, a DNA/RNA helicase, thought to have a critical function in DNA repair and mRNA biogenesis (Chen et al., 2004; Moreira et al., 2004). Potentially, missense mutations in sentaxin may render the helicase non-functional and impair the repair of mutated DNA/RNA, thus causing neuronal degeneration, although the reason for the underlying specificity for motoneurons remains unclear (Chen et al., 2004; Moreira et al., 2004).

iv) ALS8/Vesicular Associated Membrane Protein (VAPB gene)

In 2004, an ALS locus was mapped at chromosome 20q13.3 in a large Brazilian family with slowly progressive ALS, and was subsequently identified as the gene encoding vesicular associated membrane protein B (VAPB; Nishimura et al., 2004). A missense mutation has since been isolated in a highly conserved region of VAPB in the original family and six subsequent families. The presenting phenotype, from dominant inheritance of mutant VAPB, ranges from typical ALS to slowly progressive ALS or late-onset spinal muscular atrophy (Nishimura et al., 2004). Normally, VAPB is an intracellular membrane protein that has a critical function in cellular secretion and membrane transport (Soussan et al., 1999). However, the missense mutation in VAPB alters its subcellular distribution *in vitro*, inducing cytoplasmic aggregation and therefore disrupting normal VAPB function. The selective degeneration of motoneurons exposed to mutant VAPB may be related to critical threshold levels of VAPB required for intracellular trafficking (Nishimura et al., 2004).

v) Dynactin

Mutations in the gene encoding the p150 subunit of dynactin (DCTN1) on chromosome 2p13, have been discovered in families with a slowly progressing lower motoneuron disease. These mutations may affect the interaction of dynactin with both dynein and microtubules thus affecting axonal transport (Puls et al., 2003; Munch et al., 2004). Axonal transport deficits may have particularly serious consequences for motoneurons as some motoneuron axons can extend up to 1 metre in length (Shaw, 2005). In mutant SOD1 mice, deficits in axonal transport have been shown several months before symptom onset (Williamson & Cleveland, 1999).

vi) Other genetic loci and genetic risk factors/modifiers

Another candidate gene for ALS is the angiogenin gene mapped to chromosome 14q11.2 (Greenway et al., 2004). Other loci have been mapped to chromosome 9q21-22, 15q15.1-21.1, 16q12, 18q21 and 20ptel-p13, although the candidate genes have not yet been identified (for review see Shaw, 2005). Finally, several genes proposed to be risk factors in SALS or modifier genes in fALS are summarised in **Table 1.3**.

1.3.3. ALS – a non-cell autonomous disorder

1.3.3.1. Involvement of astrocytes in ALS

The degeneration of upper and lower motoneurons in ALS is accompanied by profound astrocytosis (Hirano, 1996; Schiffer et al., 1996; Hall et al., 1998). Reactive astrocytes assume a hypertrophic morphology that is associated with an increase in expression of glial fibrillary acidic protein (GFAP). Astrocyte activation is often accompanied by an up- regulation in production of cytokines, growth factors, matrix proteins, cell adhesion molecules, proteases and protease inhibitors (Ridet et al., 1997; John et al., 2003; Barbeito et al., 2004). In post-mortem spinal cord tissue from ALS patients, astrogliosis surrounds lower and upper motoneurons and can be found in the degenerating corticospinal tracts (Hirano, 1996; Schiffer et al., 1996). Furthermore, in ALS patients, the expression of the astrocyte transporter protein EAAT-2 is reduced in post-mortem spinal cord tissue, in association with a reduction in glutamate transport and an elevation in CSF glutamate levels, which indicates functional astrocyte deficits (Rothstein et al., 1991, 1992, 1995; Spreux-Varoquaux et al., 2002). Mutations in EAAT-2, as found in one sALS patient with a reduction in glutamate uptake capacity, may therefore represent a risk factor for the development of ALS (Trotti et al., 2002), although this may only have relevance for a small proportion of patients as in two large studies of familial and sporadic ALS patients no linkage has been found (Aoki et al.,

Table 1.3 – Potential genetic risk factors/modifiers in ALS

Proposed Risk Factor/Modifier Gene	Genetic loci	Function	Genetic alteration	References
NF-H	22q12.1-q13.1	Neuronal intermediate filament	KSP deletion/insertion	Figlewicz et al., 1994; Tomkins et al., 1998; Al Chalabi et al., 1999
NF-L	15p12	Neuronal intermediate filament	Deletion	Bergeron et al., 1994
Peripherin	12q12-q13	Neuronal intermediate filament	Deletion	Gros-Louis et al., 2004
VEGF	6p12	Growth factor	Single nucleotide polymorphisms in promoter	Lambrechts et al., 2003
CNTF	11q12.2	Growth factor	Loss of function mutation	Giess et al., 2002
EAAT2	11p13-p12	Astroglial glutamate transporter	Reduced expression	Trotti et al., 2001
AMPA receptor subunit GluR2	4q32-q33	Regulates calcium permeability of AMPA/KA receptors	Aberrant editing at Q/R site	Kawahara et al., 2004

1998; Jackson et al., 1999). In mutant SOD1 mice, reactive astrogliosis is evident from disease onset and increases steadily during disease progression (Hall et al., 1998; Levine et al., 1999; Alexianu et al., 2001; Elliott et al., 2001). Inclusions in astrocytes are one of the earliest pathological features seen in $SOD1^{G85R}$ mice, occurring before the appearance of symptoms, and are accompanied by reductions in GLT-1 expression by disease end-stage (Bruijn et al., 1997a). Therefore, alterations in non-neuronal cell functions are likely to contribute to ALS pathogenesis.

Astrocytes were once considered to be passive supporting cells, the 'nerve glue' (Virchow, 1958). However, there is now substantial evidence to suggest that astrocytes also provide metabolic and trophic support to neurons. Furthermore, evidence of bidirectional communication between neurons and astrocytes and their close spatial association indicates that astrocytes form an integral component of the synapse in that they act to modulate both neuronal activity and synaptic transmission (reviewed in Vernadakis, 1996; Kirchoff et al., 2001; described in more detail in **Chapter 3.1.2.**). However, considering the extensive functional interaction and close spatial association which is maintained between reactive astrocytes and degenerating motoneurons in $SOD1^{G93A}$ mice (Levine et al., 1999), it is perhaps not surprising that degenerative changes in astrocytes are seen in ALS. Indeed, the appearance of reactive astrocytosis coincident with symptom onset in mutant SOD1 mice suggests that the activation of astrocytes in ALS occurs in response to neuronal degeneration, as a significant proportion of motoneurons have already been lost by this disease stage (Chiu et al., 1995; Levine et al., 1999; Sharp et al., 2005). Activation of astrocytes in ALS may occur as a consequence of the release of pro-inflammatory cytokines and free radicals from motoneurons and microglial cells (reviewed in Barbeito et al., 2004). Rao et al, (2003) suggested that reactive oxygen species (ROS) generated by damaged

motoneurons could be released to exert oxidative damage on surrounding astrocytes. Indeed, peroxynitrite exposure is found to induce a phenotypic change that renders cultured astrocytes toxic to motoneurons (Cassina et al., 2002). However, although astrocytosis may occur secondarily to neuronal damage, there is increasing evidence to suggest that once activated, astrocytes may actively participate in the process of neuronal degeneration (Levine et al., 1999).

Evidence emerging from the study of transgenic mice supports the possibility that ALS, although a motoneuron-specific disorder, is not cell-autonomous. Expression of $SOD1^{G86R}$ under the control of the GFAP promoter produces significant astrocytosis in transgenic mice, although to a lesser extent than in $SOD1^{G86R}$ mice in which mutant SOD1 is ubiquitously expressed. Furthermore, the large motoneurons in the ventral horn display no significant morphological changes and do not undergo degeneration in these mice, therefore suggesting that mutant SOD1-expressing astrocytes alone do not mediate disease (Gong et al., 2000). However, selective neuronal expression of $SOD1^{G93A}$, using a NF-L chain promoter, similarly does not induce motoneuron degeneration in transgenic mice (Pramatarova et al., 2001), and a selective 2-fold elevation of mutant $SOD1^{G93A}$ expression in postnatal motoneurons also does not influence disease progression (Lino et al., 2002). This suggests that interaction between mutant SOD1-expressing neurons and mutant SOD1-expressing astrocytes is necessary for the development of ALS. Indeed, in an *in vitro* co-culture model, the expression of mutant SOD1 in both neuroblastoma and glioblastoma cells is necessary to induce neuronal apoptosis (Ferri et al., 2004). In 2003, the generation of chimeric mice with varying expression of mutant and endogenous SOD1 (WT) in motoneurons and non-neuronal cells, further clarified the importance of the non-neuronal environment to disease progression (Clement et al., 2003). In these mice, the presence of WT non-

neuronal cells significantly protects mutant SOD1 motoneurons from degeneration, whereas an environment of mutant SOD1-expressing non-neuronal cells induces formation of ubiquitinylated intracellular aggregates in WT motoneurons (Clement et al., 2003). These results therefore provide definitive evidence that glial cells make a significant contribution to ALS pathogenesis.

1.3.4. Disease pathogenesis

Extensive research on mutant SOD1 mice in combination with analysis of post-mortem tissue from ALS patients has given some insight into several potentially neurotoxic mechanisms that may be involved in ALS pathogenesis. These mechanisms are discussed in detail in the following sections. These mechanisms may apply to the pathogenesis of both sALS and fALS, as evidence for their involvement exists in both forms of the disease.

1.3.4.1. Oxidative stress

Under normal conditions, superoxide radicals produced by cells are rendered harmless by conversion into water and hydrogen peroxide by the activity of the SOD1 enzyme, as shown in **Figure 1.2**. However, following the discovery that the mutant SOD1 enzyme acquires a toxic gain of function, it was proposed that alterations in structural conformation induce an aberrant protein chemistry. Improper folding of the mutant SOD1 protein may reduce the selectivity of the active site, allowing interaction with abnormal substrates, for example peroxynitrite, with subsequent nitration of tyrosine residues. Alternatively, the access of hydrogen peroxide to the active site will generate highly reactive hydroxyl radicals that can oxidise essential cellular components (Beckman et al., 1993; Wiedau-Pazos., et al., 1996; **Figure 1.3**).

Figure 1.3 – Proposed aberrant chemistry of the mutant SOD1 enzyme

a) Nitration of tyrosine

$$SOD1\text{-}Cu^{2+} + ONOO^{\cdot} \longrightarrow SOD1\text{-}CuO\ldots\ldots NO^{2+}$$

$$SOD1\text{-}CuO\ldots\ldots NO^{2+} + Tyr \longrightarrow SOD1\text{-}Cu^{2+} + OH^{-} + NO_2\text{-}Tyr$$

b) Generation of hydroxyl radicals

$$SOD1\text{-}Cu^{2+} + H_2O_2 \longrightarrow SOD1\text{-}Cu^{+} + O_2^{\cdot -} + 2H^{+}$$

$$SOD1\text{-}Cu^{+} + H_2O_2 \longrightarrow SOD1\text{-}Cu^{2+} + OH^{\cdot} + OH^{-}$$

An alternative hypothesis suggests that mutations in SOD1 alter the binding of copper or zinc ions to the enzyme. Crow et al, (1997) demonstrated that mutations in SOD1 reduced the affinity of the enzyme for zinc by up to 30-fold *in vitro*. In the absence of zinc, the active copper atom could become reduced and catalyse the normal dismutase reaction in reverse, thus generating superoxide radicals. Subsequent reaction between superoxide and nitric oxide generates peroxynitrite, which can damage cellular components via tyrosine nitration (Estevez et al., 1999). Indeed, depletion of zinc from mutant SOD1 induces NO and copper-dependent toxicity in cultured motoneurons (Estevez et al., 1999). The susceptibility of motoneurons may be related to their high neurofilament content, which can compete with mutant SOD1 for zinc loading (Estevez et al., 1999).

The contribution of copper-induced toxicity in mutant SOD1-mediated ALS is controversial. In mammals, the cellular copper concentration is low (Rae et al., 1999) and copper is loaded into SOD1 via a copper chaperone (CCS) protein (Wong et al., 2000). However, ablation of CCS in mutant SOD1 mice does not affect disease progression despite a significant reduction in copper loading of mutant SOD1 (Subramaniam et al., 2002). The possibility exists that the residual, CCS-independent copper loading of the mutant SOD1 enzyme may be sufficient to exert mutant SOD1-mediated toxicity in this model (Subramaniam et al., 2002). Subsequent ablation of the copper binding site of mutant SOD1, however, does not affect disease progression in mutant SOD1 mice, which suggests that copper-mediated toxicity does not significantly contribute to ALS pathogenesis (Wang et al., 2003). Furthermore, many mutations do not reduce the affinity of mutant SOD1 for zinc in transgenic mice *in vivo*, therefore zinc deficient SOD1-mediated toxicity may not be physiologically relevant (Williamson et al., 2000). The downstream contribution of NO and peroxynitrite has also been

further examined by eliminating either neuronal or inducible NOS from mutant SOD1 mice, neither of which altered disease progression (Facchinetti et al., 1999; Son et al., 2001). In contrast, however, treatment of mutant SOD1 mice with copper chelators does exert significantly beneficial effects (Hottinger et al., 1997).

In post-mortem spinal cord tissue from sALS and fALS patients, levels of 3-nitrotyrosine are elevated in motoneurons (Abe et al., 1997; Beal et al., 1997; Ferrante et al., 1997). Similarly, in mutant SOD1 mice, free 3-nitrotyrosine immunoreactivity and markers of lipid peroxidation are elevated from a presymptomatic stage (Bruijn et al., 1997a; Hall et al., 1998). Furthermore, evidence from mutant SOD1 mice suggests that oxidative damage occurs to both mitochondria (Mattiazzi et al., 2002) as well as GLT-1 glutamate transporter proteins (Trotti et al., 1999; Vanoni et al., 2004). In contrast, there is no evidence of protein bound nitrotyrosine in either mutant SOD1 mice or post-mortem tissue from ALS patients (Bruijn et al., 1997b). Similarly no increase in hydroxyl radical production can be detected in $SOD1^{G37R}$ mice (Bruijn et al., 1997a). Therefore, the mechanism by which mutant SOD1 induces oxidative stress is controversial, although there is cellular evidence for oxidative damage. Furthermore, involvement of oxidative stress in both sALS and fALS suggests a common mechanism of motoneuron pathology.

1.3.4.2. Glutamate excitotoxicity

Glutamate is the most abundant excitatory neurotransmitter in the CNS (Heath & Shaw, 2002). However, there is substantial evidence to suggest that overactivation of glutamate receptors can induce neuronal damage, a process termed 'excitotoxicity'. Elevated extracellular glutamate, either due to an increase in release or reduction in uptake, can activate calcium-permeable glutamate receptors on the postsynaptic cell,

thus enhancing calcium influx. Excessive postsynaptic calcium can activate neurotoxic cascades, including the activation of calpains, endonucleases and phospholipases, ultimately leading to neuronal death (Choi, 1992).

Motoneurons receive glutamatergic inputs from the descending corticospinal tracts, from collaterals of the Aα fibres innervating muscle fibres and Golgi tendon organs and from excitatory interneurons in the spinal cord (Heath and Shaw, 2002). Therefore abnormalities in glutamate neurotransmission may conceivably contribute to motoneuron degeneration in ALS. Indeed, an elevation in CSF glutamate levels occurs in approximately 40% of sALS patients (Rothstein et al., 1991; Spreux-Varoquaux et al., 2002) and transcranial magnetic stimulation studies in ALS patients reveal that cortical motoneurons are hyperexcitable (Zanette et al., 2002). Furthermore, an increase in firing frequency and reduction in action potential duration in embryonic $SOD1^{G93A}$ motoneurons *in vitro* is also indicative of an increase in excitability (Pieri et al., 2003; Kuo et al., 2004).

1.3.4.2.1. Glutamate uptake transporter, GLT-1

In most CNS regions, glutamate uptake by the astroglial glutamate transporter, GLT-1 (EAAT-2) predominates (Tanaka et al., 1997). Therefore, any reduction in normal expression of this transporter may result in an elevation in extracellular glutamate and consequently may induce excitotoxicity. In 60-70% of sALS patients, there are reductions in EEAT-2 protein expression and glutamate transport in post-mortem tissue from the spinal cord and motor cortex (Rothstein et al., 1992, 1995). A mutation in EAAT-2 has also been identified in a sALS patient, with an associated reduction in glutamate uptake (Trotti et al., 2001). Similarly, glutamate uptake is diminished in symptomatic mutant SOD1 mice, which corresponds to reductions in GLT-1 expression

(Bruijn et al., 1997a; Bendotti et al., 2001; Canton et al., 2001). Selective inhibition of the GLT-1 transporter protein in mice initiates a progressive paralysis *in vivo* (Rothstein et al., 1996). Furthermore, in organotypic spinal cord cultures, chronic inhibition of glutamate transport induces selective motoneuron degeneration (Rothstein et al., 1993), whereas restoration of GLT-1 activity either by pharmacological enhancement (Rothstein et al., 2005) or by the introduction of glial progenitor cells overexpressing GLT-1, significantly increases motoneuron survival in this model (Maragakis et al., 2005).

Oxidative damage to GLT-1 transporter proteins and subsequent protein internalisation can disrupt glutamate uptake and reduce GLT-1 expression (Trotti et al., 1999; Vanoni et al., 2004). Indeed, peroxynitrite exerts a dose-dependent inhibition of glutamate transporter activity in reconstituted liposomes (Trotti et al., 1996). Similarly co-expression of GLT-1 with mutant SOD1 in *Xenopus* oocytes inhibits glutamate transport (Trotti et al., 1999). Oxidative damage to glial glutamate transporters may be mediated by free radicals generated in and transferred from motoneurons in response to glutamate. Consequent inhibition of astroglial glutamate transport would therefore elevate extracellular glutamate and amplify any damage (Rao et al., 2003). Potentially, however, a loss of neuronal regulation of glutamate transporter expression, due to motoneuron loss in ALS, may also explain the down-regulation of GLT-1 (Swanson et al., 1997).

1.3.4.2.2. Calcium permeable AMPA/KA receptors

Glutamate excitotoxicity may be mediated through the activation of ionotropic, N-methyl-D-aspartate (NMDA) receptors and α-amino-3-hydroxy-5-methyl-4-isoxazole propionic acid (AMPA)/kainate (KA) receptors, and metabotropic glutamate receptors

(reviewed in Heath & Shaw, 2002). Motoneurons are believed to be more susceptible to AMPA/KA receptor-mediated neurodegeneration (Rothstein et al., 1993; Vandenberghe et al., 1998; van den Bosch & Robberecht, 2000; van den Bosch et al., 2000). Indeed, activation of AMPA/KA receptors induces selective degeneration of cultured motoneurons *in vitro* (Rothstein et al., 1993; Carriedo et al., 1996) and in mice *in vivo* (Ikonomidou et al., 1996), an effect that is inhibited by selective AMPA/KA receptor antagonists (Vandenberghe et al., 1998; van den Bosch & Robberecht, 2000; van den Bosch et al., 2000, 2002; Van Damme et al., 2003). Furthermore, treatment of mutant SOD1 mice with AMPA/KA receptor antagonists significantly extends lifespan (Canton et al., 2001; Van Damme et al., 2003).

AMPA receptors mediate fast neurotransmission and are composed of 4 different subunits, GluR1-4, which confer different functional characteristics (Hollmann & Heinemann, 1994). The absence of the GluR2 subunit renders the receptor calcium permeable (Hollmann & Heinemann, 1994). The majority of studies indicate that motoneurons express GluR2-containing AMPA receptors (Morrison et al., 1998; Bar Peled et al., 1999; Vandenberghe et al., 2000a, 2000b; van den Bosch et al., 2000; Laslo et al., 2001; Heath et al., 2002), although there is evidence for the colocalisation of GluR2-containing and GluR2-lacking AMPA receptors on the same motoneurons (Vandenberghe et al., 2001). Recently, however, defective GluR2 editing, which would render the receptor calcium permeable, has been found selectively in motoneurons in post-mortem spinal cord tissue from ALS patients (Kawahara et al., 2004). The selective vulnerability of motoneurons may however, also be related to a higher density of calcium-permeable AMPA receptors which will result in an increase in agonist-induced calcium influx into these neurons (Carriedo et al., 1996; Vandenberghe et al., 2000b; van den Bosch et al., 2000, 2002; Van Damme et al., 2003). Furthermore,

following elevations in intracellular calcium, cultured motoneurons exhibit an increase in mitochondrial calcium buffering and free radical generation, which may inflict accumulative mitochondrial damage in comparison with other calcium-permeable AMPA/KA receptor expressing neurons (Carriedo et al., 2000).

Interestingly, reducing the calcium permeability of AMPA/KA receptors by crossing mice overexpressing the GluR2 subunit with $SOD1^{G93A}$ mice, significantly delays symptom onset and extends the lifespan of $SOD1^{G93A}$ mice by 14.3% (Tateno et al., 2004). In contrast, an acceleration in disease course and shortening of lifespan is seen in $SOD1^{G93A}$ mice following either a 2-fold increase in calcium permeability or total ablation of the GluR2 subunit (Kuner et al., 2005; Van Damme et al., 2005). However, there is no motoneuron loss in GluR2 knock-out mice, suggesting that the absence of the GluR2 subunit alone is not sufficient to induce ALS (Jia et al., 1996).

1.3.4.2.3. Expression of calcium binding proteins

In addition to mitochondrial uptake, intracellular calcium can be buffered by calcium binding proteins. Electrophysiological studies in brain slices from WT mice, however, have demonstrated a lower calcium binding capacity in specific motoneuron populations vulnerable to degeneration in ALS, in contrast to those less vulnerable motoneuron populations such as oculomotor neurons and motoneurons of Onuf's nucleus (Lips et al., 1999; Vanselow et al., 2000). Furthermore, the calcium binding proteins, parvalbumin and calbindin-D28K, are not expressed in 'vulnerable' motoneurons, but are present in motoneurons less affected in ALS (Ince et al., 1993; Alexianu et al., 1994; Elliott & Snider, 1995). Motoneurons with a low expression of calcium binding proteins may therefore have to depend to a greater extent on mitochondrial calcium uptake in order to buffer excess calcium, and this may render their mitochondria more susceptible

to damage. Indeed, as described in **Chapter 1.3.4.3.**, mitochondrial abnormalities are a common pathological feature of ALS. In support of the proposal that a decrease in calcium buffering capacity contributes to the selective vulnerability of motoneurons in ALS, it has been found that overexpression of parvalbumin protects motoneurons *in vitro* against KA-induced calcium influx (van den Bosch et al., 2002), and protects neonatal motoneurons from injury-induced motoneuron death in parvalbumin overexpressing transgenic mice (Dekkers et al., 2003). Furthermore, the survival of $SOD1^{G93A}$ mice crossed with parvalbumin overexpressing transgenic mice is also extended (Beers et al., 2001).

1.3.4.2.4. Riluzole

The role of excitotoxicity in ALS pathogenesis is demonstrated by the finding that treatment with the anti-glutamatergic agent Riluzole extends the lifespan of ALS patients. Indeed, Riluzole is the only therapy currently licensed for treatment of ALS patients. Riluzole acts to inhibit the presynaptic release of glutamate and may also modulate NMDA receptor activity (Doble et al., 1996). However, Riluzole only extends patients lifespan by 2 - 4 months (Bensimon et al., 1994; Miller et al., 2002; Traynor et al., 2003). In $SOD1^{G93A}$ mice, treatment with riluzole also delays disease onset and extends survival (Gurney et al., 1998). However, treatment combining riluzole with minocycline, a microglial inhibitor, plus nimodipine, a blocker of voltage-gated calcium channels, exerts significantly greater beneficial effects in mutant SOD1 mice on disease progression and lifespan than is achieved individually with these agents (Kriz et al., 2003). This finding therefore supports a multifactorial ALS pathogenesis and highlights the benefits of targeting multiple pathways in the design of a suitable therapy.

1.3.4.3. Normal mitochondrial function

Alterations in mitochondrial structure and function may be a critical factor contributing to ALS pathogenesis. Considering the critical role that mitochondria play in cellular physiology, it is not surprising that defects in mitochondrial function can result in disease. The primary function of mitochondria is to provide cellular ATP, although mitochondria also play significant roles in cellular calcium signalling and apoptotic cell death pathways. These functions are described in brief below (**Sections 1.3.4.3.1. – 1.3.4.3.3.**).

1.3.4.3.1. Chemiosmotic theory – the indirect coupling of electron transfer to ATP production

The primary function of mitochondria is to generate ATP and therefore provide cellular energy. In this process, acetyl coenzyme A, derived from respiratory substrates, is metabolised to carbon dioxide in the tricarboxylic acid cycle (TCA cycle). This also produces electrons that reduce NAD^+ and FAD to provide reducing equivalents for the supply of electrons to complex I (NADH dehydrogenase) and II (succinate dehydrogenase) of the electron transport chain respectively. Electrons are transferred from complexes I and II to ubisemiquinone and then to complex III (ubiquinol cytochrome c reductase), which is covalently bonded to ubisemiquinone. Electrons are finally shuttled between complex III and IV (cytochrome c oxidase) and combine with two protons and oxygen to form water. The redox potential of each electron acceptor is greater than the previous acceptor in the chain. The transfer of electrons between complexes therefore generates a free energy that is proportional to the difference in redox potential between the acceptors. This energy is used by complexes I, III and IV to pump protons from the matrix to the intermembrane space. This consequently establishes an electrochemical potential gradient that consists of a mitochondrial

membrane potential, approximately 150mV to 200mV negative to the cytosol, and a pH gradient between the cytosol and matrix (0.5 to 1.0 pH units). The coupling of electron transfer with proton translocation forms the basis of chemiosmotic theory.

The electrochemical proton gradient provides the driving force for the influx of protons through the F_1F_0 ATP synthase, a proton translocating ATPase, which is driven backwards by the proton gradient. Proton influx stimulates the phosphorylation of ADP to ATP. ATP is subsequently released from mitochondria via the ANT. Dissipation of the mitochondrial membrane potential may stimulate the ATPase to run in reverse, hydrolysing ATP and potentially depleting cellular energy.

1.3.4.3.2. Cellular calcium signalling

Another important role of mitochondria is the modulation of intracellular calcium signalling. In response to the elevation of cytoplasmic calcium above a certain 'set point' (Nicholls & Crompton, 1980), mitochondria will accumulate calcium. Under physiological conditions, mitochondrial calcium influx may provide a mechanism to couple cellular activity with ATP generation, since calcium up-regulates 3 rate limiting enzymes of the TCA cycle; pyruvate dehydrogenase, isocitrate dehydrogenase and 2-oxoglutarate dehydrogenase. Furthermore, it has been suggested that mitochondria are closely apposed to endoplasmic reticulum (ER) calcium release sites (Rizzuto et al., 1998). Therefore following release of calcium from ER, mitochondria are exposed to high local calcium concentrations therefore stimulating uptake, which can modulate cellular calcium signalling. However, calcium overloading of mitochondria is also widely implicated in mechanisms of neuronal death (reviewed in Duchen, 2004).

1.3.4.3.3. Apoptosis

In addition to the vital role that mitochondria play in ATP generation, they are also critical mediators in the initiation of apoptotic cell death. Release of cytochrome c from the intermembrane space and its translocation to the cytosol stimulates the activation of caspase 9 and subsequently initiates apoptosis, as described in **Chapter 1.2.1.i.** Furthermore, Smac/Diablo protein is also located in the intermembrane space and upon release acts to inhibit cellular inhibitors of apoptosis, therefore inducing PCD. Other intermembrane space proteins may include the pro-apoptotic molecules procaspase 9 and AIF (Duchen, 2004). Permeability of the outer mitochondrial membrane can be achieved by translocation of Bax to mitochondria, which forms a pore in the membrane (Kuwana et al., 2002). Alternatively, opening of the mitochondrial permeability transition pore increases mitochondrial permeability and can induce the release of pro-apoptotic molecules (Zamzami et al., 1996).

1.3.4.3.4. Mitochondrial abnormalities in ALS

Irregularities in mitochondrial structure, including dilated cristae and mitochondrial swelling, are found in post-mortem spinal cord tissue from sporadic and familial ALS patients (Hirano et al., 1984; Fujita et al., 1996; Sasaki & Iwata, 1996; Siklos et al., 1996). In mutant SOD1 mice, abnormalities in mitochondrial structure occur before the appearance of symptoms, and in $SOD1^{G93A}$ and $SOD1^{G37R}$ mice, symptom onset correlates with the appearance of membrane-bound vacuoles that derive from degenerating mitochondria (Dal Canto & Gurney, 1994; Wong et al., 1995; Kong & Xu et al., 1998; Bendotti et al., 2001; Jaarsma et al., 2001). These observations suggest that mitochondria may represent a primary target for mutant SOD1-mediated damage and furthermore that in ALS, mitochondrial damage may be the trigger for motoneuron degeneration.

Consistent with abnormalities in structure, alterations in mitochondrial function are also evident in ALS. Reductions in the activity of complexes I and IV in the electron transport chain are found in affected post-mortem tissue from sALS patients, symptomatic $SOD1^{G93A}$ mice and a $SOD1^{G93A}$-expressing motoneuronal cell line (Fujita et al., 1996; Swerdlow et al., 1998; Weidemann et al., 1998; Borthwick et al., 1999; Vielhaber et al., 2000; Jung et al., 2002; Mattiazzi et al., 2002; Menzies et al., 2002b; Fukada et al., 2004). Evidence also suggests that mutant SOD1 mitochondria, isolated from spinal cords of $SOD1^{G93A}$ mice, have a lower maximal respiratory rate and reduced ATP generation (Mattiazzi et al., 2002). Moreover, under resting conditions the mitochondrial calcium buffering capacity of $SOD1^{G93A}$ motoneurons is impaired with a subsequent increase in cytosolic calcium levels (Carri et al., 1997; Swerdlow et al., 1998; Kruman et al., 1999). Together with reductions in mitochondrial membrane potential and elevations in mitochondrial free radical production, this suggests that mitochondrial function is compromised in mutant SOD1-expressing motoneurons (Carri et al., 1997; Kruman et al., 1999; Rizzardini et al., 2005). Interestingly, following chronic treatment with malonate, a complex II inhibitor that induces mitochondrial inhibition and eventually ATP depletion, motoneurons in organotypic cultures are selectively vulnerable compared to interneurons (Kaal et al., 2000).

One source of superoxide production is the electron transport chain and the localised production of superoxide radicals therefore renders mitochondria highly susceptible to oxidative damage. Indeed, mitochondria from spinal cords of $SOD1^{G93A}$ mice show a significant increase in markers of protein and lipid oxidative damage (Mattiazzi et al., 2002). Interestingly, although predominantly cytosolic, 1-5% of the SOD1 enzyme exists in both the mitochondrial intermembrane space (Okado-Matsumoto & Fridovich, 2001; Sturtz et al., 2001; Higgins et al., 2002; Mattiazzi et al., 2002) and the matrix

(Vijayvergiya et al., 2005), thus providing a mechanism by which mutant SOD1 in fALS can directly inflict damage on mitochondria. Moreover, selective targeting of mutant SOD1 to mitochondria rather than the cytoplasm, nucleus or endoplasmic reticulum was found to be essential for mutant SOD1-induced toxicity in culture (Takeuchi et al., 2002). It has subsequently been shown that association of mutant SOD1 with mitochondria only occurs in the spinal cord in mutant SOD1 mice (Liu et al., 2004; Pasinelli et al., 2004; Vijayvergiya et al., 2005). This association prompts the formation of aggregates in mitochondria, which suggests that mutant SOD1 may exert mitochondrial damage by directly altering the function of mitochondrial proteins (Liu et al., 2004; Vijayvergiya et al., 2005). Indeed, it has been shown that Bcl2 is sequestered in such aggregates, therefore potentially reducing its anti-apoptotic function (Pasinelli et al., 2004).

Independently of mutant SOD1 involvement, mitochondrial calcium buffering may have a more significant role in motoneurons due to their low expression of calcium binding proteins, as discussed in **Chapter 1.3.4.2.3.**. Indeed, following AMPA/KA receptor activation and calcium influx, cultured motoneurons exhibit an increase in mitochondrial calcium buffering in comparison with other calcium permeable AMPA/KA receptor expressing neurons (Carriedo et al., 2000; Rao et al., 2003). An elevation in mitochondrial calcium uptake can subsequently stimulate free radical generation (Dykens, 1994; Castilho et al., 1995; Dugan et al., 1995) and therefore inflict mitochondrial damage. Indeed, a greater incidence of point mutations in mitochondrial DNA (mtDNA) is found in motoneurons in post-mortem spinal cord tissue from sALS patients (Wiedemann et al., 2002). Consistent with these findings, expression of sALS mtDNA in mtDNA-depleted neuroblastoma cells, replicates the ultrastructural changes in mitochondria seen in ALS patients (Swerdlow et al., 1998). Accumulated damage to

mitochondria can then further increase the susceptibility of motoneurons to glutamate excitotoxicity (Kruman et al., 1999; Kanki et al., 2004).

Mitochondrial dysfunction will have serious cellular consequences due to their role in ATP generation as well as their calcium buffering functions. In addition, disruption of structure and function may initiate apoptosis. Interestingly, the association of cytochrome c with the inner mitochondrial membrane is impaired in mitochondria from the CNS of symptomatic $SOD1^{G93A}$ mice, perhaps due to accumulative damage, thereby increasing the vulnerability of mitochondria to apoptotic stimuli (Kirkinezos et al., 2005). Therapies that aim to protect mitochondria may therefore exert significant protection in ALS. Indeed, administration of creatine, which improves mitochondrial energy buffering, significantly delays disease progression and extends the lifespan of $SOD1^{G93A}$ mice by 17% (Klivenyi et al., 1999), whereas a 9% extension is seen after treatment with minocycline, one action of which is to inhibit the release of cytochrome c from mitochondria (Zhu et al., 2002).

1.3.4.4. Altered axonal transport

One of the pathological hallmarks of ALS is the presence of abnormal accumulations of intermediate filaments (IF) in the perikarya and axons of motoneurons from post-mortem human tissue and mutant SOD1 mice (Carpenter, 1968; Hirano et al., 1996; Tu et al., 1996). These accumulations consist predominantly of neurofilaments and peripherin (Corbo & Hays, 1992; Migheli et al., 1993; Tu et al., 1996), and suggest that defects in axonal transport may contribute to ALS pathogenesis.

1.3.4.4.1. Cytoskeletal abnormalities

i) Neurofilaments

Neurofilaments are the most abundant structural protein in large calibre axons including motoneurons and are involved in determining axonal calibre and maintaining axonal transport and structure. There are three neurofilament subunits: heavy (NF–H; 115kD), medium (NF-M; 95kD) and light (NF-L; 68kD), which are synthesised in the cell body and then co-assemble into neurofilament polymers. Similar to other structural proteins, neurofilaments are transported down the axon by slow anterograde transport and undergo progressive phosphorylation (Zhang et al., 1997).

However, the presence of neurofilament accumulations in degenerating motoneurons in post-mortem spinal cord tissue of both sALS and fALS patients and in mutant SOD1 mice, suggests that slow anterograde transport may be defective in ALS. In addition, the formation of accumulations in proximal axons may act to hinder axonal transport further, therefore depriving the motoneurons of vital components necessary for normal cellular function (Collard et al., 1995; Zhang et al., 1997). Additionally these accumulations may also sequester organelles (Tu et al., 1997). In $SOD1^{G93A}$ mice the presence of accumulations correlates with symptom onset and increases during disease progression (Tu et al., 1996). Therefore, neurofilament accumulations may have a causal role in ALS. In fact it is suggested that the selective vulnerability of motoneurons in ALS is related to their high neurofilament content (Kawamura et al., 1981; Bruijn et al., 1997a). Underlying genetic alterations in neurofilament subunits may also contribute to their accumulation, by interfering with neurofilament assembly and increasing their propensity to aggregate, therefore representing a risk factor for ALS. Indeed, approximately 1% of ALS patients have missense mutations in the tail domain of the NF-H subunit (Figelwicz et al., 1994; Tomkins et al., 1998; Al Chalabi et al.,

1999). Furthermore, a 60% reduction in levels of NF-L mRNA has been reported in ALS patients (Bergeron et al., 1994).

Interestingly, overexpression of either the human NF-L or NF-H subunits in WT mice induces an accumulation of neurofilaments in motoneurons, with accompanying motoneuron and skeletal muscle dysfunction (Cote et al., 1993; Xu et al., 1993). Disruption of neurofilament polymerisation by overexpression of the NF-L subunit carrying a point mutation similarly induces the formation of neurofilament aggregates and selective motoneuron degeneration in WT mice, similar to that seen in ALS (Lee et al., 1994). This therefore suggests that accumulations of neurofilaments, by neurofilament dysregulation, are sufficient to induce motoneuron dysfunction in ALS.

Ablation of the NF-L subunit in $SOD1^{G85R}$ mice delays disease onset and extends lifespan by 15%, thus supporting the proposal that neurofilament accumulations are toxic (Williamson et al., 1998). However, perhaps surprisingly, the expression of a NF-H β galactosidase fusion protein, which acts by trapping neurofilaments in the cell body and preventing their transport into the axon, has no effect on disease progression in $SOD1^{G37R}$ mice (Eyer et al., 1998). Even more surprising, overexpression of NF-H actually induces a 65% extension in the lifespan of $SOD1^{G37R}$ mice (Couillard-Despres et al., 1998). Consistent with these findings, a delay in disease progression is seen in $SOD1^{G93A}$ mice following overexpression of NF-H or NF-L subunits (Kong & Xu, 2000). Beneficial effects are also observed in $SOD1^{G37R}$ mice overexpressing NF-L (Couillard-Despres et al., 2000). Despite the apparently contradictory results achieved in mutant SOD1 mice, in each model the perikaryal accumulation of neurofilaments is increased, and it has been suggested that these accumulations in the perikarya rather than in axons are responsible for the protective effect seen. There is a correlation

between axonal neurofilament content and the speed of axonal transport (Marszalek et al., 1996), therefore the protection mediated by perikaryal accumulation may be attributed to a reduction in axonal neurofilament content. This may relieve the burden on axonal transport, defects in which occur before disease onset in $SOD1^{G37R}$ mice, thereby preventing 'axonal strangulation' (Williamson & Cleveland, 1999). Alternatively, the presence of multiple calcium binding sites and phosphorylation sites on neurofilaments suggests that perikaryal accumulations may buffer excess calcium or dysregulated kinase activity, such as the inappropriate activation of cyclin-dependent kinase 5 that occurs in $SOD1^{G37R}$ mice (Nguyen et al., 2001). Recently however it has been shown that disease progression is significantly delayed and lifespan extended in $SOD1^{G37R}$ mice in which the tail domain of NF-H and/or NF-M have been genetically replaced. These benefits are observed despite increased tau phosphorylation, which suggests that the restoration of axonal transport underlies the protective effects of neurofilament inclusions (Lobsiger et al., 2005).

ii) Peripherin

Peripherin, a 57kD intermediate filament, is expressed at low levels in motoneurons, although, expression is increased following neuronal injury (Troy et al., 1990) or in response to inflammatory cytokines (Sterneck et al., 1996). Indeed, in post-mortem spinal cord tissue from ALS patients and in spinal cord motoneurons in $SOD1^{G37R}$ mice the expression of peripherin is up-regulated (Robertson et al., 2003), and forms a component of the majority of IF accumulations seen (Migheli et al., 1993; Tu et al., 1996). In WT mice, overexpression of peripherin induces the formation of toxic IF inclusions and selective motoneuron degeneration. This is enhanced by NF-L deficiency (Beaulieu et al., 1999), a situation that may occur in ALS patients (Bergeron et al., 1994). Motoneuron death may therefore occur as a result of the association of peripherin

with NF-M or NF-H subunits and the subsequent formation of toxic aggregates (Beaulieu et al., 1999), a mechanism that may be relevant in ALS. More recently, a toxic splice variant of peripherin, known to induce motoneuron death has been identified in motoneurons in post-mortem spinal cord tissue from ALS patients (Robertson et al., 2001, 2003). Furthermore, a truncation mutation in the peripherin gene, which disrupts the IF network, has been identified in a small proportion of ALS patients, which may represent a risk factor (Gros-Louis et al., 2004). However, contradictory to this toxic role of peripherin, neither overexpression nor ablation of peripherin affects disease progression or lifespan in $SOD1^{G37R}$ mice, which suggests that abnormal peripherin expression and its accumulation may not actually influence ALS pathogenesis (Larivière et al., 2003).

1.3.4.4.2. Altered axonal transport

The maintenance of efficient axonal transport is critical for motoneurons. Many motoneurons have extremely long axons, up to 1 metre in length, which places an enormous metabolic and structural demand on the cell. There are two main components of anterograde transport: fast transport mediated by kinesin motors, responsible for the movement of vesicles and mitochondria, and slow transport, mediated by dynein motors (Wagner et al., 2004), for the movement of the major structural proteins including neurofilaments (slow component a; 0.5mm/day), tubulin and actin (slow component b; 1-2mm/day; Hoffman & Lasek, 1975, 1980). Motoneurons also rely on dynein-mediated retrograde transport for the provision of organelles and ligands such as neurotrophins from the neuromuscular junction to the cell body (Goldstein & Yang, 2000).

Defects in axonal transport are one of the earliest abnormalities seen in mutant SOD1 mouse models of ALS (as discussed in **Chapter 1.3.4.4.1.i**). The appearance of neurofilament accumulations in degenerating motoneurons in ALS may be indicative of defects in slow anterograde transport, and may also act to further hinder axonal transport (Collard et al., 1995; Zhang et al., 1997). In support of this possibility, slow anterograde transport, particularly of tubulin, is reduced in $SOD1^{G37R}$ and $SOD1^{G85R}$ mice, several months before the onset of symptoms (Williamson & Cleveland, 1999). The discovery that the $SOD1^{G37R}$ enzyme is anterogradely transported in slow component b, suggests that the mutant enzyme may exert a direct toxic effect during its own transport (Borchelt et al., 1998). Significant reductions in fast anterograde transport have also been shown in proximal axons in post-mortem human ALS tissue (Sasaki & Iwata, 1996) and reductions in both fast and slow anterograde transport are also seen in symptomatic $SOD1^{G93A}$ mice (Collard et al., 1995; Zhang et al., 1997; Warita et al., 1999). Furthermore, reductions in retrograde transport have recently been identified as early in motoneuron development as E13, in motoneurons cultured from $SOD1^{G93A}$ mice (Kieran et al., 2005). Microarray technology on sALS post-mortem spinal cord tissue similarly revealed a reduction in dynactin expression at disease end-stage (Jiang et al., 2005).

Various transgenic mice have been generated to study the consequences of defective axonal transport on motoneuron function. Homozygous expression of a missense mutation in the dynein heavy chain (DNCHC1) gene in transgenic mice (Legs at odd angles; *Loa*) significantly reduces the rate of axonal transport in motoneurons and reduces motoneuron survival (Hafezparast et al., 2003). Similarly, targeted disruption of the dynein:dynactin complex by postnatal overexpression of the dynamitin (p50) subunit of dynactin in transgenic mice, induces a late-onset progressive motoneuron

degeneration (LaMonte et al., 2002). Dynactin is a multiprotein complex believed to increase the efficiency of the dynein motor and is involved in the interaction of dynein with both microtubules and the substrate cargo to be transported (Karki & Holzbaur et al., 1995; Waterman-Storer et al., 1995, 1997; Muresan et al., 2001). Mutations in the gene encoding the p150 subunit of dynactin (DCTN1) have subsequently been identified in families with a slowly progressing lower motoneuron disease (Puls et al., 2003; Munch et al., 2004). Together these observations indicate that disruption of axonal transport can induce a motoneuron phenotype similar to that found in ALS.

Remarkably, it has recently been shown that the deficits in retrograde transport seen in embryonic $SOD1^{G93A}$ motoneurons could be reversed by crossing the $SOD1^{G93A}$ mice with the *Loa* mice, which express a dynein mutation that also reduces retrograde transport (Hafezparast et al., 2003). This manipulation increases the lifespan of $SOD1^{G93A}$ mice by 28%. The exact mechanism underlying this restoration of axonal transport is still unclear (Kieran et al., 2005), although these results suggest that correction of the defects in axonal transport may have beneficial effects in ALS.

1.3.4.5. Protein aggregation

Protein aggregation is a well-recognised pathological feature of several neurodegenerative disorders including ALS. Intracellular cytoplasmic aggregates, known as Bunina bodies, are present in the cell bodies and proximal axons of motoneurons in post-mortem spinal cord tissue from sALS and fALS patients and also in mutant SOD1 mice (Leigh et al., 1991; Bruijn et al., 1997a; Watanabe et al., 2001; Jonsson et al., 2003). However, as with the other neurodegenerative disorders their exact contribution to disease pathogenesis is unclear. These aggregates are believed to arise from misfolded proteins, which accumulate due to either inadequate refolding by

chaperone proteins, or to reduced degradation as a result of inhibition of the proteasome (Kopito, 2000). Inclusions are generally immunoreactive for ubiquitin, suggesting that they have been targeted for proteasomal degradation (Bruijn et al., 1997a; Jaarsma et al., 2001; Watanabe et al., 2001), and molecular chaperones, such as heat shock proteins (hsps), are a common constituent of the inclusions (Shinder et al., 2001). Aggregations of misfolded proteins may exert toxicity by acquiring an aberrant chemistry, or through the sequestration of organelles or other essential proteins, and ultimately these aggregates may overburden the proteasome (Bruijn et al., 1998; Johnston et al., 2000). In contrast, it has been suggested that aggregates may also have a protective role by sequestering misfolded proteins that would otherwise exert toxic effects.

In mutant SOD1-mediated ALS, disease-causing mutations occur throughout the structure of the SOD1 protein, rather than being localised, for example, to the active site. Therefore, it has been suggested that structural alterations may modify the protein conformation and increase its propensity to aggregate (Bruijn et al., 1997a; Durham et al., 1997; Johnston et al., 2000). Indeed, the stability of mutant SOD1 proteins is reduced compared to endogenous WT SOD1 (Johnston et al., 2000; Shinder et al., 2001) and the expression of mutant SOD1 in primary motoneurons induces aggregate formation, and subsequently cell death (Durham et al., 1997). Interestingly, aggregations are not seen in cultured hippocampal cells or dorsal root ganglion cells following similar expression of mutant SOD1, therefore indicating that selective aggregate formation in motoneurons may underlie their vulnerability in ALS (Durham et al., 1997). In $SOD1^{G85R}$ mice, one of the earliest abnormalities observed is the formation of astrocytic inclusions, which increase in abundance with disease progression, and by end-stage also occur in motoneurons (Bruijn et al., 1997a). Similarly, high molecular weight aggregates containing the mutant SOD1 protein are

found in the spinal cord of presymptomatic SOD1^{G93A} mice. As disease progresses, these insoluble protein complexes are sequestered into cytoplasmic inclusion bodies, which may interfere with axonal transport (Johnston et al., 2000). Delaying the appearance of aggregates in SOD1^{G93A} mice delays the onset of symptoms, therefore indicating that protein aggregation does make a significant contribution to disease pathogenesis (Tateno et al., 2004).

Hsps act as molecular chaperones and associate with misfolded proteins to either promote their refolding or transfer to the proteasome for degradation (Shinder et al., 2001). However, the presence of hsps in mutant SOD1-containing aggregates in motoneurons suggests that this cellular defence mechanism is not sufficient to tackle the abundance of mutant SOD1 protein and this deficit in cellular chaperone proteins may underlie the presence of aggregates (Shinder et al., 2001). Surprisingly, cultured motoneurons have a high threshold for activation of HSF-1, the transcription factor that regulates the heat shock response (Batulan et al., 2003). Thus the expression of hsp70 in cultured motoneurons is unaltered in response to heat shock or exposure to glutamate, which is sufficient to elicit hsp70 up-regulation in other cell types in culture (Batulan et al., 2003). Consistent with these findings, in presymptomatic SOD1^{G93A} mice, hsp70 levels are upregulated in unaffected tissues, whereas they are unchanged in spinal cord and brain (Bruening et al., 1999). Similarly hsp70 levels are unchanged in the post-mortem spinal cord tissue from ALS patients (Batulan et al., 2003). In contrast, in symptomatic SOD1^{G93A} mice, hsp27 and αB crystalline are upregulated in motoneurons and glia (Vleminckx et al., 2002). In support of the proposal that a deficient heat shock response in motoneurons contributes to aggregate formation and subsequent motoneuron degeneration, overexpression of hsp70, either alone or in combination with hsp40, reduces the formation of mutant SOD1 aggregates in cell lines *in vitro* and

ameliorates cell death (Bruening et al., 1999; Takeuchi et al., 2002). Moreover, treatment of $SOD1^{G93A}$ mice with arimoclomol, which induces hsp expression by prolonging the activation of HSF1, delays disease progression and extends lifespan by 22% (Kieran et al., 2004). However, a 10-fold increase in the expression of hsp70 does not affect disease progression in mutant SOD1 mice (Liu et al., 2005). These findings suggest that the expression of several hsps and their co-chaperones, which would result from the activation of HSF-1, may be required to ameliorate toxicity in mutant SOD1 mice *in vivo*, rather than an increase in levels of specific hsps per se.

Therefore, the presence of protein aggregates in motoneurons of mutant SOD1 mice appears to contribute to disease pathogenesis, whereby the increasing formation of aggregates with disease progression exerts toxicity. The susceptibility of motoneurons to protein aggregation may be related to their reduced ability to induce a sufficient heat shock response and therefore to reduce the toxicity of abundantly misfolded mutant SOD1 proteins. Furthermore, the targeting of hsps to mutant SOD1 will reduce their cellular availability to chaperone other misfolded proteins, and this may also contribute to the toxicity of mutant SOD1 aggregates (Shinder et al., 2001). Recently, a specific reduction in proteasomal activities was shown in presymptomatic $SOD1^{G93A}$ mice. A reduction in the capacity for the degradation of misfolded proteins may actually initiate aggregate formation and over the disease course may eventually overwhelm the proteasome (Kabashi et al., 2004). In sALS and mutant SOD1-independent fALS, it is possible that proteins damaged by oxidative stress, for example, may aggregate and exert toxicity similar to mutant SOD1-containing aggregates.

1.3.4.6. Inflammation

In post-mortem spinal cord tissue from ALS patients there are substantial signs of inflammation including significant proliferation and accumulation of activated microglia, reactive astrocytes and $CD4^+$ and $CD8^+$ lymphocytes in areas of motoneuron degeneration (Troost et al., 1990; Engelhardt et al., 1993; Alexianu et al., 2001; McGeer & McGeer, 2002). Furthermore increases in mRNA and protein levels of inflammatory markers such as COX2 and PGE_2 are also seen in post-mortem spinal cord tissue from ALS patients (Yasojima et al., 2001; Maihofner et al., 2003). In $SOD1^{G93A}$ mice there is a correlation between disease progression and the intensity of inflammation (Hall et al., 1998; Alexianu et al., 2001; Almer et al., 2001; Elliott et al., 2001), so that reactive astrogliosis increases steadily from symptom onset. However, microglial activation is evident from a presymptomatic age and continues to increase in intensity during disease progression, paralleling the loss of motoneurons (Hall et al., 1998; Alexianu et al., 2001; Elliott et al., 2001; Olsen et al., 2001; Weydt et al., 2004). In fact, up–regulation of intracellular adhesion molecule-1 (ICAM-1) expression on microglia at 40 days is one of the earliest pathological changes in the $SOD1^{G93A}$ mice, and this up–regulation may be important in the induction of inflammatory processes (Kawasaki et al., 1993; Alexianu et al., 2001).

1.3.4.6.1. Microglial-mediated damage

In response to neuronal damage, microglia are activated, undergo rapid proliferation and migrate to the site of injury (Sargsyan et al., 2005). Activated microglia release a variety of neurotoxic mediators including pro-inflammatory cytokines, for example TNFα and IL-1β, as well as ROS and glutamate (Molina-Holgado et al., 1997; Waksman et al., 1999; Tikka & Koistinaho, 2001; Facchinetti et al., 2003). These neurotoxic agents elicit cellular damage and initiate the recruitment and activation of further microglia,

thus propagating the inflammatory response (Puffenbarger et al., 2000; Facchinetti et al., 2003). Microglia from $SOD1^{G93A}$ mice have been shown to secrete significantly more TNFα than microglia from age-matched WT mice (Weydt et al., 2004) There is also an up-regulation of TNFα mRNA and protein in the CNS of $SOD1^{G93A}$ mice (Hensley et al., 2003). Pro-inflammatory cytokines can induce COX2 expression, via transcription factor NF-κB activation (Consilvio et al., 2004; Juttler et al., 2004). COX2 activation will then increase production of prostaglandins, including PGE_2, which may actually contribute to excitotoxicity by stimulating the release of glutamate from astrocytes (Drachman & Rothstein, 2000). In addition, COX2 activation releases ROS, which may further propagate the inflammatory process (Consilvio et al., 2004).

1.3.4.6.2. Mechanisms of reactive astrocyte-induced neurotoxicity

i) Pro-inflammatory cytokines

Activated astrocytes, like microglia, release a variety of neurotoxic molecules including pro-inflammatory cytokines and ROS, which may also act to propagate the inflammatory reaction via further recruitment and activation of glial cells, and exert additional neuronal damage (Levine et al., 1999; reviewed in Barbeito et al., 2004). Indeed, there is an elevation in the expression of the inflammatory marker, COX2, and the transcription factor, NF-κB, in reactive astrocytes in post-mortem spinal cord tissue from ALS patients (Migheli et al., 1997; Maihofner et al., 2003).

ii) Nitric oxide (NO)

Under pathological conditions, the expression of inducible NOS is stimulated in activated astrocytes. Astrocyte viability is largely unaffected by NO. In contrast, NO can exert significant neuronal toxicity, via inhibition of mitochondrial respiration, the release of glutamate and subsequent depletion of cellular ATP (Bal-Price & Brown,

2001). Furthermore, NO reacts with superoxide radicals to generate peroxynitrite, which can nitrate tyrosine residues exerting substantial cellular damage. Correspondingly, levels of 3-nitrotyrosine are elevated in motoneurons in post-mortem spinal cord tissue from sALS and fALS patients, (Beal et al., 1997; Ferrante et al., 1997). Interestingly, Raoul et al, (2002) have demonstrated that mutant SOD1 motoneurons in culture are selectively vulnerable to a subtype of Fas-mediated cell death that is enhanced by NO.

iii) Reduced glutamate uptake

Oxidative damage may also reduce the expression and function of the astrocytic GLT-1 glutamate transporter protein (Trotti et al., 1996, 1999). Selective inhibition of the GLT-1 transporter in mice initiates motoneuron loss (Darman et al., 2004) and progressive paralysis *in vivo* (Rothstein et al., 1996). Reduced glutamate uptake will therefore elevate extracellular glutamate levels and potentially induce excitotoxic damage (Choi, 1992).

1.3.4.6.3. Therapies targeting inflammation

Several therapies that aim to reduce inflammation in models of ALS have been examined. Minocycline and nordihydroguaiaretic acid, potent inhibitors of microglial activation, both exert beneficial effects in mutant SOD1 mice (Kriz et al., 2002; van den Bosch et al., 2002; Zhu et al., 2002; West et al., 2004). Furthermore, selective COX2 inhibitors delay onset (Pompl et al., 2003) and extend the lifespan of $SOD1^{G93A}$ mice by 25% (Drachman et al., 2002).

In summary, multiple mechanisms are proposed to play a role in the pathogenesis of ALS, and indeed substantial evidence exists for their individual involvement, as detailed in **Chapters 1.3.4.1. – 1.3.4.6.** These neurotoxic mechanisms, however, appear to not be

mutually exclusive, as shown in **Figure 1.4**, and may in fact interact, resulting in motoneuron degeneration via either apoptosis or necrosis.

1.4. Aims of this Thesis

The aim of this Thesis is to investigate potential strategies to prevent the degeneration of motoneurons in both *in vivo* and *in vitro* models of ALS. In particular, the neuroprotective potential of the endocannabinoid system is evaluated in the transgenic $SOD1^{G93A}$ mouse model of ALS. Furthermore, the development of a co-culture model of $SOD1^{G93A}$ motoneurons and $SOD1^{G93A}$ astrocytes allows investigation into the interaction between motoneurons and astrocytes. This will increase our understanding of the influence astrocytes have on disease progression, and establish whether specific targeting of astrocytes may be an appropriate strategy to develop, to rescue motoneurons from degeneration in ALS.

Figure 1.4 – Summary of neurotoxic mechanisms proposed to contribute to ALS pathogenesis.

A variety of neurotoxic mechanisms, summarised in the diagram, are proposed to play a role in the pathogenesis of ALS, as described in **Chapters 1.3.4.1. – 1.3.4.6.**. The exact contribution of each mechanism to disease pathogenesis is unknown, although it is likely that interactions between multiple mechanisms occur. There is substantial evidence indicating that apoptosis is the final cell death pathway, however depending on the energy state of the cell necrosis may alternatively be initiated. This diagram is adapted from Shaw (2005).

$[Ca^{2+}]_c$ – cytosolic calcium levels; GLT-1 – astrocytic glutamate transporter –1;

● glutamate neurotransmitter; ▭ GLT-1; ⬭ synaptic vesicle; AMPA receptor; transported cargo; —— intermediate filament.

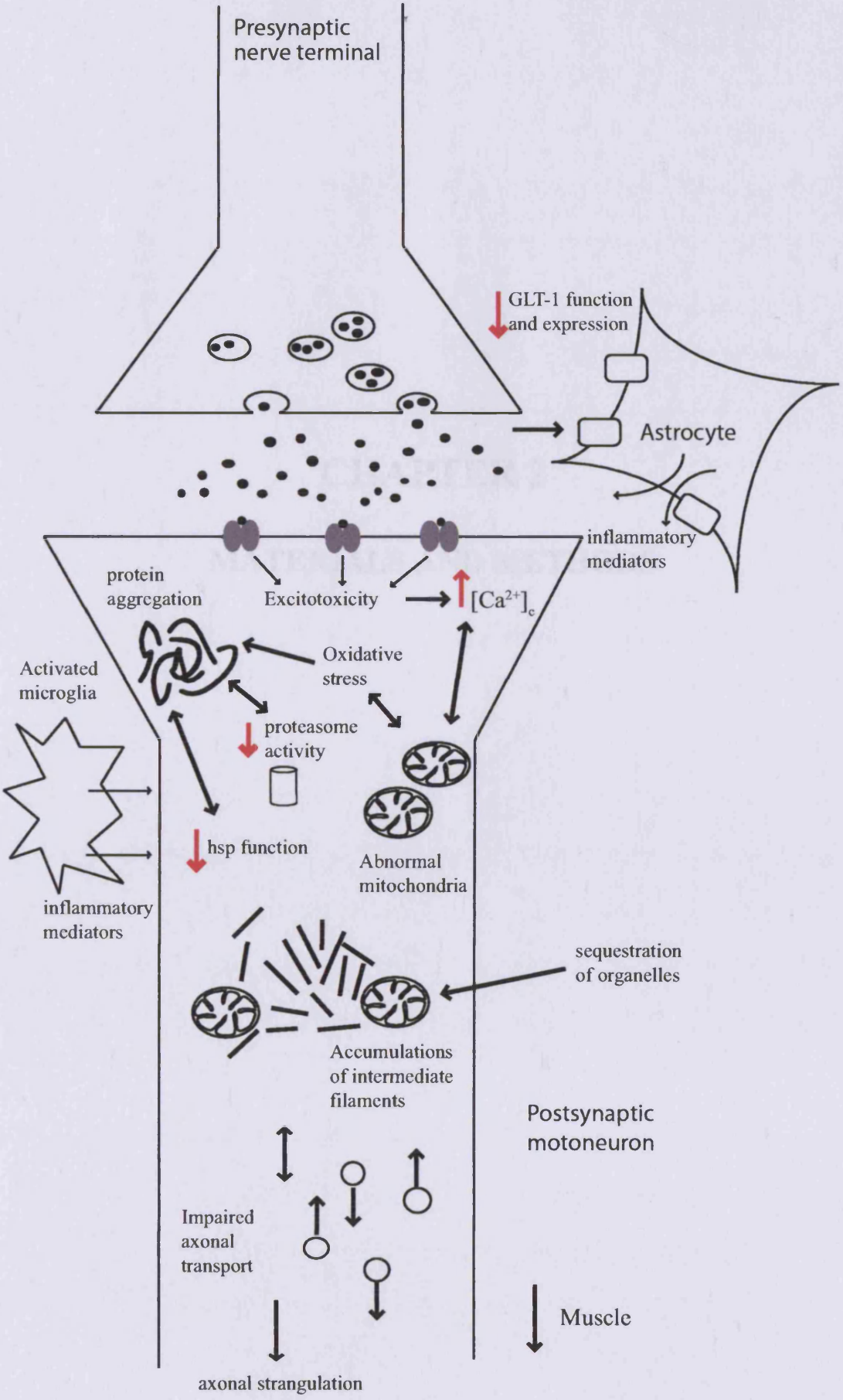
Presynaptic
nerve terminal
GLT-1 function
and expression
Astrocyte
inflammatory
mediators
protein
aggregation
Excitotoxicity
$[Ca^{2+}]_c$
Oxidative
stress
Activated
microglia
proteasome
activity
hsp function
Abnormal
mitochondria
inflammatory
mediators
sequestration
of organelles
Accumulations
of intermediate
filaments
Postsynaptic
motoneuron
Impaired
axonal
transport
Muscle
axonal strangulation

CHAPTER 2

MATERIALS AND METHODS

2. METHODS

2.1. Breeding and maintenance of transgenic mouse colonies.

a) SOD1^{G93A} colony

Transgenic mice carrying a human SOD1 gene with a G93A mutation (TgN[SOD1-G93A]1Gur) were originally purchased from Jackson Laboratories (Bar Harbour, ME). The colony was maintained by breeding male heterozygous carriers with female (C57BL/6 x SJL) F_1 hybrids. The SOD1^{G93A} mice were originally generated and characterised by Gurney et al, (1994) and contain an estimated transgene copy number of 25.

b) SOD1.*Faah* -/- and SOD1.*Cnr1* -/- colony

The *Cnr1* -/- and *Faah* -/- mice (provided by C. Ledent, Belgium and B. Cravatt, USA, respectively; Ledent et al., 1999; Cravatt et al., 2001) were backcrossed at least seven generations on to the ABH mouse background. SOD1.*Faah* +/- and SOD1.*Cnr1* +/- mice were obtained by breeding male heterozygous SOD1^{G93A} carriers with female *Faah* or CB_1 receptor knock–out mice on the ABH background. Male heterozygous carriers for both genes were backcrossed again with female *Faah* or CB_1 receptor knock-out mice to obtain an F_2 generation of SOD1.*Faah* -/- and SOD1.*Cnr1* -/- mice for use in the experiments described in this Thesis.

The animals were housed in a controlled temperature and humidity environment and maintained on a 12-hour light/dark cycle with access to food and water provided *ad libitum* via an overhead rack. At the onset of paralysis, affected animals were provided with food pellets soaked in water to ensure sufficient nourishment and hydration. All experiments were carried out under license from the Home Office in accordance with

the Animals (Scientific Procedures) Act 1986 and following approval from the Institute of Neurology Ethical Review Committee.

2.2. Characterisation of SOD1^{G93A} mice

In these experiments, high copy expressing SOD1^{G93A} mice were used (TgN[SOD1-G93A]1Gur). The disease progression in these mice has been investigated by several laboratories and **Table 2.1** summarises the key pathological changes reported to occur during the progression of the disease. The first visible sign of disease in these mice is a fine hindlimb tremor at approximately 90 days of age, which progresses to hindlimb weakness and then complete hindlimb paralysis over the next month, coupled with an inability to groom, feed or drink from the overhead rack (Gurney et al., 1994). At disease end-stage, approximately 130 days, over 70% of ventral horn motoneurons have been lost and severe muscle atrophy and paralysis is observed. For the purpose of this Thesis, disease in SOD1^{G93A} mice was defined as 4 stages: 42 - 83 days of age (presymptomatic), 84 – 111 days of age (early symptomatic), 112 – 125 days of age (late symptomatic) and 126 – 153 days of age (end-stage disease). Although the term 'symptomatic' may not be appropriate when referring to mice, in this Thesis the term 'symptomatic' is used to describe the stage at which defects in motor function are first observed, with onset of disease signs occurring around 90 days of age.

2.3. Genotyping by polymerase chain reaction of purified DNA

The mice carrying the SOD1^{G93A} transgene were identified by polymerase chain reaction (PCR) amplification of the transgene from genomic DNA. Tail snips (<0.5cm) were taken just after weaning, under ethyl chloride local anesthesia. To purify the DNA, the tails were digested for a minimum of 3 hours, with regular vortexing, in 600µl lysis buffer (consisting of 484µl nuclei lysis solution [Promega UK,

Table 2.1 – Summary of the pathological changes observed in high copy expressing $SOD1^{G93A}$ mice

Age of animal (disease stage)	Pathological change observed in $SOD1^{G93A}$ mice	References
Embryonic	Reduced rate of retrograde axonal transport Increased excitability of motoneurons	Kieran et al., 2005 Pieri et al., 2003 Kuo et al., 2004
0-39 days (presymptomatic)	Fragmentation of Golgi apparatus (31d) Vacuolation of ventral horn motoneurons due to swelling of ER and mitochondria (37d)	Mourelatos et al., 1996 Chiu et al., 1995
40-79 days (presymptomatic)	Loss of fast muscle fibre synapses (40d) ICAM expression up-regulated (40d) 40% of end-plates denervated (47d) Significant loss of gastrocnemious motor units (47d) Significant loss of corticospinal, rubrospinal, bulbospinal neurons (60d) Protein aggregates in ventral horn motoneurons (60d) Vacuolation of motor-related areas of the brain (69d)	Frey et al., 2000 Kawasaki et al., 1993 Fischer et al., 2004 Kennel et al., 1996 Zang & Cheema, 2002 Johnston et al., 2000 Chiu et al., 1995
80-120 days (symptomatic)	Significant loss of motoneurons innervating the diaphragm (82d) Neurofilament inclusions in ventral horn motoneurons (82d) Decline in constant rotarod performance (85d) 40% of ventral horn motoneurons lost (90d) Reduction in GLT-1 expression (90d) Onset of reactive gliosis (90d) Fine hindlimb tremor, muscle spasticity and hyperreflexia (91d)	Chiu et al., 1995 Tu et al., 1996 Fischer et al., 2004 Sharp et al.,2005 Rothstein et al., 2005 Olsen et al., 2001 Chiu et al., 1995
End-stage	Worsening of all disease signs >60% loss of ventral horn motoneurons Severe muscle atrophy Death – approximately 130d	Gurney et al., 1994 Chiu et al., 1995

Southampton, UK] and 116µl 0.5mM EDTA [pH 8.0]) and 17.5µl proteinase K (20mg/ml; Invitrogen, Paisley, UK) at 55°C. Following digestion, 200µl of protein precipitation solution (Promega UK, Southampton, UK) was added to each digest and the sample vortexed vigorously for 20 seconds, before chilling on ice for 5 minutes and then centrifuging at 14,000g for 6 minutes at room temperature. The supernatant containing the DNA was removed and transferred to a clean eppendorf tube, to which isopropanol (0.7-1.0x sample volume; VWR International Ltd, Poole, UK) was added and inverted gently several times. The samples were centrifuged at 14,000g for one minute at room temperature and the supernatant was decanted leaving a small DNA pellet. 600µl of 70% ethanol (VWR International Ltd, Poole, UK) was added and the DNA was rinsed by inverting the tube several times before the samples were centrifuged again at 14,000g for one minute at room temperature. The supernatant was decanted and discarded and the DNA pellet was rehydrated in 200µl sterile water.

2.5µl of each DNA sample was added to a reaction tube that contained 17.65µl sterile water, 2.5µl PCR buffer (10X), 0.75µl $MgCl_2$ (50mM), 0.5µl dNTP solution (10mM), 0.25µl of both the forward and reverse primers for the endogenous SOD1 enzyme and human mutant SOD1 enzyme (1µg/µl), and 0.1µl Taq polymerase (0.5 units) to make a final volume of 25µl. To identify the human $SOD1^{G93A}$ transgene, primers with the following sequences were used: 5' CAT CAG CCC TAA TCC ATC TGA 3' and 5' CGC GAC TAA CAA TCA AAG TGA 3'. The samples were then temperature cycled as follows: 1 cycle of 3 minutes at 95°C; 36 cycles of 30 seconds at 95°C, 30 seconds at 60°C, 45 seconds at 72°C; and one cycle of 2 minutes at 72°C. The PCR products were visualised by gel electrophoresis by running 20µl of each PCR product on a 4% agarose gel at 130mV for 40 minutes.

2.4. Primary spinal cord astrocyte cultures

Primary astrocytes were prepared based on a procotol described by Robb & Conner (1998). Two working solutions were used, referred to as Solution A (comprising 50mls of Eagle's Balanced Salt Solution [Invitrogen, Paisley, UK], supplemented with 50units/ml penicillin, 50μg/ml streptomycin, 2.5μg/ml amphotericin B, 0.3% bovine serum albumin [BSA; dissolved in L-15 medium] and 20μg/ml DNase 1) and Solution B (comprising 20mls of Solution A further supplemented with 0.25mg/ml trypsin and 0.15mg/ml DNAse 1), which was kept at 37°C until use.

P0-P2 transgenic mouse pups were decapitated and their spinal cords were dissected out and the meninges removed. The spinal cords were maintained in Hank's balanced salt solution (HBSS; Invitrogen, Paisley, UK) supplemented with 50units/ml penicillin, 50μg/ml streptomycin and 2.5μg/ml amphotericin B until genotyping was complete. A tail snip was taken from each pup to allow determination of its genotype prior to culturing, using PCR as described in **Chapter 2.3**.

The spinal cords were pooled according to genotype, either WT or $SOD1^{G93A}$, and each genotype was cultured separately. Initially, the spinal cords were transferred into sterile, phenol red free, supplemented HBSS, and chopped into smaller pieces. Spinal cord pieces were then transferred to 10mls of Solution A and triturated until homogenous. The homogenate was centrifuged at 4°C for 5 minutes at 2000rpm, and the supernatant was discarded. The pellet was resuspended in 10mls of Solution B and incubated for 10 minutes at 37°C in a 5% CO_2 humidified incubator, before centrifugation for a further 5 minutes at 2000rpm at 4°C. The supernatant was removed and the pellet resuspended in 5mls of Solution A. The resuspension was centrifuged for a further 5 minutes at 4°C at 2000rpm. Following the removal of supernatant, the final pellet was resuspended in 1ml

of Dulbecco's Modified Essential Medium (DMEM; Invitrogen, Paisley, UK; supplemented with 50units/ml penicillin, 50μg/ml streptomycin, 2.5μl/ml amphotericin B and 10% foetal calf serum). The resuspended pellet was passed through a 100μm mesh (Marathon, London, UK), and then the cell density determined using a haemocytometer. Cells were seeded onto 0.1μg/ml poly-D-lysine coated 13mm coverslips in 24 well plates at a density of $1.5x10^5$ cells/well, or 22mm coverslips in 6 well plates at a density of $5x10^5$ cells/well for survival assays and imaging experiments respectively. Cells were maintained in supplemented DMEM in a 37°C, 5% CO_2 humidified incubator for between 2 and 3 weeks until confluency was reached. Astrocytes were then placed in a 37°C, 5% CO_2 environmental shaker and rotated at 160rpm for 18 hours in order to dislodge O2A progenitor cells and microglia (Robb & Conner, 1998). The media was then rapidly exchanged for fresh media and the cultures were returned to the incubator for 7-10 days. At 3 weeks *in vitro*, mixed ventral horn cells were plated onto the enriched astrocyte layers, as described below.

To determine the percentage of astrocytes within the enriched astrocyte layer, glial cultures were immunostained for GFAP, a specific marker of astrocytes, and DAPI, a nuclear marker (0.01%, Molecular Probes, Paisley, UK), and the percentage of DAPI stained, GFAP positive cells were calculated.

2.5. Mixed ventral horn neuron cultures

Mixed motoneuron cultures were prepared using a protocol adapted from that described by Camu & Henderson (1994). Female (C57BL/6 x SJL) F_1 hybrids were time-mated with male $SOD1^{G93A}$ mice. Pregnant females were terminally anaesthetised with pentobarbitone (140mg/kg) and embryos at gestational age E12.5 were quickly removed by hysterectomy and placed in Dulbecco's phosphate buffered saline (PBS; Invitrogen,

Paisley, UK), supplemented with 50 units/ml penicillin (Invitrogen, Paisley, UK), 50μg/ml streptomycin (Invitrogen, Paisley, UK) and 2.5μg/ml amphotericin B.

The spinal cords of individual embryos were isolated under a dissection microscope, using fine forceps to carefully separate the spinal cord from the surrounding tissue. The remaining meninges plus attached dorsal root ganglia were then carefully removed to avoid damaging the spinal cord. The dorsal horn was carefully detached from the ventral portion of the spinal cord using a fine ophthalmic scalpel blade and each individual ventral horn was collected in an eppendorf containing supplemented PBS, as described above. A tail snip was also taken from each embryo to allow determination of its genotype prior to culturing, using PCR as described in **Chapter 2.3**.

The spinal cords were pooled according to genotype, either WT or $SOD1^{G93A}$, and each genotype was cultured separately. The tissue was incubated for 10 minutes at 37°C in HAM F10 modified medium (Invitrogen, Paisley, UK) containing 0.025% trypsin. The digest was transferred to complete medium (comprising L15 medium [Invitrogen, Paisley, UK] supplemented with 3.6mg/ml glucose, 0.2μM progesterone, 50units/ml penicillin [Invitrogen, Paisley, UK], 50μg/ml streptomycin [Invitrogen, Paisley, UK], 5μg/ml insulin, 100uM putrescine, 0.1mg/ml conalbumin and 2% horse serum [Invitrogen, Paisley, UK]), containing 0.125mg/ml DNase 1 and 0.4% BSA and gently dissociated three times. The cell suspension was then centrifuged through a 4% BSA cushion for 5 minutes at 1500rpm. Then following removal of the supernatant, the pellet was resuspended in complete medium (as described above), further supplemented with 0.02mg/ml DNase 1 and the cell density determined using a haemocytometer. Cells were seeded onto poly-ornithine and laminin (Invitrogen, Paisley, UK) coated 13mm coverslips in 24 well plates at a density of 7.5×10^4 cells/well, or 22mm coverslips in 6

well plates at a density of 1.5 x 10^5 cells/well for survival assays and imaging experiments respectively.

In some experiments motoneuron:astrocyte co-cultures were prepared. In these co-culture experiments, mixed ventral horn cultures were plated directly onto an enriched WT or $SOD1^{G93A}$ astrocyte layer at the densities indicated above. Cells were maintained in complete neurobasal medium ([Invitrogen, Paisley, UK] supplemented with 2% B-27 supplement [Invitrogen, Paisley, UK], 0.5mM glutamine [Invitrogen, Paisley, UK], 0.05% mercaptoethanol, 2% horse serum, 0.1ng/ml GDNF [Caltag, Silverstone, UK], 0.5ng/ml CNTF [Caltag, Silverstone, UK], 0.1ng/ml BDNF [Caltag, Silverstone, UK], 50 units/ml penicillin, 50μg/ml streptomycin and 2.5μg/ml amphotericin B) in a 37°C, 5% CO_2 humidified incubator for a minimum of 7 days in vitro (DIV) before undergoing any drug treatment or imaging protocol. The medium was replaced twice a week.

All reagents were obtained from Sigma-Aldrich, Poole, UK, unless otherwise stated.

2.6. Cellular fluorescence imaging

The cellular interaction between motoneurons and astrocytes was examined by fluorescent imaging technology using confocal microscopy and a cooled charge coupled device (CCD) camera.

2.6.1. Dye loading and drug application

Immediately prior to experimentation, coverslips of cultured cells (7-10 DIV) were removed from their culture medium and mounted in custom built imaging chambers. These chambers consisted of a circular base in which the 22mm coverslip was held

secure by a slight indentation, and a threaded top that when screwed onto the base formed a watertight seal and allowed incubation of the cells in various experimental solutions. Furthermore, a rubber ring placed between the top and base prevented the leakage of recording medium from the chamber onto the objective lens.

Once mounted in imaging chambers, cells were incubated in Hepes buffered salt solution (referred to as recording medium, RM) composed of (mM): 156 NaCl, 3 KCl, 2 $MgSO_4$, 1.25 KH_2PO_4, 2 $CaCl_2$, 10 glucose and 10 Hepes, and the pH was adjusted to 7.35 with NaOH (all Sigma Aldrich, Poole, UK). Certain experiments required the use of RM with a high potassium concentration, which was based on the standard RM with an isotonic replacement of NaCl (109mM) with KCl (50mM).

Cultures were loaded with various fluorimetric indicators that are listed in **Table 2.2** (all Molecular Probes, Paisley, UK). Tetramethylrhodamine methyl ester (TMRM) is a highly lipid soluble cation and therefore is extremely membrane permeable. In contrast, the free acid moieties of the calcium indicators (fluo 4, fura-2FF and rhod 5N) are negatively charged and water-soluble and therefore their diffusion across cellular membranes is limited. Therefore, these fluorimetric indicators were loaded as their acetoxy-methyl (AM) esters, which are membrane permeant. Exposure to endogenous cellular esterases cleaves the AM esters and generates the fluorophore intracellularly. When required, a surfactant, Pluronic F-127 (0.005%) was added to the chambers to aid the dispersion of water insoluble molecules in the aqueous RM. After the loading period, cells were washed 3 times with RM to remove background dye and were then incubated in 0.5ml of fresh RM for the duration of the experiment. At least 3 experiments were performed for each parameter studied, using cultures prepared on separate occasions.

Table 2.2 – Fluorophore loading conditions

Fluorophore	**Concentration**	**0.005% Pluronic required ?**	**Loading conditions**	**Parameter measured**
Tetramethyl-rhodamine methyl ester (TMRM)	30nM	Yes	30 mins at room temperature	Mitochondrial membrane potential
Fluo 4 AM (fluo 4)	5μM	Yes	30 mins at room temperature	Cytosolic calcium levels (high affinity)
Fura 2-FF AM (fura 2-FF)	5μM	Yes	30 mins at room temperature	Cytosolic calcium levels (low affinity)
Rhod 5N AM (rhod 5N)	5μM	Yes	30 mins at room temperature	Mitochondrial calcium levels
Dihydroethidium (HEt)	2μM	Yes	None	Free radical generation

Drugs applied during the course of the experiment were made up in 0.5ml aliquots of RM and applied by means of RM replacement. All experiments were performed at room temperature.

2.6.2. Fluorescence measurement

The majority of recordings were performed on a Zeiss 510 confocal laser scanning microscope (CLSM), however, the use of the ratiometric calcium indicator fura 2-FF required the use of a cooled charge-coupled device (CCD) camera. The general methods associated with confocal/CCD camera use are described in this section, however, details particular to one experiment are given in the individual Chapter.

i) Confocal imaging

Confocal images were produced using a Zeiss 510 CLSM (Oberkocken, Germany). This set-up comprised a Zeiss Axiovert 200M inverted microscope equipped with a quartz x40 and glass x63 plan-apochromat, oil immersion objective lenses (numerical aperture 1.3 and 1.4 respectively). Four different laser types were available for the excitation of fluorescence: UV laser (lines at 351 and 364nm), laser diode 405nm (line at 405nm), Argon laser (lines at 458, 477, 488 and 514nm) and two helium-neon lasers (lines at 543 nm and 633nm respectively).

A diagrammatic representation of the confocal microscope set-up is shown in **Figure 2.1**. The excitation wavelength provided by the laser is reflected, by means of a dichroic mirror, onto an objective lens, which focuses the illuminating light onto a small spot within the sample specimen. The diameter of the illuminated sample is determined by the numerical aperture of the objective lens. The excitation laser beam is rapidly moved across the sample area, under the control of the scan generator, which also rapidly scans

Figure 2.1 - A diagrammatic representation of the experimental confocal laser scanning microscope and the interline-transfer CCD camera set-up

a) Confocal Laser Scanning Microscope

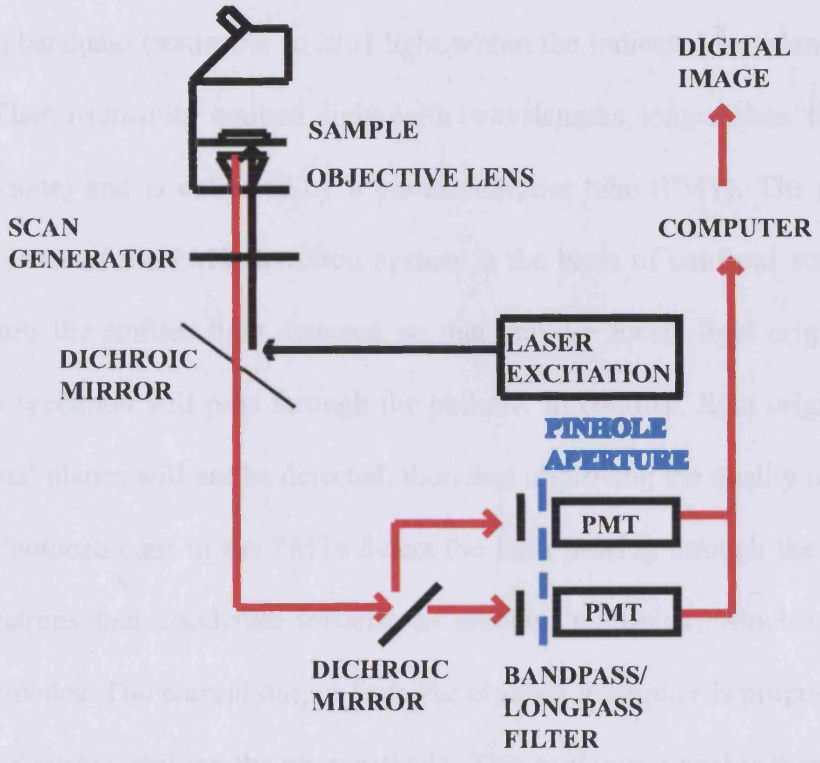

b) Interline-transfer cooled Charge Coupled Device (CCD) Camera

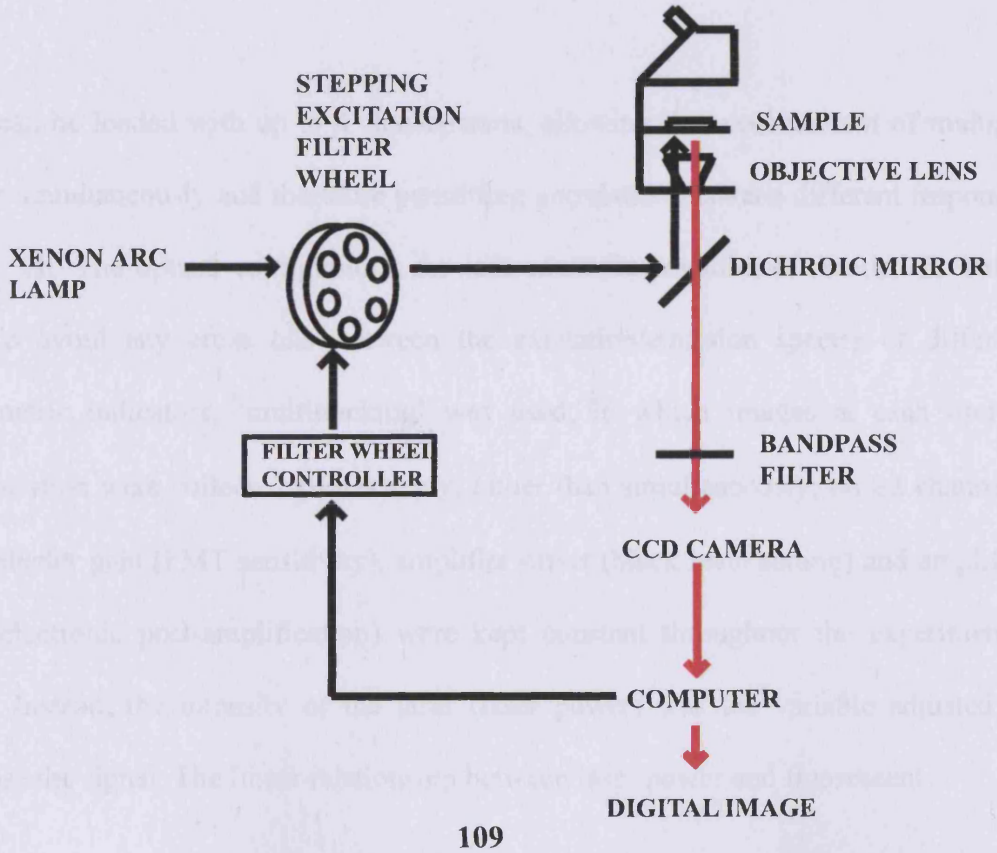

the emitted fluorescent light. Emitted fluorescence is reflected from the sample through the objective lens, the scan generator and the dichroic mirror, which separates the emitted fluorescent light from the excitation light. Emitted light passes through an appropriate bandpass (transmits emitted light within the indicated wavelength band) or longpass filter (transmits emitted light with wavelengths longer than the indicated threshold value) and is collected by a photomultiplier tube (PMT). The placing of a pinhole in front of the PMT detection system is the basis of confocal scanning. This pinhole limits the emitted light detected, so that only 'in focus' light originating from the sample specimen will pass through the pinhole. In contrast, light originating from 'out of focus' planes will not be detected, therefore improving the quality of the images obtained. Photocathodes in the PMTs detect the light passing through the pinhole and release electrons that accelerate towards an electron multiplier, which consists of a series of dynodes. The current output from the electron multiplier is proportional to the number of electrons striking the photocathode. This analogue signal is then digitised to produce an image on the computer monitor.

Cells can be loaded with up to 4 fluorophores, allowing the measurement of multiple signals simultaneously and therefore permitting correlation between different responses of the cell. The optical configuration for individual fluorophores is detailed in **Table 2.3.** To avoid any cross talk between the excitation/emission spectra of different fluorimetric indicators, 'multitracking' was used, in which images at each optical configuration were collected successively, rather than simultaneously, on ≥2 channels. The detector gain (PMT sensitivity), amplifier offset (black level setting) and amplifier gain (electronic post-amplification) were kept constant throughout the experimental series. Instead, the intensity of the laser (laser power) was the variable adjusted to optimise the signal. The linear relationship between laser power and fluorescent

Table 2.3 – The optical configurations for fluorophore use.

The optical configurations for each fluorophore are listed in the table. A dichroic mirror in the microscope separated the excitation from emission light. To prevent cross talk between the excitation/emission spectra of different fluorimetric indicators, images at each optical configuration were collected successively, rather than simultaneously, on two channels (multitracking). The emitted signal was passed through an appropriate bandpass or longpass filter and detected by a PMT.

Fluorophore	Laser excitation wavelength (nm)	Microscope dichroic filter (nm)	Bandpass/ Longpass emission filter
TMRM	543	545	LP 560
Fluo 4	488	490	BP 505-550
Fura 2-FF	340/380	510	LP 515
Rhod 5N	543	545	LP 560
HEt	543	545	BP 560-615
NADH auto-fluorescence	364	395	BP 435-485

intensity allowed correction for changes in laser power. The presence of an acousto-optic tunable filter allowed the intensity of each laser line to be independently controlled and indeed this was maintained between 0.05% and 1% of the total laser output. The pinhole was set to give an optical slice of approximately 2μM to optimise light collection.

An image (an array of 512 x 512 pixels) was acquired every 30 seconds, to minimise photodamage. However, immediately after drug application continuous scanning was implemented for 5 minutes to allow a detailed analysis of the cellular response. For the analysis of mitochondrial membrane potential, a 'z' stack of images was taken throughout the culture. Images were acquired at a scan speed of 7.86 seconds and digitised to 12 bits, which provides 4096 grey levels, therefore improving resolution. Unless otherwise stated images were acquired using the x40 objective lens.

ii) Cooled charge coupled device (CCD) camera

The CCD camera was used in association with the ratiometric calcium indicator, fura 2-FF. Fluorescent measurements were obtained on a Nikon epifluorescence inverted microscope (Tokyo, Japan) equipped with a x20 fluorite objective lens (numerical aperture 0.7). Cells were placed on the microscope stage and fluorescence excited using a 75W xenon arc lamp, the beam passing sequentially through 10nm bandpass filters centred at 340 and 380nm housed in a stepping excitation filter wheel (Cairn Research, Faversham, UK) and controlled by Acquisition Manager software (Kinetic Imaging, Liverpool, UK; see **Figure 2.1**). Sequential excitation of cells at 340nm and 380nm, which corresponds to the excitation of calcium-bound and calcium-free fura 2-FF, allowed the ratiometric measurement of fura 2-FF fluorescence. Images were acquired every 10 seconds and cells were protected from phototoxicity by interposing a

computer-controlled shutter in the light path between exposures. Excitation light was separated from emitted light by a dichroic mirror, and the emitted light was reflected through a 515nm longpass filter to a interline-transfer cooled CCD camera with a chip of 656 pixels x 494 pixels (pixel area 9.9 μm^2) and digitised to 10 bit resolution (Orca ER; Hamamatsu 4880, Welwyn Garden City, UK). All data was collected using Kinetic Imaging software (Liverpool, UK). To reduce background noise, the CCD camera was cooled by a Peltier element to a temperature of 20°C below the ambient temperature.

Imaging using the interline-transfer CCD camera is based on the transfer of accumulated charge from each photodiode to an adjacent charge transfer channel. This occurs rapidly and efficiently therefore improving the acquisition rate. Data was digitised to 10 bits and acquisition speed further improved by 'binning' the pixels, whereby square arrays of 4 pixels were averaged to produce a single data point.

2.6.3. Image processing

Images were collected using Zeiss 'LSM' software or Kinetic Imaging 'Acquisition Manager' for confocal and CCD microscopy respectively. With the exception of experiments measuring mitochondrial membrane potential, all images were analysed using Lucida version 5.0 image analysis software (Kinetic Imaging, Liverpool, UK). Initially background fluorescence was subtracted from the acquired confocal image. Motoneurons and other cells of interest were selected and the change in signal differentiated over time. Subsequently, the change in digitised signal for each region of interest was corrected for laser power and plotted in Microcal Origin 7.1. (Northampton, MA, USA).

Data acquired using fura 2-FF required an additional analysis step. Following subtraction of background fluorescence from the individual 340nm and 380nm images, the 340nm image was divided by the 380nm image to calculate the ratio of the signal generated. Subsequently the change in signal was differentiated over time and the change in digitised signal for each region of interest was plotted in Microcal Origin 7.1, as described above.

Experiments to investigate the resting mitochondrial membrane potential were analysed using Metamorph software (Universal Imaging Corporation, Downingtown, PA, USA). For each experiment a 'z' stack was taken through the culture, and this was compressed to a single image with each pixel representing the average intensity of that point through the sample. An image threshold was set at a point that represented the minimum fluorescence for that experimental culture. This threshold value was subtracted from the fluorescent signal to give a value corresponding to the mitochondrial membrane potential.

Single excitation wavelength fluorophores require extensive calibration to define the minimum and maximum fluorescence in each cell, due to the variability in fluorophore loading. The calibration takes into account the minimum fluorescence attained in the absence of calcium in the RM, and the maximum fluorescence attained in the presence of calcium and enables quantitative measurements to be made from the data acquired. However, the laborious nature of this calibration in combination with the potential risk of damaging the cultured cells warrants the representation of the fluorescence acquired from single wavelength fluorophores on an arbitrary scale, allowing only qualitative analysis. However, by averaging the data from at least 3 experiments, loading deviations should be minimised, therefore allowing quantitative analysis. The use of

the ratiometric, low affinity calcium indicator fura 2-FF provides a more accurate quantitative measurement of the change in cytosolic calcium, compared to single wavelength indicator fluo 4. However, the fura 2-FF data has not been calibrated in terms of $[Ca^{2+}]_c$ because of the uncertainty arising from the use of different calibration techniques (Henke et al., 1996). Data are therefore presented as the ratio of the signal excited at 340nm and 380nm (representing calcium-bound and calcium-free respectively) for fura 2-FF.

For all experiments, the mean values or the slope of the fitted lines (depending on experiment) were compared using either a Mann Whitney U test or a one way ANOVA incorporating a Student Newman Keuls multiple comparison test (according to individual experiments) using Sigma Stat (version 2.03, Erkrath, Germany).

2.7. Motoneuron survival *in vitro*

To assess motoneuron survival *in vitro*, cultures (7-10 DIV) were divided into a treated group, the details of treatments are given in individual Chapters, or an untreated group. The effect of treatment on motoneuron survival was assessed using the Trypan Blue exclusion method. This method involves incubation of the cultured cells in 200µl trypan blue (Sigma-Aldrich, Poole, UK) for 10 minutes at 37°C. Subsequently, the trypan blue was removed and the cells were fixed in 4% paraformaldehyde (PFA; pH7.4; Tabb Ltd, Aldermaston, UK) in 0.1M PBS for 30 minutes then rinsed in PBS and stored at 4°C until processing. To assess the effect of pharmacological treatment on motoneuron survival, the cells were immunostained for MAP-2, a pan neuronal marker, using the protocol described below (**Chapter 2.8**). Motoneurons were identified according to the morphological criteria:

i) a cell body diameter ≥ 15µm

ii) the presence of at least 3 neuritic processes

Random fields of neurons were counted and the number of surviving motoneurons was expressed as a percentage of the total number of motoneurons from an untreated culture prepared on the same occasion.

2.8. Immunocytochemistry

In the experiments described in this Thesis, immunocytochemistry was performed on both cultured motoneurons and spinal cord sections. Information regarding the specific primary antibodies used in individual experiments is detailed in the relevant Chapters.

The fixed cells or spinal cord sections were rinsed in PBS containing 0.1% Triton (Sigma-Aldrich, Poole, UK) for 15 minutes, and then incubated in a blocking solution consisting of 5% milk fat (Marvel, Premium Brands, Lincs, UK) and 3% normal serum (Vector Laboratories, Burlingame, CA, USA) in PBS (pH 7.4), for 1 hour at room temperature. The blocking solution was then removed and the cells/sections were rinsed twice with PBS containing 0.1% Triton for 5 minutes and a final rinse in PBS only, for 5 minutes. Cells/sections were then incubated overnight at 4°C in primary antibody solution made up in PBS. Following incubation, the primary antibody solution was removed and the sections were rinsed twice with PBS containing 0.1% Triton for 5 minutes and a final rinse in PBS only, for 5 minutes. Cells/sections were next incubated in secondary antibody solution (dilution 1:100) in PBS for 2 hours at room temperature. Following removal of the secondary antibody, cells/sections were incubated for 1 hour at room temperature in Avidin-Biotin complex solution (ABC; Vector Laboratories, Burlingame, CA, USA), which was prepared thirty minutes before use, and then rinsed three times in PBS for 5 minutes each. Immunostaining was visualised using fast 3,3

diaminobenzadine tablets (Sigma-Aldrich, Poole, UK), and then cells/sections were rinsed in PBS for 2 minutes, dehydrated through graded alcohols; 1 minute in 70% ethanol, 1 minute in 90% ethanol and 2 rinses in 100% ethanol for 1 minute each. Cells/sections were then cleared by incubation in histoclear for 2 minutes (2 rinses). Finally, the cultured cells plated on coverslips were removed from their 24 well plates, and mounted face down onto uncoated slides using DPX mounting solution. Alternatively, coverslips were mounted onto spinal cord sections using DPX mounting solution.

2.9. Mouse on mouse immunocytochemistry

The monoclonal antibody to the human SOD1 enzyme was raised in the mouse and therefore immunocytochemical detection of mutant SOD1 in cultured cells required the use of a mouse-on-mouse (MOM) immunodetection kit (Vector Laboratories, Burlingame, CA, USA). Cultured cells were incubated in MOM blocking reagent (consisting of 2 drops of MOM blocking reagent in 2.5ml PBS) for 1 hour at room temperature. The blocking solution was then removed and the cells were rinsed twice with PBS for 2 minutes each. Subsequently, cells were incubated in MOM diluent (consisting of 600µl of MOM protein concentrate stock solution diluted in 7.5ml PBS) for 5 minutes. The excess diluent was then removed and the primary antibody, diluted to the appropriate concentration in MOM diluent, was applied for 30 minutes. Following removal of the primary antibody, cells were rinsed twice in PBS for 2 minutes each and then incubated in MOM biotinylated anti-mouse IgG reagent (consisting of 10µl stock MOM biotinylated anti-mouse IgG reagent diluted in 2.5mls MOM diluent) for 10 minutes. Cells were then twice rinsed in PBS and incubated in ABC solution (made up 30 minutes before application) for 1 hour at room temperature. Following removal of the ABC, the cells were rinsed three times in PBS for 5 minutes

each. Immunostaining was visualised using fast 3,3 diaminobenzadine tablets (Sigma-Aldrich, Poole, UK), and then cells were rinsed in PBS for 2 minutes, dehydrated through graded alcohols; 1 minute in 70% ethanol, 1 minute in 90% ethanol and 2 rinses in 100% ethanol for 1 minute each. Cells were then cleared by incubation in histoclear for 2 minutes each (2 rinses). Finally, the cultured cells mounted on coverslips were removed from their 24 well plates and mounted face down onto uncoated slides using DPX mounting solution.

2.10. Physiological assessment of muscle function

Physiological assessment of hindlimb muscle force was assessed *in vivo* in anaesthetised mice at either 120 days of age (**Chapter 4**) or 90 days of age (**Chapter 5**). The animals were anaesthetised with 4% chloral hydrate (1ml/100g body weight, injected intraperitoneally, i.p.; Sigma-Aldrich, Poole, UK) and once reflex action to painful stimuli was absent and the animals were deeply anaesthetised, they were prepared for assessment of hindlimb muscle function. The distal tendon of the tibialis anterior (TA) and extensor digitorum longus (EDL) muscle in both hindlimbs were exposed, dissected free from surrounding tissue and cut. The sciatic nerve was exposed, sectioned and all of its branches cut, apart from the deep peroneal nerve, which innervates the TA and EDL muscles. The hindlimbs of the animals were rigidly secured to the table with stainless steel pins and the distal tendons of the TA and EDL muscle attached to an isometric force transducer (Dynamometer UFI Devices, Welwyn Garden City, UK) via thread. Once attached, the length of each muscle was adjusted to obtain maximal twitch tension. Both muscles and nerves were kept moist with saline and experiments were carried out at room temperature.

2.10.1. Muscle force

Muscle contraction was elicited by stimulation of the sciatic nerve using square wave pulses of 0.02ms duration at a supramaximal voltage (10 volts) via platinum electrodes. Maximal tetanic contraction and hence muscle force was assessed by stimulating the sciatic nerves of both hindlimbs with trains of stimuli at increasing frequencies of 40, 80 and 100 Hz for a total duration of 450ms.

2.10.2. Motor unit number

To determine the number of functional motor units in each EDL muscle, stimuli of increasing intensity were applied to the sciatic nerve. This gradual increase in intensity resulted in stepwise increments in twitch tension due to the successive recruitment of motor axons. The motor unit traces were recorded on a storage oscilloscope (Tektronix, Beaverton, OR, USA) and a photograph was taken using a Tektronix oscilloscope camera (Beaverton, OR, USA). The number of increments was counted to give an estimate of the number of motor axons present in the nerve.

2.10.3. Fatigue test

At the end of the isometric tension recordings, the resistance of the EDL muscles to fatigue during repeated stimulation was tested. The EDL muscles were stimulated over a 3 minute period, at 40Hz for a duration of 250ms every second, and contractions were recorded on a pen recorder (Lectromed Multitrace 2, Letchworth Garden City, UK). The traces obtained illustrate the fatigue pattern of the muscle in response to sustained contraction. In addition, from such traces a fatigue index (F.I.), a measure of muscle fatigability, can be calculated. The F.I. represents the decline in EDL muscle force following repeated stimulation, thus quantifying the muscle fatigue, and is calculated as follows:

$$F.I. = \frac{\text{Initial tetanic tension} - \text{tetanic tension after 3 minute stimulation}}{\text{Initial tetanic tension.}}$$

A muscle that is fatigue resistant will have an F.I. value close to 0, whereas a muscle that is fatiguable during sustained contraction will have an F.I. value close to 1.0.

2.10.4. Muscle histochemistry

Following the physiological recordings, the soleus, TA and EDL muscles were removed from both hindlimbs and weighed. The muscles were mounted in an upright position in tissue-tek (Agar Scientific, Stanstead, UK) on a piece of cork board, and snap-frozen in isopentane cooled in liquid nitrogen. Serial transverse sections (10μM) were cut on a cryostat (Bright Instrument Company, Huntingdon, UK) and mounted onto poly-lysine coated slides (VWR International, Poole, UK). Muscle sections were stained for succinate dehydrogenase (SDH) activity to evaluate the oxidative capacity of the muscle fibres. According to the protocol detailed by Nachlas et al, (1957), a 'working solution' was prepared consisting of 0.1M phosphate buffer (pH 7.6), 1M sodium succinate, 15mM nitroblue-tetrazolium, 0.1M potassium cyanide and 10mM phenazine methosulphate. This solution was filtered and stored in a darkly coloured bottle to protect the photosensitive elements from sunlight. To ensure maximal staining, the muscle sections and a small volume of the 'working solution' were incubated separately at 37°C for approximately 20 minutes. Subsequently the sections were exposed to the 'working solution' and incubated at 37°C for a further 5 minutes to develop the SDH stain. Sections were then rinsed in 0.9% saline and dehydrated by washing in alcohol of increasing concentration (70% acetone for 1 minute, 90% acetone for 1 minute and then 2 rinses in 100% ethanol for 2 minutes each). Finally, the sections were cleared in

histoclear (2 rinses for 2 minutes each) and then coverslips were mounted onto the sections using DPX mounting solution.

2.10.5. Motoneuron survival

In order to evaluate the survival of motoneurons as a consequence of the experimental conditions as detailed in this Thesis, the number of motoneurons in the sciatic pool of the lumbar spinal cord was counted. Animals were terminally anaesthetised with pentobarbitone (140mg/kg i.p.) and on cessation of reflex to painful stimuli were perfused transcardially with 0.9% NaCl and then 4% PFA. Once fixed, the spinal cords were removed and the lumbar regions (L2-L6) were post-fixed for 4-6 hours in the same fixative and then cryoprotected in sucrose (30% in PBS) overnight at 4°C.

Serial transverse sections (20μm) of lumbar spinal cord were cut on a cryostat, mounted onto poly-lysine coated slides and stained with gallocyanin, a Nissl stain (Cullings, 1963). The sections were then dehydrated in increasing concentrations of alcohol, cleared in histoclear and then coverslips were mounted onto the slides using DPX as a mounting solution. The number of surviving motoneurons in the sciatic motor pool was assessed by counting the number of Nissl-stained motoneurons in every third spinal cord section in order to avoid counting the same cell twice in consecutive sections, using a light microscope (Leica DMR). For each animal, 60 spinal cord sections were assessed. Only large polygonal neurons with a distinguishable nucleus and nucleolus, visible at high magnification were included in the counts. This method of counting has previously been used to assess motoneuron survival (White et al., 2000).

2.10.6. Statistical analysis

Statistical significance between the experimental groups was assessed either using a Mann-Whitney U test or a one-way analysis of variance (ANOVA), incorporating a Student Neuman Keuls multiple comparisons test using Sigma Stat (version 2.03, Erkrath, Germany). Significance was set at $p < 0.05$.

2.11. Transfection of primary cells using lentiviral vectors

The lentiviral vectors were generated at and supplied by Oxford Biomedica, Oxford, UK. At 1 DIV, mixed ventral horn cultures were incubated with VSV-G pseudotyped EIAV vectors encoding either GFP, lacZ, shRNA to mutant SOD1 or an empty vector. The volume of virus added to each well of a 24 well plate ($5x10^5$ cells), was calculated according to the following equation:

$$\text{Volume} = \frac{\text{Multiplicity of infection (MOI)} \times \text{Number of cells}}{\text{Titre}}$$

The viral titre ranged from $5 \times 10^8 - 1 \times 10^9$ transducing units/ml, and was consistent within each viral batch. The MOI represents the average number of phage particles that infect a single cell. To optimise transfection, 6 different MOI: 0.25, 0.5, 0.75, 1, 2.5 and 5; were tested using EIAV vectors encoding lacZ and the transfection efficiency for each MOI was calculated as described below in **Chapter 2.12**. The volume of virus required was diluted in complete neurobasal medium (as described in **Chapter 2.5**) and added to the cells via media replacement. Cells were incubated with virus for 5 hours at 37°C in a 5% CO_2 humidified incubator and then the media was replaced with fresh complete neurobasal media. Cells were left for a further 7DIV before processing.

2.12. Calculation of transfection efficiency

Initially, primary mixed ventral horn cultures were transfected using lentiviral vectors encoding lacZ to calculate the transfection efficiency. Transfection efficiency was calculated by counting the number of motoneurons in which β-galactosidase (the lacZ gene product) had mediated the hydrolysis of an X-gal stain to form a blue product, therefore indicating successful transfection. Therefore at 7DIV, primary mixed ventral horn cultures were fixed in 4% PFA for 10 minutes and then rinsed twice in PBS. The cells were then incubated in a sufficient amount of staining solution (comprising 25µl of 400mM potassium ferricyanide, 25µl of 400mM potassium ferrocyanide, 25µl of 200mM magnesium chloride and 125µl X-gal [20mg/ml] in a total volume of 2.5ml PBS) to cover the cells and left overnight at 37°C. Following removal of the staining solution, cells were fixed for 30 minutes in 4% PFA and then rinsed twice in PBS before mounting face down onto coverslips using citifluor as a mountant. The number of motoneurons successfully transfected was expressed as a percentage of the total number of motoneurons present.

2.13. Protein extraction

In order to evaluate the effect of the lentiviral vector encoding siRNA targeted to mutant SOD1, protein was extracted from transfected cells and a Western blot run to determine the levels of mutant SOD1 protein remaining. The protein extraction was performed at the Institute of Neurology and the protein samples sent to Oxford Biomedica where the Western blots were carried out.

To extract the protein from cultured mixed ventral horn cells, the media was first aspirated and the cells were rinsed in PBS. Following aspiration of the PBS, 200µl of lysis buffer (consisting of 20mM Tris-HCl pH7.5, 10mM EDTA, 1mM EGTA, 100mM

NaCl and 1% TritonX-100 in PBS), supplemented with 0.012µl proteinase inhibitor cocktail (all Sigma-Aldrich, Poole, UK), was added to each well of a 24 well plate for approximately 1 minute. The coverslips were then gently scraped to dislodge the lysed cells and the supernatant was collected into an RNAse free eppendorf and stored at –80°C prior to transfer to Oxford Biomedica. Equal amounts (10µg) of each protein sample were fractionated by SDS-PAGE. Following transfer onto a nitrocellulose membrane (Amersham Biosciences, Buckinghamshire, UK) blots were probed with rabbit anti-human SOD1 antibody (1:1000; Santa Cruz Biotechnology, Santa Cruz, CA, USA) or rabbit polyclonal anti α-actin antibody (1:1000, Sigma-Aldrich, Poole, UK) followed by a horseradish peroxidase-conjugated secondary antibody (Dako, Glostrup Denmark). Blots were developed using ECL reagent (Amersham Biosciences, Buckinghamshire, UK) and band area quantified using Image J software (NIH, Bethesda, MA, USA).

CHAPTER 3

THE INFLUENCE OF MUTANT SOD1 EXPRESSION IN ASTROCYTES ON MOTONEURON PROPERTIES IN AN *IN VITRO* MODEL OF ALS

3.1. INTRODUCTION

3.1.1. Physiological function of astrocytes in the CNS

In the vertebrate CNS, glial cells are subdivided into two distinct classes: microglia and macroglia. Microglia are macrophage-like cells that are mobilised after injury, infection or disease and have a phagocytic function. Macroglial cells consist of oligodendrocytes, which, similar to Schwann cells that are present in the periphery, function to myelinate neurons, and astrocytes, the 'supporting cells' of the CNS, the functions of which will be discussed below.

In the mature CNS, astrocytes form an interconnecting network through gap junction communication. Gap junctions consist of two hemi-channels, each comprised of a hexagonal assembly of connexin proteins that are inserted in each glial membrane and form hydrophobic pores. Gap junctions allow the transport of ions and small molecules, including signalling molecules and various metabolites, between neighbouring cells (reviewed in Giaume & McCarthy, 1996). Astrocytic processes also make contact with both blood capillaries and numerous neurons, permitting additional intercellular trafficking (reviewed in Araque et al., 2001). Furthermore, direct contact with astrocytes is necessary for the formation of tight junctions between endothelial cells, which forms the basis of the blood brain barrier. Tight junctions occlude the intercellular spaces between endothelial cells rendering the brain capillaries highly impermeable (Tao-Cheng et al., 1987).

3.1.2. Neuronal-astrocyte interaction

Initially astrocytes were thought to be passive, supporting cells in the CNS, the so called nerve "glue" (Virchow, 1958). However, there is now substantial evidence to suggest that astrocytes provide metabolic and trophic support to neurons. Furthermore, evidence

of bidirectional communication between neurons and astrocytes and their close spatial association indicates that astrocytes form an integral component of the synapse in that they act to modulate both neuronal activity and synaptic transmission (reviewed in Vernadakis, 1996; Kirchoff et al., 2001).

3.1.2.1. Neurite outgrowth

There is both *in vitro* and *in vivo* evidence to suggest that during development astrocytes are involved in axonal migration and neurite outgrowth. Astrocytes secrete a variety of growth factors, cytokines, proteases and protease inhibitors, with expression varying depending on developmental stage and the extracellular environment (Eddleston & Mucke, 1993; Mizuno et al., 1994). Furthermore, astrocytes express numerous cell adhesion molecules, including integrins, N-CAM, N-cadherin and L1 glycoprotein (Tomaselli et al., 1988; Matsunaga et al., 1988; Doherty et al., 1990, 1991; Williams et al., 1992). Astrocytes also produce various extracellular matrix molecules, thereby encouraging specific cellular interactions (Sanes, 1989; Venstrom & Reichardt, 1993; Letourneau et al., 1994). However, there is also a subpopulation of astrocytes that are restrictive to neurite outgrowth and exert axonal guidance through the formation of inhibitory boundaries, which are impenetrable to axons (Steindler et al., 1990). This is achieved by the production of non-permissive extracellular matrix molecules, such as tenascin and chondroitin sulphate proteoglycan (Snow et al., 1990; reviewed in Powell et al., 1997).

3.1.2.2. Metabolic support

The contact of astrocytic processes with both neurons and blood capillaries makes astrocytes an ideal intermediate for the provision of nutrients and other essential substances to neurons. Furthermore, the selective expression of certain metabolic

enzymes in astrocytes indicates a metabolic coupling between astrocytes and neurons. Indeed, in response to enhanced neuronal activity, glycogen stores in astrocytes are mobilised to provide glucose for neurons (Forsyth et al., 1996). Furthermore, the sodium-dependent uptake of glutamate by astrocytic transporters activates the Na^+/K^+ ATPase, stimulating glycolysis and the production of lactate, which can be used by neurons to maintain oxidative phosphorylation (Walz & Mukerji, 1988).

Neurons also rely on astrocytes for the provision of several essential precursors. For example, following uptake by astrocytic transporters, glutamate is metabolised to glutamine by glutamine synthetase, an enzyme selectively found in astrocytes and oligodendrocytes (Norenberg & Martinez-Hernandez, 1979; Tansey et al., 1991). Released glutamine is subsequently taken up by neurons and recycled to glutamate by the enzyme glutaminase (Kirchoff et al., 2001). Astrocytes also supply neurons with cysteine and glycine, which, together with glutamine, are essential for the synthesis of glutathione, therefore enhancing the antioxidant capacity of neurons (Dringen et al., 1999).

3.1.2.3. Modulation of neuronal activity and synaptic transmission

One of the primary functions of astrocytes is to maintain interstitial ionic homeostasis, in particular regulating the extracellular potassium concentration. Neuronal activity induces substantial alterations in the extracellular ionic concentration of potassium and protons, which can be detrimental to neuronal function if not regulated (Newman, 2003). Astrocytes are highly permeable to potassium and can therefore buffer changes in extracellular potassium in the synaptic cleft. Furthermore, cultured astrocytes express various ion channels and can therefore respond to changes in the extracellular ionic environment as a consequence of neuronal activity (Vernadakis, 1996).

The expression of neurotransmitter receptors on their plasma membrane provides further evidence that astrocytes are not simply a passive structure at the synapse. Activation of astrocytic ionotropic and metabotropic glutamate receptors for example, evokes an elevation in intracellular calcium levels in isolated brain slices (reviewed in Araque et al., 2001). This occurs primarily by the release of calcium from intracellular ER stores. Local elevations in astrocytic calcium levels can initiate calcium oscillations within the same cell (Pasti et al., 1997; Carmignoto, 2000) or can initiate a calcium wave that propagates to neighbouring astrocytes either by diffusion of sufficient concentrations of IP_3 through gap junctions or through the release of ATP, which can act on disconnected astrocytes (Cornell-Bell et al., 1991; Bruner & Murphy, 1993; Guthrie et al., 1999). Neuronal activity and subsequent astrocytic calcium signalling can regulate astrocyte communication either by short-term modulation of gap junction activity or long-term regulation of the expression of connexin proteins (Giaume & McCarthy, 1996).

Interestingly, in response to elevated astrocytic calcium, adjacent neurons *in vitro* show a similar increase in cytosolic calcium, an effect that is susceptible to blockade by glutamate receptor antagonists (Nedergaard, 1994; Hassinger et al., 1995; Pasti et al., 1997; Araque et al., 1998a). Indeed, cultured astrocytes have been shown to release glutamate in a calcium-dependent manner (Parpura et al., 1994). Therefore, astrocytes can potentially modulate the activity of distant synapses in addition to the active synapse through the propagation of calcium waves and the release of glutamate (Araque et al., 1999b). Astrocyte-mediated changes in neuronal calcium may influence calcium-dependent membrane transport mechanisms or the actions of metabolic or regulatory enzymes, with subsequent effects on ionic homeostasis or neurotransmitter metabolism and ultimately synaptic transmission (Araque et al., 2001).

Astrocytes can modulate synaptic transmission directly via glutamate release, which can activate postsynaptic neurons *in vitro*, eliciting a depolarising slow inward current, consequently regulating neuronal excitability (Araque et al., 1998a, 1999). Furthermore, astrocyte-derived glutamate can activate presynaptic metabotropic or ionotropic NMDA receptors subsequently depressing or enhancing neurotransmitter release, respectively (Araque et al., 1998a, 1998b). Similarly, astrocyte-derived ATP can exert stimulatory or inhibitory effects on neuronal activity (Newman, 2003). Interestingly, the extent of the astrocytic calcium response appears to be dependent on the frequency of presynaptic neuronal activity. This suggests that neuronal activity can actually regulate the extent of astrocyte-mediated modulation of synaptic transmission (Pasti et al., 1997).

Indirect modulation of synaptic transmission mediated by astrocytes occurs through the uptake of neurotransmitters and neuromodulators at the synapse, including glutamate, GABA and taurine. In most CNS regions, sodium-dependent glutamate uptake by the astroglial transporter, GLT-1 predominates (Tanaka et al., 1997), although the astroglial GLAST and the neuronal EAAC1 transporters also contribute (Rothstein et al., 1996). The uptake of glutamate into astrocytes provides a mechanism by which the action of glutamate is terminated, thereby preventing excess activation of synaptic glutamate receptors and further modulating synaptic transmission.

3.1.3. Role of astrocytes in neuronal injury

In response to a wide variety of neuronal insults, astrocytes proliferate and assume a hypertrophic morphology associated with alterations in gene expression, for example an increase in glial fibrillary acidic protein (GFAP) and vimentin expression (Ridet et al., 1997; John et al., 2003; Barbeito et al., 2004). Reactive changes in morphology are often accompanied by increased production of cytokines, growth factors, matrix

proteins, cell adhesion molecules, proteases and protease inhibitors (Ridet et al., 1997). The molecular signals that initiate reactive astrogliosis are largely undefined, although several cytokines have been implicated, including IL-1β, IFNγ, TGFβ$_1$ and TNFα (John et al., 2003). Indeed, injection of IL-1β into the CNS initiates reactive astrogliosis (Giulian et al., 1988), and in response to IL-1β astrocytes express various neurotoxic factors (Toulmond et al., 1996). Several growth factors are also implicated in the induction of reactive astrogliosis, including fibroblast growth factor-2 (FGF-2) and ciliary neurotrophic factor (CNTF), which promote morphological changes in cultured astrocytes and increase expression of GFAP (Perraud et al., 1988; Winter et al., 1995; Clatterbuck et al., 1996). However, the role of reactive astrocytosis is not fully clarified, therefore under certain circumstances reactive astrocytes may provide a permissive environment for regeneration. However, there is also evidence to suggest that astrocytosis plays an active role in neuronal degeneration (Ridet et al., 1997).

3.1.3.1. Evidence for a neuroprotective influence of reactive astrocytosis

Astrocytes have been shown to secrete various neurotrophins, including basic FGF, nerve growth factor, interleukin-6 (IL-6), and epidermal growth factor, all of which promote neuronal survival. Therefore reactive astrocytosis may actually encourage neuronal regeneration. In support of this possibility, ablation of reactive astrocytes enhances neuronal degeneration *in vivo* in response to a CNS stab injury (Bush et al., 1999). Furthermore, treatment with CNTF, an IL-6 analogue that induces astrogliosis and GFAP overexpression, can promote motoneuron survival *in vitro* (Winter et al., 1996; Albrecht et al., 2002). Similarly, induction of reactive astrogliosis via activation of the glial I_2-imidazoline receptor, protects motoneurons after axotomy, due to an associated up-regulation of GLT-1 and FGF-2 expression in astrocytes and motoneurons respectively (Casanovas et al., 2000). Indeed, functional astrocyte-induced

FGF-2 expression may exert neuroprotection via NMDA receptor suppression (Mattson et al., 1993) and increased expression of antioxidant enzymes (Mattson et al., 1995). Moreover, the up-regulation of astrocytic cell adhesion and extracellular matrix molecules will provide a suitable environment for regeneration (reviewed in Ridet et al., 1997). Indeed, following exposure to NO donors, astrocytes promote neuronal survival *in vitro* through a neurotrophic effect of the extracellular matrix molecules, fibronectin and laminin that maintain neuronal-astrocyte interaction (Tanaka et al., 1999).

Astrocytes have a higher oxidative capacity than neurons and therefore can scavenge ROS and other toxic metabolites produced by degenerating neurons (Slivka et al., 1987), thereby minimising the spread of neurodegeneration. Astrocytes are able to rapidly detoxify hydrogen peroxide via glutathione peroxidase (Dringen et al., 1998) or catalase (Desagher et al., 1996), and *in vitro* astrocytes protect neurons from NO-mediated toxicity by a glutathione-dependent mechanism (Chen et al., 2001). Astrocytes may also enhance the endogenous ability of neurons to protect against neurotoxic insults, for example by increasing the provision of antioxidant precursors. Furthermore, astrocytes can augment the heat shock response of neurons via the release and transfer of the cytoprotective heat shock protein, hsp70, to neurons (Tytell et al., 1986; Hightower & Guidon, 1989). Indeed, overexpression of Hsp70 can protect motoneurons *in vivo* after sciatic nerve crush (Kalmar et al., 2002).

A consequence of astrocyte proliferation may be enhanced glutamate uptake from the synaptic cleft. This function is vital to protect neurons from the excitotoxic effects of glutamate and the activation of downstream neurotoxic cascades (Choi, 1992). Indeed, a neuroprotective role of astrocytes has been shown in response to various excitotoxic

agents, an effect due at least partly to GLT-1-mediated uptake from the extracellular space (Sugiyama et al., 1989; Rosenberg et al., 1992; Rothstein et al., 1996).

3.1.3.2. Evidence for detrimental actions of reactive astrogliosis

There is, however, significant evidence to suggest that reactive astrocytes may actually play an active role in the induction of neuronal death. *In vitro*, resting astrocytes support neuronal growth in the absence of exogenous trophic factors. However, neuronal survival is reduced following the activation of astrocytes due to insufficient trophic support (Pehar et al., 2004). Moreover, ablation of GFAP-positive reactive astrocytes has been shown to enhance local neurite outgrowth *in vivo* following a CNS stab injury (Bush et al., 1999). Activation of astrocytes increases expression of the non-permissive molecules, GFAP and vimentin, suggesting a detrimental action of reactive astrocytes on neuronal regeneration (Emsley et al., 2004).

In addition to the trophic factors discussed in **Chapter 3.1.3.1.** activated astrocytes also release a variety of neurotoxic molecules. Pro-inflammatory cytokines, such as TNFα and IL-1β, can induce COX2 expression, via activation of the transcription factor NF-κB (Consilvio et al., 2004; Juttler et al., 2004). COX2 activation generates prostaglandins, including PGE_2, which may actually contribute to excitotoxicity by stimulating glutamate release (Drachman & Rothstein, 2000), and in addition releases reactive oxygen species (ROS), which may further propagate the inflammatory process (Consilvio et al., 2004).

Cytokine-mediated activation of inducible nitric oxide synthase (iNOS), the expression of which is restricted to astrocytes, may also contribute to neuronal degeneration. Under normal physiological conditions, NO functions as a neurotransmitter in the CNS

(Garthwaite et al., 1991; Moncada et al., 1991). However, inappropriate production of NO can induce neurotoxicity, although astrocyte viability, in contrast, appears unaffected by NO (Bolãnos et al., 1994; Stewart et al., 2000). High concentrations of NO can bind to complex IV and reversibly inhibit respiration (Brown & Cooper, 1994). Furthermore, peroxynitrite, generated via the reaction of NO with superoxide, can mediate irreversible inhibition of complexes I, II and II/III (Brookes et al., 1998; Stewart et al., 2000; Jekabsone et al., 2003). Inhibition of respiration induces mitochondrial depolarisation, which can subsequently lead to depletion of cellular ATP levels. NO may also initiate glutamate release, inducing excitotoxicity (Bal-Price & Brown, 2001). Furthermore, in models of NMDA receptor-mediated excitotoxicity, NO acts synergistically with elevated intracellular calcium to induce neuronal death *in vitro* (Hewett et al., 1994; Keelan et al., 1999; Comoletti et al., 2001; Solenski et al., 2003).

Glutamate uptake via astrocytic glutamate transporter proteins, GLT-1 and GLAST, represents another target for peroxynitrite-mediated damage (Trotti et al., 1996). Reduced expression or function of astrocytic transporters may have significant consequences for neuronal viability, as elevations in extracellular glutamate can mediate excitotoxic damage through sustained activation of neuronal glutamate receptors (Choi, 1992).

3.1.4. Involvement of astrocytes in ALS

3.1.4.1. Evidence for the involvement of astrocytes in ALS

The degeneration of upper and lower motoneurons in ALS is accompanied by profound astrocytosis in post-mortem human ALS tissue (Hirano, 1996; Schiffer et al., 1996; Hall et al., 1998). In mutant SOD1 mice reactive astrogliosis is evident from disease onset and increases steadily with disease progression (Hall et al., 1998; Levine et al., 1999;

Alexianu et al., 2001; Elliott et al., 2001). Reduced expression of the astroglial transporter protein GLT-1 in post-mortem spinal cord tissue from ALS patients, with an associated reduction in glutamate transport and corresponding elevation of CSF glutamate levels, indicates functional astrocytic deficits (Rothstein et al., 1991, 1992, 1995; Spreux-Varoquaux et al., 2002). Furthermore, a mutation in GLT-1 has been identified in one sALS patient, which reduces plasma membrane expression and glutamate uptake by the transporter (Trotti et al., 2001). Inclusions in astrocytes are one of the earliest pathological features seen in $SOD1^{G85R}$ mice, occurring before the appearance of symptoms, and are accompanied by reductions in GLT-1 expression by end-stage disease (Bruijn et al., 1997b; Rothstein et al., 2005). Moreover, increased nitrotyrosine immunoreactivity (Sasaki et al., 2001) and expression of poly (ADP-ribose) polymerase (PARP), an enzyme activated by DNA damage, are evident in astrocytes from mutant SOD1 mice, indicating that oxidative damage to astrocytes is occurring in ALS (Kim et al., 2003). Therefore alterations in non-neuronal cell functions are likely to contribute to ALS pathogenesis.

The generation of transgenic mice with the selective expression of mutant SOD1 in either motoneurons or astrocytes supports the proposal that ALS is a non-cell autonomous disorder. Expression of mutant $SOD1^{G86R}$ under the control of the GFAP promoter produces significant astrocytosis in transgenic mice, although to a lesser extent than in $SOD1^{G86R}$ mice in which mutant SOD1 is expressed ubiquitously. Furthermore, large ventral horn motoneurons display no significant morphological changes and do not undergo degeneration in these mice, therefore suggesting that mutant SOD1-expressing astrocytes alone do not mediate disease (Gong et al., 2000). However, selective neuronal expression of $SOD1^{G93A}$, using a NF-L chain promoter, similarly does not induce motoneuron degeneration in transgenic mice (Pramatarova et

al., 2001). A selective elevation of mutant $SOD1^{G93A}$ expression in postnatal motoneurons also has no influence on disease progression (Lino et al., 2001). This suggests that interaction between mutant SOD1-expressing neurons and mutant SOD1-expressing astrocytes is necessary for the development of ALS. Indeed, Ferri et al, (2004) demonstrated that for the induction of neuronal apoptosis in an *in vitro* co-culture model, the expression of mutant SOD1 in both neuroblastoma and glioblastoma cell lines is necessary. Moreover, the generation of chimeric mice, with varying expression of mutant and endogenous SOD1 (WT) in motoneurons and non-neuronal cells, further clarified the importance of the non-neuronal environment to disease progression (Clement et al., 2003). In these mice, the presence of WT non-neuronal cells significantly protects mutant SOD1 motoneurons from degeneration, whereas an environment of mutant SOD1-expressing non-neuronal cells induces the formation of ubiquitinylated intracellular aggregates in WT motoneurons (Clement et al., 2003). Together these findings provide definitive evidence that glial cells make a significant contribution to ALS pathogenesis.

The appearance of reactive astrocytosis coincidently with symptom onset in mutant SOD1 mice suggests that in ALS astrocyte activation occurs in response to neuronal degeneration, as a significant proportion of motoneurons have already been lost by the onset of disease symptoms (Chiu et al., 1995; Levine et al., 1999; Sharp et al., 2005). Activation of astrocytes in ALS may occur through the release of pro-inflammatory cytokines and free radicals by motoneurons and microglial cells (reviewed in Barbeito et al., 2004). Rao et al, (2003) suggested that ROS generated by damaged motoneurons could be released to exert oxidative damage on surrounding astrocytes. Indeed, exposure of astrocytes to peroxynitrite induces a phenotypic change that renders cultured astrocytes toxic to motoneurons (Cassina et al., 2002). Furthermore, Levine et

al, (1999) demonstrated that the processes of reactive astrocytes extend towards and wrap around degenerating motoneurons in $SOD1^{G93A}$ mice. This close spatial association combined with their extensive functional interaction provides a mechanism through which altered astrocytic function may actually actively participate in the process of neuronal degeneration (Levine et al., 1999).

3.1.4.2. Potential mechanisms of reactive astrocyte-induced toxicity in ALS

i) Production of pro-inflammatory molecules

In ALS, reactive astrocytes synthesise and secrete elevated levels of pro-inflammatory cytokines and ROS *in vitro*, which may act to propagate the inflammatory reaction via further recruitment and activation of astrocytes and microglia, thereby exerting neuronal damage (Levine et al., 1999; reviewed in Barbeito et al., 2004). Indeed, the expression of the pro-inflammatory marker COX2 and the transcription factor NF-κB are significantly increased in astrocytes in post-mortem spinal cord tissue from ALS patients (Migheli et al., 1997; Maihofner et al., 2003). COX2 activation induces the formation of prostaglandins such as PGE_2 that can stimulate the release of glutamate from astrocytes. Consistent with these findings it has been shown that selective COX2 inhibition protects motoneurons in organotypic spinal cord cultures from excitotoxic damage and extends the lifespan of $SOD1^{G93A}$ mice (Drachman & Rothstein, 2000, 2002; Pompl et al., 2002).

ii) Inducible NOS

In $SOD1^{G93A}$ mice, the expression and activity of iNOS is upregulated in astrocytes from an early symptomatic stage of disease and may contribute to disease propagation (Almer et al., 1999). Furthermore, the expression of mutant SOD1 induces activation of a glioblastoma cell line with an accompanying up-regulation of neuronal NOS (Ferri et

al., 2004). Astrocytes are relatively resistant to the toxic effects of NO (Bolanos et al., 1994). However, astrocyte-derived NO mediates motoneuron death *in vitro* (Cassina et al., 2002), possibly through irreversible damage to the mitochondrial electron transport chain (Brookes, et al., 1998; Stewart et al., 2000). Interestingly, Raoul et al, (2002) demonstrated that cultured motoneurons are selectively vulnerable to a subtype of Fas-mediated cell death that is enhanced by NO. Furthermore, expression of the $p75^{NTR}$ death receptor is upregulated in motoneurons in post-mortem spinal cord tissue from ALS patients (Seeburger et al., 1993) and activation, via NGF released by reactive astrocytes, initiates motoneuron death in a NO-dependent manner *in vitro* (Pehar et al., 2004). NO-mediated toxicity may involve the generation of peroxynitrite, which can exert substantial cellular damage, via nitration of tyrosine residues. Correspondingly, levels of 3-nitrotyrosine are elevated in motoneurons in post-mortem spinal cord tissue from sALS and fALS patients (Beal et al., 1997; Ferrante et al., 1997).

Peroxynitrite also exerts a dose-dependent inhibition of glutamate transporter activity (Trotti et al., 1996) and in *Xenopus* oocytes co-expression of GLT-1 with mutant SOD1, which may induce oxidative stress, inhibits glutamate transport (Trotti et al., 1999). Selective inhibition of the astrocytic GLT-1 transporter protein initiates motoneuron loss (Darman et al., 2004) and progressive paralysis in mice *in vivo* (Rothstein et al., 1996). Furthermore, in organotypic spinal cord cultures, chronic inhibition of glutamate transport induces selective motoneuron degeneration (Rothstein et al., 1993). Conversely, restoration of GLT-1 activity, either by pharmacological enhancement (Rothstein et al., 2005) or by introduction of glial progenitor cells overexpressing GLT-1, significantly increases motoneuron survival in this model (Maragakis et al., 2005). Elevated extracellular glutamate is hypothesised to contribute to ALS pathogenesis through the activation of neuronal glutamate receptors, as described in **Chapter**

1.3.4.2., although it may also induce astrocytic glutamate release (Levi et al., 1992), which will further exacerbate neuronal injury (Parpura et al., 1994).

3.1.4.3. Potential neuroprotective actions of reactive astrocytes in ALS

In contrast, an increase in motoneuron survival *in vivo* following peripheral nerve injury is shown in the presence of activated astrocytes, which up-regulate motoneuron FGF-2 expression (Casanovas et al., 2000). Furthermore, an increase in secretion of GDNF by reactive astrocytes exerts neuronal protection in co-cultures exposed to excitotoxic stimuli (Palantina et al., 2005).

3.1.5. Hypothesis to be tested

The majority of evidence suggests that the activation of astrocytes in the spinal cord contributes to motoneuron degeneration in ALS. To investigate the influence astrocytes may exert on motoneurons at a cellular level, a co-culture model was designed whereby WT or $SOD1^{G93A}$ motoneurons were co-cultured with WT or $SOD1^{G93A}$ astrocytes. The effect of expression of mutant SOD1 in astrocytes was then investigated on a variety of motoneuron responses under basal conditions and following excitotoxic stimuli, using confocal microscopy.

3.2. METHODS

3.2.1. Primary cultures

Primary astrocyte and motoneuron cultures were prepared as detailed in **Chapters 2.4** and **2.5** respectively. The genotype of each pup or embryo was determined prior to culturing, using PCR as described in **Chapter 2.3**, and the spinal cords were pooled according to genotype, either WT or $SOD1^{G93A}$, and each genotype was cultured separately. Astrocytes were maintained in a 37°C, 5% CO_2 humidified incubator for between 2 and 3 weeks until confluency was reached. Astrocytes were then placed in a 37°C environmental shaker and rotated at 160rpm for 18 hours in order to dislodge O2A progenitor cells and microglia (Robb & Conner, 1998). These cultures were then returned to the incubator for 7-10 days. After approximately 3 weeks *in vitro*, mixed ventral horn cells were plated onto the enriched astrocyte layers, as previously described in **Chapter 2.5**. Co-cultures were kept at 37°C in a 5% CO_2 humidified incubator for a minimum of 7 DIV before undergoing any imaging protocol or drug treatment.

3.2.2. Immunocytochemistry

Co-cultures were immunostained with a primary antibody to the human SOD1 enzyme (1:500; Sigma-Aldrich, Poole, UK). This antibody was raised in the mouse and therefore the mouse on mouse immunocytochemistry protocol was used, as detailed in **Chapter 2.9**. To determine the percentage of astrocytes within the enriched astrocyte layer, glial cultures were immunostained for GFAP (according to the protocol detailed in **Chapter 2.8**; 1:100; Chemicon) and DAPI (0.01%) and the percentage of DAPI stained, GFAP positive cells were calculated.

3.2.3. Dye loading

Co-cultured motoneurons (7-10 DIV) and astrocytes were mounted in custom built imaging chambers and bathed in standard recording medium (RM), as detailed in **Chapter 2.6**. **Table 2.2** details the loading procedure for the fluorophores used in this chapter. All experiments were performed at room temperature.

3.2.4. Confocal imaging

Dye-loaded cells were placed onto the microscope stage and the microscope optics were configured according to the fluorophores used, as detailed in **Table 2.3**. Suitable dichroic mirrors were used for each fluorophore in order to separate the excitation from the emission signal. Detector gain, amplifier offset and amplifier gain were maintained constant throughout an experimental series. In contrast, the laser power was adjusted to optimise the signal, as the linear relationship between laser power and fluorescent intensity allowed correction for changes in laser power, which was maintained between 0.05% and 1% of the total laser output. For the majority of experiments the pinhole was opened to a confocal thickness of approximately 2μM to optimise light collection. However, the pinhole was opened fully in experiments in which superoxide sensing fluorophore, HEt, was used or if NADH autofluorescence was measured.

Images were acquired every 30 seconds prior to drug addition, to minimise photodamage. Drugs were made up in 0.5ml aliquots of RM and applied by means of RM replacement. The drugs applied and their working concentrations are listed in **Table 3.1**. Following drug addition the scan interval was reduced to 0 seconds to allow detailed analysis of the response to drug addition. After 5 minutes of drug incubation, a 30 second interval between scans was re-introduced to minimise photodamage. Each signal was detected by a photomultiplier tube, after passing through an appropriate

Table 3.1 – Concentrations of drugs used in imaging experiments

Drug used	Concentration	Drug Action
Kainate	100μM	Kainate receptor agonist
Glutamate	40μM	Glutamate receptor agonist
Carbonyl cyanide p-trifluoromethoxyphenyl hydrazone (FCCP)	1μM	Mitochondrial uncoupler (proton ionophore)
Cyanide	1mM	Inhibitor of complex IV
Rotenone	20μM	Inhibitor of complex I
MK-801	20μM	NMDA receptor antagonist
CNQX	20μM	AMPA/KA receptor antagonist
MCPG	1mM	Metabotropic glutamate receptor antagonist

MK-801 - (5R,10S)-(+)-5-Methyl-10,11-dihydro-5H-dibenzo [a,d] cyclohepten-5,10-imine hydrogen maleate

CNQX – 6-cyano-2,3-dihydroxy-7-nitro-qunioxaline.

MCPG - +(RS)-α-methyl-4-carboxyphenylglycine

bandpass or longpass filter, as detailed in **Chapter 2.6.2**. Unless otherwise stated images were acquired using the x40 objective lens.

3.2.5. Imaging using the interline-transfer cooled CCD camera

Cells loaded with fura 2-FF according to **Table 2.2** were imaged using an interline-transfer cooled CCD camera, as described in **Chapter 2.6.2.ii**. Sequential excitation of cells at 340nm and 380nm, which corresponds to the excitation of calcium-bound and calcium-free fura 2-FF, allows the ratiometric measurements of fura 2-FF fluorescence. Data were acquired every 10 seconds and cells were protected from phototoxicity by interposing a computer-controlled shutter in the light path between exposures.

3.2.6. Image analysis

Images were collected using Zeiss 'LSM' software or Kinetic Imaging 'Acquisition Manager' for confocal and CCD microscopy respectively, and analysed using Lucida version 5.0 image analysis software as described in **Chapter 2.6.3**. Experiments to investigate the resting mitochondrial membrane potential were analysed using Metamorph software (Universal Imaging Corporation, Downingtown, PA, USA), as described in **Chapter 2.6.3**. At least 3 experiments were performed for each experimental parameter, using co-cultures prepared on different days.

To calculate the extent of mitochondrial membrane potential ($\Delta\Psi_m$) depolarisation, the TMRM data was normalised, whereby the resting $\Delta\Psi_m$ was given a value of 1 and the minimum $\Delta\Psi_m$ attained after the addition of the mitochondrial uncoupler, FCCP, was given a value of 0. Normalisation was carried out to account for the variation in the resting $\Delta\Psi_m$ and allowed a more comprehensive evaluation of $\Delta\Psi_m$ depolarisation.

3.2.7. Motoneuron survival *in vitro*

At 7-10 DIV, cultured motoneurons were divided into five treatment groups: no treatment, 100μM AMPA (excitotoxic agent), 200μM AMPA, 100μM hydrogen peroxide (H_2O_2; inducer of oxidative stress) or 200nM staurosporine (STN; inducer of apoptosis). Treatment was implemented for 24 hours and the effect of treatment was assessed using the Trypan Blue exclusion method, as described in **Chapter 2.7**. The cultures were then fixed using 4% PFA and immunostained for MAP-2, a pan-neuronal marker. Motoneurons surviving were subsequently identified according to morphological criteria:

i) a cell body diameter ≥ 15μm

ii) the presence of at least 3 neuritic processes.

.

3.2.8. Statistical analysis

Statistical significance between mean values or the slope of the fitted lines (depending on experiment) was assessed using a Mann-Whitney U test in Sigma Stat (version 2.03, Erkrath, Germany). Significance between baseline cytosolic and mitochondrial calcium levels was assessed using one way repeated measures ANOVA. Values are expressed as mean ± standard error of the mean (S.E.M). Significance was set at $p < 0.05$.

3.3. RESULTS

In this Chapter, a co-culture model of motoneurons and spinal cord astrocytes was developed to assess the influence of astrocytes on motoneuron degeneration in ALS. The effect of expression of mutant SOD1 in either motoneurons or astrocytes was evaluated on various cellular properties under both basal and excitotoxic conditions, using confocal microscopy in conjunction with a variety of fluorimetric indicators.

3.3.1. Co-culture immunocytochemistry

WT or $SOD1^{G93A}$ motoneurons were plated onto an enriched layer of either WT or $SOD1^{G93A}$ astrocytes and the identity of the cells in the differing co-culture conditions was confirmed by immunostaining at 7DIV. **Figure 3.1** shows examples of co-cultures immunostained for the human SOD1 antibody: **A,** WT neurons cultured on WT astrocytes (WTnWTa), **B**, SOD^{G93A} neurons on WT astrocytes (SODnWTa), **C**, WT neurons on $SOD1^{G93A}$ astrocytes (WTnSODa) and **D**, $SOD1^{G93A}$ neurons on $SOD1^{G93A}$ astrocytes (SODnSODa). The glial layer consisted of approximately 99% astrocytes and the identity of astrocytes was confirmed by GFAP immunoreactivity (data not shown). Characterisation of the co-cultures revealed that approximately 48% of the neuronal cells were motoneurons, as determined by immunostaining with the pan neuronal marker MAP-2, and morphological criteria as described in **Chapter 3.2.8.**.

3.3.2. The effect of expression of mutant SOD1 on resting cellular properties of motoneurons and astrocytes

A number of resting cellular properties were assessed at 7-10 DIV, in order to investigate the potential influence of astrocyte genotype, either WT or $SOD1^{G93A}$, on the cellular properties of both motoneurons and astrocytes in co-culture.

Figure 3.1 – Immunostaining of co-cultures with primary antibody to human SOD1

The photomicrographs show examples of the 4 different co-cultures stained with a primary antibody to human SOD1: (**A**) WT motoneurons on WT astrocytes (WTnWTa), (**B**) $SOD1^{G93A}$ motoneurons on WT astrocytes (SODnWTa), (**C**) WT motoneurons on $SOD1^{G93A}$ astrocytes (WTnSODa) and (**D**) $SOD1^{G93A}$ motoneurons on SOD^{G93A} astrocytes (SODnSODa). The arrow indicates a typical motoneuron identified according to the morphological criteria used in these experiments.

Scale bar = 50μm.

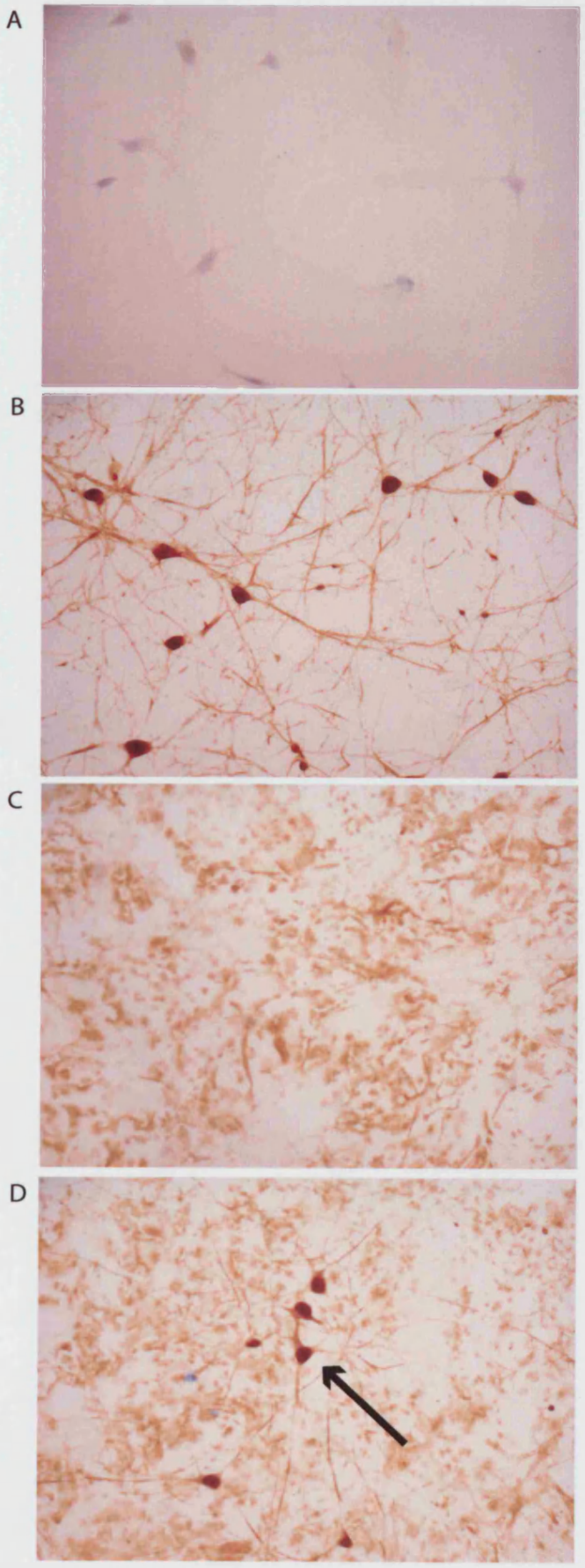
A
B
C
D

3.3.2.1. Resting cytosolic and mitochondrial calcium levels in motoneurons

Co-cultures were loaded with fura 2-FF, a low affinity, ratiometric calcium indicator, and the effect of expression of mutant SOD1 on basal cytosolic calcium levels ($[Ca^{2+}]_c$) in motoneurons was assessed. Resting $[Ca^{2+}]_c$ was expressed as a ratio between the fluorescence excited at 340nm and the fluorescence excited at 380nm. The mean basal $[Ca^{2+}]_c$ under differing co-culture conditions is summarised in **Table 3.2**. Interestingly, motoneurons from SODnSODa co-cultures ($n = 17$) had a significantly lower resting $[Ca^{2+}]_c$ compared to motoneurons from WTnWTa ($n = 18$), SODaWTn ($n = 19$) and WTnSODa ($n = 22$; $p < 0.015$) co-cultures. This finding was corroborated using fluo 4, a less quantitative, high affinity calcium indicator. The fluo 4 signal was also significantly lower, which was consistent with a lower resting $[Ca^{2+}]_c$, in motoneurons from SODnWTa and WTnSODa co-cultures than motoneurons from WTnWTa co-cultures ($p < 0.001$). However, this finding was not confirmed using the more quantitative indicator, fura 2-FF. These results indicated that the expression of mutant SOD1 protein in both motoneurons and astrocytes was required to lower $[Ca^{2+}]_c$. There were no significant differences in the resting $[Ca^{2+}]_c$ of astrocytes from any co-culture ($p > 0.2$).

Resting mitochondrial calcium levels ($[Ca^{2+}]_m$) were assessed using rhod 5N, a calcium indicator that accumulates in mitochondria, using a x63 oil immersion objective lens. Rhod 5N is sequestered into the mitochondria due to the electrochemical gradient and is then retained in the mitochondria following cleavage of the AM ester by mitochondrial esterases. Resting $[Ca^{2+}]_m$ values are summarised in **Table 3.2**. In contrast to the basal $[Ca^{2+}]_c$, resting $[Ca^{2+}]_m$ was significantly elevated in motoneurons from SODnSODa co-cultures ($n = 14$) compared to motoneurons from WTnWTa co-cultures ($n = 7$; $p < 0.005$). Interestingly, the resting $[Ca^{2+}]_m$ of motoneurons from SODnWTa ($n = 9$) and

Table 3.2 – Baseline levels of cytosolic and mitochondrial calcium in motoneurons

Cytosolic calcium levels ($[Ca^{2+}]_c$) were assessed in WT and $SOD1^{G93A}$ motoneurons cultured with either WT or $SOD1^{G93A}$ astrocytes using the ratiometric, low affinity calcium indicator, fura 2-FF. Resting $[Ca^{2+}]_c$ was expressed as a ratio between the fluorescence excited at 340nm and the fluorescence excited at 380nm and the mean values are summarised in the Table. The Table also shows the mean baseline $[Ca^{2+}]_c$ measured with fluo 4, a less quantitative fluorophore. Basal mitochondrial calcium levels ($[Ca^{2+}]_m$) were assessed using the cationic mitochondrial calcium indicator rhod 5N. The effects of expression of mutant SOD1 on the basal $[Ca^{2+}]_m$ in motoneurons are also summarised in the Table. Values represent the mean basal level ± standard error of the mean. *** $p < 0.005$ indicates a significant difference from WTnWTa. $^{+}$ $p < 0.005$ indicates a significant difference from SODnWTa. $^{\#}$ $p < 0.005$ indicates a significant difference from WTnSODa.

Cytosolic calcium		WTnWTa	SODnWTa	WTnSODa	SODnSODa
Motoneurons	**Fura 2-FF AM** ± S.E.M.	**0.483** ± 0.002	**0.475** ± 0.003	**0.481** ± 0.005	**0.455*** $^{+\#}$** ± 0.002
		n = 18	n = 19	n = 22	n = 17
	Fluo 4 AM (arbitrary units) ± S.E.M.	**2940** ± 92.46	**1756.4 ***** ± 45.94	**1113.2 ***** ± 30.79	**1216.1 ***** ± 32.2
		n = 44	n = 30	n = 17	n = 34
Mitochondrial Calcium					
Motoneurons	**Rhod 5N AM** (arbitrary units) ± S.E.M.	**305.9** ± 4.55	**437.9 ***** ± 18.68	**376.5 ***** ± 10.18	**497.3 *****$^{+}$** ± 9.71
		n = 7	n =9	n = 15	n = 14

WTnSODa (n = 15) co-cultures was also significantly higher than in WTnWTa co-cultures (n = 7; $p < 0.005$). Furthermore, motoneurons from SODnSODa co-cultures had a significantly elevated resting $[Ca^{2+}]_m$ compared to motoneurons from SODnWTa co-cultures ($p < 0.005$), indicating that the expression of mutant SOD1 protein in both astrocytes and neurons had a greater influence on resting $[Ca^{2+}]_m$ in motoneurons, although expression of mutant SOD1 protein in neurons alone did result in a significant elevation in $[Ca^{2+}]_m$ at rest.

3.3.2.2. Spontaneous calcium activity in co-cultured cells

Co-cultured cells were loaded with fluo 4 and the spontaneous calcium activity of both motoneurons and astrocytes was recorded for a minimum period of 5 minutes. Examples of typical traces from SODnSODa co-cultures are shown in **Figure 3.2** for **(A)** motoneurons and **(B)** astrocytes. A motoneuron or astrocyte was determined to show spontaneous calcium activity if a transient intracellular calcium spike reached a minimum amplitude of 150 arbitrary units (a.u.) in fluo 4 intensity during the recording, to firmly distinguish spontaneous calcium activity from background noise. This allowed quantification of the percentage of cells that showed spontaneous calcium activity, as shown in **Table 3.3**. $SOD1^{G93A}$ motoneurons showed an increase in spontaneous calcium activity compared to WT motoneurons. In contrast, $SOD1^{G93A}$ astrocytes had reduced spontaneous calcium activity compared to WT astrocytes and this reduction was enhanced if $SOD1^{G93A}$ astrocytes were cultured with $SOD1^{G93A}$ motoneurons.

3.3.2.3. Resting mitochondrial membrane potential

Co-cultures were loaded with TMRM, a highly lipid soluble, potentiometric indicator that has a single, delocalised positive charge and therefore becomes sequestered in mitochondria as a result of the electrochemical potential gradient between the cytosol

Figure 3.2 – Spontaneous calcium activity in co-cultured cells

Co-cultured were loaded with fluo 4 and the spontaneous calcium activity was recorded for a minimum period of 5 minutes. Typical traces from fluo 4 loaded (**A**) motoneurons and (**B**) astrocytes from SODnSODa co-cultures are illustrated. Each coloured trace represents the response from a single cell.

s = seconds

A

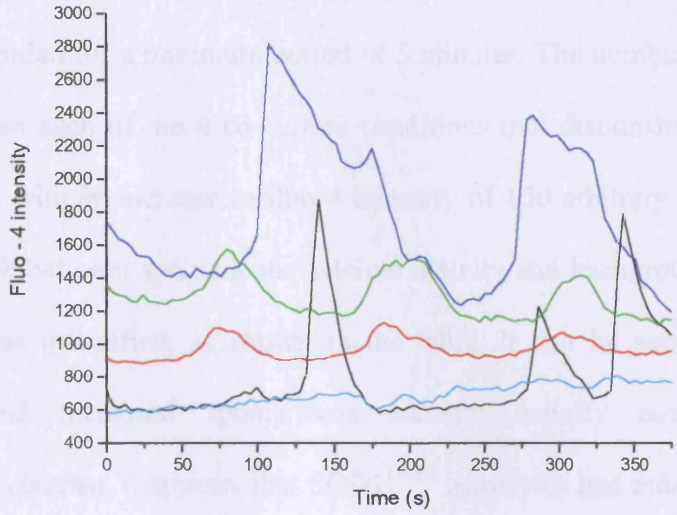
Fluo - 4 intensity
Time (s)
3000
2800
2600
2400
2200
2000
1800
1600
1400
1200
1000
800
600
400
0
50
100
150
200
250
300
350

B

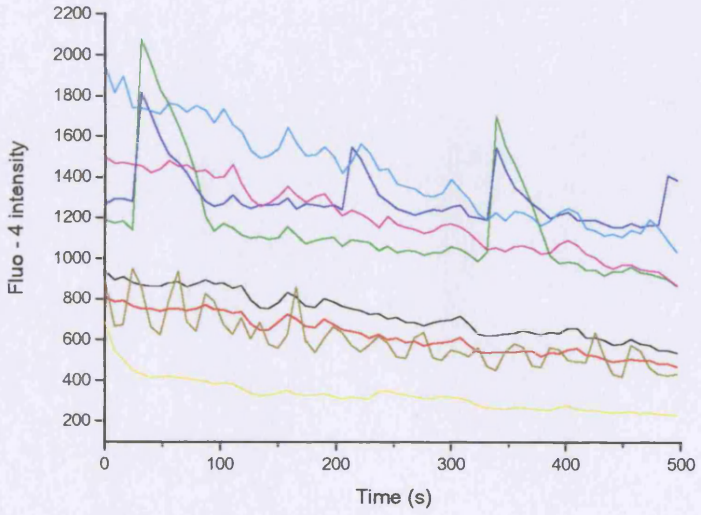
Fluo - 4 intensity
Time (s)
2200
2000
1800
1600
1400
1200
1000
800
600
400
200
0
100
200
300
400
500

Table 3.3 - Spontaneous calcium activity in co-cultured cells

The spontaneous calcium activity of motoneurons and astrocytes from fluo 4 loaded co-cultures was recorded for a minimum period of 5 minutes. The number of motoneurons or astrocytes from each of the 4 co-culture conditions that demonstrated spontaneous calcium activity, with an increase in fluo 4 intensity of 150 arbitrary units or more, to firmly distinguish between spontaneous calcium activity and background noise, during the recording was quantified, as shown in the table. It can be seen that $SOD1^{G93A}$ motoneurons had increased spontaneous calcium activity compared to WT motoneurons. In contrast, it appears that $SOD1^{G93A}$ astrocytes had reduced spontaneous calcium activity compared to WT astrocytes and this reduction was enhanced if $SOD1^{G93A}$ astrocytes were cultured with $SOD1^{G93A}$ motoneurons. Values represent the number of cells that show spontaneous calcium activity expressed as a percentage of the total number of cells from 3 different co-culture preparations. s = seconds.

	Motoneurons	Astrocytes
WTnWTa	**20.6%**	**71.4%**
SODnWTa	**31.1%**	**63.6%**
WTnSODa	**19.2%**	**69.6%**
SODnSODa	**36.8%**	**57.9%**

and mitochondria. Cells were imaged using a x63 oil immersion objective lens to obtain high spatial resolution, as shown in **Figure 3.3**. The mean resting mitochondrial membrane potential ($\Delta\Psi_m$), measured by TMRM signal, of motoneurons cultured under the different co-culture conditions is summarised in the bar chart shown in **Figure 3.4A**. Interestingly, both WT (n = 10) and $SOD1^{G93A}$ (n = 18) motoneurons co-cultured with $SOD1^{G93A}$ astrocytes had a significantly reduced resting $\Delta\Psi_m$ compared to either WT (n = 19) or $SOD1^{G93A}$ (n = 18) motoneurons co-cultured with WT astrocytes ($p < 0.005$). Therefore the TMRM signal of motoneurons in SODnSODa and WTnSODa cultures was 453.6 a.u. (± 65.7 S.E.M.) and 587.1 a.u. (± 219.8 S.E.M.) respectively compared to 2147.6 a.u. (± 392.8 S. E.M.) and 2294.2 a.u. (± 401.5) in WTnWTa and SODnWTa co-cultures at rest, respectively. The basal $\Delta\Psi_m$ of WT and $SOD1^{G93A}$ motoneurons cultured on WT astrocytes did not differ significantly ($p > 0.3$).

The resting $\Delta\Psi_m$ of astrocytes from SODnSODa co-cultures was also significantly reduced ($p < 0.01$) compared to WTnWTa or SODnWTa co-cultures. Therefore, as illustrated in **Figure 3.4B**, astrocytes from SODnSODa cultures had a resting TMRM signal of 388.8 a.u. (± 53.7) compared to 2930.5 a.u. (± 482.1) and 2528.9 a.u. (± 582.8) in astrocytes from WTnWTa and SODnWTa cultures respectively.

3.3.2.4. NADH autofluorescence

The functional operation of complex I in the mitochondrial electron transport chain relies on the transfer of electrons and protons from the TCA cycle to complex I via the pyridine nucleotide carrier, nicotinamide adenine dinucleotide (NADH). The reduced carrier, NADH, has an intrinsic autofluorescence. However, the transfer of electrons and protons to complex I oxidises NADH to NAD^+, which lacks autofluorescence. A change in fluorescence therefore indicates a shift in the balance between the reduced and

Figure 3.3 – Confocal image of a TMRM-loaded motoneuron cultured on an enriched astrocytic layer

The cationic fluorophore TMRM becomes partitioned into mitochondria due to the electrochemical potential gradient that exists between the cytosol and the mitochondria. The image was acquired on a Zeiss 510 CLSM confocal microscope using a x63 oil immersion objective lens. Scale bar = 8μm.

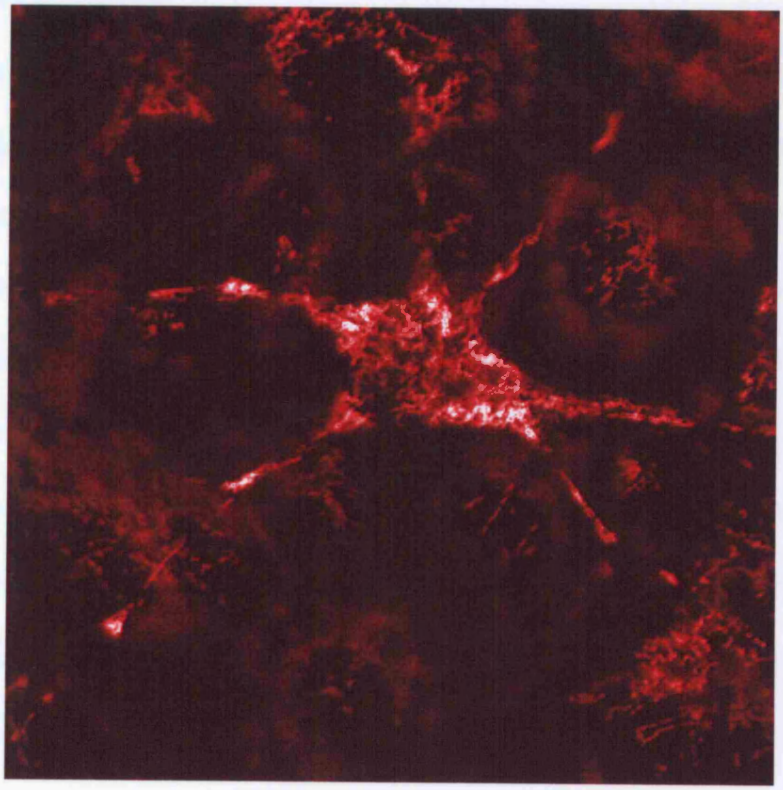

Figure 3.4 – The resting mitochondrial membrane potential of motoneurons co-cultured with astrocytes

The co-cultures were loaded with TMRM, a potentiometric indicator that becomes partitioned into mitochondria due to the electrochemical potential gradient that exists between the cytosol and the mitochondria. Images were acquired using a x63 oil immersion objective lens on a Zeiss 510 CLSM. A 'z' stack of images were taken thorough the co-culture and compressed to a single image with each pixel representing the average intensity of that point through the sample. The mean resting mitochondrial membrane potential ($\Delta\Psi_m$) from motoneurons is shown in **A**, and **B** shows the mean resting astrocytic $\Delta\Psi_m$. It can be seen that motoneurons cultured on $SOD1^{G93A}$ astrocytes had a significantly lower resting $\Delta\Psi_m$ compared to motoneurons cultured on WT astrocytes (**A**; $p < 0.005$). Similarly, the resting $\Delta\Psi_m$ of astrocytes from SODnSODa co-cultures was significantly reduced compared to astrocytes from co-cultures consisting of a WT astrocytic layer (**B**; $p < 0.01$). The values represent the mean resting $\Delta\Psi_m$, measured by TMRM signal, ± standard error of the mean. ** $p < 0.01$, *** $p < 0.005$ indicates a significant difference from motoneurons from both the WTnWTa and SODnWTa co-cultures.

A

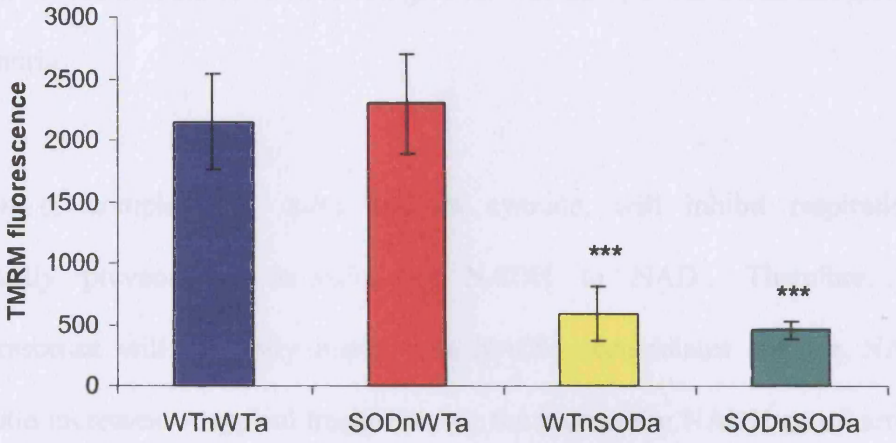
TMRM fluorescence
3000
2500
2000
1500
1000
500
0
***
***
WTnWTa
SODnWTa
WTnSODa
SODnSODa

B

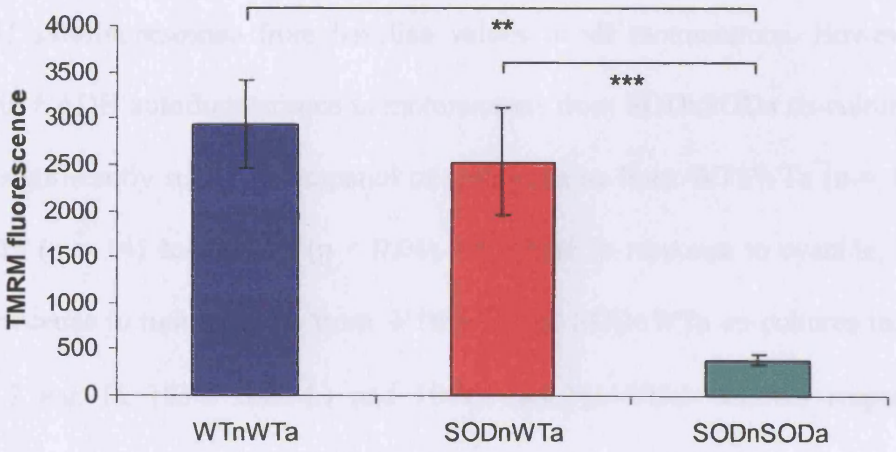
TMRM fluorescence
4000
3500
3000
2500
2000
1500
1000
500
0
**
***
WTnWTa
SODnWTa
SODnSODa

oxidised forms of the carrier. Manipulation of this system and measurement of the change in the redox state of NADH can give an indication of the metabolic state of the mitochondria.

Inhibition of complex IV, using sodium cyanide, will inhibit respiration and consequently prevent the oxidation of NADH to NAD^+. Therefore, NADH autofluorescence will generally increase as NADH accumulates and the NADH to NAD^+ ratio increases. A typical trace showing the increase in NADH autofluorescence in $SOD1^{G93A}$ motoneurons co-cultured with $SOD1^{G93A}$ astrocytes in response to cyanide is illustrated in **Figure 3.5A**. The change in NADH autofluorescence of motoneurons cultured on an enriched astrocytic layer, in response to cyanide application is shown in **Figure 3.5B**. The mean values shown in the bar chart represent the peak increase in autofluorescence, corrected for baseline values. Addition of cyanide induced an increase in NADH autofluorescence from baseline values in all motoneurons. However, the increase in NADH autofluorescence in motoneurons from SODnSODa co-cultures ($n = 10$) was significantly reduced compared to motoneurons from WTnWTa ($n = 13$) and SODnWTa ($n = 14$) co-cultures ($p < 0.04$). Therefore in response to cyanide, NADH autofluorescence in motoneurons from WTnWTa and SODnWTa co-cultures increased by 1092.7 a.u. (± 183.3 S.E.M.) and 1067.4 a.u. (± 205.3 S.E.M.) respectively, compared to an increase of only 463.4 a.u. (± 71.1 S.E.M.) in motoneurons from SODnSODa co-cultures. There was also a trend towards a lower increase in NADH autofluorescence in motoneurons from WTnSODa co-cultures (707.1 a.u. ± 177.0 S.E.M.; $n = 11$), although this did not reach statistical significance ($p > 0.1$). Baseline values did not differ significantly between experimental groups ($p > 0.1$).

Figure 3.5 – The mean increase in NADH autofluorescence of co-cultured motoneurons and astrocytes in response to the complex IV inhibitor cyanide

A typical trace of the increase in NADH autofluorescence in $SOD1^{G93A}$ motoneurons co-cultured with $SOD1^{G93A}$ astrocytes in response to cyanide is shown in **A**. The bar chart summarises the mean peak increase in NADH autofluorescence from baseline values in (**B**) motoneurons and (**C**) astrocytes in co-culture, following treatment with cyanide. All motoneurons, regardless of their own genotype or the genotype of their astrocytic layer, showed an increase in NADH autofluorescence in response to cyanide (**B**). However, the increase in NADH autofluorescence in motoneurons from SODnSODa co-cultures was lower compared to motoneurons co-cultured with WT astrocytes ($p < 0.04$). There was also a trend to a lower increase in NADH autofluorescence in motoneurons from WTnSODa co-cultures, but this did not reach significance. Similarly, in response to cyanide, the NADH autofluorescence was increased in all astrocytes (**C**). However, $SOD1^{G93A}$ astrocytes co-cultured with WT motoneurons demonstrated a lower increase following cyanide than astrocytes in the other co-cultures. Values represent the mean peak increase in NADH autofluorescence above baseline ± standard error of the mean. * $p < 0.05$.

A

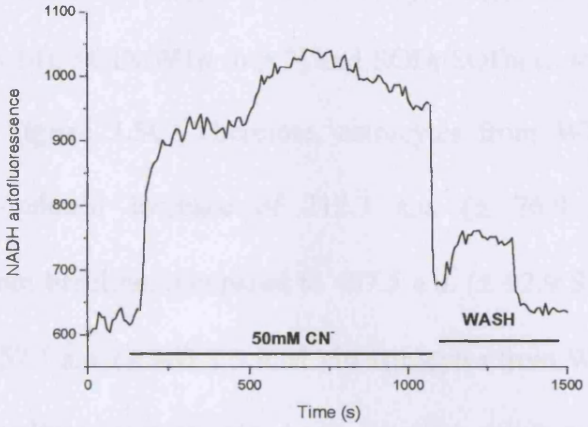
NADH autofluorescence
1100
1000
900
800
700
600
50mM CN⁻
WASH
0
500
1000
1500
Time (s)

B

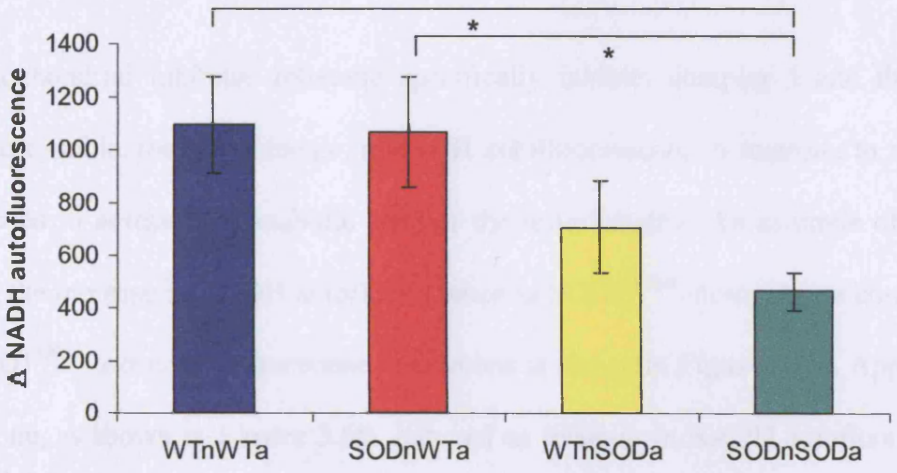
Δ NADH autofluorescence
1400
1200
1000
800
600
400
200
0
*
*
WTnWTa
SODnWTa
WTnSODa
SODnSODa

C

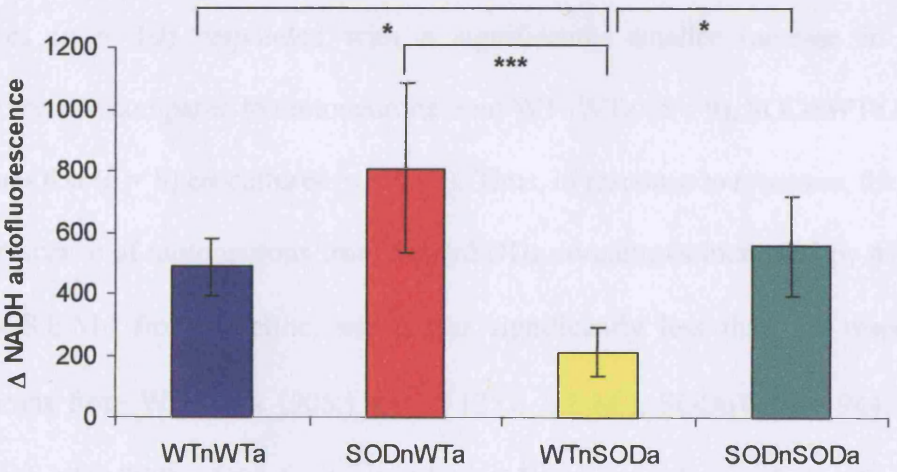
Δ NADH autofluorescence
1200
1000
800
600
400
200
0
*
***
*
WTnWTa
SODnWTa
WTnSODa
SODnSODa

Astrocytes from WTnSODa (n = 13) co-cultures exhibited significantly less of an increase in NADH autofluorescence, in response to cyanide, in comparison to astrocytes from WTnWTa (n = 14), SODnWTa (n = 7) and SODnSODa (n = 11) co-cultures ($p < 0.05$) as shown in **Figure 3.5C**. Therefore, astrocytes from WTnSODa co-cultures showed a cyanide-induced increase of 212.3 a.u. (± 76.9 S.E.M.) in NADH autofluorescence, from baseline, compared to 487.5 a.u. (± 92.9 S.E.M.), 808.7 a.u. (± 275.5 S.E.M.) and 557.1 a.u. (± 163.2 S.E.M.) in astrocytes from WTnWTa, SODnWTa and SODnSODa co-cultures respectively. Again, baseline values were not different ($p > 0.08$).

The mitochondrial inhibitor rotenone specifically inhibits complex I and therefore, similar to cyanide, the peak change in NADH autofluorescence in response to rotenone can be used to assess the metabolic state of the mitochondria. An example of a trace showing the increase in NADH autofluorescence in $SOD1^{G93A}$ motoneurons co-cultured with $SOD1^{G93A}$ astrocytes in response to rotenone is shown in **Figure 3.6A**. Application of rotenone, as shown in **Figure 3.6B**, induced an increase in NADH autofluorescence from baseline in motoneurons from all 4 co-culture conditions. However, consistent with the data recorded following exposure to cyanide, motoneurons from SODnSODa co-cultures (n = 10) responded with a significantly smaller increase in NADH autofluorescence compared to motoneurons from WTnWTa (n = 9), SODnWTa (n = 10) and WTnSODa (n = 8) co-cultures ($p < 0.03$). Thus, in response to rotenone, the NADH autofluorescence of motoneurons from SODnSODa co-cultures increased by 419.3 a.u. (± 131.4 S.E.M.) from baseline, which was significantly less than the response of motoneurons from WTnWTa (905.1 a.u. ± 125.6 S.E.M.), SODnWTa (1944.7 a.u. ± 323.8) and WTnSODa (903.1 a.u. ± 136.9 S.E.M.) co-cultures. Interestingly, the increase in NADH autofluorescence of motoneurons from SODnWTa co-cultures was

Figure 3.6 – The mean increase in NADH autofluorescence of co-cultured motoneurons in response to the complex I inhibitor rotenone

An example of a trace showing the increase in NADH autofluorescence in $SOD1^{G93A}$ motoneurons co-cultured with $SOD1^{G93A}$ astrocytes in response to rotenone is shown in **Figure 3.6A**. The bar chart (**B**) summarises the mean peak increase in NADH autofluorescence from baseline values in motoneurons cultured under the 4 different co-culture conditions, following treatment with rotenone. All motoneurons, regardless of their own genotype or the genotype of their astrocytic layer, showed an increased NADH autofluorescence in response to rotenone. However, the increase in NADH autofluorescence in motoneurons from SODnSODa co-cultures was significantly lower compared to motoneurons from all other co-cultures ($p < 0.03$). However, in contrast $SOD1^{G93A}$ motoneurons cultured with WT astrocytes showed a significantly greater increase in NADH autofluorescence in response to rotenone ($p < 0.03$). Values represent the mean peak increase in NADH autofluorescence above baseline ± standard error of the mean. * $p < 0.05$, ** $p < 0.01$, *** $p < 0.005$.

A

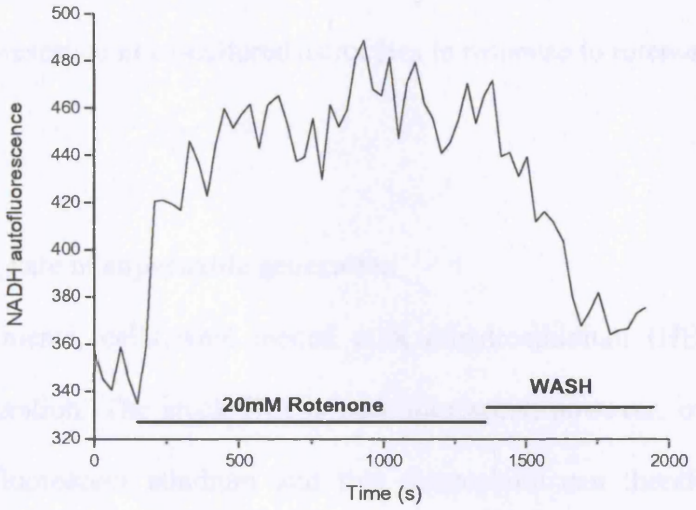
NADH autofluorescence
500
480
460
440
420
400
380
360
340
320
0
500
1000
1500
2000
Time (s)
20mM Rotenone
WASH

B

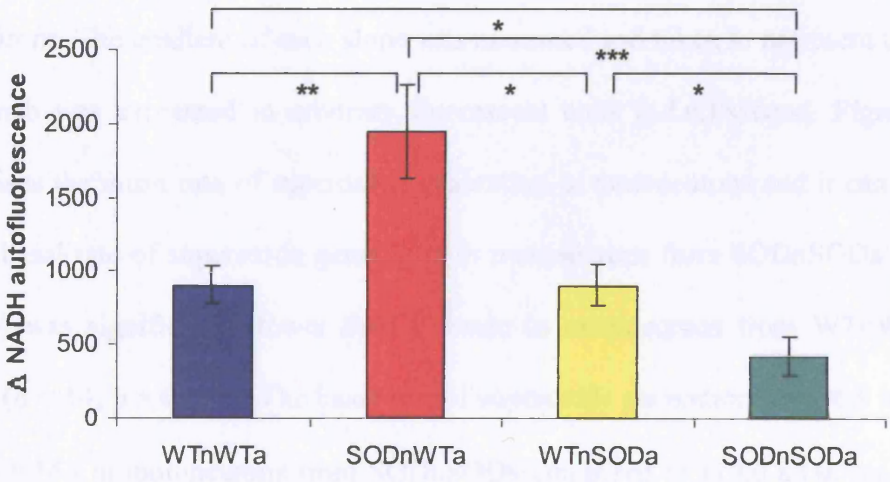
Δ NADH autofluorescence
2500
2000
1500
1000
500
0
**
*
***
*
*
WTnWTa
SODnWTa
WTnSODa
SODnSODa

significantly greater than that of motoneurons from WTnWTa and WTnSODa ($p < 0.03$) co-cultures. In contrast, there were no significant differences in the change in NADH autofluorescence in co-cultured astrocytes in response to rotenone ($p > 0.3$; data not shown).

3.3.2.5. Resting rate of superoxide generation

In these experiments, cells were loaded with dihydroethidium (HEt) a marker of superoxide generation. The stock HEt is non-fluorescent, however, oxidation of HEt generates the fluorescent ethidium and this fluorophore can therefore be used to compare rates of superoxide generation.

The basal rate of HEt oxidation in the different co-cultures was measured over a 15 minute period. **Figure 3.7A** shows typical traces from motoneurons in WTnWTa co-cultures taken from an experiment measuring the basal rate of superoxide production in motoneurons. The gradient of each slope was measured and taken to represent the basal rate, which was expressed in arbitrary fluorescent units (a.f.u.)/second. **Figure 3.7B** summarises the mean rate of superoxide generation in motoneurons and it can be seen that the basal rate of superoxide generation in motoneurons from SODnSODa cultures ($n = 20$) was significantly lower than the rate in motoneurons from WTnWTa co-cultures ($n = 14$; $p = 0.032$). The basal rate of superoxide generation was 86.9 a.f.u./sec ($\pm$ 9.8 S.E.M.) in motoneurons from SODnSODa compared to 119.0 a.f.u./sec ($\pm$ 50.0 S.E.M.) in motoneurons from WTnWTa c-cultures. The basal rate in motoneurons from SODnWTa ($n = 17$) and WTnSODa ($n = 15$) co-cultures did not differ significantly from WTnWTa ($p > 0.2$).

Figure 3.7 – The basal rate of superoxide generation in both WT and SOD1^{G93A} motoneurons co-cultured with either WT or SOD1^{G93A} astrocytes

The co-cultures were loaded with dihydroethidium (HEt), a non-fluorescent indicator that becomes fluorescent on oxidation to ethidium, and can therefore be used to compare rates of superoxide generation. The basal rate of superoxide generation was measured in motoneurons over a 15 minute period and a typical trace from WT motoneurons co-cultured with WT astrocytes is shown in **A**. The gradient of each slope was measured and taken to represent the rate of superoxide generation (expressed in arbitrary fluorescent units/second). The bar chart (**B**) summarises the mean rates of superoxide production under the different co-culture conditions. Motoneurons from SODnSODa co-cultures (n = 20) had a significantly reduced rate of superoxide generation under basal conditions ($p = 0.032$), compared to motoneurons from WTnWTa (n = 14) co-cultures, whereas the rate in motoneurons from SODnWTa (n = 17) or WTnSODa (n = 15) co-cultures was unchanged. Values represent the mean basal rate ± standard error of the mean. * $p < 0.05$.

A

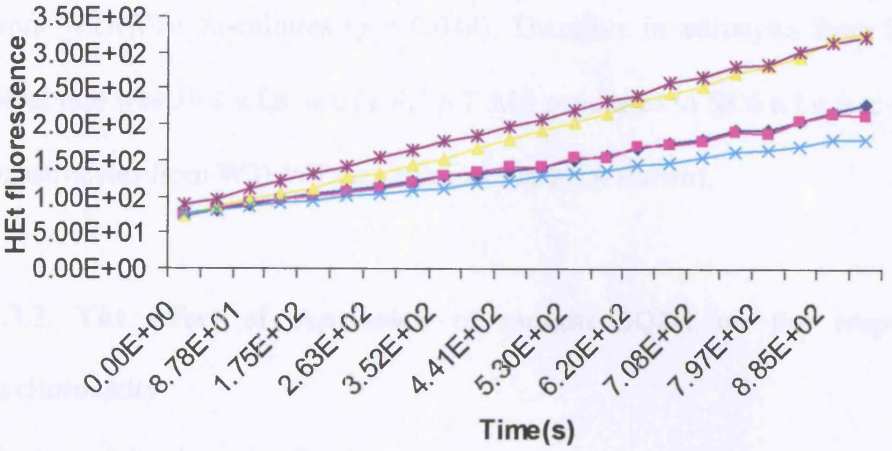
3.50E+02
3.00E+02
2.50E+02
2.00E+02
1.50E+02
1.00E+02
5.00E+01
0.00E+00
HEt fluorescence
0.00E+00
8.78E+01
1.75E+02
2.63E+02
3.52E+02
4.41E+02
5.30E+02
6.20E+02
7.08E+02
7.97E+02
8.85E+02
Time(s)

B

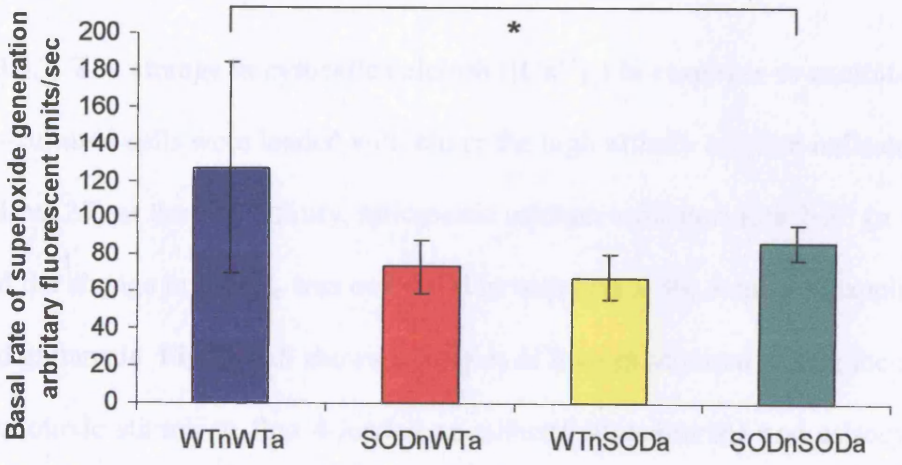
Basal rate of superoxide generation arbitary fluorescent units/sec
200
180
160
140
120
100
80
60
40
20
0
*
WTnWTa
SODnWTa
WTnSODa
SODnSODa

Similar to motoneurons, the astrocytes from SODnSODa cultures also had a significantly reduced basal rate of superoxide generation compared to the astrocytes from WTnWTa co-cultures ($p = 0.044$). Therefore in astrocytes from SODnSODa the basal rate was 39.4 a.f.u./sec (± 8.5 S.E.M.) compared to 58.6 a.f.u./sec (± 29.6 S.E.M.) in astrocytes from WTnWTa co-cultures (data not shown).

3.3.3. The effect of expression of mutant SOD1 on the response to acute excitotoxicity

Excitotoxicity is one of the neurotoxic mechanisms proposed to contribute to the pathogenesis of ALS, as described in **Chapter 1.3.4.2.**. Therefore in order to further evaluate the influence of astrocytes, the effect of expression of mutant SOD1 on the response of motoneurons under acute excitotoxic conditions was investigated next.

3.3.3.1. The change in cytosolic calcium ($[Ca^{2+}]_c$) in response to excitotoxic stimuli

Co-cultured cells were loaded with either the high affinity calcium indicator, fluo 4 (n = at least 27) or the low affinity, ratiometric calcium indicator, fura 2-FF (n = at least 11), and the change in $[Ca^{2+}]_c$ was evaluated in response to the sequential application of KA and glutamate. **Figure 3.8** shows examples of images acquired during the application of excitotoxic stimuli to fluo 4-loaded co-cultured motoneurons and astrocytes: **A**, basal $[Ca^{2+}]_c$; **B**, the change in $[Ca^{2+}]_c$ in response to KA. The mean fluo 4 trace of the $[Ca^{2+}]_c$ response of motoneurons from WTnWTa co-cultures to excitotoxic stimuli is shown in **Figure 3.9A**. The mean peak increase in $[Ca^{2+}]_c$, above baseline, in co-cultured motoneurons in response to KA is shown in **Figure 3.9B**, as measured by fluo 4 intensity. Measurement of fluo 4 intensity revealed that there was no significant difference in the change in $[Ca^{2+}]_c$ in co-cultured motoneurons in response to KA ($p > 0.15$). Similarly, **Figure 3.9C** demonstrates that there was no significant difference in

Figure 3.8 – The change in cytosolic calcium ($[Ca^{2+}]_c$) levels in fluo 4-loaded co-cultures

The sequential images show representative images taken from an experiment to measure the change in $[Ca^{2+}]_c$ in fluo 4-loaded co-cultured cells, undertaken on the confocal microscope. **A,** represents the basal $[Ca^{2+}]_c$; **B**, illustrates the increase in $[Ca^{2+}]_c$ in response to the addition of KA. Scale bar = 30μm.

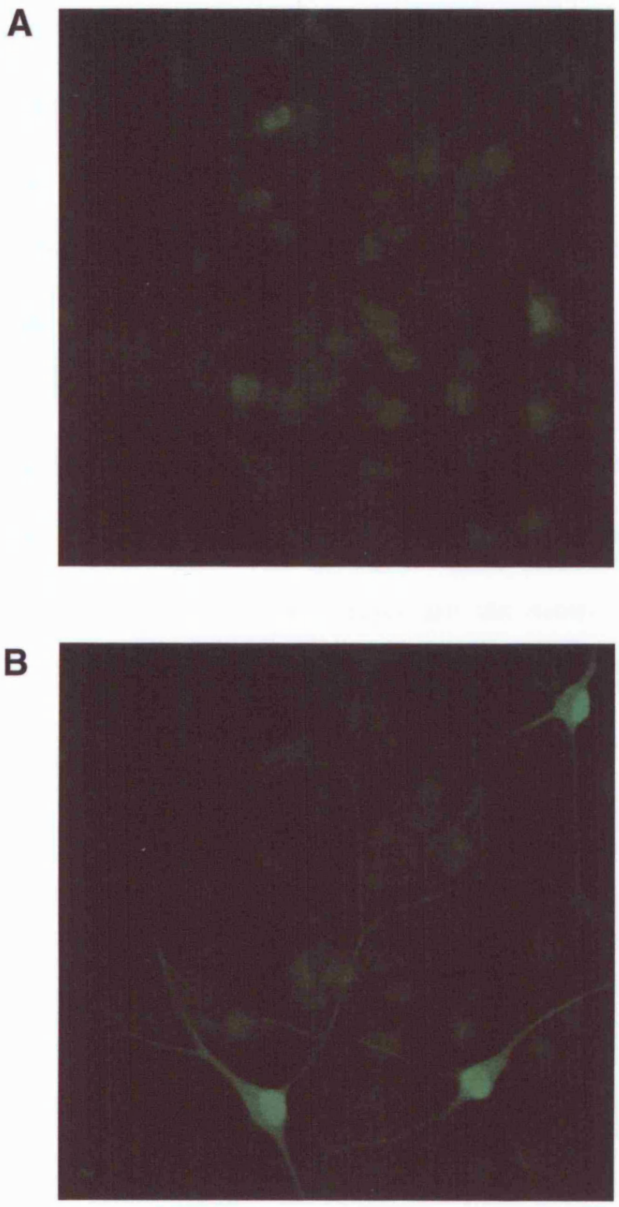
A
B

Figure 3.9 – The change in cytosolic calcium ($[Ca^{2+}]_c$) in fluo 4-loaded motoneurons in response to excitotoxic stimuli

Cells were loaded with fluo 4 (n = at least 27), a high affinity calcium indicator, and the change in fluo 4 intensity, corresponding to a change in $[Ca^{2+}]_c$, was recorded in response to sequential stimulation with KA and glutamate. **A** shows the mean fluo 4 trace from WT motoneurons co-cultured with WT astrocytes showing the change in $[Ca^{2+}]_c$ above baseline, in response to the addition of KA and then glutamate. The mean change in the levels of $[Ca^{2+}]_c$ in co-cultured motoneurons in response to KA, are summarised in the bar chart shown in **B**. The fluo 4 response to glutamate is shown in **C**, which summarises the mean change in $[Ca^{2+}]_c$ in motoneurons after the addition of glutamate, above that achieved with KA. Values are the mean change in $[Ca^{2+}]_c$ ± standard error of the mean.

GLT = glutamate, s = seconds.

A

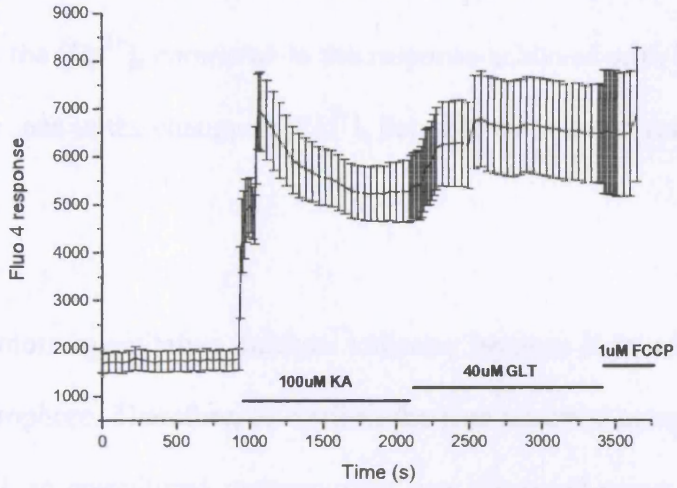
Fluo 4 response
Time (s)
100uM KA
40uM GLT
1uM FCCP

B

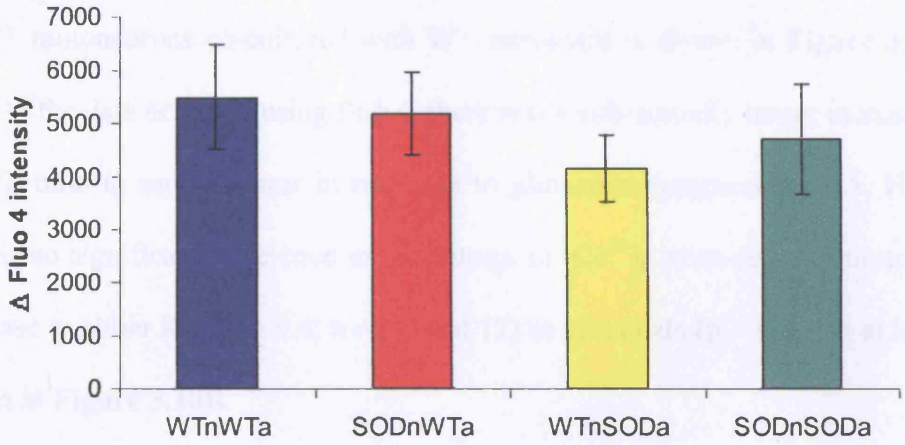
Δ Fluo 4 intensity
WTnWTa
SODnWTa
WTnSODa
SODnSODa

C

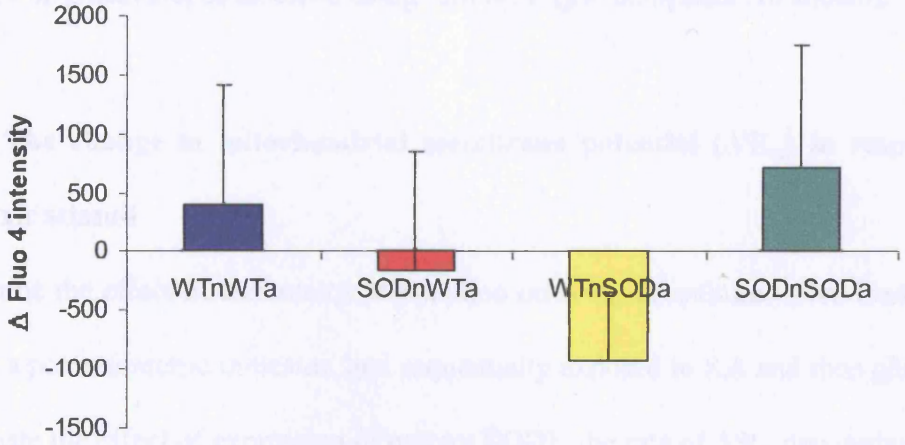
Δ Fluo 4 intensity
WTnWTa
SODnWTa
WTnSODa
SODnSODa

the change in $[Ca^{2+}]_c$ in co-cultured motoneurons in response to the sequential addition of glutamate ($p > 0.25$). It can be seen that the addition of glutamate in some cases actually reduced the $[Ca^{2+}]_c$ compared to the response achieved with KA. Similarly, no differences were seen in the change in $[Ca^{2+}]_c$ between co-cultured astrocytes ($p > 0.05$; data not shown).

Fura 2-FF is a more quantitative calcium indicator because it is a low affinity, dual wavelength fluorophore. Therefore, to confirm the data acquired using fluo 4, the mean change in $[Ca^{2+}]_c$ in co-cultured motoneurons, was measured using fura 2-FF on the cooled CCD camera. The change in $[Ca^{2+}]_c$ was expressed as a ratio between the fluorescence excited at 340nm and the fluorescence excited at 380nm. The mean trace from WT motoneurons co-cultured with WT astrocytes is shown in **Figure 3.10A**. In contrast to the data acquired using fluo 4, there was a substantially larger increase in the fura 2-FF ratio in motoneurons in response to glutamate compared to KA. However, there was no significant difference in the change in $[Ca^{2+}]_c$ in co-cultured motoneurons in response to either KA ($p > 0.4$; n = at least 17) or glutamate ($p > 0.3$; n = at least 11), as shown in **Figure 3.10B**.

There was no significant difference in the change in $[Ca^{2+}]_c$ of co-cultured astrocytes to either KA or glutamate, as assessed using fura 2-FF ($p > 0.55$; data not shown).

3.3.3.2. The change in mitochondrial membrane potential ($\Delta\Psi_m$) in response to excitotoxic stimuli

To examine the effect of excitotoxic stimulation on $\Delta\Psi_m$, co-cultures were loaded with TMRM, a potentiometric indicator, and sequentially exposed to KA and then glutamate. To evaluate the effect of expression of mutant SOD1, the rate of $\Delta\Psi_m$ depolarisation, as

Figure 3.10 –The change in cytosolic calcium ($[Ca^{2+}]_c$) in fura 2-FF loaded motoneurons in response to excitotoxic stimuli

Cells were loaded with fura 2-FF, a low affinity, ratiometric calcium indicator, and the change in $[Ca^{2+}]_c$ in response to sequential stimulation with KA and glutamate was recorded on the cooled CCD camera. The change in $[Ca^{2+}]_c$ was expressed as a ratio between the fluorescence excited at 340nm and the fluorescence excited at 380nm. The mean fura 2-FF trace from WT motoneurons co-cultured with WT astrocytes illustrating the change in $[Ca^{2+}]_c$ in response to the addition of KA and then glutamate is shown in **A.** The mean change in $[Ca^{2+}]_c$ in co-cultured motoneurons in response to both KA and glutamate is summarised in the bar chart in **B**. Values are the mean change in $[Ca^{2+}]_c \pm$ standard error of the mean.

GLT = glutamate, s = seconds.

A

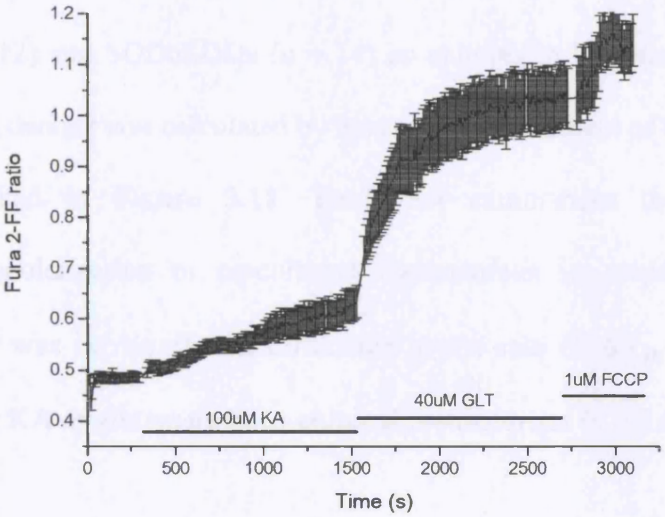
Fura 2-FF ratio
Time (s)
100uM KA
40uM GLT
1uM FCCP

B

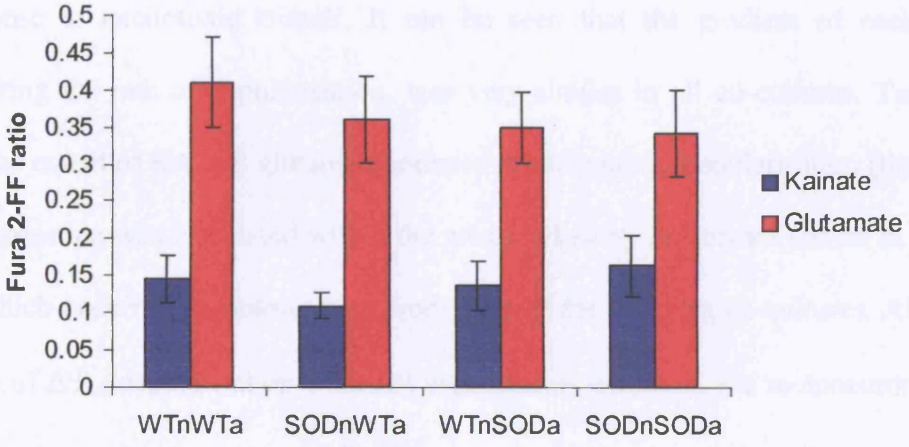
Fura 2-FF ratio
WTnWTa
SODnWTa
WTnSODa
SODnSODa
Kainate
Glutamate

measured by the rate of decline of TMRM signal, in co-cultured motoneurons was calculated in response to both KA and glutamate. **Figure 3.11** illustrates the change in TMRM signal in motoneurons from WTnWTa (n = 30), SODnWTa (n = 13), WTnSODa (n = 12) and SODnSODa (n = 14) co-cultures in response to excitotoxins. The rate of signal decline was calculated by measuring the gradient of the slope between the arrows marked in **Figure 3.11**. **Table 3.4** summarises the mean rate of mitochondrial depolarisation in co-cultured motoneurons in response to KA and glutamate. There was no significant difference in the rate of $\Delta\Psi_m$ depolarisation in response to either KA or glutamate in co-cultured motoneurons ($p > 0.06$).

To evaluate the extent of mitochondrial depolarisation, the TMRM intensities were normalised, to account for the variation in resting $\Delta\Psi_m$ between co-cultured motoneurons. **Figure 3.12** shows the normalised TMRM traces for $\Delta\Psi_m$ depolarisation in response to excitotoxic stimuli. It can be seen that the gradient of each trace, representing the rate of depolarisation, was very similar in all co-cultures. **Table 3.5** details the extent of KA and glutamate-induced mitochondrial depolarisation (the extent of depolarisation was calculated within the area marked by the arrows shown in **Figure 3.12**), which occurred in motoneurons from each of the different co-cultures. Although the rates of $\Delta\Psi_m$ depolarisation were not significantly different, the motoneurons from co-cultures containing either $SOD1^{G93A}$ neurons or astrocytes, and in particular $SOD1^{G93A}$ astrocytes, underwent a greater extent of mitochondrial depolarisation in response to KA, compared to WTnWTa co-cultures. Unfortunately due to the extensive depolarisation in response to KA, the true response to glutamate could not be evaluated from these experiments.

Figure 3.11 – Depolarisation of mitochondria in response to excitotoxic stimuli

Co-cultures were loaded with the potentiometric indicator, TMRM and the loss of $\Delta\Psi_m$ in co-cultured motoneurons, as measured by the loss of TMRM signal, was recorded in response to both KA and glutamate. The mean traces representing loss of $\Delta\Psi_m$ in co-cultured motoneurons in response to excitotoxic stimulation are shown. The arrows mark the boundaries within which the rate of mitochondrial depolarisation was calculated from the gradient of the slope, in response to kainate and glutamate.

GLT = glutamate, s = seconds.

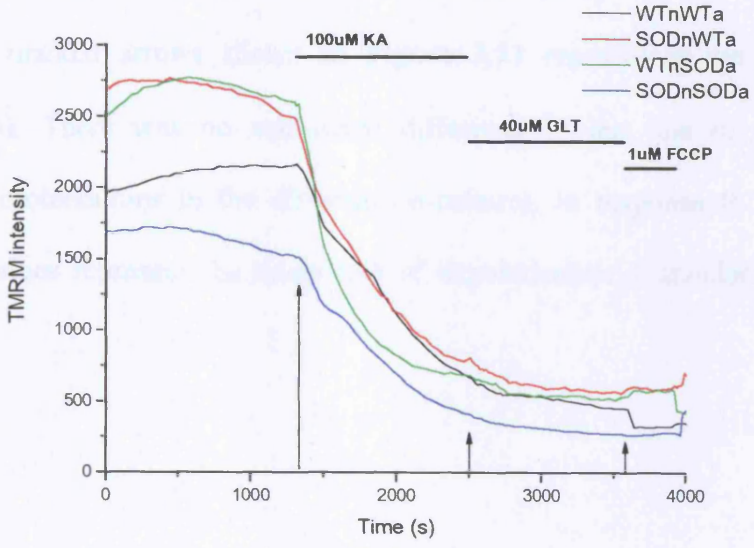
WTnWTa
SODnWTa
WTnSODa
SODnSODa
100uM KA
40uM GLT
1uM FCCP
TMRM intensity
Time (s)
0
500
1000
1500
2000
2500
3000
0
1000
2000
3000
4000

Table 3.4 – The rate of mitochondrial depolarisation in response to excitotoxic stimulation

The mean rate of mitochondrial depolarisation in co-cultured motoneurons in response to KA and glutamate is summarised in the Table (the gradient of the slope measured between the marked arrows shown in **Figure 3.11** represented the rate of $\Delta\Psi_m$ depolarisation). There was no significant difference in the rate of depolarisation between the motoneurons in the different co-cultures, in response to either KA or glutamate. Values represent the mean rate of depolarisation ± standard error of the mean.

	Kainate	Glutamate
WTnWTa	**44.7**	**5.3**
± SEM	± 6.2	± 1.7
SODnWTa	**45.8**	**4.6**
± SEM	± 8.9	± 1.4
WTnSODa	**58.7**	**4.6**
± SEM	± 13.0	± 3.0
SODnSODa	**31.3**	**3.2**
± SEM	± 3.6	± 0.7

Figure 3.12 – Normalisation of the change in mitochondrial membrane potential ($\Delta\Psi_m$) in co-cultured motoneurons in response to the sequential addition of KA and glutamate

To calculate the extent of mitochondrial depolarisation in response to excitotoxic stimuli, the change in TMRM signal was normalised, with the maximal intensity of 1 representing the resting $\Delta\Psi_m$, and the minimal intensity of 0 representing the remaining $\Delta\Psi_m$ after the addition of the mitochondrial uncoupler, FCCP. The traces show the mean normalised TMRM signals of co-cultured motoneurons in response to KA and glutamate. It can be seen that the rate of the mitochondrial depolarisation appeared similar in WTnWTa, SODnWTa, WTnSODa and SODnSODa, thus corroborating the data before normalisation as shown in **Table 3.4**. The arrows mark the boundaries within which the extent of mitochondrial depolarisation was calculated in response to KA and glutamate.

GLT = glutamate, s = seconds

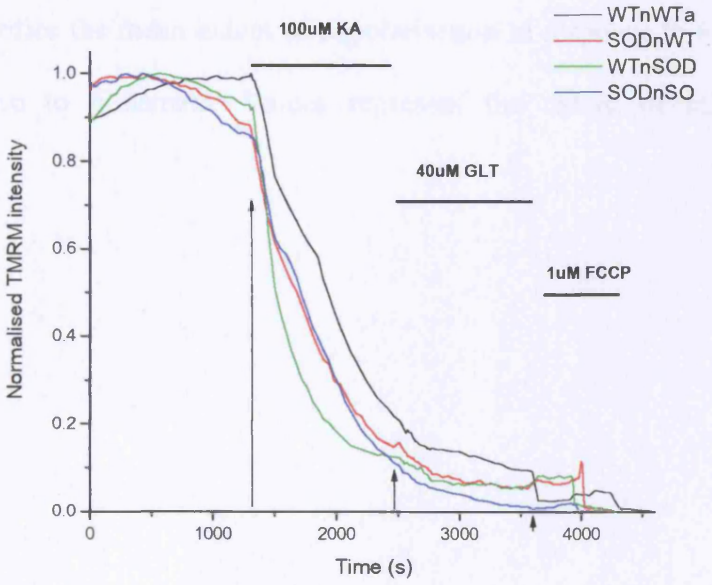
WTnWTa
SODnWT
WTnSOD
SODnSO
100uM KA
40uM GLT
1uM FCCP
Normalised TMRM intensity
1.0
0.8
0.6
0.4
0.2
0.0
0
1000
2000
3000
4000
Time (s)

Table 3.5 - The extent of mitochondrial depolarisation in response to excitotoxic stimulation

The extent of mitochondrial depolarisation was calculated in response to KA and glutamate, within the respective areas as marked by arrows, as shown in **Figure 3.12** and the Table quantifies the mean extent of depolarisation in response to KA and then the further response to glutamate. Values represent the extent of mitochondrial depolarisation.

	KAINATE	GLUTAMATE
WTnWTa	-79.1%	-90.8%
SODnWTa	-81.8%	-92.2%
WTnSODa	-86.4%	-93.1%
SODnSODa	-87.6%	-99.1%

3.3.3.3. Superoxide generation in response to excitotoxic stimuli

To evaluate the effect of mutant SOD1 expression in either motoneurons or astrocytes on the generation of superoxide in response to excitotoxic stimuli, co-cultures were loaded with HEt, and the rates of free radical generation under different co-culture conditions compared. However, Budd et al, (1997) demonstrated that to acquire an accurate measurement of oxidation rates with HEt, it was necessary to use a low concentration, since at high concentrations (10μM) oxidised ethidium could become sequestered in the mitochondria and upon depolarisation, the release of oxidised ethidium produced an unrepresentative increase in the fluorescent signal. Therefore, for these experiments, 2μM HEt was used, ensuring the increase in fluorescence was an accurate reflection of superoxide production. Furthermore, no increase in signal was seen upon addition of the mitochondrial uncoupler, FCCP, implying that excess oxidised ethidium was not being sequestered in the mitochondria.

Table 3.6 gives the rate of superoxide generation in motoneurons (**A**) and astrocytes (**B**) from WTnWTa, SODnWTa, WTnSODa and SODnSODa co-cultures under resting conditions, in response to KA and in response to glutamate. The rate of superoxide generation in WT motoneurons co-cultured with WT astrocytes ($n = 16$) in response to KA was not significantly different from the basal rate ($p > 0.9$). In contrast, there was a significant increase in the rate of superoxide generation in response to KA compared to the basal rate in motoneurons from SODnWTa ($n = 15$), WTnSODa ($n = 17$) and SODnSODa ($n = 20$) co-cultures ($p < 0.03$). In response to glutamate, with the exception of motoneurons from WTnWTa co-cultures, the rate of superoxide generation was reduced compared to the rate in response to KA ($p < 0.04$).

Table 3.6 – The rate of superoxide generation under resting conditions and in response to KA and glutamate

Table **A** summarises the rate of superoxide generation in motoneurons under basal conditions and also in response to KA and to glutamate. There was a significant increase in the rate of superoxide generation in response to KA compared to the basal rate in motoneurons from SODnWTa ($n = 15$), WTnSODa ($n = 17$) and SODnSODa ($n = 20$) co-cultures ($p < 0.03$), but not in WTnWTa co-cultures ($p > 0.9$; $n = 16$). In contrast, the rate of superoxide generation in response to glutamate in motoneurons from SODnWTa, WTnSODa and SODnSODa co-cultures was significantly lower than the rate in response to KA ($p < 0.04$), whereas the rate did not differ in motoneurons in WTnWTa co-cultures ($p > 0.9$). Table **B** summarises the rate of superoxide generation in astrocytes under basal conditions and also in response to KA and to glutamate. Astrocytes from SODnWTa ($n = 16$) co-cultures generated superoxide at a greater rate in response to KA ($p < 0.001$), and also glutamate ($p = 0.011$) compared to their basal rate of superoxide generation. In contrast, the rate of superoxide generation in astrocytes from WTnWTa ($n = 23$), WTnSODa ($n = 19$) and SODnSODa ($n = 9$) co-cultures did not differ in response to KA or glutamate compared to the baseline rate ($p > 0.1$). Values are the mean rate (a.f.u./sec) corrected for baseline ± standard error of the mean. * $p < 0.05$, ** $p < 0.01$, *** $p < 0.005$ indicates a significant difference in the observed rate compared to the rate before excitotoxin addition.

A

	Basal rate (a.f.u./sec)	Rate in response to KA (a.f.u./sec)	Rate in response to glutamate (a.f.u./sec)
WTnWTa	**119.0** ± 50.0	**117.3** ± 38.9	**112.6** ± 28.1
SODnWTa	**73.6** ± 14.3	**239.8** ± 57.8 **	**103.9** ± 22.2 *
WTnSODa	**68.1** ± 12.5	**260.3** ± 63.6 **	**133.5** ± 31.2 *
SODnSODa	**86.9** ± 9.8	**172.4** ± 35.1 *	**103.0** ±14.7*

B

	Basal rate (a.f.u./sec)	Rate in response to KA (a.f.u./sec)	Rate in response to glutamate (a.f.u./sec)
WTnWTa	**58.6** ± 29.6	**29.8** ± 12.9	**16.1** ± 3.9
SODnWTa	**5.3** ± 7.7	**80.3** ± 15.6 ***	**133.0** ± 17.0 *
WTnSODa	**22.2** ± 5.3	**61.2** ± 24.8	**105.3** ± 26.1
SODnSODa	**39.4** ± 8.5	**87.9** ± 49.3	**62.4** ± 21.1

The bar chart in **Figure 3.13A** shows the rate of superoxide generation in co-cultured motoneurons in response to both KA and glutamate, corrected for basal rate. In response to KA, the rate of superoxide generation in motoneurons from SODnWTa co-cultures was significantly greater than in motoneurons from WTnWTa co-cultures ($p = 0.027$). Thus, in response to KA, the rate of superoxide generation in WTnWTa co-cultures was -1.7 a.f.u./sec (± 35.3 S.E.M.) compared to 166.2 a.f.u./sec (± 48.6 S.E.M.) in SODnWTa co-cultures. In addition, motoneurons from WTnSODa and SODnSODa co-cultures also appeared to show a trend towards an increased rate of superoxide generation, although this did not reach statistical significance. Furthermore, analysis of the rate of superoxide generation in motoneurons in response to glutamate added sequentially to KA, revealed that there was no significant difference between SODnWTa, SODnSODa and WTnWTa co-cultures, whereas the rate in WTnSODa co-cultures was significantly less than in WTnWTa co-cultures ($p = 0.038$).

The rate of superoxide generation in astrocytes from SODnWTa co-cultures was increased in response to KA compared to the rate in this co-culture under resting conditions ($p < 0.001$; **Table 3.6B**), and the rate was further increased in response to glutamate ($p = 0.011$). No other significant differences in the rate of superoxide generation were observed for astrocytes within a particular co-culture, between the three conditions. However, in response to KA, astrocytes from SODnWTa ($n = 16$) and WTnSODa ($n = 19$) co-cultures generated superoxide at a greater rate than astrocytes from WTnWTa co-cultures ($n = 23$; $p < 0.002$; **Figure 3.13B**). The rate of superoxide generation in response to glutamate was similarly increased in astrocytes from SODnWTa compared to WTnWTa co-cultures ($p = 0.036$), but no other significant differences were observed compared to WTnWTa co-cultures ($p > 0.08$).

Figure 3.13 - The rate of superoxide generation in co-cultures in response to excitotoxic stimuli.

Co-cultures were loaded with HEt, a non-fluorescent dye that upon oxidation becomes fluorescent, and can therefore be used to compare the rate of superoxide generation between different co-culture conditions, in response to the sequential addition of KA and glutamate. The bar chart (**A**) illustrates the rate of superoxide generation that occurred, above baseline, in response to KA and glutamate in motoneurons from WTnWTa (n = 16), SODnWTa (n = 17), WTnSODa (n = 15) and SODnSODa (n = 20) co-cultures. There was a significant increase in the rate of superoxide generation in motoneurons from SODnWTa co-cultures in response to KA compared to motoneurons from WTnWTa co-cultures ($p < 0.03$). However, in response to glutamate, motoneurons from WTnSODa co-cultures showed a significantly reduced rate of superoxide generation compared to WTnWTa co-cultures ($p < 0.04$).

The bar chart in **B** illustrates the results from astrocytes. In contrast to motoneurons, astrocytes from SODnWTa (n = 16) and WTnSODa (n = 19) co-cultures generated superoxide at a significantly increased rate in response to KA, compared to astrocytes from WTnWTa (n = 23; $p \leq 0.002$) co-cultures. Similarly, astrocytes from SODnWTa co-cultures had a significantly increased rate of superoxide generation in response to glutamate compared to astrocytes from WTnWTa co-cultures ($p < 0.035$). Values are the mean rate (a.f.u./sec) above the basal rate of generation ± standard error of the mean. * $p < 0.05$.

A

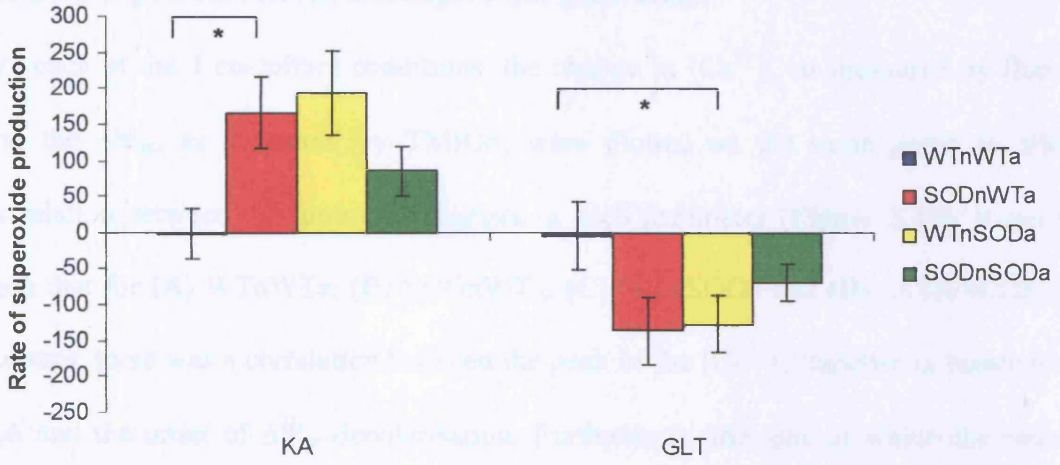
Rate of superoxide production
300
250
200
150
100
50
0
-50
-100
-150
-200
-250
*
*
KA
GLT
WTnWTa
SODnWTa
WTnSODa
SODnSODa

B

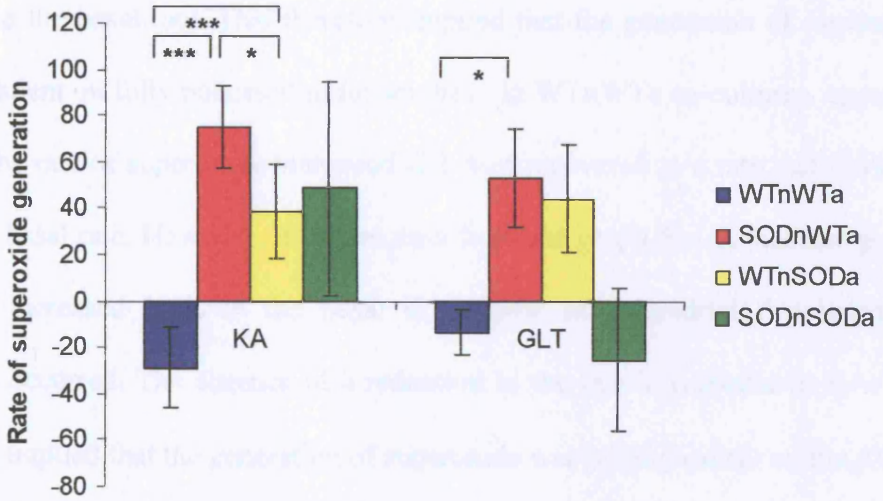
Rate of superoxide generation
120
100
80
60
40
20
0
-20
-40
-60
-80
***
***
*
*
KA
GLT
WTnWTa
SODnWTa
WTnSODa
SODnSODa

3.3.3.4. Correlation between cytosolic calcium ($[Ca^{2+}]_c$) influx, mitochondrial membrane potential ($\Delta\Psi_m$) and superoxide generation

For each of the 4 co-culture conditions, the change in $[Ca^{2+}]_c$, as measured by fluo 4, and the $\Delta\Psi_m$, as measured by TMRM, were plotted on the same graph to allow correlation between the timing of changes in each parameter (**Figure 3.14**). It can be seen that for (**A**) WTnWTa, (**B**) SODnWTa, (**C**) WTnSODa and (**D**) SODnSODa co-cultures, there was a correlation between the peak of the $[Ca^{2+}]_c$ response in response to KA and the onset of $\Delta\Psi_m$ depolarisation. Furthermore, the time at which the rate of superoxide generation increased in motoneurons, relative to the basal rate, after KA exposure, was marked on the same graph (red line). Interestingly, in SODnWTa, WTnSODa and SODnSODa co-cultures, significant mitochondrial depolarisation had already occurred by the time point at which the rate of superoxide generation increased relative to the basal rate. This therefore implied that the generation of superoxide was not dependent on fully polarised mitochondria. In WTnWTa co-cultures, upon addition of KA, the rate of superoxide plateaued and then recovered to a rate that did not differ from the basal rate. However, it can be seen from the graph that at the time point when the rate increased back to the basal rate, some mitochondrial depolarisation had similarly occurred. The absence of a reduction in the rate in response to KA, however similarly implied that the generation of superoxide was not dependent on the $\Delta\Psi_m$.

3.3.3.5. The change in mitochondrial calcium ($[Ca^{2+}]_m$) in response to excitotoxic stimuli

Co-cultured cells were loaded with the low affinity indicator, rhod 5N, which accumulates in mitochondria and can therefore be used to measure $[Ca^{2+}]_m$. An example of a typical trace from an experiment measuring changes in $[Ca^{2+}]_c$ and $[Ca^{2+}]_m$ in motoneurons in WTnWTa co-cultures is shown in **Figure 3.15A**. It can be seen that

Figure 3.14 – Temporal correlation between the change in cytosolic calcium ($[Ca^{2+}]_c$), mitochondrial membrane potential ($\Delta\Psi_m$) and the rate of superoxide generation

The increase in $[Ca^{2+}]_c$ and the depolarisation of the $\Delta\Psi_m$ were plotted on the same graph for (**A**) WTnWTa, (**B**) SODnWTa, (**C**) WTnSODa and (**D**) SODnSODa co-cultures. In addition, the time at which the rate of superoxide generation changed relative to basal levels was marked (red line) to allow a correlation between the three parameters. The peak increase in $[Ca^{2+}]_c$, as measured by fluo 4, occurred simultaneously with the onset of mitochondrial depolarisation, as measured by TMRM, in each co-culture condition. Interestingly, in SODnWTa, WTnSODa and SODnSODa co-cultures at the time point at which the rate of superoxide generation increased above basal in response to KA, significant mitochondrial depolarisation had already occurred. This implied that $\Delta\Psi_m$ was not necessary for the generation of superoxide in these conditions.

s = seconds

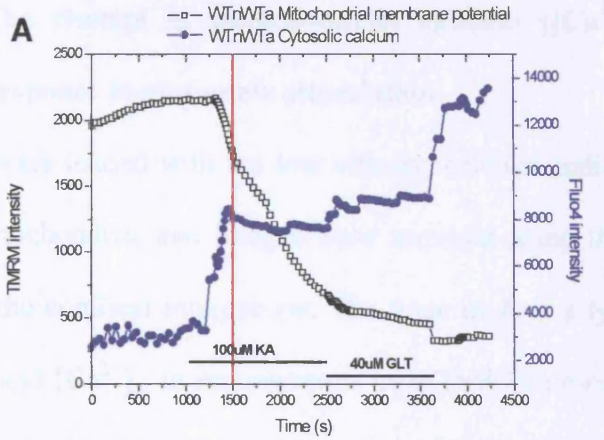
A
WTnWTa Mitochondrial membrane potential
WTnWTa Cytosolic calcium
TMRM intensity
Fluo4 intensity
100uM KA
40uM GLT
Time (s)

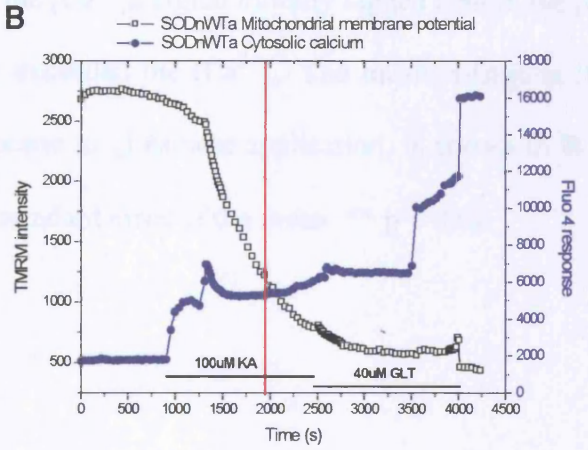
B
SODnWTa Mitochondrial membrane potential
SODnWTa Cytosolic calcium
TMRM intensity
Fluo 4 response
100uM KA
40uM GLT
Time (s)

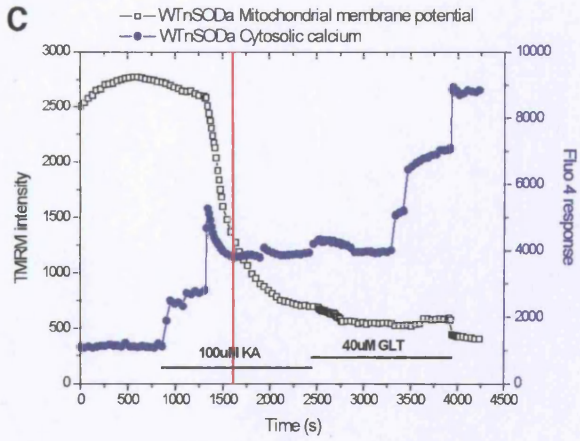
C
WTnSODa Mitochondrial membrane potential
WTnSODa Cytosolic calcium
TMRM intensity
Fluo 4 response
100uM KA
40uM GLT
Time (s)

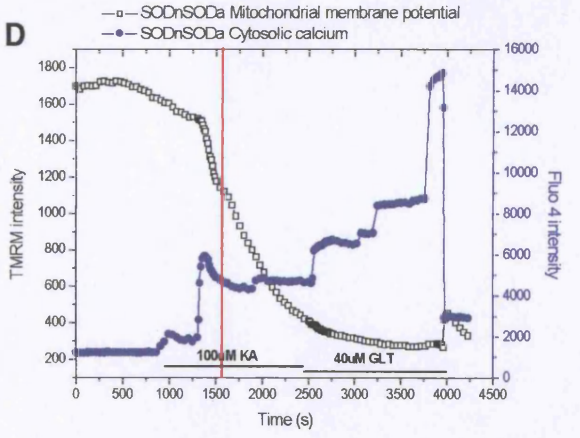
D
SODnSODa Mitochondrial membrane potential
SODnSODa Cytosolic calcium
TMRM intensity
Fluo 4 intensity
100uM KA
40uM GLT
Time (s)

Figure 3.15 – The change in mitochondrial calcium ($[Ca^{2+}]_m$) in co-cultured motoneurons in response to glutamate stimulation

Co-cultured cells were loaded with the low affinity, calcium indicator rhod 5N, which accumulates in mitochondria, and images were acquired using the x63 oil immersion objective lens on the confocal microscope. The trace in **A** is a typical example of the change in $[Ca^{2+}]_c$ and $[Ca^{2+}]_m$ in motoneurons in WTnWTa co-cultures in response to glutamate, whereby the $[Ca^{2+}]_m$ signal initially lagged behind the $[Ca^{2+}]_c$ signal and then the $[Ca^{2+}]_m$ actually exceeded the $[Ca^{2+}]_c$. The mean change in $[Ca^{2+}]_m$ in co-cultured motoneurons in response to glutamate application, is shown in **B**. Values are the mean values of $[Ca^{2+}]_m \pm$ standard error of the mean. ** $p < 0.01$.

s = seconds

A

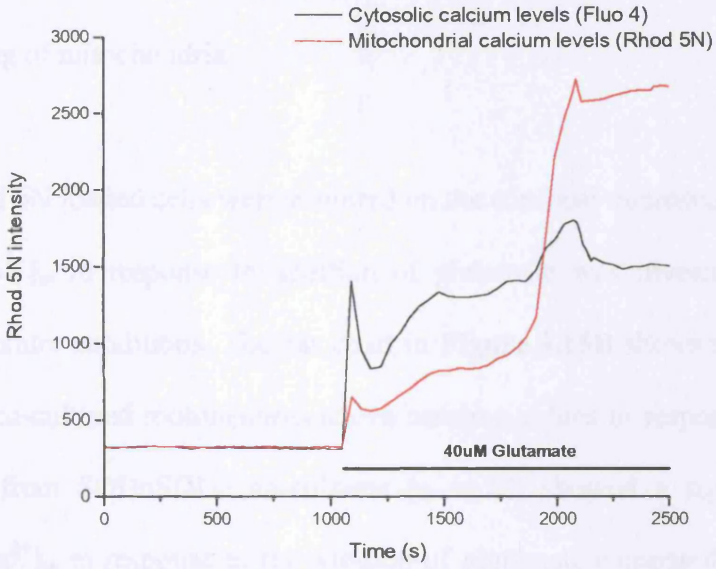
Cytosolic calcium levels (Fluo 4)
Mitochondrial calcium levels (Rhod 5N)
Rhod 5N intensity
3000
2500
2000
1500
1000
500
0
40uM Glutamate
0
500
1000
1500
2000
2500
Time (s)

B

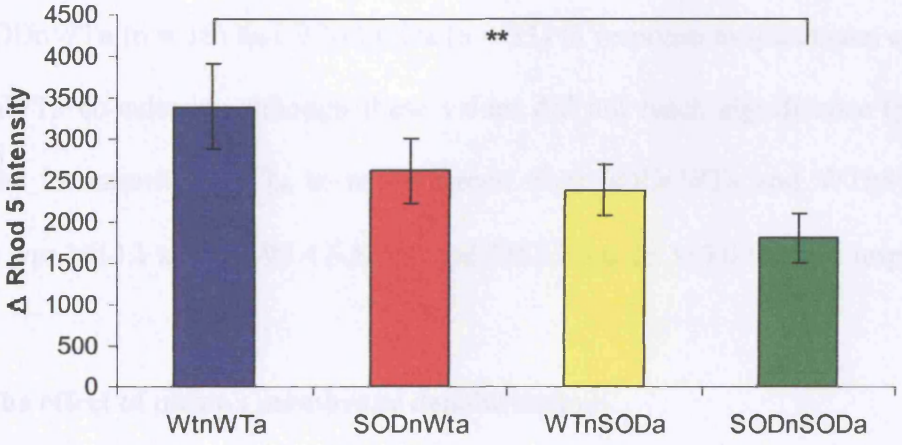
**
Δ Rhod 5 intensity
4500
4000
3500
3000
2500
2000
1500
1000
500
0
WtnWTa
SODnWta
WTnSODa
SODnSODa

the change in $[Ca^{2+}]_m$ lagged behind that of the cytosol in response to excitotoxic stimuli, and then the elevation in $[Ca^{2+}]_m$ actually exceeded that of the $[Ca^{2+}]_c$ due to calcium loading of mitochondria.

Images of rhod 5N loaded cells were acquired on the confocal microscope and the mean change in $[Ca^{2+}]_m$ in response to addition of glutamate was investigated under the differing co-culture conditions. The bar chart in **Figure 3.15B** shows the mean change in $[Ca^{2+}]_m$ of co-cultured motoneurons above baseline values in response to glutamate. Motoneurons from SODnSODa co-cultures (n = 28) showed a significantly lower increase in $[Ca^{2+}]_m$ in response to the addition of glutamate compared to motoneurons from WTnWTa (n = 15; p = 0.006) co-cultures. Therefore in response to glutamate, the $[Ca^{2+}]_m$ increased by 3386.8 a.u. (± 512.1 S.E.M.) in motoneurons from WTnWTa co-cultures, whereas this response in motoneurons from SODnSODa co-cultures was significantly lower and $[Ca^{2+}]_m$ only increased by 1800.7 a.u. (± 297.3 S.E.M.). Furthermore, there was a trend towards a lesser increase in $[Ca^{2+}]_m$ in motoneurons from SODnWTa (n = 18) and WTnSODa (n = 33) in response to glutamate, compared to WTnWTa co-cultures, although these values did not reach significance (p > 0.1). Thus, the increase in $[Ca^{2+}]_m$ in motoneurons from SODnWTa and WTnSODa co-cultures was 2614.1 a.u. (± 395.4 S.E.M.) and 2387.2 a.u. (± 310.0 S.E.M.) respectively.

3.3.4. The effect of plasma membrane depolarisation

Neuronal toxicity may be dependent on the route of calcium influx ('source specificity' hypothesis) rather than the extent of calcium influx ('calcium load' hypothesis). To test this, co-cultures were stimulated with recording medium (RM) containing depolarising concentrations of potassium (50mM), and the effects observed compared to those seen in response to KA.

3.3.4.1. Evaluation of the effect of plasma membrane depolarisation on cytosolic calcium ($[Ca^{2+}]_c$) levels

Co-cultures were loaded with the high affinity calcium indicator, fluo 4, and stimulated with RM containing 50mM potassium. In addition, the RM contained the glutamate receptor antagonists MK-801 ((5R,10S)-(+)-5-Methyl-10,11-dihydro-5H-dibenzo [a,d] cyclohepten-5,10-imine hydrogen maleate), CNQX (6-cyano-2,3-dihydroxy-7-nitro-qunioxaline) and MCPG (+(RS)-α-methyl-4-carboxyphenylglycine), to prevent activation of glutamate receptors subsequent to plasma membrane depolarisation and the potential release of glutamate. The mean increase in $[Ca^{2+}]_c$ in motoneurons following the application of a high concentration of potassium is summarised in **Table 3.7**. The mean increase in $[Ca^{2+}]_c$ following application of KA is shown for comparison. The change in $[Ca^{2+}]_c$ in motoneurons from WTnSODa and SODnWTa co-cultures was significantly less in response to potassium compared to KA application ($p < 0.02$). There was also a trend towards a lower $[Ca^{2+}]_c$ influx in motoneurons from WTnWTa and SODnSODa co-cultures in response to potassium compared to KA, although statistical significance was not reached ($p > 0.05$). Furthermore, in response to potassium, the $[Ca^{2+}]_c$ influx in motoneurons in SODnSODa co-cultures ($n = 13$) was significantly greater than in motoneurons in SODnWTa ($n = 19$; $p = 0.05$) co-cultures.

3.3.4.2. Evaluation of the effect of plasma membrane depolarisation on mitochondrial membrane potential ($\Delta\Psi_m$)

TMRM loaded co-cultures were stimulated with RM containing 50mM potassium and the effect on the $\Delta\Psi_m$ was investigated to determine if the calcium influx through voltage-gated calcium channels induced mitochondrial depolarisation. To control for the activation of glutamate receptors, subsequent to plasma membrane depolarisation and glutamate release, the RM contained MK-801, CNQX and MCPG. The rate of

Table 3.7 – Comparison of the change in cytosolic calcium ($[Ca^{2+}]_c$) in response to plasma membrane depolarisation and KA receptor activation

Co-cultures were loaded with fluo 4 and the mean change in $[Ca^{2+}]_c$ in response to RM containing high potassium concentrations (50mM) was evaluated by measuring the fluorescent intensity of fluo 4 using confocal microscopy. MK-801, CNQX and MCPG were included in the RM to prevent activation of glutamate receptors subsequent to plasma membrane depolarisation and glutamate release. The mean change in fluo 4 intensity, corresponding to levels of $[Ca^{2+}]_c$, is summarised in the Table, and the mean change in $[Ca^{2+}]_c$ in response to KA is provided for comparison. Values are the mean change in $[Ca^{2+}]_c$ ± standard error of the mean. * $p < 0.05$, *** $p < 0.005$ indicates significance between the increase in $[Ca^{2+}]_c$ in response to depolarising potassium compared to the change in response to KA. $^+$ indicates significance between motoneurons from SODnSODa and SODnWTa in response to potassium only.

K^+ = potassium

	Depolarising K^+	Kainate
WTnWTa	**2344. 2**	**5493.1**
± S.E.M.	± 582.9	± 988.7
SODnWTa	**1425.8 *****	**5192.0**
± S.E.M.	± 409.0	± 785.8
WTnSODa	**946.1 ***	**4150.3**
± S.E.M.	± 549.3	± 643.2
SODnSODa	**3581.5** $^+$	**4692.3**
± S.E.M.	± 894.7	± 1036.9

mitochondrial depolarisation in response to potassium is summarised in **Table 3.8A**, and the data from KA-induced depolarisation is provided for comparison. Motoneurons from SODnWTa (n = 19) and WTnSODa (n = 7) co-cultures showed a significantly reduced rate of mitochondrial depolarisation in response to potassium than in response to KA ($p < 0.015$). There was also a trend towards a reduced rate of mitochondrial depolarisation in response to potassium in motoneurons from WTnWTa (n = 11) and SODnSODa (n = 8) co-cultures, although this did not reach significance ($p > 0.4$). Furthermore, motoneurons from SODnSODa co-cultures had a more rapid rate of mitochondrial depolarisation in response to potassium than motoneurons from WTnSODa co-cultures ($p = 0.021$).

To examine the extent of mitochondrial depolarisation, the TMRM intensities were normalised, to account for variation in resting $\Delta\Psi_m$ between co-cultures. Examples of the normalised traces are shown in **Figure 3.16**. From traces such as these, the extent of mitochondrial depolarisation, compared to baseline was calculated in motoneurons from each of the different co-cultures and the results are summarised in **Table 3.8B**. The data acquired with KA is provided for comparison. It appears that KA induced a greater extent of mitochondrial depolarisation than that induced by high concentrations of potassium, therefore indicating that the change in $\Delta\Psi_m$ in response to KA was specific to glutamate receptor activation, rather than due to cellular depolarisation. Furthermore, in response to potassium, the extent of mitochondrial depolarisation was reduced in motoneurons from SODnWTa, WTnSODa and SODnSODa co-cultures compared to WTnWTa co-cultures.

Table 3.8 – Mitochondrial membrane potential ($\Delta\Psi_m$) depolarisation in motoneurons in response to high concentrations of potassium

Co-cultures were loaded with the potentiometric fluorophore, TMRM, and the change in TMRM signal, which corresponded to a change in $\Delta\Psi_m$, in response to high depolarising concentrations of potassium was recorded. The mean rate of $\Delta\Psi_m$ depolarisation in motoneurons in response to potassium is shown in Table **A**, and the rate in response to KA is shown for comparison. Following normalisation of the TMRM signal, the extent of $\Delta\Psi_m$ depolarisation in response to potassium was calculated and Table **B** summarises the extent of $\Delta\Psi_m$ depolarisation in response to both potassium and KA. Potassium appeared to induce less $\Delta\Psi_m$ depolarisation than KA. Values are the mean response ± standard error of the mean. * $p < 0.05$, *** $p < 0.005$ indicates a significant difference between the motoneurons of the same co-culture type in response to the two different treatments. $^+$ indicates a significant difference between motoneurons of SODnSODa and WTnSODa co-cultures in response to potassium only.

K^+ = potassium, s = seconds

A

Rate of depolarisation	WTnWTa	SODnWTa	WTnSODa	SODnSODa
In response to K^+ ± SEM	34.0 ±12.8	24.5 * ±9.3	7.6 *** ±5.3	28.1$^+$ ±4.4
In response to KA ± SEM	44. 7 ±6.2	45.8 ±8.9	58.7 ±13.0	31.3 ±3.6

B

Extent of depolarisation	WTnWTa	SODnWTa	WTnSODa	SODnSODa
Induced by K^+	73%	58%	52%	65%
Induced by KA	79.1%	81.8%	86.4%	87.6%

Figure 3.16 – Mitochondrial membrane potential ($\Delta\Psi_m$) depolarisation in motoneurons in response to high concentrations of potassium

To calculate the extent of $\Delta\Psi_m$ depolarisation in motoneurons, the TMRM data was normalised. Examples of normalised traces from motoneurons under the different co-culture conditions are shown. The arrows represent the points between which the extent of depolarisation was measured.

s = seconds

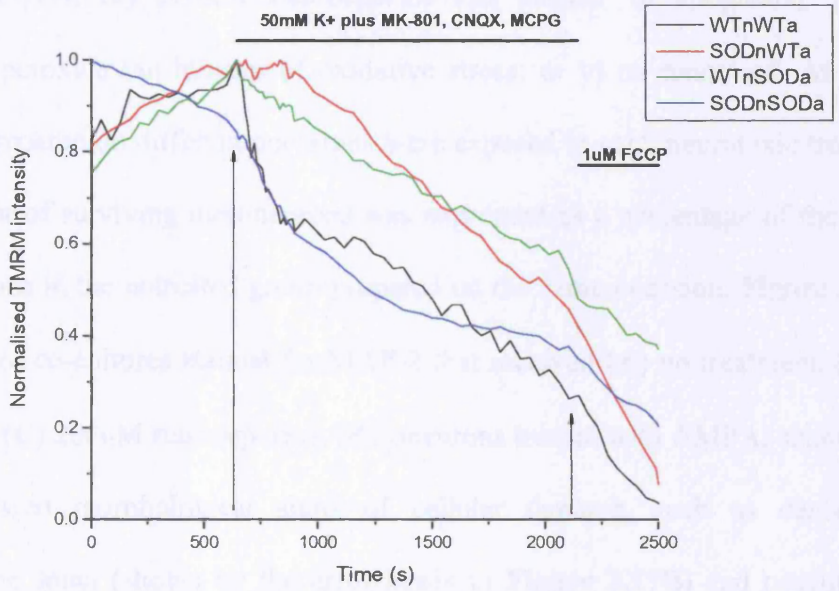
50mM K+ plus MK-801, CNQX, MCPG
1uM FCCP
WTnWTa
SODnWTa
WTnSODa
SODnSODa
Normalised TMRM intensity
Time (s)
0.0
0.2
0.4
0.6
0.8
1.0
0
500
1000
1500
2000
2500

3.3.5. The effect of expression of mutant SOD1 on motoneuron survival following exposure to neurotoxic agents

At 7DIV, motoneurons in each of the four co-culture conditions were exposed to one of the following stressful stimuli for 24 hours: i) 100μM AMPA (an excitotoxic agent), ii) 200μM AMPA, iii) 200nM staurosporine (an inducer of apoptosis), iv) 100μM hydrogen peroxide (an inducer of oxidative stress) or v) no treatment. At least 3 co-cultures prepared on different occasions were exposed to each neurotoxic treatment and the number of surviving motoneurons was expressed as a percentage of the number of motoneurons in the untreated group prepared on the same occasion. **Figure 3.17** shows examples of co-cultures stained for MAP-2 that received (**A**) no treatment, (**B**) 200μM AMPA or (**C**) 200nM staurosporine. Motoneurons treated with AMPA, staurosporine or H_2O_2 showed morphological signs of cellular damage, such as damage to the motoneuron soma (shown by the arrowheads in **Figure 3.17B**) and neuritic blebbing (shown by the arrows in **Figure 3.17C**) compared to those in the control, untreated cultures. The effect of exposure to each of these stressful stimuli on motoneuron survival in each co-culture condition was assessed and the results are summarised in **Figure 3.18**. Exposure to each of the stressful stimuli resulted in the death of a significant proportion of motoneurons in each of the co-culture conditions. Surprisingly, there was no significant difference in the number of motoneurons surviving in WTnWTa, SODnWTa, WTnSODa and SODnSODa co-cultures following exposure to excitotoxic, apoptotic or oxidative insults ($p > 0.1$), suggesting that the presence of mutant SOD1 in either motoneurons or astrocytes had no effect on their vulnerability to acute cell death agents.

Figure 3.17 – MAP-2 immunostaining of co-cultured motoneurons

The photomicrographs show examples of MAP-2 immunostained motoneurons that were (**A**) untreated, or were treated with (**B**) 200μM AMPA for 24 hours or (**C**) 200nM staurosporine for 24 hours. A substantial proportion of motoneurons died following neurotoxic treatment and the motoneurons remaining following AMPA or staurosporine treatment showed morphological signs of cellular damage, such as damage to the motoneuron soma, as shown by the arrowheads in **B**, and neuritic blebbing, as shown by the arrows in **C**, compared to those in the control untreated co-cultures (**A**). Scale bar = 50μm.

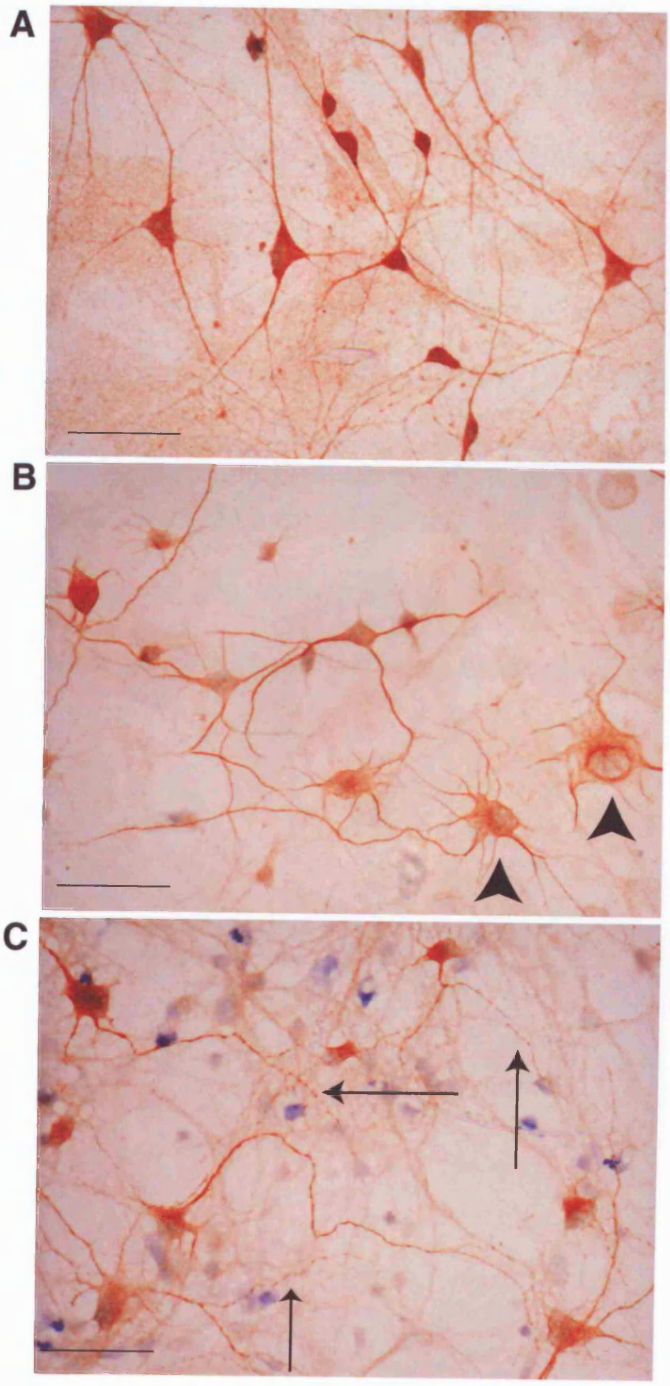
A
B
C

Figure 3.18 – The number of surviving motoneurons after exposure to stressful stimuli

Motoneurons in the various co-culture conditions were exposed to an excitotoxic (100μM or 200μM AMPA), apoptotic (200nM staurosporine) or oxidative (100μM hydrogen peroxide) insult for 24 hours. The number of surviving motoneurons was assessed using the trypan blue exclusion method and immunostained for MAP-2, a pan neuronal marker, for morphological identification. Exposure to each of the stressful stimuli induced the death of a substantial proportion of motoneurons compared to control, untreated co-cultures. However, there was no significant difference in the number of motoneurons surviving in WTnWTa, SODnWTa, WTnSODa and SODnSODa co-cultures exposed to any of the insults ($p > 0.1$). Values are the mean number of motoneurons surviving, from at least 3 different co-cultures, expressed as a percentage of the number of control motoneurons from the same preparation ± standard error of the mean.

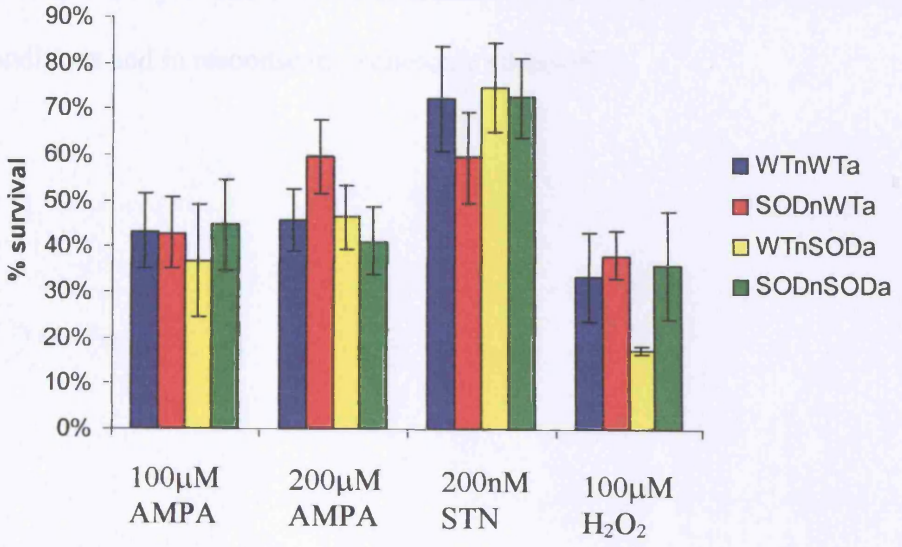
90%
80%
70%
60%
50%
40%
30%
20%
10%
0%
% survival
WTnWTa
SODnWTa
WTnSODa
SODnSODa
100µM AMPA
200µM AMPA
200nM STN
100µM H_2O_2

3.3.6. Summary of results

A number of physiological and cellular parameters of motoneurons and astrocytes under the various co-culture conditions were examined in this Chapter. The results of this Chapter are summarised in **Figure 3.19**, which illustrates the influence of mutant SOD1 expression in astrocytes and also motoneurons to the response of motoneurons under basal conditions and in response to excitotoxic stimulation.

Figure 3.19 – Summary of the influence of mutant SOD1 expression in astrocytes and motoneurons under basal conditions (A) and in response to excitotoxic stimulation (B)

A) BASAL CONDITIONS

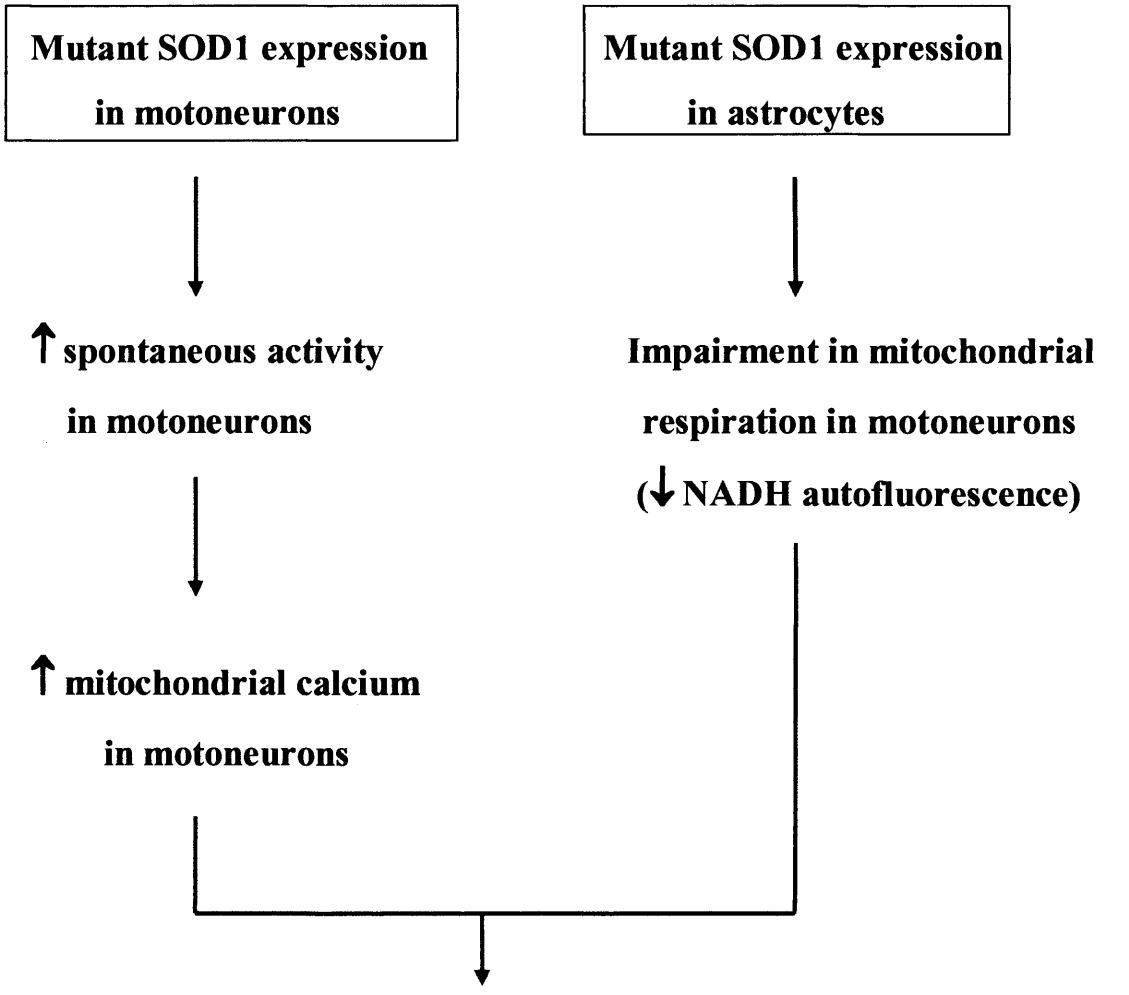

B) EXCITOTOXIC CONDITIONS

Mutant SOD1 expression in either motoneurons or astrocytes

↓

No change in $[Ca^{2+}]_c$ influx in motoneurons

No change in rate of mitochondrial depolarisation in motoneurons

BUT

↑ in extent of mitochondrial depolarisation in motoneurons

↑ rate of superoxide generation in motoneurons

3.4. DISCUSSION

In this Chapter, the role that astrocytes play in ALS pathogenesis was investigated by studying the effect of differential expression of mutant SOD1 in either motoneurons or astrocytes. Several cellular properties of motoneurons and in some cases astrocytes were examined under both resting, basal conditions and in response to excitotoxic stimuli using fluorescent imaging. The key findings are summarised in **Table 3.9**, which illustrates the responses of motoneurons in which mutant SOD1 was expressed in either motoneurons, astrocytes or both cell types, compared with motoneurons from WTnWTa co-cultures. It can be seen that in motoneurons in SODnSODa co-cultures almost every parameter investigated is significantly different from the response obtained in WTnWTa co-cultures. Thus, expression of mutant SOD1 in both motoneurons and astrocytes has serious consequences, even in embryonic motoneurons. Furthermore, expression of mutant SOD1 in either astrocytes or in motoneurons also alters some motoneuron responses suggesting that expression of the mutant SOD1 protein in either neurons or non-neuronal cells alone is sufficient to induce alterations in the cellular homeostasis of motoneurons.

The co-culture system used in this study generates four different co-culture conditions; WTnWTa, SODnWTa, WTnSODa and SODnSODa. Spinal cords astrocytes are used, in preference over for example cortical astrocytes, in order to model the natural environment of spinal motoneurons that exists *in vivo*. Furthermore, it is important to use spinal cord astrocytes as deficits in glutamate transport have been reported in spinal cord astrocytes in both post-mortem tissue from ALS patients and mutant SOD1 mice (Rothstein et al., 1992; Bruijn et al., 1997). Despite the highly simplistic nature of this co-culture system compared to the *in vivo* spinal cord, it provides an excellent model to examine the effects of mutant SOD1 expression on a cellular basis. This system permits

Table 3.9 – Summary of the alterations in cellular properties of motoneurons induced by the expression of mutant SOD1, under basal conditions and in response to excitotoxic stimuli

The Table summarises the mean alterations in cellular properties of motoneurons from SODnWTa, WTnSODa and SODnSODa co-cultures in comparison to motoneurons from WTnWTa co-cultures, under basal conditions and in response to excitotoxic stimuli.

$[Ca^{2+}]_c$ = cytosolic calcium levels, $[Ca^{2+}]_m$ = mitochondrial calcium levels, $\Delta\Psi_m$ = mitochondrial membrane potential.

	SODnWTa		WTnSODa		SODnSODa	
	Basal	Excitotoxic	Basal	Excitotoxic	Basal	Excitotoxic
$[Ca^{2+}]_c$ -						
fura 2-FF	-	-	-	-	↓	-
fluo 4	↓	-	↓	-	↓	-
$[Ca^{2+}]_m$						
(rhod 5N)	↑	-	↑	-	↑	↓
Spontaneous						
$[Ca_{2+}]_c$ (fluo 4)	↑		-		↑	
$\Delta\Psi_m$ (TMRM)						
Basal	-		↓		↓	
Rate - KA		-		-		-
Extent - KA		-		↑		↑
Superoxide						
generation						
(HEt)						
Basal	-		-		↓	
KA		↑		-		-
GLT		-		↓		-
NADH						
autofluorescence						
Cyanide	-		-		↓	
Rotenone	-		-		↓	
High K^+ (fluo 4)						
$[Ca^{2+}]_c$		-		-		-
$\Delta\Psi_m$: Rate		-		-		-
Extent		↓		↓		↓

detailed analysis of the response of individual motoneurons to the extracellular application of a variety of agents. Furthermore, confocal imaging provides the high spatial and temporal resolution to perform such experiments.

3.4.1. The effect of expression of mutant SOD1 on basal cellular properties

3.4.1.1. Basal cellular calcium levels

Even under resting conditions, expression of mutant SOD1 in motoneurons and astrocytes alters several cellular properties compared to motoneurons in WT conditions. The results show that in motoneurons in SODnSODa co-cultures there is a reduction in $[Ca^{2+}]_c$, possibly due to enhanced mitochondrial calcium uptake, since $[Ca^{2+}]_m$ is elevated. Selective expression of mutant SOD1 in either motoneurons or astrocytes also causes elevations in $[Ca^{2+}]_m$ and lower $[Ca^{2+}]_c$ at rest, although the cytosolic data, measured with fluo 4, is not observed with the more quantitative indicator fura 2-FF. However, it appears that expression of mutant SOD1 either in motoneurons or astrocytes, is sufficient to alter calcium homeostasis in motoneurons.

i) Elevated mitochondrial calcium levels ($[Ca^{2+}]_m$)

Calcium influx into mitochondria is dependent on the electrochemical potential gradient, which in turn is determined by a combination of the $\Delta\Psi_m$ and the $[Ca^{2+}]_m$ (Kapus et al., 1991). Therefore, mitochondrial hyperpolarisation may induce an elevation in calcium loading of mitochondria. However, under basal conditions the $\Delta\Psi_m$ of motoneurons from SODnWTa co-cultures does not differ significantly from WTnWTa, whereas motoneurons from WTnSODa and SODnSODa co-cultures have a reduced $\Delta\Psi_m$. This reduction in $\Delta\Psi_m$ may be a consequence of the elevated $[Ca^{2+}]_m$, as calcium influx into mitochondria, through the uniporter, will induce depolarisation of the $\Delta\Psi_m$. Mitochondrial depolarisation can subsequently inhibit the electrogenic

Na^+/Ca^{2+} exchanger consequently reducing calcium efflux (Montero et al., 2001). Therefore, an elevated $[Ca^{2+}]_m$ influx may, via the induction of a slight mitochondrial depolarisation, slow the re-equilibration of calcium between the mitochondria and cytosol, thereby increasing resting $[Ca^{2+}]_m$.

ii) Spontaneous calcium activity

Although mitochondrial hyperpolarisation may be the driving force for elevated $[Ca^{2+}]_m$ uptake in mutant SOD1-expressing co-cultures, it is more likely that the increase in $[Ca^{2+}]_m$ is due to increased spontaneous calcium activity observed when mutant SOD1 is expressed in motoneurons or in astrocytes but only when co-cultured with WT motoneurons. Typically, transient elevations in $[Ca^{2+}]_c$ are reflected by more prolonged changes in $[Ca^{2+}]_m$ and consequently changes in mitochondrial metabolism (Hajnoczky et al., 1995; Robb-Gaspers et al., 1998). Therefore, an increase in the frequency of intracellular calcium transients may result in augmentation of $[Ca^{2+}]_m$ loading. Indeed, mutant SOD1 motoneurons, which show the greatest spontaneous calcium activity, consistently have the highest $[Ca^{2+}]_m$ under basal conditions.

The increased spontaneous activity seen in mutant SOD1 motoneurons may be due to an increased persistent sodium conductance, which would induce motoneuron depolarisation and increase the probability of opening of voltage-gated calcium channels. Previous reports have found that mutant SOD1 motoneurons show an increase in spontaneous excitability (Pieri et al., 2003; Kuo et al., 2004). In mutant SOD1 mice this enhanced excitability of motoneurons may be further exacerbated by a reduction in the functioning of the Na^+/K^+ ATPase towards end-stage of disease (Ellis et al., 2003). As a result of the increased spontaneous excitability of mutant SOD1 motoneurons, the probability of opening of voltage-gated potassium channels is also likely to be

increased, resulting in elevated extracellular potassium levels. Thus, in the presence of mutant SOD1-expressing motoneurons, astrocytes may buffer excess potassium, which will reduce their spontaneous activity. In contrast, when co-cultured with WT motoneurons, the spontaneous activity of mutant SOD1 astrocytes will not be suppressed in this way. Since astrocyte calcium signalling can modulate neuronal activity (see **Chapter 3.1.2.3**), the increase in spontaneous activity of astrocytes may result in increased $[Ca^{2+}]_m$ in motoneurons, as observed in WTnSODa co-cultures.

iii) Consequences of elevated mitochondrial calcium levels ($[Ca^{2+}]_m$)

Under normal physiological conditions, the uptake of calcium by mitochondria provides a mechanism by which increased cellular activity is coupled with an up-regulation of mitochondrial metabolism. However, elevated $[Ca^{2+}]_m$ has also been implicated in many pathological conditions. Indeed, inhibition of $[Ca^{2+}]_m$ uptake has neuroprotective effects following exposure to excitotoxic levels of glutamate (Stout et al., 1998). There are several mechanisms by which elevated $[Ca^{2+}]_m$ may be damaging to cellular function. Uptake of calcium may activate many calcium-dependent processes, particularly if high $[Ca^{2+}]_m$ is maintained. For example, a correlation between calcium uptake and NO production in endothelial cell mitochondria has been shown (Dedkova et al., 2004), which suggests that the calcium-dependent mitochondrial isoform of nitric oxide synthase (mtNOS) might be a target for the elevated $[Ca^{2+}]_m$. The high calcium affinity of mtNOS (Giulivi, 2003) coupled with elevated resting $[Ca^{2+}]_m$, implies that in the present study, mtNOS may be activated in the mutant SOD1-expressing co-cultures even under basal conditions. NO may then damage both the respiratory chain (Stewart et al., 2000; Jekabsone et al., 2003), and the Na^+/Ca^{2+} exchanger (Castilho et al., 1999), resulting in mitochondrial depolarisation (Ghafourifar & Richter, 1997). Elevated $[Ca^{2+}]_m$ can also increase production of ROS (Dykens, 1994; Castilho et al., 1995;

Dugan et al., 1995). If this occurs in combination with calcium-induced depletion of glutathione reductase and glutathione peroxidase activity, which has been shown to occur in isolated rat brain mitochondria (Zoccarato et al., 2004), subsequent damage to mitochondria will occur. Furthermore, high $[Ca^{2+}]_{m,}$ under certain conditions can induce opening of the mPTP, which can initiate cell death pathways (Halestrap et al., 2002).

Therefore, elevated $[Ca^{2+}]_m$ in motoneurons even under basal conditions, may initiate a variety of potentially neurotoxic mechanisms that can inflict cumulative damage. In addition, these motoneurons will also have a reduced mitochondrial buffering capacity due to a reduced driving force for calcium uptake into mitochondria, which again may increase their susceptibility to further stressful stimuli. This is particularly important for motoneurons, which not only have a high metabolic demand but also rely to a greater extent on mitochondrial buffering, due to the reduced cytosolic expression of calcium buffering proteins (Ince et al., 1993; Alexianu et al., 1994; Elliott & Snider, 1995).

Previous studies have reported an elevation in $[Ca^{2+}]_c$ as a consequence of mutant SOD1 expression, which is proposed to be related to a reduced mitochondrial calcium buffering capacity (Carri et al., 1997; Kruman et al., 1999). However, culture differences, both in terms of cell types and culture conditions may explain the discrepancy between these studies and the present data.

3.4.1.2. Mitochondrial status under basal conditions

In addition to elevated $[Ca^{2+}]_m$, motoneurons co-cultured with mutant SOD1 astrocytes have a reduced $\Delta\Psi_m$ under basal conditions. As discussed above, the elevation in basal $[Ca^{2+}]_m$ may contribute to the observed mitochondrial depolarisation in motoneurons. However, the $\Delta\Psi_m$ of motoneurons from SODnWTa co-cultures, which also display

elevated $[Ca^{2+}]_m$ at rest, is the same as that of motoneurons in WTnWTa co-cultures. Therefore it appears that the expression of mutant SOD1 in astrocytes confers an additional property, which results in mitochondrial depolarisation in motoneurons under basal conditions.

i) Respiratory chain defects

Inhibition of respiration by cyanide or rotenone induces an increase in NADH autofluorescence as a consequence of an accumulation of NADH, due to the inability of complex I to oxidise NADH to NAD^+. In motoneurons in SODnSODa co-cultures, there is a reduced change in NADH autofluorescence in response to cyanide or rotenone, inhibitors of complexes IV and I of the respiratory chain respectively. Furthermore, a smaller change in NADH autofluorescence in response to cyanide is also observed in motoneurons from WTnSODa co-cultures, although this does not reach statistical significance. The smaller increase in NADH autofluorescence in motoneurons from SODnSODa, and to some extent in WTnSODa co-cultures, suggests that expression of mutant SOD1 in astrocytes results in functional alterations in the electron transport chain, particularly in complex I. Reduced oxidation of NADH, possibly due to either a reduction in the availability of mitochondrial substrates or to a defect in the electron transport chain, would lower the pool of NAD^+ available for reduction, and consequently reduce the change in NADH autofluorescence that is observed upon respiratory inhibition. Further experiments will be required to distinguish between these two possibilities, but both indicate a disruption in mitochondrial function.

Therefore, in motoneurons co-cultured with mutant SOD1 astrocytes the combination of elevated $[Ca^{2+}]_m$ together with defects in the electron transport chain, perhaps in complex I, may induce mitochondrial depolarisation under basal conditions.

Motoneurons from SODnWTa co-cultures demonstrate elevated resting $[Ca^{2+}]_m$ but there is no indication of electron transport chain damage and consequently no reduction in $\Delta\Psi_m$ is observed.

Reductions in complex I and IV activities have been found in affected tissue from ALS patients, symptomatic $SOD1^{G93A}$ mice and a $SOD1^{G93A}$-expressing motoneuronal cell line (Fujita et al., 1996; Swerdlow et al., 1998; Weidemann et al., 1998; Borthwick et al., 1999; Vielhaber et al., 2000; Jung et al., 2002; Mattiazzi et al., 2002; Menzies et al., 2002; Fukada et al., 2004). Furthermore, mitochondria from the spinal cords of symptomatic $SOD1^{G93A}$ mice have a low maximal respiratory rate and reduced ATP generation, which will result in energy depletion (Mattiazzi et al., 2002). Finally, a reduction in the $\Delta\Psi_m$ of motoneurons due to mutant SOD1 expression under basal conditions has also been previously shown (Carri et al., 1997; Kruman et al., 1999; Rizzardini et al., 2005). However, in those studies the reduction in $\Delta\Psi_m$ is attributed to the expression of mutant SOD1 in motoneurons. The results of this Chapter, in contrast, suggest that the expression of mutant SOD1 in astrocytes is the critical factor that induces alterations in mitochondrial function in motoneurons.

ii) Astrocyte-mediated toxicity

In this study, expression of mutant SOD1 in astrocytes is sufficient to induce defects in the electron transport chain that, in combination with elevated $[Ca^{2+}]_m$, ultimately results in the mitochondrial depolarisation of co-cultured motoneurons. The expression of mutant SOD1 in a glioblastoma cell line is sufficient to induce cellular activation and the subsequent production of NO (Ferri et al., 2004). Astrocyte-derived NO (via iNOS stimulation) can diffuse to neighbouring motoneurons and has been shown to inhibit mitochondrial respiration (Bal-Price & Brown, 2001). NO-mediated damage to the

electron transport chain can occur via both a direct and indirect mechanism. NO can compete with molecular oxygen for binding to complex IV, and reversibly inhibit respiration (Brown & Cooper, 1994). However, the reaction of NO with superoxide generates peroxynitrite, which can mediate substantial cellular damage including irreversible inhibition of complexes I, II/III and IV (Brown & Cooper, 1994; Brookes et al., 1998; Stewart et al., 2000; Jekabsone et al., 2003). NO-mediated respiratory inhibition can induce mitochondrial depolarisation and subsequently increase ROS production, and furthermore may also stimulate the release of glutamate (Bal-Price & Brown, 2001; Votyakova & Reynolds, 2001). A contribution of mtNOS to mitochondrial damage is also possible, since this enzyme may be activated in response to elevated $[Ca^{2+}]_m$, and will generate NO inside the mitochondria, in close proximity to the electron transport chain (Giulivi, 2003).

Reactive astrocytes also release a variety of proinflammatory cytokines that can induce COX2 expression, via activation of the transcription factor NF-κB (Consilvio et al., 2004; Juttler et al., 2004). COX2 activation will increase production of prostaglandins, including PGE_2, which may contribute to excitotoxicity by stimulating the release of glutamate from astrocytes (Drachman & Rothstein, 2000), and in addition releases ROS, which may further propagate the inflammatory process and exert neurotoxicity (Consilvio et al., 2004). Therefore, the data presented in this Chapter suggests that mutant SOD1 expression in astrocytes can have significantly detrimental effects on adjacent motoneurons.

However, under basal conditions, the mutant SOD1-induced defect in respiration and elevation in $[Ca^{2+}]_m$, with resulting mitochondrial depolarisation, does not appear to affect motoneuron viability *in vitro*. Indeed, there is no difference in motoneuron

survival in any of the 4 co-culture conditions. However, it is possible that over time the reduced efficiency of respiration in depolarised mitochondria may reduce ATP generation, therefore depleting cellular energy and eventually initiating necrosis.

3.4.1.3. Basal cellular superoxide production

The electron transport chain in mitochondria is regarded as the main cellular source of superoxide. The release of unpaired electrons from complexes I and III during oxidative phosphorylation, can react with oxygen to generate superoxide, which can subsequently exert cellular damage. A combination of highly susceptible mitochondrial components with the localised production of superoxide renders mitochondria highly vulnerable to oxidative damage.

In both motoneurons and astrocytes from SODnSODa co-cultures, the rate of superoxide generation under basal conditions is less than in WTnWTa co-cultures. This selective reduction in oxidation rates may be related to the increased expression of the mutant SOD1 enzyme in these co-cultures as the mutant $SOD1^{G93A}$ protein has been shown to retain full enzymatic activity (Gurney et al., 1994). In both SODnWTa and WTnSODa co-cultures, there is also a trend towards a reduced basal rate of superoxide generation, which may be related to the increased expression of the mutant SOD1 enzyme. An alternative possibility is that the reduced rate of superoxide production is a consequence of the partial depolarisation of the mitochondria from both motoneurons and astrocytes in SODnSODa co-cultures. The generation of superoxide from complex I has a $\Delta\Psi_m$-dependent and independent component. Therefore the production of ROS via the succinate-driven transfer of electrons from complex II to I is highly $\Delta\Psi_m$ dependent, with mitochondrial depolarisation inhibiting superoxide production. In contrast, ROS

production mediated by complex III is independent of $\Delta\Psi_m$ (Votyakova & Reynolds, 2001).

However, in contrast to the results that are presented in this Chapter, Kruman et al, (1999) reported an increased rate of superoxide production in primary $SOD1^{G93A}$ motoneurons under basal conditions. However, this result is observed in motoneurons cultured without an enriched astrocyte layer. Furthermore, Swerdlow et al, (1998) reported an increase in the rate of free radical scavenging activity in platelets expressing mtDNA from sALS patients, which has been taken to imply a greater free radical production. However, if this assumption is correct then it applies to all free radicals and not just superoxide. Perhaps investigation into total free radical production may reveal an increase in the co-cultures.

3.4.2. The effect of expression of mutant SOD1 on the response of motoneurons to excitotoxicity

3.4.2.1. Cellular calcium levels

In these experiments the different co-cultures are exposed to excitotoxic stimuli, initially KA followed by glutamate, and the cellular response of motoneurons and astrocytes are assessed. KA is used as a specific glutamate receptor agonist since it has been proposed that motoneurons show a selective vulnerability to AMPA/KA receptor-mediated excitotoxicity, and the subsequent application of glutamate allows investigation into whether a secondary response is observed to a physiological agonist.

Expression of mutant SOD1 has no effect on the $[Ca^{2+}]_c$ influx into either motoneurons or astrocytes following exposure to KA and glutamate. Thus, the peak $[Ca^{2+}]_c$ influx induced by the sequential addition of KA and glutamate in both motoneurons and

astrocytes is the same in all co-culture conditions. Thus, although there is considerable evidence to indicate that glutamate excitotoxicity plays a role in ALS, as discussed in detail in **Chapter 1.3.4.2.**, the current experiments do not detect any differential vulnerability of mutant SOD1-expressing motoneurons to KA or glutamate compared to WT motoneurons. This implies that the expression of mutant SOD1 does not increase the selective vulnerability of motoneurons to excitotoxicity. In ALS, motoneurons, which have a number of characteristics that render them more susceptible to glutamate, including a reduction in expression of calcium binding proteins (Ince et al., 1993; Alexianu et al., 1994; Elliott & Snider, 1995) and an increased density of AMPA/KA receptors (Carriedo et al., 1996; Vandenberghe et al., 2000b; van den Bosch et al., 2000, 2002; Van Damme et al., 2003), are exposed to greater levels of glutamate than motoneurons in normal spinal cord. The results of the experiments in this Chapter however, suggest that mutant SOD1 toxicity does not involve an elevated susceptibility to glutamate, at least in an acute, *in vitro* model. However, accumulative effects of the expression of mutant SOD1 over time on the vulnerability of motoneurons to excitotoxicity cannot be excluded.

As with some of the basal data obtained in experiments described in this Chapter, the data on glutamate-induced $[Ca^{2+}]_c$ influx contrasts to that reported by Kruman et al, (1999), in which a given concentration of glutamate not only induces a greater $[Ca^{2+}]_c$ influx, but also a greater production of ROS and an increased mitochondrial depolarisation in primary $SOD1^{G93A}$ motoneuron monocultures. However, Stout et al, (1998) demonstrated that increased $[Ca^{2+}]_c$ itself might not be neurotoxic and suggest that the extent of $[Ca^{2+}]_m$ loading determines toxicity since they found that inhibition of $[Ca^{2+}]_m$ uptake, and the subsequent sustained elevation in $[Ca^{2+}]_c$, is neuroprotective. Alternatively, calcium-mediated neurotoxicity may be determined by the inability of the

cell to return $[Ca^{2+}]_c$ to baseline due to defects in calcium extrusion. Mitochondrial depolarisation, induced by calcium uptake, may inhibit calcium extrusion mechanisms, since the Na^+/Ca^{2+} exchanger and Ca^{2+}/H^+ pump are both ATP dependent (Montero et al., 2001). The contribution of such mechanisms to excitotoxicity-induced motoneuron toxicity requires further investigation.

3.4.2.2. Mitochondrial depolarisation in response to excitotoxicity

Expression of mutant SOD1 in motoneurons and astrocytes not only has no effect on changes in $[Ca^{2+}]_c$ but also does not affect the rate of mitochondrial depolarisation in response to either KA or glutamate. Normalisation of the data to account for variability in the resting $\Delta\Psi_m$, however, reveals that in response to the same $[Ca^{2+}]_c$ influx, mitochondria from motoneurons in WTnSODa and SODnSODa co-cultures depolarise to a greater extent in response to KA than in WTnWTa co-cultures. Previously, Kruman et al, (1999) have also shown a greater loss of $\Delta\Psi_m$ in response to glutamate in $SOD1^{G93A}$ motoneurons.

The greater susceptibility of these mitochondria to depolarisation in response to excitotoxicity may be related to their underlying resting mitochondrial defects, including; elevated $[Ca^{2+}]_m$, possible defects in the electron transport chain complex activity and reduced $\Delta\Psi_m$. Therefore, the mitochondria from motoneurons co-cultured with mutant SOD1-expressing astrocytes are already altered even under basal conditions, which suggests that they may have been less able to withstand an excitotoxic insult. The release of NO and proinflammatory cytokines by mutant SOD1 astrocytes, in combination with an elevation in $[Ca^{2+}]_m$, may exert mitochondrial toxicity that underlies this selective vulnerability, as described in **Chapter 3.4.1.2**. Keelan et al, (1999) proposed that mitochondrial depolarisation following NMDA

receptor activation, requires the combination of NO with an innocuous calcium load. Indeed, the $[Ca^{2+}]_c$ influx in response to excitotoxicity may combine with NO derived from mutant SOD1 astrocytes to induce a greater extent of mitochondrial depolarisation in mutant SOD1 astrocyte containing co-cultures. The complete mitochondrial depolarisation in SODnSODa co-cultures following glutamate exposure may represent the opening of the mPTP, a large conductance pore that spans the inner and outer mitochondrial membranes. High $[Ca^{2+}]_m$ in combination with oxidative stress, ATP depletion, high inorganic phosphate and mitochondrial depolarisation can trigger the opening of the mPTP and ultimately mitochondrial death (Halestrap et al., 2002). The release of cytochrome c from the mitochondria may also stimulate apoptosis (De Giorgi et al., 2002), or alternatively, the resultant collapse of $\Delta\Psi_m$ and ATP depletion may eventually initiate necrotic cell death (Sullivan et al., 2005).

3.4.2.3. Cellular superoxide production in response to excitotoxicity

In contrast to $[Ca^{2+}]_c$ and mitochondrial membrane potential depolarisation, expression of mutant SOD1 in motoneurons, astrocytes or both cell types has a significant effect on the rate of superoxide generation following exposure to KA and glutamate. Thus, in response to stimulation with KA, the rate of superoxide generation is significantly increased in motoneurons from SODnWTa, WTnSODa and SODnSODa co-cultures compared to their individual basal rates, but not in WTnWTa co-cultures. However, when compared directly to WTnWTa co-cultures, the rate is only increased in response to KA in motoneurons from SODnWTa co-cultures, although there is a trend towards an increased rate of superoxide production in motoneurons from WTnSODa and SODnSODa co-cultures as well. Similarly in astrocytes, the rate at which superoxide is generated is increased in SODnWTa and WTnSODa co-cultures following KA exposure, compared to WTnWTa, although again a trend towards an increased rate is

also observed in astrocytes in SODnSODa co-cultures. Thus, expression of mutant SOD1 appears to increase the rate of superoxide production in motoneurons and astrocytes in response to KA stimulation. However, these results may actually be an underestimation of the level of free radical production since HEt is an indicator of superoxide production alone. An elevated free radical generation in mutant SOD1 motoneurons has been previously shown following glutamate stimulation (Kruman et al., 1999), consistent with these results. Similarly, markers of oxidative damage are increased in mitochondria isolated from the brain and spinal cord of symptomatic $SOD1^{G93A}$ mice (Mattiazzi et al., 2002).

The increase in superoxide production together with further mitochondrial depolarisation in mutant SOD1-expressing co-cultures is perhaps surprising due to the dependence of free radical production on $\Delta\Psi_m$. However, enhanced free radical generation has previously been associated with mitochondrial depolarisation induced by NMDA receptor (Solenski et al., 2003) and AMPA/KA receptor activation (Rao et al., 2003). Furthermore, Lafon-Cazal et al, (1993) demonstrated an enhancement in free radical generation that is delayed in relation to mitochondrial depolarisation. More recently it has been suggested that a component of mitochondrial ROS generation occurs independently of the $\Delta\Psi_m$. Votyakova & Reynolds, (2001) demonstrated that ROS production driven by complex I substrates glutamate and malate, occurs independently of $\Delta\Psi_m$. Furthermore, in the same study, the $\Delta\Psi_m$-independent production of ROS is enhanced in the presence of complex I inhibition (Votyakova & Reynolds, 2001). As described earlier, there appears to be a defect in mitochondrial respiration in motoneurons co-cultured with mutant SOD1 astrocytes, possibly mediated by iNOS activation. Therefore NO-mediated damage to the electron transport chain may induce an increased rate of superoxide generation in mutant SOD1-expressing astrocyte

co-cultures, despite depolarised mitochondria. Whereas in motoneurons in SODnWTa co-cultures, elevated $[Ca^{2+}]_m$ and mtNOS activation may be responsible for increased superoxide production (Dykens, 1994; Castilho et al., 1995; Dugan et al., 1995). Indeed, the increase in superoxide generation despite a significant reduction in $\Delta\Psi_m$ implies that under these co-culture conditions, a significant proportion of $\Delta\Psi_m$-independent superoxide production occurs. Potentially, the production of free radicals from arachidonic acid metabolism, xanthine oxidase and NADPH oxidase, which are mitochondrial-independent sources, may also contribute to the observed increase in superoxide generation.

In motoneurons in mutant SOD1-expressing co-cultures, the rate of superoxide generation in response to glutamate is significantly reduced compared to the rate in response to KA. This may be indicative of reduced mitochondrial viability. Indeed, the almost complete loss of $\Delta\Psi_m$ in motoneurons in SODnSODa co-cultures in response to glutamate may reflect the opening of the mPTP. Calcium extrusion mechanisms are sensitive to ROS-induced damage. Therefore, enhanced ROS production may impair the cellular clearance of calcium, further increasing intracellular calcium concentrations, so that the combination of ROS and calcium can induce mPTP opening (Castilho et al., 1999; reviewed in Duchen, 2004).

3.4.2.4. Mitochondrial calcium levels

In all co-culture conditions, glutamate stimulation induces significant $[Ca^{2+}]_m$ loading. However, the loading of $[Ca^{2+}]_m$ in motoneurons from SODnSODa co-cultures is less than that in motoneurons in WTnWTa co-cultures. This is in contrast to the results obtained under basal conditions, which show that motoneurons in SODnSODa co-cultures have significantly elevated $[Ca^{2+}]_m$. However, there may be a causal link

between the two values as increased $[Ca^{2+}]_m$ at rest can induce partial mitochondrial depolarisation and reduce the subsequent driving force for calcium influx into mitochondria, which is dependent on both the $\Delta\Psi_m$ and the $[Ca^{2+}]_m$ (Kapus et al., 1991). Therefore, in response to glutamate stimulation, the mitochondria of motoneurons in SODnSODa co-cultures will have a reduced capacity for calcium influx. The resting $[Ca^{2+}]_m$ in motoneurons in SODnWTa and WTnSODa co-cultures are also elevated, and there is a tendency for a lower $[Ca^{2+}]_m$ influx in motoneurons in these co-cultures in response to glutamate.

These observations may at first appear to contradict the prevailing view that $[Ca^{2+}]_m$ overloading is associated with neuronal death and conversely that inhibition of $[Ca^{2+}]_m$ uptake has neuroprotective effects (Stout et al., 1998; Rodrigo et al., 2002). Therefore, the fact that mutant SOD1 motoneurons have a reduced $[Ca^{2+}]_m$ loading in response to glutamate in the co-culture set up in this study may be considered surprising. However, as discussed above, mutant SOD1 motoneurons co-cultured with mutant SOD1 astrocytes exhibit several mitochondrial defects even under basal, resting conditions. This suggests that they might have a particular vulnerability to further insults. Indeed a greater extent of mitochondrial depolarisation and increased superoxide production are observed in motoneurons in SODnSODa co-cultures in response to excitotoxicity. It is possible that a toxic threshold for $[Ca^{2+}]_m$ exists in motoneurons and once reached, calcium-dependent deleterious processes are activated. Therefore, the pre-existing mitochondrial defects in combination with only a reduced $[Ca^{2+}]_m$ influx in response to excitotoxicity, may be sufficient to induce mitochondrial depolarisation resulting in cytochrome c release and apoptosis, or energy depletion and necrotic cell death.

3.4.2.5. Response to depolarisation of the plasma membrane

A critical factor influencing the effects of $[Ca^{2+}]_c$ influx may be the source through which the calcium enters the cell ('source specificity' hypothesis; Sattler et al., 1998), rather than the extent of the calcium influx ('calcium load' hypothesis; Lu et al., 1996). The basis of the 'source specificity' hypothesis is that distinct neurotoxic signalling pathways may be activated in response to calcium influx via a specialised route (Sattler et al., 1998), for example AMPA/KA receptors in motoneurons. In contrast, an equivalent calcium influx through an alternative pathway, for example voltage-gated calcium channels, may lack neurotoxic actions. Therefore in this study, the change in $[Ca^{2+}]_c$ and extent of mitochondrial depolarisation is also investigated in response to high concentrations of potassium, which acts to depolarise the plasma membrane.

The results show that there is a greater $[Ca^{2+}]_c$ influx and rate of mitochondrial depolarisation in motoneurons in response to KA compared to potassium in all co-culture conditions, although in homogeneous WT or $SOD1^{G93A}$ co-cultures these results do not reach significance. However, the extent of mitochondrial depolarisation in motoneurons is greater in response to KA compared to potassium in all co-cultures. This suggests that both mutant SOD1-expressing and WT motoneurons have an increased vulnerability to KA over potassium-induced depolarisation. However, potassium does induce prolonged mitochondrial depolarisation in motoneurons. This is in contrast to mitochondria in hippocampal neurons that have been shown to not depolarise in response to potassium, despite a significant elevation in $[Ca^{2+}]_c$ (Keelan et al., 1999). Previously, Roy et al, (1998) reported that calcium influx via voltage-gated calcium channels contributes to the toxicity of $SOD1^{G93A}$ expression.

3.4.2.6. Survival assay

In addition to fluorescent imaging of motoneurons in co-cultures the effect of expression of mutant SOD1 in astrocytes on the susceptibility of motoneurons to a number of toxic insults is also examined. In contrast to the data acquired by fluorescent imaging, 24 hour exposure to neurotoxic agents, reveals no differences in motoneuron survival in any of the co-culture conditions. These results imply that the expression of mutant SOD1 in motoneurons or astrocytes does not increase vulnerability of motoneurons to cell death. However, it is more likely that such cell death assays are too crude to identify subtle but significant changes in motoneurons that may accumulate over time, to gradually increase the vulnerability of motoneurons to cell death.

3.5. Overall summary of results

3.5.1. Susceptibility of motoneurons to mitochondrial damage

The results of this Chapter indicate that mutant SOD1 astrocytes exert a deleterious influence on the mitochondrial function of mutant SOD1 motoneurons, inducing defects in several mitochondrial parameters even under basal conditions. However, following acute excitotoxic stimulation, the influence of mutant SOD1-expressing astrocytes is less clear, although it appears that expression of mutant SOD1 in either motoneurons or astrocytes is sufficient to induce the observed changes.

Motoneurons have a very high metabolic rate and are therefore particularly vulnerable to mitochondrial inhibition. Interestingly, irregularities in mitochondrial structure, including dilated cristae and mitochondrial swelling, have previously been identified in motoneurons in post-mortem tissue from sporadic and familial ALS patients (Hirano et al., 1984; Fujita et al., 1996; Sasaki & Iwata, 1996; Siklos et al., 1996). In mutant SOD1 mice, one of the earliest pathological signs are abnormalities in mitochondrial structure

associated with altered function, occurring even before the appearance of symptoms (as discussed in **Chapter 1.3.4.3.**; Dal Canto & Gurney, 1994; Wong et al., 1995; Kong & Xu et al., 1998; Bendotti et al., 2001; Jaarsma et al., 2001). Moreover, there is some evidence to suggest that mutant SOD1 may specifically associate with mitochondria in the spinal cord of mutant SOD1 mice (Liu et al., 2004; Pasinelli et al., 2004). Furthermore, proteomic analysis of NSC34 cells reveals significant mitochondrial deficits induced by mutant SOD1 expression (Kirby et al., 2005). Thus, together with the results of the present study, an increasing body of evidence now suggests that mitochondria may be a primary target in ALS. The results shown here provide a functional basis for the morphological and proteomic changes previously reported by other authors.

3.5.2. The contribution of astrocytes to ALS pathogenesis

The evidence presented in this Chapter supports a toxic role of mutant SOD1 astrocytes on mutant SOD1 motoneurons under basal conditions. These findings are consistent with increasing evidence that suggests that ALS is a non-cell autonomous disorder. In a series of elegant experiments, Clement et al, (2003) generated chimeric mice that have varying expression of mutant SOD1 and endogenous WT SOD1 in motoneurons and non-neuronal cells. In these mice, mutant SOD1 expressing non-neuronal cells are found to exert detrimental effects on WT motoneurons. In contrast, an environment of WT non-neuronal cells protects mutant SOD1 motoneurons from degeneration. Similarly, it has also been shown that the selective expression of mutant SOD1 in either motoneurons or astrocytes *in vivo* is not sufficient to induce motoneuron pathology, indicating that interaction between mutant SOD1-expressing neurons and astrocytes is required for the development of ALS (Gong et al., 2001; Pramatarova et al., 2001; Lino et al., 2002).

Considering the close spatial association and extensive functional interaction between neurons and astrocytes, which is maintained in ALS (Levine et al., 1999), it is perhaps not surprising that degenerative changes are also seen in astrocytes. Rao et al, (2003) demonstrated that free radicals generated through the activation of AMPA/KA receptors in motoneurons could be released to exert oxidative damage on neighbouring astrocytes. Furthermore, activated astrocytes release a variety of neurotoxic molecules, including pro-inflammatory cytokines and NO, which can exert neuronal damage (reviewed in Barbeito et al., 2004). This may initiate a self-propagating cycle of damage between motoneurons and astrocytes.

3.6. CONCLUSION

In ALS, significant astrocytic pathology accompanies motoneuron degeneration in the spinal cord. Recently it has been suggested that alterations in non-neuronal cell functions are likely to contribute to ALS pathogenesis. The data presented in this Chapter suggest that the expression of the mutant SOD1 enzyme, particularly in astrocytes, appears to exert potentially deleterious effects on the mitochondrial function of both motoneurons and astrocytes under basal conditions. Alterations in cellular homeostasis induced by activated astrocytes may therefore increase the intrinsic vulnerability of motoneurons and astrocytes to the neurotoxic mechanisms thought to play a role in ALS pathogenesis.

CHAPTER 4

THE NEUROPROTECTIVE EFFECTS OF CANNABINOIDS IN THE SOD1^{G93A} MOUSE MODEL OF ALS

4.1. INTRODUCTION

In the experiments described in this Chapter the neuroprotective potential of cannabinoids was investigated in an *in vivo* model of ALS, by treatment of $SOD1^{G93A}$ mice with a synthetic cannabinoid.

4.1.1. Cannabinoids

Cannabis is a widely used illicit recreational drug recognised for its ability to induce a mildly euphoric relaxation with associated alterations in perception, cognition, memory and motor skills (Kumar et al., 2001). However, for centuries *cannabis sativa* has also been used as a treatment for epilepsy (reviewed in Mechoulam & Lichtman, 2003). More recently the therapeutic potential of cannabis has been further recognised by its use as an analgesic, an anti-emetic and an appetite stimulant for AIDS and cancer patients (Kumar et al., 2001). *Cannabis sativa* is composed of over 60 cannabinoid compounds that are responsible for the induction of its therapeutic and psychoactive effects. The main psychoactive component, Δ^9-tetrahydrocannabinol (Δ^9-THC), was isolated and synthesised in 1964 (Gaoni & Mechoulam). Other derivatives such as cannabidiol (CBD), the main non-psychoactive component, may modulate the response to Δ^9-THC (Wade et al., 2004) and indeed may also have therapeutic potential (Zuardi et al., 1991).

The prescriptive use of cannabis is banned in the UK under the 1971 Misuse of Drugs Act. However illegal self-medication has continued with reports of beneficial effects, particularly the alleviation of muscle spasticity by multiple sclerosis (MS) patients. As a result, several clinical trials have been initiated. An oromucosal spray combining Δ^9-THC and CBD under a self–titrating dosing regimen significantly reduces spasticity according to the Visual Analogue Scale (Wade et al., 2004). In contrast, synthetic oral

Δ^9-THC (Marinol) does not affect spasticity as assessed by the Ashworth score of spasticity (Zajicek et al., 2003). However, the patients involved in this trial did report reduced pain levels following cannabinoid treatment (Zajicek et al., 2003). Furthermore, clinical trials testing the analgesic capacity of cannabinoid extracts in conditions of acute and chronic pain report significant cannabinoid-mediated pain relief (Kumar et al., 2001; Berman et al., 2004). Thus, as a consequence of several successful clinical trials it is now apparent that cannabinoids may have an even greater therapeutic potential than previously thought.

4.1.2. Cannabinoid receptor pharmacology and modulation of neuronal activity

Until the late 1980s Δ^9-THC was believed to exert its effects via incorporation into biological membranes due to its high lipophilicity. However, Devane et al, (1988) demonstrated specific binding of CP 55,940, a synthetic cannabinoid, to rat brain membranes in a dose-dependent, saturable and enantioselective manner, all characteristic features of receptor interaction. Indeed, following identification of specific binding sites for CP 55,940 throughout the CNS (Herkenham et al., 1990), the CB_1 receptor was isolated and cloned (Matsuda et al., 1990). Subsequently a second cannabinoid receptor, the CB_2 receptor (with 68% homology to the CB_1 receptor) was identified (Kaminski et al., 1992) and cloned from peripheral immune cells (Munro et al., 1993). Due to the relatively recent discovery of cannabinoid receptors, developments in this research area are still ongoing and as a consequence there may be other, as yet unidentified cannabinoid receptors. Indeed a putative 'CB_3' receptor has been described in the brains of mice lacking the CB_1 receptor (Di Marzo et al., 2000; Breivogel et al., 2001; Monory et al., 2002).

Cannabinoid receptors are coupled to inhibitory GTP binding proteins, $G_{i/o}$ (Matsuda et al., 1990; Schatz et al., 1992). Therefore activation of CB_1 and CB_2 receptors inhibits adenylate cyclase activity in a pertussis toxin sensitive manner (Howlett & Fleming, 1984, 1985; Bidaut-Russell et al., 1990; Vogel et al., 1993). This reduction in cAMP levels, and subsequent inhibition of protein phosphorylation, may inhibit neuronal activity by activation of A-type potassium channels (Deadwyler et al., 1995). In addition, CB_1, but not CB_2, receptor coupled G_i proteins mediate inhibition of voltage gated N- and P-/Q- type calcium channels (Caulfield & Brown, 1992; Mackie & Hille, 1992; Mackie et al., 1995; Twitchell et al., 1997; Shen & Thayer, 1998a) and activation of inwardly rectifying potassium channels (Mackie et al., 1995), independent of adenylate cyclase inhibition. Thus activation of CB_1 receptors can reduce neuronal excitability and may suppress neurotransmitter release. Indeed cannabinoids have been shown to inhibit the release of neurotransmitters *in vitro* (Shen et al., 1996; Gessa et al., 1998; Levenes et al., 1998; Nicholson et al., 2003). Furthermore, the endogenous ligand anandamide and synthetic cannabinoid receptor agonist WIN55,212-2 have been shown to directly interact with, and inhibit, sodium channels and T-type calcium channels, actions which would also reduce neuronal excitability and further hinder action potential propagation (Chemin et al., 2001; Nicholson et al., 2003).

However, there is increasing evidence that cannabinoids may also have a stimulatory influence on neuronal activity. Under conditions in which $G_{i/o}$ proteins are inhibited or indeed absent, CB_1 receptors have been shown to couple to G_s proteins, stimulatory GTP binding proteins, increasing intracellular cAMP levels (Felder et al., 1998; Maneuf & Brotchie, 1997; Hampson et al., 1998a). Coupling to G_s proteins and consequential cAMP elevation is theorised to underlie an observed stimulatory effect of cannabinoids on calcium influx (Sugiura et al., 1996; Rubovitch et al., 2002; Bash et al., 2003).

Activation of protein kinase A (PKA), by cAMP, phosphorylates and activates L-type calcium channels inducing a calcium influx (Rubovitch et al., 2002). Alternatively, protein kinase C-mediated phosphorylation of mitogen activated protein kinases (MAPK) may also modulate activation of L-type calcium channels, inducing calcium influx via a CB_1 receptor-coupled, $G_{i/o}$ protein-mediated mechanism (Rubovitch et al., 2004). Furthermore, an interaction between CB_1 receptors and phospholipase C (PLC) can induce calcium release from inositol (1,4,5) tris-phosphate (IP_3) regulated stores (Netzeband et al., 1999). Enhanced calcium influx may underlie the reported stimulation of neurotransmitter release mediated by cannabinoids (Acquas et al., 2000; Ferraro et al., 2001). The ability of CB_1 receptors to couple to more than one G protein may have relevance under pathological conditions. Indeed, elevated cAMP during reperfusion is believed to improve functional outcome after ischaemic injury (Block et al., 1997).

Several other signalling pathways may also contribute to the effects of CB_1 receptor activation. Induction of mRNA expression of immediate early genes (IEGs), such as *c-fos*, involved in neuroprotection against excitotoxicity (Marsicano et al., 2003), and *Krox 24*, a growth related gene (Bouaboula et al., 1995a), by CB_1 receptor activation is mediated by G_i protein-dependent activation of extracellular signal regulated kinase (ERK; Marsicano et al., 2003) and MAPK respectively (Bouaboula et al., 1995b). ERK activation via CB_1 receptor stimulation also plays a more direct role in the control over cell fate when induced by ceramide synthesis. In cultured astrocytes, brief exposure to cannabinoids induces a transient increase in ceramide generation through the coupling of the adaptor protein FAN (factor associated with neutral sphingomyelinase activation) to the CB_1 receptor, resulting in sphingomyelin hydrolysis in a G_i protein independent manner (Sanchez et al., 2001). Ceramide production is involved in the stimulation of glucose metabolism and glycogen synthesis (Sanchez et al., 1998). However, prolonged

cannabinoid exposure initiates *de novo* synthesis and accumulation of ceramide, which induces sustained ERK activation, and under such circumstances apoptosis can be induced (Galve-Roperh et al., 2000; Guzman et al., 2001). **Figure 4.1** summarises the cellular consequences of cannabinoid receptor activation.

4.1.3. Endocannabinoid synthesis

The discovery of a receptor based signalling cascade activated by cannabinoid agonists added further weight to the hypothesised existence of endogenous metabolites capable of activating cannabinoid receptors. Indeed, displacement of radiolabelled cannabinoid ligands by fractions extracted from porcine brain and canine gut led to the identification of two endocannabinoids, arachidonyl ethanolamide (anandamide; AEA) and 2-ararachidonylglycerol (2-AG) respectively (Devane et al., 1992; Mechoulam et al., 1995; Sugiura et al., 1995). Three further substances, homo-γ-linolenylethanolamide and docosatetraenylethanolamide, both structurally related to AEA (Hanus et al., 1993) and 2-arachidonyl glyceryl ether (Hanus et al., 2001) have subsequently been identified as endocannabinoids. Meanwhile in 2002, *O*-arachidonoyl ethanolamine (virhodamine), another structural analogue of AEA was discovered. However, virhodamine has been shown to have antagonistic properties at CB_1 receptors, in contrast to AEA, although it acts as a full agonist at CB_2 receptors similarly to AEA (Porter et al., 2002).

Endocannabinoids are synthesised in a calcium-dependent manner (Di Marzo et al., 1994; Cadas et al., 1996). Confirmation of their activity at cannabinoid receptors (CB_1 and CB_2 receptors; Devane et al., 1992; Felder et al., 1993; Vogel et al., 1993; Felder et al., 1995; Slipetz et al., 1995), and identification of uptake transporters and degradation mechanisms (Di Marzo et al., 1994) have confirmed their status as neurotransmitters (discussed in more detail in **Chapter 5.1.2. – 5.1.4.**). However, there is also evidence

Figure 4.1 – The cellular pathways of cannabinoid receptor activation

Activation of cannabinoid receptors 1 and 2 (CB_1 and CB_2) by either endogenous or exogenous cannabinoids stimulates many cellular pathways that are summarised in the flow diagram. Each pathway is described in more detail in **Chapter 4.1.2**.

FAN – factor associated with neutral sphingomyelinase activation; MAPK – mitogen activated protein kinase; ERK – extracellular activated protein kinase; A.C. – adenylate cyclase; PKA – protein kinase A; PKC – protein kinase C; PLC – phospholipase C; DAG – diacylglycerol; IP_3 – inositol (1,4,5) tris-phosphate.

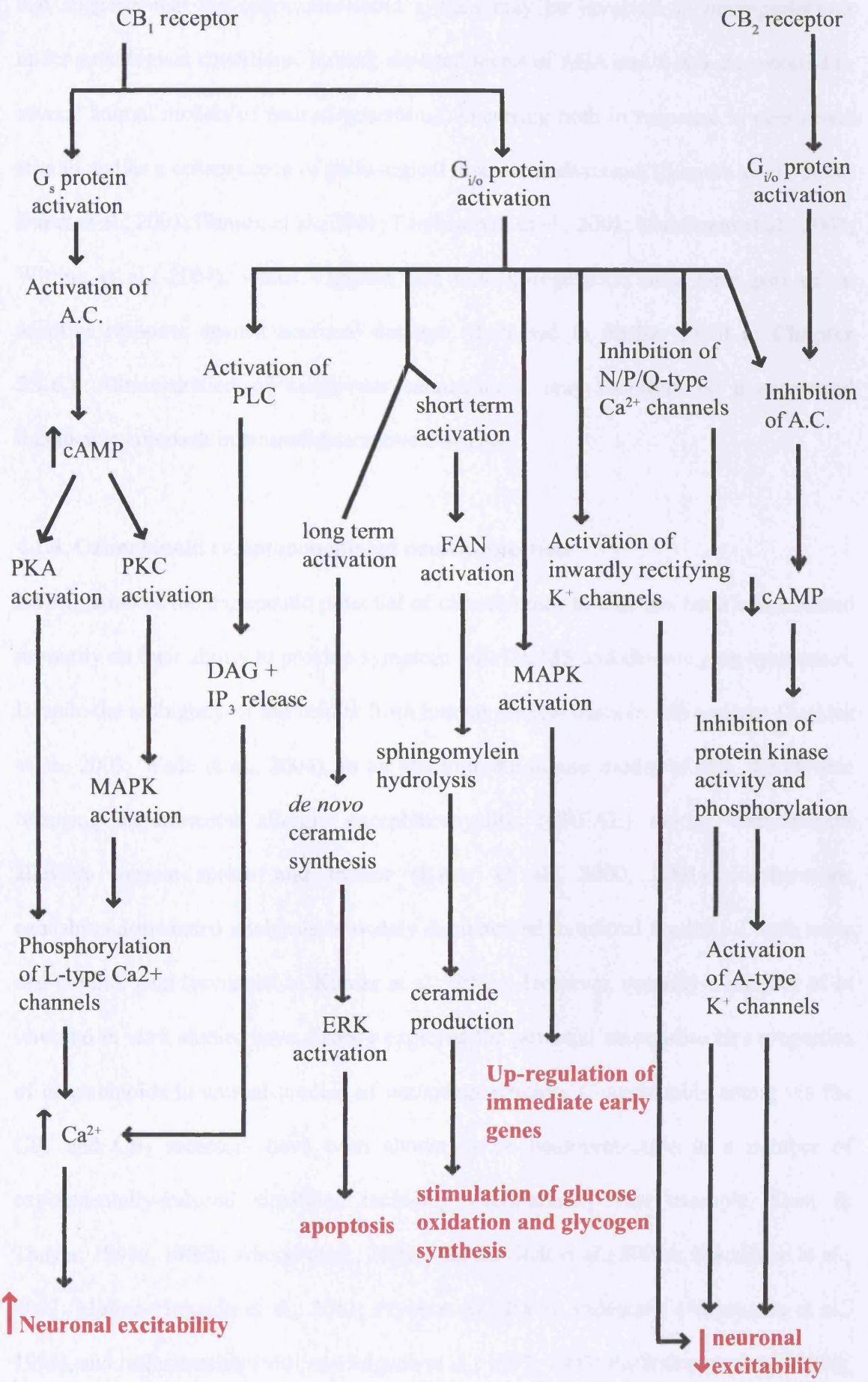
CB1 receptor
CB2 receptor
Gs protein activation
Gi/o protein activation
Gi/o protein activation
Activation of A.C.
Activation of PLC
short term activation
Inhibition of N/P/Q-type Ca2+ channels
Inhibition of A.C.
cAMP
long term activation
FAN activation
Activation of inwardly rectifying K+ channels
PKA activation
PKC activation
DAG + IP3 release
MAPK activation
cAMP
MAPK activation
Inhibition of protein kinase activity and phosphorylation
de novo ceramide synthesis
sphingomylein hydrolysis
Phosphorylation of L-type Ca2+ channels
ceramide production
Activation of A-type K+ channels
ERK activation
Up-regulation of immediate early genes
Ca2+
apoptosis
stimulation of glucose oxidation and glycogen synthesis
Neuronal excitability
neuronal excitability

that suggests that the endocannabinoid system may be involved in neuroprotection under pathological conditions. Indeed, elevated levels of AEA and 2-AG are reported in several animal models of neurodegeneration, occurring both in response to neurotoxic stimuli and as a consequence of pathological disease mechanisms (Sugiura et al., 2000; Baker et al., 2001; Hansen et al., 2001; Panikashvili et al., 2001; Marsicano et al., 2003; Witting et al., 2004), which suggests that this up-regulation may form part of an adaptive response against neuronal damage (discussed in further detail in **Chapter 5.1.6.**). Administration of exogenous cannabinoids may therefore be a successful therapeutic approach in neurodegenerative diseases.

4.1.4. Cannabinoid receptor-mediated neuroprotection

Investigation of the therapeutic potential of cannabinoids to date has been concentrated primarily on their ability to provide symptom relief in MS and chronic pain syndromes. Despite the ambiguity of the results from human clinical trials in MS patients (Zajicek et al., 2003; Wade et al., 2004), in an autoimmune mouse model of MS, the chronic relapsing experimental allergic encephalomyelitis (CREAE) model, cannabinoids alleviate muscle spasm and tremor (Baker et al., 2000, 2001). Furthermore, cannabinoid-mediated analgesia is widely documented in animal models of both acute and chronic pain (reviewed in Kumar et al., 2001). However, recently a number of *in vivo* and *in vitro* studies have directly explored the potential neuroprotective properties of cannabinoids in animal models of neurodegeneration. Cannabinoids acting via the CB_1 and CB_2 receptors have been shown to be neuroprotective in a number of experimentally-induced situations including excitotoxicity (for example, Shen & Thayer, 1998a, 1998b; Abood et al., 2001; van der Stelt et al., 2001a; Marsicano et al., 2003; Molina–Holgado et al., 2003; Pryce et al., 2003), ischaemia (Nagayama et al., 1999), and inflammation (Molina-Holgado et al., 1997, 2003; Puffenbarger et al., 2000;

Baker et al., 2001; Klegeris et al., 2003; Pryce et al., 2003) and following acute brain trauma (Panikashvili et al., 2001). These neuroprotective effects of cannabinoids can be mediated either via the CB_1 or the CB_2 receptor.

4.1.4.1. CB_1 receptor-mediated neuroprotection

In the CNS, the predominant cannabinoid receptor subtype is the CB_1 receptor (Matsuda et al., 1990). Autoradiographical studies reveal a widespread distribution of the CB_1 receptor in the CNS with the highest densities found in areas including the basal ganglia, the molecular layers of the cerebellum and in portions of the hippocampus (Herkenham et al., 1990, 1991). This localisation in the CNS correlates with the observed effects of cannabis on movement, cognition and memory (Herkenham et al., 1991). Neuronal expression of CB_1 receptors occurs on both the cell soma and neurites (Westlake et al., 1994; Twitchell et al., 1997; Tsou et al., 1998; Ong & Mackie, 1999). Cultured astrocytes and microglial have also been shown to express CB_1 receptors (Molina-Holgado et al., 2002; Facchinetti et al., 2003; Walter et al., 2003).

Activation of CB_1 receptors on presynaptic terminals will act to reduce neuronal excitability by inducing alterations in calcium and potassium permeability, as discussed in **Chapter 4.1.2.** (Caulfield & Brown, 1992; Mackie & Hille, 1992; Mackie et al., 1995; Twitchell et al., 1997; Shen & Thayer, 1998a). This raises the threshold for neurotransmitter release, consequently reducing presynaptic release (Shen et al., 1996; Gessa et al., 1998; Levenes et al., 1998; Nicholson et al., 2003). Therefore under conditions of excitotoxicity, which is suggested to contribute to the pathogenesis of many neurodegenerative diseases, activation of CB_1 receptors may reduce presynaptic glutamate release. In addition, activation of postsynaptic CB_1 receptors may also reduce excitotoxicity-induced postsynaptic calcium influx via inhibition of voltage gated N-

and P/Q- type calcium channels (Caulfield & Brown, 1992; Mackie & Hille, 1992; Mackie et al., 1995; Twitchell et al., 1997; Hampson et al., 1998a; Abood et al., 2001). Interestingly, due to the activity-dependent nature of their synthesis, it is possible that endocannabinoid synthesis will be increased under excitotoxic conditions (Di Marzo et al., 1994; Cadas et al., 1996). Indeed following injection of excitotoxins into the CNS of mice, levels of the endocannabinoids, AEA and 2-AG, are increased (Sugiura et al., 2000; Hansen et al 2001; Panikashvili et al., 2001; Marsicano et al., 2003), suggesting a role for endocannabinoids in protection against excitotoxicity.

In support of a CB_1 receptor-mediated neuroprotective effect, results have shown that injection of kainate (KA) into the CNS of CB_1 receptor knock-out mice produces a more extreme behavioural reaction and greater mortality than in wild-type (WT) mice (Marsicano et al 2003; Pryce et al., 2003). More specifically, Marsicano et al, (2003) generated a conditional knock–out mouse model in which only CB_1 receptors on glutamatergic neurons of the forebrain were deleted. Administration of KA to these mice induces seizures that are significantly worse in than in mice with a full complement of CB_1 receptors. In addition to the immediate benefits, CB_1 receptor activation under excitotoxic conditions also induces an up-regulation of IEGs, c-fos and Krox-24, which may be involved in the initiation of long-term adaptive changes (Bouaboula et al., 1995; Marsicano et al., 2003). These results imply that CB_1 receptors, particularly those located on glutamatergic neurons, play a role in endogenous protection against excitotoxicity and represent a system that may be suitable for therapeutic manipulation by administration of exogenous cannabinoid agonists.

4.1.4.2. CB_2 receptor-mediated neuroprotection

CB_2 receptors are primarily regarded as peripheral cannabinoid receptors (Howlett et al., 2002) and under normal healthy circumstances, CB_2 receptors are not detected in the CNS (Walter & Stella, 2004). However, CB_2 receptors have recently been identified on the plasma membrane of cultured rodent microglial cells (Facchinetti et al., 2003; Walter et al., 2003; Carrier et al., 2004), and cultured human microglia cells have been found to express CB_2 receptor mRNA and protein (Klegeris et al., 2003).

Microglia have a dual and conflicting role in neurodegeneration. Following neuronal damage, microglia become activated and undergo rapid proliferation and migration to the site of injury (Sargsyan et al., 2005). Activated microglia release a variety of neurotoxic mediators including reactive oxygen species (ROS), pro-inflammatory cytokines, such as TNFα and IL-1β, and glutamate (Molina-Holgado et al., 1997; Waksman et al., 1999; Facchinetti et al., 2003). Such mediators are involved in phagocytosis, to remove degenerating neurons and thus potentially aid recovery. However, they can also play a role in the propagation of inflammatory processes, which would hinder protective mechanisms (McGeer and McGeer, 2002; Consilvio et al., 2004; Sargsyan et al., 2005). Microglia can therefore have a neuroprotective or neurotoxic influence, the outcome of which is likely to be dependent on many interacting factors (Sargsyan et al., 2005).

The anti-inflammatory action of cannabinoids is based on their ability to reduce the release of neurotoxic mediators from microglia. Stimulation of microglia *in vitro* with lipopolysaccahride induces an up-regulation of TNFα and IL-1β mRNA expression in microglia (Puffenbarger et al., 2000; Facchinetti et al., 2003). Treatment with cannabinoid receptor agonists, however, dose-dependently reduces the expression and

release of pro-inflammatory cytokines (Puffenbarger et al., 2000; Facchinetti et al., 2003) via a CB_2 receptor-mediated mechanism (Klegeris et al., 2003). Indeed, cannabinoids actually reduce microglial activation (Arevalo-Martin et al., 2003), thus limiting propagation of the inflammatory response. In the CREAE autoimmune model of MS, WIN55,212-2, a synthetic cannabinoid agonist, reduces tremor and spasticity, whereas a CB_2 receptor antagonist worsens such symptoms (Baker et al., 2000, 2001). Meanwhile, in the Theiler's virus MS autoimmune model, various cannabinoid agonists reduce both microglial and T-lymphocyte activation in the spinal cord with concomitant reduction in CNS mRNA for TNFα and Il-1β (Croxford & Miller, 2003).

4.1.5. Cannabinoid receptor independent neuroprotection

Cannabinoid receptor agonists may also act by receptor-independent anti-oxidant actions. Hampson et al., (1998b) reported a potent anti-oxidant capacity of Δ^9-THC and CBD, comparable to the anti-oxidant butylated hydroxytoluene. Furthermore CBD, a non-receptor binding cannabinoid, exerts greater neuronal protection than that achieved with vitamin E, a known antioxidant, in response to an excitotoxic insult (Hampson et al., 1998b). Meanwhile, Δ^9-THC and CP 55,940 show receptor-independent anti-oxidant activity *in vitro*, in response to oxidative stress mediated by serum deprivation or hydrogen peroxide exposure respectively (Chen & Buck, 2000; Marsicano et al., 2002).

4.1.6. Evidence supporting the use of cannabinoid therapy in ALS

The discovery of endocannabinoid up-regulation in response to pathological conditions and the identification of mechanisms by which cannabinoids can exert neuroprotective effects in a receptor-dependent and independent manner, suggests that the cannabinoid system may be a therapeutic target in ALS. In summary, CB_1 receptor activation may

inhibit glutamate release from presynaptic nerve terminals and reduce the postsynaptic calcium influx in response to glutamate receptor stimulation. Meanwhile, CB_2 receptors may influence inflammation, whereby receptor activation will reduce microglial activation and subsequently inhibit their secretion of neurotoxic mediators. Lastly, cannabinoid agents may also exert anti-oxidant actions by a receptor-independent mechanism. Although the pathogenic mechanisms in ALS are still not fully understood there is significant evidence, as described in **Chapter 1.3.4**, which indicates that excitotoxicity, inflammation and oxidative stress may all contribute to disease pathogenesis.

4.1.6.1. CB_1 receptor involvement – potential anti-excitotoxic action

Motoneurons receive glutamatergic inputs from the descending corticospinal tracts, from collaterals of the Aα fibres innervating muscle fibres and Golgi tendon organs and from excitatory interneurons in the spinal cord (Heath and Shaw, 2002). Elevated synaptic glutamate, due to increased release or reduced uptake, will enhance postsynaptic calcium influx via activation of calcium-permeable glutamate receptors and subsequent depolarisation–induced activation of voltage-gated calcium channels. Excessive calcium can then activate neurotoxic cascades in the postsynaptic cell ultimately resulting in neuronal death (Choi et al., 1992).

CB_1 receptors are expressed on the cell soma and neurites of motoneurons cultured from the spinal cord (Abood et al., 2001), although the levels of expression in the ventral horn of the spinal cord are relatively low compared to the basal ganglia (Herkenham et al., 1991). However, following peripheral nerve injury in WT mice, expression of CB_1 receptors in the spinal cord increases (Lim et al., 2003). Furthermore, the finding that CB_1 receptors are expressed on microglia also suggests that during disease progression,

overall CB_1 receptor density in the spinal cord may increase due to the influx of microglia to areas affected in ALS.

In the spinal cord, pre- and postsynaptic CB_1 receptors may be activated either by endocannabinoids, the synthesis of which is elevated under excitotoxic conditions (Sugiura et al., 2000; Hansen et al 2001; Panikashvili et al., 2001; Marsicano et al., 2003), or alternatively by the administration of exogenous cannabinoids. This may then provide neuroprotection via dual modulation of neuronal excitability. CB_1 receptor-mediated presynaptic regulation of calcium and potassium permeability may inhibit glutamate release from the nerve terminal. In addition, inhibition of postsynaptic voltage-gated calcium channels will reduce the calcium influx into the postsynaptic cell (Caulfield & Mackie 1992; Mackie & Hille, 1992; Mackie et al., 1995; Twitchell et al., 1997; Hampson et al., 1998a; Shen & Thayer, 1998a; Abood et al., 2001), as described in greater detail in **Chapter 4.1.2.** An inhibitory effect of cannabinoids on non-neuronal cells, via CB_1 receptors, may similarly act to reduce glutamate release, contributing to an anti-excitotoxic effect (Tikka et al., 2002). In models of ALS, there is evidence to suggest that cannabinoids may be neuroprotective. Indeed, treatment of mouse mixed spinal cord cultures with Δ^9-THC exerts neuroprotection against direct KA-induced toxicity (Abood et al., 2001). Furthermore, treatment of $SOD1^{G93A}$ mice with Δ^9-THC delays disease progression (Raman et al., 2004).

4.1.6.2. CB_2 receptor involvement – potential anti-inflammatory action

In the post-mortem spinal cords of ALS patients there are substantial signs of inflammation including significant proliferation and accumulation of activated microglia, reactive astrocytes and $CD4^+$ and $CD8^+$ lymphocytes in areas of motoneuron degeneration (Troost et al., 1990; Engelhardt et al., 1993; Alexianu et al., 2001; McGeer

& McGeer, 2002). Furthermore increased mRNA and protein levels of inflammatory markers such as COX2 and PGE_2 are seen in the post-mortem spinal cords of ALS patients (Yasojima et al., 2001; Maihofner et al., 2003). Similar neuroinflammatory changes are seen in the mutant SOD1 mouse models of ALS where a correlation between the intensity of inflammation and disease progression is reported (Hall et al., 1998; Alexianu et al., 2001; Almer et al., 2001; Elliott et al., 2001).

Recent studies using immunocytochemistry have demonstrated the expression of CB_2 receptors on microglia (Facchinetti et al., 2003; Klegeris et al., 2003; Walter et al., 2003; Carrier et al., 2004). Interestingly, in response to peripheral nerve injury there is a simultaneous increase in the presence of activated microglia and the expression of CB_2 receptors in the rat spinal cord (Zhang et al., 2003). In mutant SOD1 mice, the presence of activated microglia increases from a presymptomatic stage (Hall et al., 1998; Alexianu et al., 2001; Almer et al., 2001), therefore it is likely that CB_2 receptor expression will also increase. Activated microglia can exert either protective or toxic effects depending on various interacting factors (Sargsyan et al., 2005). However, it is unlikely that microglia exert a neuroprotective effect in ALS, as in $SOD1^{G93A}$ mice there is a concurrent increase in the presence of activated microglia with the loss of motoneurons (Hall et al., 1998; Alexianu et al., 2001; Weydt et al., 2004). Upon activation, microglia release a variety of pro-inflammatory cytokines, including TNFα and IL-1β, that cause neuronal damage and the recruitment of further microglia (Puffenbarger et al., 2000; Facchinetti et al., 2003). However, cannabinoids can limit the propagation of this inflammatory response by inhibiting microglial activation (Arevalo-Martin et al., 2003) and subsequently reducing the expression and release of pro-inflammatory cytokines (Puffenbarger et al., 2000; Facchinetti et al., 2003) via a CB_2 receptor-mediated mechanism (Klegeris et al., 2003). Furthermore, CB_2 receptor

activation will also inhibit the release of ROS from microglia, consequently reducing oxidative damage (Tikka & Koistinaho, 2001).

Previously, minocycline and nordihydroguaiaretic acid (NDGA), potent inhibitors of microglial activation, have been shown to exert beneficial effects in mutant SOD1 mice (Kriz et al., 2002; van den Bosch et al., 2002; Zhu et al., 2002; West et al., 2004). Furthermore, selective inhibitors of the COX2 enzyme, which act to inhibit inflammation, have been shown to delay disease onset and extend survival in mutant SOD1 mice (Drachman et al., 2002; Pompl et al., 2002). Therefore, cannabinoids, acting via the CB_2 receptor, may have therapeutic effects in ALS by inhibiting microglial activation and reducing inflammation.

4.1.6.3. Cannabinoid receptor-independent involvement – potential anti-oxidant action

Mutations in the SOD1 enzyme structure may increase aberrant interactions with abnormal substrates such as peroxynitrite or hydrogen peroxide, or alternatively impede the binding of copper or zinc ions to the enzyme. A consequence of the gain of function acquired by the mutant SOD1 enzyme may therefore be to increase oxidative stress as discussed in **Chapter 1.3.4.1.**. Therefore anti-oxidant agents targeted at reducing oxidative stress may be an effective therapy in ALS. Cannabinoids, including Δ^9-THC and CP 55,940, can exert anti-oxidant actions, via a cannabinoid receptor-independent mechanism, in models of oxidative stress *in vitro* (Chen & Buck, 2000; Marsicano et al., 2002). Furthermore, treatment of $SOD1^{G93A}$ mice with CBD significantly delays disease progression, although does not increase lifespan (Weydt et al., 2005).

4.1.7. Hypothesis to be tested

In ALS, multiple pathways are believed to contribute to disease pathogenesis (reviewed in Bruijn et al., 2004). Previous studies have shown that cannabinoids can exert neuroprotection under conditions of excitotoxicity, inflammation and oxidative stress. Therefore in this study the effect of R(+)-WIN55,212-2, a synthetic aminoalkylindole that acts as a full agonist at CB_1 and CB_2 receptors (D'ambra et al., 1992), was investigated in the SOD^{G93A} mouse model of ALS. The therapeutic potential of R(+)-WIN55,212-2 was examined in terms of its ability to delay disease progression, as assessed by effects on muscle function and motoneuron survival, and ultimately to extend the lifespan of $SOD1^{G93A}$ mice.

4.2. METHODS

4.2.1. Breeding and maintenance of transgenic mouse colonies

Transgenic mice carrying a human SOD1 gene with a G93A mutation (TgN[SOD1-G93A]1Gur) were maintained as described in **Chapter 2.1a**. Individual animals were genotyped by PCR using DNA extracted from tail snips, as described in **Chapter 2.3**.

4.2.2. Analysis of endocannabinoid levels with disease progression in $SOD1^{G93A}$ mice

This analysis was performed in collaboration with Professor Vincenzo Di Marzo's group at the Endocannabinoid Research Group, Istituto di Chimica Biomolecolare, Naples, Italy, on tissue extracted from $SOD1^{G93A}$ mice at the Institute of Neurology, UK.

The levels of endocannabinoids in the spinal cords of WT and $SOD1^{G93A}$ mice were assessed at 40, 90 or 120 days of age (n = at least 3 in each group). The mice were killed by overdose of pentobarbitone anaesthetic (Fort Dodge Animal Health, Southampton, UK) and their spinal cords rapidly dissected and immediately frozen in liquid nitrogen. Post-mortem delay between onset of dissection and freezing of dissected tissue in liquid nitrogen was estimated to be between 5 and 10 minutes. Tissues were dounce-homogenized with chloroform/methanol/Tris-HCl 50 mM, pH 7.4 (1/1/1 by volume) containing 5 pmol of octa-deuterated (d8)-anandamide and 50 pmol of d8-2-arachidonoylglycerol (Cayman Chemicals, Ann Arbor, MI, USA) as internal standards. Lipid-containing organic phase was dried down, weighed and pre-purified by open-bed chromatography on silica gel, and analyzed by liquid chromatography-atmospheric pressure chemical ionization-mass spectrometry (LC-APCI-MS) using a Shimadzu high-performance liquid chromatography (HPLC) apparatus (LC-10ADVP)

coupled to a Shimadzu quadrupole mass spectrometer (LCMS-2010) via a Shimadzu APCI interface (Kyoto, Japan). Mass spectrometry analyses were carried out in the selected ion-monitoring mode. Temperature of the APCI source was 400°C; HPLC column was a Phenomenex (i.d.= 3μm, length 150mm, section 4.5 mm) reverse phase column. AEA (retention time of 14.5 min) and 2-AG (retention time of 17.0 min) quasi-molecular ions were quantified by isotope dilution with the above-mentioned deuterated standards and their amounts in pmols and nmols respectively, normalized per mg of lipid extract. The endocannabinoid extraction and quantification was performed by Professor Vincenzo Di Marzo and colleagues.

4.2.3. WIN55,212-2 preparation and treatment protocol

The synthetic cannabinoid receptor agonist R(+)-WIN55,212-2 (Tocris, Bristol, U.K.) was dissolved in a vehicle which consisted of ethanol, cremaphor (Fluka Biochemika, Buchs, Switzerland), DMSO and PBS (ratio 1: 1 : 1 : 17). WT and $SOD1^{G93A}$ mice of both sexes were divided into four treatment groups:

1. Treatment with 0.1 ml WIN55,212-2 (5mg/kg) injected i.p. once daily from 40 days of age (presymptomatic; n = 15);
2. Treatment with 0.1 ml WIN55,212-2 (5mg/kg) i.p. once daily from 90 days of age (early symptomatic; n = 19);
3. Treatment with 0.1ml vehicle i.p. from 40 days of age (n = 11);
4. No treatment to serve as untreated controls (n = 32).

Each of the treatment groups were further subdivided into 2 subgroups in order to study **i)** disease progression and **ii)** lifespan.

4.2.4. Assessment of disease progression

The progression of disease in $SOD1^{G93A}$ mice in this study was evaluated by repeated assessment of body weight and spontaneous locomotor activity over the course of disease. In addition the effect of treatment with WIN55,212-2 on disease progression was also assessed at 120 days of age, a relatively late stage of the disease, by examination of muscle force and phenotype, motor unit and motoneuron survival as described in **Chapters 2.10.1 – 2.10.5**.

4.2.4.1. Body weight

Experimental animals were weighed on a weekly basis until disease onset at which point the mice were weighed twice a week and a weekly average taken to monitor the loss of body weight with disease progression. At the onset of body weight decline, mice were weighed on a daily basis.

4.2.4.2. Spontaneous locomotor activity

Locomotor activity was evaluated by monitoring the experimental animals in an activity chamber. After an initial equilibration period of 5 – 10 minutes, the distance travelled (cm) over a further 5 minutes in a 27 x 27 cm open-field activity monitor (Med Associates, Georgia, VT, USA) was recorded.

Assessment of locomotor activity was undertaken at least 24 hours after the previous injection of WIN55,212-2 or vehicle to ensure no residual drug effects were observed.

4.2.5. Lifespan analysis

The lifespan of $SOD1^{G93A}$ mice was determined as the number of days the animals survived for before reaching an end-point that agreed with Home Office guidelines, namely when the animal:

i) had lost ≥ 20% of its maximal body weight

ii) was unable to perform the righting reflex in less than 30 seconds (unable to right itself when placed on its side). WT mice are able to complete this task in < 2 seconds.

The effect of WIN55,212-2 treatment on the lifespan of $SOD1^{G93A}$ mice was assessed under the same criteria, and the animals were culled when they reached this end-point, and lifespan recorded.

4.2.6. Statistical analysis

Statistical significance between the experimental groups was assessed using a Mann-Whitney U test. Spontaneous locomotor activity assessments were compared by one-way analysis of variance (ANOVA) repeated measures, incorporating a Student Neuman Keuls multiple comparisons test. Endocannabinoid levels were compared by one-way ANOVA, incorporating a Student Neuman Keuls multiple comparisons test. Values are expressed as mean ± standard error of the mean (S.E.M). Significance was set at $p < 0.05$.

4.3. RESULTS

In this Chapter levels of endocannabinoids in SOD1^{G93A} and WT littermates were assessed in order to establish any changes in endocannabinoid levels associated with disease progression. Furthermore, the therapeutic potential of WIN55,212-2 in SOD1^{G93A} mice was assessed by examining disease progression, muscle function and motoneuron survival after treatment from a presymptomatic (40 days) or symptomatic (90 days) age.

4.3.1. Endocannabinoid levels in SOD1^{G93A} mice during disease progression

In order to assess whether endocannabinoid levels varied during disease progression in the colony of SOD1^{G93A} mice used in these experiments, we measured levels of endocannabinoids in both WT and SOD1^{G93A} mice at various ages. The levels of the endocannabinoids, AEA and 2-AG, were measured in the spinal cord of WT and SOD1^{G93A} mice at 40 days (presymptomatic), 90 days (early symptomatic) and 120 days of age (end-stage). There was no significant difference in the levels of AEA and 2-AG in the spinal cord between WT and SOD1^{G93A} mice at 40 days ($p > 0.1$). However, as shown in **Figure 4.2**, levels of AEA in the spinal cord of SOD1^{G93A} mice at 90 and 120 days of age were significantly elevated over 2 fold in comparison to WT mice ($p < 0.05$; 18.1±2.3 pmol/g and 14.9±2.4pmol/g compared to 8.0 ±2.3 pmol/g and 6.9±1.7pmol/g respectively). Spinal cord levels of 2-AG were only elevated towards the end-stage of disease, and were significantly higher in 120 day old SOD1^{G93A} mice compared to WT ($p = 0.003$; 6.7±0.7 nmol/g compared to 4.4±0.5 nmol/g respectively). Thus, as previously shown (Witting et al., 2004), there was a clear increase in the levels of endocannabinoids in the spinal cord of SOD1^{G93A} mice during the symptomatic phase of disease.

Figure 4.2 - Levels of endocannabinoids in spinal cords of WT and SOD1^{G93A} mice

Levels of the endocannabinoids (**A**) anandamide (AEA) and (**B**) 2-arachidonoylglycerol (2-AG) were analyzed in spinal cord extracts from WT and SOD1^{G93A} mice at 40, 90 and 120 days of age (n = at least 3 in each case). Levels were expressed as the concentration of endocannabinoid per gram of tissue. There was a clear increase in the levels of AEA in symptomatic SOD1^{G93A} mice. Levels of 2-AG appeared to increase in SOD1^{G93A} mice only during the late stages of disease (120 days). Prior to the onset of disease symptoms, levels of AEA and 2-AG were no different from WT. Error bars represent standard error of the mean. * $p < 0.05$, *** $p < 0.005$.

A

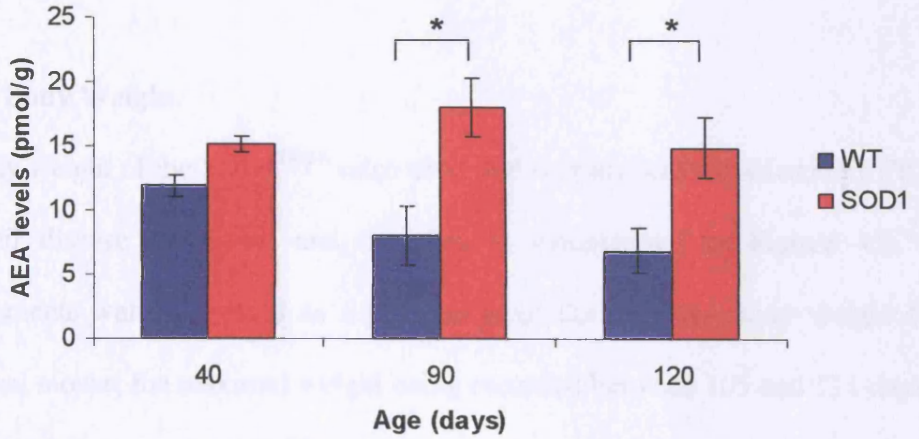
25
20
15
10
5
0
AEA levels (pmol/g)
*
*
40
90
120
Age (days)
WT
SOD1

B

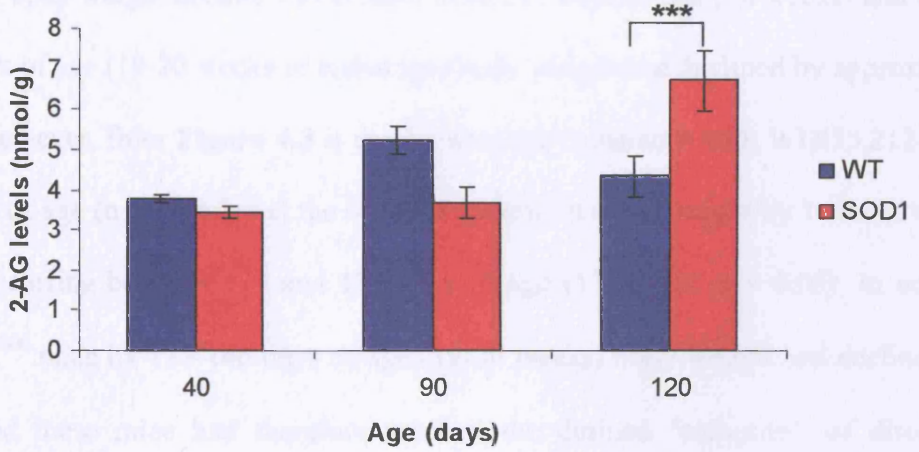
8
7
6
5
4
3
2
1
0
2-AG levels (nmol/g)
***
40
90
120
Age (days)
WT
SOD1

4.3.2. Assessment of disease progression in SOD1^{G93A} mice.

SOD1^{G93A} mice treated with WIN55,212-2 from 40 or 90 days of age and their untreated littermates were monitored on a daily basis and various parameters checked regularly to assess disease progression.

4.3.2.1. Body Weight.

The body weight of the SOD1^{G93A} mice used in this study was recorded from 70 days of age until disease end-point, and the data is summarised in **Figure 4.3**. Weight measurements were expressed as a percentage of the maximal body weight for each individual mouse, the maximal weight being recorded between 105 and 111 days of age (15 weeks) in untreated SOD1^{G93A} mice. Treatment with WIN55,212-2 from 40 days of age was found to significantly delay the decline in body weight that usually occurs in SOD1^{G93A} mice during disease progression. In untreated SOD1^{G93A} mice ($n = 9$) the onset of body weight decline was evident from 112 days of age (16 weeks) and by 133-146 days of age (19-20 weeks or end-stage) body weight had declined by approximately 20%. However, from **Figure 4.3** it can be seen that treatment with WIN55,212-2 from 40 days of age ($n = 9$) delayed the onset of decline in body weight by 1 week, with the onset occurring between 119 and 125 days of age (17 weeks; $p < 0.05$). In untreated SOD1^{G93A} mice by 133-146 days of age (19-20 weeks) body weight had declined by $\geq$ 20% and these mice had therefore reached the defined 'end-point' of disease. In contrast, in SOD1^{G93A} mice treated with WIN55,212-2 from 40 days of age, body weight did not drop below 20% of the maximum until 140 days of age (20 weeks), and even when the mice were unable to right themselves within 30 seconds (the second definition of 'end-stage') they still maintained significantly more body weight than untreated SOD1^{G93A} mice, which were culled one week earlier. In contrast, treatment

Figure 4.3 – The effect of WIN55,212-2 on the decline in body weight of SOD1^{G93A} mice

The body weight of SOD1^{G93A} mice treated from 40 and 90 days of age with WIN55,212-2 and their untreated SOD1^{G93A} littermates was recorded weekly from 70 days of age (10 weeks) until disease end-point, as shown in the graph. Body weight was expressed as a percentage of the maximal weight of each individual animal. As a consequence of disease progression the body weight of untreated SOD1^{G93A} mice (n = 9) declined from 112 days of age (16 weeks) onwards. However, treatment with WIN55,212-2 from 40 days of age (n = 9) significantly delayed the decline in body weight of SOD1^{G93A} mice. In contrast, treatment with WIN55,212-2 from 90 days of age (n = 8) had no effect on the loss of weight observed in SOD1^{G93A} mice. Error bars = standard error of the mean. * $p < 0.05$.

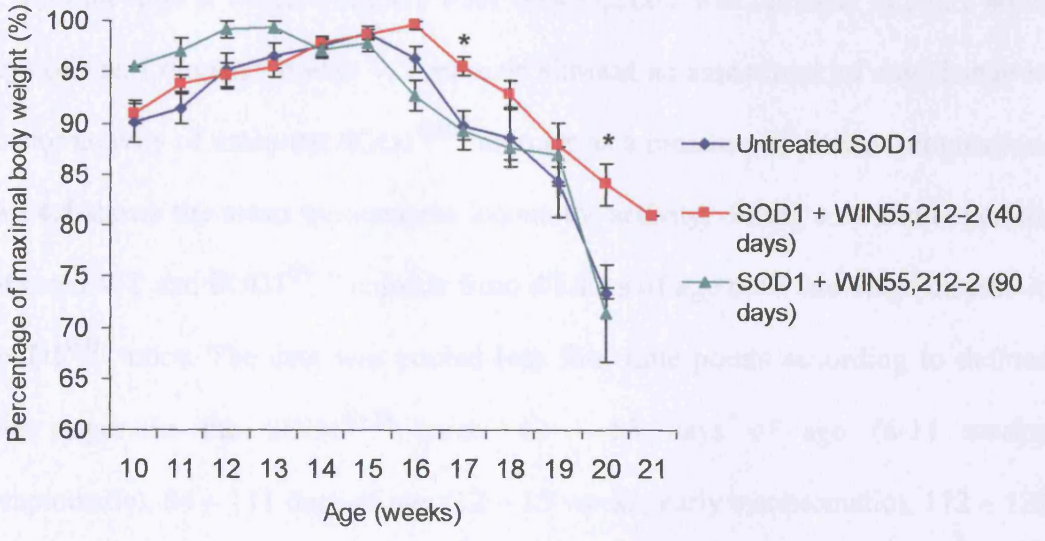
Percentage of maximal body weight (%)
100
95
90
85
80
75
70
65
60
10 11 12 13 14 15 16 17 18 19 20 21
Age (weeks)
*
*
Untreated SOD1
SOD1 + WIN55,212-2 (40 days)
SOD1 + WIN55,212-2 (90 days)

with WIN55,212-2 from 90 days of age (n = 8), had no effect on the decline in body weight seen with disease progression in $SOD1^{G93A}$ mice ($p > 0.05$). Similarly, treatment of $SOD1^{G93A}$ mice with vehicle had no effect on the decline of body weight ($p > 0.05$; data not shown).

4.3.2.2. Locomotor activity

The spontaneous locomotor activity of WT and $SOD1^{G93A}$ mice was measured twice a week from the time at which treatment with WIN55,212-2 was initiated, at either 40 or 90 days of age. Comparison with WT animals allowed an assessment of any change in locomotor activity of untreated $SOD1^{G93A}$ animals as a measure of disease progression. **Figure 4.4** shows the mean spontaneous locomotor activity, during a 5-minute period, of untreated WT and $SOD1^{G93A}$ animals from 40 days of age until end-stage disease in the $SOD1^{G93A}$ mice. The data was pooled into four time points according to defined disease stages in the $SOD1^{G93A}$ mice: 42 - 83 days of age (6-11 weeks; presymptomatic), 84 – 111 days of age (12 – 15 weeks; early symptomatic), 112 – 125 days of age (16 – 17 weeks; late symptomatic) and 126 – 153 days of age (18-21 weeks; end-stage disease). It can be seen in **Figure 4.4** that there was no significant difference in spontaneous locomotor activity between WT and $SOD1^{G93A}$ mice until 111 days of age (15 weeks). By 112 – 125 days of age (16-17 weeks), a late symptomatic stage of disease, $SOD1^{G93A}$ mice showed a significant reduction in locomotor activity (343.0 ± 61.0cm; n = 12) compared to age-matched WT mice (676.8 ± 95.3cm; n = 8; p = 0.005). Similarly at the disease end-stage, as may be expected from the progressive paralysis that occurs, the spontaneous locomotor activity of $SOD1^{G93A}$ mice was significantly less than that of WT mice ($p < 0.001$). Whereas WT mice travelled 744.2cm (± 102.8 S.E.M.) in 5 minutes, $SOD1^{G93A}$ mice between 126-153 days of age (18 – 21 weeks) only travelled 152.8cm (± 28.2 S.E.M.).

Figure 4.4 – The spontaneous locomotor activity of WT and SOD1^{G93A} mice

As a measure of disease progression, the locomotor activity (centimetres travelled) of untreated WT and SOD1^{G93A} mice was recorded over a 5 minute period in an activity chamber from 6 weeks of age until the disease end-point of the SOD1^{G93A} mice. The graph shows a comparison of WT and SOD1^{G93A} activity grouped according to the disease stage of the SOD1^{G93A} mice: 42 - 83 days of age (presymptomatic), 84 – 111 days of age (early symptomatic), 112 – 125 days of age (late symptomatic) and 126 – 153 days of age (end-stage disease). It can be seen that WT mice (n = 8) showed no significant change in locomotor activity with increasing age. In contrast, within the duration of the study there was a progressive decline in the spontaneous locomotor activity of untreated SOD1^{G93A} mice (n = 12) during disease progression, as paralysis of the hindlimb muscles increased. Values are the mean response ± standard error of the mean. cm = centimetres. * $p < 0.05$, *** $p < 0.005$.

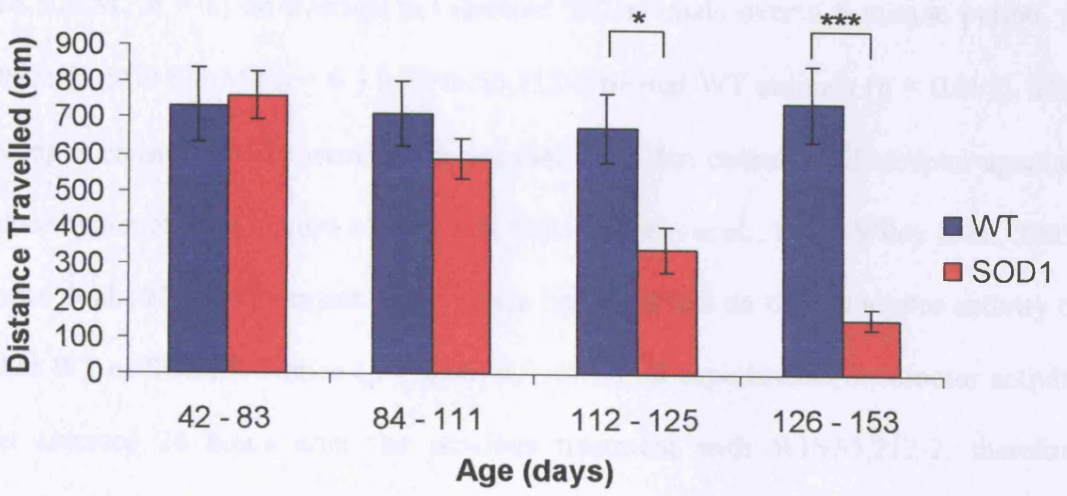
*
***
900
800
700
600
500
400
300
200
100
0
Distance Travelled (cm)
WT
SOD1
42 - 83
84 - 111
112 - 125
126 - 153
Age (days)

The effect of treatment with WIN55,212-2 from 40 days of age on locomotor activity in WT mice was assessed next. Locomotor activity did not differ significantly in WT mice (n = 8) during the study period, as shown in **Figure 4.4**. Therefore all activity recordings were pooled, and the effect of treatment with WIN55,212-2 or vehicle was assessed and the results are summarised in **Figure 4.5**. It can be seen that treatment with WIN55,212-2 significantly reduced locomotor activity in WT animals from 718cm (± 52.8 S.E.M.; n = 8) on average in untreated WT animals over a 5 minute period, to 406cm (± 35.0 S.E.M.; n = 6) in WIN55,212-2 treated WT animals ($p < 0.001$). This finding is consistent with previous reports that show that cannabinoid receptor agonists induce hypomotility (Sulcova et al., 1998; Sañudo–Peña et al., 2000; Wiley et al., 2003; Drews et al., 2005). Treatment with vehicle had no effect on the locomotor activity of either WT or $SOD1^{G93A}$ mice ($p > 0.06$; n = 6). In all experiments, locomotor activity was assessed 24 hours after the previous treatment with WIN55,212-2, therefore avoiding measurement of the immediate drug effects on activity levels, rather than the overall effect of WIN55,212-2 on locomotor activity of the mice.

$SOD1^{G93A}$ mice treated with WIN55,212-2 from 40 days of age showed reduced spontaneous locomotor activity between the ages of 46 and 111 days (6 - 11 weeks) compared to untreated $SOD1^{G93A}$ littermates, as shown in **Figure 4.6**. Whereas untreated presymptomatic and early symptomatic $SOD1^{G93A}$ mice travelled 761.3cm (± 64.0 S.E.M.; n = 12) and 589.6cm (± 54.4 S.E.M.; n = 12) respectively, over a 5 minute period, $SOD1^{G93A}$ mice treated with WIN55,212-2 from 40 days of age, travelled 541.9cm (± 61.2 S.E.M.; n = 12 ; $p = 0.016$) and 398.3cm (± 37.4 S.E.M.; n = 12; $p = 0.047$) respectively. However, from 112 days of age (16 weeks; a late symptomatic disease stage) there was no significant difference in spontaneous locomotor activity between treated and untreated $SOD1^{G93A}$ littermates ($p > 0.5$). Therefore the significant

Figure 4.5 – The effect of WIN55,212-2 treatment on the spontaneous locomotor activity of WT mice

The spontaneous locomotor activity of WT mice was recorded from 40 days of age until the maximal survival time of $SOD1^{G93A}$ littermates (approximately 140 days). Locomotor activity did not differ significantly in WT mice (n = 8) during the study period, as shown in **Figure 4.4**. Therefore all activity recordings were pooled, and the effect of treatment with WIN55,212-2 or vehicle was assessed and the results are summarised in the bar chart. Treatment with WIN55,212-2 significantly reduced the spontaneous locomotor activity of WT mice (n = 6). In contrast, treatment with vehicle had no effect on the activity levels of WT mice even over a prolonged period of time (n = 6). Values are the mean response ± standard error of the mean. cm = centimetres. *** $p < 0.005$.

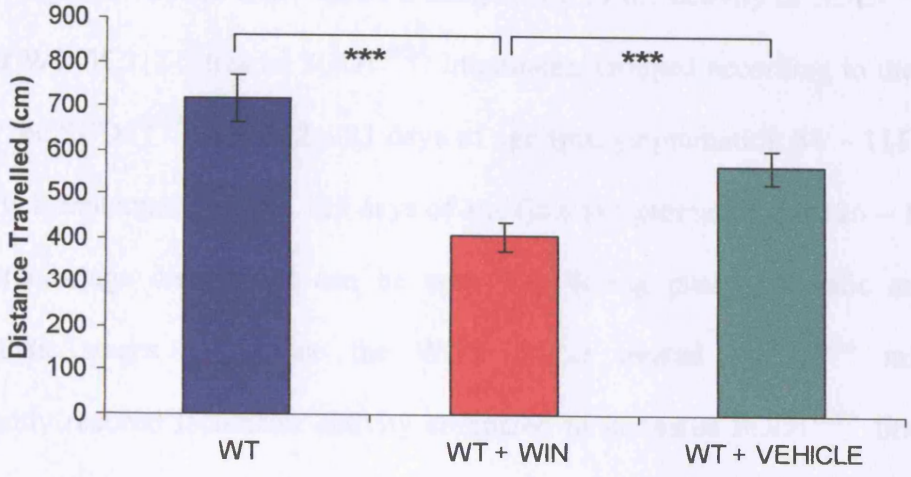
900
800
700
600
500
400
300
200
100
0
Distance Travelled (cm)
***
***
WT
WT + WIN
WT + VEHICLE

Figure 4.6 - The effect of treatment with WIN55,212-2 from 40 days of age on the spontaneous locomotor activity levels of SOD1^{G93A} mice

As a measure of disease progression the locomotor activity (in centimetres travelled) of SOD1^{G93A} mice over a 5 minute period in an activity chamber was recorded from 42 days of age (6 weeks) until disease end-point. Furthermore the effect of treatment with WIN55,212-2 from 40 days of age on the spontaneous activity levels of SOD1^{G93A} mice was investigated. The bar chart shows a comparison of the activity of SOD1^{G93A} mice and their WIN55,212-2 treated SOD1^{G93A} littermates, grouped according to the disease stage of the SOD1^{G93A} mice: 42 - 83 days of age (presymptomatic), 84 – 111 days of age (early symptomatic), 112 – 125 days of age (late symptomatic) and 126 – 153 days of age (end-stage disease). It can be seen that during presymptomatic and early symptomatic stages of disease the WIN55,212-2 treated SOD1^{G93A} mice had significantly reduced locomotor activity compared to untreated SOD1^{G93A} littermates. However, this hypomotile effect was lost with further disease progression. Values are the mean response ($n = 12$) ± standard error of the mean. * $p < 0.05$.

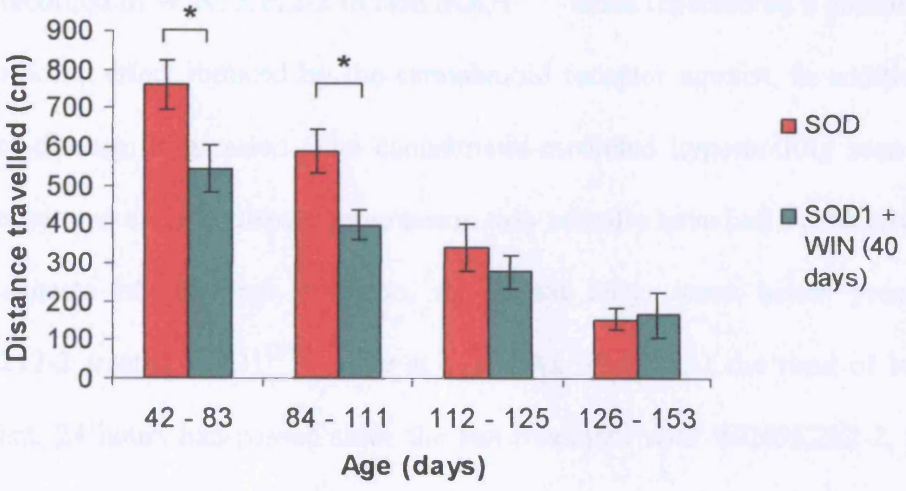
900
800
700
600
500
400
300
200
100
0
Distance travelled (cm)
*
*
42 - 83
84 - 111
112 - 125
126 - 153
Age (days)
SOD
SOD1 + WIN (40 days)

hypomotile effect induced by WIN55,212-2 on SOD1^{G93A} mice appeared to be lost at a late symptomatic stage of the disease, when hindlimb dysfunction was becoming prevalent. However, from the results observed in WT mice treated with WIN55,212-2 it was possible that at a late symptomatic stage of disease, the spontaneous locomotor activity recorded in WIN55,212-2 treated SOD1^{G93A} mice represented a combination of the hypomotile effect induced by the cannabinoid receptor agonist, in addition to the effects of disease progression. The cannabinoid-mediated hypomotility seen prior to disease onset and early in disease progression may actually have had a protective role as certain aspects of hindlimb function, as shown later, were better preserved in WIN55,212-2 treated SOD1^{G93A} mice at 120 days of age. At the time of locomotor assessment, 24 hours had passed since the last treatment with WIN55,212-2, therefore avoiding measurement of the immediate drug effects on activity levels, rather than the overall effect on locomotor activity of the SOD1^{G93A} mice.

The effect of treatment with WIN55,212-2 from 90 days of age, a symptomatic stage of disease, on locomotor activity was also examined. The spontaneous locomotor activity of SOD1^{G93A} mice treated with WIN55,212-2 from 90 days of age ($n = 6$) did not differ significantly from untreated SOD1^{G93A} mice ($n = 12$) at any stage ($p > 0.2$), as shown in **Figure 4.7**. In this study SOD1^{G93A} mice were already symptomatic by the time treatment was initiated. Thus no reduction in activity was observed in SOD1^{G93A} mice treated with WIN55,212-2 after symptom onset compared to untreated SOD1^{G93A} littermates.

Figure 4.7 – The effect of treatment with WIN55,212-2 from 90 days of age on the spontaneous locomotor activity of SOD1^{G93A} mice

The spontaneous locomotor activity of SOD1^{G93A} mice treated with WIN55,212-2 from 90 days of age and their untreated SOD1^{G93A} littermates was recorded from the onset of treatment until the disease end-point. The graph shows a comparison of the activity of SOD1^{G93A} mice (n = 12) and their WIN55,212-2 treated SOD1^{G93A} littermates (n = 6), grouped according to the disease stage of the SOD1^{G93A} mice: 90 – 111 days of age (early symptomatic), 112 – 125 days of age (late symptomatic) and 126 – 153 days of age (end-stage disease). It can be seen that treatment with WIN55,212-2 had no significant effect on the locomotor activity of SOD1^{G93A} mice over this time period. Values are the mean response ± standard error of the mean. cm = centimetres.

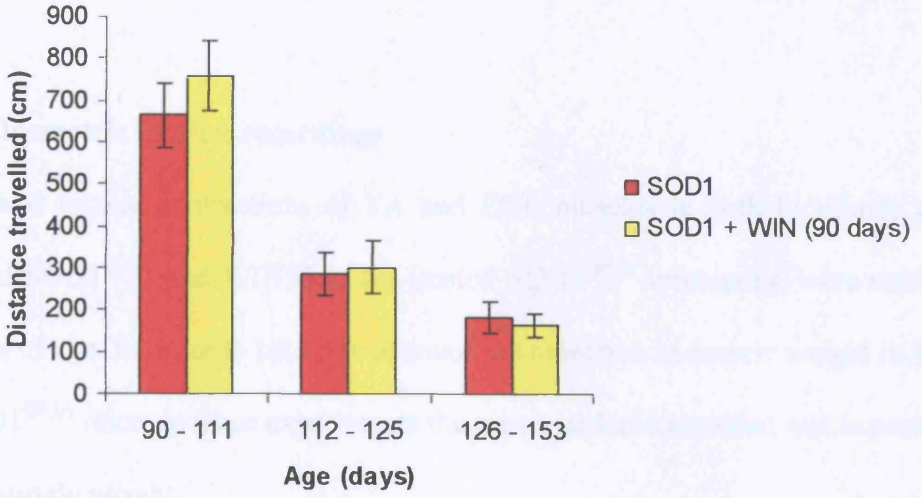
900
800
700
600
500
400
300
200
100
0
Distance travelled (cm)
90 - 111
112 - 125
126 - 153
Age (days)
SOD1
SOD1 + WIN (90 days)

4.3.3. Hindlimb muscle function in SOD1^{G93A} mice at 120 days of age

The effect of treatment with WIN55,212-2 from 40 or 90 days of age on the function of the hindlimb TA and EDL muscles of SOD1^{G93A} mice was assessed at 120 days of age, a relatively late stage of disease, by *in vivo* physiological recordings of muscle contractions.

4.3.3.1. Isometric tension recordings

Twitch and tetanic contractions of TA and EDL muscles in both hindlimbs of WT, untreated SOD1^{G93A} and WIN55,212-2 treated SOD1^{G93A} littermates, were recorded at 120 days of age. In order to take into account the reduction in muscle weight in 120 day old SOD1^{G93A} mice, in these experiments the maximal force recorded was expressed per 100mg muscle weight.

i) Twitch force

The mean twitch tension of TA muscles elicited by stimulation of the sciatic nerve of WT, SOD1^{G93A} and WIN55,212-2 treated SOD1^{G93A} littermates is summarised in **Figure 4.8**. By 120 days of age, the mean twitch tension of TA muscles from SOD1^{G93A} mice was significantly reduced compared to WT littermates. Thus TA muscles from WT mice produced a mean twitch force of 68.4g (± 5.3 S.E.M. per 100mg TA muscle; n = 10), whereas in SOD1^{G93A} mice this was reduced to 34.4g (± 5.8 S.E.M. per 100mg TA muscle; n = 14; $p < 0.001$). This represented a 49.7% reduction in maximal twitch tension in SOD1^{G93A} TA muscles compared with WT at 120 days of age. Treatment with WIN55,212-2 significantly reduced the loss in twitch force in TA muscles of SOD1^{G93A} mice. Thus, following treatment from 90 days of age the twitch force of TA muscles of SOD1^{G93A} mice was 51.13g (± 6.5 S.E.M. per 100mg TA muscle; n = 16; $p = 0.026$), representing a loss of only 25.2% of the twitch response attained in WT mice.

Figure 4.8 – The twitch tension of TA muscles from WT, untreated SOD1^{G93A} and WIN55,212-2 treated SOD1^{G93A} mice at 120 days of age

The maximal twitch tension of TA muscles was elicited by stimulation of the sciatic nerve by a single square pulse of 0.02ms duration at a supramaximal voltage. The mean twitch tension of TA muscles from WT (n = 10), SOD1^{G93A} (n = 14) and WIN55,212-2 treated SOD1^{G93A} mice (40 days, n = 9; 90 days, n = 16) are summarised in the bar chart. Force was expressed per 100mg muscle weight to take into account the reduction in muscle weight in 120 day old SOD1^{G93A} mice. At 120 days, the twitch tension of TA muscles was substantially reduced in SOD1^{G93A} mice compared to WT. However, treatment with WIN55,212-2 from 90 days of age significantly prevented this decline in twitch tension. Treatment from 40 days, in contrast, had no effect on twitch tension. g = grams. Values represent the mean response ± standard error of the mean. * $p < 0.05$, ** $p < 0.01$, *** $p < 0.005$.

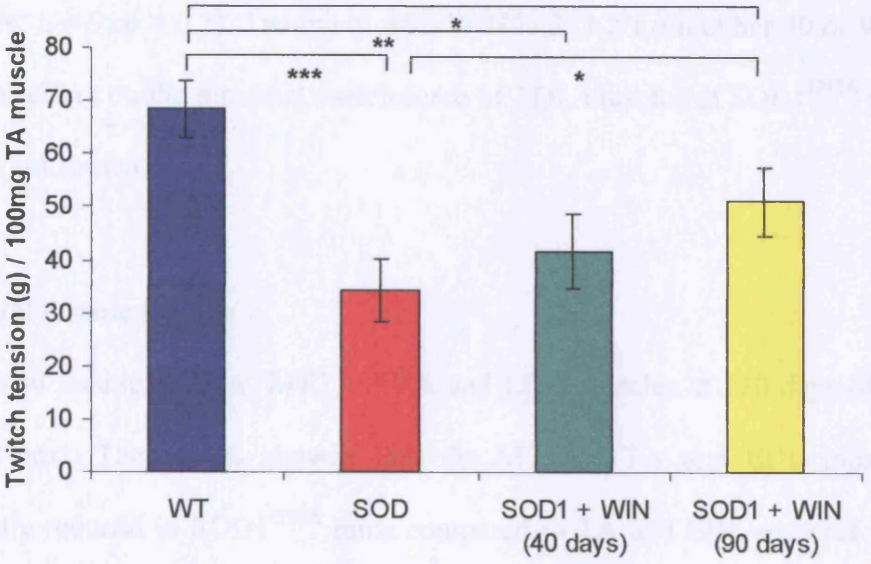
Twitch tension (g) / 100mg TA muscle
80
70
60
50
40
30
20
10
0
***
**
*
*
WT
SOD
SOD1 + WIN (40 days)
SOD1 + WIN (90 days)

Therefore the twitch response of TA muscles from $SOD1^{G93A}$ mice treated with WIN55,212-2 from 90 days of age was 49% greater than in untreated $SOD1^{G93A}$ littermates. Surprisingly, treatment with WIN55,212-2 from 40 days of age had no significant effect on the twitch force of TA muscles (41.49g ± 7.1 S.E.M. per 100mg TA muscle; $n = 9$; $p > 0.2$). Treatment with WIN55,212-2 from either 40 or 90 days of age had no effect on the maximal twitch force of EDL muscles of $SOD1^{G93A}$ mice ($p > 0.07$; data not shown).

ii) Maximal tetanic tension

The maximal tetanic tension (MTT) of TA and EDL muscles at 120 days of age was examined next. The results showed that the MTT of TA and EDL muscles was significantly reduced in $SOD1^{G93A}$ mice compared to TA and EDL muscles from WT mice, as shown in **Figure 4.9 and Figure 4.10** respectively ($p < 0.005$). TA muscles from 120 day old WT mice produced a MTT of 276.6g (± 12.0 S.E.M. per 100mg TA muscle; $n = 9$), whereas TA muscles from $SOD1^{G93A}$ mice produced a maximal force of only 90.7g (± 15.0 S.E.M. per 100mg TA muscle; $n = 14$), a reduction of 67.2%. The MTT of EDL muscles in untreated $SOD1^{G93A}$ mice at this stage was also significantly reduced compared to WT littermates. Therefore WT EDL muscles produced a MTT of 305.94g (± 16.8 S.E.M. per 100mg EDL muscle; $n = 10$), whereas in $SOD1^{G93A}$ mice the MTT of EDL muscles was just 175.68g (± 14.8 S.E.M. per 100mg EDL muscle; $n = 13$), a reduction of 42.6%. Treatment with WIN55,212-2 from 90 days, however, significantly prevented the decline in hindlimb muscle force so that the MTT of TA and EDL muscles at 120 days was 157.0g (± 19.8 S.E.M.; $p = 0.005$; $n = 16$) and 243.4g (± 27.8 S.E.M.; $p = 0.044$; $n = 16$), a reduction of only 43.2% and 20.4% respectively compared to WT muscles. Thus the MTT of $SOD1^{G93A}$ TA and EDL muscles treated with WIN55,212-2 (from 90 days) was significantly greater than in the untreated

Figure 4.9 – Maximal tetanic force of TA muscles from WT, untreated SOD1^{G93A} and WIN55,212-2 treated SOD1^{G93A} mice at 120 days of age

Maximal tetanic tension (MTT) of TA muscles was elicited by increasing the frequency of stimulation of the sciatic nerve (40, 80 and 100Hz). The bar chart summarises the results of the MTT of TA muscles from WT (n = 9), SOD1^{G93A} (n = 14) and WIN55,212-2 treated SOD1^{G93A} mice (n = 16) at 120 days of age. Force was expressed per 100mg muscle weight to take into account the reduction in muscle weight in 120 day old SOD1^{G93A} mice. As a function of disease progression the MTT of TA muscles from untreated SOD1^{G93A} mice was significantly less than in WT littermates. However, treatment with WIN55,212-2 from 90 days of age prevented the decline in muscle force and TA muscles in treated SOD1^{G93A} mice were significantly stronger than in their untreated SOD1^{G93A} littermates. In contrast, treatment with WIN55,212-2 from 40 days of age had no effect on muscle force. g = grams. Values are the mean MTT of TA muscles ± standard error of the mean. * $p < 0.05$, ** $p < 0.01$, *** $p < 0.005$.

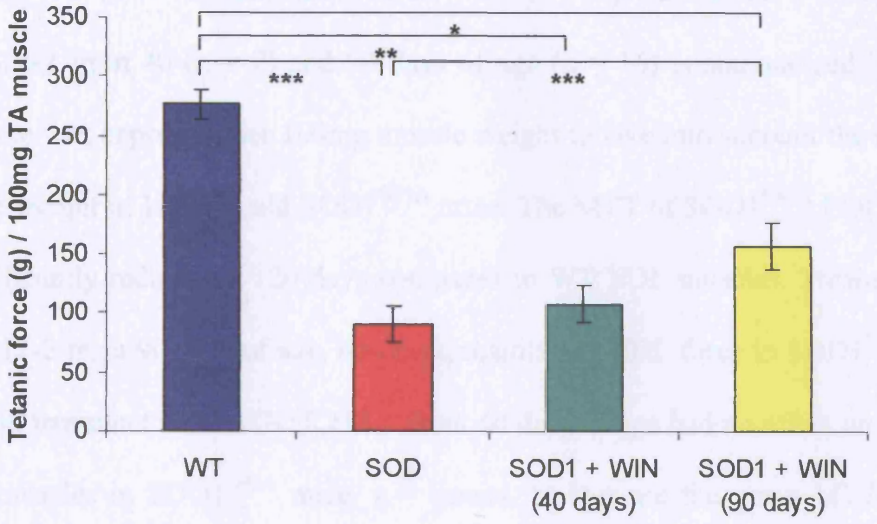
Tetanic force (g) / 100mg TA muscle
350
300
250
200
150
100
50
0
*
**
***
***
WT
SOD
SOD1 + WIN (40 days)
SOD1 + WIN (90 days)

Figure 4.10 – The effect of treatment with WIN55,212-2 on the maximal tetanic tension of EDL muscles from SOD1^{G93A} mice

Maximal tetanic tension (MTT) of EDL muscles was elicited by increasing the frequency of stimulation of the sciatic nerve (40, 80 and 100Hz). The MTT of EDL muscles in WT (n = 10), untreated SOD1^{G93A} (n = 13) and SOD1^{G93A} treated with WIN55,212-2 from 40 (n = 7) and 90 days of age (n = 16) is summarised in the bar chart. Force was expressed per 100mg muscle weight to take into account the reduction in muscle weight in 120 day old SOD1^{G93A} mice. The MTT of SOD1^{G93A} EDL muscles was significantly reduced at 120 days compared to WT EDL muscles. Treatment with WIN55,212-2 from 90 days of age, however, maintained EDL force in SOD1^{G93A} mice. In contrast, treatment with WIN55,212-2 from 40 days of age had no effect on the force of EDL muscles in SOD1^{G93A} mice. g = grams. Values are the mean MTT of EDL muscles ± standard error of the mean. * $p< 0.05$, *** $p< 0.005$.

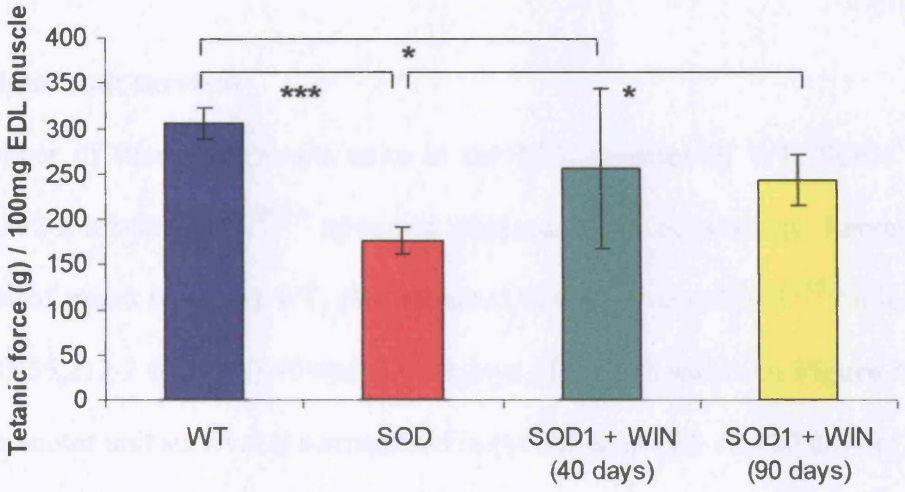
Tetanic force (g) / 100mg EDL muscle
400
350
300
250
200
150
100
50
0
***
*
*
WT
SOD
SOD1 + WIN (40 days)
SOD1 + WIN (90 days)

$SOD1^{G93A}$ mice. Indeed muscle force was improved by 73.1% and 38.5% in TA and EDL muscles respectively, compared to muscles in untreated $SOD1^{G93A}$ mice. Surprisingly treatment with WIN55,212-2 from 40 days of age did not significantly affect the MTT of $SOD1^{G93A}$ TA and EDL muscles ($p > 0.25$). Twitch and tetanic tensions of $SOD1^{G93A}$ TA and EDL muscles were also unaffected by treatment with vehicle ($p > 0.05$; data not shown).

4.3.4. Motor unit survival

The number of functional motor units in the EDL muscles of WT, $SOD1^{G93A}$ and WIN55,212-2 treated $SOD1^{G93A}$ mice was assessed at 120 days of age. Representative examples of traces from (**A**) WT, (**B**) untreated $SOD1^{G93A}$ and $SOD1^{G93A}$ mice treated with WIN55,212-2 from (**C**) 40 and (**D**) 90 days of age are shown in **Figure 4.11**, and the mean motor unit survival is summarised in the bar chart (**E**). At 120 days of age WT EDL muscles had on average 29 (± 0.9 S.E.M., n = 10) motor units compared to only 12 (± 0.9 S.E.M.; n = 18) in untreated $SOD1^{G93A}$ mice. Treatment with WIN55,212-2 significantly improved motor unit survival and in 120 day old $SOD1^{G93A}$ mice 16 (± 1.7 S.E.M.; n = 9; p = 0.04) and 20 (± 0.9 S.E.M.; n = 16; $p<0.001$) motor units survived following treatment from 40 and 90 days of age respectively.

4.3.5. Muscle fatigue characteristics

In $SOD1^{G93A}$ mice alterations in the contractile characteristics of EDL muscles are known to occur as disease progresses (Derave et al., 2003; Sharp et al., 2005). The effect of treatment with WIN55,212-2 on these disease related changes in muscle phenotype were examined next. Repeated stimulation of the sciatic nerve to the EDL muscle over a 3 minute period elicits a characteristic fatigue trace as shown in **Figure 4.12.** The Figure shows examples of the fatigue traces of EDL muscles from (**A**) WT,

Figure 4.11 – The number of motor units in EDL muscles of WT, untreated SOD1^{G93A} and WIN55,212-2 treated SOD1^{G93A} mice at 120 days of age

Stimulation of the sciatic nerve with increasing intensity produces stepwise increments in twitch tension of EDL muscles that corresponds to the successive recruitment of motor axons. Representative motor unit traces from EDL muscles from **(A)** WT, **(B)** untreated SOD1^{G93A} and SOD1^{G93A} mice treated with WIN55,212-2 from **(C)** 40 and **(D)** 90 days of age are shown. The number of functional motor units was determined by counting the increments in twitch tension and the mean values are summarised in the bar chart **(E)**. Horizontal scale bar = 10 milliseconds. g = grams. Values shown are the mean ± standard error of the mean. * $p < 0.05$, *** $p < 0.005$.

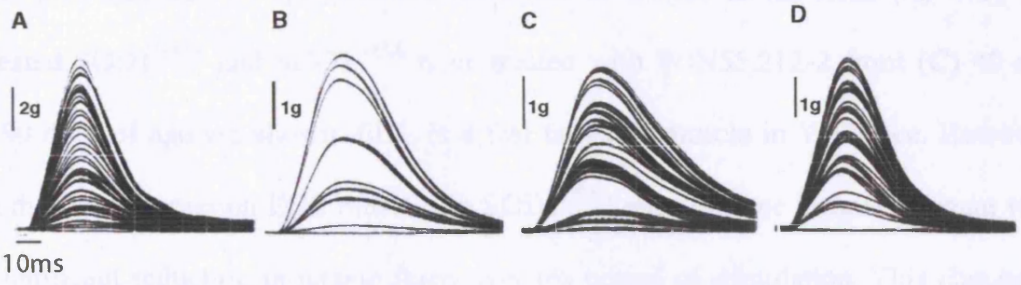
A
B
C
D
2g
1g
1g
1g
10ms

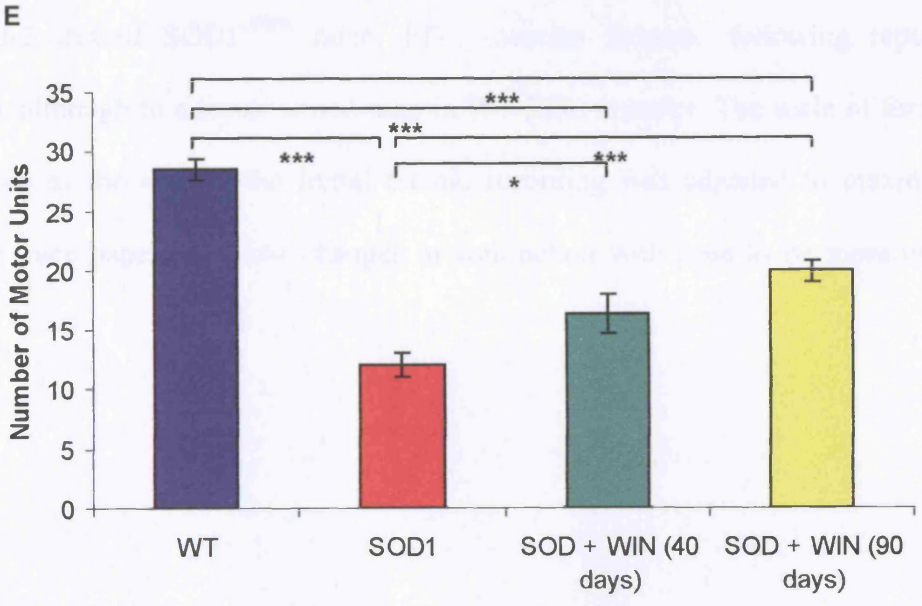
E
Number of Motor Units
35
30
25
20
15
10
5
0
***
***
***
***
*
WT
SOD1
SOD + WIN (40 days)
SOD + WIN (90 days)

Figure 4.12 – Fatigue traces from WT, untreated SOD1^{G93A} and WIN55,212-2 treated SOD1^{G93A} mice at 120 days of age

Repeated stimulation of the EDL muscle via the sciatic nerve over a 3 minute period elicits a fatigue trace. Representative examples of fatigue traces from (**A**) WT, (**B**) untreated SOD1^{G93A} and SOD1^{G93A} mice treated with WIN55,212-2 from (**C**) 40 and (**D**) 90 days of age are shown. EDL is a fast fatigable muscle in WT mice. However, with disease progression EDL muscles in SOD1^{G93A} mice became fatigue resistant with no significant reduction in tetanic force over the period of stimulation. This change in the fatigue characteristics of EDL muscles in SOD1^{G93A} mice did not occur to the same extent in EDL muscles from SOD1^{G93A} mice treated with WIN55,212-2. Thus in WIN55,212-2 treated SOD1^{G93A} mice, EDL muscles fatigued following repeated stimulation, although to a lesser extent than in WT EDL muscles. The scale of force is not indicated as the size of the initial tetanic recording was adjusted to maximally occupy the trace paper, to allow changes in contraction with time to be more easily visible.

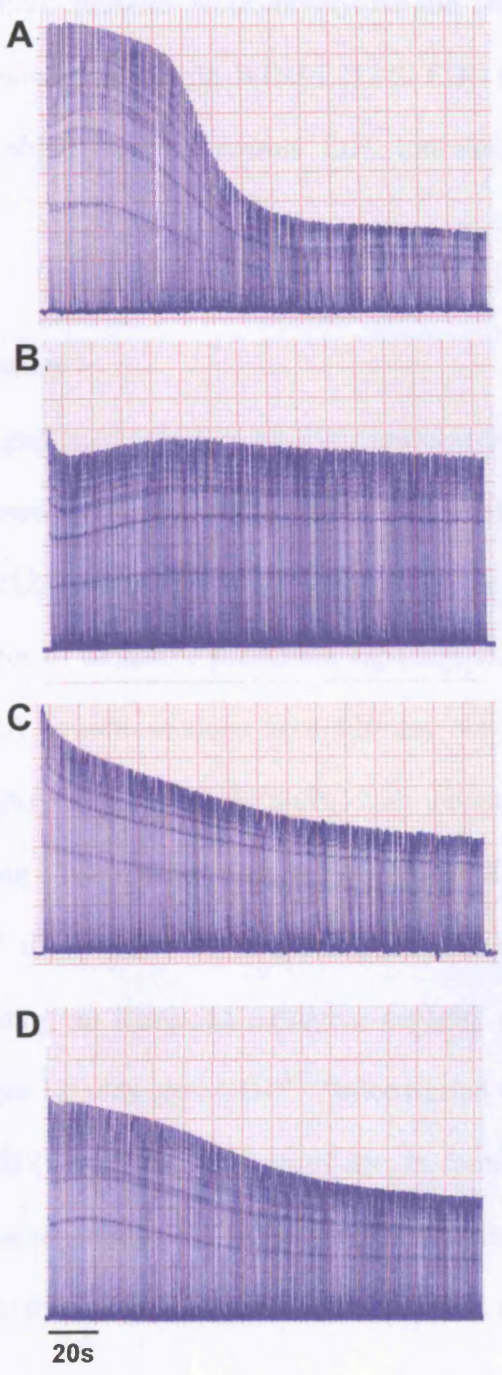
A
B
C
D
20s

(**B**) $SOD1^{G93A}$ and $SOD1^{G93A}$ mice treated with WIN55,212-2 from (**C**) 40 and (**D**) 90 days. EDL is normally a fast muscle that fatigues rapidly when subjected to repeated stimulation, as seen in **Figure 4.12A**. In contrast, in untreated $SOD1^{G93A}$ mice in the late stages of disease, EDL muscles were largely fatigue resistant (**Figure 4.12B**). However, in $SOD1^{G93A}$ mice treated with WIN55,212-2, EDL muscles showed fatigue characteristics that resembled those of normal EDL muscles, as shown in **Figures 4.12C** and **D**.

4.3.6. Muscle histochemistry

The changes in the fatigue characteristics of EDL muscles of $SOD1^{G93A}$ mice were reflected in the histochemical properties of the muscle fibres. EDL muscles from WT, $SOD1^{G93A}$ and WIN55,212-2 treated $SOD1^{G93A}$ mice were sectioned and stained for SDH activity, an indicator of oxidative metabolic capacity, as shown in **Figure 4.13**. SDH staining of WT EDL muscle sections from 120 day old mice revealed a mosaic pattern of lightly and darkly stained muscle fibres, with the majority of fibres staining lightly for SDH, indicating a low oxidative capacity (**Figure 4.13A**). In EDL muscles of 120 day old $SOD1^{G93A}$ mice, however, a greater proportion of fibres were more intensely stained, indicating an increased oxidative capacity of these fibres (**Figure 4.13B**). EDL muscles from 120 day old $SOD1^{G93A}$ mice treated with WIN55,212-2 from 40 (**Figure 4.13C**) and 90 (**Figure 4.13D**) days of age, in contrast, showed a pattern of SDH staining more characteristic of WT EDL muscles, so that a greater proportion of fibres were lightly stained than in the untreated $SOD1^{G93A}$ EDL muscle.

Figure 4.13 – Succinate dehydrogenase staining of EDL muscle sections from WT, untreated SOD1^{G93A} and WIN55,212-2 treated SOD1^{G93A} mice

EDL muscle sections from (**A**) WT, (**B**) untreated SOD1^{G93A} and SOD1^{G93A} mice treated with WIN55,212-2 from (**C**) 40 and (**D**) 90 days of age were sectioned on a cryostat and stained for succinate dehydrogenase (SDH) activity, an indicator of oxidative capacity. WT EDL muscles showed a mosaic pattern of SDH activity, with the majority of fibres staining lightly. A greater proportion of untreated SOD1^{G93A} EDL muscle fibres, however, had an increased oxidative capacity, reflected by more intense staining for SDH activity. In contrast, EDL muscles from 120 day old SOD1^{G93A} mice treated with WIN55,212-2 showed a pattern of SDH staining that was more characteristic of WT EDL muscles, with a greater proportion of fibres lightly stained. Scale bar = 200μm.

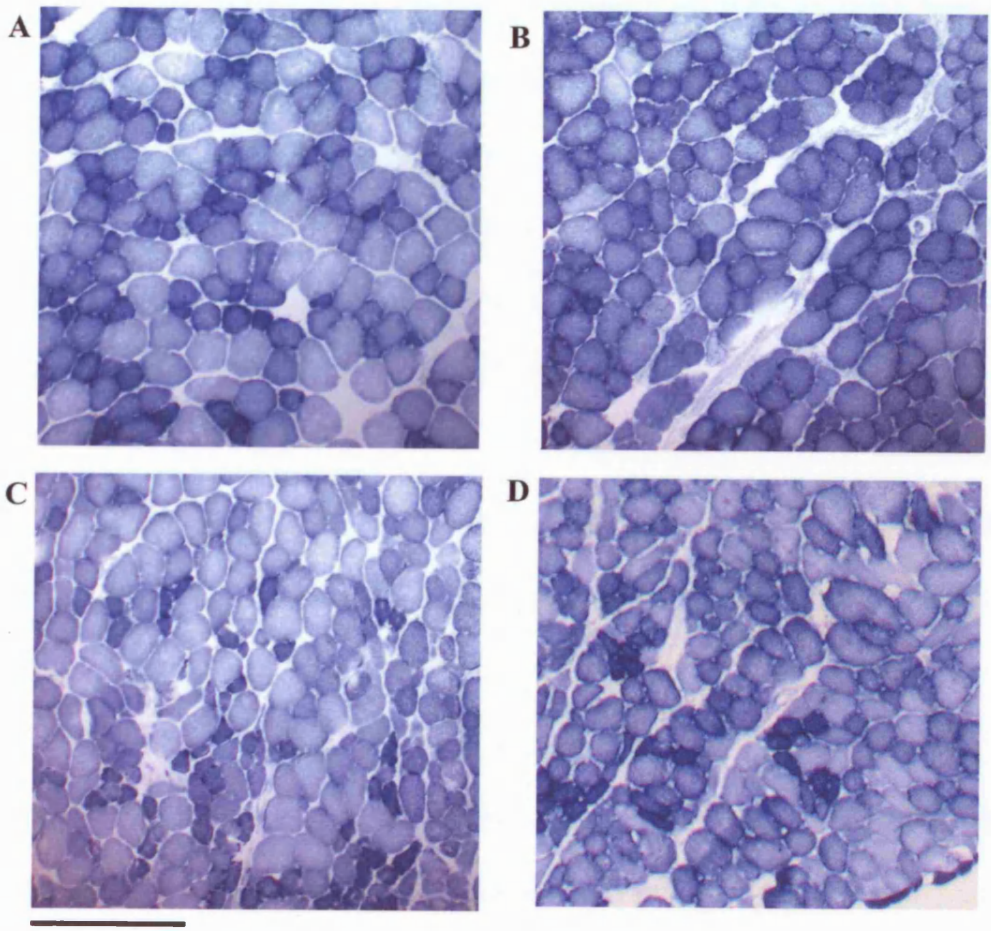
A
B
C
D

4.3.7. Motoneuron survival

The effect of treatment with WIN55,212-2 on motoneuron survival was assessed in 120 day old $SOD1^{G93A}$ mice, by counting the number of motoneurons in the sciatic pool in each ventral horn. **Figure 4.14** shows examples of Nissl - stained spinal cord sections from (**A**) WT, (**B**) $SOD1^{G93A}$ and $SOD1^{G93A}$ treated with WIN 55,212-2 from (**C**) 40 and (**D**) 90 days of age. The improvement in motor unit survival observed in WIN55,212-2 treated $SOD1^{G93A}$ mice was reflected in an increase in motoneuron survival, and the results are summarised in the bar chart (**E**). At 120 days of age a significant number of motoneurons in the sciatic pool had already died in untreated $SOD1^{G93A}$ mice, so that only 140 (± 6.7 S.E.M.; n = 12; $p < 0.001$) motoneurons survived compared to 369 (± 12.9 S.E.M.; n = 8) in the spinal cords of WT littermates, a reduction in motoneuron survival of 62.1%. However, treatment with WIN55,212-2 from both 40 and 90 days of age rescued a significant proportion of motoneurons so that 271 (± 7.5 S.E.M.; n = 8; $p < 0.001$) and 199 (± 10.2 S.E.M.; n = 16; $p < 0.001$) motoneurons survived, a loss of only 26.6% and 46.1% respectively, compared to WT littermates. Thus treatment with WIN55,212-2 protected motoneurons from cell death in $SOD1^{G93A}$ mice, and 93% and 42% more motoneurons survived following treatment from 40 and 90 days respectively, compared to their untreated $SOD1^{G93A}$ littermates.

In addition, the number of motoneurons surviving in the sciatic pool at the end-stage of disease was also assessed (**Figure 4.15**). The number of motoneurons surviving in the spinal cord of end-stage $SOD1^{G93A}$ mice treated with WIN55,212-2 from 40 days of age was significantly greater than in untreated $SOD1^{G93A}$ littermates. Thus, 122 motoneurons (± 6.9 S.E.M.; n = 12; $p = 0.035$) survived in end-stage spinal cord of $SOD1^{G93A}$ mice treated with WIN55,212-2 from 40 days of age, compared to 96 motoneurons (± 7.6 S.E.M.; n = 12) in untreated $SOD1^{G93A}$ littermates, representing a

Figure 4.14 – Motoneuron survival in WT, untreated SOD1^{G93A} and WIN55,212-2 treated SOD1^{G93A} mice at 120 days of age

Motoneuron survival at 120 days of age was assessed by counting the number of Nissl-stained motoneurons in the sciatic motor pool (dotted areas) of (**A**) WT, (**B**) untreated SOD1^{G93A} and SOD1^{G93A} mice treated with WIN55,212-2 from (**C**) 40 and (**D**) 90 days of age. The mean motoneuron survival is summarised in the bar chart (**E**). At 120 days of age SOD1^{G93A} mice (n = 12) had lost a substantial proportion of their sciatic motoneurons compared to WT mice (n = 8). However, treatment with WIN55,212-2 had neuroprotective effects and significantly more motoneurons survived in treated SOD1^{G93A} mice at 120 days of age. Indeed, WIN55,212-2 treatment from 40 (n = 8) and 90 (n = 16) days rescued 93% and 42% of motoneurons respectively. Values are the mean ± standard error of the mean. Scale bar = 100μm. *** $p < 0.005$. There was a significant difference between the mean values of each of the experimental groups.

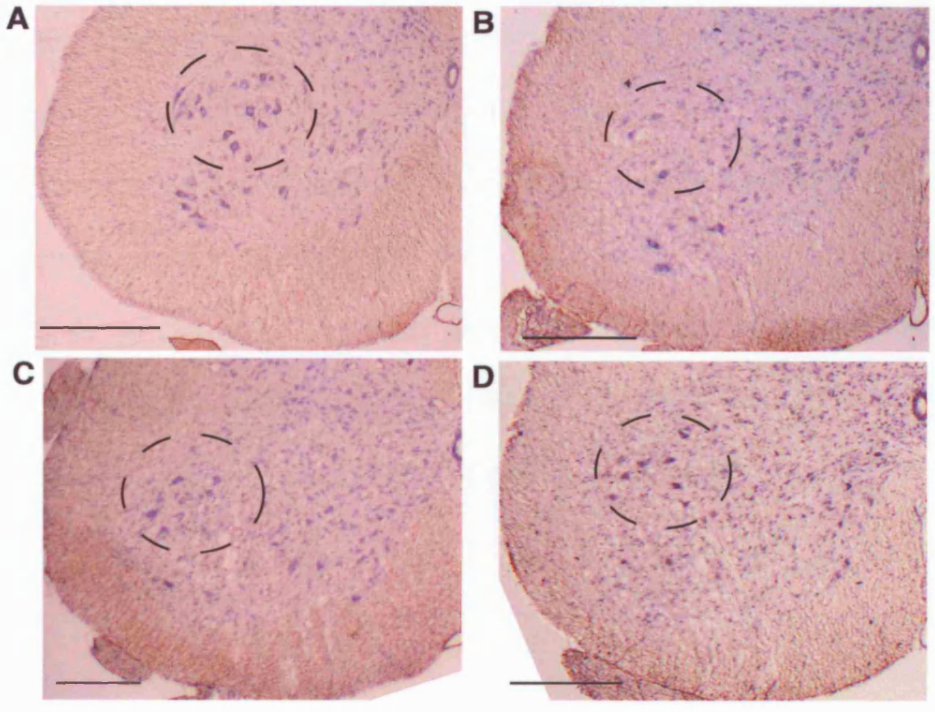
A
B
C
D

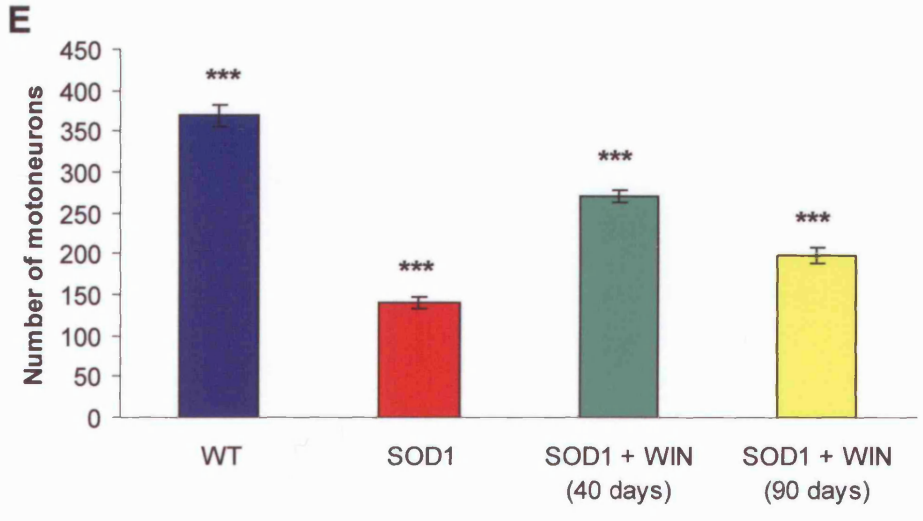
E
Number of motoneurons
450
400
350
300
250
200
150
100
50
0
***
***
***
***
WT
SOD1
SOD1 + WIN (40 days)
SOD1 + WIN (90 days)

Figure 4.15 – Motoneuron survival in end-stage untreated SOD1^{G93A} mice and SOD1^{G93A} mice treated with WIN55,212-2

Motoneuron survival was assessed by counting the number of Nissl-stained motoneurons in the sciatic pool of untreated SOD1^{G93A} and WIN55,212-2 treated SOD1^{G93A} mice at the end-stage of disease. It can be seen that even at the end-stage of disease, treatment with WIN55,212-2 from 40 days of age rescued a significant proportion of sciatic motoneurons in SOD1^{G93A} mice. However, no increase in motoneuron survival was seen in the group treated with WIN55,212-2 from 90 days of age. Values are the mean ± standard error of the mean. * $p < 0.05$.

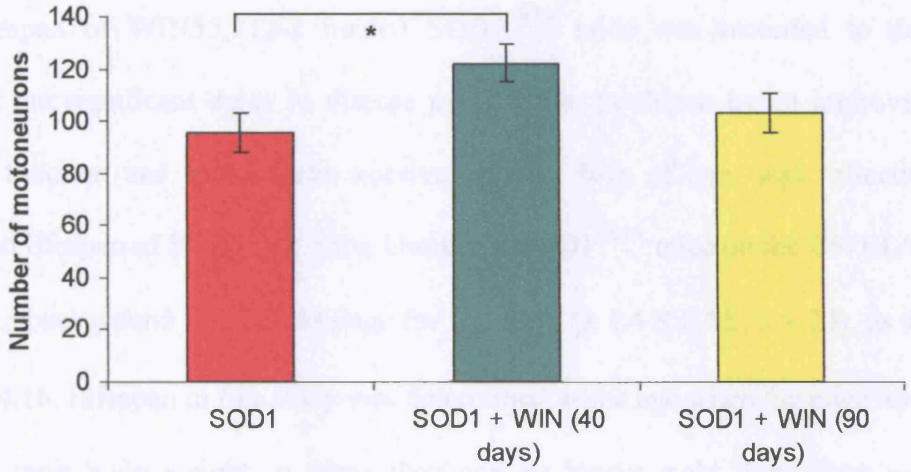
Number of motoneurons
140
120
100
80
60
40
20
0
*
SOD1
SOD1 + WIN (40 days)
SOD1 + WIN (90 days)

27.9% increase in motoneuron survival. However the improvement in motoneuron survival seen at 120 days following treatment with WIN55,212-2 from 90 days of age, was not maintained and only 103 motoneurons (± 7.5 S.E.M.; n = 6; p > 0.4) survived at the end-stage.

4.3.8. The effect of WIN55,212-2 treatment on the lifespan of SOD1^{G93A} mice

The lifespan of WIN55,212-2 treated SOD1^{G93A} mice was recorded to determine whether the significant delay in disease progression, as shown by an improvement in muscle function and motoneuron survival at 120 days of age, was reflected in an increased lifespan of SOD1^{G93A} mice. Untreated SOD1^{G93A} mice on the C57BL/6 x SJL F_1 hybrid background lived on average for 131 days (± 1.4 S.E.M.; n = 23), as shown in **Figure 4.16**. Lifespan in this study was determined as the age when the mice have lost ≥ 20% of their body weight or when they can no longer right themselves within 30 seconds when placed on their sides. Treatment with WIN55,212-2, from either 40 or 90 days of age, had no significant effect on lifespan and treated SOD1^{G93A} mice had an average lifespan of 131 days (± 3.4 S.E.M.; n = 10; p > 0.5) and 134 days (± 2.3 S.E.M.; n = 10; p > 0.1) respectively, although at each time point examined, except end-stage, more treated SOD1^{G93A} mice survived.

Figure 4.16 – The effect of WIN55,212-2 treatment on the lifespan of SOD1^{G93A} mice

The effect of treatment with WIN55,212-2 on the lifespan of SOD1^{G93A} mice was investigated. At weekly time intervals, the number of animals surviving in each experimental group was expressed as a percentage of the total number of animals in that group, as shown in the graph. Although there is a slight shift to the right in the lifespan curve of SOD1^{G93A} mice treated with WIN55,212-2 from 40 or 90 days of age, there was no significant increase in survival. The value at each time point represents the mean survival of each group of experimental mice.

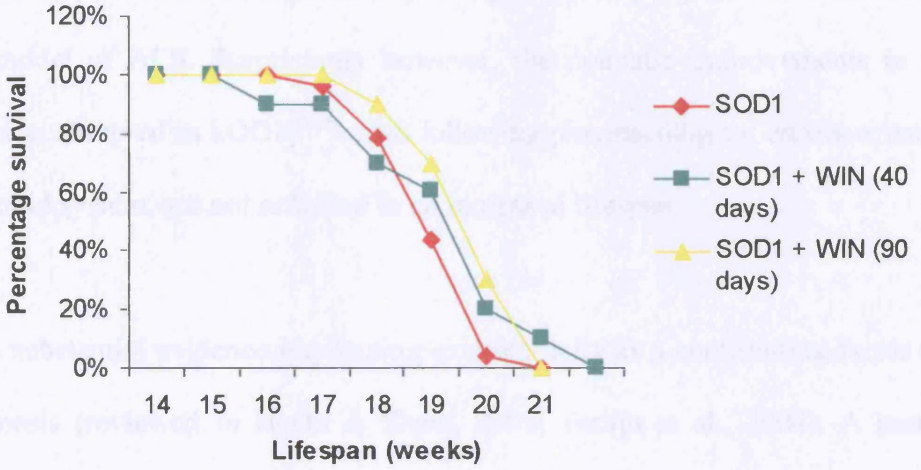
120%
100%
80%
60%
40%
20%
0%
Percentage survival
14
15
16
17
18
19
20
21
Lifespan (weeks)
SOD1
SOD1 + WIN (40 days)
SOD1 + WIN (90 days)

4.4. DISCUSSION

The availability of transgenic mice expressing mutations in Cu/Zn SOD1 enzyme has enabled considerable research into the disease pathogenesis of ALS (Gurney et al., 1994; Ripps et al., 1995; Wong et al., 1995; Bruijn et al., 1998). These mice also provide a useful model in which to test potential therapeutic agents. Indeed, the results of this Chapter show that administration of the exogenous cannabinoid WIN55,212-2, even after symptom onset, significantly delays disease progression in the $SOD1^{G93A}$ mouse model of ALS. Surprisingly however, the dramatic improvements in disease progression observed in $SOD1^{G93A}$ mice following pharmacological enhancement of the cannabinoid system, are not reflected in an increased lifespan.

There is substantial evidence implicating excitotoxicity as a contributing factor to ALS pathogenesis (reviewed in Heath & Shaw, 2002; Bruijn et al., 2004). A number of therapies aimed at reducing excitotoxicity have previously been shown to have beneficial effects in animal models of ALS (Gurney et al., 1998; Canton et al., 2001; Van Damme et al., 2003). However, in ALS patients', treatment with the anti – glutamatergic agent Riluzole has only limited effects, with patient lifespan extended by only 2-4 months (Bensimon et al., 1994; Riviere et al., 1998; Miller et al., 2002; Traynor et al., 2003). Cannabinoids have been shown to reduce excitotoxicity in a number of models of neuronal death via a CB_1 receptor-dependent mechanism (for example Hampson et al., 1998a; Shen & Thayer, 1998b; Abood et al., 2001; Marsicano et al., 2003; Pryce et al., 2003). However, they also exhibit other potentially beneficial effects. For example they are known to have anti-inflammatory (reviewed in Walter & Stella, 2004) and anti-oxidant properties (Hampson et al., 1998b; Chen & Buck, 2000; Marsicano et al., 2002), which in view of the role of these pathogenic mechanisms in ALS, may be particularly relevant. This combination of potential neuroprotective

mechanisms, against inflammation and oxidative stress in addition to excitotoxicity, suggest that cannabinoids may have a greater impact on disease progression in ALS than therapies that target excitotoxicity alone. Indeed, the combination of riluzole, minocycline, an inhibitor of microglial activation, and nimodipine, a blocker of voltage-gated calcium channels, delays disease onset and extends survival in $SOD1^{G37R}$ mice to a greater extent than achieved individually with these agents, thus highlighting the benefits of targeting multiple pathways (Kriz et al., 2003).

4.4.1. Up-regulation of endocannabinoids in symptomatic $SOD1^{G93A}$ mice

The results of this study show an increase in levels of the endocannabinoids, AEA and 2-AG, in the spinal cord of $SOD1^{G93A}$ mice during the symptomatic stages of disease in contrast to presymptomatic stages. This is consistent with the observations of Witting et al, (2004), who also reported elevated levels of endocannabinoids in the spinal cord of symptomatic $SOD1^{G93A}$ mice. It is possible that this is an adaptive response aimed at counteracting excitotoxicity, similar to that observed in the hippocampus of mice treated with KA (Marsicano et al., 2003). However, such an endogenous response is clearly not sufficient to counteract the progression of disease. Administration of an exogenous cannabinoid may therefore act to boost this endogenous protective mechanism, and the results presented in this Chapter show that treatment with WIN55,212-2 significantly delays disease progression in the $SOD1^{G93A}$ mice, maintaining muscle function and delaying motoneuron degeneration. It is interesting to note that in response to peripheral nerve injury, both CB_1 and CB_2 receptors are up-regulated in the spinal cord, on neurons and microglial respectively (Lim et al., 2003; Zhang et al., 2003). This suggests that the pool of cannabinoid receptors available for activation in areas affected in ALS may actually increase with disease progression, at least initially.

4.4.2. The effect of WIN55,212-2 treatment on hindlimb muscle force

Treatment of $SOD1^{G93A}$ mice with WIN55,212-2 from 40 or 90 days of age, a presymptomatic and early symptomatic stage respectively, has significantly beneficial effects on muscle force. In 120 day old $SOD1^{G93A}$ mice, muscle force is substantially reduced compared to WT mice. Indeed, the maximal tetanic force of TA and EDL muscles of $SOD1^{G93A}$ mice is reduced by 67% and 43% respectively, compared to WT muscle force. Sharp et al, (2005) similarly reported a greater vulnerability of TA muscles in $SOD1^{G93A}$ mice. This increased vulnerability of TA muscles may be related to the larger peripheral field of motoneurons innervating the TA muscle compared to EDL, which therefore may render these motoneurons more vulnerable to pathogenic mechanisms, for example oxidative stress. A previous study reported an increased vulnerability of fast twitch EDL muscles, compared to slow twitch soleus muscles in $SOD1^{G93A}$ mice (Derave et al., 2003). This further supports the link between motor unit susceptibility in ALS and their functional size and perhaps phenotype.

Treatment with WIN55,212-2 from 90 days of age prevents the reduction in muscle force in $SOD1^{G93A}$ mice. Thus, the twitch force of TA muscles is 49% greater than in untreated $SOD1^{G93A}$ littermates and tetanic force is 73% greater. Similarly the maximal tetanic force of EDL muscles in $SOD1^{G93A}$ mice treated with WIN55,212-2 from 90 days of age, is 39% greater than EDL muscles in untreated $SOD1^{G93A}$ mice. Since TA muscles of $SOD1^{G93A}$ mice are affected earlier and to a greater extent than EDL muscles, any beneficial effects of WIN55,212-2 may have a comparatively greater impact on TA than EDL muscles.

Treatment with WIN55,212-2 from 40 days has no effect on the decline in force of either TA or EDL muscles in $SOD1^{G93A}$ mice. In view of the positive effects of

treatment from 90 days, this is a surprising finding, although WIN55,212-2 treatment from 40 days does exert beneficial effects on other muscle characteristics.

4.4.3. The effect of WIN55,212-2 treatment on muscle contractile characteristics

Treatment with WIN55,212-2 from either 40 days or 90 days prevents the appearance of disease-induced changes in the fatigue characteristics of EDL muscles. EDL muscles are normally fast muscles that fatigue rapidly when repeatedly stimulated due to the low oxidative capacity of the muscle fibres. However, as a consequence of disease progression in $SOD1^{G93A}$ mice, EDL muscle fibres undergo a phenotypic change and become fatigue resistant (Derave et al., 2003; Sharp et al., 2005). Histochemical staining for SDH activity reveals an increased proportion of more intensely stained muscle fibres in EDL muscles from $SOD1^{G93A}$ mice. This indicates that these muscle fibres have a higher oxidative capacity than normal, a characteristic more typical of slow muscle fibres, which have the capability to maintain contraction for extended periods of time (Navarrete & Vrbova, 1983).

Muscle fibre phenotype is normally determined by the activity of innervating motoneurons (Navarrete & Vrbova, 1984). During development, all motoneurons are initially tonically active with a low frequency of firing (Navarrete & Vrbova, 1983). However, during the first few weeks of postnatal development motoneurons differentiate, becoming either phasic, high frequency firing motor units (fast motoneurons) or remaining tonically-active motor units, but with an increased duration of low frequency firing (slow motoneurons). As a consequence of this change in motoneuron firing pattern, the muscle fibres these motoneurons innervate differentiate into fast and slow muscle fibres respectively (Navarrete & Vrbova, 1983). Interruption of this nerve-muscle interaction during early postnatal development, for example by

peripheral nerve injury, has been shown to have more severe consequences for fast muscles than slow muscles. Therefore as a result of injury, fast muscles generate significantly less force than normal and also become fatigue resistant, with a fatigue pattern more typical of slow muscles. In contrast, following neonatal nerve injury, although significantly weaker than normal, slow muscles remain virtually unchanged (Lowrie et al., 1982, 1987). This injury-induced change in fast muscle phenotype may be the result of a change in the activity pattern of those motoneurons that survive injury, since fast motoneurons that survive become more active (Navarrete & Vrbova, 1984). In contrast, muscle fibres during the period of separation remain unchanged. Therefore upon reinnervation there will be a large mismatch in the characteristics of fast muscles and motoneurons innervating them, which may be detrimental to the muscles (Navarrete & Vrbova, 1984).

It is possible that in $SOD1^{G93A}$ mice, as a consequence of motoneuron degeneration, the remaining motoneurons also become more active, as observed following nerve injury (Navarrete & Vrbova, 1984). Such a change in motoneuron activity would directly affect muscle fibre phenotype. Alternatively, there may be a selective loss of motoneuron subtypes. Indeed, Frey et al, (2000) demonstrate a selective loss of fast neuromuscular synapses in $SOD1^{G93A}$ mice from as early as 40 days of age, suggesting a preferential degeneration of fast motoneurons. Furthermore, Atkin et al, (2005) show a preferential vulnerability of fast twitch muscle fibres by analysis of single muscle fibre contractile properties in $SOD1^{G93A}$ mice at the end-stage of disease. Such selective degeneration of fast motoneurons would also explain the change in EDL muscle phenotype observed here in $SOD1^{G93A}$ mice, as remaining muscle fibre innervation would be from slow motoneurons. Another possibility for the observed change in muscle fibre phenotype in $SOD1^{G93A}$ mice may be that during the

denervation/reinnervation that occurs in SOD1^{G93A} mice (Sharp et al., 2005), EDL muscle fibres become selectively reinnervated by fatigue resistant motoneurons, as a result of collateral sprouting of slow motoneuron axons, thus altering muscle phenotype.

Alternatively, independent of motor unit activity, it is possible that biochemical changes in the skeletal muscles may also be involved in the change in muscle fibre phenotype in SOD1^{G93A} mice. Overexpression of uncoupling protein 1 in skeletal muscle has been shown to result in a reduction in muscle mass and also induces a change in muscle fibre phenotype from fast glycolytic fibres to slow oxidative fibres as a result of the chronic uncoupling of mitochondria (Couplan et al., 2002). In presymptomatic SOD1^{G85R} mice, the levels of uncoupling protein 3 are up-regulated in skeletal muscle, resulting in the functional uncoupling of mitochondria in these muscles, and this may contribute to the changes seen in muscle fibre phenotype with disease progression (Dupuis et al., 2003).

In EDL muscles from SOD1^{G93A} mice treated with WIN55,212-2 from either 40 or 90 days, repeated stimulation produces fatigue characteristics that resemble those of normal EDL muscles, indicating that WIN55,212-2 treatment has delayed the deleterious changes in muscle fibre phenotype in SOD1^{G93A} mice. Similarly, SDH staining reveals that EDL muscle fibres from SOD1^{G93A} mice treated with WIN55,212-2 retain the mosaic pattern of lightly and darkly stained fibres, with a predominance of light staining, characteristic of WT EDL muscle fibres. Therefore, in WIN55,212-2 treated SOD1^{G93A} mice, EDL remains a fast, fatigable muscle with a relatively low oxidative capacity. This observation may be a direct consequence of increased motoneuron survival in these SOD1^{G93A} mice.

4.4.4. The neuroprotective effect of WIN55,212-2 treatment in SOD1^{G93A} mice

The results show that in SOD1^{G93A} mice at 120 days of age, more than 60% of motor units and the same proportion of motoneurons have already died. This is in agreement with previous reports (Kieran et al., 2004; Sharp et al., 2005). However, treatment with WIN55,212-2 rescues a significant proportion of motor units. Thus following treatment with WIN55,212-2 from 40 or 90 days of age only approximately 43% and 30% of motor units are lost respectively. This increase in motor unit survival is reflected in a dramatic increase in motoneuron survival in WIN55,212-2 treated SOD1^{G93A} mice, particularly following treatment from 40 days of age. Thus only 27% of motoneurons die in SOD1^{G93A} mice treated with WIN55,212-2 from 40 days and only 46% of motoneurons die in mice treated from 90 days of age.

4.4.5. The effect of WIN55,212-2 treatment on locomotor activity

It is interesting that SOD1^{G93A} mice treated with WIN55,212-2 from 40 days of age are significantly less active at a presymptomatic and early symptomatic stage of disease than untreated SOD1^{G93A} mice. Cannabinoid-induced inhibition of movement is a widely recognised effect (Baker et al., 2003). However, reports suggest that there is actually a biphasic locomotor response to cannabinoids, with low doses stimulating locomotor activity and high doses exhibiting an inhibitory action (Sulcova et al., 1998; Sañudo–Peña et al., 2000; Wiley et al., 2003; Drews et al., 2005). Although it has been shown that repeated administration of Δ^9-THC can actually stimulate locomotor activity (Wiley, 2003), this study was only carried out over a period of 5 days, in contrast to the 1-3 months duration in the experiments described in this Chapter.

The relationship between ALS and general exercise, both prior to and after disease onset, remains controversial. Several studies claim to link excessive vigorous exercise,

both occupational and recreational, with an increased risk of developing ALS (Scarmeas et al., 2002; Piazza et al., 2004). In contrast, it has also been proposed that physical exercise may be a therapy for ALS patients in an attempt to increase/preserve muscle strength (Drory et al., 2001). The present data suggests that reduced activity levels after disease onset may be protective by preserving hindlimb muscle function, whereas reduced activity levels before disease onset may actually have deleterious effects. Treatment from 90 days of age significantly improves all aspects of muscle function even at a late stage of disease (120 days of age). Cannabinoid-induced inhibition of neurotransmitter release may reduce the input firing frequency from motoneurons to muscle fibres, which consequently would reduce their activity and induce hypomotility. As discussed earlier, increased motoneuron activity due to disease progression may be the process underlying the increased fatigue resistance of EDL muscles in $SOD1^{G93A}$ mice, therefore the hypomotility induced by WIN55,212-2 may delay such deleterious changes. Reduced input to motoneurons may also help to prevent excitotoxic damage and may contribute to the neuroprotective effects observed here. However, treatment from 40 days did not affect muscle force despite exerting beneficial effects on the fatigue characteristics of EDL muscles in $SOD1^{G93A}$ mice. This suggests that prolonged hypomotility induced by WIN55212,2 may actually prevent the preservation of muscle force seen following treatment from 90 days.

4.4.6. The effect of WIN55,212-2 treatment on the lifespan of $SOD1^{G93A}$ mice

Surprisingly, the significant improvements seen in muscle function and motoneuron survival at 120 days of age, following treatment with WIN55,212-2, are not reflected in an increase in lifespan of $SOD1^{G93A}$ mice. The failure of WIN55,212-2 to affect lifespan is particularly surprising considering the significant increase in motoneuron survival at end-stage disease in mice treated from 40 days of age. These results are however

consistent with previous studies in which Δ^9-THC and cannabinol delay the onset of disease in $SOD1^{G93A}$ mice but do not significantly extend lifespan (Raman et al., 2004; Weydt et al., 2005). However the present study extends these observations to confirm that cannabinoid treatment preserves body weight, muscle function and motoneuron survival at a late stage of disease, thereby significantly increasing the "quality of life" of $SOD1^{G93A}$ mice. Therefore, treatment of $SOD1^{G93A}$ mice with WIN55,212-2, a synthetic cannabinoid, significantly delays the disease progression, via the maintenance of muscle force and the preservation of motoneuron survival. However, these improvements are not reflected by an increase in lifespan of the $SOD1^{G93A}$ mice.

4.4.7. Mechanism of cannabinoid-mediated neuroprotection

4.4.7.1. CB_1 receptor-mediated neuroprotection

Cannabinoids exert their effects primarily by activation of CB_1 and CB_2 receptors, located predominantly in the CNS (Herkenham et al., 1991) and on cells of the immune system (Howlett et al., 2002) respectively. Cannabinoid receptor agonists have been shown to inhibit neurotransmitter release via activation of presynaptic CB_1 receptors (Shen et al, 1996; Gessa et al., 1998; Levenes et al., 1998; Nicholson et al., 2003). Furthermore, activation of postsynaptic CB_1 receptors may reduce excitotoxicity-induced postsynaptic calcium influx via inhibition of voltage gated N- and P-/Q- type calcium channels (Caulfield & Brown, 1992; Mackie & Hille, 1992; Twitchell et al., 1997; Shen & Thayer, 1998a; Abood et al., 2001; Hampson & Grimaldi, 2001). It was therefore hypothesised that exogenous WIN55,212-2 may act via the CB_1 receptor to inhibit glutamate neurotransmission and thus limit excitotoxicity in the $SOD1^{G93A}$ model of ALS. Indeed, many *in vivo* and *in vitro* studies have shown neuroprotective actions of cannabinoids under excitotoxic conditions, via a CB_1 receptor-dependent mechanism (for example, Shen & Thayer, 1998a, 1998b; Abood et al., 2001; van der

Stelt et al., 2001a; Marsicano et al., 2003; Molina–Holgado et al., 2003; Pryce et al., 2003). Furthermore, injection of KA into the CNS of CB_1 receptor knock-out mice elicits a more severe response than in WT mice (Marsicano et al., 2003; Pryce et al., 2003). In addition, Parmentier – Batteur et al (2002) reported an increase in neurological damage in CB_1 receptor knock-out mice after either middle cerebral artery occlusion or NMDA injection, therefore highlighting the role of this receptor in neuroprotection.

4.4.7.2. CB_2 receptor-mediated neuroprotection

Other studies have demonstrated neuroprotective effects of cannabinoids in the presence of CB_1 receptor antagonism, indicating a non-CB_1 receptor-mediated effect (Nagayama et al., 1999; Klegeris et al., 2003; van der Stelt et al., 2001b). CB_2 receptors were initially thought to be located only in the immune system (reviewed in Howlett et al., 2002). However, CB_2 receptors have recently been localised to rodent microglia *in vitro* (Facchinetti et al., 2003; Walter et al., 2003; Carrier et al., 2004) and to human microglia (Benito et al., 2003; Klegeris et al., 2003). Therefore, CB_2 receptor activation may also contribute to the effects of cannabinoids in the CNS. Indeed, microglial expression of CB_2 receptors has been shown to be up-regulated in the lumbar spinal cord of rats following peripheral nerve injury (Zhang et al., 2003).

Several lines of evidence indicate that inflammation may also play a role in ALS (McGeer & McGeer, 2002). In the post-mortem spinal cords of ALS patients there are abundant signs of inflammation, with reactive astrocytes, activated microglia and $CD4^+$ and $CD8^+$ T-lymphocytes present in areas of motoneuron degeneration (Troost et al., 1990; Engelhardt et al., 1993; Alexianu et al., 2001; Yasojima et al., 2001; McGeer & McGeer, 2002; Zhang et al., 2005). Furthermore, increased mRNA and protein levels of

inflammatory markers such as COX2, PGE_2 and TNFα are also seen in the post-mortem spinal cords of ALS patients (Poloni et al., 2000; Yasojima et al., 2001; Maihofner et al., 2003).

In $SOD1^{G93A}$ mice there is a correlation between disease progression and the intensity of inflammation (Hall et al., 1998; Alexianu et al., 2001; Almer et al., 2001). Reactive astrogliosis increases steadily from disease onset, whereas microglial activation is evident from a presymptomatic age of 60 days and continues to increase in intensity with disease progression, paralleling the loss of motoneurons (Hall et al., 1998; Alexianu et al., 2001; Elliott et al., 2001; Olsen et al., 2001; Weydt et al., 2004). The contribution of glial cells to disease progression in ALS is highlighted by studies in which *in vivo* expression of the mutant SOD1 protein under the control of a neuronal promoter does not result in development of motor neuron disease (Pramatarova et al., 2001; Lino et al., 2002). This indicates that expression of the mutant SOD1 protein is required in both motoneurons and glial cells for disease to manifest. The up–regulation of intracellular adhesion molecule-1 (ICAM-1) expression on microglia at 40 days is in fact one of the earliest pathological changes seen in the $SOD1^{G93A}$ mice (Alexianu et al., 2001). Such up–regulation may be important in the induction of inflammatory processes (Kawasaki et al., 1993; Alexianu et al., 2001). Microglia are also implicated in the propagation of inflammation, whereby microglial activation induces the release of pro-inflammatory cytokines, ROS and glutamate which initiate the recruitment and activation of further microglia, and in addition can also elicit cellular damage (Molina-Holgado et al., 1997; Tikka & Koistinaho, 2001). Microglia from $SOD1^{G93A}$ mice have been shown to secrete significantly more TNFα than age-matched WT microglia (Weydt et al., 2004) and there is a significant up-regulation of TNFα mRNA and protein in the CNS of $SOD1^{G93A}$ mice (Hensley et al., 2003). Pro-inflammatory

cytokines, such as TNFα and IL-1β, can induce COX2 expression, via activation of the transcription factor NF-κB (Consilvio et al., 2004; Juttler et al., 2004). Activation of COX2 will then increase production of prostaglandins, including PGE2, which may actually contribute to excitotoxicity by stimulating the release of glutamate from astrocytes (Drachman & Rothstein, 2000), and in addition releases ROS, which may further propagate the inflammatory process (Consilvio et al., 2004).

Minocycline, a potent inhibitor of microglial activation, has been shown to inhibit neuronal death induced by exposure to cerebrospinal fluid from ALS patients (Tikka et al., 2002) and also delay onset and extend survival by 9-16% in mutant SOD1 mice (Kriz et al., 2002; van den Bosch et al., 2002; Zhu et al., 2002). Similarly, NDGA, an inhibitor of 5-lipoxygenase, which acts to suppress microglial activation by reducing TNFα release, extended the lifespan of $SOD1^{G93A}$ mice by 32% (West et al., 2004). Other inhibitors of inflammation have also been shown to have beneficial effects in ALS models. In a model of chronic motoneuron degeneration the selective COX2 inhibitor SC236 prevents motoneuron loss (Drachman & Rothstein, 2000), whereas *in vivo,* selective COX2 inhibitors delay onset (Pompl et al., 2003) and extend the lifespan of $SOD1^{G93A}$ mice by 25% (Drachman et al., 2002). However, recently a clinical trial using celebrex (a selective COX2 inhibitor) failed to have any significant effect on muscle function in ALS patients. At this stage it is not clear whether the lack of effects observed are actually due to poor bioavailability of the drug, an incorrect dosage regimen or even a inappropriately designed trial and also whether this negative result is solely related to celebrex or to all COX2 inhibitors (www.alsa.org).

Cannabinoids have also been shown to reduce microglial activation (Arevalo-Martin et al., 2003) and reduce both mRNA expression and release of pro-inflammatory cytokines

from microglia (Puffenbarger et al., 2000; Croxford & Miller, 2003; Facchinetti et al., 2003) via a CB_2 receptor-mediated mechanism (Klegeris et al., 2003). Furthermore, Molina-Holgado et al, (2003) suggest that cannabinoids antagonise the actions of the pro-inflammatory mediator IL-1β via a CB_1 or CB_2 receptor-induced increase in Il-1 receptor antagonist, thus reducing inflammation. There is also evidence to suggest that cannabinoids can inhibit activation of the transcription factor NF-κB, in a CB_1 receptor-dependent manner, which may also suppress inflammation by reducing the expression of the COX2 enzyme, nitric oxide and expression of pro-inflammatory cytokine TNFα, for example (Waksman et al., 1999; Juttler et al., 2004). In addition to these anti-inflammatory actions, an inhibitory effect of cannabinoids on microglia may also limit their release of glutamate and ROS, thus lowering the potential contribution of excitotoxicity and oxidative stress to disease pathogenesis (Molina-Holgado et al., 1997, 2002; Waksman et al., 1999; Tikka et al., 2002).

4.4.7.3. Other potential targets

Another possible target mediating the effect of WIN55,212-2 in nervous tissue is the as yet unidentified, G protein coupled cannabinoid "CB_3" receptor that has been pharmacologically characterised in the brain of CB_1 receptor knock-out mice (Di Marzo et al., 2000; Breivogel et al., 2001; Monory et al., 2002). This receptor is activated to the same extent by AEA and WIN55,212-2, but not by other synthetic cannabinoids or Δ^9-THC. It is insensitive to CB_1 and CB_2 receptor antagonists and is not coupled to the inhibition of adenylate cyclase (Monory et al., 2002), unlike the existing cannabinoid receptors. There is, however, evidence to suggest that this receptor may be selectively coupled to the inhibition of glutamate release in the mouse hippocampus (Hajos et al., 2001).

Cannabinoids have also been shown to act via receptor-independent mechanisms. Δ^9-THC and CBD have been ascribed an anti-oxidant capacity equivalent to that of butylated hydroxytoluene, a known anti-oxidant (Hampson et al., 1998b; Chen & Buck, 2000). Indeed, CBD, a non-receptor binding cannabinoid, exerts significant neuroprotection in models of serum deprivation and hydrogen peroxide-induced oxidative stress (Chen & Buck, 2000; Marsicano et al., 2002) and NMDA/AMPA-mediated excitotoxicity (Hampson et al., 1998b). Δ^9-THC achieves similar levels of neuroprotection in these models but these effects are insensitive to CB_1 receptor antagonism, are not stereoselective and are achieved at concentrations significantly higher than that required for receptor binding (Chen & Buck, 2000). Meanwhile, the synthetic cannabinoid, CP 55,940, exerts an equivalent degree of neuroprotection in WT and CB_1 receptor knock-out cerebellar granule neurons, suggesting that CB_1 receptors are not involved (Marsicano et al., 2002). However, it is unlikely that anti-oxidant activity contributes to the neuroprotection mediated by WIN55,212-2 in this ALS model, as the anti-oxidant mediated neuroprotection of CBD, Δ^9-THC and CP 55,940 has been shown to be dependent on the presence of a phenol ring in their structure and WIN55,212-2, an aminoalkylindole, lacks a phenol ring.

4.5. CONCLUSION

Treatment with WIN55,212-2, from either 40 or 90 days, a presymptomatic or symptomatic age respectively, delays disease progression in $SOD1^{G93A}$ mice. At 120 days of age, a relatively late stage of disease, muscle function and motoneuron survival are significantly improved in WIN55,212-2 treated $SOD1^{G93A}$ mice compared to their untreated $SOD1^{G93A}$ littermates. However, despite these significant improvements, no increase in lifespan is observed. These results may have relevance for the treatment of

ALS, as the clear increase in muscle function induced by WIN55,212-2 may translate to a significant improvement in patient "quality of life".

CHAPTER 5

THE EFFECTS OF GENETIC MANIPULATION OF THE ENDOCANNABINOID SYSTEM IN THE SOD1^{G93A} MOUSE MODEL OF ALS

5.1. INTRODUCTION

The results presented in **Chapter 4** demonstrated that administration of an exogenous synthetic cannabinoid receptor agonist, WIN55,212-2, to symptomatic $SOD1^{G93A}$ mice has significant neuroprotective effects, but no impact on lifespan. Therefore the effect of genetically enhancing endocannabinoid levels in $SOD1^{G93A}$ mice was examined next, in order to establish whether this would have a greater impact on disease than pharmacological treatment. Furthermore, in order to elucidate the mechanism by which cannabinoids exert their neuroprotective capabilities, the CB_1 receptor was genetically ablated in $SOD1^{G93A}$ mice and the effect of this manipulation on disease progression was assessed.

5.1.1. Endocannabinoids

The discovery of cannabinoid receptors in the early 1990s (Matsuda et al., 1990; Munro et al., 1993) initiated extensive research into the existence of endogenous modulators of the cannabinoid system. In 1992, arachidonoyl ethanolamine (anandamide; AEA), the first endocannabinoid, was identified (Devane et al., 1992), followed by 2-arachidonoyl glycerol (2-AG), 2-arachidonoyl glycerol ether, homo-γ-linolenylethanolamide, docosatetraenylethanolamide and *O*-arachidonoyl ethanolamine, comprising a family of lipid-derived neurotransmitters (Devane et al., 1992; Hanus et al., 1993, 2001; Mechoulam et al., 1995; Sugiura et al., 1995; Porter et al., 2002). In animal models, administration of synthetic AEA or 2-AG reproduces the characteristic behavioural effects of plant-derived and synthetic cannabinoids for example, hypomotility, analgesia and hypothermia (Fride & Mechoulam, 1993; Di Marzo et al., 1998). Two further endocannabinoids, oleoylethanolamide (OEA) and palmitoylethanolamide (PEA), have also been characterised although they do not activate the known cannabinoid receptors (Freund et al., 2003).

The ability of AEA and 2-AG to displace [^{3}H]HU-243, a specific cannabinoid receptor agonist, demonstrates their efficacy at both CB_1 and CB_2 receptors (Devane et al., 1992; Felder et al., 1993; Vogel et al., 1993; Felder et al., 1995; Slipetz et al., 1995). The functional coupling between endocannabinoid-mediated cannabinoid receptor binding and the activation of $G_{i/o}$ proteins is shown by significant inhibition of adenylate cyclase activity in a pertussis toxin sensitive manner (Vogel et al., 1993; Pertwee et al., 1994; Felder et al., 1995; Slipetz et al., 1995). CNS levels of 2-AG are elevated approximately 200 fold over AEA concentrations (Sugiura et al., 1995; Stella et al., 1997). Furthermore, 2-AG can fully activate both G_i and G_o binding proteins. AEA can similarly activate G_i proteins fully, but in contrast mediates only partial activation of G_o proteins (McAllister & Glass, 2002). This differential regulation of G protein activation, together with differing CNS concentrations, may permit some control over the effects exerted by endocannabinoids in different cell types (McAllister & Glass, 2002).

5.1.2. Endocannabinoid synthesis

The cellular synthesis of endocannabinoids occurs on demand, in response to neuronal depolarisation and the subsequent increase in intracellular calcium (Di Marzo et al., 1994; Cadas et al., 1996). The synthetic pathways of AEA and 2-AG are summarised in **Figure 5.1** and **Figure 5.2** respectively. In contrast, the biosynthetic pathways of the other identified endocannabinoids are not yet fully understood (De Petrocellis et al., 2004).

AEA and other N-acyl ethanolamines (NAEs) are derived from phospholipid precursors, the N-acyl phosphatidylethanolamines (NAPEs), by the action of an N-acyl phosphatidylethanolamine-selective phospholipase D (NAPE-PLD), a member of the

Figure 5.1 – Synthetic and degradation pathways of anandamide

The diagram details the pathways and enzymatic reactions involved in the synthesis and degradation of anandamide (AEA). AEA is derived from its corresponding N – acyl phosphatidylethanolamine (NAPE) precursor, N-arachidonoyl phosphatidylethanolamine, by calcium-dependent hydrolysis of the NAPE phosphodiester bond, a reaction catalysed by NAPE-phospholipase D (Di Marzo et al., 1994; Cadas et al., 1997; Okamoto et al., 2004). This forms N-arachidonoyl ethanolamine (AEA) and phosphatidic acid. The NAPE precursor of AEA is in turn generated by the N-acyl transferase mediated transfer of a fatty acid group from *sn*-1 phosphatidylcholine to the amino group of phosphatidylethanolamine (Cadas et al., 1997; Di Marzo et al., 2004). Following the release of AEA and its subsequent re-uptake by the putative endocannabinoid membrane transporter (Di Marzo et al., 1994), AEA is hydrolysed by fatty acid amide hydrolase to form ethanolamine and arachidonic acid (Di Marzo et al., 1994; Cravatt et al., 1996).

Pathways of anandamide synthesis and degradation

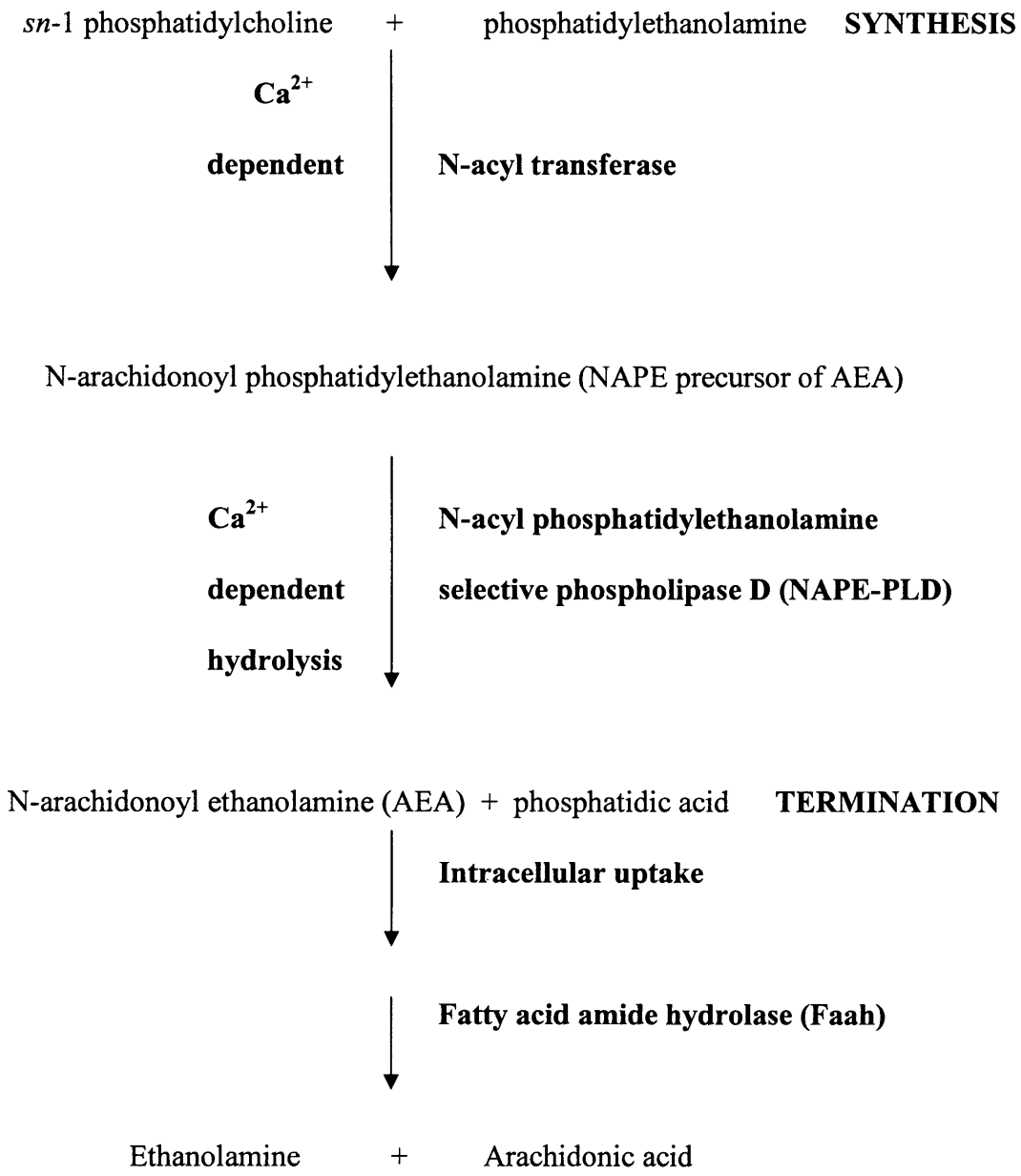

zinc metallohydrolase enzyme family (Okamoto et al., 2004). NAPE-PLD catalyses the calcium-dependent hydrolysis of the NAPE phosphodiester bond to generate the corresponding NAE and phosphatidic acid (Di Marzo et al., 1994). The action of NAPE-PLD is not specific to one NAPE and this enzyme is therefore responsible for the generation of all NAEs, including N-arachidonoyl ethanolamine (AEA), N-palmitoyl ethanolamine, N-stearoyl ethanolamine and N-oleoyl ethanolamine (Cadas et al., 1997; Okamoto et al., 2004). Generation of NAPEs is also calcium-dependent, therefore to avoid depletion, synthesis of the precursor pool of NAPEs occurs under the same conditions that stimulate endocannabinoid synthesis. NAPEs are synthesised by the calcium-dependent transfer of a fatty acid acyl group from phosphatidylcholine to the amino group of a phosphatidylethanolamine, catalysed by an uncharacterised N-acyl transferase enzyme (Cadas et al., 1997; Di Marzo et al., 2004).

In contrast, there are two possible mechanisms by which 2-AG may be synthesised, as shown in **Figure 5.2**. The calcium-dependent hydrolysis of *sn*-1-acyl-2-arachidonoyl glycerol (diacylglycerol; DAG) by the action of membrane bound diacylglycerol lipases (DAGL), isoforms α and β, can generate 2-AG (Bisogno et al., 2003; Di Marzo et al., 2004). DAG in turn is generated, along with inositol (1,4,5) tris-phosphate (IP_3), by phospholipase C (PLC) mediated hydrolysis of a particular subset of membrane phospholipids, the phosphatidylinositols (Stella et al., 1997). Alternatively, phosphatidylinositols may be hydrolysed by phospholipase A_1 to generate 2-arachidonoyl lysophospholipid, which can be subsequently hydrolysed to 2-AG by the action of lyso-PLC (Freund et al., 2003; Piomelli, 2003). Evidence for this pathway occurring *in vivo*, however, is lacking.

Figure 5.2 – Synthetic and degradation pathways of 2-arachidonoyl glycerol

This diagram represents the synthetic and degradation pathways of 2-arachidonoyl glycerol (2-AG). 2-AG can be derived from the calcium-dependent hydrolysis of *sn*-1-acyl-2-arachidonoyl glycerol (DAG), catalysed by diacylglycerol lipases (DAGL; Bisogno et al., 2003; Di Marzo et al., 2004). DAG is generated from phospholipase C-mediated breakdown of phosphatidylinositols, phospholipid components of cellular membranes, along with inositol (1,4,5) tris-phosphate (IP_3; Stella et al., 1997). Alternatively, 2-AG can be synthesised by phospholipase A_1-mediated hydrolysis of phosphatidylinositols to generate 2-arachidonoyl lysophospholipid, which can be subsequently broken down to form 2-AG by the action of lyso-phospholipase C (Freund et al., 2003; Piomelli, 2003). Following the release of 2-AG and its re-uptake by the putative endocannabinoid membrane transporter (Di Marzo et al., 1994), 2-AG is hydrolysed by the action of monoacylglycerol lipase to form glycerol and arachidonic acid (Karlsson et al., 1997; Dinh et al., 2002).

Pathways of 2-AG synthesis and degradation

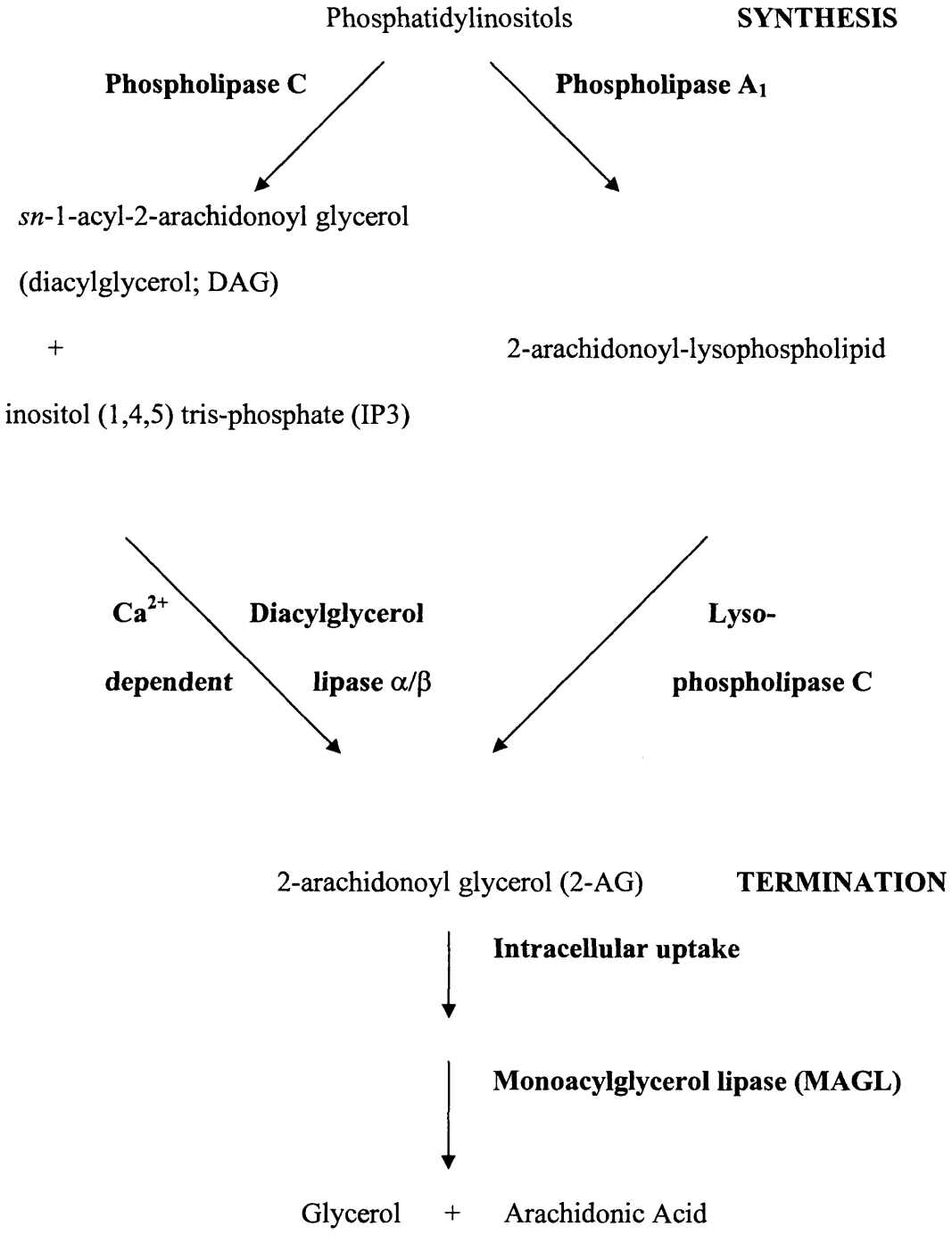

The existence of different biosynthetic pathways for AEA and 2-AG suggests that these endocannabinoids may operate independently of each other and may actually be responsible for the regulation of different physiological functions. This possibility is supported by the fact that calcium entry through ionotropic glutamate receptors is sufficient to initiate the synthesis of 2-AG, whereas the synthesis of AEA and other NAEs requires the activation of both ionotropic glutamate and acetylcholine receptors (Stella & Piomelli, 2001), which again suggests a differential regulation of endocannabinoid synthesis under certain conditions.

Endocannabinoids can also be synthesised in a calcium-independent manner through the activation of postsynaptic metabotropic glutamate receptors (Cadas et al., 1996; Maejima et al., 2001). Activation of group I metabotropic glutamate receptors, coupled to $G_{q/11}$, stimulates the activation of $PLC_{\beta s}$ subunits, thus producing DAG from membrane phospholipids and subsequently forming 2-AG (Maejima et al., 2001). Furthermore, the production of IP_3 via PLC activity will induce calcium release from intracellular stores, potentially stimulating the calcium-dependent synthesis of both AEA and 2-AG (Freund et al., 2003). There is also evidence suggesting that group I metabotropic glutamate receptors are coupled to the activation of protein kinase A (PKA) though adenylate cyclase stimulation and the subsequent elevation in cAMP levels (Cadas et al., 1996). This transduction pathway may potentiate the activity of N-acyl transferase, enhancing AEA formation (Azad et al., 2004).

5.1.3. Endocannabinoid reuptake

In the CNS, endocannabinoids are synthesised by neurons, astrocytes and microglia (Di Marzo et al., 1994; Walter et al., 2003). Following synthesis, in contrast to most other neurotransmitters, endocannabinoids are released by a non-vesicular mechanism into the

extracellular space, permitting activation of cannabinoid receptors (Di Marzo et al., 1994). However, subsequent reuptake and hydrolysis of endocannabinoids occurs rapidly, so that for example, the biological action of AEA is less than 5 minutes in duration (Di Marzo et al, 1994; Willoughby et al., 1997; Cravatt et al., 2001). Initially it was thought that termination of the actions of endocannabinoids occurred by simple diffusion across plasma membranes, with intracellular hydrolysis acting as the driving force for diffusion (Glaser et al., 2003). However, AEA accumulation has been shown to be identical in WT neurons and in neurons lacking fatty acid amide hydrolase (Faah), the enzyme responsible for AEA hydrolysis, indicating that internalisation is not driven by hydrolysis (Fegley et al., 2004). Furthermore, endocannabinoid uptake has characteristics typical of carrier-mediated uptake: selectivity, saturation at 37°C, rapid action and temperature dependency (Di Marzo et al., 1994; Beltramo et al., 1997; Hillard et al., 1997). Uptake, however, is not dependent on cellular ATP suggesting a mechanism of facilitated diffusion rather than active uptake (Hillard et al., 1997), with the direction of transport depending on the endocannabinoid concentration gradient. Alternatively, it has been suggested that the binding of endocannabinoids to a lipid binding protein may act as the driving force for cellular uptake (Fegley et al., 2004; Ortega-Gutierrez et al., 2004). In 1997, AM404, a competitive inhibitor of endocannabinoid uptake, was developed based on the structure of AEA (Beltramo et al., 1997). Administration of AM404 potentiates the effects of AEA in both *in vitro* and *in vivo* studies and provides pharmacological evidence for the existence of an endogenous endocannabinoid membrane transporter (EMT; Beltramo et al., 1997; Calignano et al., 1997) that is believed to be involved in the release as well as reuptake of endocannabinoids (Hillard et al., 1997). However, despite substantial evidence for its existence, no transporter protein has ever been isolated.

5.1.4. Endocannabinoid hydrolysis

Termination of endocannabinoid action occurs by intracellular hydrolysis that follows cellular reuptake (as shown in **Figures 5.1** & **5.2**; Di Marzo et al., 1994; Goparaju et al., 1999; Dinh et al., 2002). The Faah enzyme, identified and cloned from rat liver microsomes in 1996 (Cravatt et al., 1996), is responsible for the hydrolysis of AEA into ethanolamine and arachidonic acid (Di Marzo et al., 1994; Cravatt et al., 1996). 2-AG in contrast, is hydrolysed by monoacylglycerol lipase (MAGL; Dinh et al., 2002) into glycerol and arachidonic acid (Karlsson et al., 1997).

Regional CB_1 receptor expression in the CNS co-localises with that of both the Faah and MAGL enzymes, although the two degradative enzymes show a complementary neuronal distribution (Dinh et al., 2002; Gulyas et al., 2004). The Faah enzyme is found predominantly postsynaptically with a somatodendritic localisation (Egertova et al., 2003). At an ultrastructural level Faah is associated with smooth endoplasmic reticulum and the outer membranes of mitochondria (Gulyas et al., 2004). Faah activity has also been demonstrated in glial cells (Di Marzo et al., 1994). Meanwhile, MAGL has an almost exclusive presynaptic location (Gulyas et al., 2004). This segregation of the main endocannabinoid hydrolysing enzymes again suggests differential functions for AEA and 2-AG (Gulyas et al., 2004).

The generation of *Faah* -/- mice in 2001, as described by Cravatt et al, allowed further examination of the physiological role of AEA and other Faah-hydrolysed NAEs, such as OEA and PEA. Hydrolysis rates in *Faah* -/- mice are reduced by between 50 – 100 fold and levels of AEA and the other Faah-hydrolysed NAEs are consequently elevated 10 - 15 fold in the CNS (Cravatt et al., 2001). *Faah* -/- mice are viable, fertile and display normal cage behaviour and lifespan (Cravatt et al., 2001). Importantly in the *Faah* -/-

mice the CB_1 receptor system is functionally equivalent to that in WT mice (Lichtman et al., 2002). Indeed, administration of exogenous AEA to *Faah* -/- mice induces CB_1 receptor-mediated analgesia, hypomotility, catalepsy and hypothermia (Cravatt et al., 2001). Furthermore, *Faah* -/- mice actually demonstrate a reduced basal sensitivity to pain following thermal and chemically noxious stimuli, an effect partially reversed by CB_1 receptor antagonism. This demonstrates the CB_1 receptor-mediated effect of AEA in the endogenous response to pain and also highlights the regulatory role of Faah in this response (Cravatt et al., 2001; Lichtman et al., 2004).

Clement et al, (2003) however, demonstrated an increased susceptibility of *Faah* -/- mice to kainate (KA) induced seizures, which was ascribed to AEA-mediated inhibition of GABA release in the hippocampus. This is in contrast to the generally accepted anti-convulsant properties of cannabinoids (reviewed in Mechoulam & Lichtman, 2003) and in addition also contradicts their implicated role in an endogenous neuroprotective mechanism against excitotoxicity (Sugiura et al., 2000; Hansen et al 2001b; Panikashvili et al., 2001; Marsicano et al., 2003). However, the overall neuroprotective influence of endocannabinoids will also depend on the contribution of those not hydrolysed by Faah, for example, 2-AG. In addition, the final outcome may actually depend on the regional distribution of endocannabinoid synthesis in the CNS (Cravatt & Lichtman, 2003).

5.1.5. The physiological role of endocannabinoids

Since endocannabinoids have only been relatively recently discovered, their physiological functions are not yet fully understood. However, the use of selective pharmaceutical inhibitors and the availability of animal models in which the

cannabinoid system has been genetically manipulated have provided some insight into the physiological significance of endocannabinoids.

5.1.5.1. Endocannabinoid sites of action

Endocannabinoid-mediated activation of CB_1 and CB_2 receptors, as described in **Chapter 4.1.2.**, will exert, in brief, the following effects:

i) Inhibition of adenylate cyclase activity with consequent reduction in cAMP levels

ii) Activation of A- type potassium channels

iii) CB_1 receptor-mediated inhibition of voltage gated N-, P- and Q- type calcium channels and stimulation of inwardly rectifying potassium channels

iv) CB_1 receptor-mediated activation of MAPK

v) CB_1 receptor-induced up-regulation of immediate early genes, for example c-fos

vi) Potential stimulatory effects on calcium mobilisation dependent on elevated cAMP levels, and a combination of PKA/PKC and PLC activation that may occur under certain circumstances (as described in more detail in **Chapter 4.1.2.**).

There is also increasing evidence for other, uncloned, cannabinoid receptors that may account for several of the effects exerted by endocannabinoids. The "CB_3" receptor has been pharmacologically characterised in the brains of CB_1 receptor knock-out (*Cnr1* -/-) mice (Di Marzo et al., 2000; Breivogel et al., 2001; Monory et al., 2002). This receptor subtype is activated only by AEA and WIN55,212-2 and has been suggested to be responsible for mediating cannabinoid-induced inhibition of glutamatergic neurotransmission (Hajos et al., 2001; Hajos & Freud, 2002). Furthermore, this receptor subtype, or alternatively an unidentified receptor subtype, may underlie the selective

ability of AEA to inhibit gap junction permeability in striatal astrocytes and consequently reduce calcium propagation within this astrocytic network (Venance et al., 1995).

Jarai et al, (1999) identified a potential endothelial cannabinoid receptor subtype in rat mesenteric arteries, activated by AEA and abnormal-cannabidiol, a non-cannabinoid receptor binding cannabinoid. AEA-mediated mesenteric vasodilation was maintained in *Cnr1 -/- Cnr2 -/-* mice, which implicates a currently unidentified receptor subtype in this effect (Jarai et al., 1999). However, it has been suggested that AEA-mediated vasodilation is in fact mediated by activation of the vanilloid receptor, VR1 (or TRPV1) receptor and subsequent release of calcitonin gene related peptide (CGRP; Zygmunt et al., 1999). AEA has been identified as an endogenous ligand for the VR1 receptor and may in fact exert a number of cannabinoid receptor-independent effects, through this receptor (Zygmunt et al., 1999; Smart et al., 2000). VR1 receptors are calcium permeable, non-selective cation channels (Zygmunt et al., 1999; Smart et al., 2000), activation of which will induce an intracellular calcium influx, neuronal depolarisation and subsequently increase excitability (Smart et al., 2000). However, VR1 channels also undergo rapid desensitisation and therefore AEA-mediated activation may in fact induce their desensitisation and paradoxically reduce neuronal excitability (Veldhuis et al., 2003). Indeed, arvanil, a potent CB_1 and VR1 receptor agonist has neuroprotective effects in an animal model of ouabain-mediated excitotoxicity, acting through both CB_1 and VR1 receptors (Veldhuis et al., 2003). Meanwhile, capsazepine, a VR1 receptor antagonist, also had direct neuroprotective effects in this model (Veldhuis et al., 2003).

Furthermore, AEA interacts with several ion channels providing a receptor-independent mechanism through which endocannabinoids can modulate neuronal function. For

example, AEA directly inhibits TASK-1, a background potassium channel that is involved in setting the neuronal resting membrane potential (Maingret et al., 2001). Somatic motoneurons and cerebellar granule neurons express high levels of TASK-1 and inhibition of this current induces depolarisation and increases neuronal excitability (Maingret et al., 2001). AEA can also directly inhibit sodium channels and T-type calcium channels, which may reduce neuronal excitability (Chemin et al., 2001; Nicholson et al., 2003).

Prior to enzymatic hydrolysis, the arachidonoyl moiety of endocannabinoids is subject to oxidation by enzymes of the prostaglandin system, for example, COX-2, and lipoxygenases (Kozak et al., 2000; Veldhuis et al., 2003). Interestingly some of these oxidative products have activity at molecular targets distinct from the cannabinoid receptors. For example, the 15-(S)-hydroxy derivative of 2-AG, formed by 2-AG lipoxygenation, can activate peroxisome proliferation activator receptor-α (Kozak et al., 2002). Furthermore, 12-Hydroxy-N-arachidonoylethanolamine (12-HAEA), an oxygenation product of AEA, reduces oedema in a model of excitotoxicity via a CB_1 receptor-independent mechanism, and 15-HAEA actually potentiates the protective effects of AEA in this model (Veldhuis et al., 2003). These metabolites may contribute to the recognised actions of endocannabinoids.

5.1.5.2. Physiological functions of endocannabinoids

The endocannabinoid system is highly conserved within vertebrates, and is also present in invertebrates, indicating the physiological importance of endocannabinoids (De Petrocellis et al., 2004). The generation of knock-out mice in which the CB_1 and CB_2 receptors have been ablated, has enabled a more thorough evaluation of the physiological role of endocannabinoids (Ledent et al., 1999; Zimmer et al., 1999;

Buckley et al., 2000). *Cnr1* -/- mice are healthy, viable and fertile, however, they show an increased rate of spontaneous mortality therefore highlighting the physiological importance of the CB_1 receptor (Zimmer et al., 1999). Furthermore, *Cnr1* -/- mice demonstrate a reduction in locomotor activity, lower analgesic sensitivity and a reduction in addictive behaviours (Ledent et al., 1999; Zimmer et al., 1999 Pryce et al., 2003), suggesting that such behaviours are under the control of the CB_1 receptors. *Cnr2* -/- mice appear normal and have demonstrated a role for the CB_2 receptor in the inhibitory action of cannabinoids on T lymphocyte activation (Buckley et al., 2000). Limited research has been performed on mice deficient in both CB_1 and CB_2 receptors. However, they appear to display no gross defects and are healthy and fertile (Jarai et al., 1999). The physiological functions of endocannabinoids characterised thus far are summarised in **Table 5.1**.

5.1.5.3. Entourage effects

In vivo and *in vitro* studies of 2-AG have shown that the action of 2-AG is greatly enhanced when it is combined with 2-linoleoyl-glycerol and 2-palmitoyl-glycerol, two 2-acyl-glycerol esters lacking cannabinoid receptor activity. However, when applied in combination with 2-AG they enhance the hypomotile, hypothermic and analgesic effects of 2-AG *in vivo*, partially due to the inhibition of 2-AG hydrolysis (Ben-Shabat et al., 1998). Lipoxygenase metabolism of AEA generates 12-HAEA and 15-HAEA (Veldhuis et al., 2003) and 15-HAEA has been shown to potentiate the actions of AEA in an ouabain model of excitotoxicity (Veldhuis et al., 2003). Furthermore, OEA competes with AEA for Faah-mediated hydrolysis thus prolonging the actions of AEA (Mechoulam et al., 1997).

Table 5.1 – A summary of the main physiological functions of endocannabinoids.

Physiological actions	Endo-cannabinoid involved	Functions	References
Neuro-modulation	2-AG	Presynaptic inhibition of neurotransmitter release via CB_1 receptor activation (DSI/DSE)	Kreitzer & Regehr, 2001. Maejima et al., 2001 Ohno-Shosaku et al., 2001 Wilson & Nicoll, 2002
LTP	AEA/2-AG	Inhibition of LTP via CB_1 receptor-mediated inhibition of glutamate release	Ameri et al., 1999 Reibaud et al., 1999 Auclair et al., 2000 Slanina et al., 2005
		Induction of LTP via CB_1 receptor-mediated inhibition of GABA release	Wigstrom & Gustafsson, 1985 Wilson & Nicoll, 2001
Aversive memories	AEA/2-AG	Abolition of memory associated fear via CB_1 receptor-mediated inhibition of GABA release	Marsicano et al., 2003
Movement	AEA	Activation of CB_1 receptors in basal ganglia	Herkenham et al., 1991
		Hypomotility mediated via VR1 receptor activation	Sulcova et al., 1998 De Lago et al., 2004
		Hypermotility mediated via TASK-1 channel inhibition	Maingret et al., 2001 Ledent et al., 1999 Zimmer et al., 1999
Anti-nociception	AEA	Analgesia via CB_1 receptor-mediated modulation of neurotransmission in the descending tracts from PAG to spinal cord	Walker et al., 1999 Zimmer et al., 1999 Cravatt et al., 2001 Freund et al., 2003
Brain development	2-AG	Axonal guidance or growth of developing neurons	Fernandez-Ruiz et al., 2000 Bisogno et al., 2003 Williams et al., 2003
	AEA/2-AG	Neurogenesis via CB_1 receptor-mediated ERK activation	Fernandez-Ruiz et al., 2000 Jin et al., 2004
	AEA/2-AG	Developmental elimination of climbing fibre synapses	Maejima et al., 2001

Feeding	AEA/2-AG	Stimulation of feeding via CB_1 receptor-mediated alteration in expression of hypothalamic neuropeptides	Williams et al., 1998 Di Marzo et al., 2001 Cota et al., 2003 Ravinet Trillou et al., 2004 Gamber et al., 2005
	AEA/2-AG	Stimulation of lipogenesis via CB_1 receptor activation	Cota et al., 2003 Ravinet Trillou et al., 2004
	OEA	Satiety via PPARα activation and up-regulation of lipid metabolism genes	Rodriguez de Fonseca et al., 2001 Fu et al., 2005
Sleep	AEA	Sleep induction via CB_1 receptor activation	Santucci et al., 1996 Cravatt et al., 1995 Mechoulam et al., 1997
Blood pressure	AEA/2-AG	Vasodilation via CB_1 receptor-mediated inhibition of NE release	Varga et al., 1995
	AEA	Vasodilation via VR1 receptor-mediated release of CGRP	Jarai et al., 1999 Wagner et al., 1999
Inflammation	AEA/2-AG	Immunosuppression via CB_2 receptor activation	Molina-Holgado et al., 1997 Buckley et al., 2000 Baker et al., 2001
	PEA	Anti-inflammatory action	Skaper et al., 1996
Bone density	AEA/2-AG	Control of bone density via CB_1 receptor-mediated stimulation of osteoclast formation	Idris et al., 2005
Addiction	AEA	Susceptibility to addiction due to Faah enzyme polymorphism	Sipe et al., 2002

Abbreviations: DSI – depolarisation-induced suppression of inhibition, DSE – depolarisation-induced suppression of excitation, LTP – long term potentiation, GABA – gamma amino butyric acid, PAG – periaqueductal grey matter, PPARα - peroxisome proliferator-activated receptor-alpha, NE – norepinephrine.

5.1.6. The pathophysiological role of endocannabinoids

There is increasing evidence to suggest that endocannabinoids may contribute to an endogenous protective response, initiated under pathological conditions. In the post-mortem brain of rodents there is a rapid accumulation of both NAPEs and NAEs (Hansen et al., 2001a, 2001b; Sugiura et al., 2001). Furthermore, levels of AEA and 2-AG are up-regulated following injection of excitotoxins into the CNS of rodents (Sugiura et al., 2000; Hansen et al., 2001b; Marsicano et al., 2003), following induction of ischaemia (Muthian et al., 2004) and after traumatic brain injury (Panikashvili et al., 2001; Hansen et al., 2001a). Additionally, as shown in **Chapter 4** and also by Witting et al, (2004), the levels of AEA and 2-AG are increased in late symptomatic $SOD1^{G93A}$ mice, and spastic mice in the CREAE model of MS also have elevated endocannabinoid levels (Baker et al., 2001). Therefore, following various pathological stimuli and in several models of neurodegenerative disease, endocannabinoid levels are up-regulated. This up-regulation may therefore be regarded as an adaptive response aimed at counteracting ongoing pathogenesis and exerting a neuroprotective effect.

5.1.7. Hypothesis to be tested

Endocannabinoids levels are elevated in response to various pathological conditions, which suggests that they form the basis of an endogenous neuroprotective mechanism. Therefore in this study, the effect of elevating endogenous AEA levels was investigated in $SOD1^{G93A}$ mice via genetic ablation of the Faah enzyme, which elevates AEA levels in the CNS between 10 and 15 fold (Cravatt et al., 2001). Furthermore, to further examine the neuroprotective mechanisms exerted by cannabinoids, the contribution of the CB_1 receptor was investigated by genetically ablating the CB_1 receptor in $SOD1^{G93A}$ mice. The therapeutic effect of this genetic manipulation of the endocannabinoid system on disease progression and lifespan in $SOD1^{G93A}$ mice was examined.

5.2. METHODS

5.2.1. Breeding and maintenance of transgenic mouse colonies

Transgenic mice carrying a human SOD1 gene with a G93A mutation (TgN[SOD1-G93A]1Gur) were maintained as described in **Chapter 2.1a**. Individual animals were genotyped by PCR using DNA extracted from tail snips for both the expression of the human $SOD1^{G93A}$ transgene, as described in **Chapter 2.3**, as well as for either the presence of a disrupted Faah allele or the neo cassette inserted to disrupt the CB_1 receptor gene. The *Faah* -/- and *Cnr1* -/- PCR amplifications were undertaken by Mr Gareth Pryce in the Department of Inflammation at the Institute of Neurology.

To identify *Faah* -/- mice the primers used were 5' TAACTAGGCAGTCTGACTCTAG 3', and 5' TTTGTCACGTCCTGCACGACG 3'. The samples were then temperature sampled as follows: 1 precycle for 2 minutes at 94°C, and then 35 cycles of 1 minute at 94°C, 1 minute at 50°C and 30 seconds at 72°C. The primers used for *Cnr1* -/- mice were 5'GATCCAGAACATCAGGTAGG 3' and 5' AAGGAAGGGTGAGAACAGAG 3'. The samples were then temperature cycled as follows: 1 precycle for 2 minutes at 94°C and then 30 cycles of 30 seconds at 55°C, 1 minute at 55°C and 30 seconds at 72°C. The PCR products were visualised by gel electrophoresis by running 20µl of each PCR product on a 2% agarose gel at 130mV for 40 minutes.

The mice lacking the fatty acid amide hydrolase gene (*Faah* -/-) and mice lacking the CB_1 receptor gene (*Cnr1* -/-) were obtained from Professor David Baker, Institute of Neurology, for use in this project (originally donated by Dr. B. Cravatt, La Jolla, CA and Dr. C. Ledent, Brussels, Belgium, respectively). The generation of *Faah* -/- and *Cnr1* -/- mice has been previously described in detail by Cravatt et al, (2001) and

Ledent et al, (1999) respectively. Briefly, *Faah* -/- mice were generated by insertion of a PGK-Neo cassette (consisting of a phosphoglycerate kinase promoter driving the neomycin phosphotransferase gene) between *Eco*RI and *Eco*RV sites located 2.3kb apart, replacing the first FAAH exon (encoding amino acids 1-65) and approximately 2kb of upstream sequence. For the generation of the *Cnr1* -/- mice, a PGK-Neo cassette was inserted between AvrII and SfiI sites located 1073 base pairs apart on the single coding exon, replacing the first 233 codons of the gene.

Faah -/- and *Cnr1* -/- mice were backcrossed for at least seven generations onto the ABH mouse background to minimise genetic heterogeneity. SOD1.*Faah* +/- and SOD1.*Cnr1* +/- mice were obtained by breeding male heterozygous $SOD1^{G93A}$ carriers with female Faah or CB_1 receptor knock–out mice (F_1 generation). Male heterozygous carriers for both genes were backcrossed again with female Faah or CB_1 receptor knock-outs to obtain a F_2 generation of SOD1.*Faah* -/- and SOD1.*Cnr1* -/- mice for use in this study. For these breeding experiments we also crossed the control $SOD1^{G93A}$ mice onto the ABH background of the ABH.*Faah* -/- and ABH.*Cnr1* -/- mice. Male F_1 generation ABH.$SOD1^{G93A}$ mice were then backcrossed with female ABH mice to generate an F_2 generation of ABH.$SOD1^{G93A}$ mice. Therefore in these experiments described here, all mice were from an F_2 generation irrespective of genotype.

5.2.2. Experimental groups

To examine the effect of Faah or CB_1 receptor ablation on the disease progression in $SOD1^{G93A}$ mice, animals were divided into two experimental groups to study disease progression, by analysis of either:

a) hindlimb muscle function and motoneuron survival at 90 days of age, as described in **Chapters 2.10.1 – 2.10.5.**, or

b) lifespan of the $SOD1^{G93A}$ mice.

In this study, disease progression was assessed at an early symptomatic stage of disease, at 90 days of age, which enabled us to observe any positive or negative effects of Faah or CB_1 receptor ablation on disease progression.

5.2.3. Assessment of body weight

As a measure of disease progression, in this study a record of body weight of each animal was kept from 70 days of age. Each animal was weighed twice a week and a weekly average was taken to monitor the loss of body weight over time. At the onset of body weight decline, mice were weighed on a daily basis.

5.2.4. Spinal cord immunocytochemistry

Cross sections of spinal cord were immunostained with primary antibodies to GFAP (1:100; Chemicon) according to the protocol detailed in **Chapter 2.8.**

5.2.5. Lifespan analysis

The lifespan or disease end-point, of $ABH.SOD1^{G93A}$ (F_2 generation) mice was determined as the number of days the animals lived for before reaching an end-point that met Home Office guidelines, namely when the animal:

a) had lost ≥ 20% of its maximal body weight

b) was unable to perform the righting reflex in less than 30 seconds.

The effect of Faah or CB_1 receptor ablation on the lifespan of $SOD1^{G93A}$ mice was assessed under the same criteria, and the animals were culled when they reached this end-point, and lifespan recorded.

5.2.6. Statistical analysis

Statistical significance between the experimental groups was assessed by one-way analysis of variance (ANOVA) incorporating a Student Neuman Keuls multiple comparisons test. Values are expressed as mean ± standard error of the mean (S.E.M.). Significance was set at $p < 0.05$.

5.3. RESULTS

In this Chapter, the effects of raising the levels of the endocannabinoid, AEA, in $SOD1^{G93A}$ mice were assessed by breeding $SOD1^{G93A}$ mice with mice lacking the fatty acid amide hydrolase enzyme (*Faah* -/-). Faah is normally responsible for the hydrolysis of AEA, and in *Faah* -/- mice, brain AEA levels are elevated between 10 and 15 fold (Cravatt et al., 2001). In addition in a separate set of experiments, to further elucidate the neuroprotective mechanism of action of endogenous and exogenous cannabinoids on disease progression in $SOD1^{G93A}$ mice, we bred $SOD1^{G93A}$ mice with mice lacking the CB_1 receptor gene (*Cnr1* -/-).

For these breeding experiments we crossed the control $SOD1^{G93A}$ mice onto the ABH background of the ABH.*Faah* -/- and ABH.*Cnr1* -/- mice. Disease progression, including muscle function and motoneuron survival, in SOD1.*Faah* -/- and SOD1.*Cnr1* -/- mice was assessed at an early symptomatic stage of disease, at 90 days of age, rather than a late stage of disease, to enable us to observe any positive or negative effects of Faah or CB_1 receptor ablation on disease progression. The SOD1.*Faah* -/- and SOD1.*Cnr1* -/- mice used in this study were all F_2 generation offspring and were therefore compared to F_2 generation ABH.$SOD1^{G93A}$ (ABH.SOD1) and ABH.WT mice. However, the data acquired from *in vivo* physiological assessment of both F_1 and F_2 generation ABH.SOD1 or ABH.WT mice revealed that there were no significant differences between generations and this data was therefore pooled.

5.3.1. Assessment of body weight decline in $SOD1^{G93A}$ mice

$SOD1^{G93A}$ mice, in which either the Faah enzyme or the CB_1 receptor had been ablated, were monitored on a daily basis and their body weight was measured regularly to assess the progression of disease.

The body weight of the SOD1^{G93A} mice bred onto the ABH background was recorded weekly from 70 days of age until disease end-point and the data is summarised in **Figure 5.3.** Body weight measurements were expressed as a percentage of the maximal body weight for each individual mouse, the maximal weight being recorded between 85 and 91 days of age (13 weeks) in the control ABH.SOD1 mice. The onset of body weight loss in the ABH.SOD1 mice (n = 5) occurred between 105 and 111 days of age (15 weeks) and by 119 – 125 days (17 weeks) body weight had declined by approximately 20%. From **Figure 5.3.** it can be seen that ablation of the Faah enzyme had no effect on the rate of decline in body weight. Therefore, in SOD1.*Faah* -/- mice (n = 8) the onset of body weight loss occurred between 105 and 111 days of age (15 weeks) and the rate of weight loss was rapid, similar to ABH.SOD1 mice, with approximately 20% of body weight being lost by 119 – 125 days of age (17 weeks). However, ablation of the CB_1 receptor (n = 8) significantly delayed the loss in body weight that occurred in ABH.SOD1 mice with disease progression. Therefore, a significant reduction in body weight did not occur in SOD1.*Cnr1* -/- mice until 119 – 125 days of age (17 weeks) and body weight did not decline by ≥ 20% until 147 – 153 days of age (21 weeks). In fact, from 112 days of age onwards, the body weight of SOD1.*Cnr1* -/- was significantly greater than in SOD1.*Faah* -/- mice ($p < 0.025$).

5.3.2. Hindlimb muscle function in SOD1^{G93A} mice at 90 days of age

The effect of genetically ablating either the Faah enzyme or the CB_1 receptor in SOD1^{G93A} mice on the ABH background was assessed on hindlimb muscle function at 90 days of age, an early symptomatic stage of disease.

Figure 5.3 - The effect of *Faah* and CB_1 receptor ablation on the decline in body weight of ABH.SOD1 mice

The body weight of ABH.SOD1, SOD1.*Faah* -/- and SOD1.*Cnr1* -/- mice was recorded weekly from 70 days of age (10 weeks) until disease end-point, as shown in the graph. Body weight was expressed as a percentage of the maximal body weight of each individual animal. As a consequence of disease progression, the body weight of ABH.SOD1 mice (n = 5) declined from 105 days of age (15 weeks) onwards. Genetic ablation of the Faah enzyme had no significant effect on the decline in body weight of $SOD1^{G93A}$ mice (n = 8). In contrast ablation of the CB_1 receptor significantly delayed the loss of body weight observed in $SOD1^{G93A}$ mice (n = 8). Values are the mean body weight at each age ± standard error of the mean. * $p < 0.05$.

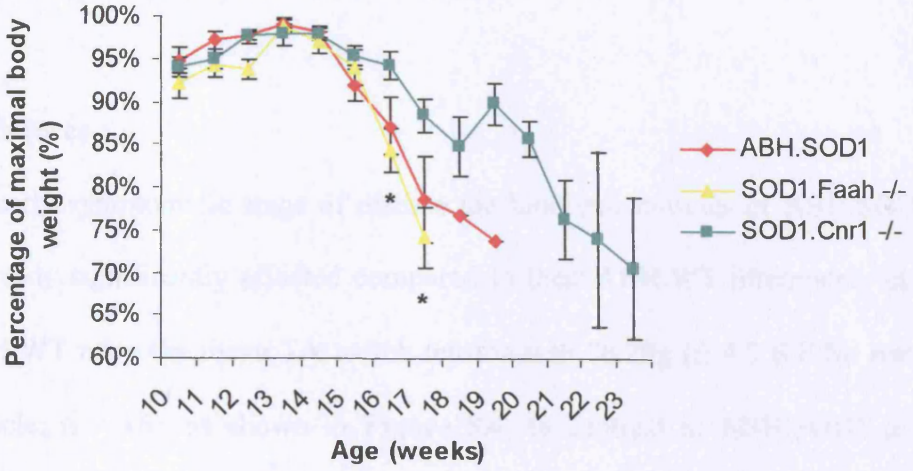
Percentage of maximal body weight (%)
100%
95%
90%
85%
80%
75%
70%
65%
60%
10
11
12
13
14
15
16
17
18
19
20
21
22
23
Age (weeks)
*
*
ABH.SOD1
SOD1.Faah -/-
SOD1.Cnr1 -/-

5.3.2.1. Isometric tension recordings

Twitch and tetanic contractions of TA and EDL muscles in both hindlimbs of ABH.WT, ABH.SOD1, SOD1.*Faah* -/- and SOD1.*Cnr1* -/- mice, were recorded at 90 days of age. All forces were expressed per 100mg muscle weight to take into account any reduction in muscle weight in 90 day old $SOD1^{G93A}$ mice.

i) Twitch force

At this early symptomatic stage of disease the hindlimb muscles of ABH.SOD1 mice were already significantly affected compared to their ABH.WT littermates. In 90 day old ABH.WT mice the mean TA twitch tension was 76.29g (± 4.2 S.E.M. per 100mg TA muscle; n = 16), as shown in **Figure 5.4**. In contrast in ABH.SOD1 mice, TA generated only 26.05g (± 2.6 S.E.M. per 100mg TA muscle; n = 18; $p < 0.001$) of twitch force, a reduction of 65.9% compared to the WT control. In contrast, the twitch force of TA muscles from SOD1.*Faah* -/- mice was less affected. Thus in SOD1.*Faah* -/- mice at 90 days of age, TA generated 62.63g (± 3.9 S.E.M. per 100mg TA muscle; n = 9; $p < 0.02$) of twitch force, representing a reduction of only 17.8%. However, the twitch tension of TA muscles from SOD1.*Cnr1* -/- mice at 90 days of age was very similar to that in ABH.SOD1 mice, generating only 33.0g (± 4.3 S.E.M. per 100mg TA muscle; n = 10) of force, a reduction of 56.7% compared to ABH.WT ($p < 0.001$).

ii) Maximal tetanic tension

The maximal tetanic tension (MTT) of TA and EDL muscles from ABH.SOD1 mice at 90 days of age was significantly reduced ($p < 0.005$) compared to ABH.WT mice, as shown in **Figures 5.5** and **5.6** respectively. Thus by 90 days of age, the MTT of TA muscles from ABH.WT mice was 286.8g (± 11.7 S.E.M. per 100mg TA muscle; n = 16), compared to 118.4g (± 12.8 S.E.M. per 100mg TA muscle; n = 16) in ABH.SOD1

Figure 5.4 – The twitch tension of TA muscles from ABH.WT, ABH.SOD1, SOD1.*Faah* -/- and SOD1.*Cnr1* -/- mice at 90 days of age

The maximal twitch tension of TA muscles was elicited by stimulation of the sciatic nerve by a single square pulse of 0.02ms duration at a supramaximal voltage. The mean twitch tension of TA muscles from ABH.WT (n = 16), ABH.SOD1 (n = 18), SOD1.*Faah* -/- (n = 9) and SOD1.*Cnr1* -/- mice (n = 10) are summarised in the bar chart. Force was expressed per 100mg muscle weight to take into account the reduction in muscle weight in 90 day old ABH.SOD1 mice. At 90 days of age, the twitch tension of TA muscles from ABH.SOD1 mice was substantially reduced compared to ABH.WT TA muscles. However, the reduction in twitch force in SOD1.*Faah* -/- mice was significantly less than in ABH.SOD1 mice. Ablation of the CB_1 receptor, however, had no significant effect on the reduction in twitch tension in $SOD1^{G93A}$ mice by 90 days of age. g = grams. Values represent the mean response ± standard error of the mean.

* $p < 0.05$, *** $p < 0.005$.

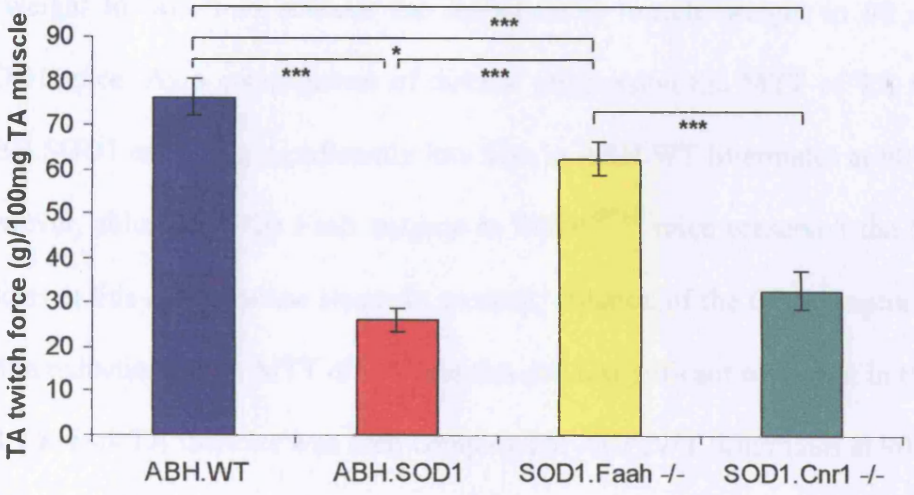
TA twitch force (g)/100mg TA muscle
90
80
70
60
50
40
30
20
10
0
***
*
***
***
***
ABH.WT
ABH.SOD1
SOD1.Faah -/-
SOD1.Cnr1 -/-

Figure 5.5 – Maximal tetanic force of TA muscles from ABH.WT, ABH.SOD1, SOD1.*Faah* -/- and SOD1.*Cnr1* -/- mice at 90 days of age

Maximal tetanic tension (MTT) of TA muscles was elicited by increasing the frequency of stimulation of the sciatic nerve (40, 80 and 100Hz). The bar chart summarises the MTT of TA muscles from ABH.WT (n = 16), ABH.SOD1 (n = 16), SOD1.*Faah* -/- (n = 9) and SOD1.*Cnr1* -/- (n = 9) mice at 90 days of age. Force was expressed per 100mg muscle weight to take into account the reduction in muscle weight in 90 day old ABH.SOD1 mice. As a consequence of disease progression the MTT of TA muscles from ABH.SOD1 mice was significantly less than in ABH.WT littermates at 90 days of age. However, ablation of the Faah enzyme in $SOD1^{G93A}$ mice preserved the MTT of TA muscles at this early disease stage. In contrast, ablation of the CB_1 receptor did not prevent the reduction in the MTT of TA muscles and a significant reduction in the MTT of SOD1.*Cnr1* -/- TA muscles was seen compared to ABH.WT littermates at 90 days of age. g = grams. Values are the mean MTT of TA muscles ± standard error of the mean. *** $p < 0.005$.

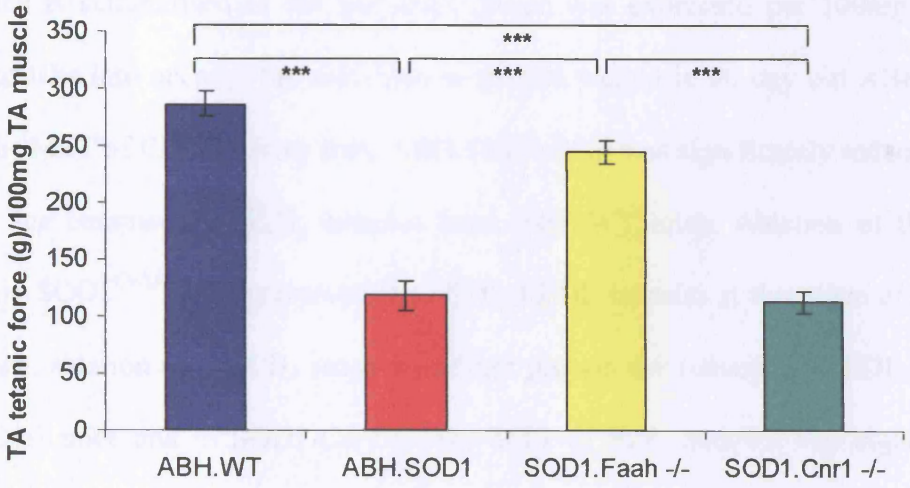
TA tetanic force (g)/100mg TA muscle
350
300
250
200
150
100
50
0
***
***
***
***
ABH.WT
ABH.SOD1
SOD1.Faah -/-
SOD1.Cnr1 -/-

Figure 5.6 – The effect of genetic ablation of either the Faah enzyme or the CB_1 receptor on the maximal tetanic tension of EDL muscles from ABH.SOD1 mice

Maximal tetanic tension (MTT) of EDL muscles was elicited by increasing the frequency of stimulation of the sciatic nerve (40, 80 and 100Hz). The MTT of ABH.WT (n = 16), ABH.SOD1 (n = 16), SOD1.*Faah* -/- (n = 9) and SOD1.*Cnr1* -/- (n = 9) mice is summarised in the bar chart. Force was expressed per 100mg muscle weight to take into account the reduction in muscle weight in 90 day old ABH.SOD1 mice. The MTT of EDL muscles from ABH.SOD1 mice was significantly reduced at 90 days of age compared to EDL muscles from ABH.WT mice. Ablation of the Faah enzyme in $SOD1^{G93A}$ mice preserved the MTT of EDL muscles at this stage of disease. In contrast, ablation of the CB_1 receptor did not prevent the reduction in EDL force in ABH.SOD1 mice and in SOD1.*Cnr1* -/- the MTT of EDL muscles was significantly lower than in ABH.WT mice. g = grams. Values are the mean MTT of EDL muscles ± standard error of the mean. * $p < 0.05$, *** $p < 0.005$.

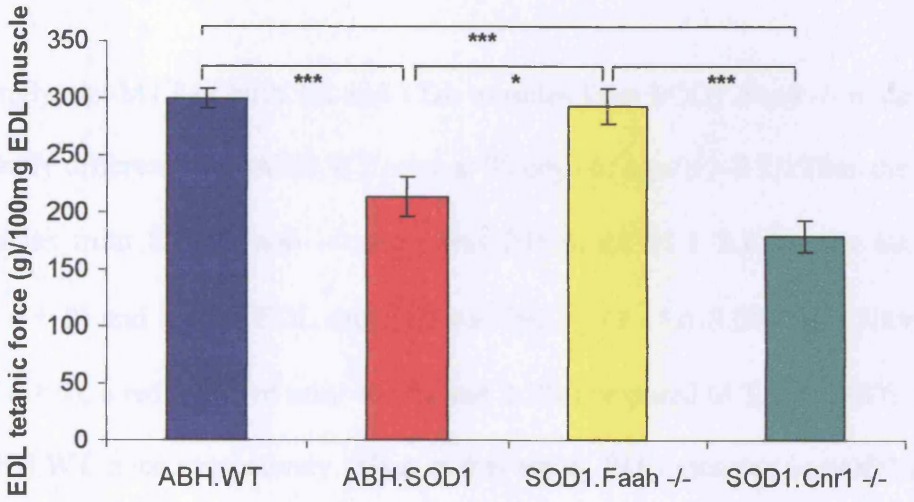
EDL tetanic force (g)/100mg EDL muscle
350
300
250
200
150
100
50
0
***
***
*
***
ABH.WT
ABH.SOD1
SOD1.Faah -/-
SOD1.Cnr1 -/-

mice, a reduction in maximal force of 58.7%. EDL muscles of 90 day old ABH.SOD1 mice were less affected than TA muscles, as observed in **Chapter 4.3.3.** in 120 day old $SOD1^{G93A}$ mice. Whereas EDL muscles in ABH.WT mice generated 300.4g (± 16.9 S.E.M. per 100mg EDL muscle; n = 16) of force, this was reduced to 213.6g (± 16.9 S.E.M. per 100mg EDL muscle; n = 16; $p < 0.005$) in EDL muscles from ABH.SOD1 mice at 90 days of age, a reduction of 28.9%.

Surprisingly, the MTT of both TA and EDL muscles from SOD1.*Faah* -/- mice was not significantly different from ABH.WT mice at 90 days of age ($p > 0.1$). Thus the MTT of TA muscles from SOD1.*Faah* -/- mice was 244.8g (± 11.1 S.E.M. per 100mg TA muscle; n = 9) and that of EDL muscles was 292.4g (± 15.6 S.E.M. per 100mg EDL muscle; n = 9), a reduction of only 14.6% and 2.7% compared to TA and EDL muscles from ABH.WT mice respectively. Thus at this stage, EDL muscles in SOD1.*Faah* -/- mice were as strong as EDL muscles in ABH.WT mice. Muscle force in SOD1.*Cnr1* -/- mice, however, was significantly reduced at 90 days of age. The MTT of TA muscles from SOD1.*Cnr1* -/- mice was only 40.6% of that in ABH.WT mice, generating only 113.4g (± 9.4 S.E.M. per 100mg TA muscle; n = 9; $p < 0.005$) of force. Similarly, EDL muscles were significantly weaker with an MTT of 179.7g (± 14.3 S.E.M. per 100mg EDL muscle; n = 9; $p < 0.005$), a reduction of 40.2% compared to EDL muscles in ABH.WT mice. Interestingly, the MTT of SOD.*Cnr1* -/- hindlimb muscles did not differ significantly from muscles in ABH.SOD1 mice ($p > 0.1$), suggesting that ablation of the CB_1 receptor had no effect on the progression of hindlimb paralysis. In contrast, ablation of the Faah enzyme completely delayed the decline in muscle function and indeed the muscle force of SOD1.*Faah* -/- mice was indistinguishable from ABH.WT, suggesting that elevation of endocannabinoid levels exerted significant beneficial effects at this early stage of disease.

5.3.3. Motor unit survival

The number of functional motor units in each experimental group was assessed at 90 days of age. **Figure 5.7** shows representative traces from (**A**) ABH.WT, (**B**) ABH.SOD1, (**C**) SOD1.*Faah* -/- and (**D**) SOD1.*Cnr1* -/- mice, and the mean number of surviving motor units are summarised in the bar chart (**E**). At 90 days of age ABH.WT mice had, on average, 31 motor units (± 0.9 S.E.M.; n = 16) compared to only 21 (± 1.2 S.E.M.; n = 19; $p < 0.005$) in ABH.SOD1 mice. Ablation of the Faah enzyme resulted in a significant increase in survival of motor units in $SOD1^{G93A}$ mice, so that 27 (± 1.5 S.E.M.; n = 10) motor units survived, a value not significantly different from the ABH.WT mice ($p > 0.1$). However, in $SOD1^{G93A}$ mice in which the CB_1 receptor had been ablated, a significant number of motor units were already lost by 90 days of age. Thus EDL muscles from SOD1.*Cnr1* -/- mice had only 19 (± 1.4 S.E.M.; n = 10) functional motor units, which was significantly less than the number of motor units in EDL muscles of ABH.WT mice ($p < 0.005$).

5.3.4. Muscle fatigue characteristics

Repeated stimulation of the nerve innervating the EDL muscle produces a fatigue trace as shown in **Figure 5.8** for (**A**) ABH.WT, (**B**) ABH.SOD1, (**C**) SOD1.*Faah* -/- and (**D**) SOD1.*Cnr1* -/- EDL muscles. The bar chart, shown in **Figure 5.9**, summarises the fatigue index (F.I.), which gives a measure of the fatigability of the EDL muscles. EDL muscles are normally fast muscles that fatigue rapidly when subjected to repeated stimulation (**Figure 5.8A**) and in this study ABH.WT EDL muscles had a F.I. of 0.62 (± 0.02 S.E.M.; n = 16). In contrast, the EDL muscles from ABH.SOD1 mice at 90 days of age, an early symptomatic age, were largely fatigue resistant (**Figure 5.8B**) and had a F.I. value of 0.33 (± 0.05 S.E.M.; n = 18; $p = 0.005$), indicating that significant changes

Figure 5.7 – The number of motor units in EDL muscles of ABH.WT, ABH.SOD1, SOD1.*Faah* -/- and SOD1.*Cnr1* -/- mice at 90 days of age

Stimulation of the sciatic nerve with increasing intensity produced stepwise increments in twitch tension of EDL muscles that corresponded to the successive recruitment of motor axons. Representative motor unit traces from EDL muscles from (**A**) ABH.WT (n = 16), (**B**) ABH.SOD1 (n = 19), (**C**) SOD1.*Faah* -/- (n = 10) and (**D**) SOD1.*Cnr1* -/- (n = 10) mice are shown. The number of functional motor units was determined by counting the number of increments in twitch tension and the mean values are summarised in the bar chart (**E**). Horizontal scale bar = 10 milliseconds. Vertical scale bars = 1 gram. g = grams. Values shown are the mean ± standard error of the mean. *** $p < 0.005$.

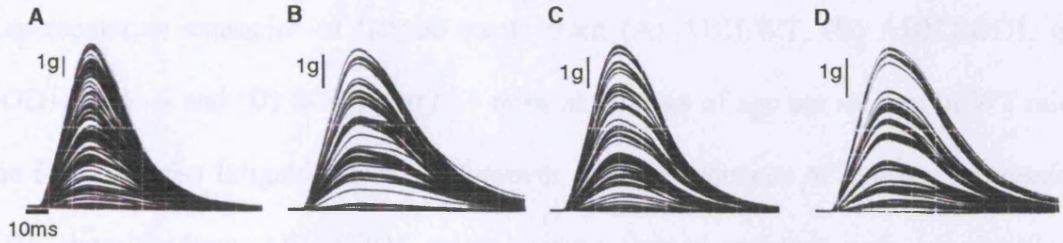
A
B
C
D
1g
1g
1g
1g
10ms

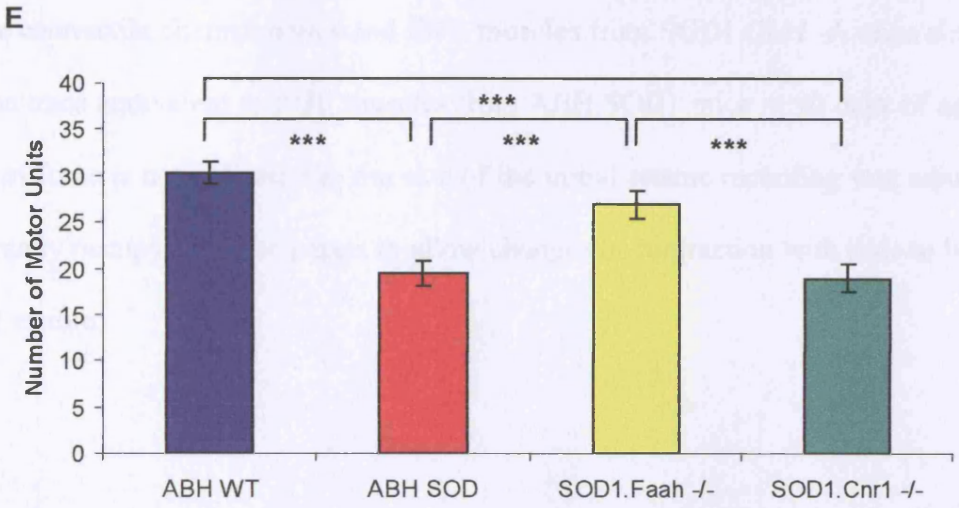
E
Number of Motor Units
40
35
30
25
20
15
10
5
0
***
***
***
***
ABH WT
ABH SOD
SOD1.Faah -/-
SOD1.Cnr1 -/-

Figure 5.8 – Fatigue traces from ABH.WT, ABH.SOD1, SOD1.*Faah* -/- and SOD1.*Cnr1* -/- mice at 90 days of age

Repeated stimulation of the EDL muscle over a 3 minute period elicited a fatigue trace. Representative examples of fatigue traces from (**A**) ABH.WT, (**B**) ABH.SOD1, (**C**) SOD1.*Faah* -/- and (**D**) SOD1.*Cnr1* -/- mice at 90 days of age are shown. In WT mice, the EDL is a fast fatigable muscle. However as a consequence of disease progression, EDL muscles from ABH.SOD1 mice became fatigue resistant with no significant reduction in tetanic force over the duration of stimulation. This change in the fatigue pattern of EDL muscles from ABH.SOD1 mice did not occur to the same extent in EDL muscles from SOD1.*Faah* -/- mice. However, ablation of the CB_1 receptor had no effect on the contractile characteristics and EDL muscles from SOD1.*Cnr1* -/- mice showed a fatigue trace equivalent to EDL muscles from ABH.SOD1 mice at 90 days of age. The scale of force is not indicated as the size of the initial tetanic recording was adjusted to maximally occupy the trace paper, to allow changes in contraction with time to be more easily visible.

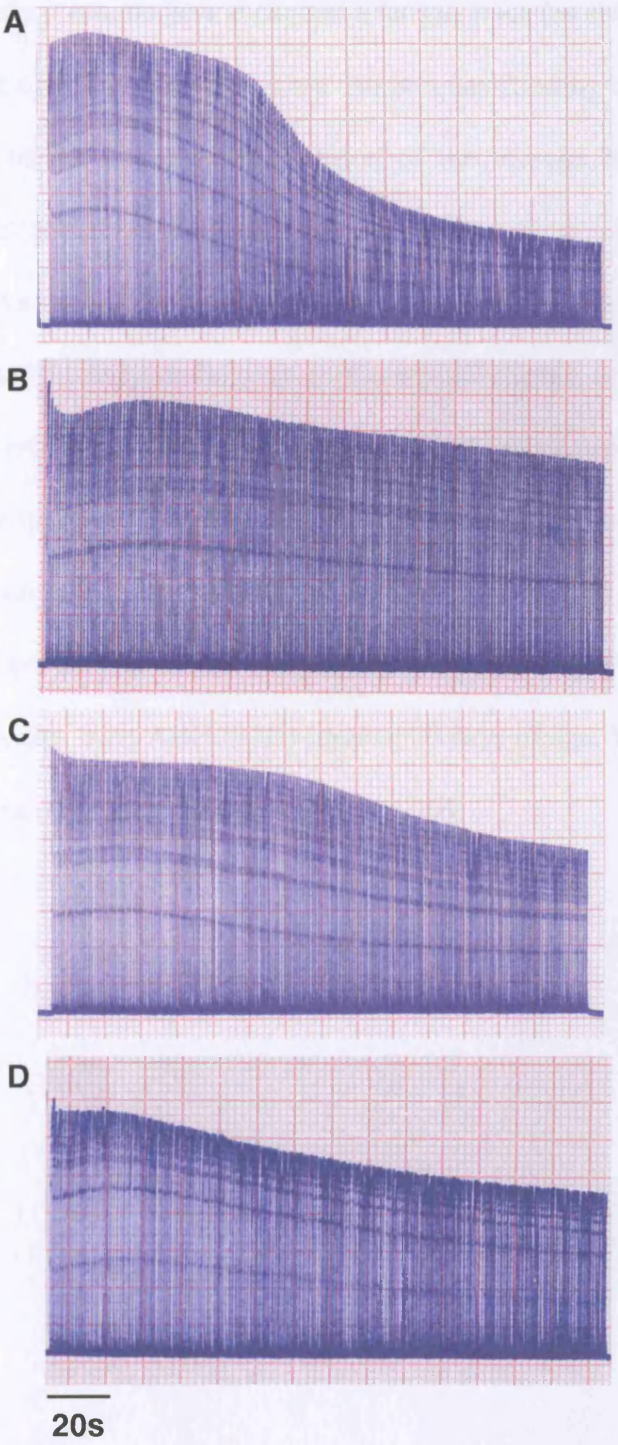
A
B
C
D
20s

Figure 5.9 – Fatigue index of EDL muscles from ABH.WT, ABH.SOD1, SOD1.*Faah* -/- and SOD1.*Cnr1* -/- mice at 90 days of age

A fatigue index (F.I.) is a measure of the fatigability of a muscle. Repeated stimulation of EDL muscles over a 3 minute period elicited a fatigue trace (as shown in **Figure 5.8**). The decline in force over this period of time can be quantified by expressing the final force as a fraction of the initial tetanic tension of the muscle. Normally WT EDL muscles are fast fatigable muscles with an F.I. approaching 1.0, whereas fatigue resistant muscles have an F.I. approaching 0. By 90 days of age the EDL muscles from ABH.SOD1 mice had already undergone a phenotypic change as a consequence of disease progression and were largely fatigue resistant, as can be seen by the significant reduction in F.I. compared to ABH.WT EDL muscles. Ablation of the Faah enzyme lessened this reduction in F.I. in ABH.SOD1 EDL muscles, whereas ablation of the CB_1 receptor had no effect on the deleterious changes in contractile characteristics that occurred in EDL muscles from ABH.SOD1 mice at 90 days of age. Values are the mean ± standard error of the mean. * $p < 0.005$, *** $p < 0.005$.

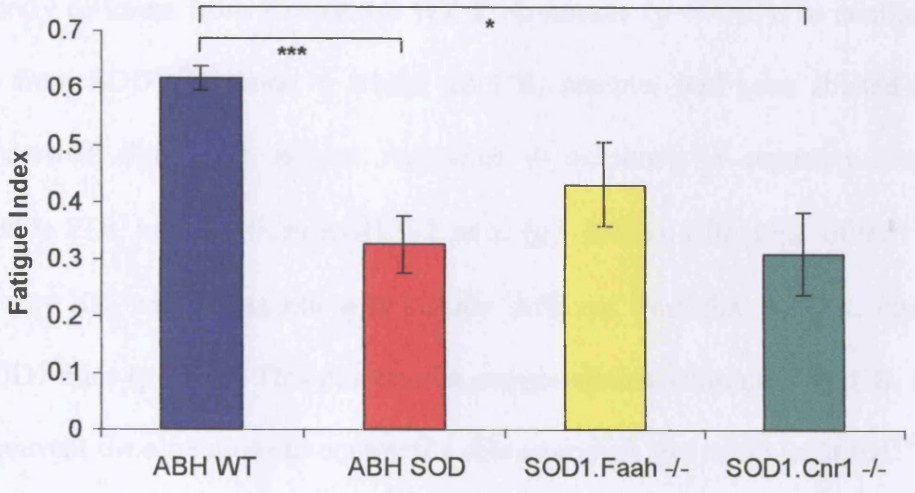
0.7
0.6
0.5
0.4
0.3
0.2
0.1
0
Fatigue Index
***
*
ABH WT
ABH SOD
SOD1.Faah -/-
SOD1.Cnr1 -/-

in the contractile characteristics of hindlimb muscles had already occurred at this early stage of disease. However, the fatigue pattern of EDL muscles from $SOD1^{G93A}$ mice in which the Faah enzyme has been ablated resembled that of ABH.WT EDL muscles (**Figure 5.8C**), and had a F.I. of 0.43 (± 0.07 S.E.M.; n = 10), which was not significantly different from that of the WT EDL muscle ($p > 0.05$). In contrast, EDL muscles from $SOD1^{G93A}$ mice in which the CB_1 receptor had been ablated (**Figure 5.8D**), showed significant fatigue resistance in response to repeated stimulation compared to EDL muscles from ABH.WT mice ($p = 0.015$), with a F.I. of 0.31 (± 0.07 S.E.M.; n = 10), which was not significantly different from that of EDL muscles in ABH.SOD1 mice ($p > 0.7$). This observation suggested that ablation of the CB_1 receptor did not prevent the alterations in contractile characteristics that occur in $SOD1^{G93A}$ mice as a consequence of disease progression. However, elevation of endocannabinoid levels by ablation of Faah, appeared to delay these deleterious changes in hindlimb contractile characteristics.

5.3.5. Muscle histochemistry

Histochemical staining of EDL muscle sections for SDH activity, an indicator of oxidative capacity, revealed patterns of staining as shown in **Figure 5.10**, which are consistent with the changes in contractile characteristics of EDL muscles described above. SDH staining of EDL muscle sections from ABH.WT mice (**Figure 5.10A**) revealed a mosaic pattern of lightly and darkly stained muscles fibres, with the majority of fibres staining lightly for SDH, indicating a low oxidative capacity. In contrast, a greater proportion of EDL muscle fibres from 90 day old ABH.SOD1 mice (**Figure 5.10B**) stained more intensely for SDH. However, the pattern of SDH staining in EDL muscle fibres from SOD1.*Faah* -/- mice (**Figure 5.10C**) resembled that of EDL muscles from ABH.WT mice, with the majority of fibres lightly stained. In contrast, ablation of

Figure 5.10 – SDH staining of EDL muscle sections from ABH.WT, ABH.SOD1, SOD1.*Faah* -/- and SOD1.*Cnr1* -/- mice

EDL muscles from (**A**) ABH.WT, (**B**) ABH.SOD1, (**C**) SOD1.*Faah* -/- and (**D**) SOD1.*Cnr1* -/- mice were cut on a cryostat and stained for SDH activity, an indicator of oxidative capacity. ABH.WT EDL muscles showed a mosaic pattern of SDH activity, with the majority of fibres staining lightly for SDH. In EDL muscles from ABH.SOD1 mice, a greater proportion of muscle fibres were intensely stained for SDH, reflecting an increased oxidative capacity. Ablation of the Faah enzyme largely prevented this change in muscle fibre phenotype so that EDL muscles from 90 day old SOD1.*Faah* -/- mice showed a pattern of SDH staining that was more characteristic of EDL muscles from WT mice, with a greater proportion of fibres lightly stained. In contrast, ablation of the CB_1 receptor had no significant effect on the oxidative capacity of EDL muscle fibres at 90 days of age and the pattern of SDH staining in EDL muscle sections from SOD1.*Cnr1* –/– mice resembled that seen in ABH.SOD1 EDL muscle sections. Scale bar = 200μm.

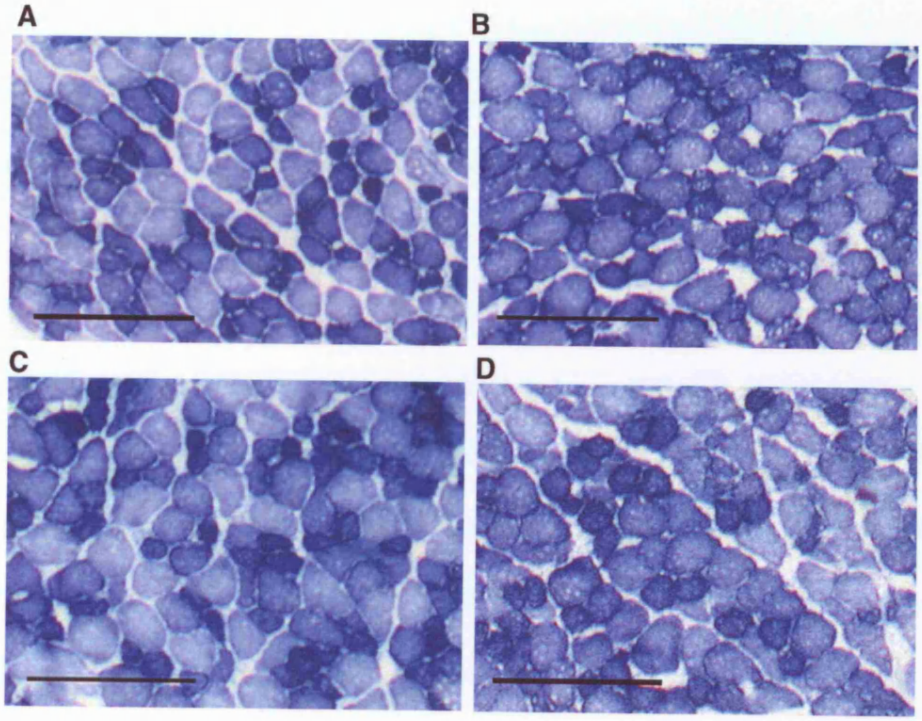
A
B
C
D

the CB_1 receptor had no effect on the oxidative capacity of the EDL muscle fibres and the pattern of SDH staining in SOD1.*Cnr1* -/- mice (**Figure 5.10D**) resembled that of ABH.SOD1 EDL muscles fibres at 90 days of age, indicating increased oxidative capacity compared to muscles from ABH.WT mice.

5.3.6. Motoneuron survival

Motoneuron survival was assessed morphologically by counting the number of Nissl-stained motoneurons in a section of the sciatic motor pool in the lumbar spinal cord. **Figure 5.11** shows examples of Nissl-stained motoneurons in spinal cord sections from (**A**) ABH.WT, (**B**) ABH.SOD1, (**C**) SOD1.*Faah* -/- and (**D**) SOD1.*Cnr1* -/- mice. **Figure 5.11E** summarises the mean motoneuron survival for each genotype. It can be seen that significant motoneuron death had already occurred by 90 days of age in $SOD1^{G93A}$ mice. Only 245 (± 13.6 S.E.M.; n = 20) motoneurons survived in ABH.SOD1 mice compared to 358 (± 13.8 S.E.M.; n = 10) in their ABH.WT littermates ($p < 0.001$), a reduction of 32%. In the SOD1.*Faah* -/- mice, however, genetic elevation of endocannabinoid levels delayed motoneuron loss at this stage of disease and 305 (± 18.1 S.E.M.; n = 10) motoneurons survived, a reduction of only 14.8% compared to the ABH.WT mice ($p = 0.04$). However, in SOD1.*Cnr1* -/- mice the absence of the CB_1 receptor did not affect motoneuron survival in $SOD1^{G93A}$ mice and at 90 days only 217 (± 12.8 S.E.M.; n = 10) motoneurons survived, which represents a reduction of 39.4%, compared to ABH.WT mice ($p < 0.001$).

In addition, the number of motoneurons surviving in the sciatic motor pool at the end-stage of disease in $SOD1^{G93A}$ mice on the ABH background was also assessed, and the results are summarised in **Figure 5.12**. In ABH.SOD1 mice, only 145 (± 8.2 S.E.M.; n = 6) motoneurons survived at disease end-stage. In $SOD1^{G93A}$ mice in which the Faah

Figure 5.11 – Sciatic motoneuron survival in ABH.WT, ABH.SOD1, SOD1.*Faah* -/- and SOD1.*Cnr1* -/- mice at 90 days of age

Motoneuron survival at 90 days of age was assessed by counting the number of Nissl stained motoneurons in the sciatic motor pool (dotted areas) of (**A**) ABH.WT, (**B**) ABH.SOD1, (**C**) SOD1.*Faah* -/- and (**D**) SOD1.*Cnr1* -/- mice at 90 days of age. The mean motoneuron survival is summarised in the bar chart (**E**). At 90 days of age, ABH.SOD1 mice (n = 20) had lost a significant proportion of their sciatic motoneurons compared with ABH.WT mice (n = 10). However, ablation of the Faah enzyme exerted neuroprotective effects and significantly more motoneurons survived in SOD1.*Faah* -/- mice (n = 10) than in the ABH.SOD1 mice at 90 days of age. In contrast, ablation of the CB_1 receptor did not affect motoneuron survival in $SOD1^{G93A}$ mice (n = 10) and the number of motoneurons surviving in SOD1.*Cnr1* -/- mice was not substantially different to ABH.SOD1 mice. Values are the mean ± standard error of the mean. Scale bar = 100μm. * $p < 0.05$, *** $p < 0.005$.

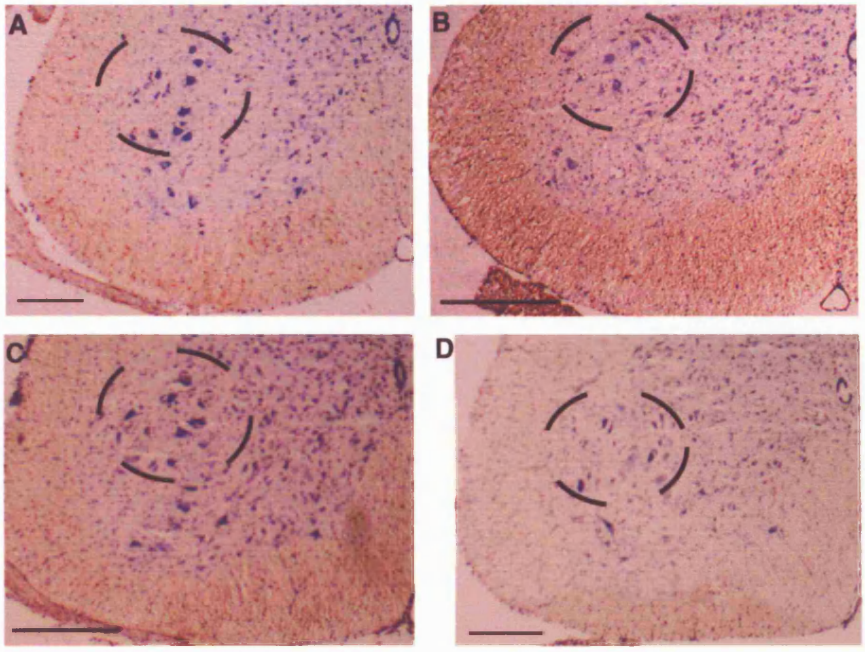
A
B
C
D

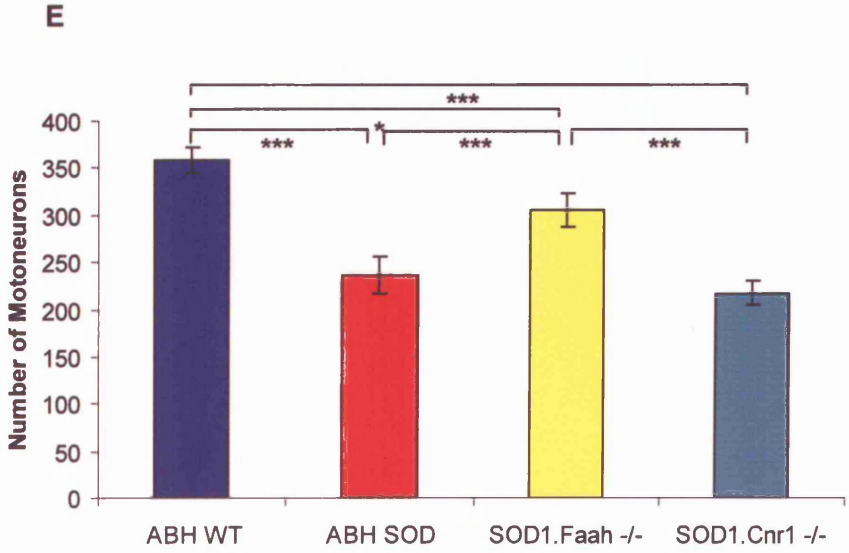
E
Number of Motoneurons
400
350
300
250
200
150
100
50
0
***
*
***
***
***
ABH WT
ABH SOD
SOD1.Faah -/-
SOD1.Cnr1 -/-

Figure 5.12 – Motoneuron survival in end-stage ABH.SOD1, SOD1.*Faah* -/- and SOD1.*Cnr1* -/- mice

Motoneuron survival was assessed by counting the number of Nissl-stained motoneurons in the sciatic pool of ABH.SOD1, SOD1.*Faah* -/- and SOD1.*Cnr1*-/- mice at the disease end-stage. It can be seen that ablation of either the Faah enzyme or CB_1 receptor had no effect on the number of sciatic motoneurons surviving at the end-stage of disease. Values are the mean ± standard error of the mean.

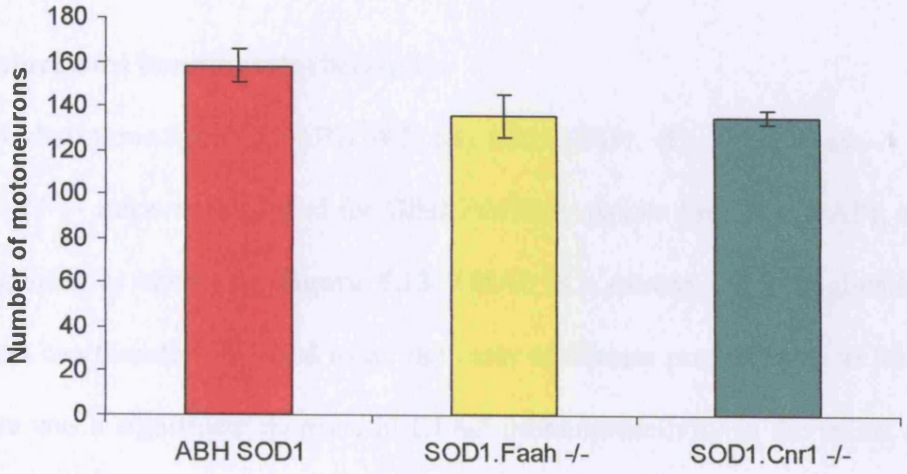
Number of motoneurons
180
160
140
120
100
80
60
40
20
0
ABH SOD1
SOD1.Faah -/-
SOD1.Cnr1 -/-

enzyme had been ablated, there was no significant difference in the number of motoneurons surviving at disease end-stage and 136 (± 9.8 S.E.M.; n = 12) motoneurons survived ($p > 0.7$). Similarly, 135 (± 3.3 S.E.M.; n = 6) motoneurons survived in SOD1.*Cnr1* -/- at end stage, which was not significantly different from that of ABH.SOD1 mice ($p > 0.7$).

5.3.7. Spinal cord immunocytochemistry

Spinal cord sections from (**A**) ABH.WT, (**B**) ABH.SOD1, (**C**) SOD1.*Faah* -/- and (**D**) SOD1.*Cnr1* -/- mice were stained for Glial Fibrillary Acidic Protein (GFAP), a marker of astrogliosis, as shown in **Figure 5.13**. GFAP is a measure of astrogliosis and its expression can therefore be used as an indicator of disease progression. At 90 days of age, there was a significant increase in GFAP immunoreactivity in the spinal cords of ABH.SOD1 mice compared to ABH.WT mice. However, in SOD1.*Faah* -/- spinal cords, there was substantially less GFAP immunoreactivity, and therefore astrogliosis, at this stage of disease. In contrast, in the spinal cords of SOD1.*Cnr1* -/- mice, GFAP immunoreactivity appeared significantly elevated compared to spinal cords of ABH.WT mice.

5.3.8. The effect of Faah or CB_1 receptor ablation on the lifespan of ABH.SOD1 mice

We next examined the effect of genetic manipulation of the endocannabinoid system on the lifespan of the $SOD1^{G93A}$ mice, and the results are summarised in **Figure 5.14**. In these experiments, $SOD1^{G93A}$ mice were bred onto the ABH background of the *Faah* -/- and *Cnr1* -/- mice and F_2 generation animals were used in all experiments. In this colony the lifespan of the F_2 generation ABH.SOD1 mice was reduced compared to that of $SOD1^{G93A}$ mice bred onto the traditional (C57BL/6 x SJL) F_1 background. Thus, the

Figure 5.13 – The expression of GFAP in the spinal cords of ABH.WT, ABH.SOD1, SOD1.*Faah* -/- and SOD1.*Cnr1* -/- mice

The photomicrographs show examples of cross sections of the lumbar spinal cord immunostained for GFAP, a marker of astrogliosis, and counterstained for Nissl, from (**A**) ABH.WT, (**B**) ABH.SOD1, (**C**) SOD1.*Faah* -/- and (**D**) SOD1.*Cnr1* -/- mice at 90 days of age. It can be seen that there was a significant increase in GFAP immunoreactivity in the ventral horn of ABH.SOD1 mice compared to ABH.WT at 90 days of age. However, GFAP immunoreactivity was significantly lower in the SOD1.*Faah* -/- mice. In contrast, astrogliosis in SOD1.*Cnr1* -/- mice at 90 days of age resembled that in ABH.SOD1 spinal cord and was significantly increased compared to ABH.WT. Scale bar = 200μm.

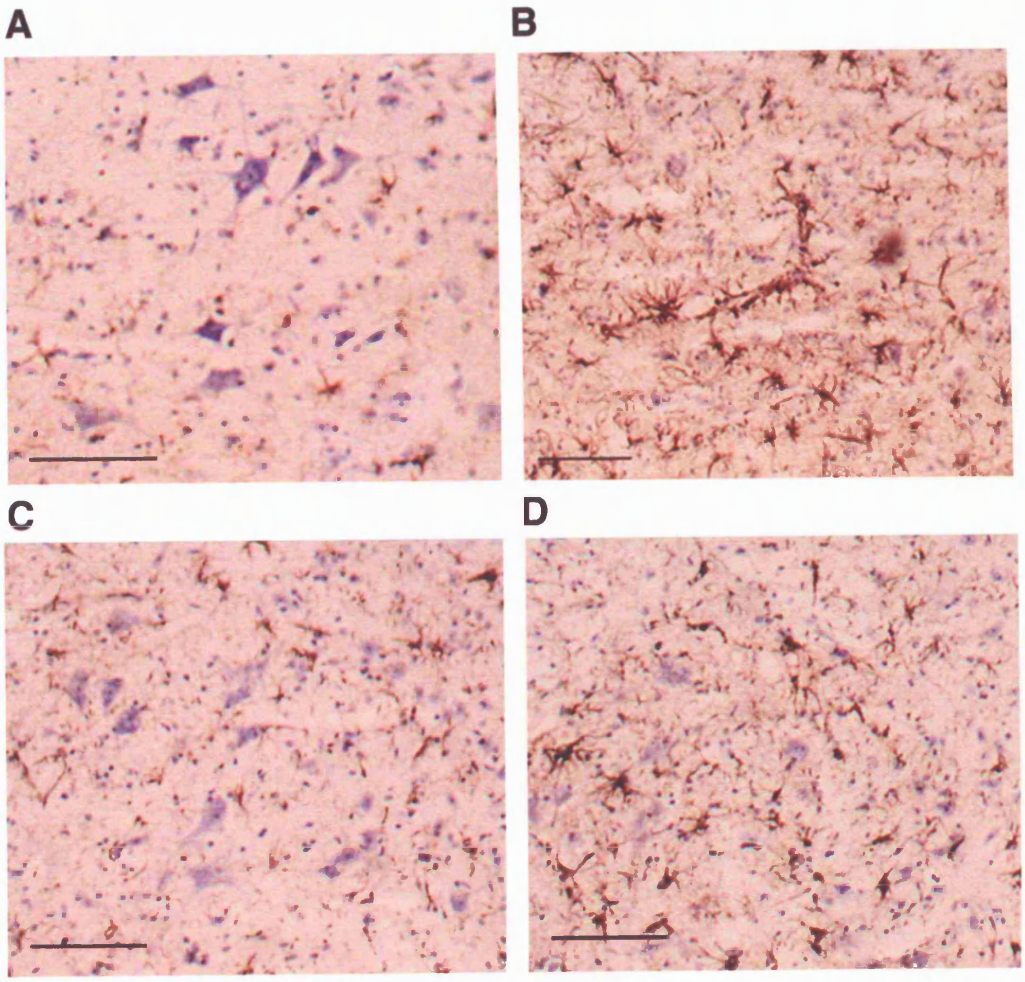
A
B
C
D

Figure 5.14 – The effect of genetic manipulation of the endocannabinoid system on the lifespan of ABH.SOD1 mice

The lifespan of SOD1.*Faah* -/- and SOD1.*Cnr1* -/- mice was recorded to determine whether genetic manipulation of the endocannabinoid system had any significant effects on the lifespan of ABH.SOD1 mice. The lifespan of F_2 generation $SOD1^{G93A}$ mice bred onto the ABH background of the *Faah* -/- and *Cnr1* -/- mice was significantly less than $SOD1^{G93A}$ mice on the (C57BL/6 x SJL) F_1 background ($p = 0.01$). Lifespan in this study was determined as the age when mice have lost ≥ 20% of their body weight or when they can no longer right themselves within 30 seconds of being placed on their sides. Despite the significant amelioration of disease signs at 90 days of age achieved with ablation of the Faah enzyme, this was not reflected by an extension in lifespan of the SOD1.*Faah* -/- mice ($p = 0.4$). In contrast, despite there being no significant improvements in disease signs at 90 days of age, SOD1.*Cnr1* -/- mice had a significantly extended lifespan compared to ABH.SOD1 mice ($p = 0.03$). The value at each time point represents the mean survival of each group of experimental mice.

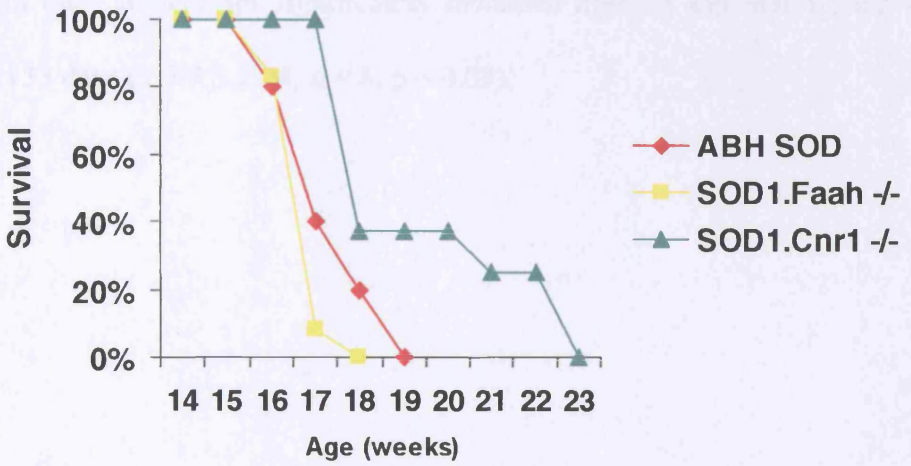
100%
80%
60%
40%
20%
0%
Survival
14 15 16 17 18 19 20 21 22 23
Age (weeks)
ABH SOD
SOD1.Faah -/-
SOD1.Cnr1 -/-

F_2 generation of ABH.SOD1^{G93A} mice lived for 118 days (± 4.2 S.E.M.; n = 5) compared to 131 days (± 1.4 S.E.M.; n = 23) for SOD1^{G93A} mice on the (C57BL/6 x SJL) F_1 background (p = 0.011). Surprisingly, despite the dramatic improvement in disease signs observed at 90 days of age in SOD1.*Faah* -/- mice, ablation of the Faah enzyme had no significant effect on lifespan (p = 0.4) and SOD1.*Faah* -/- animals lived on average for 114 days (± 1.5 S.E.M.; n = 12). Conversely, although we observed no difference in disease signs between ABH.SOD1 and SOD1.*Cnr1* -/- at 90 days of age, ablation of the CB_1 receptor significantly increased lifespan and SOD1.*Cnr1* -/- mice lived for 133 days (± 5.9 S.E.M; n = 8; p = 0.03).

5.4. DISCUSSION

The results presented in this Chapter show that genetic augmentation of endogenous levels of AEA, via ablation of the Faah enzyme, almost completely ameliorated disease signs in 90 day old $SOD1^{G93A}$ mice. However, the dramatic reduction in disease progression observed in $SOD1^{G93A}$ mice following genetic enhancement of the cannabinoid system, were not reflected in an increased lifespan. Interestingly, ablation of the CB_1 receptor had neither a positive or negative effect on disease progression in $SOD1^{G93A}$ mice. However, in contrast to SOD1.*Faah* -/- mice, in which AEA levels were augmented, or to $SOD1^{G93A}$ mice treated with WIN55,212-2, ablation of the CB_1 receptor significantly extended the lifespan of $SOD1^{G93A}$ mice.

Under various pathological conditions, such as excitotoxicity, inflammation and brain trauma, the synthesis of endocannabinoids is up-regulated in the CNS (Sugiura et al., 2000; Baker et al., 2001; Hansen et al., 2001b ; Panikashvili et al., 2001; Marsicano et al., 2003; Muthian et al., 2004). This up-regulation may therefore constitute an endogenous protective mechanism that can be activated in response to a variety of pathological stimuli. The results presented in **Chapter 4** (see **Figure 4.1**) show that both AEA and 2-AG, the two most widely studied endocannabinoids, are up-regulated in the spinal cords of symptomatic $SOD1^{G93A}$ mice. A similar pattern of endocannabinoid elevation has also been reported by Witting et al, (2004). Although, the pathogenic mechanisms underlying ALS are still far from understood there is substantial evidence that indicates that glutamate excitotoxicity, inflammation and oxidative stress are all involved (reviewed by Bruijn et al., 2004). The elevation in endocannabinoid levels observed in the spinal cord of the $SOD1^{G93A}$ mice may therefore be regarded as an adaptive response aimed at counteracting the pathological processes underlying ALS. However, this protective endogenous response is clearly not sufficient

to counteract these pathological mechanisms in the long-term. Nevertheless, the results of this study show that genetic elevation of AEA levels, and therefore enhancement of the endocannabinoid-mediated protective response is neuroprotective, particularly in the early stages of disease and indicate that augmentation of this response may have therapeutic potential.

5.4.1. The effects of genetically manipulating the cannabinoid system on hindlimb muscle force

At 90 days of age, the MTT of both TA and EDL muscles are significantly reduced in ABH.SOD1 mice compared to the hindlimb muscles of ABH.WT littermates. Similar to results in $SOD1^{G93A}$ mice on the C57BL/6 x SJL F_1 background, TA muscles from ABH.SOD1 mice are significantly more affected than EDL muscles even at this early stage of disease. Sharp et al, (2005) also reported a greater deficit in TA muscles than EDL muscles at 90 days of age in $SOD1^{G93A}$ mice on the C57BL/6 x SJL F_1 background. Therefore the MTT of TA and EDL muscles from ABH.SOD1 mice is only 41.3% and 71.1% of the MTT of these muscles in ABH.WT mice respectively.

Elevation of AEA levels, as a consequence of ablation of the Faah enzyme, prevents the loss in muscle force that occurs in $SOD1^{G93A}$ mice during disease progression. Indeed, the TA and EDL muscles in SOD1.*Faah* -/- mice are as strong as the respective muscles in ABH.WT mice. Therefore, augmenting the increase in endogenous endocannabinoid levels that occurs in $SOD1^{G93A}$ mice during disease progression, by ablation of the Faah enzyme, prevents any loss in muscle force at an early stage of disease.

In contrast, ablation of the CB_1 receptor has no effect on the maximal hindlimb muscle force of $SOD1^{G93A}$ mice. The MTT of TA and EDL muscles in SOD1.*Cnr1* -/- mice is

similar to that in ABH.SOD1 mice, so that these muscles are significantly weaker than in their ABH.WT littermates. This result suggests that the beneficial effects of cannabinoids observed here following treatment with either WIN55,212-2 or following ablation of Faah, are not mediated by the CB_1 receptor. If the CB_1 receptor mediated the beneficial effects of endocannabinoids then ablation of this receptor subtype would be expected to result in an acceleration of disease progression. Therefore, the lack of effect seen following CB_1 receptor ablation implies that activation of this receptor subtype may not contribute to the protective effects mediated by cannabinoids.

5.4.2. The effect of genetically manipulating the cannabinoid system on muscle contractile characteristics

Normally, EDL muscles are fast, fatigable muscles. However, as a consequence of disease progression the EDL muscles in $SOD1^{G93A}$ mice become largely fatigue resistant as shown in **Chapter 4.3.5**. Interestingly, the results of this Chapter show that by 90 days of age, an early symptomatic stage of disease, EDL muscles from ABH.SOD1 mice are already largely fatigue resistant. This data is consistent with a previous study by Sharp et al, (2005), in which EDL muscles from $SOD1^{G93A}$ mice, on the C57BL/6 x SJL F_1 background, have increased fatigue resistance compared to WT EDL muscles at 90 days of age. Thus, significant changes in the contractile characteristics have already occurred in $SOD1^{G93A}$ mice by this stage.

Consistent with the muscle force data, however, the fatigue pattern of EDL muscles from SOD1.*Faah* -/- mice does not differ significantly from that seen in ABH.WT mice. Thus, elevation of AEA levels appears to delay the deleterious changes in contractile characteristics in EDL hindlimb muscles that occur in $SOD1^{G93A}$ mice at this early stage of disease. In contrast, EDL muscles from SOD1.*Cnr1* -/- mice are fatigue resistant by

90 days of age, similar to EDL muscles from ABH.SOD1 mice, implying that ablation of the CB_1 receptor does not alter the progression of changes occurring in muscle contractile characteristics in the $SOD1^{G93A}$ mice.

The pattern of SDH staining of EDL muscles fibres from ABH.WT, ABH.SOD1, SOD1.*Faah* -/- and SOD1.*Cnr1* -/- is consistent with the EDL muscle fatigue data. Therefore, whereas ABH.WT EDL muscle fibres stain lightly for SDH, indicating a low oxidative capacity, EDL muscles from ABH.SOD1 mice at 90 days of age, in contrast, have a greater proportion of muscle fibres that are darkly stained suggesting that they have a higher oxidative capacity. EDL muscle fibres from SOD1.*Faah* -/- mice resemble WT EDL, with the majority of fibres lightly stained, indicating that SOD1.*Faah* -/- EDL muscle fibres have not undergone the deleterious changes in muscle fibre phenotype that have already occurred in the EDL muscles of ABH.SOD1 mice by this stage. This provides further evidence to suggest that elevation of endogenous AEA levels has a significantly beneficial effect on muscle function in $SOD1^{G93A}$ mice, as in SOD1.*Faah* -/- mice the EDL muscles remain fast, fatigable muscles with a relatively low oxidative capacity. The pattern of SDH staining of EDL muscles from SOD1.*Cnr1* -/- mice, in contrast, is similar to that seen in ABH.SOD1 EDL muscles. Therefore, ablation of the CB_1 receptor has no effect on the changes in the muscle fibre phenotype of EDL muscles that occur by 90 days of age in the $SOD1^{G93A}$ mice.

5.4.3. The effect of genetically manipulating the cannabinoid system on the survival of functional motor units in $SOD1^{G93A}$ mice

At 90 days of age, at the onset of observable disease symptoms, 32% of motor units have already been lost in ABH.SOD1 mice, compared to their ABH.WT littermates. In

contrast, at this stage no motor unit loss occurs in SOD1^{G93A} mice in which the Faah enzyme has been genetically ablated. Genetic ablation of the CB_1 receptor, however, has no effect on motor unit survival and at 90 days of age SOD1.*Cnr1* -/- mice have lost 39% of their functional motor units, which is similar to the motor unit loss that occurs in ABH.SOD1 mice. Therefore, consistent with the muscle function studies, ablation of the Faah enzyme has dramatic protective effects on motor unit survival, whereas ablation of the CB_1 receptor does not influence disease progression at 90 days of age in ABH.SOD1 mice.

5.4.4. The effect of genetic manipulation of the cannabinoid system on the survival of sciatic motoneurons

The increase in motor unit survival observed in SOD1.*Faah* -/- mice is reflected in a significant increase in survival of motoneurons in the spinal cord. Thus, in ABH.SOD1 mice at 90 days of age, 32% of motoneurons have already died compared to their ABH.WT littermates. In contrast, in SOD1.*Faah* -/- mice only 14.8% of motoneurons have been lost at this early stage of disease compared to ABH.WT mice. However, the survival of sciatic motoneurons in SOD1.*Cnr1* -/- mice at 90 days of age does not differ significantly from ABH.SOD1 mice, and 39.4% fewer motoneurons survive in SOD1.*Cnr1* -/- mice at 90 days of age compared to ABH.WT mice.

Surprisingly, the significant increase in motoneuron survival observed in SOD1.*Faah* -/- mice at 90 days of age is not maintained, in the long-term. Thus, at the end-stage of disease there is no significant difference in motoneuron survival between ABH.SOD1, SOD1.*Faah* -/- and SOD.*Cnr1* -/- mice.

5.4.5. The effect of genetically manipulating the cannabinoid system on the lifespan of SOD1^{G93A} mice on the ABH background

Both the ABH.*Faah* -/- and ABH.*Cnr1* -/- mice used in this study have a normal lifespan. However, it is interesting to note that the F_2 generation of SOD1^{G93A} mice on the ABH background show a significant reduction in lifespan compared to SOD1^{G93A} mice on the C57BL/6 x SJL F_1 hybrid background. This may result from a reduced level of BL/6 in the genetic background of these F_2 generation ABH.SOD1 mice, due to backcrossing onto the ABH background. Previously, the genetic background of SOD1^{G93A} mice has been shown to have significant effects on their lifespan. Indeed, in a study by Heiman-Patterson et al, (2005), SOD1^{G93A} mice on the C57BL/6 x SJL background live on average for 130.2 days (± 11.2) compared to 143.6 days (± 7.5) on the C57BL/6 background. The extension in lifespan in SOD1^{G93A} mice on the C57BL/6 background is related to a reduced level of SJL, which confers a less severe phenotype (Heiman-Patterson et al., 2005).

Surprisingly, despite the significant amelioration in disease progression in SOD1.*Faah* –/– mice observed at 90 days, these effects are not reflected in an increase in the lifespan of SOD1.*Faah* -/- mice. This is consistent with the results shown in **Chapter 4**, whereby administration of an exogenous cannabinoid, WIN55,212-2, delays disease progression at 120 days of age, but does not significantly extend lifespan. Similarly, disease progression is delayed in SOD1^{G93A} mice treated with Δ^9-THC or CBD, but there is no significant extension of lifespan (Raman et al., 2004; Weydt et al., 2005). Interestingly, it can be seen from the results in this Chapter that while ablation of the CB_1 receptor in SOD1^{G93A} mice has no effect on disease progression at 90 days of age, there is a significant increase in the lifespan of these mice. Indeed, the lifespan of SOD1.*Cnr1* -/- mice is extended by 13%, similar to that of SOD1^{G93A} mice treated with

the anti-excitotoxic agents, riluzole and RPR119990, and the microglial inhibitor, minocycline (Gurney et al., 1998; Canton et al., 2001; van den Bosch et al., 2002).

5.4.6. Why might ablation of the CB_1 receptor significantly extend lifespan?

The observation that CB_1 receptor ablation significantly extends lifespan without affecting disease progression at an early stage of disease suggests that CB_1 receptor activation does not play a role in the cellular defence mechanism of motoneurons in $SOD1^{G93A}$ mice. Furthermore, contrary to current opinion, the neuroprotective effects of cannabinoids, achieved either by treatment with WIN55,212-2 or elevation of endocannabinoids following ablation of Faah, may not be mediated by the CB_1 receptor. These results therefore suggest that inhibition or blockade of the CB_1 receptor may actually have a neuroprotective effect.

These results are therefore in contrast to studies in which an increase in neurological damage is seen in *Cnr1* -/- mice after middle cerebral artery occlusion or NMDA injection, (Parmentier–Batteur et al., 2002). Furthermore, injection of KA into the CNS of *Cnr1* -/- mice produces a more extreme behavioural reaction and mortality than in WT mice (Marsicano et al., 2003; Pryce et al., 2003), therefore highlighting the role of this receptor in neuroprotection. However, other reports support the possibility that blockade of CB_1 receptors may be neuroprotective. Treatment with a CB_1 receptor antagonist alone reduces neurological damage following an intrastriatal NMDA injection in neonatal rats (Hansen et al., 2002). Similarly, neuroprotection in an animal model of permanent or transient middle cerebral artery occlusion is elicited via blockade of CB_1 receptors (Muthian et al., 2004). Interestingly in both of these models, similarly to the $SOD1^{G93A}$ mice, levels of AEA are elevated, suggesting that an underlying

endocannabinoid-mediated toxic mechanism may be exerted by activation of CB_1 receptors.

Indeed, activation of CB_1 receptors has been reported to exert neurotoxic effects via the stimulation of an increased calcium influx (Chan et al., 1998; Netzeband et al., 1999; Klegeris et al., 2003). *In vitro* studies have also shown that AEA can induce apoptosis in many cell types (Zhu et al., 1998; Sarker et al., 2000), and it has been suggested that the immunosuppressive effects of AEA may result from the induction of apoptosis in immune cells (Zhu et al., 1998; Do et al., 2004), although the involvement of cannabinoid receptors in this effect is controversial (Movsesyan et al., 2004). Furthermore, *Faah -/-* mice are more susceptible to KA-induced seizures (Clement et al., 2003). Together these observations suggest a potentially neurotoxic role for elevated endocannabinoids, in contrast to their generally accepted neuroprotective role.

Nevertheless, the results here clearly show that elevated levels of cannabinoids are neuroprotective. However, the extended lifespan of SOD1.*Cnr1 -/-* mice suggests that these neuroprotective effects are not mediated via the CB_1 receptor. Therefore, it is possible that the beneficial effects observed with increased endocannabinoid levels are in fact mediated via the CB_2 receptor. Other authors have demonstrated neuroprotective effects of cannabinoids in the presence of CB_1 receptor antagonism, also suggesting a non-CB_1 receptor mediated effect (Nagayama et al., 1999; van der Stelt et al., 2001; Klegeris et al., 2003). Activation of CB_2 receptors may inhibit inflammatory processes and indeed, there is significant evidence to suggest that inflammation plays a role in ALS pathogenesis, as described in detail in **Chapter 4.4.7.2.**. Markers of inflammation, for example reactive astrocytes and microglia, are prevalent in the post-mortem spinal cords from ALS patients concurrent with elevated levels of inflammatory mediators

(Alexianu et al., 2001; Yasojima et al., 2001; McGeer & McGeer, 2002; Maihofner et al., 2003). Similarly, in $SOD1^{G93A}$ mice there is a correlation between disease progression and the intensity of inflammation (Hall et al., 1998; Alexianu et al., 2001; Almer et al., 2001). Interestingly, in post-mortem brains from Alzheimer's disease (AD) patients, expression of CB_2 receptors and the Faah enzyme are elevated in microglia and astrocytes associated with neuritic plaques (Benito et al., 2003). In a model of peripheral nerve injury, CB_2 receptor expression is elevated in the rat spinal cord due to the influx of activated microglia (Zhang et al., 2003). Furthermore, another study reports a reduction in functional CB_1 receptors in the post-mortem brains of AD patients (Ramirez et al., 2005). Together with the findings of the present study, these observations suggest that pharmaceutical targeting of the CB_2 receptor may be beneficial in neurodegenerative conditions where inflammation plays a significant role (Benito et al., 2003; Zhang et al., 2003; Ramirez et al., 2005).

5.4.7. How may CB_2 receptor activation exert neuroprotective effects?

Cannabinoid-mediated activation of CB_2 receptors located on microglia (Benito et al., 2003; Klegeris et al., 2003) inhibits microglial activation (Arevalo-Martin et al., 2003) and reduces both mRNA expression and release of pro-inflammatory cytokines from microglia (Puffenbarger et al., 2000; Croxford & Miller, 2003; Facchinetti et al., 2003; Klegeris et al., 2003). Furthermore, an inhibitory effect of cannabinoids on microglia may also limit their release of glutamate and reactive oxygen species, therefore reducing the potential contribution of excitotoxicity and oxidative stress to disease pathogenesis (Molina-Holgado et al., 1997; Waksman et al., 1999; Tikka et al., 2002). Previously therapies targeting inflammation such as minocycline and NDGA, which are inhibitors of microglia, and selective COX2 inhibitors have had beneficial effects in mutant SOD1 mice (Drachman et al., 2002; Kriz et al., 2002; Pompl et al., 2002; van den Bosch et al.,

2002; Zhu et al., 2002; West et al., 2004). The present study provides evidence that elevated endocannabinoids, via Faah ablation, act to reduce inflammation as GFAP immunoreactivity, a marker of astrogliosis, is significantly reduced in SOD1.*Faah* -/- mice compared to ABH.SOD1 mice. Therefore further investigation into the therapeutic potential of specific CB_2 receptor agonists in ALS is warranted.

It is possible that other receptor subtypes may also contribute to the neuroprotective effects of elevated AEA observed in this study. For example, activation of the putative "CB_3" receptor, characterised in the brains of *Cnr1* -/- mice, by AEA may contribute to the neuroprotection seen in SOD1.*Faah* -/- mice (Di Marzo et al., 2000; Breivogel et al., 2001; Monory et al., 2002). This receptor subtype may mediate cannabinoid-induced inhibition of glutamate neurotransmission (Hajos et al., 2001; Hajos & Freud, 2002) therefore reducing excitotoxicity. Alternatively, the ability of AEA to activate VR1 receptors may also be involved (Zygmunt et al., 1999; Smart et al., 2000). VR1 receptors are coupled to non-selective cation channels, thus receptor activation may induce neuronal excitability by increasing calcium influx. However, VR1 receptors are believed to undergo rapid desensitisation, therefore prolonged activation of VR1 receptors by elevated endogenous AEA may induce receptor desensitisation and consequently reduce neuronal excitability (Zygmunt et al., 1999). Indeed, blockade of VR1 receptors has previously been shown to have neuroprotective effects *in vivo* (Veldhuis et al., 2003). Potentially AEA-mediated inhibition of sodium and T-type calcium channels, acting to reduce neuronal excitability may also contribute to the effects of AEA seen in the SOD1.*Faah* -/- mice (Chemin et al., 2001; Nicholson et al., 2003), whereas inhibition of the TASK-1 channel with excitatory consequences is unlikely to be involved (Maingret et al., 2001). Finally, a contribution of the oxidative products of AEA hydrolysis to the neuroprotective effects in this study must also be

considered, in particular 12-HAEA, which has exerted anti-oedematous effects in an animal model of excitotoxicity (Veldhuis et al., 2003).

5.4.8. The therapeutic potential of the Faah enzyme

The results of this study identify for the first time the Faah enzyme as a novel therapeutic target in ALS. In this study, genetic deletion of the *Faah* gene, which is known to bring about a 10 – 15 fold elevation of AEA levels in the CNS (Cravatt et al., 2001), exerts a dramatic neuroprotective effect in $SOD1^{G93A}$ mice, at least at 90 days of age. Recently a class of highly selective and reversible *O*-arylcarbamate inhibitors of the Faah enzyme have been developed (Kathuria et al., 2003; Fegley et al., 2005), which will further aid research in this field. Within 2 hours of application, URB597, a member of the *O*-arylcarbamate inhibitor family, induces a 3-5 fold elevation in the CNS concentration of AEA and other NAEs hydrolysed by Faah, for example the non-receptor binding endocannabinoids, OEA and PEA (Cravatt et al., 2003). Selective pharmaceutical (Baker et al., 2001) and genetic inhibition of Faah activity (Massa et al., 2004) has been shown to ameliorate symptoms in an autoimmune rodent model of inflammation. Meanwhile, Faah inhibitors have also been proposed as potential therapies in the treatment of anxiety attacks (Kathuria et al., 2003)

In spite of the dramatic effects on disease signs observed in 90 day old SOD1.*Faah* -/- mice, there is no increase in lifespan, suggesting that endocannabinoids may only be therapeutic in the early stages of disease. This effect may be related to the appearance of activated microglia from a presymptomatic stage in mutant SOD1 mice onwards (Hall et al., 1998; Alexianu et al., 2001; Elliott et al., 2001; Olsen et al., 2001; Weydt et al., 2004). Therefore the protective effects mediated via endocannabinoid-induced activation of CB_2 receptors on microglia may also be initiated at a presymptomatic

stage. However, with further disease progression and the initiation of other pathological changes, the protective effects of endocannabinoids may then be overwhelmed. Nevertheless, ablation of Faah and the subsequent increase in endogenous AEA, does significantly delay disease onset. Therefore pharmacological inactivation of Faah may be particularly effective if used in combination with agents that act on mechanisms active during later stages of the disease such as heat shock protein co-inducers (Kieran et al., 2004) or glutamate inhibitors (Canton et al., 2001; Van Damme et al., 2003).

Recognition of the abundance of endocannabinoids in the CNS coupled with an increasing understanding of their physiological functions, has now established a role for endocannabinoids as modulators of neuronal activity. The precise elucidation of their mechanisms of synthesis, uptake and degradation has facilitated the development of pharmaceutical agents targeting particular steps of each pathway, in addition to permitting further assessment of the role of the endocannabinoid system. Therefore agents acting simultaneously to inhibit the hydrolysis or reuptake of several endocannabinoids may exert greater neuroprotective effects than observed with genetic inhibition of the Faah enzyme. Furthermore, the existence of different synthetic and degradative pathways for AEA and 2-AG may suggest a differential regulation of endocannabinoid functions in different areas of the CNS. Therefore, it is possible that the neuroprotective effects of 2-AG may be greater than those seen with AEA in this model of ALS.

5.5. CONCLUSION

In conclusion, the results from this Chapter show that increased tone of the endocannabinoid system obtained by ablation of the Faah enzyme, similar to that seen following treatment with synthetic cannabinoids such as WIN55,212-2, ameliorates

disease symptoms, at least in the short term. These neuroprotective effects appear to be mediated by a non–CB_1 receptor dependent mechanism. Our results therefore identify the Faah enzyme and possibly the CB_2 receptor as potential therapeutic targets in ALS. Manipulation of the endocannabinoid system alone or in combination with other therapeutic agents targeted at alternative mechanisms hypothesised to contribute to ALS pathogenesis is warranted in an attempt to further increase lifespan as well as quality of life.

CHAPTER 6

THE SILENCING OF HUMAN MUTANT SOD1^{G93A} *IN VITRO* USING siRNA EXPRESSING LENTIVIRAL VECTORS

6.1. INTRODUCTION

In this Chapter, the ability of siRNA technology to successfully ablate human mutant SOD1 protein was investigated in primary mixed ventral horn $SOD1^{G93A}$ cultures. This project was carried out in collaboration with Dr Mimoun Azzouz from Oxford Biomedica (Oxford, UK). In these experiments the primary cell culture and viral transfection procedures were undertaken at the Institute of Neurology and the generation of lentiviral vectors and the protein analysis was carried by out by Dr Azzouz and colleagues at Oxford Biomedica.

6.1.1. ALS therapies

The mutant SOD1 transgenic mouse model of fALS provides the best available model of ALS in which to test neuroprotective strategies. **Table 6.1** shows a selective list of potential neuroprotective agents that have been tested in mutant SOD1 mice. However to date, the translation of the positive effects observed in mutant SOD1 mice to humans has failed to materialise. There may be several reasons for this discrepancy. For example, it is possible that one major hurdle is the bioavailability of pharmacological agents and also the targeting of therapies to motoneurons within the human CNS. A recent attempt to overcome this problem has involved the use of viral vectors. Indeed, viral gene therapy is being extensively studied as a delivery method for therapeutic agents.

Viral vectors can infect non-dividing as well as dividing cells, therefore making them suitable candidates for the treatment of neurodegenerative disease. Replication deficient viruses can be manipulated to express a gene of interest that can be introduced directly into the patient. Alternatively, cells can be removed from patients, for example bone marrow cells, and injected with viral vectors *ex vivo* prior to transplantation back into

Table 6.1 - Pharmacological therapies tested in mutant SOD1 mice for the treatment of ALS

In these studies, the onset of pharmacological treatment is at a presymptomatic stage in mutant SOD1 mice unless otherwise stated.

Pathogenic mechanism targeted Drug name	**Mechanism of action**	**Extension in lifespan (%)**	**Reference**
Oxidative stress			
d-penicillamine	Copper chelator	8	Hottinger et al., 1997
AR-R 17,477	Inhibits neuronal NOS activity	13	Facchinetti et al., 1999
Excitotoxicity			
Riluzole	Inhibition of glutamate release, modulation of NMDA receptor function	10.5	Gurney et al., 1998
RPR 119990	AMPA receptor antagonist	12.7	Canton et al.,2001
NBQX	AMPA/KA receptor antagonist	10	Van Damme et al., 2003
β-lactam antibiotics (treatment onset at early symptomatic stage)	Upregulation of GLT-1	8	Rothstein et al., 2005
Mitochondrial dysfunction			
Bcl-2 overexpression	Inhibits caspase/apoptosis activation	15	Kostic et al., 1997
Creatine	Stabilisation of mitochondrial creatine kinase	17.8	Klivenyi et al., 1999
Protein aggregation			
Arimoclomol	HSP co-inducer	22	Kieran et al., 2004

Inflammation			
Celecoxib	COX2 inhibitor	25	Drachman et al., 2002
Minocycline	Microglial inhibition, inhibition of cytochrome c release.	9-16	Kriz et al., 2002; van den Bosch et al., 2002; Zhu et al., 2002
NDGA (treatment onset at early symptomatic stage)	Inhibition of TNFα release	32	West et al., 2004
Other targeted mechanisms			
ICE inhibition	Inhibits caspase 1	8	Friedlander et al., 1997
WHI-PI3I	Janus kinase inhibitor	49	Trieu et al., 2000
VEGF (in mutant SOD1 rats from 85d)	Growth factor	8	Storkebaum et al., 2005
ZVAD-fmk	Broad spectrum caspase inhibitor	22	Li et al., 2000
Combination therapy			
Riluzole, minocycline and nimodipine – targeting excitotoxicity and inflammation	Inhibition of glutamate release, inhibition of microglial activation and inhibition of voltage-gated calcium channels	13	Kriz et al., 2003
Viral therapies			
AAV – Bcl2	Inhibits apoptosis induction	0	Azzouz et al., 2000
AAV – GDNF	Neurotrophic factor	14	Wang et al., 2002
Ad – GDNF	Neurotrophic factor	12	Acsadi et al., 2002
AAV – IGF –1 (treatment onset at early symptomatic stage)	Neurotrophic factor and inhibits caspase activation	18	Kaspar et al., 2003
LV- VEGF (treatment onset at early symptomatic stage)	Growth Factor	15	Azzouz et al., 2004
LV – shRNA to mutant SOD1	Ablation of mutant SOD1	77	Ralph et al., 2005b

the patient. Several laboratories have attempted viral gene therapy in models of ALS. Lentiviral vectors expressing a recombinant GDNF transgene successfully transfect motoneurons *in vitro* and significantly increase their survival in the presence of exogenous trophic factor deprivation (Cisterni et al., 2000). Indeed, virus based GDNF is as effective in promoting survival as exogenous GDNF (Cisterni et al., 2000). *In vivo*, the local injection of lentivirus-encoding GDNF into the lumbar spinal cord of $SOD1^{G93A}$ mice at 35 days of age induces strong transgene expression that persists until 120 days of age. However, despite maintained elevations in GDNF, no significant benefit is observed in terms of disease progression or lumbar motoneuron survival, although a significant protection of facial motoneurons occurs (Guillot et al., 2004). In contrast, intraspinal injection of recombinant adeno-associated virus (AAV) expressing Bcl2 significantly increases motoneuron survival in the lumbar spinal cord of $SOD1^{G93A}$ mice (Azzouz et al., 2000). Similarly, injection of Bcl2 expressing adenovirus (Ad) into the tongue of $SOD1^{G93A}$ mice significantly protects motoneurons in the hypoglossal nucleus (Yamashita et al., 2002).

Intraspinal injection, however, is not likely to be an acceptable delivery route for human gene therapy due to the risks associated with such an approach. Instead the peripheral administration of viral vectors via intramuscular injection would have greater transfer to the clinic. In mutant SOD1 mice, following the intramuscular injection of a GDNF-expressing Ad or AAV vector, GDNF is retrogradely transported to the motoneurons of the spinal cord (Acsadi et al., 2002; Manabe et al., 2002; Wang et al., 2002; Lu et al., 2003). Sustained expression of GDNF in the muscles and spinal cord significantly delays disease onset and extends survival of $SOD1^{G93A}$ mice by 12% or 14% following intramuscular delivery of Ad-GDNF (Acsadi et al., 2002) or AAV-GDNF respectively (Wang et al., 2002).

Intramuscular viral therapies have also been shown to be effective if administered at the time of disease onset. Indeed, injection of AAV expressing insulin-like growth factor-1 (IGF-1) induces significant expression and secretion of IGF-1 in spinal motoneurons, consequently delaying disease onset and extending lifespan of $SOD1^{G93A}$ mice by 18% (Kaspar et al., 2003). This neuroprotective effect is due to a combination of the trophic effects of IGF-1 and its anti-apoptotic actions. Furthermore, this effect is dependent on the retrograde transport of viral vectors encoding IGF-1 to the spinal cord in addition to IGF-1 expression in the muscle fibres (Kaspar et al., 2003). Similarly, retrograde transport of a lentiviral vector encoding VEGF from hindlimb and facial muscles of $SOD1^{G93A}$ mice significantly delays disease progression and is accompanied by a 15% extension in lifespan, despite treatment being initiated after disease onset, at 90 days of age (Azzouz et al., 2004).

6.1.2. Lentiviral-based therapy

The ability of viral vectors to infect non-dividing cells provides a mechanism to induce the expression of a gene of interest in non-mitotic, adult neuronal cells. This offers a significant advantage over other therapeutic strategies. Viral vectors can consist of either capsid virions, for example Ad and AAV, or envelope virions, for example lentiviruses and herpes simplex virus (Davidson & Breakefield, 2003). The individual attributes of the most commonly used viral vectors are listed in **Table 6.2**.

In the experiments in this Chapter, lentiviral vectors are used as the gene delivery agent. Lentiviral vectors are retroviral vectors that stably integrate the gene of interest into the host genome, via reverse transcription of the viral RNA. This provides stable, long-term expression of therapeutic molecules, circumventing the problem of maintaining treatment by repeated therapy. Indeed the expression of genes encoded by lentiviral

Table 6.2. The attributes of commonly used viral vectors

Type of viral vector	Type of virus	Transgene expression	Transgene capacity	Immune reaction	Transduction capacity of non-dividing cells
Recombinant adenovirus (Ad)	Capsid virion	Long-term	Large (up to 36kb)	Substantial immune response although reduced upon removal of Ad genomic sequences	Efficient and can be retrogradely transported
Adeno-associated virus (AAV)	Capsid virion	Long-term under mammalian promoter although generally extra-chromosomal	Small (4-5kb)	Low	Selective neuronal efficiency
Lentivirus	Enveloped virion	Long-term	Moderate (up to 8kb)	Very low	Efficient and can be retrogradely transported
Recombinant herpes simplex virus	Enveloped virion	Long-term	Large (up to 50kb)	Low but risk of expression of viral genes	Efficient and capable of retrograde and anterograde transport within the CNS

vectors has been shown up to 1 year after transfection (Wong et al., 2003). Lentiviral vectors have a moderate cloning capacity (approximately 8kb) and show a very high transduction efficiency of neuronal cells. The need for cell division is bypassed by lentiviruses via the formation of a preintegration complex, which docks at the nuclear membrane and passes through the nuclear pore in an ATP-dependent manner (Martin-Rendon et al., 2001). To avoid safety concerns over the use of HIV-based vectors, non-primate vectors, for example equine infectious anaemia virus (EIAV), have been developed, which have also been rendered replication deficient and are therefore unable to replicate in human cells. These vectors also exert minimal inflammatory and immunological responses (Wong et al., 2003).

Another benefit of lentiviral vectors is the potential for manipulation of the glycoprotein components of the viral envelope. This manipulation can induce the interaction of viral vectors with specific receptors on the plasma membrane of target cells, therefore potentially allowing the targeting of selective populations of cells for gene therapy. For example, after intramuscular injection, viral vectors pseudotyped with a Rabies-G viral envelope will be retrogradely transported from muscles to the innervating motoneurons in the spinal cord. In contrast, viral vectors that are pseudotyped with the vesicular stomatitis virus-G envelope protein (VSV-G) will be confined to the muscle and are not retrogradely transported to the spinal cord (Martin-Rendon et al., 2001; Mazarakis et al., 2001; Kaspar et al., 2003). Therefore, their low toxicity combined with the ability to target motoneurons after intramuscular injection, suggests that lentiviral vectors may be an ideal vector for the treatment of ALS.

6.1.3. Small interfering RNA technology

RNA interference refers to the ability of small, endogenous or exogenous RNA molecules to induce specific, post-translational silencing of selective, sequence-matched mRNAs (Fire et al, 1998). Endogenous RNA interference is involved in the regulation of gene expression, the maintenance of genome stability and possibly as a defence mechanism against RNA viruses (Denli & Hannon, 2003). However, the treatment of *Caenorhabditis elegans* with double stranded RNA (dsRNA), which initiated the degradation of endogenous, sequence-matched mRNA, indicated that this endogenous system could be successfully manipulated to induce specific gene silencing (Fire et al, 1998). It was subsequently discovered that the silencing effect *in vivo* is mediated by small interfering RNA (siRNA) duplexes of 21-23 nucleotides in length, which are formed by the cleavage of exogenous dsRNA (Zamore et al., 2001). This initiated the development of synthetic siRNA duplexes, 21 base pairs in length, which upon direct transfection of mammalian cell lines induce specific down-regulation of sequence specific genes (Elbashir et al., 2001). More recently, short hairpin RNAs (shRNA), which consist of a sense and anti-sense strand, joined by a loop region and under the control of an RNA polymerase III promoter, have been developed. *In vivo* transcription of shRNAs from expression vectors generates siRNA and subsequently induces specific gene silencing (Brummelkamp et al., 2002). The mechanism underlying siRNA-mediated gene silencing is proposed to involve the cytoplasmic cleavage of shRNA by an RNase III enzyme (DICER), therefore generating siRNA molecules. Following degradation of the sense strand, the anti-sense strand associates with an RNA-induced silencing complex (RISC). The RISC complex is subsequently targeted to the siRNA sequence-matched mRNA, and this mRNA is then cleaved and degraded (Ralph et al., 2005a). This mechanism is summarised in **Figure 6.1**.

Figure 6.1 – Mechanism of action of siRNA

The intracellular mechanism of siRNA-induced selective gene silencing is summarised in the diagram, which is adapted from Ralph et al (2005a). Following viral delivery of targeted shRNA molecules, they are cleaved intracellularly to form specific siRNA molecules, which can subsequently associate with RISC and induce degradation of sequence-matched mRNA.

RISC - RNA-induced silencing complex; shRNA - short-hairpin RNA; siRNA – small interfering RNA.

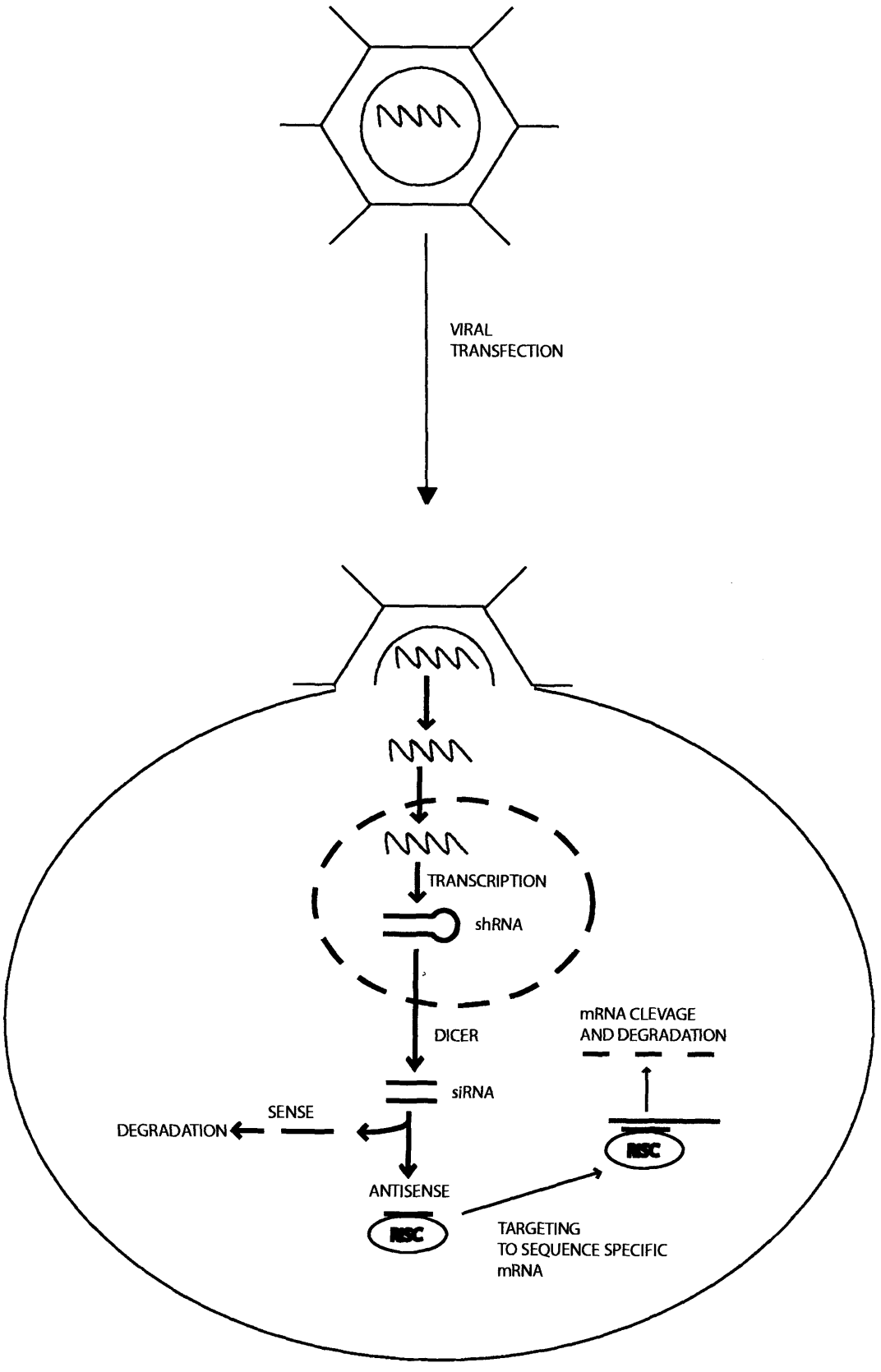
VIRAL
TRANSFECTION
TRANSCRIPTION
shRNA
DICER
siRNA
SENSE
DEGRADATION
ANTISENSE
RISC
mRNA CLEVAGE
AND DEGRADATION
RISC
TARGETING
TO SEQUENCE SPECIFIC
mRNA

The use of siRNA technology to induce long-term gene silencing may therefore provide a novel mechanism for the development of a therapy for dominantly inherited neurodegenerative conditions. Furthermore, the use of viral vectors to express siRNA overcomes the problem of transfecting non-mitotic, adult neurons. Indeed, injection of AAV expressing siRNA targeted against the human mutant form of ataxin-1 significantly reduces the cerebellar pathology and improves motor co-ordination in a mouse model of spinocerebellar ataxia type 1 (Xia et al., 2004). Moreover, specific targeting of siRNA against a mutation in the APP gene implicated in a Swedish form of Alzheimer's disease successfully ablates expression in Cos-7 cells *in vitro*, although the *in vivo* effects remain to be elucidated (Miller et al., 2004).

siRNA technology may therefore prove to be an effective therapy in ALS as although ALS is a predominantly sporadic disorder, approximately 10% of cases have a family history consistent with mendelian inheritance. Currently 11 candidate genes have been identified in familial ALS, although the existence of further causative genes is likely. Therefore, siRNA technology may prove to be a suitable approach for the treatment of some cases of familial ALS, by reducing the expression of specific genes known to be involved. In mutant SOD1-mediated ALS, the mutant SOD1 enzyme acquires a toxic gain of function and therefore ablation has the potential to exert significant beneficial effects. Indeed, in contrast to the ubiquitous expression of mutant SOD1, selective expression in either astrocytes or motoneurons, does not initiate motoneuron degeneration in transgenic mice (Gong et al., 2000; Pramatarova et al., 2001; Lino et al., 2002). Selective ablation of mutant SOD1 *in vitro* has previously been shown by transfection of siRNA targeted to mutant SOD1 (Ding et al., 2003; Maxwell et al., 2004). Furthermore, selective ablation of mutant SOD1 protein significantly protects $SOD1^{G37R}$ expressing N2a cells from cyclosporine-induced toxicity (Maxwell et al.,

2004). Therefore, potentially ablation of mutant SOD1 *in vivo* may have neuroprotective effects in transgenic mutant SOD1 mice.

6.1.4. Hypothesis to be tested

In this study the potential capability of EIAV lentiviral vectors to transfect primary motoneurons is tested *in vitro*. Furthermore, the ability of siRNA to ablate mutant SOD1 protein in $SOD1^{G93A}$ mixed ventral horn cultures is assessed. This project formed part of a pilot study to ensure specific *in vitro* ablation of mutant SOD1, before the initiation and completion of an *in vivo* study by Oxford Biomedica (Ralph et al., 2005b).

6.2. METHODS

6.2.1. pONY8.7-H1SOD1KO vectors

The design and construction of the pONY8.7-H1SOD1KO vectors, which encode siRNA targeted to mutant SOD1, was undertaken at Oxford Biomedica. The lentiviral vectors used were non-primate lentiviruses derived from EIAV. To optimise safety all viral proteins had been removed from EIAV except *gag* and *pol*, and the accessory gene, *rev*, which represent the minimal requirement for gene transfer. Furthermore, the virus had been rendered replication defective by deletions from the 5' and 3' long terminal repeats. Finally, the EIAV virus was pseudotyped with a vesicular stomatitis virus-G envelope protein (VSV-G), which permits transduction of neuronal cells and long-term expression of the transgene (Martin-Rendon et al., 2001), and reduces the probability of reformation of replication competent EIAV (Mitrophanous et al., 1999). Viral titres were estimated by real time quantitative reverse transcriptase PCR by comparison with a previously quantified vector, pONY8.0GFP (Mazarakis et al., 2001), and then normalised for viral RNA (Martin-Rendon et al., 2002). Viral titres used in these experiments were in the range of $5 \times 10^8 - 1 \times 10^9$ transducing units/ml.

To determine transfection capability of EIAV vectors in mixed ventral horn cultures, lentiviral vectors expressing green fluorescent protein (GFP) or lacZ were constructed initially, which permitted the calculation of transfection efficiency.

Putative small interfering RNA (siRNA) target sequences were designed against the human SOD1 gene using online algorithms (Dharmacon, Lafayette, CO, USA). Sequences were determined to be unique to the human SOD1 gene by BLAST searching of the GenBank database. The target sequence of the siRNA used in this study was 5'-GCATTAAAGGACTGACTGA-3'. Subsequently, oligonucleotide primers were

designed corresponding to the sense and antisense sequences of the siRNA target site of interest and separated by a hairpin loop sequence (Brummelkamp et al., 2002). The primers were annealed and cloned into the EIAV vector downstream of a ribonuclease P RNA component H1 (RPPH1) promoter, which had been amplified from human embryonic kidney cell 293T (HEK293T) cell line. **Figure 6.2** provides a diagrammatic representation of the vector used including the mutant SOD1 specific siRNA sequence.

6.2.2. Mixed ventral horn cultures

Mixed motoneuron cultures were prepared using a protocol adapted from that described by Camu & Henderson (1994). The genotype of each embryo was determined prior to culturing, using PCR as described in **Chapter 2.3**, and the spinal cords were pooled according to genotype, either WT or $SOD1^{G93A}$, and each genotype was cultured separately, as detailed in **Chapter 2.5**. Cells were maintained at 37°C in a 5% CO_2 humidified incubator and media replaced twice a week.

6.2.3. Viral transfection

At 1DIV, $SOD1^{G93A}$ mixed ventral horn cultures were incubated with VSV-G pseudotyped EIAV vectors expressing either GFP, lacZ, shRNA to mutant SOD1 or an empty vector. The volume of virus added to each well of a 24 well plate (5×10^5 cells), was calculated according to the following equation:

$$\text{Volume} = \frac{\text{Multiplicity of infection (MOI)} \times \text{Number of cells}}{\text{Titre}}$$

Figure 6.2 – EIAV lentiviral vector encoding siRNA to mutant SOD1^{G93A}

Putative small interfering RNA (siRNA) target sequences were designed against the human SOD1 gene. Oligonucleotide primers were designed corresponding to the sense and antisense sequences of the siRNA target site of interest (EIAV-SOD1HP1) and separated by a hairpin loop sequence. The primers were annealed and cloned into the EIAV vector downstream from RPPH1 (encoding ribonuclease P RNA component H1) promoter, as shown. Following transcription shRNA molecules targeted to mutant SOD1^{G93A} were generated. LacZ was incorporated to enable detection of the vector and therefore successful transfection (in some experiments this was replaced with GFP). Control vectors were also constructed containing an empty expression cassette.

SIN-LTR, self-inactivating long terminal repeat; Ψ, EIAV packaging signal; CMV, cytomegalovirus promoter; EIAV-SOD1HP1 treated.

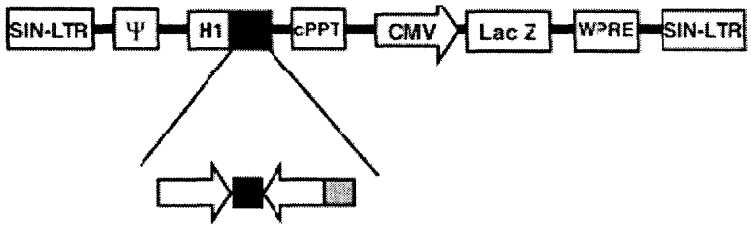

EIAV-SOD1HP1

GATCCCC GCATTAAAGGACTGACTGA TTCAAGAGA TCAGTCAGTCCTTTAATGC TTTTT GGAAA
GGG CGTAATTTCCTGACTGACT AAGTTCTCT AGTCAGTCAGGAAATTACG AAAAA CTTTGATC

Sense Loop Antisense

The viral titre ranged from 5 x 10^8 – 1 x 10^9 transducing units/ml, and was consistent within each viral batch. Initially, using lacZ encoding EIAV vectors, the MOI was varied (between 0.5 and 5) and transfection efficiency calculated for each MOI to allow optimisation of the transfection, as described in **Chapter 2.12** and **6.2.5**. The required volume of virus was diluted into 0.5ml complete neurobasal media and added to the cells via media replacement. Mixed ventral horn cultures were incubated for 5 hours at 37°C in a 5% CO_2 humidified incubator and then the media was replaced with fresh complete neurobasal media. Cells were left for a further 7DIV before processing.

6.2.4. Immunocytochemistry

EIAV-lacZ transfected cultures were double immunostained with primary antibodies to β-galactosidase (1:500, AbCam, Cambridge, UK) and the motoneuron specific marker choline acetyltransferase (ChAT; 1:100, Chemicon, Temecula, CA, USA), according to the protocol detailed in **Chapter 2.8**.

6.2.5. Calculation of transfection efficiency

EIAV-lacZ transfected cultures were processed for Xgal, as described in **Chapter 2.12**. Successful transfection was indicated by the formation of a blue product due to β-galactosidase (the lacZ gene product) mediated hydrolysis of Xgal. The number of motoneurons that stained blue was expressed as a percentage of the total number of motoneurons present. Following calculation of the transfection efficiency, in the remainder of the experiments, cells were transduced with VSV-G pseudotyped vectors using an MOI of 2.5 transducing units/cell.

6.2.6. Protein extraction

Following transfection at 1DIV, mixed ventral horn cultures were left for a further 7DIV before processing. $SOD1^{G93A}$ motoneurons transfected with either lentiviruses expressing shRNA targeted to mutant SOD1 or an empty vector, were lysed and the protein extracted, as described in **Chapter 2.13**. Samples were then frozen at –80°C and sent to Oxford Biomedica on dry ice for analysis of $SOD1^{G93A}$ protein levels.

6.2.7. Statistical analysis

Statistical significance was assessed using a Mann-Whitney U test (Sigma Stat, version 2.03, Erkrath, Germany). Values are expressed as the mean ± standard error of the mean (S.E.M). Significance was set at $p < 0.05$.

6.3. RESULTS

In this Chapter, lentiviral vectors expressing shRNA targeted to human mutant SOD1 were assessed in their ability to ablate $SOD1^{G93A}$ protein in mixed ventral horn cultures.

6.3.1. Assessment of transfection

Initially, it was necessary to determine the ability of EIAV lentiviral vectors to transduce primary motoneurons in culture. Therefore, GFP encoding EIAV vectors were incubated with mixed ventral horn cultures, with GFP expression indicating successful transfection. The photomicrograph in **Figure 6.3** shows primary motoneurons successfully transfected with GFP-encoding EIAV vectors. In a separate set of experiments, cultures were transfected with lacZ-encoding EIAV vectors and double immunolabelling was performed to confirm that the cells transfected were motoneurons. Therefore, cultures were immunostained for ChAT, a marker of cholinergic neurons that can be used to identify motoneurons, and β-galactosidase, the lacZ gene product, which indicated successful transfection. Indeed, double labelling of motoneurons was observed, as shown in **Figure 6.4**.

6.3.2. Transfection efficiency

Mixed ventral horn cultures were transfected with lacZ-encoding EIAV vectors and 7 days later were processed for Xgal, as described in **Chapter 2.12**. The formation of a blue product indicated successful transfection and the number of transfected motoneurons, identified by the morphological criteria listed in **Chapter 2.7**, were calculated as a percentage of the total number of motoneurons. The photomicrographs in **Figure 6.5** show transfected motoneurons in which Xgal has been hydrolysed to a blue product. The percentage of transfected motoneurons at differing MOIs are shown

Figure 6.3 - Motoneurons successfully transfected with GFP-encoding EIAV lentiviral vectors

The photomicrograph shows primary motoneurons in culture that have been transfected with GFP-encoding EIAV vectors. The expression of GFP indicates that the motoneurons have been successfully transfected with the lentiviral vector.

Scale bar = 20μm

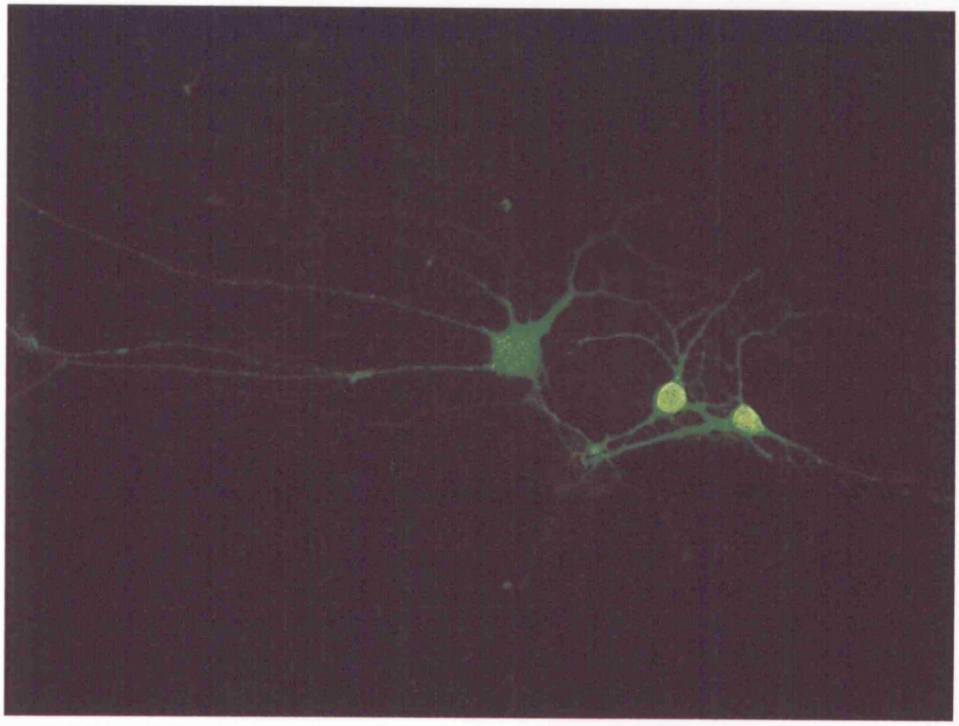

Figure 6.4 – Double-immunolabelling of motoneurons in culture

The photomicrographs show a primary motoneuron in culture that has been stained for **(A)** ChAT, a marker of ACh synthesis and therefore motoneurons, and **(B)** β-galactosidase, the lacZ gene product. The overlay between the immunostaining for ChAT and β-galactosidase is shown in image **C**. The merged image shows a complete overlap of ChAT and β-galactosidase immunostaining, which therefore indicates that motoneurons have been successfully transfected with lacZ-encoding EIAV vectors.

Scale bar = 20μm

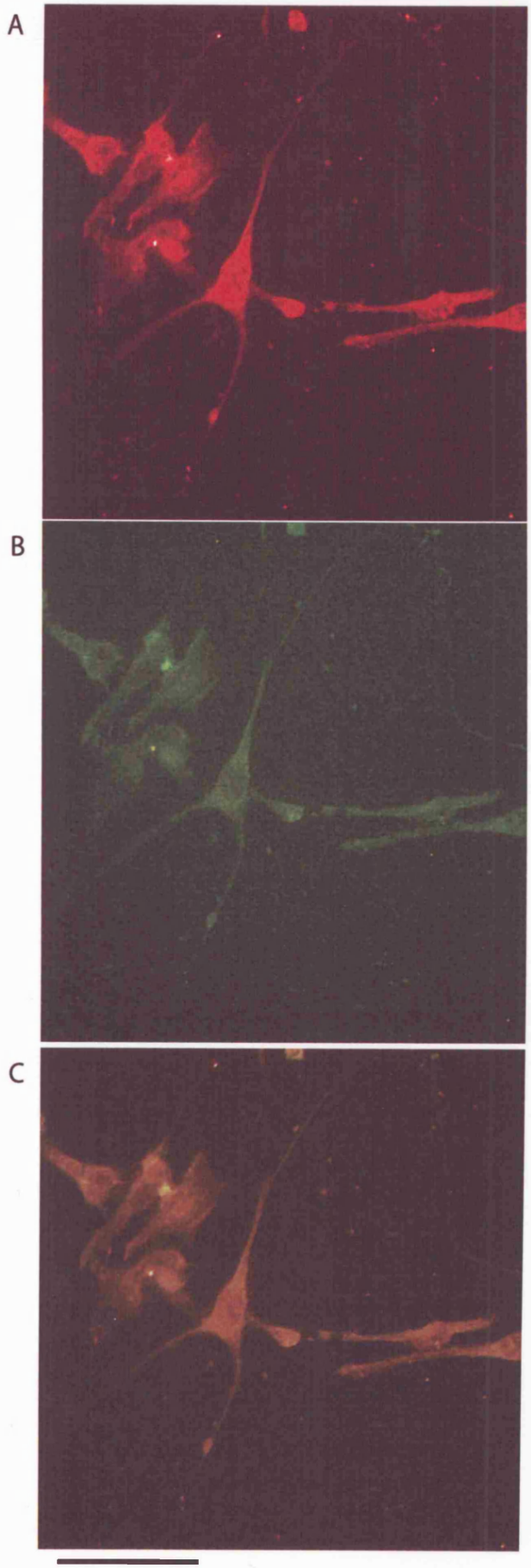
A
B
C

Figure 6.5 – Motoneurons transfected with lacZ-encoding EIAV vectors

The photomicrographs show motoneurons at different magnifications (using the x20 and x40 objective lenses), successfully transfected with lacZ-encoding EIAV vectors, which is indicated by the formation of a blue product. It can be seen in (**A**) that many neurons in the mixed ventral horn cultures are successful transfected. Transfected motoneurons, with significant nuclear staining, are shown at higher magnification in (**B**). The processing of mixed ventral horn cultures for Xgal staining was used to determine the transfection efficiency.

Scale bar = 50μm

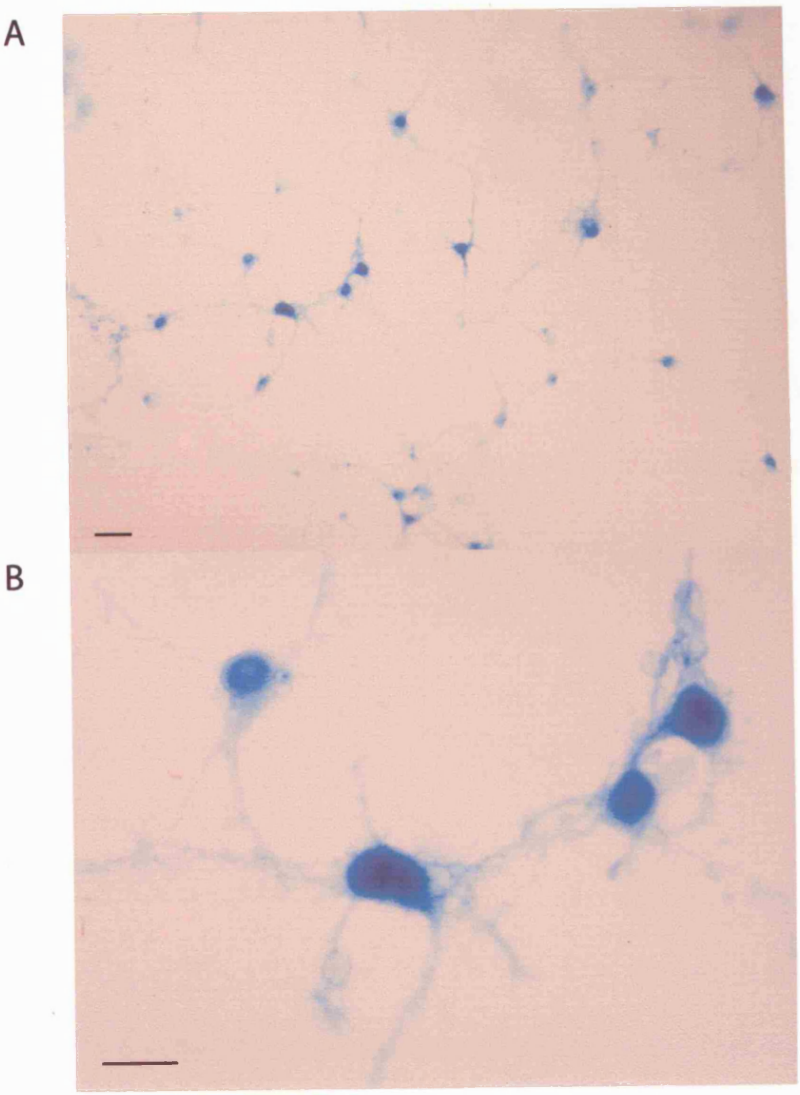
A
B

in **Table 6.3.**. However, the decision regarding the optimal MOI was based not only on the percentage of motoneurons that had been successfully transfected but also required an assessment of the viability of the motoneurons after transfection. Thus in random fields of neurons, the general health of motoneurons was assessed and for example, signs of membrane blebbing and underdeveloped neurites were taken to represent reduced motoneuron viability. An individual MOI was therefore deemed toxic *in vitro* if greater than 10% of motoneurons in a particular culture showed signs of reduced viability. Using these criteria, an MOI of 2.5, which successfully transfected 69% of motoneurons, was chosen for the remaining experiments. In contrast, an MOI of 5, which produced higher transfection efficiency, also produced signs of motoneuron toxicity *in vitro*.

6.3.3. Ablation of mutant SOD1

At 1 DIV, mixed ventral horn $SOD1^{G93A}$ cultures were transfected with either EIAV vectors-encoding siRNA targeted to mutant SOD1 or an empty vector (MOI 2.5). At 7 days post-transfection, cells were lysed and protein was extracted. The analysis of protein levels was undertaken at Oxford Biomedica. **Figure 6.6A** gives an example of a typical Western blot measuring mutant SOD1 protein levels in the $SOD1^{G93A}$ cultures, and the densities are quantified in the bar chart in **Figure 6.6B**. Transfection with EIAV expressing an empty vector did not significantly lower mutant SOD1 protein levels in mixed ventral horn cultures ($p = 0.142$). In contrast, transfection with shRNA targeted to mutant SOD1 significantly ablated the expression of the mutant SOD1 protein ($p < 0.02$). Indeed, mutant SOD1 protein levels were reduced by 70% (± 0.06 S.E.M.) compared to untransfected mixed ventral horn cultures.

Table 6.3 – Transfection efficiency of EIAV vectors in motoneurons

The Table summarises the number of motoneurons successfully transfected with lacZ-encoding EIAV vectors, expressed as a percentage of the total number of motoneurons in the cultures. To optimise the transfection procedure, varying multiplicities of infection (MOI) were used. An MOI of 2.5 was finally chosen for the remainder of the experiments due to the high transfection efficiency and a lack of side effects achieved using this MOI.

Multiplicity of Infection (MOI)	Percentage of motoneurons successfully transfected
0.25	23.6
0.5	44.0
0.75	48.8
1	60.8
2.5	69.0
5	77.8

Figure 6.6 – Ablation of mutant SOD1 protein by siRNA-expressing EIAV vectors

Following transfection with either siRNA targeted to mutant SOD1, or an empty vector, cultures were processed for protein extraction and western blot analysis. An example of a typical western blot is shown in **A**, where the levels of mutant SOD1 protein were measured in mixed ventral horn cultures, either untransfected, or transfected with either an empty vector or shRNA. β-actin protein levels were also calculated to correct for loading. The bar chart (**B**) quantifies the ablation of mutant SOD1 protein by the shRNA-expressing lentiviral vectors. It can be seen that transfection with a lentivirus expressing an empty vector did not reduce mutant SOD1 protein levels. However, siRNA targeted to mutant SOD1, ablated protein levels by approximately 70%. Values are the mean of 3 experiments ± standard error of the mean. * $p < 0.05$.

A

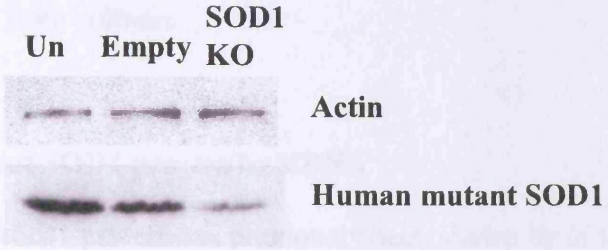
Un
Empty
SOD1 KO
Actin
Human mutant SOD1

B

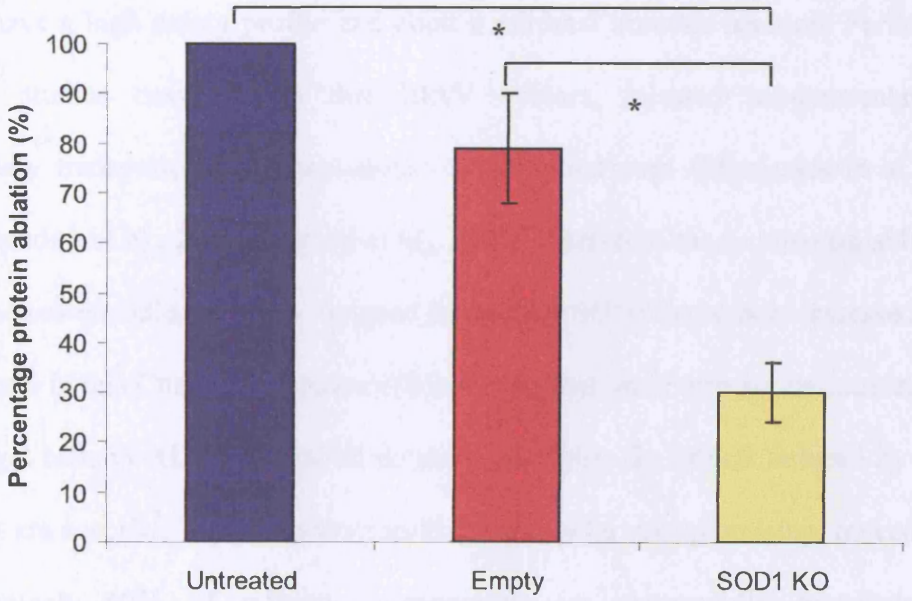
Percentage protein ablation (%)
100
90
80
70
60
50
40
30
20
10
0
*
*
Untreated
Empty
SOD1 KO

6.4. DISCUSSION

The results presented in this Chapter show that primary motoneurons can be successfully transfected by EIAV lentiviral vectors *in vitro*. Furthermore, transfection with shRNA targeted to mutant SOD1 successfully ablates the expression of $SOD1^{G93A}$ protein in mixed ventral horn cultures.

6.4.1. Ablation of mutant SOD1 protein by siRNA

The ablation of mutant SOD1 protein has previously been shown by *in vitro* transfection of siRNA targeted to specific mutant SOD1 sequences in both a neural and a HEK cell line (Ding et al., 2003; Maxwell et al., 2004). However, the data presented in this Chapter represents part of an initial investigation into the development of EIAV vectors as a method of therapeutic delivery to ALS patients (Ralph et al., 2005b). Indeed, EIAV vectors have a high safety profile and elicit a minimal immune reaction. Furthermore, previous studies have shown that EIAV vectors, injected intramuscularly are retrogradely transported to motoneurons of the spinal cord (Mazarakis et al., 2001; Martin-Rendon et al., 2001; Azzouz et al., 2004). Therefore the *in vitro* capabilities of EIAV vectors-encoding shRNA targeted to mutant SOD1 have been assessed in the experiments in this Chapter, to ensure efficient transfection of primary motoneurons, the main target cells in ALS, and also to determine whether the effects induced by siRNA treatment are specific. These *in vitro* results proved to be very promising. Indeed, using this approach, 69% of primary motoneurons are successfully transfected and approximately 70% of the mutant SOD1 protein is ablated. These results indicate that administration of siRNA can effectively silence mutant SOD1 expression in primary motoneurons *in vitro*. The percentage of mutant SOD1 protein ablated in our mixed ventral horn cultures using lentiviral vectors is equivalent to that obtained in other

studies. Raoul et al, (2005) similarly use lentiviral vectors expressing shRNA to mutant SOD1, and report a 70% protein ablation in purified motoneurons.

6.4.2. Ablation of mutant SOD1 *in vivo*

In mutant SOD1-mediated ALS, the mutant SOD1 enzyme acquires a toxic gain of function. However, it has been shown that expression of mutant SOD1 enzyme is necessary in both motoneurons and astrocytes for the disease to manifest. Indeed, transgenic mice expressing mutant SOD1 selectively in either motoneurons or astrocytes fail to develop motoneuron disease (Gong et al., 2000; Pramatarova et al., 2001; Lino et al., 2002). This implies that ablation of mutant SOD1 *in vivo* potentially may have therapeutic value in mutant SOD1-mediated ALS.

The success of siRNA-mediated ablation of mutant SOD1 *in vitro* has been extended in an *in vivo* study carried out by Dr Mimoun Azzouz and colleagues at Oxford Biomedica, to examine the ability of siRNA to silence mutant SOD1 in $SOD1^{G93A}$ mice (Ralph et al., 2005b). In this study, $SOD1^{G93A}$ mice receive an intramuscular injection of siRNA-encoding EIAV vectors into the diaphragm, intercostal, facial, tongue and hindlimb muscles at 7 days of age. Modification of the vectors from the *in vitro* study includes the replacement of the VSV-G envelope with a pseudotyped Rabies-G envelope, which allows retrograde transport of the viral vector from muscle fibres to motoneurons in the spinal cord. Indeed, over 50% of ventral horn motoneurons are transfected for more than 7 months (the duration of the study; Ralph et al., 2005b). Ablation of mutant SOD1 protein (40% ablation after 2 weeks) exerts significant neuroprotective effects in $SOD1^{G93A}$ mice, in which disease onset is delayed by 115% and survival extended by 77% (Ralph et al., 2005b). This is the greatest extension in lifespan observed with any therapeutic manipulation in mutant SOD1 mice to date.

Indeed, it has actually been suggested that the death of the shRNA treated $SOD1^{G93A}$ mice may not have been a consequence of motoneuron degeneration, due to the significant increase in motoneuron survival at disease end-stage compared to untreated $SOD1^{G93A}$ mice (Ralph et al., 2005b). A concurrent study by Raoul et al, (2005) similarly demonstrates ablation of mutant SOD1 in $SOD1^{G93A}$ mice via bilateral intraspinal injection of an HIV-derived lentiviral vector encoding siRNA to mutant SOD1. 15 days post-injection, mutant SOD1 protein levels are reduced by 52% and this translates to a 20% delay in disease onset, with significant neuroprotection and preservation of motor function. This method results in the transfection of both motoneurons and glial cells (Raoul et al., 2005), whereas the retrograde transfer of EIAV vectors only transfects motoneurons (Ralph et al., 2005b). Potentially therefore, modification of EIAV vectors to also infect non-neuronal cells might exert further beneficial effects. Intramuscular injection of $SOD1^{G93A}$ mice with AAV-expressing siRNA, shown in a subsequent study, similarly ablates mutant SOD1 protein in spinal motoneurons and preserves motor function (Miller et al., 2005).

6.4.3. Potential relevance to the clinical situation

The development of a viral vector system that can be injected intramuscularly to apply treatment to motoneurons in the spinal cord may be a significant advance in the development of therapies for ALS. Indeed, EIAV vectors pseudotyped with a Rabies-G envelope can specifically target motoneurons innervating the injected muscles and they can induce stable, efficient and long-term expression of the transgene in motoneurons and muscle fibres (Mitrophanous et al., 1999; Mazarakis et al., 2001; Azzouz et al., 2004; Ralph et al., 2005b). A study by Kaspar et al, (2003) highlights the importance of retrograde transport of the viral vector to the motoneurons. Expression of IGF-1 in motoneurons and muscle fibres following intramuscular injection extends lifespan of

$SOD1^{G93A}$ mice by 22%, whereas IGF-1 expression localised only to muscle fibres extends lifespan by only 7% (Kaspar et al., 2003). Furthermore, an intramuscular injection would be significantly less risky than an intraspinal injection. The ability to target selective neuronal populations will also reduce the risk of adverse side effects due to non-specific drug application (Ralph et al., 2005b). Interestingly, EIAV vectors encoding VEGF are currently in clinical development for the treatment of ALS (Ralph et al., 2005b). However, there are several hurdles to overcome before siRNA targeting mutant SOD1 can be used in patients. For example, over 100 mutations are known to exist in the SOD1 gene, therefore to provide a cost effective strategy, an siRNA targeted to both mutant SOD1 and endogenous SOD1 would probably be necessary to ensure ablation of all mutant forms of SOD1. However, the detrimental effects of ablating endogenous SOD1 are unknown in patients, although no phenotype is evident in mice (Reaume et al., 1996). Indeed, it may be necessary to incorporate a replacement endogenous SOD1 transgene in the same therapy (Ralph et al., 2005b).

6.5. CONCLUSION

In this Chapter, the successful transfection of primary motoneurons *in vitro* has been shown with an EIAV lentiviral vector. Furthermore, the transfection of an EIAV vector encoding shRNA targeted to mutant SOD1 significantly ablates the mutant $SOD1^{G93A}$ protein in mixed ventral horn cultures. This study has since been extended in an *in vivo* study, which demonstrates that ablation of the $SOD1^{G93A}$ protein significantly delays disease onset and extends the survival of $SOD1^{G93A}$ mice by 77% (Ralph et al., 2005b). Potentially, this therapy may prove to be suitable for use in ALS patients.

CHAPTER 7

GENERAL DISCUSSION

7.1. Aims of this Thesis

The aim of the experiments described in this Thesis using both *in vitro* and *in vivo* models, was to investigate mechanisms that may play a role in the disease pathogenesis of ALS and to evaluate potential neuroprotective agents. Indeed, in **Chapter 3**, a co-culture model of spinal cord motoneurons and astrocytes was developed to investigate the role of astrocytes in ALS. Confocal fluorescence microscopy was used to study the influence of expression of mutant SOD1 in astrocytes on the resting cellular properties of motoneurons. Furthermore, the effect of mutant SOD1 expression on the cellular response of motoneurons to excitotoxic conditions was also explored.

Currently, the only available therapy for ALS is riluzole, an anti-excitotoxic agent. However, riluzole extends patient lifespan by only 2-4 months, and so the development of alterative and more effective therapies is essential. Cannabinoids have been shown to exhibit anti-excitotoxic, anti-inflammatory and anti-oxidant actions, all of which are neuroprotective mechanisms that may have relevance to the treatment of ALS. This suggests that cannabinoids may exert greater benefits in ALS than therapies that target excitotoxicity alone. Therefore in **Chapter 4**, the neuroprotective effects of WIN55,212-2, a synthetic cannabinoid, were evaluated in the $SOD1^{G93A}$ mouse model of ALS. In **Chapter 5**, the endocannabinoid system was genetically augmented to establish whether this would have a greater impact on disease than pharmacological treatment. Therefore $SOD1^{G93A}$ mice were bred with mice in which the endogenous Faah enzyme, which is responsible for the hydrolysis of the endocannabinoid anandamide (AEA), was genetically ablated thereby increasing AEA levels. In addition, in an attempt to elucidate the mechanism of action of cannabinoids, $SOD1^{G93A}$ mice were also bred with mice lacking the CB_1 receptor in **Chapter 5**. The consequences of

these pharmacological and genetic manipulations were assessed in $SOD1^{G93A}$ mice in terms of muscle function and motoneuron survival in addition to lifespan.

The potential of lentiviral vectors to deliver therapeutic agents to motoneurons was investigated in **Chapter 6**, in collaboration with colleagues from Oxford Biomedica. The experiments described in this Chapter were designed to test the ability of EIAV vectors to transfect motoneurons. Furthermore, the ability of siRNA to ablate mutant SOD1 protein in primary $SOD1^{G93A}$ motoneurons was investigated. These experiments formed the basis of a study undertaken at Oxford Biomedica to investigate the ability of these vectors to ablate mutant SOD1 expression *in vivo* in $SOD1^{G93A}$ mice. Furthermore, the consequences of mutant SOD1 ablation were investigated on disease progression and lifespan in $SOD1^{G93A}$ mice.

7.2. Does the expression of mutant SOD1 in astrocytes influence the cellular properties of motoneurons?

There is increasing evidence that suggests that ALS is a non-cell autonomous disorder. In contrast to the ubiquitous expression of mutant SOD1, selective expression of mutant SOD1 in either astrocytes or motoneurons alone does not result in motoneuron degeneration in transgenic mice (Gong et al., 2000; Pramatarova et al., 2001; Lino et al., 2001). Therefore, in **Chapter 3** the effect of mutant SOD1 expression in astrocytes was investigated on both the basal cellular properties of motoneurons and their response to excitotoxic stimulation in an *in vitro* co-culture model.

Under basal conditions, the expression of mutant SOD1 protein in spinal cord astrocytes induced impairment of the electron transport chain in co-cultured motoneurons. This defect in combination with an elevation in mitochondrial calcium loading at rest,

induced by the expression of mutant SOD1 in either motoneurons or astrocytes, stimulated depolarisation of mitochondria in the co-cultured motoneurons. Therefore, the presence of mutant SOD1-expressing astrocytes was sufficient to significantly alter the cellular homeostasis of motoneurons under basal conditions.

In response to acute excitotoxic stimulation, the influence of mutant SOD1-expressing astrocytes on motoneurons was less clear. Indeed, cultures expressing mutant SOD1 protein were more vulnerable to excitotoxicity, in terms of mitochondrial depolarisation and superoxide generation. However, this effect was not specific to mutant SOD1 expression in astrocytes, and the expression of mutant SOD1 protein in motoneurons was also sufficient to induce increased susceptibility to an acute excitotoxic insult.

These results therefore suggest that mutant SOD1-expressing astrocytes induce functional deficits in mitochondria in motoneurons under basal conditions. It is possible that these defects increase the vulnerability of motoneurons to the progressive, accumulative neurotoxicity that occurs in ALS.

7.3. Are cannabinoids neuroprotective in the SOD1^{G93A} mouse model of ALS?

Cannabinoids have been shown to exert neuroprotective effects in several *in vivo* and *in vitro* models, and in **Chapter 4** their potential to protect motoneurons in SOD1^{G93A} mice was investigated. In SOD1^{G93A} mice, an up-regulation of endocannabinoids in the spinal cord occurs during disease progression and it is possible that this represents an endogenous cellular defence mechanism to protect neurons from damage. However, this was not sufficient to halt disease progression in SOD1^{G93A} mice. Therefore in order to boost this endogenous protective mechanism, SOD1^{G93A} mice were treated with WIN55,212-2, a synthetic CB_1 and CB_2 receptor agonist, in **Chapter 4**.

The results of the experiments in **Chapter 4** demonstrated that treatment with WIN55,212-2, even after the onset of disease, prevented the decline in muscle function that occurs with disease progression. Moreover, this treatment improved motoneuron survival in $SOD1^{G93A}$ mice at 120 days of age, a relatively late stage of disease. However, despite these significant improvements observed at 120 days of age, WIN55,212-2 did not extend the lifespan of $SOD1^{G93A}$ mice. Cannabinoids are known to have anti-excitotoxic actions, via activation of the CB_1 receptor or putative 'CB_3' receptor, anti-inflammatory actions via the CB_2 receptor, as well as receptor-independent antioxidant actions. It is likely that the neuroprotective actions of WIN55,212-2 observed in the study presented in **Chapter 4** are exerted through activation of CB_1 or CB_2 receptors, since WIN55,212-2 does not exert antioxidant actions (Hampson et al., 1998).

7.4. Does enhancement of the endocannabinoid system exert neuroprotection in $SOD1^{G93A}$ mice?

In the experiments described in **Chapter 4**, the endocannabinoid system was augmented by pharmacological manipulation. However, despite significant improvements in disease signs, WIN55,212-2 did not increase the lifespan of $SOD1^{G93A}$ mice. Therefore in **Chapter 5** the endocannabinoid system was augmented by genetic ablation of the Faah enzyme to establish whether this would have a greater impact on disease than pharmacological treatment. The Faah enzyme is responsible for the hydrolysis of the endocannabinoid AEA. Therefore mice in which the *Faah* enzyme has been ablated have a 10-15 fold increase in AEA levels in the CNS. Therefore in **Chapter 5**, $SOD1^{G93A}$ mice were crossed with Faah knock-out mice and the effects of the consequential ablation of Faah on $SOD1^{G93A}$ mice was investigated at 90 days of age, an early symptomatic stage of disease.

Ablation of Faah had significant beneficial effects in SOD1^{G93A} mice. Indeed, at 90 days SOD1.*Faah* -/- mice were almost indistinguishable from WT mice in terms of muscle function and motoneuron survival. However, as observed following pharmacological enhancement of the endocannabinoid system, ablation of the Faah enzyme did not extend the lifespan of SOD1^{G93A} mice.

Therefore, the results of **Chapters 4 and 5** together show that enhancement of the endocannabinoid system has neuroprotective effects in SOD1^{G93A} mice, and may indeed significantly improve the quality of life of these mice. This may therefore prove to be a valuable therapy in ALS patients. However, it appears that cannabinoid treatment is most effective at the early symptomatic stages of disease and therefore may have greater therapeutic effects if used in combination with agents that act on mechanisms active during later stages of the disease such as heat shock protein co-inducers (Kieran et al., 2004) or glutamate inhibitors (Canton et al., 2001; Van Damme et al., 2003).

7.5. Are the neuroprotective effects of cannabinoids in SOD1^{G93A} mice mediated through the CB_1 receptor?

The neuroprotective effects of pharmacological and genetic augmentation of the endocannabinoid system are likely to be mediated primarily through CB_1 or CB_2 receptors. To investigate this neuroprotective effect further, in **Chapter 5** the effects of breeding SOD1^{G93A} mice with mice in which the CB_1 receptor had been ablated, were examined. Activation of the CB_1 receptor can exert anti-excitotoxic actions via inhibition of the presynaptic release of glutamate and also by reducing postsynaptic calcium influx via an inhibition of voltage-gated N- and P-/Q- type calcium channels. Therefore, it was proposed that this mechanism would significantly contribute to the

neuroprotective effects of cannabinoids in $SOD1^{G93A}$ mice, so that in SOD1.*Cnr1* -/- mice, an acceleration in disease might be predicted.

Since it was possible that disease progression would be much more rapid in these mice the effects of ablating the CB_1 receptor in $SOD1^{G93A}$ mice were assessed at 90 days of age, usually an early symptomatic stage of disease. Surprisingly, ablation of the CB_1 receptor had no significant effect on disease progression in $SOD1^{G93A}$ mice at this stage. Indeed, SOD1.*Cnr1*-/- mice did not differ significantly from $SOD1^{G93A}$ mice in terms of muscle function or motoneuron survival at 90 days of age. Moreover, despite the lack of improvement in disease signs at 90 days of age, ablation of the CB_1 receptor significantly extended the survival of $SOD1^{G93A}$ mice, increasing lifespan by 13%.

These results suggest that activation of the CB_1 receptor may actually exert deleterious effects in $SOD1^{G93A}$ mice. Therefore, inhibition of the CB_1 receptor may have beneficial effects in this model. Furthermore, these results also suggest that the neuroprotection exerted by WIN55,212-2 and Faah enzyme ablation may not be mediated via activation of the CB_1 receptor and suggest a role for CB_2 receptor activation in mediating the observed neuroprotective effects. Activation of CB_2 receptors, located on microglia, is known to reduce microglial activation. Thus, the pharmacological targeting of the CB_2 receptor may be a valid approach to reduce inflammation. Therefore, the results of **Chapter 5** identify the CB_2 receptor as a potential therapeutic target in ALS.

7.6. Are lentiviral vectors encoding siRNA targeted to mutant SOD1 able to successfully ablate human mutant SOD1 protein *in vitro*?

In mutant SOD1-mediated ALS, the mutant SOD1 enzyme acquires a toxic gain of function, therefore ablation of mutant SOD1 may have therapeutic value in ALS. To

investigate this, a collaborative project was initiated with Dr Mimoun Azzouz and colleagues at Oxford Biomedica. As described in **Chapter 6**, the ability of EIAV vectors to successfully transfect motoneurons *in vitro* was first evaluated. Furthermore, EIAV vectors encoding siRNA targeted to mutant SOD1 were then tested for their ability to ablate mutant SOD1 *in vitro*.

The results described in **Chapter 6** show that 69% of primary motoneurons were successfully transfected with EIAV vectors. Furthermore, siRNA targeted to mutant SOD1 successfully ablated mutant SOD1 protein, to 30% of the original levels. The success of these *in vitro* experiments subsequently initiated an *in vivo* study at Oxford Biomedica to investigate the effect of ablation of mutant SOD1 in $SOD1^{G93A}$ mice. This study showed that ablation of mutant SOD1 *in vivo* increased motoneuron survival and extended the lifespan of $SOD1^{G93A}$ mice by 77% (Ralph et al., 2005b).

7.7. Conclusions

In summary, the results from this Thesis suggest that:

i) Mutant SOD1 expression in astrocytes has a significant influence on the mitochondrial function of motoneurons, suggesting that astrocytes play a significant role in motoneuron degeneration in ALS.

ii) Enhancement of the endocannabinoid system, either by pharmacological or genetic manipulation, can delay the disease-associated decline in muscle function and motoneuron survival, therefore potentially improving quality of life.

iii) Blockade of the CB_1 receptor, or stimulation of the CB_2 receptor may have significant therapeutic benefit in ALS

iv) Viral-mediated delivery of therapeutic agents may obviate the need for repeated treatments and minimise side effects by targeting specific neuronal populations. Furthermore, the ablation of mutant SOD1 using siRNA technology represents a novel therapy for the treatment of ALS.

These results highlight the role of non-neuronal cells in ALS pathogenesis and suggest that targeting of both astrocytes and microglia may be beneficial as a therapeutic approach in ALS.

REFERENCES

Abe, K., Pan, L. H., Watanabe, M., Konno, H., Kato, T., & Itoyama, Y. (1997). Upregulation of protein-tyrosine nitration in the anterior horn cells of amyotrophic lateral sclerosis. *Neurol.Res.* **19**, 124-128.

Abood, M. E., Rizvi, G., Sallapudi, N., & McAllister, S. D. (2001). Activation of the CB1 cannabinoid receptor protects cultured mouse spinal neurons against excitotoxicity. *Neurosci.Lett.* **309**, 197-201.

Acquas, E., Pisanu, A., Marrocu, P., & Di Chiara, G. (2000). Cannabinoid CB(1) receptor agonists increase rat cortical and hippocampal acetylcholine release in vivo. *Eur.J.Pharmacol.* **401**, 179-185.

Acsadi, G., Anguelov, R. A., Yang, H., Toth, G., Thomas, R., Jani, A., Wang, Y., Ianakova, E., Mohammad, S., Lewis, R. A., & Shy, M. E. (2002). Increased survival and function of SOD1 mice after glial cell-derived neurotrophic factor gene therapy. *Hum.Gene Ther.* **13**, 1047-1059.

Al Chalabi, A., Andersen, P. M., Nilsson, P., Chioza, B., Andersson, J. L., Russ, C., Shaw, C. E., Powell, J. F., & Leigh, P. N. (1999). Deletions of the heavy neurofilament subunit tail in amyotrophic lateral sclerosis. *Hum.Mol.Genet.* **8**, 157-164.

Albrecht, P. J., Dahl, J. P., Stoltzfus, O. K., Levenson, R., & Levison, S. W. (2002). Ciliary neurotrophic factor activates spinal cord astrocytes, stimulating their production and release of fibroblast growth factor-2, to increase motor neuron survival. *Exp.Neurol.* **173**, 46-62.

Alexianu, M. E., Ho, B. K., Mohamed, A. H., La, B., V, Smith, R. G., & Appel, S. H. (1994). The role of calcium-binding proteins in selective motoneuron vulnerability in amyotrophic lateral sclerosis. *Ann.Neurol.* **36**, 846-858.

Alexianu, M. E., Kozovska, M., & Appel, S. H. (2001). Immune reactivity in a mouse model of familial ALS correlates with disease progression. *Neurology* **57**, 1282-1289.

Allen, E. R. & Pepe, F. A. (1965). Ultrastructure of developing muscle cells in the chick embryo. *Am.J.Anat.* **116**, 115-147.

Almer, G., Vukosavic, S., Romero, N., & Przedborski, S. (1999). Inducible nitric oxide synthase up-regulation in a transgenic mouse model of familial amyotrophic lateral sclerosis. *J.Neurochem.* **72**, 2415-2425.

Almer, G., Guegan, C., Teismann, P., Naini, A., Rosoklija, G., Hays, A. P., Chen, C., & Przedborski, S. (2001). Increased expression of the pro-inflammatory enzyme cyclooxygenase-2 in amyotrophic lateral sclerosis. *Ann.Neurol.* **49**, 176-185.

Ameri, A., Wilhelm, A., & Simmet, T. (1999). Effects of the endogeneous cannabinoid, anandamide, on neuronal activity in rat hippocampal slices. *Br.J.Pharmacol.* **126**,.1831-1839.

Anderson, M. J. & Cohen, M. W. (1977). Nerve-induced and spontaneous redistribution of acetylcholine receptors on cultured muscle cells. *J.Physiol* **268**, 757-773.

Aoki, M. Lin, C. L., Rothstein, J. D., Geller, B. A., Hosler, B. A., Munsat, T. L., Horvitz, H. R. & Brown, R. H. Jr. (1998). Mutations in the glutamate transporter EAAT2 gene do not cause abnormal EAAT2 transcripts in amyotrophic lateral sclerosis. *Ann. Neurol.*, **43(5)**, 645-653.

Araque, A., Parpura, V., Sanzgiri, R. P., & Haydon, P. G. (1998). Glutamate-dependent astrocyte modulation of synaptic transmission between cultured hippocampal neurons. *Eur.J.Neurosci.* **10**, 2129-2142.

Araque, A., Sanzgiri, R. P., Parpura, V., & Haydon, P. G. (1998). Calcium elevation in astrocytes causes an NMDA receptor-dependent increase in the frequency of miniature synaptic currents in cultured hippocampal neurons. *J.Neurosci.* **18**, 6822-6829.

Araque, A., Parpura, V., Sanzgiri, R. P., & Haydon, P. G. (1999). Tripartite synapses: glia, the unacknowledged partner. *Trends Neurosci.* **22**, 208-215.

Araque, A., Sanzgiri, R. P., Parpura, V., & Haydon, P. G. (1999). Astrocyte-induced modulation of synaptic transmission. *Can.J.Physiol Pharmacol.* **77**, 699-706.

Araque, A., Carmignoto, G., & Haydon, P. G. (2001). Dynamic signaling between astrocytes and neurons. *Annu.Rev.Physiol* **63**, 795-813.

Arevalo-Martin, A., Vela, J. M., Molina-Holgado, E., Borrell, J., & Guaza, C. (2003). Therapeutic action of cannabinoids in a murine model of multiple sclerosis. *J.Neurosci.* **23**, 2511-2516.

Atkin, J. D., Scott, R. L., West, J. M., Lopes, E., Quah, A. K., & Cheema, S. S. (2005). Properties of slow- and fast-twitch muscle fibres in a mouse model of amyotrophic lateral sclerosis. *Neuromuscul.Disord.* **15**, 377-388.

Auclair, N., Otani, S., Soubrie, P., & Crepel, F. (2000). Cannabinoids modulate synaptic strength and plasticity at glutamatergic synapses of rat prefrontal cortex pyramidal neurons. *J.Neurophysiol.* **83**, 3287-3293.

Azad, S. C., Monory, K., Marsicano, G., Cravatt, B. F., Lutz, B., Zieglgansberger, W., & Rammes, G. (2004). Circuitry for associative plasticity in the amygdala involves endocannabinoid signaling. *J.Neurosci.* **24**, 9953-9961.

Azzouz, M., Poindron, P., Guettier, S., Leclerc, N., Andres, C., Warter, J. M., & Borg, J. (2000). Prevention of mutant SOD1 motoneuron degeneration by copper chelators in vitro. *J.Neurobiol.* **42**, 49-55.

Azzouz, M., Ralph, G. S., Storkebaum, E., Walmsley, L. E., Mitrophanous, K. A., Kingsman, S. M., Carmeliet, P., & Mazarakis, N. D. (2004). VEGF delivery with retrogradely transported lentivector prolongs survival in a mouse ALS model. *Nature* **429**, 413-417.

Baker, D., Pryce, G., Croxford, J. L., Brown, P., Pertwee, R. G., Huffman, J. W., & Layward, L. (2000). Cannabinoids control spasticity and tremor in a multiple sclerosis model. *Nature* **404**, 84-87.

Baker, D., Pryce, G., Croxford, J. L., Brown, P., Pertwee, R. G., Makriyannis, A., Khanolkar, A., Layward, L., Fezza, F., Bisogno, T., & Di, Marzo, V (2001).

Endocannabinoids control spasticity in a multiple sclerosis model. *FASEB J.* **15**, 300-302.

Baker, D., Pryce, G., Giovannoni, G., & Thompson, A. J. (2003). The therapeutic potential of cannabis. *Lancet Neurol.* **2**, 291-298.

Bal-Price, A. & Brown, G. C. (2001). Inflammatory neurodegeneration mediated by nitric oxide from activated glia-inhibiting neuronal respiration, causing glutamate release and excitotoxicity. *J.Neurosci.* **21**, 6480-6491.

Balice-Gordon, R. J. & Thompson, W. J. (1988). Synaptic rearrangements and alterations in motor unit properties in neonatal rat extensor digitorum longus muscle. *J.Physiol* **398**, 191-210.

Banks, G. B. & Noakes, P. G. (2002). Elucidating the molecular mechanisms that underlie the target control of motoneuron death. *Int.J.Dev.Biol.* **46**, 551-558.

Bar-Peled, O., O'Brien, R. J., Morrison, J. H., & Rothstein, J. D. (1999). Cultured motor neurons possess calcium-permeable AMPA/kainate receptors. *Neuroreport* **10**, 855-859.

Barbeito, L. H., Pehar, M., Cassina, P., Vargas, M. R., Peluffo, H., Viera, L., Estevez, A. G., & Beckman, J. S. (2004). A role for astrocytes in motor neuron loss in amyotrophic lateral sclerosis. *Brain Res.Brain Res.Rev.* **47**, 263-274.

Bash, R., Rubovitch, V., Gafni, M., & Sarne, Y. (2003). The stimulatory effect of cannabinoids on calcium uptake is mediated by Gs GTP-binding proteins and cAMP formation. *Neurosignals.* **12**, 39-44.

Batulan, Z., Shinder, G. A., Minotti, S., He, B. P., Doroudchi, M. M., Nalbantoglu, J., Strong, M. J., & Durham, H. D. (2003). High threshold for induction of the stress response in motor neurons is associated with failure to activate HSF1. *J.Neurosci.* **23**, 5789-5798.

Beal, M. F., Ferrante, R. J., Browne, S. E., Matthews, R. T., Kowall, N. W., & Brown, R. H., Jr. (1997). Increased 3-nitrotyrosine in both sporadic and familial amyotrophic lateral sclerosis. *Ann.Neurol.* **42**, 644-654.

Beaulieu, J. M., Nguyen, M. D., & Julien, J. P. (1999). Late onset of motor neurons in mice overexpressing wild-type peripherin. *J.Cell Biol.* **147**, 531-544.

Beckman, J. S., Carson, M., Smith, C. D., & Koppenol, W. H. (1993). ALS, SOD and peroxynitrite. *Nature* **364**, 584.

Beers, D. R., Ho, B. K., Siklos, L., Alexianu, M. E., Mosier, D. R., Mohamed, A. H., Otsuka, Y., Kozovska, M. E., McAlhany, R. E., Smith, R. G., & Appel, S. H. (2001). Parvalbumin overexpression alters immune-mediated increases in intracellular calcium, and delays disease onset in a transgenic model of familial amyotrophic lateral sclerosis. *J.Neurochem.* **79**, 499-509.

Beltramo, M., Stella, N., Calignano, A., Lin, S. Y., Makriyannis, A., & Piomelli, D. (1997). Functional role of high-affinity anandamide transport, as revealed by selective inhibition. *Science* **277**, 1094-1097.

Ben Shabat, S., Fride, E., Sheskin, T., Tamiri, T., Rhee, M. H., Vogel, Z., Bisogno, T., De Petrocellis, L., Di Marzo, V., & Mechoulam, R. (1998). An entourage effect: inactive endogenous fatty acid glycerol esters enhance 2-arachidonoyl-glycerol cannabinoid activity. *Eur.J.Pharmacol.* **353**, 23-31.

Bendotti, C., Calvaresi, N., Chiveri, L., Prelle, A., Moggio, M., Braga, M., Silani, V., & De Biasi, S. (2001). Early vacuolization and mitochondrial damage in motor neurons of FALS mice are not associated with apoptosis or with changes in cytochrome oxidase histochemical reactivity. *J.Neurol.Sci.* **191**, 25-33.

Benito, C., Nunez, E., Tolon, R. M., Carrier, E. J., Rabano, A., Hillard, C. J., & Romero, J. (2003). Cannabinoid CB2 receptors and fatty acid amide hydrolase are selectively overexpressed in neuritic plaque-associated glia in Alzheimer's disease brains. *J.Neurosci.* **23**, 11136-11141.

Bensimon, G., Lacomblez, L., & Meininger, V. (1994). A controlled trial of riluzole in amyotrophic lateral sclerosis. ALS/Riluzole Study Group. *N.Engl.J.Med.* **330**, 585-591.

Bergeron, C., Beric-Maskarel, K., Muntasser, S., Weyer, L., Somerville, M. J., & Percy, M. E. (1994). Neurofilament light and polyadenylated mRNA levels are decreased in amyotrophic lateral sclerosis motor neurons. *J.Neuropathol.Exp.Neurol.* **53**, 221-230.

Berman, J. S., Symonds, C., & Birch, R. (2004). Efficacy of two cannabis based medicinal extracts for relief of central neuropathic pain from brachial plexus avulsion: results of a randomised controlled trial. *Pain* **112**, 299-306.

Bidaut-Russell, M., Devane, W. A., & Howlett, A. C. (1990). Cannabinoid receptors and modulation of cyclic AMP accumulation in the rat brain. *J.Neurochem.* **55**, 21-26.

Bisogno, T., Howell, F., Williams, G., Minassi, A., Cascio, M. G., Ligresti, A., Matias, I., Schiano-Moriello, A., Paul, P., Williams, E. J., Gangadharan, U., Hobbs, C., Di, Marzo, V., & Doherty, P. (2003). Cloning of the first sn1-DAG lipases points to the spatial and temporal regulation of endocannabinoid signaling in the brain. *J.Cell Biol.* **163**, 463-468.

Block, F., Tondar, A., Schmidt, W., & Schwarz, M. (1997). Delayed treatment with rolipram protects against neuronal damage following global ischemia in rats. *Neuroreport* **8**, 3829-3832.

Bolanos, J. P., Peuchen, S., Heales, S. J., Land, J. M., & Clark, J. B. (1994). Nitric oxide-mediated inhibition of the mitochondrial respiratory chain in cultured astrocytes. *J.Neurochem.* **63**, 910-916.

Borchelt, D. R., Lee, M. K., Slunt, H. S., Guarnieri, M., Xu, Z. S., Wong, P. C., Brown, R. H. Jr., Price, D. L., Sisodia, S. S. & Cleveland, D. W. (1994). Superoxide dismutase 1 with mutations linked to familial amyotrophic lateral sclerosis possesses significant activity. *Proc. Natl. Acad. Sci.* **91 (17)**, 8292 - 8296.

Borchelt, D. R., Wong, P. C., Becher, M. W., Pardo, C. A., Lee, M. K., Xu, Z. S., Thinakaran, G., Jenkins, N. A., Copeland, N. G., Sisodia, S. S., Cleveland, D. W., Price, D. L., & Hoffman, P. N. (1998). Axonal transport of mutant superoxide dismutase 1 and focal axonal abnormalities in the proximal axons of transgenic mice. *Neurobiol.Dis.* **5**, 27-35.

Borthwick, G. M., Johnson, M. A., Ince, P. G., Shaw, P. J., & Turnbull, D. M. (1999). Mitochondrial enzyme activity in amyotrophic lateral sclerosis: implications for the role of mitochondria in neuronal cell death. *Ann.Neurol.* **46**, 787-790.

Bouaboula, M., Poinot-Chazel, C., Bourrie, B., Canat, X., Calandra, B., Rinaldi-Carmona, M., Le Fur, G., & Casellas, P. (1995). Activation of mitogen-activated protein kinases by stimulation of the central cannabinoid receptor CB1. *Biochem.J.* **312 (Pt 2)**, 637-641.

Bouaboula, M., Bourrie, B., Rinaldi-Carmona, M., Shire, D., Le Fur, G., & Casellas, P. (1995). Stimulation of cannabinoid receptor CB1 induces krox-24 expression in human astrocytoma cells. *J.Biol.Chem.* **270**, 13973-13980.

Breivogel, C. S., Griffin, G., Di Marzo, V., & Martin, B. R. (2001). Evidence for a new G protein-coupled cannabinoid receptor in mouse brain. *Mol.Pharmacol.* **60**, 155-163.

Briscoe, J. & Ericson, J. (1999). The specification of neuronal identity by graded Sonic Hedgehog signalling. *Semin.Cell Dev.Biol.* **10**, 353-362.

Briscoe, J., Pierani, A., Jessell, T. M., & Ericson, J. (2000). A homeodomain protein code specifies progenitor cell identity and neuronal fate in the ventral neural tube. *Cell* **101**, 435-445.

Briscoe, J. & Ericson, J. (2001). Specification of neuronal fates in the ventral neural tube. *Curr.Opin.Neurobiol.* **11**, 43-49.

Brookes, P. S., Land, J. M., Clark, J. B., & Heales, S. J. (1998). Peroxynitrite and brain mitochondria: evidence for increased proton leak. *J.Neurochem.* **70**, 2195-2202.

Brown, G. C. & Cooper, C. E. (1994). Nanomolar concentrations of nitric oxide reversibly inhibit synaptosomal respiration by competing with oxygen at cytochrome oxidase. *FEBS Lett.* **356**, 295-298.

Brown, M. C., Jansen, J. K., & Van Essen, D. (1976). Polyneuronal innervation of skeletal muscle in new-born rats and its elimination during maturation. *J.Physiol* **261**, 387-422.

Bruening, W., Roy, J., Giasson, B., Figlewicz, D. A., Mushynski, W. E., & Durham, H. D. (1999). Up-regulation of protein chaperones preserves viability of cells expressing toxic Cu/Zn-superoxide dismutase mutants associated with amyotrophic lateral sclerosis. *J.Neurochem.* **72**, 693-699.

Bruijn, L. I., Becher, M. W., Lee, M. K., Anderson, K. L., Jenkins, N. A., Copeland, N. G., Sisodia, S. S., Rothstein, J. D., Borchelt, D. R., Price, D. L., & Cleveland, D. W. (1997). ALS-linked SOD1 mutant G85R mediates damage to astrocytes and promotes rapidly progressive disease with SOD1-containing inclusions. *Neuron* **18**, 327-338.

Bruijn, L. I., Beal, M. F., Becher, M. W., Schulz, J. B., Wong, P. C., Price, D. L., & Cleveland, D. W. (1997). Elevated free nitrotyrosine levels, but not protein-bound nitrotyrosine or hydroxyl radicals, throughout amyotrophic lateral sclerosis (ALS)-like disease implicate tyrosine nitration as an aberrant in vivo property of one familial ALS-linked superoxide dismutase 1 mutant. *Proc.Natl.Acad.Sci.U.S.A* **94**, 7606-7611.

Bruijn, L. I., Houseweart, M. K., Kato, S., Anderson, K. L., Anderson, S. D., Ohama, E., Reaume, A. G., Scott, R. W., & Cleveland, D. W. (1998). Aggregation and motor neuron toxicity of an ALS-linked SOD1 mutant independent from wild-type SOD1. *Science* **281**, 1851-1854.

Bruijn, L. I., Miller, T. M., & Cleveland, D. W. (2004). Unraveling the mechanisms involved in motor neuron degeneration in ALS. *Annu.Rev.Neurosci.* **27**, 723-749.

Brummelkamp, T. R., Bernards, R., & Agami, R. (2002). A system for stable expression of short interfering RNAs in mammalian cells. *Science* **296**, 550-553.

Bruner, G. & Murphy, S. (1993). Purinergic P2Y receptors on astrocytes are directly coupled to phospholipase A2. *Glia* **7**, 219-224.

Brzin, M., Sketelj, J., Tennyson, V. M., Kiauta, T., & Budininkas-Schoenebeck, M. (1981). Activity, molecular forms, and cytochemistry of cholinesterases in developing rat diaphragm. *Muscle Nerve* **4**, 505-513.

Buckingham, M., Bajard, L., Chang, T., Daubas, P., Hadchouel, J., Meilhac, S., Montarras, D., Rocancourt, D., & Relaix, F. (2003). The formation of skeletal muscle: from somite to limb. *J.Anat.* **202**, 59-68.

Buckley, N. E., McCoy, K. L., Mezey, E., Bonner, T., Zimmer, A., Felder, C. C., Glass, M., & Zimmer, A. (2000). Immunomodulation by cannabinoids is absent in mice deficient for the cannabinoid CB(2) receptor. *Eur.J.Pharmacol.* **396**, 141-149.

Buffelli, M., Burgess, R. W., Feng, G., Lobe, C. G., Lichtman, J. W., & Sanes, J. R. (2003). Genetic evidence that relative synaptic efficacy biases the outcome of synaptic competition. *Nature* **424**, 430-434.

Bush, T. G., Puvanachandra, N., Horner, C. H., Polito, A., Ostenfeld, T., Svendsen, C. N., Mucke, L., Johnson, M. H., & Sofroniew, M. V. (1999). Leukocyte infiltration, neuronal degeneration, and neurite outgrowth after ablation of scar-forming, reactive astrocytes in adult transgenic mice. *Neuron* **23**, 297-308.

Cadas, H., Gaillet, S., Beltramo, M., Venance, L., & Piomelli, D. (1996). Biosynthesis of an endogenous cannabinoid precursor in neurons and its control by calcium and cAMP. *J.Neurosci.* **16**, 3934-3942.

Cadas, H., di Tomaso, E., & Piomelli, D. (1997). Occurrence and biosynthesis of endogenous cannabinoid precursor, N-arachidonoyl phosphatidylethanolamine, in rat brain. *J.Neurosci.* **17**, 1226-1242.

Cai, H., Lin, X., Xie, C., Laird, F. M., Lai, C., Wen, H., Chiang, H. C., Shim, H., Farah, M. H., Hoke, A., Price, D. L., & Wong, P. C. (2005). Loss of ALS2 function is insufficient to trigger motor neuron degeneration in knock-out mice but predisposes neurons to oxidative stress. *J.Neurosci.* **25**, 7567-7574.

Calignano, A., La Rana, G., Beltramo, M., Makriyannis, A., & Piomelli, D. (1997). Potentiation of anandamide hypotension by the transport inhibitor, AM404. *Eur.J.Pharmacol.* **337**, R1-R2.

Campagna, J. A., Prevette, D., Oppenheim, R. W., & Bixby, J. L. (1997). Target contact regulates expression of synaptotagmin genes in spinal motor neurons in vivo. *Mol.Cell Neurosci.* **8**, 377-388.

Camu, W. & Henderson, C. E. (1994). Rapid purification of embryonic rat motoneurons: an in vitro model for studying MND/ALS pathogenesis. *J.Neurol.Sci.* **124** Suppl, 73-74.

Canton, T., Pratt, J., Stutzmann, J. M., Imperato, A., & Boireau, A. (1998). Glutamate uptake is decreased tardively in the spinal cord of FALS mice. *Neuroreport* **9**, 775-778.

Canton, T., Bohme, G. A., Boireau, A., Bordier, F., Mignani, S., Jimonet, P., Jahn, G., Alavijeh, M., Stygall, J., Roberts, S., Brealey, C., Vuilhorgne, M., Debono, M. W., Le Guern, S., Laville, M., Briet, D., Roux, M., Stutzmann, J. M., & Pratt, J. (2001). RPR 119990, a novel alpha-amino-3-hydroxy-5-methyl-4-isoxazolepropionic acid antagonist: synthesis, pharmacological properties, and activity in an animal model of amyotrophic lateral sclerosis. *J.Pharmacol.Exp.Ther.* **299**, 314-322.

Carmignoto, G. (2000). Astrocyte-neurone crosstalk: variants of the same language? *Trends Pharmacol.Sci.* **21**, 373-375.

Caroni, P. & Becker, M. (1992). The downregulation of growth-associated proteins in motoneurons at the onset of synapse elimination is controlled by muscle activity and IGF1. *J.Neurosci.* **12**, 3849-3861.

Carpenter, S. (1968). Proximal axonal enlargement in motor neuron disease. *Neurology* **18**, 841-851.

Carri, M. T., Ferri, A., Battistoni, A., Famhy, L., Gabbianelli, R., Poccia, F., & Rotilio, G. (1997). Expression of a Cu,Zn superoxide dismutase typical of familial amyotrophic lateral sclerosis induces mitochondrial alteration and increase of cytosolic Ca2+ concentration in transfected neuroblastoma SH-SY5Y cells. *FEBS Lett.* **414**, 365-368.

Carriedo, S. G., Yin, H. Z., & Weiss, J. H. (1996). Motor neurons are selectively vulnerable to AMPA/kainate receptor-mediated injury in vitro. *J.Neurosci.* **16**, 4069-4079.

Carriedo, S. G., Sensi, S. L., Yin, H. Z., & Weiss, J. H. (2000). AMPA exposures induce mitochondrial Ca(2+) overload and ROS generation in spinal motor neurons in vitro. *J.Neurosci.* **20**, 240-250.

Carrier, E. J., Kearn, C. S., Barkmeier, A. J., Breese, N. M., Yang, W., Nithipatikom, K., Pfister, S. L., Campbell, W. B., & Hillard, C. J. (2004). Cultured rat microglial cells synthesize the endocannabinoid 2-arachidonylglycerol, which increases proliferation via a CB2 receptor-dependent mechanism. *Mol.Pharmacol.* **65**, 999-1007.

Casanovas, A., Olmos, G., Ribera, J., Boronat, M. A., Esquerda, J. E., & Garcia-Sevilla, J. A. (2000). Induction of reactive astrocytosis and prevention of motoneuron cell death by the I(2)-imidazoline receptor ligand LSL 60101. *Br.J.Pharmacol.* **130**, 1767-1776.

Cassina, P., Peluffo, H., Pehar, M., Martinez-Palma, L., Ressia, A., Beckman, J. S., Estevez, A. G., & Barbeito, L. (2002). Peroxynitrite triggers a phenotypic transformation in spinal cord astrocytes that induces motor neuron apoptosis. *J.Neurosci.Res.* **67**, 21-29.

Castilho, R. F., Kowaltowski, A. J., Meinicke, A. R., Bechara, E. J., & Vercesi, A. E. (1995). Permeabilization of the inner mitochondrial membrane by Ca2+ ions is stimulated by t-butyl hydroperoxide and mediated by reactive oxygen species generated by mitochondria. *Free Radic.Biol.Med.* **18**, 479-486.

Castilho, R. F., Ward, M. W., & Nicholls, D. G. (1999). Oxidative stress, mitochondrial function, and acute glutamate excitotoxicity in cultured cerebellar granule cells. *J.Neurochem.* **72**, 1394-1401.

Caulfield, M. P. & Brown, D. A. (1992). Cannabinoid receptor agonists inhibit Ca current in NG108-15 neuroblastoma cells via a pertussis toxin-sensitive mechanism. *Br.J.Pharmacol.* **106**, 231-232.

Chan, G. C., Hinds, T. R., Impey, S., & Storm, D. R. (1998). Hippocampal neurotoxicity of Delta9-tetrahydrocannabinol. *J.Neurosci.* **18**, 5322-5332.

Chemin, J., Monteil, A., Perez-Reyes, E., Nargeot, J., & Lory, P. (2001). Direct inhibition of T-type calcium channels by the endogenous cannabinoid anandamide. *EMBO J.* **20**, 7033-7040.

Chen, Y. & Buck, J. (2000). Cannabinoids protect cells from oxidative cell death: a receptor-independent mechanism. *J.Pharmacol.Exp.Ther.* **293**, 807-812.

Chen, Y., Chan, P. H., & Swanson, R. A. (2001). Astrocytes overexpressing Cu,Zn superoxide dismutase have increased resistance to oxidative injury. *Glia* **33**, 343-347.

Chen, Y. Z., Bennett, C. L., Huynh, H. M., Blair, I. P., Puls, I., Irobi, J., Dierick, I., Abel, A., Kennerson, M. L., Rabin, B. A., Nicholson, G. A., Auer-Grumbach, M., Wagner, K., De Jonghe, P., Griffin, J. W., Fischbeck, K. H., Timmerman, V., Cornblath, D. R., & Chance, P. F. (2004). DNA/RNA helicase gene mutations in a form of juvenile amyotrophic lateral sclerosis (ALS4). *Am.J.Hum.Genet.* **74**, 1128-1135.

Chiu, A. Y., Zhai, P., Dal Canto, M. C., Peters, T. M., Kwon, Y. W., Prattis, S. M., & Gurney, M. E. (1995). Age-dependent penetrance of disease in a transgenic mouse model of familial amyotrophic lateral sclerosis. *Mol.Cell Neurosci.* **6**, 349-362.

Choi, D. W. (1992). Excitotoxic cell death. *J.Neurobiol.* **23**, 1261-1276.

Chow, I. & Poo, M. M. (1985). Release of acetylcholine from embryonic neurons upon contact with muscle cell. *J.Neurosci.* **5**, 1076-1082.

Christ, B. & Brand-Saberi, B. (2002). Limb muscle development. *Int.J.Dev.Biol.* **46**, 905-914.

Cisterni, C., Henderson, C. E., Aebischer, P., Pettmann, B., & Deglon, N. (2000). Efficient gene transfer and expression of biologically active glial cell line-derived neurotrophic factor in rat motoneurons transduced wit lentiviral vectors. *J.Neurochem.* **74**, 1820-1828.

Clatterbuck, R. E., Price, D. L., & Koliatsos, V. E. (1996). Ciliary neurotrophic factor stimulates the expression of glial fibrillary acidic protein by brain astrocytes in vivo. *J.Comp Neurol.* **369**, 543-551.

Clement, A. B., Hawkins, E. G., Lichtman, A. H. & Cravatt, B. F. (2003). Increased seizure susceptibility and proconvulsant activity of anandamide in mice lacking fatty acid amide hydrolase. *J. Neurosci.* **23(9)**, 3916-3927.

Clement, A. M., Nguyen, M. D., Roberts, E. A., Garcia, M. L., Boillee, S., Rule, M., McMahon, A. P., Doucette, W., Siwek, D., Ferrante, R. J., Brown, R. H., Jr., Julien, J. P., Goldstein, L. S., & Cleveland, D. W. (2003). Wild-type nonneuronal cells extend survival of SOD1 mutant motor neurons in ALS mice. *Science* **302**, 113-117.

Cleveland, D. W. & Rothstein, J. D. (2001). From Charcot to Lou Gehrig: deciphering selective motor neuron death in ALS. *Nat.Rev.Neurosci.* **2**, 806-819.

Colamarino, S. A. & Tessier-Lavigne, M. (1995). The role of the floor plate in axon guidance. *Annu.Rev.Neurosci.* **18**, 497-529.

Collard, J. F., Cote, F., & Julien, J. P. (1995). Defective axonal transport in a transgenic mouse model of amyotrophic lateral sclerosis. *Nature* **375**, 61-64.

Comoletti, D., Muzio, V., Capobianco, A., Ravizza, T., & Mennini, T. (2001). Nitric oxide produced by non-motoneuron cells enhances rat embryonic motoneuron sensitivity to excitotoxins: comparison in mixed neuron/glia or purified cultures. *J.Neurol.Sci.* **192**, 61-69.

Condon, K., Silberstein, L., Blau, H. M., & Thompson, W. J. (1990). Differentiation of fiber types in aneural musculature of the prenatal rat hindlimb. *Dev.Biol.* **138**, 275-295.

Connold, A. L., Evers, J. V., & Vrbova, G. (1986). Effect of low calcium and protease inhibitors on synapse elimination during postnatal development in the rat soleus muscle. *Brain Res.* **393**, 99-107.

Consilvio, C., Vincent, A. M., & Feldman, E. L. (2004). Neuroinflammation, COX-2, and ALS--a dual role? *Exp.Neurol.* **187**, 1-10.

Copray, J. C., Jaarsma, D., Kust, B. M., Bruggeman, R. W., Mantingh, I., Brouwer, N., & Boddeke, H. W. (2003). Expression of the low affinity neurotrophin receptor p75 in spinal motoneurons in a transgenic mouse model for amyotrophic lateral sclerosis. *Neuroscience* **116**, 685-694.

Corbo, M. & Hays, A. P. (1992). Peripherin and neurofilament protein coexist in spinal spheroids of motor neuron disease. *J.Neuropathol.Exp.Neurol.* **51**, 531-537.

Cornell-Bell, A. H. & Finkbeiner, S. M. (1991). Ca2+ waves in astrocytes. *Cell Calcium* **12**, 185-204.

Cota, D., Marsicano, G., Tschop, M., Grubler, Y., Flachskamm, C., Schubert, M., Auer, D., Yassouridis, A., Thone-Reineke, C., Ortmann, S., Tomassoni, F., Cervino, C., Nisoli, E., Linthorst, A. C., Pasquali, R., Lutz, B., Stalla, G. K., & Pagotto, U. (2003). The endogenous cannabinoid system affects energy balance via central orexigenic drive and peripheral lipogenesis. *J.Clin.Invest* **112**, 423-431.

Cote, F., Collard, J. F., & Julien, J. P. (1993). Progressive neuronopathy in transgenic mice expressing the human neurofilament heavy gene: a mouse model of amyotrophic lateral sclerosis. *Cell* **73**, 35-46.

Couillard-Despres, S., Zhu, Q., Wong, P. C., Price, D. L., Cleveland, D. W., & Julien, J. P. (1998). Protective effect of neurofilament heavy gene overexpression in motor neuron disease induced by mutant superoxide dismutase. *Proc.Natl.Acad.Sci.U.S.A* **95**, 9626-9630.

Couillard-Despres, S., Meier, J., & Julien, J. P. (2000). Extra axonal neurofilaments do not exacerbate disease caused by mutant Cu,Zn superoxide dismutase. *Neurobiol.Dis.* **7**, 462-470.

Couplan, E., Gelly, C., Goubern, M., Fleury, C., Quesson, B., Silberberg, M., Thiaudiere, E., Mateo, P., Lonchampt, M., Levens, N., De Montrion, C., Ortmann, S., Klaus, S., Gonzalez-Barroso, M. D., Cassard-Doulcier, A. M., Ricquier, D., Bigard, A. X., Diolez, P., & Bouillaud, F. (2002). High level of uncoupling protein 1 expression in muscle of transgenic mice selectively affects muscles at rest and decreases their IIb fiber content. *J.Biol.Chem.* **277**, 43079-43088.

Cozzolino, M., Ferri, A., Ferraro, E., Rotilio, G., Cecconi, F., & Carri, M. T. (2006). Apaf1 mediates apoptosis and mitochondrial damage induced by mutant human SOD1s typical of familial amyotrophic lateral sclerosis. *Neurobiol.Dis.* **21(1)**, 69-79.

Cravatt, B. F., Prospero-Garcia, O., Siuzdak, G., Gilula, N. B., Henriksen, S. J., Boger, D. L., & Lerner, R. A. (1995). Chemical characterization of a family of brain lipids that induce sleep. *Science* **268**, 1506-1509.

Cravatt, B. F., Giang, D. K., Mayfield, S. P., Boger, D. L., Lerner, R. A., & Gilula, N. B. (1996). Molecular characterization of an enzyme that degrades neuromodulatory fatty-acid amides. *Nature* **384**, 83-87.

Cravatt, B. F., Demarest, K., Patricelli, M. P., Bracey, M. H., Giang, D. K., Martin, B. R., & Lichtman, A. H. (2001). Supersensitivity to anandamide and enhanced endogenous cannabinoid signaling in mice lacking fatty acid amide hydrolase. *Proc.Natl.Acad.Sci.U.S.A* **98**, 9371-9376.

Cravatt, B. F. & Lichtman, A. H. (2003). Fatty acid amide hydrolase: an emerging therapeutic target in the endocannabinoid system. *Curr.Opin.Chem.Biol.* **7**, 469-475.

Crow, J. P., Sampson, J. B., Zhuang, Y., Thompson, J. A., & Beckman, J. S. (1997). Decreased zinc affinity of amyotrophic lateral sclerosis-associated superoxide dismutase mutants leads to enhanced catalysis of tyrosine nitration by peroxynitrite. *J.Neurochem.* **69**, 1936-1944.

Croxford, J. L. & Miller, S. D. (2003). Immunoregulation of a viral model of multiple sclerosis using the synthetic cannabinoid R+WIN55,212. *J.Clin.Invest* **111**, 1231-1240.

Culling, C. F. A. Handbook of Histopathological Techniques 2nd edition. 362-363. 1963. London, Butterworths.

D'Ambra, T. E., Estep, K. G., Bell, M. R., Eissenstat, M. A., Josef, K. A., Ward, S. J., Haycock, D. A., Baizman, E. R., Casiano, F. M., Beglin, N. C., & . (1992). Conformationally restrained analogues of pravadoline: nanomolar potent, enantioselective, (aminoalkyl)indole agonists of the cannabinoid receptor. *J.Med.Chem.* **35**, 124-135.

Dai, Z. & Peng, H. B. (1993). Elevation in presynaptic Ca2+ level accompanying initial nerve-muscle contact in tissue culture. *Neuron* **10**, 827-837.

Dal Canto, M. C. & Gurney, M. E. (1994). Development of central nervous system pathology in a murine transgenic model of human amyotrophic lateral sclerosis. *Am.J.Pathol.* **145**, 1271-1279.

Dal Canto, M. C. & Gurney, M. E. (1995). Neuropathological changes in two lines of mice carrying a transgene for mutant human Cu,Zn SOD, and in mice overexpressing wild type human SOD: a model of familial amyotrophic lateral sclerosis (FALS). *Brain Res.* **676**, 25-40.

Darman, J., Backovic, S., Dike, S., Maragakis, N. J., Krishnan, C., Rothstein, J. D., Irani, D. N., & Kerr, D. A. (2004). Viral-induced spinal motor neuron death is non-cell autonomous and involves glutamate excitotoxicity. *J.Neurosci.* **24**, 7566-7575.

Dasen, J. S., Liu, J. P., & Jessell, T. M. (2003). Motor neuron columnar fate imposed by sequential phases of Hox-c activity. *Nature* **425**, 926-933.

Davidson, B. L. & Breakefield, X. O. (2003). Viral vectors for gene delivery to the nervous system. *Nat.Rev.Neurosci.* **4**, 353-364.

De Giorgi, F., Lartigue, L., Bauer, M. K., Schubert, A., Grimm, S., Hanson, G. T., Remington, S. J., Youle, R. J., & Ichas, F. (2002). The permeability transition pore signals apoptosis by directing Bax translocation and multimerization. *FASEB J.* **16**, 607-609.

De Lago, E., de Miguel, R., Lastres-Becker, I., Ramos, J. A., & Fernandez-Ruiz, J. (2004). Involvement of vanilloid-like receptors in the effects of anandamide on motor behavior and nigrostriatal dopaminergic activity: in vivo and in vitro evidence. *Brain Res.* **1007**, 152-159.

De Petrocellis, L., Cascio, M. G., & Di Marzo, V. (2004). The endocannabinoid system: a general view and latest additions. *Br.J.Pharmacol.* **141**, 765-774.

Deadwyler, S. A., Hampson, R. E., Mu, J., Whyte, A., & Childers, S. (1995). Cannabinoids modulate voltage sensitive potassium A-current in hippocampal neurons via a cAMP-dependent process. *J.Pharmacol.Exp.Ther.* **273**, 734-743.

Dedkova, E. N., Ji, X., Lipsius, S. L., & Blatter, L. A. (2004). Mitochondrial calcium uptake stimulates nitric oxide production in mitochondria of bovine vascular endothelial cells. *Am.J.Physiol Cell Physiol* **286**, C406-C415.

Dekkers, J., Bayley, P., Dick, J. R., Schwaller, B., Berchtold, M. W., & Greensmith, L. (2004). Over-expression of parvalbumin in transgenic mice rescues motoneurons from injury-induced cell death. *Neuroscience* **123**, 459-466.

Deng, H. X., Hentati, A., Tainer, J. A., Iqbal, Z., Cayabyab, A., Hung, W. Y., Getzoff, E. D., Hu, P., Herzfeldt, B., Roos, R. P., & . (1993). Amyotrophic lateral sclerosis and structural defects in Cu,Zn superoxide dismutase. *Science* **261**, 1047-1051.

Denli, A. M. & Hannon, G. J. (2003). RNAi: an ever-growing puzzle. *Trends Biochem.Sci.* **28**, 196-201.

Dennis, M. J., Ziskind-Conhaim, L., & Harris, A. J. (1981). Development of neuromuscular junctions in rat embryos. *Dev.Biol.* **81**, 266-279.

Derave, W., van den Bosch. L., Lemmens, G., Eijnde, B. O., Robberecht, W., & Hespel, P. (2003). Skeletal muscle properties in a transgenic mouse model for amyotrophic lateral sclerosis: effects of creatine treatment. *Neurobiol.Dis.* **13**, 264-272.

Desagher, S., Glowinski, J., & Premont, J. (1996). Astrocytes protect neurons from hydrogen peroxide toxicity. *J.Neurosci.* **16**, 2553-2562.

Devane, W. A., Hanus, L., Breuer, A., Pertwee, R. G., Stevenson, L. A., Griffin, G., Gibson, D., Mandelbaum, A., Etinger, A., & Mechoulam, R. (1992). Isolation and structure of a brain constituent that binds to the cannabinoid receptor. *Science* **258**, 1946-1949.

Di, Marzo, V, Fontana, A., Cadas, H., Schinelli, S., Cimino, G., Schwartz, J. C., & Piomelli, D. (1994). Formation and inactivation of endogenous cannabinoid anandamide in central neurons. *Nature* **372**, 686-691.

Di, Marzo, V, Melck, D., Bisogno, T., & De Petrocellis, L. (1998). Endocannabinoids: endogenous cannabinoid receptor ligands with neuromodulatory action. *Trends Neurosci.* **21**, 521-528.

Di, Marzo, V, Breivogel, C. S., Tao, Q., Bridgen, D. T., Razdan, R. K., Zimmer, A. M., Zimmer, A., & Martin, B. R. (2000). Levels, metabolism, and pharmacological activity of anandamide in CB(1) cannabinoid receptor knockout mice: evidence for non-CB(1), non-CB(2) receptor-mediated actions of anandamide in mouse brain. *J.Neurochem.* **75**, 2434-2444.

Di, Marzo, V, Goparaju, S. K., Wang, L., Liu, J., Batkai, S., Jarai, Z., Fezza, F., Miura, G. I., Palmiter, R. D., Sugiura, T., & Kunos, G. (2001). Leptin-regulated endocannabinoids are involved in maintaining food intake. *Nature* **410**, 822-825.

Di, Marzo, V, Bifulco, M., & De Petrocellis, L. (2004). The endocannabinoid system and its therapeutic exploitation. *Nat.Rev.Drug Discov.* **3**, 771-784.

Diamond, J. & Miledi, R. (1962). A study of foetal and new-born rat muscle fibres. *J.Physiol (Paris)* **162**, 393-408.

Ding, H., Schwarz, D. S., Keene, A., Affar, e. B., Fenton, L., Xia, X., Shi, Y., Zamore, P. D., & Xu, Z. (2003). Selective silencing by RNAi of a dominant allele that causes amyotrophic lateral sclerosis. *Aging Cell* **2**, 209-217.

Dinh, T. P., Carpenter, D., Leslie, F. M., Freund, T. F., Katona, I., Sensi, S. L., Kathuria, S., & Piomelli, D. (2002). Brain monoglyceride lipase participating in endocannabinoid inactivation. *Proc.Natl.Acad.Sci.U.S.A* **99**, 10819-10824.

Do, Y. McKallip, R. J., Nagarkatti, M. & Nagarkatti, P. S. (2004). Activation through cannabinoid receptors 1 and 2 on dendritic cells triggers NF-kappaB-dependent apoptosis:novel role for endogenous and exogenous cannabinoids in immunoregulation. *J. Immunol.* **173(4)**, 2372-2382.

Doble, A. (1996). The pharmacology and mechanism of action of riluzole. *Neurology.* **47(6 Suppl 4)**, S233-241.

Doherty, P., Fruns, M., Seaton, P., Dickson, G., Barton, C. H., Sears, T. A., & Walsh, F. S. (1990). A threshold effect of the major isoforms of NCAM on neurite outgrowth. *Nature* **343**, 464-466.

Doherty, P., Rowett, L. H., Moore, S. E., Mann, D. A., & Walsh, F. S. (1991). Neurite outgrowth in response to transfected N-CAM and N-cadherin reveals fundamental differences in neuronal responsiveness to CAMs. *Neuron* **6**, 247-258.

Drachman, D. B. & Rothstein, J. D. (2000). Inhibition of cyclooxygenase-2 protects motor neurons in an organotypic model of amyotrophic lateral sclerosis. *Ann.Neurol.* **48**, 792-795.

Drachman, D. B., Frank, K., Dykes-Hoberg, M., Teismann, P., Almer, G., Przedborski, S., & Rothstein, J. D. (2002). Cyclooxygenase 2 inhibition protects motor neurons and prolongs survival in a transgenic mouse model of ALS. *Ann.Neurol.* **52**, 771-778.

Drews, E., Schneider, M., & Koch, M. (2005). Effects of the cannabinoid receptor agonist WIN 55,212-2 on operant behavior and locomotor activity in rats. *Pharmacol.Biochem.Behav.* **80**, 145-150.

Dringen, R., Kussmaul, L., & Hamprecht, B. (1998). Rapid clearance of tertiary butyl hydroperoxide by cultured astroglial cells via oxidation of glutathione. *Glia* **23**, 139-145.

Dringen, R., Pfeiffer, B., & Hamprecht, B. (1999). Synthesis of the antioxidant glutathione in neurons: supply by astrocytes of CysGly as precursor for neuronal glutathione. *J.Neurosci.* **19**, 562-569.

Drory, V. E., Goltsman, E., Reznik, J. G., Mosek, A., & Korczyn, A. D. (2001). The value of muscle exercise in patients with amyotrophic lateral sclerosis. *J.Neurol.Sci.* **191**, 133-137.

Dryden, W. F., Erulkar, S. D., & Haba, G. D. L. (1974). Properties of Cell-Membrane of Developing Skeletal-Muscle Fibers in Culture and Its Sensitivity to Acetylcholine. *Clin. Exp. Pharmacol. Physiol.* **1**, 369-387.

Duchen, M. R. (2004). Mitochondria in health and disease: perspectives on a new mitochondrial biology. *Mol.Aspects Med.* **25**, 365-451.

Dugan, L. L., Sensi, S. L., Canzoniero, L. M., Handran, S. D., Rothman, S. M., Lin, T. S., Goldberg, M. P., & Choi, D. W. (1995). Mitochondrial production of reactive oxygen species in cortical neurons following exposure to N-methyl-D-aspartate. *J.Neurosci.* **15**, 6377-6388.

Dupuis, L., Oudart, H., Rene, F., De Aguilar, J. L., & Loeffler, J. P. (2004). Evidence for defective energy homeostasis in amyotrophic lateral sclerosis: Benefit of a high-energy diet in a transgenic mouse model. *Proc.Natl.Acad.Sci.U.S.A* **101**, 11159-11164.

Durham, H. D., Roy, J., Dong, L., & Figlewicz, D. A. (1997). Aggregation of mutant Cu/Zn superoxide dismutase proteins in a culture model of ALS. *J.Neuropathol.Exp.Neurol.* **56**, 523-530.

Duxson, M. J. (1982). The effect of postsynaptic block on development of the neuromuscular junction in postnatal rats. *J.Neurocytol.* **11**, 395-408.

Dykens, J. A. (1994). Isolated cerebral and cerebellar mitochondria produce free radicals when exposed to elevated CA2+ and Na+: implications for neurodegeneration. *J.Neurochem.* **63**, 584-591.

Eddleston, M. & Mucke, L. (1993). Molecular profile of reactive astrocytes--implications for their role in neurologic disease. *Neuroscience* **54**, 15-36.

Egertova, M., Cravatt, B. F., & Elphick, M. R. (2003). Comparative analysis of fatty acid amide hydrolase and cb(1) cannabinoid receptor expression in the mouse brain: evidence of a widespread role for fatty acid amide hydrolase in regulation of endocannabinoid signaling. *Neuroscience* **119**, 481-496.

Elbashir, S. M., Harborth, J., Lendeckel, W., Yalcin, A., Weber, K., & Tuschl, T. (2001). Duplexes of 21-nucleotide RNAs mediate RNA interference in cultured mammalian cells. *Nature* **411**, 494-498.

Elliott, J. L. & Snider, W. D. (1995). Parvalbumin is a marker of ALS-resistant motor neurons. *Neuroreport* **6**, 449-452.

Elliott, J. L. (2001). Cytokine upregulation in a murine model of familial amyotrophic lateral sclerosis. *Brain Res.Mol.Brain Res.* **95**, 172-178.

Ellis, D. Z., Rabe, J., & Sweadner, K. J. (2003). Global loss of Na,K-ATPase and its nitric oxide-mediated regulation in a transgenic mouse model of amyotrophic lateral sclerosis. *J.Neurosci.* **23**, 43-51.

Emsley, J. G., Arlotta, P., & Macklis, J. D. (2004). Star-cross'd neurons: astroglial effects on neural repair in the adult mammalian CNS. *Trends Neurosci.* **27**, 238-240.

Engelhardt, J. I., Tajti, J., & Appel, S. H. (1993). Lymphocytic infiltrates in the spinal cord in amyotrophic lateral sclerosis. *Arch.Neurol.* **50**, 30-36.

Epstein, J. A., Shapiro, D. N., Cheng, J., Lam, P. Y., & Maas, R. L. (1996). Pax3 modulates expression of the c-Met receptor during limb muscle development. *Proc.Natl.Acad.Sci.U.S.A* **93**, 4213-4218.

Eskes, R., Desagher, S., Antonsson, B., & Martinou, J. C. (2000). Bid induces the oligomerization and insertion of Bax into the outer mitochondrial membrane. *Mol.Cell Biol.* **20**, 929-935.

Estevez, A. G., Crow, J. P., Sampson, J. B., Reiter, C., Zhuang, Y., Richardson, G. J., Tarpey, M. M., Barbeito, L., & Beckman, J. S. (1999). Induction of nitric oxide-dependent apoptosis in motor neurons by zinc-deficient superoxide dismutase. *Science* **286**, 2498-2500.

Etienne-Manneville, S. & Hall, A. (2002). Rho GTPases in cell biology. *Nature* **420**, 629-635.

Eyer, J., Cleveland, D. W., Wong, P. C., & Peterson, A. C. (1998). Pathogenesis of two axonopathies does not require axonal neurofilaments. *Nature* **391**, 584-587.

Facchinetti, F., Sasaki, M., Cutting, F. B., Zhai, P., MacDonald, J. E., Reif, D., Beal, M. F., Huang, P. L., Dawson, T. M., Gurney, M. E., & Dawson, V. L. (1999). Lack of

involvement of neuronal nitric oxide synthase in the pathogenesis of a transgenic mouse model of familial amyotrophic lateral sclerosis. *Neuroscience* **90**, 1483-1492.

Facchinetti, F., Del Giudice, E., Furegato, S., Passarotto, M., & Leon, A. (2003). Cannabinoids ablate release of TNFalpha in rat microglial cells stimulated with lypopolysaccharide. *Glia* **41**, 161-168.

Fambrough, D. & Rash, J. E. (1971). Development of acetylcholine sensitivity during myogenesis. *Dev.Biol.* **26**, 55-68.

Fambrough, D. M. (1979). Control of acetylcholine receptors in skeletal muscle. *Physiol Rev.* **59**, 165-227.

Fegley, D., Kathuria, S., Mercier, R., Li, C., Goutopoulos, A., Makriyannis, A., & Piomelli, D. (2004). Anandamide transport is independent of fatty-acid amide hydrolase activity and is blocked by the hydrolysis-resistant inhibitor AM1172. *Proc.Natl.Acad.Sci.U.S.A* **101**, 8756-8761.

Fegley, D., Gaetani, S., Duranti, A., Tontini, A., Mor, M., Tarzia, G., & Piomelli, D. (2005). Characterization of the fatty acid amide hydrolase inhibitor cyclohexyl carbamic acid 3'-carbamoyl-biphenyl-3-yl ester (URB597): effects on anandamide and oleoylethanolamide deactivation. *J.Pharmacol.Exp.Ther.* **313**, 352-358.

Felder, C. C., Briley, E. M., Axelrod, J., Simpson, J. T., Mackie, K., & Devane, W. A. (1993). Anandamide, an endogenous cannabimimetic eicosanoid, binds to the cloned human cannabinoid receptor and stimulates receptor-mediated signal transduction. *Proc.Natl.Acad.Sci.U.S.A* **90**, 7656-7660.

Felder, C. C., Joyce, K. E., Briley, E. M., Mansouri, J., Mackie, K., Blond, O., Lai, Y., Ma, A. L., & Mitchell, R. L. (1995). Comparison of the pharmacology and signal transduction of the human cannabinoid CB1 and CB2 receptors. *Mol.Pharmacol.* **48**, 443-450.

Felder, C. C., Joyce, K. E., Briley, E. M., Glass, M., Mackie, K. P., Fahey, K. J., Cullinan, G. J., Hunden, D. C., Johnson, D. W., Chaney, M. O., Koppel, G. A., & Brownstein, M. (1998). LY320135, a novel cannabinoid CB1 receptor antagonist, unmasks coupling of the CB1 receptor to stimulation of cAMP accumulation. *J.Pharmacol.Exp.Ther.* **284**, 291-297.

Fernandez-Ruiz, J., Berrendero, F., Hernandez, M. L., & Ramos, J. A. (2000). The endogenous cannabinoid system and brain development. *Trends Neurosci.* **23**, 14-20.

Ferrante, R. J., Browne, S. E., Shinobu, L. A., Bowling, A. C., Baik, M. J., MacGarvey, U., Kowall, N. W., Brown, R. H., Jr., & Beal, M. F. (1997). Evidence of increased oxidative damage in both sporadic and familial amyotrophic lateral sclerosis. *J.Neurochem.* **69**, 2064-2074.

Ferraro, L., Tomasini, M. C., Gessa, G. L., Bebe, B. W., Tanganelli, S., & Antonelli, T. (2001). The cannabinoid receptor agonist WIN 55,212-2 regulates glutamate transmission in rat cerebral cortex: an in vivo and in vitro study. *Cereb.Cortex* **11**, 728-733.

Ferri, A., Nencini, M., Casciati, A., Cozzolino, M., Angelini, D. F., Longone, P., Spalloni, A., Rotilio, G., & Carri, M. T. (2004). Cell death in amyotrophic lateral sclerosis: interplay between neuronal and glial cells. *FASEB J.* **18**, 1261-1263.

Ferri, K. F. & Kroemer, G. (2001). Organelle-specific initiation of cell death pathways. *Nat.Cell Biol.* **3**, E255-E263.

Figlewicz, D. A., Krizus, A., Martinoli, M. G., Meininger, V., Dib, M., Rouleau, G. A., & Julien, J. P. (1994). Variants of the heavy neurofilament subunit are associated with the development of amyotrophic lateral sclerosis. *Hum.Mol.Genet.* **3**, 1757-1761.

Fire, A., Xu, S., Montgomery, M. K., Kostas, S. A., Driver, S. E., & Mello, C. C. (1998). Potent and specific genetic interference by double-stranded RNA in Caenorhabditis elegans. *Nature* **391**, 806-811.

Fischer, L. R., Culver, D. G., Tennant, P., Davis, A. A., Wang, M., Castellano-Sanchez, A., Khan, J., Polak, M. A., & Glass, J. D. (2004). Amyotrophic lateral sclerosis is a distal axonopathy: evidence in mice and man. *Exp.Neurol.* **185**, 232-240.

Forsyth, R. J., Bartlett, K., & Eyre, J. (1996). Dephosphorylation of 2-deoxyglucose 6-phosphate and 2-deoxyglucose export from cultured astrocytes. *Neurochem.Int.* **28**, 243-250.

Fredette, B. J. & Landmesser, L. T. (1991). Relationship of primary and secondary myogenesis to fiber type development in embryonic chick muscle. *Dev.Biol.* **143**, 1-18.

Freund, T. F., Katona, I., & Piomelli, D. (2003). Role of endogenous cannabinoids in synaptic signaling. *Physiol Rev.* **83**, 1017-1066.

Frey, D., Schneider, C., Xu, L., Borg, J., Spooren, W., & Caroni, P. (2000). Early and selective loss of neuromuscular synapse subtypes with low sprouting competence in motoneuron diseases. *J.Neurosci.* **20**, 2534-2542.

Fride, E. & Mechoulam, R. (1993). Pharmacological activity of the cannabinoid receptor agonist, anandamide, a brain constituent. *Eur.J.Pharmacol.* **231**, 313-314.

Friedlander, R. M., Brown, R. H., Gagliardini, V., Wang, J., & Yuan, J. (1997). Inhibition of ICE slows ALS in mice. *Nature* **388**, 31.

Friedlander, R. M. (2003). Apoptosis and caspases in neurodegenerative diseases. *N.Engl.J.Med.* **348** , 1365-1375.

Fu, J., Oveisi, F., Gaetani, S., Lin, E., & Piomelli, D. (2005). Oleoylethanolamide, an endogenous PPAR-alpha agonist, lowers body weight and hyperlipidemia in obese rats. *Neuropharmacology* **48**, 1147-1153.

Fujita, K., Yamauchi, M., Shibayama, K., Ando, M., Honda, M., & Nagata, Y. (1996). Decreased cytochrome c oxidase activity but unchanged superoxide dismutase and glutathione peroxidase activities in the spinal cords of patients with amyotrophic lateral sclerosis. *J.Neurosci.Res.* **45**, 276-281.

Fukada, K., Zhang, F., Vien, A., Cashman, N. R., & Zhu, H. (2004). Mitochondrial proteomic analysis of a cell line model of familial amyotrophic lateral sclerosis. *Mol.Cell Proteomics.* **3**, 1211-1223.

Fukaya, M., Hayashi, Y., & Watanabe, M. (2005). NR2 to NR3B subunit switchover of NMDA receptors in early postnatal motoneurons. *Eur.J.Neurosci.* **21**, 1432-1436.

Funte, L. R. & Haydon, P. G. (1993). Synaptic target contact enhances presynaptic calcium influx by activating cAMP-dependent protein kinase during synaptogenesis. *Neuron* **10**, 1069-1078.

Galve-Roperh, I., Sanchez, C., Cortes, M. L., del Pulgar, T. G., Izquierdo, M., & Guzman, M. (2000). Anti-tumoral action of cannabinoids: involvement of sustained ceramide accumulation and extracellular signal-regulated kinase activation. *Nat.Med.* **6**, 313-319.

Gamber, K. M., Macarthur, H., & Westfall, T. C. (2005). Cannabinoids augment the release of neuropeptide Y in the rat hypothalamus. *Neuropharmacology* **49**, 646-652.

Gaoni, Y. & Mechoulam, R. (1964). Isolation Structure + Partial Synthesis of Active Constituent of Hashish. *J.Am.Chem.Soc.* **86**, 1646-7.

Garthwaite, J. (1991). Glutamate, nitric oxide and cell-cell signalling in the nervous system. *Trends Neurosci.* **14**, 60-67.

Gautam, M., Noakes, P. G., Mudd, J., Nichol, M., Chu, G. C., Sanes, J. R., & Merlie, J. P. (1995). Failure of postsynaptic specialization to develop at neuromuscular junctions of rapsyn-deficient mice. *Nature* **377**, 232-236.

Gessa, G. L., Casu, M. A., Carta, G., & Mascia, M. S. (1998). Cannabinoids decrease acetylcholine release in the medial-prefrontal cortex and hippocampus, reversal by SR 141716A. *Eur.J.Pharmacol.* **355**, 119-124.

Ghafourifar, P. & Richter, C. (1997). Nitric oxide synthase activity in mitochondria. *FEBS Lett.* **418**, 291-296.

Giaume, C. & McCarthy, K. D. (1996). Control of gap-junctional communication in astrocytic networks. *Trends Neurosci.* **19**, 319-325.

Giess, R., Holtmann, B., Braga, M., Grimm, T., Muller-Myhsok, B., Toyka, K. V., & Sendtner, M. (2002). Early onset of severe familial amyotrophic lateral sclerosis with a SOD-1 mutation: potential impact of CNTF as a candidate modifier gene. *Am.J.Hum.Genet.* **70**, 1277-1286.

Gillingwater, T. H. & Ribchester, R. R. (2003). The relationship of neuromuscular synapse elimination to synaptic degeneration and pathology: insights from WldS and other mutant mice. *J.Neurocytol.* **32**, 863-881.

Giulian, D., Woodward, J., Young, D. G., Krebs, J. F., & Lachman, L. B. (1988). Interleukin-1 injected into mammalian brain stimulates astrogliosis and neovascularization. *J.Neurosci.* **8**, 2485-2490.

Giulivi, C. (2003). Characterization and function of mitochondrial nitric-oxide synthase. *Free Radic.Biol.Med.* **34**, 397-408.

Glaser, S. T., Abumrad, N. A., Fatade, F., Kaczocha, M., Studholme, K. M., & Deutsch, D. G. (2003). Evidence against the presence of an anandamide transporter. *Proc.Natl.Acad.Sci.U.S.A* **100**, 4269-4274.

Goldstein, L. S. & Yang, Z. (2000). Microtubule-based transport systems in neurons: the roles of kinesins and dyneins. *Annu.Rev.Neurosci.* **23**, 39-71.

Gong, Y. H., Parsadanian, A. S., Andreeva, A., Snider, W. D., & Elliott, J. L. (2000). Restricted expression of G86R Cu/Zn superoxide dismutase in astrocytes results in astrocytosis but does not cause motoneuron degeneration. *J.Neurosci.* **20**, 660-665.

Gonoi, T., Sherman, S. J., & Catterall, W. A. (1985). Voltage clamp analysis of tetrodotoxin-sensitive and -insensitive sodium channels in rat muscle cells developing in vitro. *J.Neurosci.* **5**, 2559-2564.

Gonoi, T. & Hasegawa, S. (1988). Post-natal disappearance of transient calcium channels in mouse skeletal muscle: effects of denervation and culture. *J.Physiol* **401**, 617-637.

Goparaju, S. K., Ueda, N., Taniguchi, K., & Yamamoto, S. (1999). Enzymes of porcine brain hydrolyzing 2-arachidonoylglycerol, an endogenous ligand of cannabinoid receptors. *Biochem.Pharmacol.* **57**, 417-423.

Greensmith, L., Mentis, G. Z., & Vrbova, G. (1994). Blockade of N-methyl-D-aspartate receptors by MK-801 (dizocilpine maleate) rescues motoneurones in developing rats. *Brain Res.Dev.Brain Res.* **81**, 162-170.

Greensmith, L. & Vrbova, G. (1996). Motoneurone survival: a functional approach. *Trends Neurosci.* **19**, 450-455.

Greenway, M. J., Alexander, M. D., Ennis, S., Traynor, B. J., Corr, B., Frost, E., Green, A., & Hardiman, O. (2004). A novel candidate region for ALS on chromosome 14q11.2. *Neurology* **63**, 1936-1938.

Gros-Louis, F., Lariviere, R., Gowing, G., Laurent, S., Camu, W., Bouchard, J. P., Meininger, V., Rouleau, G. A., & Julien, J. P. (2004). A frameshift deletion in peripherin gene associated with amyotrophic lateral sclerosis. *J.Biol.Chem.* **279**, 45951-45956.

Guegan, C., Vila, M., Rosoklija, G., Hays, A. P., & Przedborski, S. (2001). Recruitment of the mitochondrial-dependent apoptotic pathway in amyotrophic lateral sclerosis. *J.Neurosci.* **21**, 6569-6576.

Guegan, C. & Przedborski, S. (2003). Programmed cell death in amyotrophic lateral sclerosis. *J.Clin.Invest* **111**, 153-161.

Guillot, S., Azzouz, M., Deglon, N., Zurn, A., & Aebischer, P. (2004). Local GDNF expression mediated by lentiviral vector protects facial nerve motoneurons but not spinal motoneurons in SOD1(G93A) transgenic mice. *Neurobiol.Dis.* **16**, 139-149.

Gulyas, A. I., Cravatt, B. F., Bracey, M. H., Dinh, T. P., Piomelli, D., Boscia, F., & Freund, T. F. (2004). Segregation of two endocannabinoid-hydrolyzing enzymes into pre- and postsynaptic compartments in the rat hippocampus, cerebellum and amygdala. *Eur.J.Neurosci.* **20**, 441-458.

Gurney, M. E., Pu, H., Chiu, A. Y., Dal Canto, M. C., Polchow, C. Y., Alexander, D. D., Caliendo, J., Hentati, A., Kwon, Y. W., Deng, H. X., & . (1994). Motor neuron

degeneration in mice that express a human Cu,Zn superoxide dismutase mutation. *Science* **264**, 1772-1775.

Gurney, M. E., Fleck, T. J., Himes, C. S., & Hall, E. D. (1998). Riluzole preserves motor function in a transgenic model of familial amyotrophic lateral sclerosis. *Neurology* **50**, 62-66.

Guthrie, P. B., Knappenberger, J., Segal, M., Bennett, M. V., Charles, A. C., & Kater, S. B. (1999). ATP released from astrocytes mediates glial calcium waves. *J.Neurosci.* **19**, 520-528.

Gutmann, E. & Young, J. Z. The reinnervation of muscles after various periods of atrophy. *J.Anat.* **78**, 15-43. 1944.

Guzman, M., Galve-Roperh, I., & Sanchez, C. (2001). Ceramide: a new second messenger of cannabinoid action. *Trends Pharmacol.Sci.* **22**, 19-22.

Hadano, S., Hand, C. K., Osuga, H., Yanagisawa, Y., Otomo, A., Devon, R. S., Miyamoto, N., Showguchi-Miyata, J., Okada, Y., Singaraja, R., Figlewicz, D. A., Kwiatkowski, T., Hosler, B. A., Sagie, T., Skaug, J., Nasir, J., Brown, R. H., Jr., Scherer, S. W., Rouleau, G. A., Hayden, M. R., & Ikeda, J. E. (2001). A gene encoding a putative GTPase regulator is mutated in familial amyotrophic lateral sclerosis 2. *Nat.Genet.* **29**, 166-173.

Hafezparast, M., Klocke, R., Ruhrberg, C., Marquardt, A., Ahmad-Annuar, A., Bowen, S., Lalli, G., Witherden, A. S., Hummerich, H., Nicholson, S., Morgan, P. J., Oozageer, R., Priestley, J. V., Averill, S., King, V. R., Ball, S., Peters, J., Toda, T., Yamamoto, A., Hiraoka, Y., Augustin, M., Korthaus, D., Wattler, S., Wabnitz, P., Dickneite, C., Lampel, S., Boehme, F., Peraus, G., Popp, A., Rudelius, M., Schlegel, J., Fuchs, H., Hrabe, d. A., Schiavo, G., Shima, D. T., Russ, A. P., Stumm, G., Martin, J. E., & Fisher, E. M. (2003). Mutations in dynein link motor neuron degeneration to defects in retrograde transport. *Science* **300**, 808-812.

Hajnoczky, G., Robb-Gaspers, L. D., Seitz, M. B., & Thomas, A. P. (1995). Decoding of cytosolic calcium oscillations in the mitochondria. *Cell* **82**, 415-424.

Hajos, N., Ledent, C., & Freund, T. F. (2001). Novel cannabinoid-sensitive receptor mediates inhibition of glutamatergic synaptic transmission in the hippocampus. *Neuroscience* **106**, 1-4.

Hajos, N. & Freund, T. F. (2002). Pharmacological separation of cannabinoid sensitive receptors on hippocampal excitatory and inhibitory fibers. *Neuropharmacology* **43**, 503-510.

Halestrap, A. P., McStay, G. P., & Clarke, S. J. (2002). The permeability transition pore complex: another view. *Biochimie* **84**, 153-166.

Hall, A. & Nobes, C. D. (2000). Rho GTPases: molecular switches that control the organization and dynamics of the actin cytoskeleton. *Philos.Trans.R.Soc.Lond B Biol.Sci.* **355**, 965-970.

Hall, E. D., Oostveen, J. A., & Gurney, M. E. (1998). Relationship of microglial and astrocytic activation to disease onset and progression in a transgenic model of familial ALS. *Glia* **23**, 249-256.

Hamburger, V. Motor and sensory hyperplasia following limb bud transplants in chick embryos. *Physiol.Zool.* **12**, 268-284. 1939.

Hampson, A. J., Grimaldi, M., Axelrod, J., & Wink, D. (1998). Cannabidiol and (-) Delta9-tetrahydrocannabinol are neuroprotective antioxidants. *Proc.Natl.Acad.Sci.U.S.A* **95**, 8268-8273.

Hampson, A. J., Bornheim, L. M., Scanziani, M., Yost, C. S., Gray, A. T., Hansen, B. M., Leonoudakis, D. J., & Bickler, P. E. (1998). Dual effects of anandamide on NMDA receptor-mediated responses and neurotransmission. *J.Neurochem.* **70**, 671-676.

Hampson, A. J. & Grimaldi, M. (2001). Cannabinoid receptor activation and elevated cyclic AMP reduce glutamate neurotoxicity. *Eur.J.Neurosci.* **13**, 1529-1536.

Hansen, H. H., Schmid, P. C., Bittigau, P., Lastres-Becker, I., Berrendero, F., Manzanares, J., Ikonomidou, C., Schmid, H. H., Fernandez-Ruiz, J. J., & Hansen, H. S. (2001). Anandamide, but not 2-arachidonoylglycerol, accumulates during in vivo neurodegeneration. *J.Neurochem.* **78**, 1415-1427.

Hansen, H. H., Ikonomidou, C., Bittigau, P., Hansen, S. H., & Hansen, H. S. (2001). Accumulation of the anandamide precursor and other N-acylethanolamine phospholipids in infant rat models of in vivo necrotic and apoptotic neuronal death. *J.Neurochem.* **76**, 39-46.

Hansen, H. H., Azcoitia, I., Pons, S., Romero, J., Garcia-Segura, L. M., Ramos, J. A., Hansen, H. S., & Fernandez-Ruiz, J. (2002). Blockade of cannabinoid CB(1) receptor function protects against in vivo disseminating brain damage following NMDA-induced excitotoxicity. *J.Neurochem.* **82**, 154-158.

Hanus, L., Gopher, A., Almog, S., & Mechoulam, R. (1993). Two new unsaturated fatty acid ethanolamides in brain that bind to the cannabinoid receptor. *J.Med.Chem.* **36**, 3032-3034.

Hanus, L., Abu-Lafi, S., Fride, E., Breuer, A., Vogel, Z., Shalev, D. E., Kustanovich, I., & Mechoulam, R. (2001). 2-arachidonyl glyceryl ether, an endogenous agonist of the cannabinoid CB1 receptor. *Proc.Natl.Acad.Sci.U.S.A* **98**, 3662-3665.

Hassinger, T. D., Atkinson, P. B., Strecker, G. J., Whalen, L. R., Dudek, F. E., Kossel, A. H., & Kater, S. B. (1995). Evidence for glutamate-mediated activation of hippocampal neurons by glial calcium waves. *J.Neurobiol.* **28**, 159-170.

Heath, P. R., Tomkins, J., Ince, P. G., & Shaw, P. J. (2002). Quantitative assessment of AMPA receptor mRNA in human spinal motor neurons isolated by laser capture microdissection. *Neuroreport* **13**, 1753-1757.

Heath, P. R. & Shaw, P. J. (2002). Update on the glutamatergic neurotransmitter system and the role of excitotoxicity in amyotrophic lateral sclerosis. *Muscle Nerve* **26**, 438-458.

Heiman-Patterson, T. D., Deitch, J. S., Blankenhorn, E. P., Erwin, K. L., Perreault, M. J., Alexander, B. K., Byers, N., Toman, I., & Alexander, G. M. (2005). Background and gender effects on survival in the TgN(SOD1-G93A)1Gur mouse model of ALS. *J.Neurol.Sci.* **236**, 1-7.

Henke, W., Cetinsoy, C., Jung, K., & Loening, S. (1996). Non-hyperbolic calcium calibration curve of Fura-2: implications for the reliability of quantitative Ca2+ measurements. *Cell Calcium* **20**, 287-292.

Hensley, K., Fedynyshyn, J., Ferrell, S., Floyd, R. A., Gordon, B., Grammas, P., Hamdheydari, L., Mhatre, M., Mou, S., Pye, Q. N., Stewart, C., West, M., West, S., & Williamson, K. S. (2003). Message and protein-level elevation of tumor necrosis factor alpha (TNF alpha) and TNF alpha-modulating cytokines in spinal cords of the G93A-SOD1 mouse model for amyotrophic lateral sclerosis. *Neurobiol.Dis.* **14**, 74-80.

Herkenham, M., Lynn, A. B., Little, M. D., Johnson, M. R., Melvin, L. S., de Costa, B. R., & Rice, K. C. (1990). Cannabinoid receptor localization in brain. *Proc.Natl.Acad.Sci.U.S.A* **87**, 1932-1936.

Herkenham, M., Lynn, A. B., Johnson, M. R., Melvin, L. S., de Costa, B. R., & Rice, K. C. (1991). Characterization and localization of cannabinoid receptors in rat brain: a quantitative in vitro autoradiographic study. *J.Neurosci.* **11**, 563-583.

Hewett, S. J., Csernansky, C. A., & Choi, D. W. (1994). Selective potentiation of NMDA-induced neuronal injury following induction of astrocytic iNOS. *Neuron* **13**, 487-494.

Higgins, C. M., Jung, C., Ding, H., & Xu, Z. (2002). Mutant Cu, Zn superoxide dismutase that causes motoneuron degeneration is present in mitochondria in the CNS. *J.Neurosci.* **22**, RC215.

Hightower, L. E. & Guidon, P. T., Jr. (1989). Selective release from cultured mammalian cells of heat-shock (stress) proteins that resemble glia-axon transfer proteins. *J.Cell Physiol* **138**, 257-266.

Hillard, C. J., Edgemond, W. S., Jarrahian, A., & Campbell, W. B. (1997). Accumulation of N-arachidonoylethanolamine (anandamide) into cerebellar granule cells occurs via facilitated diffusion. *J.Neurochem.* **69**, 631-638.

Hirano, A., Donnenfeld, H., Sasaki, S., & Nakano, I. (1984). Fine structural observations of neurofilamentous changes in amyotrophic lateral sclerosis. *J.Neuropathol.Exp.Neurol.* **43**, 461-470.

Hirano, A. (1996). Neuropathology of ALS: an overview. *Neurology* **47**, S63-S66.

Hoch, W. (2003). Molecular dissection of neuromuscular junction formation. *Trends Neurosci.* **26**, 335-337.

Hoffman, P. N. & Lasek, R. J. (1975). The slow component of axonal transport. Identification of major structural polypeptides of the axon and their generality among mammalian neurons. *J.Cell Biol.* **66**, 351-366.

Hoffman, P. N. & Lasek, R. J. (1980). Axonal transport of the cytoskeleton in regenerating motor neurons: constancy and change. *Brain Res.* **202**, 317-333.

Hollmann, M. & Heinemann, S. (1994). Cloned glutamate receptors. *Annu.Rev.Neurosci.* **17**, 31-108.

Holtzer, H., Marshall, J. M., Jr., & Finck, H. (1957). An analysis of myogenesis by the use of fluorescent antimyosin. *J.Biophys.Biochem.Cytol.* **3**, 705-724.

Hottinger, A. F., Fine, E. G., Gurney, M. E., Zurn, A. D., & Aebischer, P. (1997). The copper chelator d-penicillamine delays onset of disease and extends survival in a transgenic mouse model of familial amyotrophic lateral sclerosis. *Eur.J.Neurosci.* **9**, 1548-1551.

Howlett, A. C. & Fleming, R. M. (1984). Cannabinoid inhibition of adenylate cyclase. Pharmacology of the response in neuroblastoma cell membranes. *Mol.Pharmacol.* **26**, 532-538.

Howlett, A. C., Barth, F., Bonner, T. I., Cabral, G., Casellas, P., Devane, W. A., Felder, C. C., Herkenham, M., Mackie, K., Martin, B. R., Mechoulam, R., & Pertwee, R. G. (2002). International Union of Pharmacology. XXVII. Classification of cannabinoid receptors. *Pharmacol.Rev.* **54**, 161-202.

Howlett, A. C., Breivogel, C. S., Childers, S. R., Deadwyler, S. A., Hampson, R. E., & Porrino, L. J. (2004). Cannabinoid physiology and pharmacology: 30 years of progress. *Neuropharmacology* **47 Suppl 1**, 345-358.

Hume, R. I., Role, L. W., & Fischbach, G. D. (1983). Acetylcholine release from growth cones detected with patches of acetylcholine receptor-rich membranes. *Nature* **305**, 632-634.

Idris, A. I., 't Hof, R. J., Greig, I. R., Ridge, S. A., Baker, D., Ross, R. A., & Ralston, S. H. (2005). Regulation of bone mass, bone loss and osteoclast activity by cannabinoid receptors. *Nat.Med.* **11**, 774-779.

Ikonomidou, C., Qin, Q. Y., Labruyere, J., & Olney, J. W. (1996). Motor neuron degeneration induced by excitotoxin agonists has features in common with those seen in the SOD-1 transgenic mouse model of amyotrophic lateral sclerosis. *J.Neuropathol.Exp.Neurol.* **55**, 211-224.

Ince, P., Stout, N., Shaw, P., Slade, J., Hunziker, W., Heizmann, C. W., & Baimbridge, K. G. (1993). Parvalbumin and calbindin D-28k in the human motor system and in motor neuron disease. *Neuropathol.Appl.Neurobiol.* **19**, 291-299.

Inoue, H., Tsukita, K., Iwasato, T., Suzuki, Y., Tomioka, M., Tateno, M., Nagao, M., Kawata, A., Saido, T. C., Miura, M., Misawa, H., Itohara, S., & Takahashi, R. (2003). The crucial role of caspase-9 in the disease progression of a transgenic ALS mouse model. *EMBO J.* **22**, 6665-6674.

Jaarsma, D., Rognoni, F., van Duijn, W., Verspaget, H. W., Haasdijk, E. D., & Holstege, J. C. (2001). CuZn superoxide dismutase (SOD1) accumulates in vacuolated mitochondria in transgenic mice expressing amyotrophic lateral sclerosis-linked SOD1 mutations. *Acta Neuropathol.(Berl)* **102**, 293-305.

Jackson, M., Steers, G., Leigh, P. N. & Morrison , K. E. (1999). Polymorphisms in the glutamate transporter gene EAAT2 in European ALS patients. *J. Neurol.* **246(12),** 1140-1144.

Jarai, Z., Wagner, J. A., Varga, K., Lake, K. D., Compton, D. R., Martin, B. R., Zimmer, A. M., Bonner, T. I., Buckley, N. E., Mezey, E., Razdan, R. K., Zimmer, A., &

Kunos, G. (1999). Cannabinoid-induced mesenteric vasodilation through an endothelial site distinct from CB1 or CB2 receptors. *Proc.Natl.Acad.Sci.U.S.A* **96**, 14136-14141.

Jekabsone, A., Ivanoviene, L., Brown, G. C., & Borutaite, V. (2003). Nitric oxide and calcium together inactivate mitochondrial complex I and induce cytochrome c release. *J.Mol.Cell Cardiol.* **35**, 803-809.

Jia, Z., Agopyan, N., Miu, P., Xiong, Z., Henderson, J., Gerlai, R., Taverna, F. A., Velumian, A., MacDonald, J., Carlen, P., Abramow-Newerly, W., & Roder, J. (1996). Enhanced LTP in mice deficient in the AMPA receptor GluR2. *Neuron* **17**, 945-956.

Jiang, Y. M., Yamamoto, M., Kobayashi, Y., Yoshihara, T., Liang, Y., Terao, S., Takeuchi, H., Ishigaki, S., Katsuno, M., Adachi, H., Niwa, J., Tanaka, F., Doyu, M., Yoshida, M., Hashizume, Y., & Sobue, G. (2005). Gene expression profile of spinal motor neurons in sporadic amyotrophic lateral sclerosis. *Ann.Neurol.* **57**, 236-251.

Jin, K., Xie, L., Kim, S. H., Parmentier-Batteur, S., Sun, Y., Mao, X. O., Childs, J., & Greenberg, D. A. (2004). Defective adult neurogenesis in CB1 cannabinoid receptor knockout mice. *Mol.Pharmacol.* **66**, 204-208.

John, G. R., Lee, S. C., & Brosnan, C. F. (2003). Cytokines: powerful regulators of glial cell activation. *Neuroscientist.* **9**, 10-22.

Johnston, J. A., Dalton, M. J., Gurney, M. E., & Kopito, R. R. (2000). Formation of high molecular weight complexes of mutant Cu, Zn-superoxide dismutase in a mouse model for familial amyotrophic lateral sclerosis. *Proc.Natl.Acad.Sci.U.S.A* **97**, 12571-12576.

Jonsson, P. A., Ernhill, K., Andersen, P. M., Bergemalm, D., Brannstrom, T., Gredal, O., Nilsson, P., & Marklund, S. L. (2004). Minute quantities of misfolded mutant superoxide dismutase-1 cause amyotrophic lateral sclerosis. *Brain* **127**, 73-88.

Jung, C., Higgins, C. M., & Xu, Z. (2002). Mitochondrial electron transport chain complex dysfunction in a transgenic mouse model for amyotrophic lateral sclerosis. *J.Neurochem.* **83**, 535-545.

Juttler, E., Potrovita, I., Tarabin, V., Prinz, S., Dong-Si, T., Fink, G., & Schwaninger, M. (2004). The cannabinoid dexanabinol is an inhibitor of the nuclear factor-kappa B (NF-kappa B). *Neuropharmacology* **47**, 580-592.

Kaal, E. C., Vlug, A. S., Versleijen, M. W., Kuilman, M., Joosten, E. A., & Bar, P. R. (2000). Chronic mitochondrial inhibition induces selective motoneuron death in vitro: a new model for amyotrophic lateral sclerosis. *J.Neurochem.* **74**, 1158-1165.

Kabashi, E., Agar, J. N., Taylor, D. M., Minotti, S., & Durham, H. D. (2004). Focal dysfunction of the proteasome: a pathogenic factor in a mouse model of amyotrophic lateral sclerosis. *J.Neurochem.* **89**, 1325-1335.

Kalmar, B., Burnstock, G., Vrbova, G., Urbanics, R., Csermely, P., & Greensmith, L. (2002). Upregulation of heat shock proteins rescues motoneurones from axotomy-induced cell death in neonatal rats. *Exp.Neurol.* **176**, 87-97.

Kaminski, N. E., Abood, M. E., Kessler, F. K., Martin, B. R., & Schatz, A. R. (1992). Identification of a functionally relevant cannabinoid receptor on mouse spleen cells that is involved in cannabinoid-mediated immune modulation. *Mol.Pharmacol.* **42**, 736-742.

Kanekura, K., Hashimoto, Y., Niikura, T., Aiso, S., Matsuoka, M., & Nishimoto, I. (2004). Alsin, the product of ALS2 gene, suppresses SOD1 mutant neurotoxicity through RhoGEF domain by interacting with SOD1 mutants. *J.Biol.Chem.* **279**, 19247-19256.

Kanki, R., Nakamizo, T., Yamashita, H., Kihara, T., Sawada, H., Uemura, K., Kawamata, J., Shibasaki, H., Akaike, A., & Shimohama, S. (2004). Effects of mitochondrial dysfunction on glutamate receptor-mediated neurotoxicity in cultured rat spinal motor neurons. *Brain Res.* **1015**, 73-81.

Kapus, A., Szaszi, K., Kaldi, K., Ligeti, E., & Fonyo, A. (1991). Is the mitochondrial Ca2+ uniporter a voltage-modulated transport pathway? *FEBS Lett.* **282**, 61-64.

Karki, S. & Holzbaur, E. L. (1995). Affinity chromatography demonstrates a direct binding between cytoplasmic dynein and the dynactin complex. *J.Biol.Chem.* **270**, 28806-28811.

Karlsson, M., Contreras, J. A., Hellman, U., Tornqvist, H., & Holm, C. (1997). cDNA cloning, tissue distribution, and identification of the catalytic triad of monoglyceride lipase. Evolutionary relationship to esterases, lysophospholipases, and haloperoxidases. *J.Biol.Chem.* **272**, 27218-27223.

Kaspar, B. K., Llado, J., Sherkat, N., Rothstein, J. D., & Gage, F. H. (2003). Retrograde viral delivery of IGF-1 prolongs survival in a mouse ALS model. *Science* **301**, 839-842.

Kasthuri, N. & Lichtman, J. W. (2003). The role of neuronal identity in synaptic competition. *Nature* **424**, 426-430.

Kathuria, S., Gaetani, S., Fegley, D., Valino, F., Duranti, A., Tontini, A., Mor, M., Tarzia, G., La Rana, G., Calignano, A., Giustino, A., Tattoli, M., Palmery, M., Cuomo, V., & Piomelli, D. (2003). Modulation of anxiety through blockade of anandamide hydrolysis. *Nat.Med.* **9**, 76-81.

Kawahara, Y., Ito, K., Sun, H., Aizawa, H., Kanazawa, I., & Kwak, S. (2004). Glutamate receptors: RNA editing and death of motor neurons. *Nature* **427**, 801.

Kawamura, Y., Dyck, P. J., Shimono, M., Okazaki, H., Tateishi, J., & Doi, H. (1981). Morphometric comparison of the vulnerability of peripheral motor and sensory neurons in amyotrophic lateral sclerosis. *J.Neuropathol.Exp.Neurol.* **40**, 667-675.

Kawasaki, K., Yaoita, E., Yamamoto, T., Tamatani, T., Miyasaka, M., & Kihara, I. (1993). Antibodies against intercellular adhesion molecule-1 and lymphocyte function-associated antigen-1 prevent glomerular injury in rat experimental crescentic glomerulonephritis. *J.Immunol.* **150**, 1074-1083.

Keelan, J., Vergun, O., & Duchen, M. R. (1999). Excitotoxic mitochondrial depolarisation requires both calcium and nitric oxide in rat hippocampal neurons. *J.Physiol* **520 Pt 3**, 797-813.

Kennel, P. F., Finiels, F., Revah, F., & Mallet, J. (1996). Neuromuscular function impairment is not caused by motor neurone loss in FALS mice: an electromyographic study. *Neuroreport* **7**, 1427-1431.

Kerr, J. F., Wyllie, A. H., & Currie, A. R. (1972). Apoptosis: a basic biological phenomenon with wide-ranging implications in tissue kinetics. *Br.J.Cancer* **26**, 239-257.

Kieran, D., Kalmar, B., Dick, J. R., Riddoch-Contreras, J., Burnstock, G., & Greensmith, L. (2004). Treatment with arimoclomol, a coinducer of heat shock proteins, delays disease progression in ALS mice. *Nat.Med.* **10**, 402-405.

Kieran, D. & Greensmith, L. (2004). Inhibition of calpains, by treatment with leupeptin, improves motoneuron survival and muscle function in models of motoneuron degeneration. *Neuroscience* **125**, 427-439.

Kieran, D., Hafezparast, M., Bohnert, S., Dick, J. R., Martin, J., Schiavo, G., Fisher, E. M., & Greensmith, L. (2005). A mutation in dynein rescues axonal transport defects and extends the life span of ALS mice. *J.Cell Biol.* **169**, 561-567.

Kim, S. H., Henkel, J. S., Beers, D. R., Sengun, I. S., Simpson, E. P., Goodman, J. C., Engelhardt, J. I., Siklos, L., & Appel, S. H. (2003). PARP expression is increased in astrocytes but decreased in motor neurons in the spinal cord of sporadic ALS patients. *J.Neuropathol.Exp.Neurol.* **62**, 88-103.

Kirby, J., Halligan, E., Baptista, M. J., Allen, S., Heath, P. R., Holden, H., Barber, S. C., Loynes, C. A., Wood-Allum, C. A., Lunec, J., & Shaw, P. J. (2005). Mutant SOD1 alters the motor neuronal transcriptome: implications for familial ALS. *Brain* **128**, 1686-1706.

Kirchhoff, F., Dringen, R., & Giaume, C. (2001). Pathways of neuron-astrocyte interactions and their possible role in neuroprotection. *Eur.Arch.Psychiatry Clin.Neurosci.* **251**, 159-169.

Kirkinezos, I. G., Bacman, S. R., Hernandez, D., Oca-Cossio, J., Arias, L. J., Perez-Pinzon, M. A., Bradley, W. G., & Moraes, C. T. (2005). Cytochrome c association with the inner mitochondrial membrane is impaired in the CNS of G93A-SOD1 mice. *J.Neurosci.* **25**, 164-172.

Klegeris, A., Bissonnette, C. J., & McGeer, P. L. (2003). Reduction of human monocytic cell neurotoxicity and cytokine secretion by ligands of the cannabinoid-type CB2 receptor. *Br.J.Pharmacol.* **139**, 775-786.

Klivenyi, P., Ferrante, R. J., Matthews, R. T., Bogdanov, M. B., Klein, A. M., Andreassen, O. A., Mueller, G., Wermer, M., Kaddurah-Daouk, R., & Beal, M. F. (1999). Neuroprotective effects of creatine in a transgenic animal model of amyotrophic lateral sclerosis. *Nat.Med.* **5**, 347-350.

Kong, J. & Xu, Z. (1998). Massive mitochondrial degeneration in motor neurons triggers the onset of amyotrophic lateral sclerosis in mice expressing a mutant SOD1. *J.Neurosci.* **18** , 3241-3250.

Kong, J. & Xu, Z. (2000). Overexpression of neurofilament subunit NF-L and NF-H extends survival of a mouse model for amyotrophic lateral sclerosis. *Neurosci.Lett.* **281**, 72-74.

Kopito, R. R. (2000). Aggresomes, inclusion bodies and protein aggregation. *Trends Cell Biol.* **10**, 524-530.

Kostic, V., Jackson-Lewis, V., de Bilbao, F., Dubois-Dauphin, M., & Przedborski, S. (1997). Bcl-2: prolonging life in a transgenic mouse model of familial amyotrophic lateral sclerosis. *Science* **277**, 559-562.

Kozak, K. R., Rowlinson, S. W., & Marnett, L. J. (2000). Oxygenation of the endocannabinoid, 2-arachidonylglycerol, to glyceryl prostaglandins by cyclooxygenase-2. *J.Biol.Chem.* **275**, 33744-33749.

Kozak, K. R., Crews, B. C., Morrow, J. D., Wang, L. H., Ma, Y. H., Weinander, R., Jakobsson, P. J. & Marnett, L. J. (2002). Metabolism of the endocannabinoids, 2-arachidonylglycerol and anandamide, into prostaglandin, thromboxane, and prostacyclin glycerol esters and ethanolamides. *J. Biol. Chem.* **277 (47)**, 44877-44885.

Kreitzer, A. C. & Regehr, W. G. (2001). Retrograde inhibition of presynaptic calcium influx by endogenous cannabinoids at excitatory synapses onto Purkinje cells. *Neuron* **29**, 717-727.

Kriz, J., Nguyen, M. D., & Julien, J. P. (2002). Minocycline slows disease progression in a mouse model of amyotrophic lateral sclerosis. *Neurobiol.Dis.* **10**, 268-278.

Kriz, J., Gowing, G., & Julien, J. P. (2003). Efficient three-drug cocktail for disease induced by mutant superoxide dismutase. *Ann.Neurol.* **53**, 429-436.

Kruman, I. I., Pedersen, W. A., Springer, J. E., & Mattson, M. P. (1999). ALS-linked Cu/Zn-SOD mutation increases vulnerability of motor neurons to excitotoxicity by a mechanism involving increased oxidative stress and perturbed calcium homeostasis. *Exp.Neurol.* **160**, 28-39.

Kumar, R. N., Chambers, W. A., & Pertwee, R. G. (2001). Pharmacological actions and therapeutic uses of cannabis and cannabinoids. *Anaesthesia* **56**, 1059-1068.

Kuner, R., Groom, A. J., Bresink, I., Kornau, H. C., Stefovska, V., Muller, G., Hartmann, B., Tschauner, K., Waibel, S., Ludolph, A. C., Ikonomidou, C., Seeburg, P. H., & Turski, L. (2005). Late-onset motoneuron disease caused by a functionally modified AMPA receptor subunit. *Proc.Natl.Acad.Sci.U.S.A* **102**, 5826-5831.

Kuo, J. J., Schonewille, M., Siddique, T., Schults, A. N., Fu, R., Bar, P. R., Anelli, R., Heckman, C. J., & Kroese, A. B. (2004). Hyperexcitability of cultured spinal motoneurons from presymptomatic ALS mice. *J.Neurophysiol.* **91**, 571-575.

Kuwana, T., Mackey, M. R., Perkins, G., Ellisman, M. H., Latterich, M., Schneiter, R., Green, D. R., & Newmeyer, D. D. (2002). Bid, Bax, and lipids cooperate to form supramolecular openings in the outer mitochondrial membrane. *Cell* **111**, 331-342.

Lafon-Cazal, M., Pietri, S., Culcasi, M., & Bockaert, J. (1993). NMDA-dependent superoxide production and neurotoxicity. *Nature* **364**, 535-537.

Lambrechts, D., Storkebaum, E., Morimoto, M., Del Favero, J., Desmet, F., Marklund, S. L., Wyns, S., Thijs, V., Andersson, J., van, Marion, I., Al Chalabi, A., Bornes, S., Musson, R., Hansen, V., Beckman, L., Adolfsson, R., Pall, H. S., Prats, H., Vermeire, S., Rutgeerts, P., Katayama, S., Awata, T., Leigh, N., Lang-Lazdunski, L., Dewerchin, M., Shaw, C., Moons, L., Vlietinck, R., Morrison, K. E., Robberecht, W., Van Broeckhoven, C., Collen, D., Andersen, P. M., & Carmeliet, P. (2003). VEGF is a modifier of amyotrophic lateral sclerosis in mice and humans and protects motoneurons against ischemic death. *Nat.Genet.* **34**, 383-394.

LaMonte, B. H., Wallace, K. E., Holloway, B. A., Shelly, S. S., Ascano, J., Tokito, M., Van Winkle, T., Howland, D. S., & Holzbaur, E. L. (2002). Disruption of dynein/dynactin inhibits axonal transport in motor neurons causing late-onset progressive degeneration. *Neuron* **34**, 715-727.

Lariviere, R. C., Beaulieu, J. M., Nguyen, M. D., & Julien, J. P. (2003). Peripherin is not a contributing factor to motor neuron disease in a mouse model of amyotrophic lateral sclerosis caused by mutant superoxide dismutase. *Neurobiol.Dis.* **13**, 158-166.

Laslo, P., Lipski, J., Nicholson, L. F., Miles, G. B., & Funk, G. D. (2001). GluR2 AMPA receptor subunit expression in motoneurons at low and high risk for degeneration in amyotrophic lateral sclerosis. *Exp.Neurol.* **169**, 461-471.

Ledent, C., Valverde, O., Cossu, G., Petitet, F., Aubert, J. F., Beslot, F., Bohme, G. A., Imperato, A., Pedrazzini, T., Roques, B. P., Vassart, G., Fratta, W., & Parmentier, M. (1999). Unresponsiveness to cannabinoids and reduced addictive effects of opiates in CB1 receptor knockout mice. *Science* **283**, 401-404.

Lee, M. K., Marszalek, J. R., & Cleveland, D. W. (1994). A mutant neurofilament subunit causes massive, selective motor neuron death: implications for the pathogenesis of human motor neuron disease. *Neuron* **13**, 975-988.

Leigh, P. N. & Swash, M. (1991). Cytoskeletal pathology in motor neuron diseases. *Adv. Neurol.* **56**, 115-124.

Leigh, P. N., Whitwell, H., Garofalo, O., Buller, J., Swash, M., Martin, J. E., Gallo, J. M., Weller, R. O., & Anderton, B. H. (1991). Ubiquitin-immunoreactive intraneuronal inclusions in amyotrophic lateral sclerosis. Morphology, distribution, and specificity. *Brain* **114 (Pt 2)**, 775-788.

Letourneau, P. C., Condic, M. L., & Snow, D. M. (1994). Interactions of developing neurons with the extracellular matrix. *J.Neurosci.* **14**, 915-928.

Levenes, C., Daniel, H., Soubrie, P., & Crepel, F. (1998). Cannabinoids decrease excitatory synaptic transmission and impair long-term depression in rat cerebellar Purkinje cells. *J.Physiol* **510 (Pt 3)**, 867-879.

Levi, G., Gallo, V., & Patrizio, M. (1992). Release of exogenous and endogenous neurotransmitter amino acids from cultured astrocytes. *Prog.Brain Res.* **94**, 243-250.

Levine, J. B., Kong, J., Nadler, M., & Xu, Z. (1999). Astrocytes interact intimately with degenerating motor neurons in mouse amyotrophic lateral sclerosis (ALS). *Glia* **28**, 215-224.

Li, M., Ona, V. O., Guegan, C., Chen, M., Jackson-Lewis, V., Andrews, L. J., Olszewski, A. J., Stieg, P. E., Lee, J. P., Przedborski, S., & Friedlander, R. M. (2000). Functional role of caspase-1 and caspase-3 in an ALS transgenic mouse model. *Science* **288**, 335-339.

Lichtman, A. H., Hawkins, E. G., Griffin, G., & Cravatt, B. F. (2002). Pharmacological activity of fatty acid amides is regulated, but not mediated, by fatty acid amide hydrolase in vivo. *J.Pharmacol.Exp.Ther.* **302**, 73-79.

Lichtman, A. H., Shelton, C. C., Advani, T., & Cravatt, B. F. (2004). Mice lacking fatty acid amide hydrolase exhibit a cannabinoid receptor-mediated phenotypic hypoalgesia. *Pain* **109**, 319-327.

Lim, G., Sung, B., Ji, R. R., & Mao, J. (2003). Upregulation of spinal cannabinoid-1-receptors following nerve injury enhances the effects of Win 55,212-2 on neuropathic pain behaviors in rats. *Pain* **105**, 275-283.

Lin, J. H., Saito, T., Anderson, D. J., Lance-Jones, C., Jessell, T. M., & Arber, S. (1998). Functionally related motor neuron pool and muscle sensory afferent subtypes defined by coordinate ETS gene expression. *Cell* **95**, 393-407.

Lino, M. M., Schneider, C., & Caroni, P. (2002). Accumulation of SOD1 mutants in postnatal motoneurons does not cause motoneuron pathology or motoneuron disease. *J.Neurosci.* **22**, 4825-4832.

Lips, M. B. & Keller, B. U. (1999). Activity-related calcium dynamics in motoneurons of the nucleus hypoglossus from mouse. *J.Neurophysiol.* **82**, 2936-2946.

Liu, J., Lillo, C., Jonsson, P. A., Vande, V. C., Ward, C. M., Miller, T. M., Subramaniam, J. R., Rothstein, J. D., Marklund, S., Andersen, P. M., Brannstrom, T., Gredal, O., Wong, P. C., Williams, D. S., & Cleveland, D. W. (2004). Toxicity of familial ALS-linked SOD1 mutants from selective recruitment to spinal mitochondria. *Neuron* **43**, 5-17.

Liu, J., Shinobu, L. A., Ward, C. M., Young, D., & Cleveland, D. W. (2005). Elevation of the Hsp70 chaperone does not effect toxicity in mouse models of familial amyotrophic lateral sclerosis. *J.Neurochem.* **93**, 875-882.

Lobsiger, C. S., Garcia, M. L., Ward, C. M., & Cleveland, D. W. (2005). Altered axonal architecture by removal of the heavily phosphorylated neurofilament tail domains strongly slows superoxide dismutase 1 mutant-mediated ALS. *Proc.Natl.Acad.Sci.U.S.A* **102**, 10351-10356.

Loeb, J. A. & Fischbach, G. D. (1995). ARIA can be released from extracellular matrix through cleavage of a heparin-binding domain. *J.Cell Biol.* **130**, 127-135.

Lowrie, M. B., Krishnan, S., & Vrbova, G. (1982). Recovery of slow and fast muscles following nerve injury during early post-natal development in the rat. *J.Physiol* **331**, 51-66.

Lowrie, M. B., Krishnan, S., & Vrbova, G. (1987). Permanent changes in muscle and motoneurones induced by nerve injury during a critical period of development of the rat. *Brain Res.* **428**, 91-101.

Lu, Y. M., Yin, H. Z., Chiang, J., & Weiss, J. H. (1996). Ca(2+)-permeable AMPA/kainate and NMDA channels: high rate of Ca2+ influx underlies potent induction of injury. *J.Neurosci.* **16**, 5457-5465.

Lu, Y. Y., Wang, L. J., Muramatsu, S., Ikeguchi, K., Fujimoto, K., Okada, T., Mizukami, H., Matsushita, T., Hanazono, Y., Kume, A., Nagatsu, T., Ozawa, K., & Nakano, I. (2003). Intramuscular injection of AAV-GDNF results in sustained expression of transgenic GDNF, and its delivery to spinal motoneurons by retrograde transport. *Neurosci.Res.* **45**, 33-40.

Mackie, K. & Hille, B. (1992). Cannabinoids inhibit N-type calcium channels in neuroblastoma-glioma cells. *Proc.Natl.Acad.Sci.U.S.A* **89**, 3825-3829.

Mackie, K., Lai, Y., Westenbroek, R., & Mitchell, R. (1995). Cannabinoids activate an inwardly rectifying potassium conductance and inhibit Q-type calcium currents in AtT20 cells transfected with rat brain cannabinoid receptor. *J.Neurosci.* **15**, 6552-6561.

Maejima, T., Hashimoto, K., Yoshida, T., Aiba, A., & Kano, M. (2001). Presynaptic inhibition caused by retrograde signal from metabotropic glutamate to cannabinoid receptors. *Neuron* **31**, 463-475.

Maihofner, C., Probst-Cousin, S., Bergmann, M., Neuhuber, W., Neundorfer, B., & Heuss, D. (2003). Expression and localization of cyclooxygenase-1 and -2 in human sporadic amyotrophic lateral sclerosis. *Eur.J.Neurosci.* **18**, 1527-1534.

Maingret, F., Patel, A. J., Lazdunski, M., & Honore, E. (2001). The endocannabinoid anandamide is a direct and selective blocker of the background K(+) channel TASK-1. *EMBO J.* **20** , 47-54.

Manabe, Y., Nagano, I., Gazi, M. S., Murakami, T., Shiote, M., Shoji, M., Kitagawa, H., Setoguchi, Y., & Abe, K. (2002). Adenovirus-mediated gene transfer of glial cell line-derived neurotrophic factor prevents motor neuron loss of transgenic model mice for amyotrophic lateral sclerosis. *Apoptosis.* **7**, 329-334.

Maneuf, Y. P. & Brotchie, J. M. (1997). Paradoxical action of the cannabinoid WIN 55,212-2 in stimulated and basal cyclic AMP accumulation in rat globus pallidus slices. *Br.J.Pharmacol.* **120**, 1397-1398.

Maragakis, N. J., Rao, M. S., Llado, J., Wong, V., Xue, H., Pardo, A., Herring, J., Kerr, D., Coccia, C., & Rothstein, J. D. (2005). Glial restricted precursors protect against chronic glutamate neurotoxicity of motor neurons in vitro. *Glia* **50**, 145-159.

Marsicano, G., Moosmann, B., Hermann, H., Lutz, B., & Behl, C. (2002). Neuroprotective properties of cannabinoids against oxidative stress: role of the cannabinoid receptor CB1. *J.Neurochem.* **80**, 448-456.

Marsicano, G., Wotjak, C. T., Azad, S. C., Bisogno, T., Rammes, G., Cascio, M. G., Hermann, H., Tang, J., Hofmann, C., Zieglgansberger, W., Di Marzo, V., & Lutz, B. (2002). The endogenous cannabinoid system controls extinction of aversive memories. *Nature* **418**, 530-534.

Marsicano, G., Goodenough, S., Monory, K., Hermann, H., Eder, M., Cannich, A., Azad, S. C., Cascio, M. G., Gutierrez, S. O., van der Stelt. M., Lopez-Rodriguez, M. L., Casanova, E., Schutz, G., Zieglgansberger, W., Di Marzo, V., Behl, C., & Lutz, B.

(2003). CB1 cannabinoid receptors and on-demand defense against excitotoxicity. *Science* **302**, 84-88

Marszalek, J. R., Williamson, T. L., Lee, M. K., Xu, Z., Hoffman, P. N., Becher, M. W., Crawford, T. O., & Cleveland, D. W. (1996). Neurofilament subunit NF-H modulates axonal diameter by selectively slowing neurofilament transport. *J.Cell Biol.* **135**, 711-724.

Martin-Rendon, E., Azzouz, M., & Mazarakis, N. D. (2001). Lentiviral vectors for the treatment of neurodegenerative diseases. *Curr.Opin.Mol.Ther.* **3**, 476-481.

Martin-Rendon, E., White, L. J., Olsen, A., Mitrophanous, K. A., & Mazarakis, N. D. (2002). New methods to titrate EIAV-based lentiviral vectors. *Mol.Ther.* **5**, 566-570.

Martin, L. J. (1999). Neuronal death in amyotrophic lateral sclerosis is apoptosis: possible contribution of a programmed cell death mechanism. *J.Neuropathol.Exp.Neurol.* **58**, 459-471.

Martinou, J. C., Falls, D. L., Fischbach, G. D., & Merlie, J. P. (1991). Acetylcholine receptor-inducing activity stimulates expression of the epsilon-subunit gene of the muscle acetylcholine receptor. *Proc.Natl.Acad.Sci.U.S.A* **88**, 7669-7673.

Massa, F., Marsicano, G., Hermann, H., Cannich, A., Monory, K., Cravatt, B. F., Ferri, G. L., Sibaev, A., Storr, M., & Lutz, B. (2004). The endogenous cannabinoid system protects against colonic inflammation. *J.Clin.Invest* **113**, 1202-1209.

Matsuda, L. A., Lolait, S. J., Brownstein, M. J., Young, A. C., & Bonner, T. I. (1990). Structure of a cannabinoid receptor and functional expression of the cloned cDNA. *Nature* **346**, 561-564.

Matsunaga, M., Hatta, K., Nagafuchi, A., & Takeichi, M. (1988). Guidance of optic nerve fibres by N-cadherin adhesion molecules. *Nature* **334**, 62-64.

Mattiazzi, M., D'Aurelio, M., Gajewski, C. D., Martushova, K., Kiaei, M., Beal, M. F., & Manfredi, G. (2002). Mutated human SOD1 causes dysfunction of oxidative phosphorylation in mitochondria of transgenic mice. *J.Biol.Chem.* **277**, 29626-29633.

Mattson, M. P., Kumar, K. N., Wang, H., Cheng, B., & Michaelis, E. K. (1993). Basic FGF regulates the expression of a functional 71 kDa NMDA receptor protein that mediates calcium influx and neurotoxicity in hippocampal neurons. *J.Neurosci.* **13**, 4575-4588.

Mattson, M. P., Lovell, M. A., Furukawa, K., & Markesbery, W. R. (1995). Neurotrophic factors attenuate glutamate-induced accumulation of peroxides, elevation of intracellular Ca2+ concentration, and neurotoxicity and increase antioxidant enzyme activities in hippocampal neurons. *J.Neurochem.* **65**, 1740-1751.

Maxwell, M. M., Pasinelli, P., Kazantsev, A. G., & Brown, R. H., Jr. (2004). RNA interference-mediated silencing of mutant superoxide dismutase rescues cyclosporin A-induced death in cultured neuroblastoma cells. *Proc.Natl.Acad.Sci.U.S.A* **101**, 3178-3183.

Mazarakis, N. D., Azzouz, M., Rohll, J. B., Ellard, F. M., Wilkes, F. J., Olsen, A. L., Carter, E. E., Barber, R. D., Baban, D. F., Kingsman, S. M., Kingsman, A. J., O'Malley,

K., & Mitrophanous, K. A. (2001). Rabies virus glycoprotein pseudotyping of lentiviral vectors enables retrograde axonal transport and access to the nervous system after peripheral delivery. *Hum.Mol.Genet.* **10**, 2109-2121.

McAllister, S. D. & Glass, M. (2002). CB(1) and CB(2) receptor-mediated signalling: a focus on endocannabinoids. *Prostaglandins Leukot.Essent.Fatty Acids* **66**, 161-171.

McGeer, P. L. & McGeer, E. G. (2002). Inflammatory processes in amyotrophic lateral sclerosis. *Muscle Nerve* **26**, 459-470.

Mechoulam, R., Ben Shabat, S., Hanus, L., Ligumsky, M., Kaminski, N. E., Schatz, A. R., Gopher, A., Almog, S., Martin, B. R., Compton, D. R., & . (1995). Identification of an endogenous 2-monoglyceride, present in canine gut, that binds to cannabinoid receptors. *Biochem.Pharmacol.* **50**, 83-90.

Mechoulam, R., Fride, E., Hanus, L., Sheskin, T., Bisogno, T., Di Marzo, V., Bayewitch, M., & Vogel, Z. (1997). Anandamide may mediate sleep induction. *Nature* **389**, 25-26.

Mechoulam, R. & Lichtman, A. H. (2003). Neuroscience. Stout guards of the central nervous system. *Science* **302**, 65-67.

Menzies, F. M., Cookson, M. R., Taylor, R. W., Turnbull, D. M., Chrzanowska-Lightowlers, Z. M., Dong, L., Figlewicz, D. A., & Shaw, P. J. (2002). Mitochondrial dysfunction in a cell culture model of familial amyotrophic lateral sclerosis. *Brain* **125**, 1522-1533.

Merlie, J. P., Isenberg, K. E., Russell, S. D., & Sanes, J. R. (1984). Denervation supersensitivity in skeletal muscle: analysis with a cloned cDNA probe. *J.Cell Biol.* **99**, 332-335.

Merlie, J. P. & Sanes, J. R. (1985). Concentration of acetylcholine receptor mRNA in synaptic regions of adult muscle fibres. *Nature* **317**, 66-68.

Migheli, A., Pezzulo, T., Attanasio, A., & Schiffer, D. (1993). Peripherin immunoreactive structures in amyotrophic lateral sclerosis. *Lab Invest* **68**, 185-191.

Migheli, A., Piva, R., Atzori, C., Troost, D., & Schiffer, D. (1997). c-Jun, JNK/SAPK kinases and transcription factor NF-kappa B are selectively activated in astrocytes, but not motor neurons, in amyotrophic lateral sclerosis. *J.Neuropathol.Exp.Neurol.* **56**, 1314-1322.

Miller, R. G., Mitchell, J. D., Lyon, M., & Moore, D. H. (2002). Riluzole for amyotrophic lateral sclerosis (ALS)/motor neuron disease (MND). *Cochrane.Database.Syst.Rev.* **CD001447.**

Miller, T. M., Kaspar, B. K., Kops, G. J., Yamanaka, K., Christian, L. J., Gage, F. H., & Cleveland, D. W. (2005). Virus-delivered small RNA silencing sustains strength in amyotrophic lateral sclerosis. *Ann.Neurol.* **57**, 773-776.

Miller, V. M., Gouvion, C. M., Davidson, B. L., & Paulson, H. L. (2004). Targeting Alzheimer's disease genes with RNA interference: an efficient strategy for silencing mutant alleles. *Nucleic Acids Res.* **32**, 661-668.

Misgeld, T., Burgess, R. W., Lewis, R. M., Cunningham, J. M., Lichtman, J. W., & Sanes, J. R. (2002). Roles of neurotransmitter in synapse formation: development of neuromuscular junctions lacking choline acetyltransferase. *Neuron* **36**, 635-648.

Mitrophanous, K., Yoon, S., Rohll, J., Patil, D., Wilkes, F., Kim, V., Kingsman, S., Kingsman, A., & Mazarakis, N. (1999). Stable gene transfer to the nervous system using a non-primate lentiviral vector. *Gene Ther.* **6**, 1808-1818.

Mizuno, T., Sawada, M., Suzumura, A., & Marunouchi, T. (1994). Expression of cytokines during glial differentiation. *Brain Res.* **656**, 141-146.

Molina-Holgado, F., Lledo, A., & Guaza, C. (1997). Anandamide suppresses nitric oxide and TNF-alpha responses to Theiler's virus or endotoxin in astrocytes. *Neuroreport* **8**, 1929-1933.

Molina-Holgado, F., Molina-Holgado, E., Guaza, C., & Rothwell, N. J. (2002). Role of CB1 and CB2 receptors in the inhibitory effects of cannabinoids on lipopolysaccharide-induced nitric oxide release in astrocyte cultures. *J.Neurosci.Res.* **67**, 829-836.

Molina-Holgado, F., Pinteaux, E., Moore, J. D., Molina-Holgado, E., Guaza, C., Gibson, R. M., & Rothwell, N. J. (2003). Endogenous interleukin-1 receptor antagonist mediates anti-inflammatory and neuroprotective actions of cannabinoids in neurons and glia. *J.Neurosci.* **23**, 6470-6474.

Moncada, S., Palmer, R. M., & Higgs, E. A. (1991). Nitric oxide: physiology, pathophysiology, and pharmacology. *Pharmacol.Rev.* **43**, 109-142.

Monory, K., Tzavara, E. T., Lexime, J., Ledent, C., Parmentier, M., Borsodi, A., & Hanoune, J. (2002). Novel, not adenylyl cyclase-coupled cannabinoid binding site in cerebellum of mice. *Biochem.Biophys.Res.Commun.* **292**, 231-235.

Montero, M., Alonso, M. T., Albillos, A., Garcia-Sancho, J., & Alvarez, J. (2001). Mitochondrial Ca(2+)-induced Ca(2+) release mediated by the Ca(2+) uniporter. *Mol.Biol.Cell* **12**, 63-71.

Moreira, M. C., Klur, S., Watanabe, M., Nemeth, A. H., Le, B., I, Moniz, J. C., Tranchant, C., Aubourg, P., Tazir, M., Schols, L., Pandolfo, M., Schulz, J. B., Pouget, J., Calvas, P., Shizuka-Ikeda, M., Shoji, M., Tanaka, M., Izatt, L., Shaw, C. E., M'Zahem, A., Dunne, E., Bomont, P., Benhassine, T., Bouslam, N., Stevanin, G., Brice, A., Guimaraes, J., Mendonca, P., Barbot, C., Coutinho, P., Sequeiros, J., Durr, A., Warter, J. M., & Koenig, M. (2004). Senataxin, the ortholog of a yeast RNA helicase, is mutant in ataxia-ocular apraxia 2. *Nat.Genet.* **36**, 225-227.

Morrison, B. M., Janssen, W. G., Gordon, J. W., & Morrison, J. H. (1998). Light and electron microscopic distribution of the AMPA receptor subunit, GluR2, in the spinal cord of control and G86R mutant superoxide dismutase transgenic mice. *J.Comp Neurol.* **395**, 523-534.

Mourelatos, Z., Gonatas, N. K., Stieber, A., Gurney, M. E., & Dal Canto, M. C. (1996). The Golgi apparatus of spinal cord motor neurons in transgenic mice expressing mutant Cu,Zn superoxide dismutase becomes fragmented in early, preclinical stages of the disease. *Proc.Natl.Acad.Sci.U.S.A* **93**, 5472-5477.

Munch, C., Sedlmeier, R., Meyer, T., Homberg, V., Sperfeld, A. D., Kurt, A., Prudlo, J., Peraus, G., Hanemann, C. O., Stumm, G., & Ludolph, A. C. (2004). Point mutations of the p150 subunit of dynactin (DCTN1) gene in ALS. *Neurology* **63**, 724-726.

Munro, S., Thomas, K. L., & Abu-Shaar, M. (1993). Molecular characterization of a peripheral receptor for cannabinoids. *Nature* **365**, 61-65.

Muresan, V., Stankewich, M. C., Steffen, W., Morrow, J. S., Holzbaur, E. L., & Schnapp, B. J. (2001). Dynactin-dependent, dynein-driven vesicle transport in the absence of membrane proteins: a role for spectrin and acidic phospholipids. *Mol.Cell* **7**, 173-183.

Muthian, S., Rademacher, D. J., Roelke, C. T., Gross, G. J., & Hillard, C. J. (2004). Anandamide content is increased and CB(1) cannabinoid receptor blockade is protective during transient, focal cerebral ischemia. *Neuroscience* **129**, 743-750.

Nachlas, M. M., Tsou, K. C., De Souza, E., Cheng, C. S., & Seligman, A. M. (1957). Cytochemical demonstration of succinic dehydrogenase by the use of a new p-nitrophenyl substituted ditetrazole. *J.Histochem.Cytochem.* **5**, 420-436.

Nagayama, T., Sinor, A. D., Simon, R. P., Chen, J., Graham, S. H., Jin, K., & Greenberg, D. A. (1999). Cannabinoids and neuroprotection in global and focal cerebral ischemia and in neuronal cultures. *J.Neurosci.* **19**, 2987-2995.

Navarrete, R. & Vrbova, G. (1983). Changes of Activity Patterns in Slow and Fast Muscles During Postnatal-Development. *Dev.Brain Res.* **8**, 11-19.

Navarrete, R. & Vrbova, G. (1984). Differential effect of nerve injury at birth on the activity pattern of reinnervated slow and fast muscles of the rat. *J.Physiol* **351**, 675-685.

Nedergaard, M. (1994). Direct signaling from astrocytes to neurons in cultures of mammalian brain cells. *Science* **263**, 1768-1771.

Netzeband, J. G., Conroy, S. M., Parsons, K. L., & Gruol, D. L. (1999). Cannabinoids enhance NMDA-elicited Ca2+ signals in cerebellar granule neurons in culture. *J.Neurosci.* **19**, 8765-8777.

Newman, E. A. (2003). New roles for astrocytes: regulation of synaptic transmission. *Trends Neurosci.* **26**, 536-542.

Nguyen, M. D., Lariviere, R. C., & Julien, J. P. (2001). Deregulation of Cdk5 in a mouse model of ALS: toxicity alleviated by perikaryal neurofilament inclusions. *Neuron* **30**, 135-147.

Nicholls, D. G. & Crompton, M. (1980). Mitochondrial calcium transport. *FEBS Lett.* **111**, 261-268.

Nicholson, R. A., Liao, C., Zheng, J., David, L. S., Coyne, L., Errington, A. C., Singh, G., & Lees, G. (2003). Sodium channel inhibition by anandamide and synthetic cannabimimetics in brain. *Brain Res.* **978**, 194-204.

Nicotera, P., Leist, M., & Manzo, L. (1999). Neuronal cell death: a demise with different shapes. *Trends Pharmacol.Sci.* **20**, 46-51.

Nishimura, A. L., Mitne-Neto, M., Silva, H. C., Richieri-Costa, A., Middleton, S., Cascio, D., Kok, F., Oliveira, J. R., Gillingwater, T., Webb, J., Skehel, P., & Zatz, M. (2004). A mutation in the vesicle-trafficking protein VAPB causes late-onset spinal muscular atrophy and amyotrophic lateral sclerosis. *Am.J.Hum.Genet.* **75**, 822-831.

Nitkin, R. M., Smith, M. A., Magill, C., Fallon, J. R., Yao, Y. M., Wallace, B. G., & McMahan, U. J. (1987). Identification of agrin, a synaptic organizing protein from Torpedo electric organ. *J.Cell Biol.* **105**, 2471-2478.

Norenberg, M. D. & Martinez-Hernandez, A. (1979). Fine structural localization of glutamine synthetase in astrocytes of rat brain. *Brain Res.* **161**, 303-310.

O'Brien, R. A. & Vrbova, G. (1978). Acetylcholine synthesis in nerve endings to slow and fast muscles of developing chicks: effect of muscle activity. *Neuroscience* **3**, 1227-1230.

Ohno-Shosaku, T., Maejima, T., & Kano, M. (2001). Endogenous cannabinoids mediate retrograde signals from depolarized postsynaptic neurons to presynaptic terminals. *Neuron* **29**, 729-738.

Okado-Matsumoto, A. & Fridovich, I. (2002). Amyotrophic lateral sclerosis: a proposed mechanism. *Proc.Natl.Acad.Sci.U.S.A* **99**, 9010-9014.

Okamoto, Y., Morishita, J., Tsuboi, K., Tonai, T., & Ueda, N. (2004). Molecular characterization of a phospholipase D generating anandamide and its congeners. *J.Biol.Chem.* **279**, 5298-5305.

Olsen, M. K., Roberds, S. L., Ellerbrock, B. R., Fleck, T. J., McKinley, D. K., & Gurney, M. E. (2001). Disease mechanisms revealed by transcription profiling in SOD1-G93A transgenic mouse spinal cord. *Ann.Neurol.* **50**, 730-740.

Ong, W. Y. & Mackie, K. (1999). A light and electron microscopic study of the CB1 cannabinoid receptor in the primate spinal cord. *J.Neurocytol.* **28**, 39-45.

Oppenheim, R. W. (1987). Muscle activity and motor neuron death in the spinal cord of the chick embryo. *Ciba Found.Symp.* **126**, 96-112.

Oppenheim, R. W. (1991). Cell death during development of the nervous system. *Annu.Rev.Neurosci.* **14**, 453-501.

Oppenheim, R. W., Homma, S., Marti, E., Prevette, D., Wang, S., Yaginuma, H., & McMahon, A. P. (1999). Modulation of early but not later stages of programmed cell death in embryonic avian spinal cord by sonic hedgehog. *Mol.Cell Neurosci.* **13**, 348-361.

Orrenius, S., Zhivotovsky, B., & Nicotera, P. (2003). Regulation of cell death: the calcium-apoptosis link. *Nat.Rev.Mol.Cell Biol.* **4**, 552-565.

Ortega-Gutierrez, S., Hawkins, E. G., Viso, A., Lopez-Rodriguez, M. L., & Cravatt, B. F. (2004). Comparison of anandamide transport in FAAH wild-type and knockout neurons: evidence for contributions by both FAAH and the CB1 receptor to anandamide uptake. *Biochemistry* **43**, 8184-8190.

Otomo, A., Hadano, S., Okada, T., Mizumura, H., Kunita, R., Nishijima, H., Showguchi-Miyata, J., Yanagisawa, Y., Kohiki, E., Suga, E., Yasuda, M., Osuga, H., Nishimoto, T., Narumiya, S., & Ikeda, J. E. (2003). ALS2, a novel guanine nucleotide exchange factor for the small GTPase Rab5, is implicated in endosomal dynamics. *Hum.Mol.Genet.* **12**, 1671-1687.

Panikashvili, D., Simeonidou, C., Ben Shabat, S., Hanus, L., Breuer, A., Mechoulam, R., & Shohami, E. (2001). An endogenous cannabinoid (2-AG) is neuroprotective after brain injury. *Nature* **413**, 527-531.

Parmentier-Batteur, S., Jin, K., Mao, X. O., Xie, L., & Greenberg, D. A. (2002). Increased severity of stroke in CB1 cannabinoid receptor knock-out mice. *J.Neurosci.* **22**, 9771-9775.

Parpura, V., Basarsky, T. A., Liu, F., Jeftinija, K., Jeftinija, S., & Haydon, P. G. (1994). Glutamate-mediated astrocyte-neuron signalling. *Nature* **369**, 744-747.

Pasinelli, P., Borchelt, D. R., Houseweart, M. K., Cleveland, D. W., & Brown, R. H., Jr. (1998). Caspase-1 is activated in neural cells and tissue with amyotrophic lateral sclerosis-associated mutations in copper-zinc superoxide dismutase. *Proc.Natl.Acad.Sci.U.S.A* **95**, 15763-15768.

Pasinelli, P., Houseweart, M. K., Brown, R. H., Jr., & Cleveland, D. W. (2000). Caspase-1 and -3 are sequentially activated in motor neuron death in Cu,Zn superoxide dismutase-mediated familial amyotrophic lateral sclerosis. *Proc.Natl.Acad.Sci.U.S.A* **97**, 13901-13906.

Pasinelli, P., Belford, M. E., Lennon, N., Bacskai, B. J., Hyman, B. T., Trotti, D., & Brown, R. H., Jr. (2004). Amyotrophic lateral sclerosis-associated SOD1 mutant proteins bind and aggregate with Bcl-2 in spinal cord mitochondria. *Neuron* **43**, 19-30.

Pasti, L., Volterra, A., Pozzan, T., & Carmignoto, G. (1997). Intracellular calcium oscillations in astrocytes: a highly plastic, bidirectional form of communication between neurons and astrocytes in situ. *J.Neurosci.* **17**, 7817-7830.

Pehar, M., Cassina, P., Vargas, M. R., Castellanos, R., Viera, L., Beckman, J. S., Estevez, A. G., & Barbeito, L. (2004). Astrocytic production of nerve growth factor in motor neuron apoptosis: implications for amyotrophic lateral sclerosis. *J.Neurochem.* **89**, 464-473.

Peng, H. B., Cheng, P. C., & Luther, P. W. (1981). Formation of ACh receptor clusters induced by positively charged latex beads. *Nature* **292**, 831-834.

Perraud, F., Labourdette, G., Miehe, M., Loret, C., & Sensenbrenner, M. (1988). Comparison of the morphological effects of acidic and basic fibroblast growth factors on rat astroblasts in culture. *J.Neurosci.Res.* **20**, 1-11.

Pertwee, R., Griffin, G., Hanus, L., & Mechoulam, R. (1994). Effects of two endogenous fatty acid ethanolamides on mouse vasa deferentia. *Eur.J.Pharmacol.* **259**, 115-120.

Pettmann, B. & Henderson, C. E. (1998). Neuronal cell death. *Neuron* **20**, 633-647.

Phelps, P. E., Barber, R. P., Houser, C. R., Crawford, G. D., Salvaterra, P. M., & Vaughn, J. E. (1984). Postnatal development of neurons containing choline acetyltransferase in rat spinal cord: an immunocytochemical study. *J.Comp Neurol.* **229**, 347-361.

Piazza, O., Siren, A. L., & Ehrenreich, H. (2004). Soccer, neurotrauma and amyotrophic lateral sclerosis: is there a connection? *Curr.Med.Res.Opin.* **20**, 505-508.

Pieri, M., Albo, F., Gaetti, C., Spalloni, A., Bengtson, C. P., Longone, P., Cavalcanti, S., & Zona, C. (2003). Altered excitability of motor neurons in a transgenic mouse model of familial amyotrophic lateral sclerosis. *Neurosci.Lett.* **351**, 153-156.

Piomelli, D. (2003). The molecular logic of endocannabinoid signalling. *Nat.Rev.Neurosci.* **4**, 873-884.

Platania, P., Seminara, G., Aronica, E., Troost, D., Vincenza, C. M., & Angela, S. M. (2005). 17beta-estradiol rescues spinal motoneurons from AMPA-induced toxicity: A role for glial cells. *Neurobiol.Dis.* **20(2)**, 461-70.

Poloni, M., Facchetti, D., Mai, R., Micheli, A., Agnoletti, L., Francolini, G., Mora, G., Camana, C., Mazzini, L., & Bachetti, T. (2000). Circulating levels of tumour necrosis factor-alpha and its soluble receptors are increased in the blood of patients with amyotrophic lateral sclerosis. *Neurosci.Lett.* **287**, 211-214.

Pompl, P. N., Ho, L., Bianchi, M., McManus, T., Qin, W., & Pasinetti, G. M. (2003). A therapeutic role for cyclooxygenase-2 inhibitors in a transgenic mouse model of amyotrophic lateral sclerosis. *FASEB J.* **17**, 725-727.

Porter, A. C., Sauer, J. M., Knierman, M. D., Becker, G. W., Berna, M. J., Bao, J., Nomikos, G. G., Carter, P., Bymaster, F. P., Leese, A. B., & Felder, C. C. (2002). Characterization of a novel endocannabinoid, virodhamine, with antagonist activity at the CB1 receptor. *J.Pharmacol.Exp.Ther.* **301**, 1020-1024.

Powell, E. M., Meiners, S., DiProspero, N. A., & Geller, H. M. (1997). Mechanisms of astrocyte-directed neurite guidance. *Cell Tissue Res.* **290**, 385-393.

Pramatarova, A., Laganiere, J., Roussel, J., Brisebois, K., & Rouleau, G. A. (2001). Neuron-specific expression of mutant superoxide dismutase 1 in transgenic mice does not lead to motor impairment. *J.Neurosci.* **21**, 3369-3374.

Price, S. R. & Briscoe, J. (2004). The generation and diversification of spinal motor neurons: signals and responses. *Mech.Dev.* **121**, 1103-1115.

Pryce, G., Ahmed, Z., Hankey, D. J., Jackson, S. J., Croxford, J. L., Pocock, J. M., Ledent, C., Petzold, A., Thompson, A. J., Giovannoni, G., Cuzner, M. L., & Baker, D. (2003). Cannabinoids inhibit neurodegeneration in models of multiple sclerosis. *Brain* **126**, 2191-2202.

Przybylski, R. J. & Blumberg, J. M. (1966). Ultrastructural aspects of myogenesis in the chick. *Lab Invest* **15**, 836-863.

Puffenbarger, R. A., Boothe, A. C., & Cabral, G. A. (2000). Cannabinoids inhibit LPS inducible cytokine mRNA expression in rat microglial cells. *Glia* **29**, 58-69.

Puls, I., Jonnakuty, C., LaMonte, B. H., Holzbaur, E. L., Tokito, M., Mann, E., Floeter, M. K., Bidus, K., Drayna, D., Oh, S. J., Brown, R. H., Jr., Ludlow, C. L., & Fischbeck, K. H. (2003). Mutant dynactin in motor neuron disease. *Nat.Genet.* **33**, 455-456.

Purves, R. D. & Vrbova, G. (1974). Some characteristics of myotubes cultured from slow and fast chick muscles. *J.Cell Physiol* **84**, 97-100.

Rabizadeh, S., Gralla, E. B., Borchelt, D. R., Gwinn, R., Valentine, J. S., Sisodia, S., Wong, P., Lee, M., Hahn, H., & Bredesen, D. E. (1995). Mutations associated with amyotrophic lateral sclerosis convert superoxide dismutase from an antiapoptotic gene to a proapoptotic gene: studies in yeast and neural cells. *Proc.Natl.Acad.Sci.U.S.A* **92**, 3024-3028.

Rae, T. D., Schmidt, P. J., Pufahl, R. A., Culotta, V. C., & O'Halloran, T. V. (1999). Undetectable intracellular free copper: the requirement of a copper chaperone for superoxide dismutase. *Science* **284**, 805-808.

Ralph, G. S., Mazarakis, N. D., & Azzouz, M. (2005). Therapeutic gene silencing in neurological disorders, using interfering RNA. *J.Mol.Med.* **83**, 413-419.

Ralph, G. S., Radcliffe, P. A., Day, D. M., Carthy, J. M., Leroux, M. A., Lee, D. C., Wong, L. F., Bilsland, L. G., Greensmith, L., Kingsman, S. M., Mitrophanous, K. A., Mazarakis, N. D., & Azzouz, M. (2005). Silencing mutant SOD1 using RNAi protects against neurodegeneration and extends survival in an ALS model. *Nat.Med.* **11**, 429-433.

Raman, C., McAllister, S. D., Rizvi, G., Patel, S. G., Moore, D. H., & Abood, M. E. (2004). Amyotrophic lateral sclerosis: delayed disease progression in mice by treatment with a cannabinoid. *Amyotroph.Lateral.Scler.Other Motor Neuron Disord.* **5**, 33-39.

Ramirez, B. G., Blazquez, C., Gomez, d. P., Guzman, M., & de Ceballos, M. L. (2005). Prevention of Alzheimer's disease pathology by cannabinoids: neuroprotection mediated by blockade of microglial activation. *J.Neurosci.* **25**, 1904-1913.

Rao, S. D., Yin, H. Z., & Weiss, J. H. (2003). Disruption of glial glutamate transport by reactive oxygen species produced in motor neurons. *J.Neurosci.* **23**, 2627-2633.

Raoul, C., Henderson, C. E., & Pettmann, B. (1999). Programmed cell death of embryonic motoneurons triggered through the Fas death receptor. *J.Cell Biol.* **147**, 1049-1062.

Raoul, C., Estevez, A. G., Nishimune, H., Cleveland, D. W., deLapeyriere, O., Henderson, C. E., Haase, G., & Pettmann, B. (2002). Motoneuron death triggered by a specific pathway downstream of Fas. potentiation by ALS-linked SOD1 mutations. *Neuron* **35**, 1067-1083.

Raoul, C., Abbas-Terki, T., Bensadoun, J. C., Guillot, S., Haase, G., Szulc, J., Henderson, C. E., & Aebischer, P. (2005). Lentiviral-mediated silencing of SOD1 through RNA interference retards disease onset and progression in a mouse model of ALS. *Nat.Med.* **11**, 423-428.

Ravinet, T. C., Delgorge, C., Menet, C., Arnone, M., & Soubrie, P. (2004). CB1 cannabinoid receptor knockout in mice leads to leanness, resistance to diet-induced obesity and enhanced leptin sensitivity. *Int.J.Obes.Relat Metab Disord.* **28**, 640-648.

Reaume, A. G., Elliott, J. L., Hoffman, E. K., Kowall, N. W., Ferrante, R. J., Siwek, D. F., Wilcox, H. M., Flood, D. G., Beal, M. F., Brown, R. H., Jr., Scott, R. W., & Snider, W. D. (1996). Motor neurons in Cu/Zn superoxide dismutase-deficient mice develop normally but exhibit enhanced cell death after axonal injury. *Nat.Genet.* **13**, 43-47.

Redfern, P. A. (1970). Neuromuscular transmission in new-born rats. *J.Physiol* **209**, 701-709.

Reibaud, M., Obinu, M. C., Ledent, C., Parmentier, M., Bohme, G. A., & Imperato, A. (1999). Enhancement of memory in cannabinoid CB1 receptor knock-out mice. *Eur.J.Pharmacol.* **379** , R1-R2.

Ridet, J. L., Malhotra, S. K., Privat, A., & Gage, F. H. (1997). Reactive astrocytes: cellular and molecular cues to biological function. *Trends Neurosci.* **20**, 570-577.

Ripps, M. E., Huntley, G. W., Hof, P. R., Morrison, J. H., & Gordon, J. W. (1995). Transgenic mice expressing an altered murine superoxide dismutase gene provide an animal model of amyotrophic lateral sclerosis. *Proc.Natl.Acad.Sci.U.S.A* **92**, 689-693.

Riviere, M., Meininger, V., Zeisser, P., & Munsat, T. (1998). An analysis of extended survival in patients with amyotrophic lateral sclerosis treated with riluzole. *Arch.Neurol.* **55**, 526-528.

Rizzardini, M., Mangolini, A., Lupi, M., Ubezio, P., Bendotti, C., & Cantoni, L. (2005). Low levels of ALS-linked Cu/Zn superoxide dismutase increase the production of reactive oxygen species and cause mitochondrial damage and death in motor neuron-like cells. *J.Neurol.Sci.* **232**, 95-103.

Rizzuto, R., Pinton, P., Carrington, W., Fay, F. S., Fogarty, K. E., Lifshitz, L. M., Tuft, R. A., & Pozzan, T. (1998). Close contacts with the endoplasmic reticulum as determinants of mitochondrial Ca2+ responses. *Science* **280**, 1763-1766.

Robb-Gaspers, L. D., Burnett, P., Rutter, G. A., Denton, R. M., Rizzuto, R., & Thomas, A. P. (1998). Integrating cytosolic calcium signals into mitochondrial metabolic responses. *EMBO J.* **17**, 4987-5000.

Robb, S. J. & Connor, J. R. (1998). An in vitro model for analysis of oxidative death in primary mouse astrocytes. *Brain Res.* **788**, 125-132.

Robertson, J., Beaulieu, J. M., Doroudchi, M. M., Durham, H. D., Julien, J. P., & Mushynski, W. E. (2001). Apoptotic death of neurons exhibiting peripherin aggregates is mediated by the proinflammatory cytokine tumor necrosis factor-alpha. *J.Cell Biol.* **155**, 217-226.

Robertson, J., Doroudchi, M. M., Nguyen, M. D., Durham, H. D., Strong, M. J., Shaw, G., Julien, J. P., & Mushynski, W. E. (2003). A neurotoxic peripherin splice variant in a mouse model of ALS. *J.Cell Biol.* **160**, 939-949.

Robitaille, R., Garcia, M. L., Kaczorowski, G. J., & Charlton, M. P. (1993). Functional colocalization of calcium and calcium-gated potassium channels in control of transmitter release. *Neuron* **11**, 645-655.

Rodrigo, G. C., Lawrence, C. L., & Standen, N. B. (2002). Dinitrophenol pretreatment of rat ventricular myocytes protects against damage by metabolic inhibition and reperfusion. *J.Mol.Cell Cardiol.* **34**, 555-569.

Rodriguez, d. F., Navarro, M., Gomez, R., Escuredo, L., Nava, F., Fu, J., Murillo-Rodriguez, E., Giuffrida, A., LoVerme, J., Gaetani, S., Kathuria, S., Gall, C., & Piomelli, D. (2001). An anorexic lipid mediator regulated by feeding. *Nature* **414**, 209-212.

Romanes, G. J. (1946). Motor Localization and the Effects of Nerve Injury on the Ventral Horn Cells of the Spinal Cord. *J. Anat.* **80**, 117.

Rosen, D. R., Siddique, T., Patterson, D., Figlewicz, D. A., Sapp, P., Hentati, A., Donaldson, D., Goto, J., O'Regan, J. P., Deng, H. X., & . (1993). Mutations in Cu/Zn superoxide dismutase gene are associated with familial amyotrophic lateral sclerosis. *Nature* **362**, 59-62.

Rosenberg, P. A., Amin, S., & Leitner, M. (1992). Glutamate uptake disguises neurotoxic potency of glutamate agonists in cerebral cortex in dissociated cell culture. *J.Neurosci.* **12**, 56-61.

Ross, J. J., Duxson, M. J., & Harris, A. J. (1987). Formation of primary and secondary myotubes in rat lumbrical muscles. *Development* **100**, 383-394.

Rothstein, J. D., Kuncl, R., Chaudhry, V., Clawson, L., Cornblath, D. R., Coyle, J. T., & Drachman, D. B. (1991). Excitatory amino acids in amyotrophic lateral sclerosis: an update. *Ann.Neurol.* **30**, 224-225.

Rothstein, J. D., Martin, L. J., & Kuncl, R. W. (1992). Decreased glutamate transport by the brain and spinal cord in amyotrophic lateral sclerosis. *N.Engl.J.Med.* **326**, 1464-1468.

Rothstein, J. D., Jin, L., Dykes-Hoberg, M., & Kuncl, R. W. (1993). Chronic inhibition of glutamate uptake produces a model of slow neurotoxicity. *Proc.Natl.Acad.Sci.U.S.A* **90**, 6591-6595.

Rothstein, J. D., Van Kammen, M., Levey, A. I., Martin, L. J., & Kuncl, R. W. (1995). Selective loss of glial glutamate transporter GLT-1 in amyotrophic lateral sclerosis. *Ann.Neurol.* **38**, 73-84.

Rothstein, J. D., Dykes-Hoberg, M., Pardo, C. A., Bristol, L. A., Jin, L., Kuncl, R. W., Kanai, Y., Hediger, M. A., Wang, Y., Schielke, J. P., & Welty, D. F. (1996). Knockout of glutamate transporters reveals a major role for astroglial transport in excitotoxicity and clearance of glutamate. *Neuron* **16**, 675-686.

Rothstein, J. D., Patel, S., Regan, M. R., Haenggeli, C., Huang, Y. H., Bergles, D. E., Jin, L., Dykes, H. M., Vidensky, S., Chung, D. S., Toan, S. V., Bruijn, L. I., Su, Z. Z., Gupta, P., & Fisher, P. B. (2005). Beta-lactam antibiotics offer neuroprotection by increasing glutamate transporter expression. *Nature* **433**, 73-77.

Rowland, L. P. & Shneider, N. A. (2001). Amyotrophic Lateral Sclerosis. *N. Eng. J. Med.* **344(22)**, 1688-1700.

Roy, J., Minotti, S., Dong, L., Figlewicz, D. A., & Durham, H. D. (1998). Glutamate potentiates the toxicity of mutant Cu/Zn-superoxide dismutase in motor neurons by postsynaptic calcium-dependent mechanisms. *J.Neurosci.* **18**, 9673-9684.

Rubovitch, V., Gafni, M., & Sarne, Y. (2002). The cannabinoid agonist DALN positively modulates L-type voltage-dependent calcium-channels in N18TG2 neuroblastoma cells. *Brain Res.Mol.Brain Res.* **101**, 93-102.

Rubovitch, V., Gafni, M., & Sarne, Y. (2004). The involvement of VEGF receptors and MAPK in the cannabinoid potentiation of Ca2+ flux into N18TG2 neuroblastoma cells. *Brain Res.Mol.Brain Res.* **120**, 138-144.

Sanchez, C., Galve-Roperh, I., Canova, C., Brachet, P., & Guzman, M. (1998). Delta9-tetrahydrocannabinol induces apoptosis in C6 glioma cells. *FEBS Lett.* **436**, 6-10.

Sanchez, C., Rueda, D., Segui, B., Galve-Roperh, I., Levade, T., & Guzman, M. (2001). The CB(1) cannabinoid receptor of astrocytes is coupled to sphingomyelin hydrolysis through the adaptor protein fan. *Mol.Pharmacol.* **59**, 955-959.

Sanes, J. R. (1989). Extracellular matrix molecules that influence neural development. *Annu.Rev.Neurosci.* **12**, 491-516.

Sanes, J. R. & Lichtman, J. W. (1999). Development of the vertebrate neuromuscular junction. *Annu.Rev.Neurosci.* **22**, 389-442.

Santucci, V., Storme, J. J., Soubrie, P., & Le Fur, G. (1996). Arousal-enhancing properties of the CB1 cannabinoid receptor antagonist SR 141716A in rats as assessed by electroencephalographic spectral and sleep-waking cycle analysis. *Life Sci.* **58**, L103-L110.

Sanudo-Pena, M. C., Romero, J., Seale, G. E., Fernandez-Ruiz, J. J., & Walker, J. M. (2000). Activational role of cannabinoids on movement. *Eur.J.Pharmacol.* **391**, 269-274.

Sargsyan, S. A., Monk, P. N., & Shaw, P. J. (2005). Microglia as potential contributors to motor neuron injury in amyotrophic lateral sclerosis. *Glia* **51**, 241-253.

Sarker, K. P., Obara, S., Nakata, M., Kitajima, I., & Maruyama, I. (2000). Anandamide induces apoptosis of PC-12 cells: involvement of superoxide and caspase-3. *FEBS Lett.* **472**, 39-44.

Sasaki, S. & Iwata, M. (1996). Ultrastructural study of synapses in the anterior horn neurons of patients with amyotrophic lateral sclerosis. *Neurosci.Lett.* **204**, 53-56.

Sasaki, S. & Iwata, M. (1996). Impairment of fast axonal transport in the proximal axons of anterior horn neurons in amyotrophic lateral sclerosis. *Neurology* **47**, 535-540.

Sasaki, S., Warita, H., Abe, K., & Iwata, M. (2001). Inducible nitric oxide synthase (iNOS) and nitrotyrosine immunoreactivity in the spinal cords of transgenic mice with a G93A mutant SOD1 gene. *J.Neuropathol.Exp.Neurol.* **60**, 839-846.

Sattler, R., Charlton, M. P., Hafner, M., & Tymianski, M. (1998). Distinct influx pathways, not calcium load, determine neuronal vulnerability to calcium neurotoxicity. *J.Neurochem.* **71**, 2349-2364.

Scarmeas, N., Shih, T., Stern, Y., Ottman, R., & Rowland, L. P. (2002). Premorbid weight, body mass, and varsity athletics in ALS. *Neurology* **59**, 773-775.

Schatz, A. R., Kessler, F. K., & Kaminski, N. E. (1992). Inhibition of adenylate cyclase by delta 9-tetrahydrocannabinol in mouse spleen cells: a potential mechanism for cannabinoid-mediated immunosuppression. *Life Sci.* **51**, L25-L30.

Schiffer, D., Cordera, S., Cavalla, P., & Migheli, A. (1996). Reactive astrogliosis of the spinal cord in amyotrophic lateral sclerosis. *J.Neurol.Sci.* **139 Suppl**, 27-33.

Schudt, C., Gaertner, U., Dolken, G., & Pette, D. (1975). Calcium-related changes of enzyme activities in energy metabolism of cultured embryonic chick myoblasts and myotubes. *Eur.J.Biochem.* **60**, 579-586.

Seeburger, J. L., Tarras, S., Natter, H., & Springer, J. E. (1993). Spinal cord motoneurons express p75NGFR and p145trkB mRNA in amyotrophic lateral sclerosis. *Brain Res.* **621**, 111-115.

Sharp, P. S., Dick, J. R., & Greensmith, L. (2005). The effect of peripheral nerve injury on disease progression in the $SOD1^{G93A}$ mouse model of amyotrophic lateral sclerosis. *Neuroscience* **130**, 897-910.

Shaw, P. J. (2005). Molecular and cellular pathways of neurodegeneration in motor neurone disease. *J.Neurol.Neurosurg.Psychiatry* **76**, 1046-1057.

Shen, M., Piser, T. M., Seybold, V. S., & Thayer, S. A. (1996). Cannabinoid receptor agonists inhibit glutamatergic synaptic transmission in rat hippocampal cultures. *J.Neurosci.* **16**, 4322-4334.

Shen, M. & Thayer, S. A. (1998). The cannabinoid agonist Win55,212-2 inhibits calcium channels by receptor-mediated and direct pathways in cultured rat hippocampal neurons. *Brain Res.* **783**, 77-84.

Shen, M. & Thayer, S. A. (1998). Cannabinoid receptor agonists protect cultured rat hippocampal neurons from excitotoxicity. *Mol.Pharmacol.* **54**, 459-462.

Shinder, G. A., Lacourse, M. C., Minotti, S., & Durham, H. D. (2001). Mutant Cu/Zn-superoxide dismutase proteins have altered solubility and interact with heat shock/stress proteins in models of amyotrophic lateral sclerosis. *J.Biol.Chem.* **276**, 12791-12796.

Siklos, L., Engelhardt, J., Harati, Y., Smith, R. G., Joo, F., & Appel, S. H. (1996). Ultrastructural evidence for altered calcium in motor nerve terminals in amyotropic lateral sclerosis. *Ann.Neurol.* **39**, 203-216.

Sipe, J. C., Chiang, K., Gerber, A. L., Beutler, E., & Cravatt, B. F. (2002). A missense mutation in human fatty acid amide hydrolase associated with problem drug use. *Proc.Natl.Acad.Sci.U.S.A* **99**, 8394-8399.

Skaper, S. D., Buriani, A., Dal Toso, R., Petrelli, L., Romanello, S., Facci, L., & Leon, A. (1996). The ALIAmide palmitoylethanolamide and cannabinoids, but not anandamide, are protective in a delayed postglutamate paradigm of excitotoxic death in cerebellar granule neurons. *Proc.Natl.Acad.Sci.U.S.A* **93**, 3984-3989.

Slanina, K. A., Roberto, M., & Schweitzer, P. (2005). Endocannabinoids restrict hippocampal long-term potentiation via CB1. *Neuropharmacology*. **49(5)**, 660-8.

Slipetz, D. M., O'Neill, G. P., Favreau, L., Dufresne, C., Gallant, M., Gareau, Y., Guay, D., Labelle, M., & Metters, K. M. (1995). Activation of the human peripheral cannabinoid receptor results in inhibition of adenylyl cyclase. *Mol.Pharmacol.* **48**, 352-361.

Slivka, A., Mytilineou, C., & Cohen, G. (1987). Histochemical evaluation of glutathione in brain. *Brain Res.* **409**, 275-284.

Smart, D., Gunthorpe, M. J., Jerman, J. C., Nasir, S., Gray, J., Muir, A. I., Chambers, J. K., Randall, A. D., & Davis, J. B. (2000). The endogenous lipid anandamide is a full agonist at the human vanilloid receptor (hVR1). *Br.J.Pharmacol.* **129**, 227-230.

Snow, D. M., Lemmon, V., Carrino, D. A., Caplan, A. I., & Silver, J. (1990). Sulfated proteoglycans in astroglial barriers inhibit neurite outgrowth in vitro. *Exp.Neurol.* **109**, 111-130.

Sockanathan, S., Perlmann, T., & Jessell, T. M. (2003). Retinoid receptor signaling in postmitotic motor neurons regulates rostrocaudal positional identity and axonal projection pattern. *Neuron* **40**, 97-111.

Solenski, N. J., Kostecki, V. K., Dovey, S., & Periasamy, A. (2003). Nitric-oxide-induced depolarization of neuronal mitochondria: implications for neuronal cell death. *Mol.Cell Neurosci.* **24**, 1151-1169.

Son, M., Fathallah-Shaykh, H. M., & Elliott, J. L. (2001). Survival in a transgenic model of FALS is independent of iNOS expression. *Ann.Neurol.* **50**, 273.

Soussan, L., Burakov, D., Daniels, M. P., Toister-Achituv, M., Porat, A., Yarden, Y., & Elazar, Z. (1999). ERG30, a VAP-33-related protein, functions in protein transport mediated by COPI vesicles. *J.Cell Biol.* **146**, 301-311.

Sperandio, S., de, B., I, & Bredesen, D. E. (2000). An alternative, nonapoptotic form of programmed cell death. *Proc.Natl.Acad.Sci.U.S.A* **97**, 14376-14381.

Spreux-Varoquaux, O., Bensimon, G., Lacomblez, L., Salachas, F., Pradat, P. F., Le Forestier, N., Marouan, A., Dib, M., & Meininger, V. (2002). Glutamate levels in cerebrospinal fluid in amyotrophic lateral sclerosis: a reappraisal using a new HPLC method with coulometric detection in a large cohort of patients. *J.Neurol.Sci.* **193**, 73-78.

Steindler, D. A., O'Brien, T. F., Laywell, E., Harrington, K., Faissner, A., & Schachner, M. (1990). Boundaries during normal and abnormal brain development: in vivo and in vitro studies of glia and glycoconjugates. *Exp.Neurol.* **109**, 35-56.

Stella, N., Schweitzer, P., & Piomelli, D. (1997). A second endogenous cannabinoid that modulates long-term potentiation. *Nature* **388**, 773-778.

Stella, N. & Piomelli, D. (2001). Receptor-dependent formation of endogenous cannabinoids in cortical neurons. *Eur.J.Pharmacol.* **425**, 189-196.

Sterneck, E., Kaplan, D. R., & Johnson, P. F. (1996). Interleukin-6 induces expression of peripherin and cooperates with Trk receptor signaling to promote neuronal differentiation in PC12 cells. *J.Neurochem.* **67**, 1365-1374.

Stewart, V. C., Sharpe, M. A., Clark, J. B., & Heales, S. J. (2000). Astrocyte-derived nitric oxide causes both reversible and irreversible damage to the neuronal mitochondrial respiratory chain. *J.Neurochem.* **75**, 694-700.

Storkebaum, E., Lambrechts, D., Dewerchin, M., Moreno-Murciano, M. P., Appelmans, S., Oh, H., Van Damme, P., Rutten, B., Man, W. Y., De Mol, M., Wyns, S., Manka, D., Vermeulen, K., van den Bosch. L., Mertens, N., Schmitz, C., Robberecht, W., Conway, E. M., Collen, D., Moons, L., & Carmeliet, P. (2005). Treatment of motoneuron degeneration by intracerebroventricular delivery of VEGF in a rat model of ALS. *Nat.Neurosci.* **8**, 85-92.

Stout, A. K., Raphael, H. M., Kanterewicz, B. I., Klann, E., & Reynolds, I. J. (1998). Glutamate-induced neuron death requires mitochondrial calcium uptake. *Nat.Neurosci.* **1**, 366-373.

Sturtz, L. A., Diekert, K., Jensen, L. T., Lill, R., & Culotta, V. C. (2001). A fraction of yeast Cu,Zn-superoxide dismutase and its metallochaperone, CCS, localize to the intermembrane space of mitochondria. A physiological role for SOD1 in guarding against mitochondrial oxidative damage. *J.Biol.Chem.* **276**, 38084-38089.

Subramaniam, J. R., Lyons, W. E., Liu, J., Bartnikas, T. B., Rothstein, J., Price, D. L., Cleveland, D. W., Gitlin, J. D., & Wong, P. C. (2002). Mutant SOD1 causes motor neuron disease independent of copper chaperone-mediated copper loading. *Nat.Neurosci.* **5**, 301-307.

Sugiura, T., Kondo, S., Sukagawa, A., Nakane, S., Shinoda, A., Itoh, K., Yamashita, A., & Waku, K. (1995). 2-Arachidonoylglycerol: a possible endogenous cannabinoid receptor ligand in brain. *Biochem.Biophys.Res.Commun.* **215**, 89-97.

Sugiura, T., Kodaka, T., Kondo, S., Tonegawa, T., Nakane, S., Kishimoto, S., Yamashita, A., & Waku, K. (1996). 2-Arachidonoylglycerol, a putative endogenous cannabinoid receptor ligand, induces rapid, transient elevation of intracellular free Ca2+ in neuroblastoma x glioma hybrid NG108-15 cells. *Biochem.Biophys.Res.Commun.* **229**, 58-64.

Sugiura, T., Yoshinaga, N., Kondo, S., Waku, K., & Ishima, Y. (2000). Generation of 2-arachidonoylglycerol, an endogenous cannabinoid receptor ligand, in picrotoxinin-administered rat brain. *Biochem.Biophys.Res.Commun.* **271**, 654-658.

Sugiura, T., Yoshinaga, N., & Waku, K. (2001). Rapid generation of 2-arachidonoylglycerol, an endogenous cannabinoid receptor ligand, in rat brain after decapitation. *Neurosci.Lett.* **297**, 175-178.

Sugiyama, K., Brunori, A., & Mayer, M. L. (1989). Glial uptake of excitatory amino acids influences neuronal survival in cultures of mouse hippocampus. *Neuroscience* **32**, 779-791.

Sulcova, E., Mechoulam, R., & Fride, E. (1998). Biphasic effects of anandamide. *Pharmacol.Biochem.Behav.* **59**, 347-352.

Sullivan, P. G., Rabchevsky, A. G., Waldmeier, P. C., & Springer, J. E. (2005). Mitochondrial permeability transition in CNS trauma: cause or effect of neuronal cell death? *J.Neurosci.Res.* **79**, 231-239.

Swanson, R. A., Liu, J., Miller, J. W., Rothstein, J. D., Farrell, K., Stein, B. A., & Longuemare, M. C. (1997). Neuronal regulation of glutamate transporter subtype expression in astrocytes. *J.Neurosci.* **17**, 932-940.

Swerdlow, R. H., Parks, J. K., Cassarino, D. S., Trimmer, P. A., Miller, S. W., Maguire, D. J., Sheehan, J. P., Maguire, R. S., Pattee, G., Juel, V. C., Phillips, L. H., Tuttle, J. B., Bennett, J. P., Jr., Davis, R. E., & Parker, W. D., Jr. (1998). Mitochondria in sporadic amyotrophic lateral sclerosis. *Exp.Neurol.* **153**, 135-142.

Syntichaki, P. & Tavernarakis, N. (2002). Death by necrosis. Uncontrollable catastrophe, or is there order behind the chaos? *EMBO Rep.* **3**, 604-609.

Syntichaki, P. & Tavernarakis, N. (2003). The biochemistry of neuronal necrosis: rogue biology? *Nat.Rev.Neurosci.* **4**, 672-684.

Takahashi, T., Nakajima, Y., Hirosawa, K., Nakajima, S., & Onodera, K. (1987). Structure and physiology of developing neuromuscular synapses in culture. *J.Neurosci.* **7**, 473-481.

Takeuchi, H., Kobayashi, Y., Ishigaki, S., Doyu, M., & Sobue, G. (2002). Mitochondrial localization of mutant superoxide dismutase 1 triggers caspase-dependent cell death in a cellular model of familial amyotrophic lateral sclerosis. *J.Biol.Chem.* **277**, 50966-50972.

Takeuchi, H., Kobayashi, Y., Yoshihara, T., Niwa, J., Doyu, M., Ohtsuka, K., & Sobue, G. (2002). Hsp70 and Hsp40 improve neurite outgrowth and suppress intracytoplasmic aggregate formation in cultured neuronal cells expressing mutant SOD1. *Brain Res.* **949**, 11-22.

Tanabe, Y., William, C., & Jessell, T. M. (1998). Specification of motor neuron identity by the MNR2 homeodomain protein. *Cell* **95**, 67-80.

Tanaka, J., Toku, K., Zhang, B., Ishihara, K., Sakanaka, M., & Maeda, N. (1999). Astrocytes prevent neuronal death induced by reactive oxygen and nitrogen species. *Glia* **28**, 85-96.

Tanaka, K., Watase, K., Manabe, T., Yamada, K., Watanabe, M., Takahashi, K., Iwama, H., Nishikawa, T., Ichihara, N., Kikuchi, T., Okuyama, S., Kawashima, N., Hori, S., Takimoto, M., & Wada, K. (1997). Epilepsy and exacerbation of brain injury in mice lacking the glutamate transporter GLT-1. *Science* **276**, 1699-1702.

Tansey, F. A., Farooq, M., & Cammer, W. (1991). Glutamine synthetase in oligodendrocytes and astrocytes: new biochemical and immunocytochemical evidence. *J.Neurochem.* **56**, 266-272.

Tao-Cheng, J. H., Nagy, Z., & Brightman, M. W. (1987). Tight junctions of brain endothelium in vitro are enhanced by astroglia. *J.Neurosci.* **7**, 3293-3299.

Tateno, M., Sadakata, H., Tanaka, M., Itohara, S., Shin, R. M., Miura, M., Masuda, M., Aosaki, T., Urushitani, M., Misawa, H., & Takahashi, R. (2004). Calcium-permeable

AMPA receptors promote misfolding of mutant SOD1 protein and development of amyotrophic lateral sclerosis in a transgenic mouse model. *Hum.Mol.Genet.* **13**, 2183-2196.

Tikka, T. M. & Koistinaho, J. E. (2001). Minocycline provides neuroprotection against N-methyl-D-aspartate neurotoxicity by inhibiting microglia. *J.Immunol.* **166**, 7527-7533.

Tikka, T. M., Vartiainen, N. E., Goldsteins, G., Oja, S. S., Andersen, P. M., Marklund, S. L., & Koistinaho, J. (2002). Minocycline prevents neurotoxicity induced by cerebrospinal fluid from patients with motor neurone disease. *Brain* **125**, 722-731.

Tomaselli, K. J., Neugebauer, K. M., Bixby, J. L., Lilien, J., & Reichardt, L. F. (1988). N-cadherin and integrins: two receptor systems that mediate neuronal process outgrowth on astrocyte surfaces. *Neuron* **1**, 33-43.

Tomkins, J., Usher, P., Slade, J. Y., Ince, P. G., Curtis, A., Bushby, K., & Shaw, P. J. (1998). Novel insertion in the KSP region of the neurofilament heavy gene in amyotrophic lateral sclerosis (ALS). *Neuroreport* **9**, 3967-3970.

Topp, J. D., Gray, N. W., Gerard, R. D., & Horazdovsky, B. F. (2004). Alsin is a Rab5 and Rac1 guanine nucleotide exchange factor. *J.Biol.Chem.* **279**, 24612-24623.

Toulmond, S., Parnet, P., & Linthorst, A. C. (1996). When cytokines get on your nerves: cytokine networks and CNS pathologies. *Trends Neurosci.* **19**, 409-410.

Traynor, B. J., Alexander, M., Corr, B., Frost, E., & Hardiman, O. (2003). An outcome study of riluzole in amyotrophic lateral sclerosis--a population-based study in Ireland, 1996-2000. *J.Neurol.* **250**, 473-479.

Trieu, V. N., Liu, R., Liu, X. P., & Uckun, F. M. (2000). A specific inhibitor of janus kinase-3 increases survival in a transgenic mouse model of amyotrophic lateral sclerosis. *Biochem.Biophys.Res.Commun.* **267**, 22-25.

Troost, D., van den Oord, J. J., & Vianney de Jong, J. M. (1990). Immunohistochemical characterization of the inflammatory infiltrate in amyotrophic lateral sclerosis. *Neuropathol.Appl.Neurobiol.* **16**, 401-410.

Trotti, D., Rossi, D., Gjesdal, O., Levy, L. M., Racagni, G., Danbolt, N. C., & Volterra, A. (1996). Peroxynitrite inhibits glutamate transporter subtypes. *J.Biol.Chem.* **271**, 5976-5979.

Trotti, D., Rolfs, A., Danbolt, N. C., Brown, R. H., Jr., & Hediger, M. A. (1999). SOD1 mutants linked to amyotrophic lateral sclerosis selectively inactivate a glial glutamate transporter. *Nat.Neurosci.* **2**, 848.

Trotti, D., Aoki, M., Pasinelli, P., Berger, U. V., Danbolt, N. C., Brown, R. H., Jr., & Hediger, M. A. (2001). Amyotrophic lateral sclerosis-linked glutamate transporter mutant has impaired glutamate clearance capacity. *J.Biol.Chem.* **276**, 576-582.

Troy, C. M., Muma, N. A., Greene, L. A., Price, D. L., & Shelanski, M. L. (1990). Regulation of peripherin and neurofilament expression in regenerating rat motor neurons. *Brain Res.* **529**, 232-238.

Tsou, K., Brown, S., Sanudo-Pena, M. C., Mackie, K., & Walker, J. M. (1998). Immunohistochemical distribution of cannabinoid CB1 receptors in the rat central nervous system. *Neuroscience* **83**, 393-411.

Tu, P. H., Raju, P., Robinson, K. A., Gurney, M. E., Trojanowski, J. Q., & Lee, V. M. (1996). Transgenic mice carrying a human mutant superoxide dismutase transgene develop neuronal cytoskeletal pathology resembling human amyotrophic lateral sclerosis lesions. *Proc.Natl.Acad.Sci.U.S.A* **93**, 3155-3160.

Tu, P. H., Robinson, K. A., de Snoo, F., Eyer, J., Peterson, A., Lee, V. M., & Trojanowski, J. Q. (1997). Selective degeneration of Purkinje cells with Lewy body-like inclusions in aged NFHLACZ transgenic mice. *J.Neurosci.* **17**, 1064-1074.

Tudor, E. L., Perkinton, M. S., Schmidt, A., Ackerley, S., Brownlees, J., Jacobsen, N. J., Byers, H. L., Ward, M., Hall, A., Leigh, P. N., Shaw, C. E., McLoughlin, D. M., & Miller, C. C. (2005). ALS2/Alsin Regulates Rac-PAK Signaling and Neurite Outgrowth. *J.Biol.Chem.* **280**, 34735-34740.

Twitchell, W., Brown, S., & Mackie, K. (1997). Cannabinoids inhibit N- and P/Q-type calcium channels in cultured rat hippocampal neurons. *J.Neurophysiol.* **78**, 43-50.

Tyc, F. & Vrbova, G. (1995). Stabilisation of neuromuscular junctions by leupeptin increases motor unit size in partially denervated rat muscles. *Brain Res.Dev.Brain Res.* **88**, 186-193.

Tytell, M., Greenberg, S. G., & Lasek, R. J. (1986). Heat shock-like protein is transferred from glia to axon. *Brain Res.* **363**, 161-164.

Van Damme, P., Leyssen, M., Callewaert, G., Robberecht, W., & van den Bosch. L. (2003). The AMPA receptor antagonist NBQX prolongs survival in a transgenic mouse model of amyotrophic lateral sclerosis. *Neurosci.Lett.* **343**, 81-84.

Van Damme, P., Braeken, D., Callewaert, G., Robberecht, W., & van den Bosch. L. (2005). GluR2 deficiency accelerates motor neuron degeneration in a mouse model of amyotrophic lateral sclerosis. *J.Neuropathol.Exp.Neurol.* **64**, 605-612.

van den Bosch. L. & Robberecht, W. (2000). Different receptors mediate motor neuron death induced by short and long exposures to excitotoxicity. *Brain Res.Bull.* **53**, 383-388.

van den Bosch. L., Vandenberghe, W., Klaassen, H., Van Houtte, E., & Robberecht, W. (2000). Ca(2+)-permeable AMPA receptors and selective vulnerability of motor neurons. *J.Neurol.Sci.* **180**, 29-34.

van den Bosch. L., Van Damme, P., Vleminckx, V., Van Houtte, E., Lemmens, G., Missiaen, L., Callewaert, G., & Robberecht, W. (2002). An alpha-mercaptoacrylic acid derivative (PD150606) inhibits selective motor neuron death via inhibition of kainite induced Ca2+ influx and not via calpain inhibition. *Neuropharmacology* **42**, 706-713.

van den Bosch. L., Tilkin, P., Lemmens, G., & Robberecht, W. (2002). Minocycline delays disease onset and mortality in a transgenic model of ALS. *Neuroreport* **13**, 1067-1070.

van den Bosch. L., Schwaller, B., Vleminckx, V., Meijers, B., Stork, S., Ruehlicke, T., Van Houtte, E., Klaassen, H., Celio, M. R., Missiaen, L., Robberecht, W., & Berchtold, M. W. (2002). Protective effect of parvalbumin on excitotoxic motor neuron death. *Exp.Neurol.* **174**, 150-161.

van der Stelt. M., Veldhuis, W. B., Bar, P. R., Veldink, G. A., Vliegenthart, J. F., & Nicolay, K. (2001). Neuroprotection by Delta9-tetrahydrocannabinol, the main active compound in marijuana, against ouabain-induced in vivo excitotoxicity. *J.Neurosci.* **21**, 6475-6479.

van der Stelt. M., Veldhuis, W. B., van Haaften, G. W., Fezza, F., Bisogno, T., Bar, P. R., Veldink, G. A., Vliegenthart, J. F., Di Marzo, V., & Nicolay, K. (2001). Exogenous anandamide protects rat brain against acute neuronal injury in vivo. *J.Neurosci.* **21**, 8765-8771.

Vandenberghe, W., van den Bosch. L., & Robberecht, W. (1998). Glial cells potentiate kainate-induced neuronal death in a motoneuron-enriched spinal coculture system. *Brain Res.* **807**, 1-10.

Vandenberghe, W., Robberecht, W., & Brorson, J. R. (2000). AMPA receptor calcium permeability, GluR2 expression, and selective motoneuron vulnerability. *J.Neurosci.* **20**, 123-132.

Vandenberghe, W., Ihle, E. C., Patneau, D. K., Robberecht, W., & Brorson, J. R. (2000). AMPA receptor current density, not desensitization, predicts selective motoneuron vulnerability. *J.Neurosci.* **20**, 7158-7166.

Vandenberghe, W., Bindokas, V. P., Miller, R. J., Robberecht, W., & Brorson, J. R. (2001). Subcellular localization of calcium-permeable AMPA receptors in spinal motoneurons. *Eur.J.Neurosci.* **14**, 305-314.

Vanoni, C., Massari, S., Losa, M., Carrega, P., Perego, C., Conforti, L., & Pietrini, G. (2004). Increased internalisation and degradation of GLT-1 glial glutamate transporter in a cell model for familial amyotrophic lateral sclerosis (ALS). *J.Cell Sci.* **117**, 5417-5426.

Vanselow, B. K. & Keller, B. U. (2000). Calcium dynamics and buffering in oculomotor neurones from mouse that are particularly resistant during amyotrophic lateral sclerosis (ALS)-related motoneurone disease. *J.Physiol* **525 Pt 2**, 433-445.

Varga, K., Lake, K., Martin, B. R., & Kunos, G. (1995). Novel antagonist implicates the CB1 cannabinoid receptor in the hypotensive action of anandamide. *Eur.J.Pharmacol.* **278**, 279-283.

Veldhuis, W. B., van der Stelt. M., Wadman, M. W., van Zadelhoff, G., Maccarrone, M., Fezza, F., Veldink, G. A., Vliegenthart, J. F., Bar, P. R., Nicolay, K., & Di Marzo, V. (2003). Neuroprotection by the endogenous cannabinoid anandamide and arvanil against in vivo excitotoxicity in the rat: role of vanilloid receptors and lipoxygenases. *J.Neurosci.* **23**, 4127-4133.

Venance, L., Piomelli, D., Glowinski, J., & Giaume, C. (1995). Inhibition by anandamide of gap junctions and intercellular calcium signalling in striatal astrocytes. *Nature* **376**, 590-594.

Venstrom, K. A. & Reichardt, L. F. (1993). Extracellular matrix. 2: Role of extracellular matrix molecules and their receptors in the nervous system. *FASEB J.* **7**, 996-1003.

Vernadakis, A. (1996). Glia-neuron intercommunications and synaptic plasticity. *Prog.Neurobiol.* **49** , 185-214.

Vielhaber, S., Kunz, D., Winkler, K., Wiedemann, F. R., Kirches, E., Feistner, H., Heinze, H. J., Elger, C. E., Schubert, W., & Kunz, W. S. (2000). Mitochondrial DNA abnormalities in skeletal muscle of patients with sporadic amyotrophic lateral sclerosis. *Brain* **123 (Pt 7)**, 1339-1348.

Vijayvergiya, C., Beal, M. F., Buck, J., & Manfredi, G. (2005). Mutant superoxide dismutase 1 forms aggregates in the brain mitochondrial matrix of amyotrophic lateral sclerosis mice. *J.Neurosci.* **25**, 2463-2470.

Vleminckx, V., Van Damme, P., Goffin, K., Delye, H., van den Bosch. L., & Robberecht, W. (2002). Upregulation of HSP27 in a transgenic model of ALS. *J.Neuropathol.Exp.Neurol.* **61**, 968-974.

Vogel, Z., Barg, J., Levy, R., Saya, D., Heldman, E., & Mechoulam, R. (1993). Anandamide, a brain endogenous compound, interacts specifically with cannabinoid receptors and inhibits adenylate cyclase. *J.Neurochem.* **61**, 352-355.

Votyakova, T. V. & Reynolds, I. J. (2001). DeltaPsi(m)-Dependent and -independent production of reactive oxygen species by rat brain mitochondria. *J.Neurochem.* **79**, 266-277.

Vukosavic, S., Stefanis, L., Jackson-Lewis, V., Guegan, C., Romero, N., Chen, C., Dubois-Dauphin, M., & Przedborski, S. (2000). Delaying caspase activation by Bcl-2: A clue to disease retardation in a transgenic mouse model of amyotrophic lateral sclerosis. *J.Neurosci.* **20**, 9119-9125.

Wade, D. T., Makela, P., Robson, P., House, H., & Bateman, C. (2004). Do cannabis-based medicinal extracts have general or specific effects on symptoms in multiple sclerosis? A double-blind, randomized, placebo-controlled study on 160 patients. *Mult.Scler.* **10**, 434-441.

Wagner, J. A., Varga, K., Jarai, Z., & Kunos, G. (1999). Mesenteric vasodilation mediated by endothelial anandamide receptors. *Hypertension* **33**, 429-434.

Wagner, O. I., Ascano, J., Tokito, M., Leterrier, J. F., Janmey, P. A., & Holzbaur, E. L. (2004). The interaction of neurofilaments with the microtubule motor cytoplasmic dynein. *Mol.Biol.Cell* **15**, 5092-5100.

Waksman, Y., Olson, J. M., Carlisle, S. J., & Cabral, G. A. (1999). The central cannabinoid receptor (CB1) mediates inhibition of nitric oxide production by rat microglial cells. *J.Pharmacol.Exp.Ther.* **288**, 1357-1366.

Walker, J. M., Huang, S. M., Strangman, N. M., Tsou, K., & Sanudo-Pena, M. C. (1999). Pain modulation by release of the endogenous cannabinoid anandamide. *Proc.Natl.Acad.Sci.U.S.A* **96**, 12198-12203.

Walter, L., Franklin, A., Witting, A., Wade, C., Xie, Y., Kunos, G., Mackie, K., & Stella, N. (2003). Nonpsychotropic cannabinoid receptors regulate microglial cell migration. *J.Neurosci.* **23**, 1398-1405.

Walter, L. & Stella, N. (2004). Cannabinoids and neuroinflammation. *Br.J.Pharmacol.* **141**, 775-785.

Walz, W. & Mukerji, S. (1988). Lactate production and release in cultured astrocytes. *Neurosci.Lett.* **86**, 296-300.

Wang, L. J., Lu, Y. Y., Muramatsu, S., Ikeguchi, K., Fujimoto, K., Okada, T., Mizukami, H., Matsushita, T., Hanazono, Y., Kume, A., Nagatsu, T., Ozawa, K., & Nakano, I. (2002). Neuroprotective effects of glial cell line-derived neurotrophic factor mediated by an adeno-associated virus vector in a transgenic animal model of amyotrophic lateral sclerosis. *J.Neurosci.* **22**, 6920-6928.

Warita, H., Itoyama, Y., & Abe, K. (1999). Selective impairment of fast anterograde axonal transport in the peripheral nerves of asymptomatic transgenic mice with a G93A mutant SOD1 gene. *Brain Res.* **819**, 120-131.

Watanabe, M., Dykes-Hoberg, M., Culotta, V. C., Price, D. L., Wong, P. C., & Rothstein, J. D. (2001). Histological evidence of protein aggregation in mutant SOD1 transgenic mice and in amyotrophic lateral sclerosis neural tissues. *Neurobiol.Dis.* **8**, 933-941.

Waterman-Storer, C. M., Karki, S., & Holzbaur, E. L. (1995). The p150Glued component of the dynactin complex binds to both microtubules and the actin-related protein centractin (Arp-1). *Proc.Natl.Acad.Sci.U.S.A* **92**, 1634-1638.

Waterman-Storer, C. M., Karki, S. B., Kuznetsov, S. A., Tabb, J. S., Weiss, D. G., Langford, G. M., & Holzbaur, E. L. (1997). The interaction between cytoplasmic dynein and dynactin is required for fast axonal transport. *Proc.Natl.Acad.Sci.U.S.A* **94**, 12180-12185.

West, M., Mhatre, M., Ceballos, A., Floyd, R. A., Grammas, P., Gabbita, S. P., Hamdheydari, L., Mai, T., Mou, S., Pye, Q. N., Stewart, C., West, S., Williamson, K. S., Zemlan, F., & Hensley, K. (2004). The arachidonic acid 5-lipoxygenase inhibitor nordihydroguaiaretic acid inhibits tumor necrosis factor alpha activation of microglia and extends survival of G93A-SOD1 transgenic mice. *J.Neurochem.* **91**, 133-143.

Westlake, T. M., Howlett, A. C., Bonner, T. I., Matsuda, L. A., & Herkenham, M. (1994). Cannabinoid receptor binding and messenger RNA expression in human brain: an in vitro receptor autoradiography and in situ hybridization histochemistry study of normal aged and Alzheimer's brains. *Neuroscience* **63**, 637-652.

Weydt, P., Yuen, E. C., Ransom, B. R., & Moller, T. (2004). Increased cytotoxic potential of microglia from ALS-transgenic mice. *Glia* **48**, 179-182.

Weydt, P., Hong, S., Witting, A., Moller, T., Stella, N., & Kliot, M. (2005). Cannabinol delays symptom onset in SOD1 (G93A) transgenic mice without affecting survival. *Amyotroph.Lateral.Scler.Other Motor Neuron Disord.* **6**, 182-184.

White, C. M., Greensmith, L., & Vrbova, G. (2000). Repeated stimuli for axonal growth causes motoneuron death in adult rats: the effect of botulinum toxin followed by partial denervation. *Neuroscience* **95**, 1101-1109.

Wiedau-Pazos, M., Goto, J. J., Rabizadeh, S., Gralla, E. B., Roe, J. A., Lee, M. K., Valentine, J. S., & Bredesen, D. E. (1996). Altered reactivity of superoxide dismutase in familial amyotrophic lateral sclerosis. *Science* **271**, 515-518.

Wiedemann, F. R., Winkler, K., Kuznetsov, A. V., Bartels, C., Vielhaber, S., Feistner, H., & Kunz, W. S. (1998). Impairment of mitochondrial function in skeletal muscle of patients with amyotrophic lateral sclerosis. *J.Neurol.Sci.* **156**, 65-72.

Wiedemann, F. R., Manfredi, G., Mawrin, C., Beal, M. F., & Schon, E. A. (2002). Mitochondrial DNA and respiratory chain function in spinal cords of ALS patients. *J.Neurochem.* **80**, 616-625.

Wigstrom, H. & Gustafsson, B. (1985). Facilitation of hippocampal long-lasting potentiation by GABA antagonists. *Acta Physiol Scand.* **125**, 159-172.

Wiley, J. L. (2003). Sex-dependent effects of delta 9-tetrahydrocannabinol on locomotor activity in mice. *Neurosci.Lett.* **352**, 77-80.

Williams, C. M., Rogers, P. J., & Kirkham, T. C. (1998). Hyperphagia in pre-fed rats following oral delta9-THC. *Physiol Behav.* **65**, 343-346.

Williams, E. J., Doherty, P., Turner, G., Reid, R. A., Hemperly, J. J., & Walsh, F. S. (1992). Calcium influx into neurons can solely account for cell contact-dependent neurite outgrowth stimulated by transfected L1. *J.Cell Biol.* **119**, 883-892.

Williams, E. J., Walsh, F. S., & Doherty, P. (2003). The FGF receptor uses the endocannabinoid signaling system to couple to an axonal growth response. *J.Cell Biol.* **160**, 481-486.

Williamson, T. L., Bruijn, L. I., Zhu, Q., Anderson, K. L., Anderson, S. D., Julien, J. P., & Cleveland, D. W. (1998). Absence of neurofilaments reduces the selective vulnerability of motor neurons and slows disease caused by a familial amyotrophic lateral sclerosis-linked superoxide dismutase 1 mutant. *Proc.Natl.Acad.Sci.U.S.A* **95**, 9631-9636.

Williamson, T. L. & Cleveland, D. W. (1999). Slowing of axonal transport is a very early event in the toxicity of ALS-linked SOD1 mutants to motor neurons. *Nat.Neurosci.* **2**, 50-56.

Willoughby, K. A., Moore, S. F., Martin, B. R., & Ellis, E. F. (1997). The biodisposition and metabolism of anandamide in mice. *J.Pharmacol.Exp.Ther.* **282**, 243-247.

Wilson, R. I. & Nicoll, R. A. (2001). Endogenous cannabinoids mediate retrograde signalling at hippocampal synapses. *Nature* **410**, 588-592.

Wilson, R. I. & Nicoll, R. A. (2002). Endocannabinoid signaling in the brain. *Science* **296**, 678-682.

Wilson, S. J. & Harris, A. J. (1993). Formation of myotubes in aneural rat muscles. *Dev.Biol.* **156**, 509-518.

Winter, C. G., Saotome, Y., Levison, S. W., & Hirsh, D. (1995). A role for ciliary neurotrophic factor as an inducer of reactive gliosis, the glial response to central nervous system injury. *Proc.Natl.Acad.Sci.U.S.A* **92**, 5865-5869.

Witting, A., Weydt, P., Hong, S., Kliot, M., Moller, T., & Stella, N. (2004). Endocannabinoids accumulate in spinal cord of SOD1 transgenic mice. *J.Neurochem.* **89**, 1555-1557.

Wong, L. F., Azzouz, M., Walmsley, L. E., Askham, Z., Wilkes, F. J., Mitrophanous, K. A., Kingsman, S. M., & Mazarakis, N. D. (2004). Transduction patterns of pseudotyped lentiviral vectors in the nervous system. *Mol.Ther.* **9**, 101-111.

Wong, P. C., Pardo, C. A., Borchelt, D. R., Lee, M. K., Copeland, N. G., Jenkins, N. A., Sisodia, S. S., Cleveland, D. W., & Price, D. L. (1995). An adverse property of a familial ALS-linked SOD1 mutation causes motor neuron disease characterized by vacuolar degeneration of mitochondria. *Neuron* **14**, 1105-1116.

Wong, P. C., Waggoner, D., Subramaniam, J. R., Tessarollo, L., Bartnikas, T. B., Culotta, V. C., Price, D. L., Rothstein, J., & Gitlin, J. D. (2000). Copper chaperone for superoxide dismutase is essential to activate mammalian Cu/Zn superoxide dismutase. *Proc.Natl.Acad.Sci.U.S.A* **97**, 2886-2891.

Wyllie, A. H., Kerr, J. F., & Currie, A. R. (1980). Cell death: the significance of apoptosis. *Int.Rev.Cytol.* **68**, 251-306.

Xia, H., Mao, Q., Eliason, S. L., Harper, S. Q., Martins, I. H., Orr, H. T., Paulson, H. L., Yang, L., Kotin, R. M., & Davidson, B. L. (2004). RNAi suppresses polyglutamine-induced neurodegeneration in a model of spinocerebellar ataxia. *Nat.Med.* **10**, 816-820.

Xie, Z. P. & Poo, M. M. (1986). Initial events in the formation of neuromuscular synapse: rapid induction of acetylcholine release from embryonic neuron. *Proc.Natl.Acad.Sci.U.S.A* **83**, 7069-7073.

Xu, Z., Cork, L. C., Griffin, J. W., & Cleveland, D. W. (1993). Increased expression of neurofilament subunit NF-L produces morphological alterations that resemble the pathology of human motor neuron disease. *Cell* **73**, 23-33.

Yaffe, D. (1969). Cellular aspects of muscle differentiation in vitro. *Curr.Top.Dev.Biol.* **4**, 37-77.

Yamanaka, K., Vande, V. C., Eymard-Pierre, E., Bertini, E., Boespflug-Tanguy, O., & Cleveland, D. W. (2003). Unstable mutants in the peripheral endosomal membrane component ALS2 cause early-onset motor neuron disease. *Proc.Natl.Acad.Sci.U.S.A* **100**, 16041-16046.

Yamashima, T. (2000). Implication of cysteine proteases calpain, cathepsin and caspase in ischemic neuronal death of primates. *Prog.Neurobiol.* **62**, 273-295.

Yamashita, S., Mita, S., Kato, S., Okado, H., Ohama, E., & Uchino, M. (2002). Effect on motor neuron survival in mutant SOD1 (G93A) transgenic mice by Bcl-2 expression using retrograde axonal transport of adenoviral vectors. *Neurosci.Lett.* **328**, 289-293.

Yang, Y., Hentati, A., Deng, H. X., Dabbagh, O., Sasaki, T., Hirano, M., Hung, W. Y., Ouahchi, K., Yan, J., Azim, A. C., Cole, N., Gascon, G., Yagmour, A., Ben Hamida, M., Pericak-Vance, M., Hentati, F., & Siddique, T. (2001). The gene encoding alsin, a protein with three guanine-nucleotide exchange factor domains, is mutated in a form of recessive amyotrophic lateral sclerosis. *Nat.Genet.* **29**, 160-165.

Yasojima, K., Tourtellotte, W. W., McGeer, E. G., & McGeer, P. L. (2001). Marked increase in cyclooxygenase-2 in ALS spinal cord: implications for therapy. *Neurology* **57**, 952-956.

Young, S. H. & Poo, M. M. (1983). Spontaneous release of transmitter from growth cones of embryonic neurones. *Nature* **305**, 634-637.

Zajicek, J., Fox, P., Sanders, H., Wright, D., Vickery, J., Nunn, A., & Thompson, A. (2003). Cannabinoids for treatment of spasticity and other symptoms related to multiple sclerosis (CAMS study): multicentre randomised placebo-controlled trial. *Lancet* **362**, 1517-1526.

Zamore, P. D. (2001). RNA interference: listening to the sound of silence. *Nat.Struct.Biol.* **8**, 746-750.

Zamzami, N., Marchetti, P., Castedo, M., Hirsch, T., Susin, S. A., Masse, B., & Kroemer, G. (1996). Inhibitors of permeability transition interfere with the disruption of the mitochondrial transmembrane potential during apoptosis. *FEBS Lett.* **384**, 53-57.

Zanette, G., Tamburin, S., Manganotti, P., Refatti, N., Forgione, A., & Rizzuto, N. (2002). Different mechanisms contribute to motor cortex hyperexcitability in amyotrophic lateral sclerosis. *Clin.Neurophysiol.* **113**, 1688-1697.

Zang, D. W. & Cheema, S. S. (2002). Degeneration of corticospinal and bulbospinal systems in the superoxide dismutase 1(G93A G1H) transgenic mouse model of familial amyotrophic lateral sclerosis. *Neurosci.Lett.* **332**, 99-102.

Zhang, B., Tu, P., Abtahian, F., Trojanowski, J. Q., & Lee, V. M. (1997). Neurofilaments and orthograde transport are reduced in ventral root axons of transgenic mice that express human SOD1 with a G93A mutation. *J.Cell Biol.* **139**, 1307-1315.

Zhang, J., Hoffert, C., Vu, H. K., Groblewski, T., Ahmad, S., & O'Donnell, D. (2003). Induction of CB2 receptor expression in the rat spinal cord of neuropathic but not inflammatory chronic pain models. *Eur.J.Neurosci.* **17**, 2750-2754.

Zhang, R., Gascon, R., Miller, R. G., Gelinas, D. F., Mass, J., Hadlock, K., Jin, X., Reis, J., Narvaez, A., & McGrath, M. S. (2005). Evidence for systemic immune system alterations in sporadic amyotrophic lateral sclerosis (sALS). *J.Neuroimmunol.* **159**, 215-224.

Zhu, S., Stavrovskaya, I. G., Drozda, M., Kim, B. Y., Ona, V., Li, M., Sarang, S., Liu, A. S., Hartley, D. M., Wu, d. C., Gullans, S., Ferrante, R. J., Przedborski, S., Kristal, B. S., & Friedlander, R. M. (2002). Minocycline inhibits cytochrome c release and delays progression of amyotrophic lateral sclerosis in mice. *Nature* **417**, 74-78.

Zhu, W., Friedman, H., & Klein, T. W. (1998). Delta9-tetrahydrocannabinol induces apoptosis in macrophages and lymphocytes: involvement of Bcl-2 and caspase-1. *J.Pharmacol.Exp.Ther.* **286**, 1103-1109.

Zimmer, A., Zimmer, A. M., Hohmann, A. G., Herkenham, M., & Bonner, T. I. (1999). Increased mortality, hypoactivity, and hypoalgesia in cannabinoid CB1 receptor knockout mice. *Proc.Natl.Acad.Sci.U.S.A* **96**, 5780-5785.

Zoccarato, F., Cavallini, L., & Alexandre, A. (2004). Respiration-dependent removal of exogenous H2O2 in brain mitochondria: inhibition by Ca2+. *J.Biol.Chem.* **279**, 4166-4174.

Zoubine, M. N., Ma, J. Y., Smirnova, I. V., Citron, B. A., & Festoff, B. W. (1996). A molecular mechanism for synapse elimination: novel inhibition of locally generated thrombin delays synapse loss in neonatal mouse muscle. *Dev.Biol.* **179**, 447-457.

Zuardi, A. W., Rodrigues, J. A., & Cunha, J. M. (1991). Effects of cannabidiol in animal models predictive of antipsychotic activity. *Psychopharmacology (Berl)* **104**, 260-264.

Zygmunt, P. M., Petersson, J., Andersson, D. A., Chuang, H., Sorgard, M., Di Marzo, V., Julius, D., & Hogestatt, E. D. (1999). Vanilloid receptors on sensory nerves mediate the vasodilator action of anandamide. *Nature* **400**, 452-457.